LMSC-F087173

CR 183535

Solar Array Flight Experiment

Final Report

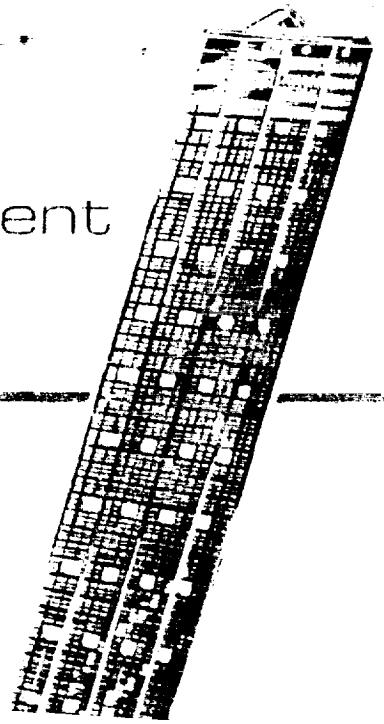

Contract NAS-8-31352

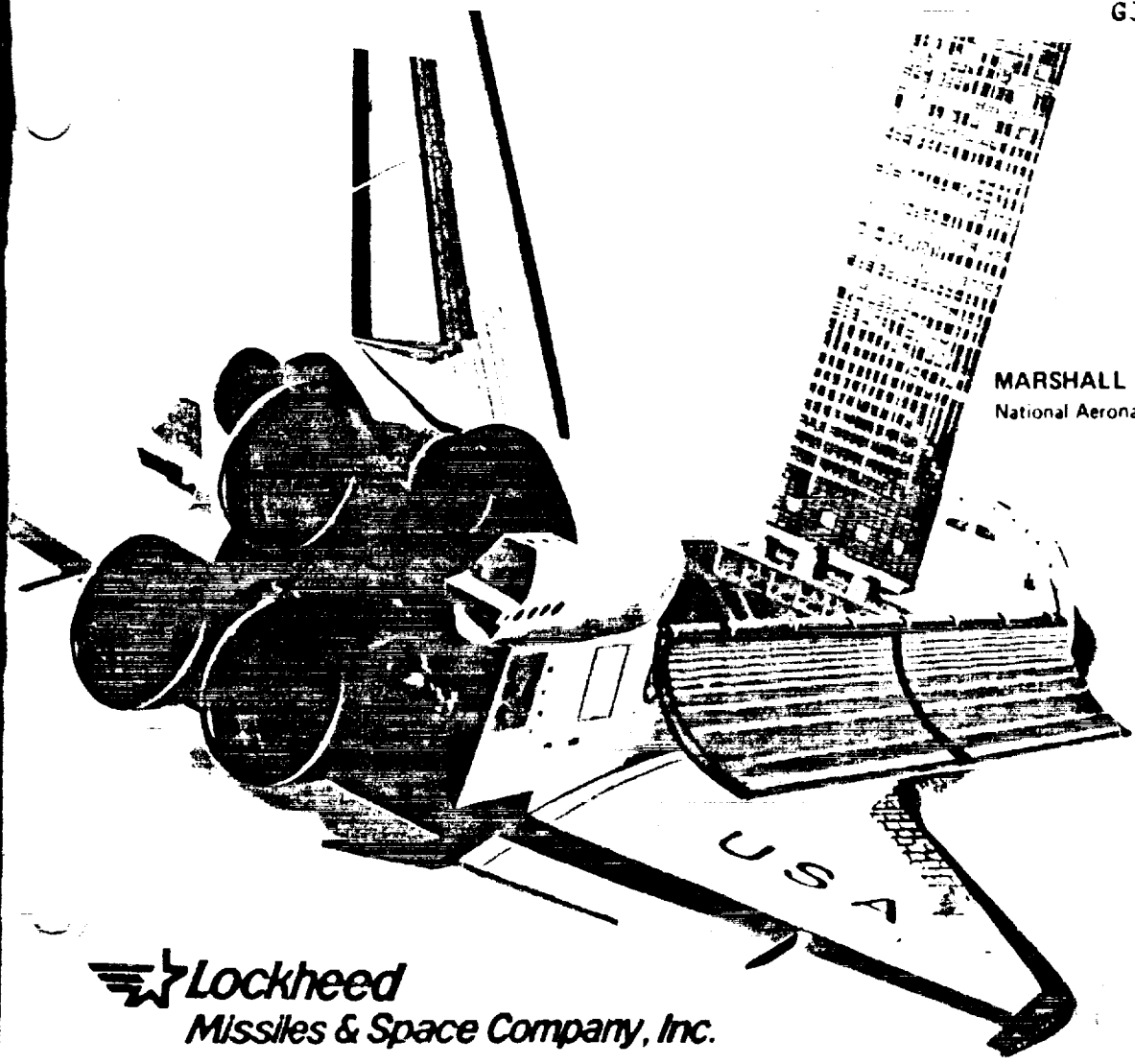

submitted to:

NASA

MARSHALL SPACE FLIGHT CENTER
National Aeronautics and Space Administration

April 1986

Lockheed
Missiles & Space Company, Inc.

267

SUMMARY

Emerging satellite designs require increasing amounts of electrical power to operate spacecraft instruments and to provide environments suitable for human habitation. In the past, electrical power has been generated by covering rigid "honeycomb" panels with solar cells. This technology results in unacceptable weight and volume penalties when large amounts of power are required.

To fill the need for large-area, lightweight solar arrays, Lockheed Missiles & Space Company, Inc. (LMSC), has developed a fabrication technique in which solar cells are attached to a copper printed circuit laminated to a plastic sheet. The result is a flexible solar array with one-tenth the stowed volume and one-third the weight of comparably sized rigid arrays. An automated welding process developed to attach the cells to the printed circuit guarantees repeatable welds that are more tolerant of severe environments than conventional soldered connections.

To demonstrate the flight readiness of this technology, the Solar Array Flight Experiment (SAFE) was developed under contract to NASA Marshall Space Flight Center (MSFC) and flown on the space shuttle Discovery in September 1984. The SAFE wing had 84 panels and, when fully extended, was 13.5 feet wide and over 100 feet long. To reduce costs, only one of the 84 panels was fully populated with active solar cells.

While in orbit the array was extended and retracted four times over a three-day period. While the array was extended, the orbiter Vernier Reaction Control System (VRCS) thrusters were fired in a programmed fashion on 14 occasions so that the dynamic behavior of this large space structure could be evaluated.

The tests showed the modes and frequencies of the array to be very close to preflight predictions. Structural damping, however, was higher than anticipated. Electrical performance of the active solar panel was also tested. The power output of the panel while on orbit matched that measured in preflight tests. On return to Earth, the power output was found to be unchanged and the cells undamaged by the flight environments. Thus, the flight test of the array was a complete success.

This report describes the flight performance and postflight data evaluation. It is submitted to NASA-MSFC by LMSC in partial fulfillment of the requirements of contract NAS 8-31352.

Final Report

LMSC-F087173

Table of Contents

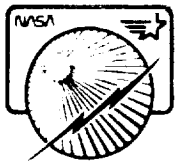

ACRONYMS AND ABBREVIATIONS

CG	Center of Gravity
DAE	Dynamics Augmentation Experiment
DAS	Data Acquisition System
GMT	Greenwich Mean Time
IV	Current Versus Voltage Curves
LaRC	Langley Research Center
LMSC	Lockheed Missiles & Space Co., Inc.
MET	Mission Elapsed Time
MSFC	Marshall Space Flight Center
PSD	Power Spectral Density
SAFE	Solar Array Flight Experiment
TBE	Teledyne Brown Engineering
VRCS	Vernier Reaction Control System

Final Report

LMSC-F087173

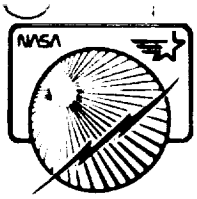

Section 1
Introduction

Section 1
INTRODUCTION

1.1 MISSION OBJECTIVES

In September 1984, the Solar Array Flight Experiment (SAFE) was carried into orbit on Shuttle mission STS-41D. The SAFE was a large-area, lightweight solar array wing capable of being populated with enough solar cells to produce more than 12.5 kilowatts of power. Over a three-day period, numerous tests were performed on the wing to demonstrate the readiness of large-area, lightweight, solar array technology. The specific objectives of the tests on the SAFE were:

a. To demonstrate the deployment, retraction, and restowage of the array
b. To measure the dynamic behavior of a large, flexible space structure
c. To measure the on-orbit electrical and thermal performance of the array

The SAFE mission was a success, and this final report describes the results of flight operations and postflight tests and analysis.

1.2 EXPERIMENT DESCRIPTION

The SAFE wing assembly is shown deployed from the orbiter cargo bay in Fig. 1-1. The axis system shown in this figure is used exclusively in this report. The components of the SAFE wing assembly are shown in Fig. 1-2. Dimensions of the stowed array are shown in Fig. 1-3 and dimensions of the array deployed to the 70- and 100-percent positions are shown in Figs. 1-4 and 1-5, respectively. The mass properties shown in these figures are summarized in Table 1-1.

The principal component of the SAFE hardware is the blanket, 13.5 feet wide by 101 feet long, made of two 1.0-mil sheets of Kapton with a copper printed circuit laminated between them. The blanket comprises 84 panels that fold like an accordion when stowed. When extended, the panels form a flat surface with the solar cells mounted on one side. The cells are attached to the blanket by welding them to the copper printed circuit through properly placed holes in the Kapton. The printed circuit connects the cells in series and in parallel strings to achieve the desired current and voltage output. A cross-section view of an active solar cell attached to the blanket is shown in Fig. 1-6.

On the SAFE wing, only the third panel from the wing tip was completely covered with active solar cells. One half contained cells that measure 2 × 4 cm, and the other half contained cells that measure 5.9 × 5.9 cm. Except for a small patch of very thin 2 × 2 cm cells on the outermost panel, the remainder of the blanket was covered with glass and aluminum platelets that simulated the weight and thickness of active solar cells. These simulators were used to save cost on the experiment.

The solar array blanket is extended and retracted by a coilable fiberglass mast that attaches through a rigid cover to the outermost panel of the blanket. The mast consists of three fiberglass longeron members, each continuous over the length of the mast. At nine-inch stations along their length, the longerons are connected by a triangle of fiberglass batten members. Three pairs of stranded stainless steel diagonal wires connect the intersections of the battens and longerons between adjacent stations. Rollers are located at the outside of all three longerons at each station location. The mast is initially stowed by coiling it in torsion and placing it in the bottom of the stowage canister. Extension is caused by the action of a motor-driven rotating section on the upper end of the stowage canister. The rotating section has internal threads that engage the rollers on the longerons. As the section rotates, the rollers are pulled up through the threads of the rotating nut, and the coiled longerons are allowed to straighten. The configuration of the canister, rotating section, and longerons is shown in Fig. 1-7. Reversing the rotation of the threaded section drives the rollers back into the canister, causing the longerons to resume their coiled configuration.

When the blanket is fully stowed, the panels are folded within a containment box. The cover of the containment box applies a preload force to prevent the panels from shifting

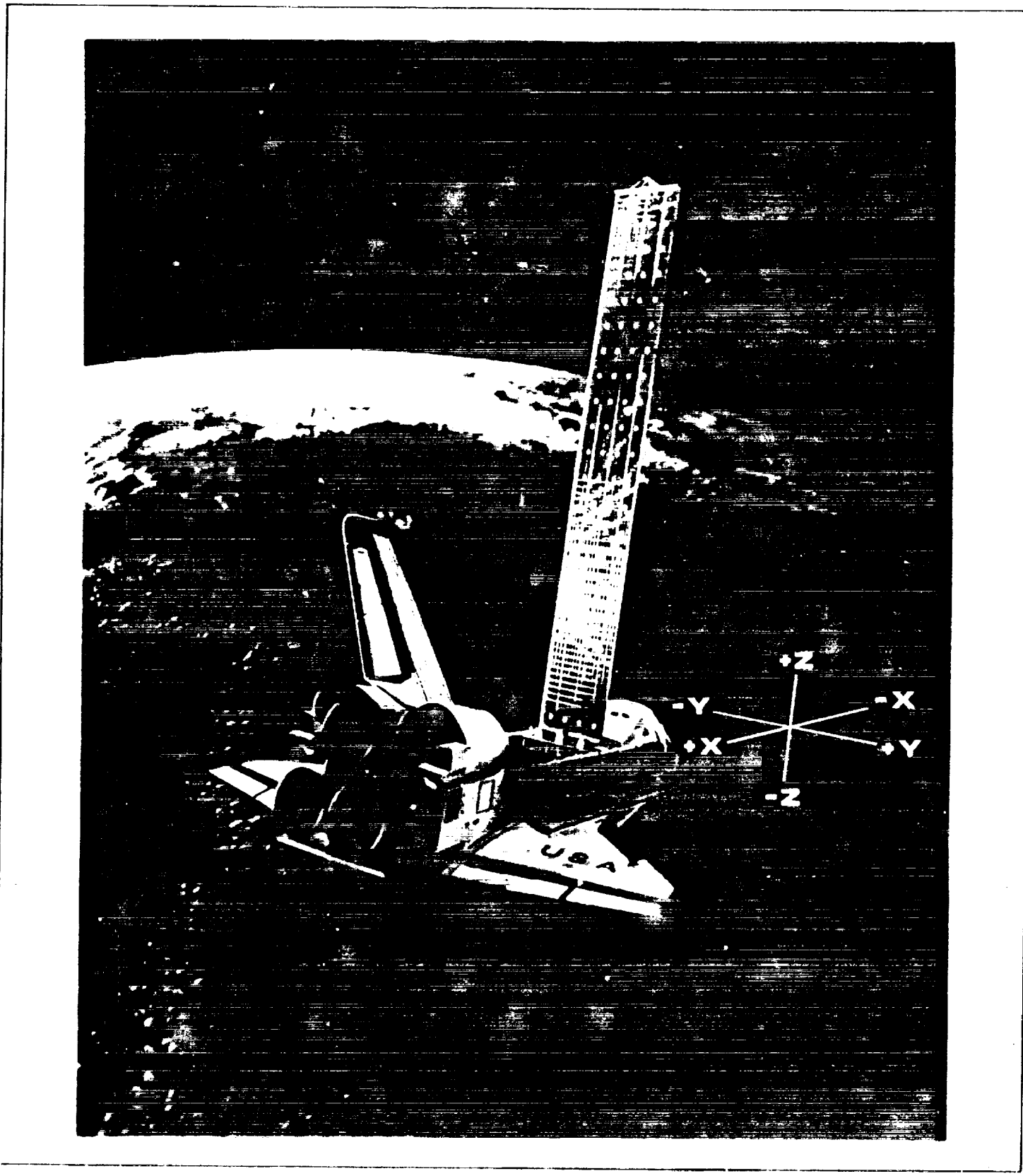

Fig. 1-1 Axis System Used for Final Report

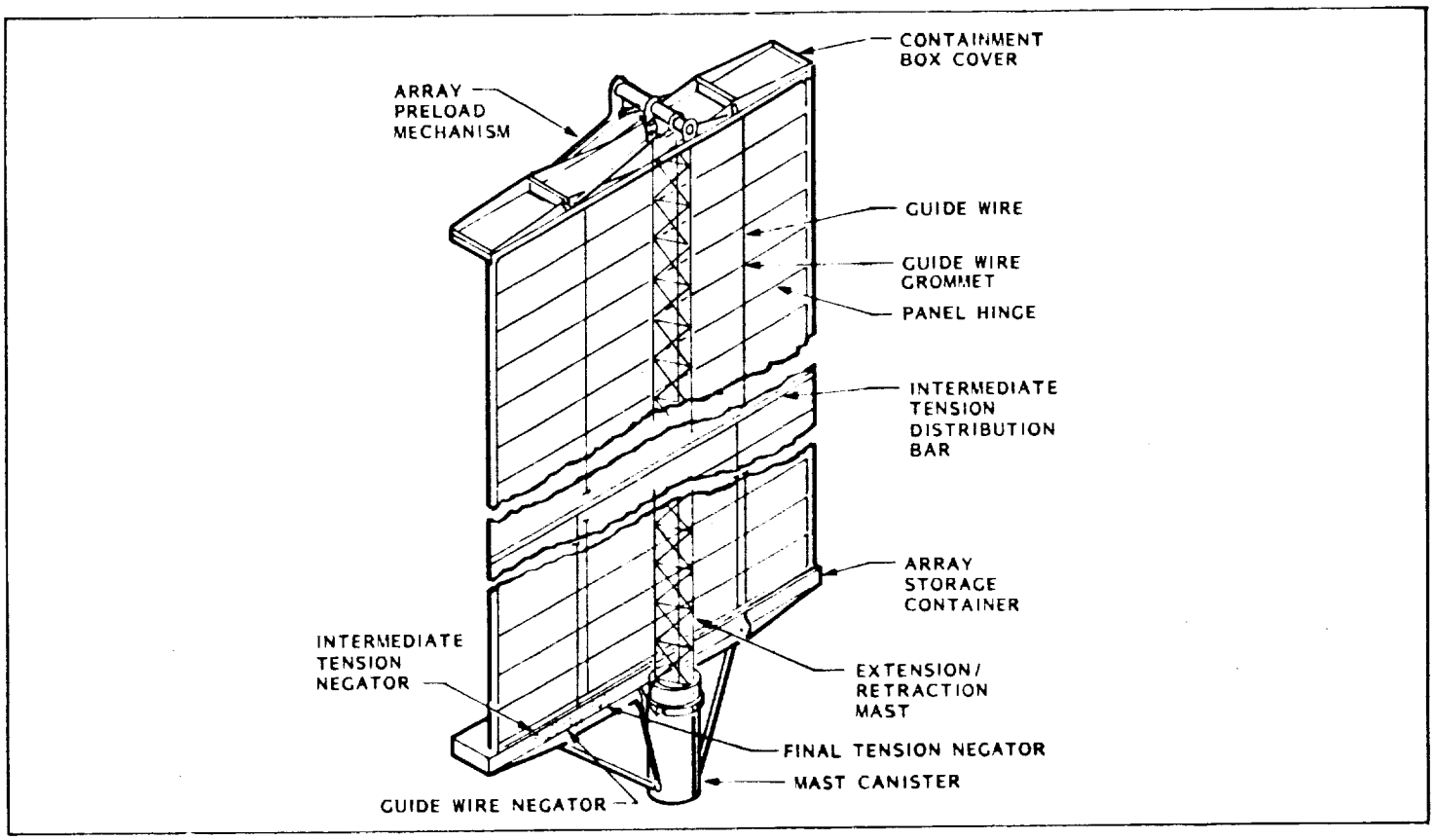

Fig. 1-2 SAFE Wing Assembly

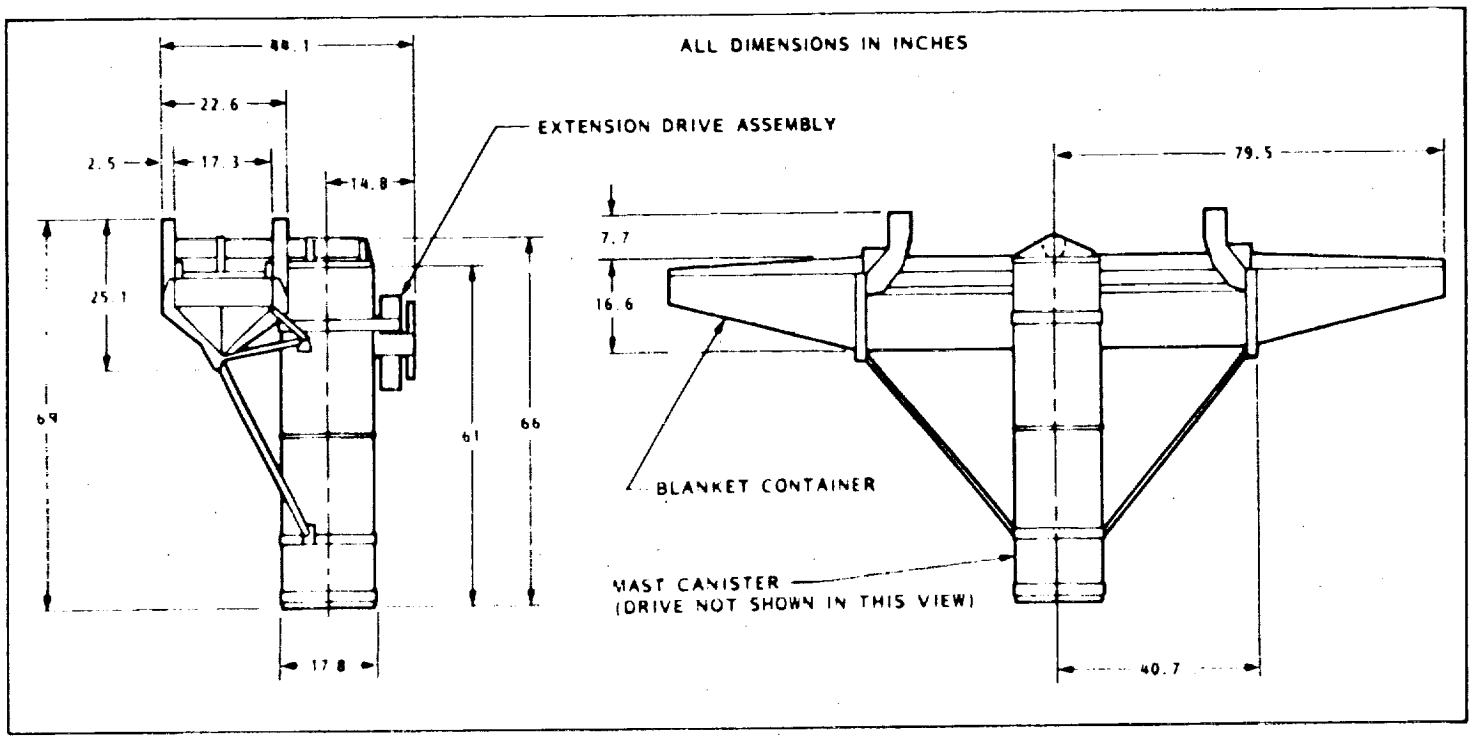

Fig. 1-3 Dimensions of the Stored SAFE Array

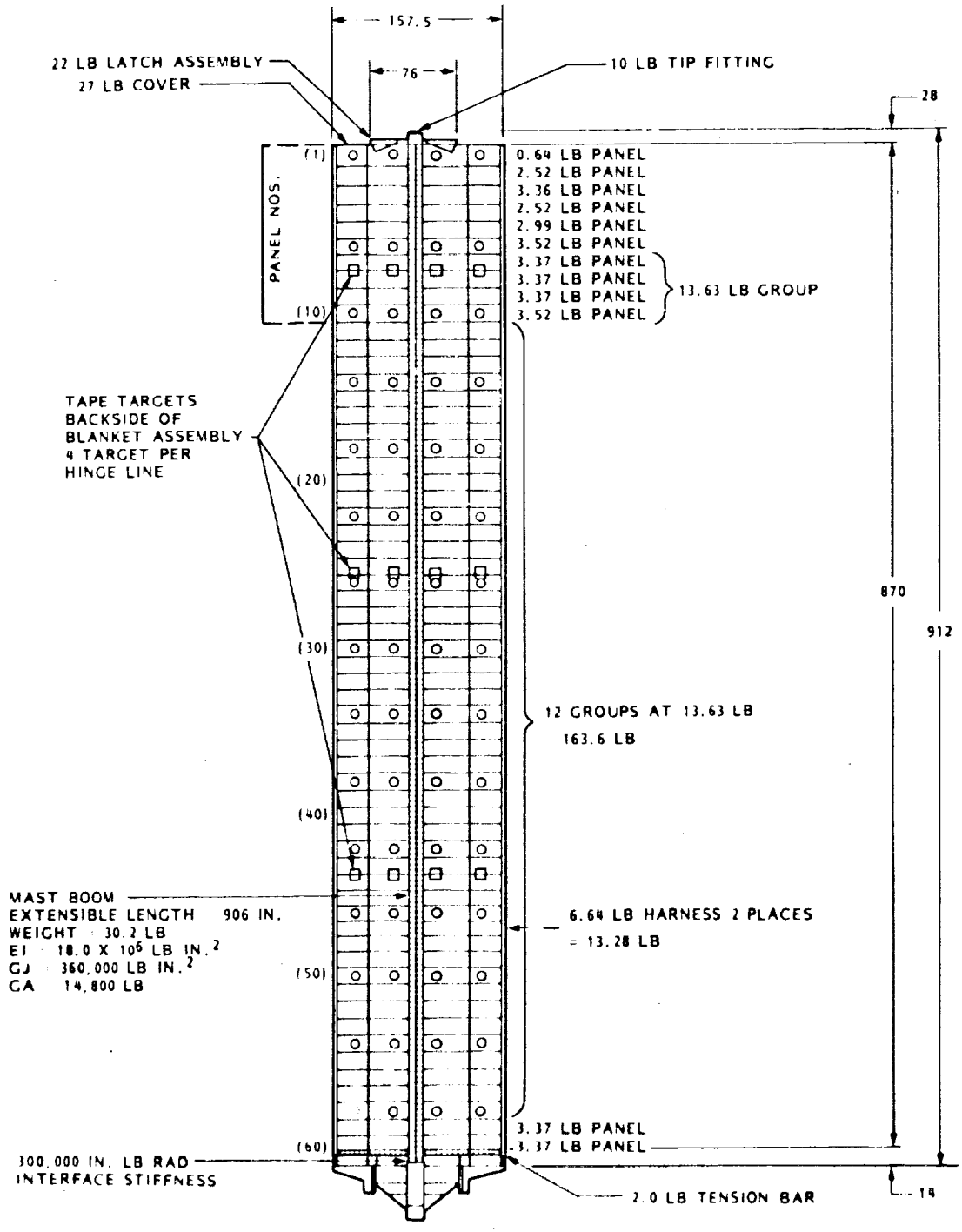

Fig. 1-4 Dimensions of the Array at 70-Percent-Extended Position

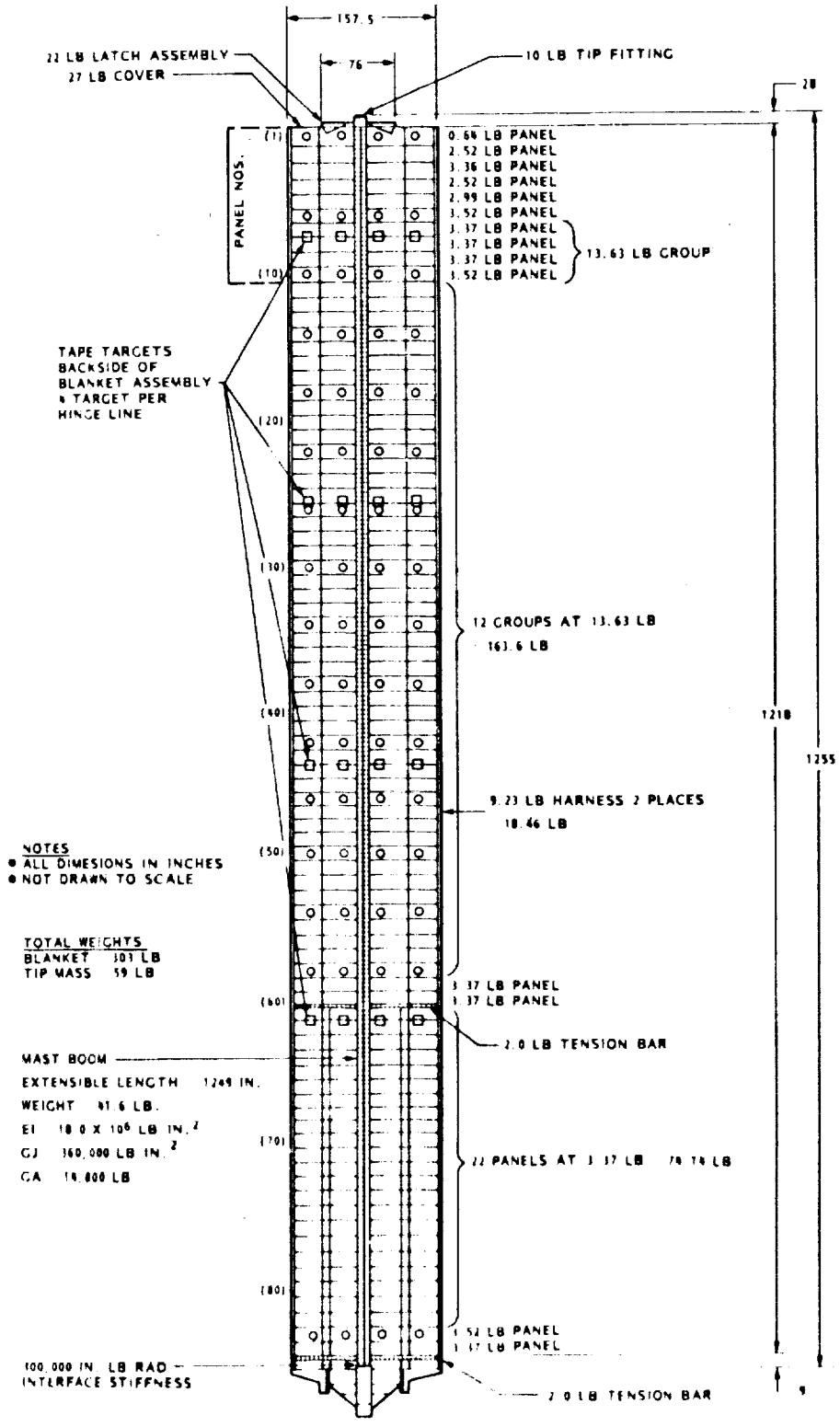

Fig. 1-5 Dimensions of the Array at 100-Percent-Extended Position

Table 1-1

SAFE WEIGHT SUMMARY

Components	Weight (lb)
Experiment Total	940.0
Support Structure & Separation System	270.0
Separable Wing Assembly	670.0
Blanket	303.0
Panels	280.5
Harness	18.5
Tension Bars	4.0
Container	90.5
Base Hardware	43.5
Tension System	18.5
Latch System	16.0
Support Struts	9.0
Cover	27.0
Tip Hardware	32.0
Latch System	22.0
Tip Fitting	10.0
Mast	122.0
Boom	45.0
Canister	49.0
Drive	25.0
Lock	3.0
Jettison Capability	34.0
Grapple	21.0
Grapple Fitting	7.0
Rear Support	6.0
Wires & Connectors	7.0
Misc. Fasteners & Adhesives	11.0

Table 1-1 SAFE WEIGHT SUMMARY

about inside the container. In the first few inches of extension, the mast unlatches the cover of the containment box and releases the preload force on the panels. Continued mast extension causes the box cover and outermost panels to be pulled out of the containment box. The motion of the box cover also pulls out guide wires which pass through grommets at alternate panel hinge lines. The guide wires are tensioned by negator assemblies in the bottom of the containment box. These wires restrict out-of-plane motion of the blanket until, at the 70-percent-deployed position, a tension bar applies a pull force on the deployed panels to hold them flat. Continued mast extension causes the remainder of the panels to exit the containment box. These panels are held flat by a force applied to the blanket at the 100-percent position by a second tension bar. Upon retraction, small springs at the panel hinge lines cause the panels to refold in the proper direction. The lower 30 percent of the panels fold into the containment box first, followed by the upper 70 percent. Upon reaching the fully stowed position, the mast causes the box cover to latch in place with a preload force applied to the panels.

The SAFE wing is attached to the side of a support structure, and the support structure is attached to a truss within the orbiter cargo bay. Special release fittings on the support structure permit the SAFE wing to be separated from the support structure in the event of an on-orbit malfunction. A grapple fitting is provided so that the separated structure can be maneuvered away from the orbiter by the remote manipulator arm.

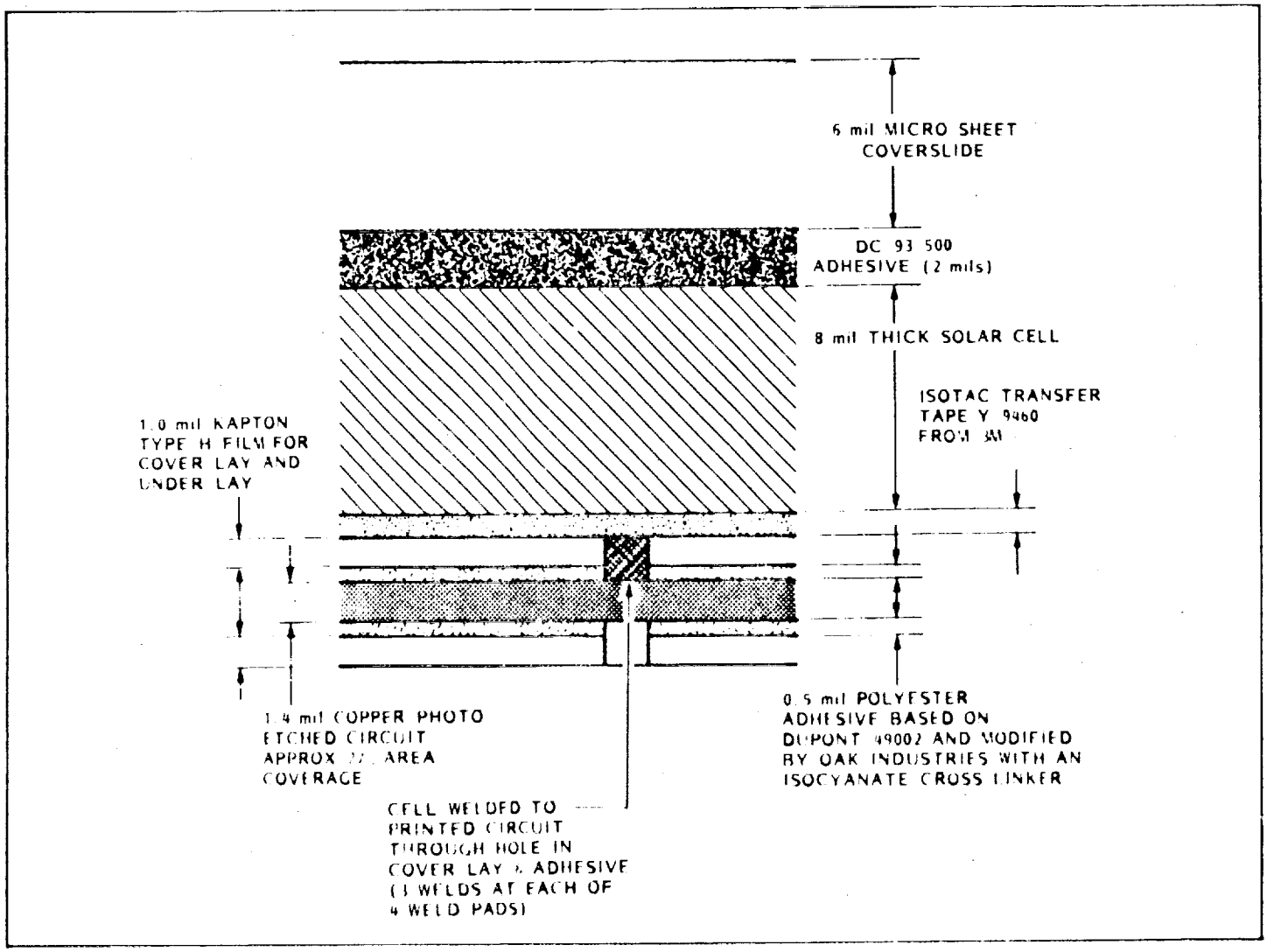

Fig. 1-6 Cross Section of Solar Cell Attachment to Blanket

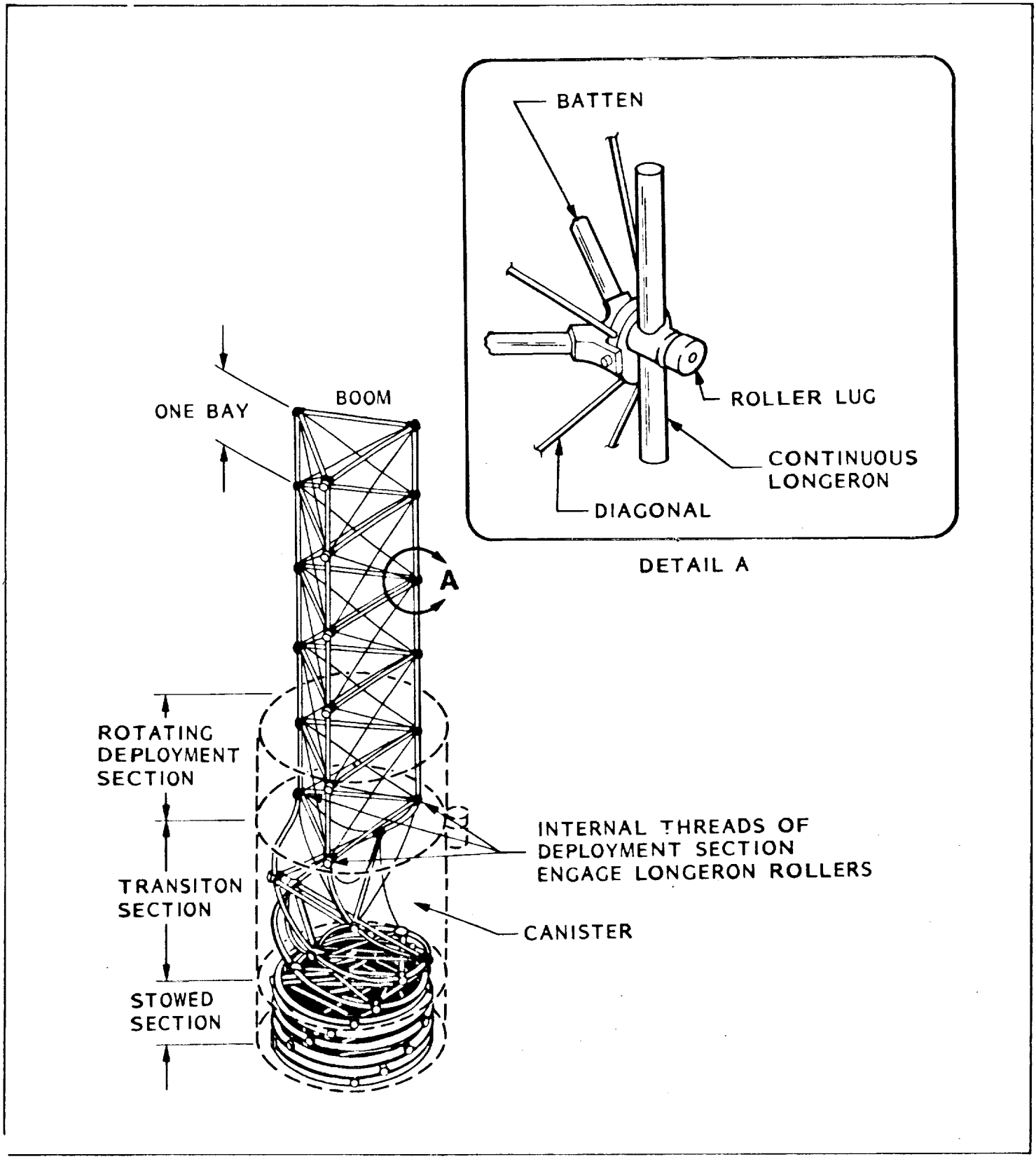

Fig. 1-7 Mast Canister and Extension Mast

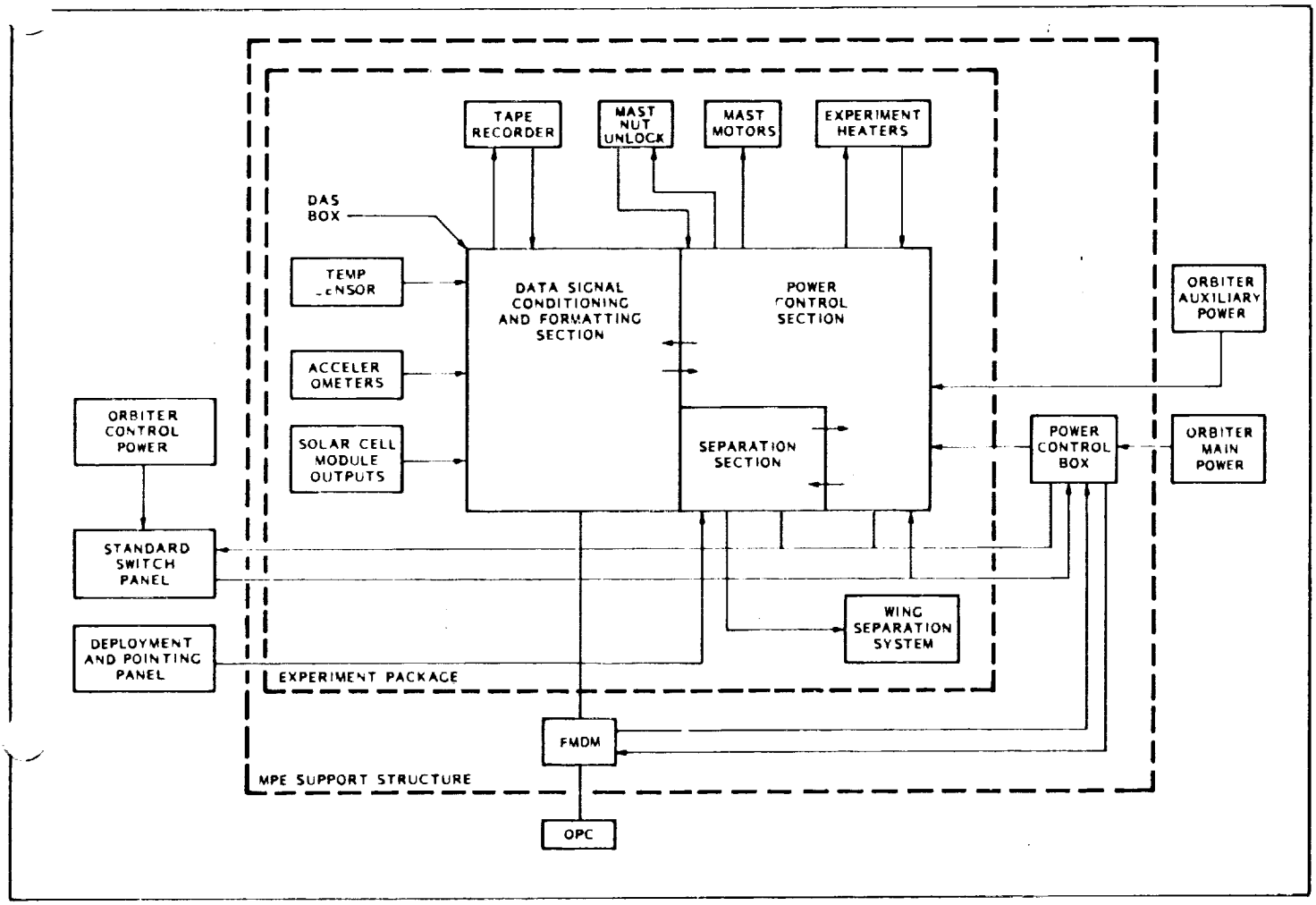

Fig. 1-8 Schematic of DAS and Orbiter Control

Also mounted on the support structure is the Data Acquisition System (DAS) box. The DAS box not only processes the instrumentation data for recording but also is the primary electrical interface between the orbiter and the SAFE wing. A schematic showing the interaction of the DAS box with the orbiter and the SAFE wing is shown in Fig. 1-8. The tape recorder used to record the instrumentation data processed by the DAS is a Mark V-Type 4200 produced by Lockheed Electronics Corporation.

Final Report

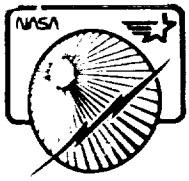

Section 2
Flight Performance and Data Evaluation

Section 2
FLIGHT PERFORMANCE AND DATA EVALUATION

Flight testing of the SAFE was performed on September 1, 2, and 3, 1984. During this time, 31 tests were performed. These included extension/retraction tests, Dynamics Augmentation Experiment (DAE) dynamics tests, photogrammetry tests, and solar cell performance tests. During these tests, data in the form of temperatures, mast-base and mast-tip accelerations, current and voltage produced by the solar cells, current used by the mast motors, and various other electrical signals were recorded by the tape recorder. This data is evaluated and compared with analytical predictions in the following subsections.

2.1 OPERATIONS PERFORMED ON ORBIT

The operations performed on orbit with the SAFE are listed in Table 2-1 in the order they occurred. For convenience, these operations are numbered according to the data file number used by MSFC in transmitting the data. Also listed in this table are the approximate Greenwich Mean Time (GMT) and Mission Elapsed Time (MET) for the start of each operation. Throughout this report, the operations performed on the experiment will be referenced according to the number listed in this table. Numerical designators on data files refer to operations listed in the table with the same numerical designator. Also, if the GMT or MET of interest is known, the operation in process at the time can be determined from the table.

2.2 OBSERVED PERFORMANCE ON ORBIT

In addition to the traditional data collected from instruments, many of the operations performed on the wing assembly were recorded on video tape and downlinked to the personnel at the mission support center. Also, the crew contributed many of their observations during air-to-ground transmissions. A significant contribution by the crew was the realtime monitoring of mast-tip motion with the Nikon camera and 500-mm lens during the daylight dynamics tests. Furthermore, a subset of the instrumentation data was periodically displayed in realtime to ground support personnel. A summary of the array behavior based on these information sources alone is presented in the following paragraphs. Only observed behavior is reported here; discussion and explanation of the behavior is delayed until Section 2.4.

During the first extension of the array from the stowed position to 70-percent extended (operation 2), sticking between adjacent panels caused nonuniform unfolding motion of the blanket. This sticking was also observed in the lower 30 percent of the panels in the first extension from the 70-percent position to the 100-percent position (operation 16). In all subsequent extensions, the panels unfolded in a uniform, accordion fashion. The sticking had previously been observed in ground test, but the motion was more dramatic in the flight zero-g environment. At no time did the sticking cause an operational problem or threaten successful array extension. Motor current during all extensions and retractions compared closely with that measured during ground test.

When deployed to the 70-percent position, the array appeared to be slightly but uniformly twisted. The twist was such that the starboard edge of the blanket was farther from the crew cabin than the port edge. This twist appeared essentially constant throughout the mission.

Panel oscillation was observed during the last 15 or 20 feet of the array-retraction events. The crew reported a similar

Table 2-1 SUMMARY OF SAFE OPERATIONS

File	Operation	GMT	MET
1	Unlock Mast	245:16:41:34	2:03:59:43
2	1st Extension	245:17:34:43	2:04:52:52
3	1st Retraction	245:17:59:39	2:05:17:48
4	2nd Extension	245:19:04:52	2:06:23:01
5	SAE Dyn 70% O/P	245:19:25:27	2:06:43:36
6	DAE Dyn 70% O/P	245:20:13:27	2:07:31:36
7	2nd Retraction	245:20:48:45	2:08:06:54
8	3rd Extension	246:10:40:07	2:21:58:16
9	Solar Cell Modules	246:11:27:54	2:22:46:03
10	SAE Dyn 70% M/M	246:13:29:27	3:00:47:36
11	DAE Dyn 70% M/M	246:14:21:55	3:01:40:04
12	SAE Dyn 70% O/P	246:15:00:26	3:02:18:35
13	DAE Dyn 70% I/P	246:15:52:32	3:03:10:41
14	SAE Dyn 70% M/M	246:16:30:22	3:03:48:31
15	DAE Dyn 70% M/M	246:17:23:04	3:04:41:13
16	1st Extension to 100%	246:17:53:12	3:05:11:21
17	SAE Dyn 100% O/P	246:18:06:29	3:05:24:38
18	1st Retract 100% to 70%	246:18:18:42	3:05:36:51
19	2nd Extension to 100%	246:19:16:58	3:06:35:07
20	SAE Dyn 100% M/M	246:19:31:29	3:06:49:38
21	2nd Retract 100% to 70%	246:19:47:19	3:07:05:28
22	Retract 70% to 0%	246:19:54:28	3:07:12:37
23	4th Extension	247:14:37:15	4:01:55:24
24	Solar Cell Modules	247:14:49:58	4:02:08:07
25	Solar Cell Modules	247:15:39:15	4:02:57:24
26	DAE Dyn 70% M/M	247:16:02:11	4:03:20:20
27	SAE Dyn 70% M/M	247:16:37:24	4:03:55:33
28	DAE Dyn 70% I/P	247:17:32:39	4:04:50:48
29	SAE Dyn 70% I/P	247:18:07:22	4:05:25:31
30	Last Retraction	247:18:19:19	4:05:37:28
31	Lock Mast	247:19:50:09	4:07:08:18

cillation shortly after the start of retraction from the 70-percent position, but this observation was not included in the downlinked video tape coverage. The panel oscillation during the last 15 or 20 feet of retraction began small and then grew until the panels were nearly slapping each other in an "accordion" mode. No similar motion was observed during extension events. As with the panel sticking behavior, the panel oscillation caused no operational problems and no abnormal motor-current usage.

With the array extended to the 70-percent position, the crew reported that the blanket curved about its longitudinal axis (about the mast) after coming out of the darkness. The curvature was such that the edges of the blanket were closer to the crew cabin than was the center of the blanket. The orbiter was in a tail-to-Earth attitude at the time of this report. After approximately ten minutes in the daylight in this attitude, the crew reported that the blanket had flattened out. The crew observed the curvature during the darkness by using a flashlight and turning on the cargo bay lights. This behavior, curving in the darkness and flattening in the daylight, was repeated for each orbit while in the tail-to-Earth attitude.

Later in the mission, when the orbiter was oriented with its tail to the sun for the solar cell performance test, the blanket remained curved for the entire daylight portion of the orbit. In this attitude, the curvature appeared more severe than observed earlier. In no case did the blanket curvature impair the deployed array performance or the panel folding behavior during extension or retraction.

In general, the array-tip displacements during dynamic tests were smaller than the values computed in preflight analysis. This difference was desirable since the flight rules would not permit maneuvering the orbiter with the array extended unless preflight predictions were verified to be accurate or conservative. That measured deflections were smaller than computed deflections was not surprising since the computations were performed using 0.5 percent modal damping to be conservative in mast longeron load predictions. For the out-of-plane tests, the measured and computed tip displacements matched more closely than for the in-plane or multimodal tests.

While the magnitude of the tip deflections was adequate for verification of the dynamic models, larger tip deflections with more cycles of motion in the free decay period were desired for enhanced demonstration of the capabilities of the DAE and photogrammetric measurement systems. Therefore, the programmed thruster firings for operations 26, 27, 28, and 29 were modified to produce a 50-percent increase in tip displacement as predicted with a response model using 0.5 percent modal damping. These changes to the thruster firings did not produce the desired increase in tip displacements. The measured peak displacements were no larger, and in some cases smaller, than those measured in the previous tests.

Temperatures for the monitored components remained well within their operational limits throughout the flight. Motor temperatures during the extension and retraction events were normally in the +20°F to +30°F range. The tape recorder also stayed in this general temperature range most of the time. The heaters for the motors and tape recorder came on several times during one short period of the flight. The heaters for the DAS box were never active because the box remained near +40°F for the entire flight.

The retraction of the mast from the soft-stop position to the hard-retract position was performed in operation 31. This event went smoothly, and peak motor current was somewhat less than measured in ground test. The microswitch signals indicated that the mast and locking levers were in the stowed position and ready for landing.

2.3 DESCRIPTION OF DATA

A large quantity of data from a variety of sources has been received for evaluating the flight performance of the SAFE. Much of this data has been carefully scrutinized. Other data sets were intended primarily as diagnostic tools, and, since no operational problems were encountered, these have received little attention. Listed in this subsection are the data sets received by LMSC for evaluating the experiment performance. Absent from this list are data from the DAE or the photogrammetric experiments. Although there has been some verbal communication with the Principal Investigators for these experiments and some preliminary reports have been exchanged, the integration of the LMSC data evaluation with the DAE and photogrammetric data is the responsibility of MSFC. Their summary report will be issued separately.

Visual data consist of the following:

- Color positives, 35 mm, of exposures taken with the Nikon camera and 500-mm lens for the first dynamics test at 70-percent extension (operation 5) and the first dynamics test at 100-percent extension (operation 17): sixty-four exposures for each test at two-second intervals at the 70-percent position and at four-second intervals at the 100-percent position
- Twenty-eight video tapes from the orbiter video cameras in the cargo bay, each tape approximately 20 to 30 minutes in duration
- Two video tapes of the downlinked video coverage
- Color prints from a 70-mm Hasselblad camera

Accelerometer data consist of the following:

- Plots of acceleration versus time for the three base accelerometers and three tip accelerometers during each extension, retraction, and dynamics test

- panded scale plots of acceleration versus time for the ...ree base and three tip accelerometers during the period of the forcing function for each dynamics test
- Power Spectral Densities (PSDs) of the acceleration data from the tip accelerometers during each accelerometer test
- Base motion acceleration of the orbiter for the firing of each of the vernier thrusters used in the dynamics tests
- Firing time and duration data for each of the vernier thrusters used in the dynamics tests

Temperature data consist of the following:

- Plots of temperature versus time for each of the three groups of solar cells during each performance test
- Plots of temperature versus time for the container cover, motor 1, motor 2, the DAS box, and tape recorder for each extension, retraction, dynamics test, and solar cell performance test

Electrical data consist of the following:

- Current versus voltage plots for each of the three groups of ...ar cells during each performance test
- Plots of motor current versus time f... each extension and retraction event and PSDs of these plots
- Plots of voltage versus time for the +12V, −15V, Gnd, +5V, +15V, 28V Pri, and 28V Aux during each extension, retraction, and dynamics test
- Listing of the discrete signal values

Miscellaneous data consist of the following:

- Flight operations log
- Video tape log
- Computer listing of orbiter attitude parameters during the flight

2.4 COMPARISON OF FLIGHT DATA AND ANALYTICAL PREDICTIONS

Reconciliation of flight data with analytical predictions is a fundamental objective of this report. Explanations for nearly all differences between the flight behavior and preflight ex...tations have been developed from the postflight testing and data analysis. These explanations are contained in the following subsections.

2.4.1 Wing Extension and Retraction Behavior

As mentioned in Section 2.2, sticking between adjacent panels caused nonuniform unfolding of the panels during the first extension from stowed to the 70-percent position and during the first extension from the 70-percent to the 100-percent position. This sticking behavior had previously been observed in ground test. It is caused by trace amounts of stray adhesive, most likely Isotac transfer adhesive, used extensively in the construction of the blanket. The adhesive is only 0.5-mil thick and nearly clear so that trace amounts are very difficult to locate and remove. Since the blanket was stowed for approximately eight months before flight with a 3000-pound preload applied, the adhesive had opportunity to stick adjacent panels together. The zero-g environment of flight caused more dramatic unfolding irregularities than in ground test, but at no time did the irregularities cause any operational problems. Since the full preload was never reapplied until the last retraction event, the extensions following the first extension to 70 percent and the first extension from 70 percent to 100 percent exhibited no sticking. In these extensions, the panel motion was regular and accordion-like.

The panel motion in the retraction events was well behaved except for an oscillation that began developing when the mast was extended 15 to 20 feet. The oscillation grew in magnitude as retraction continued and then decreased near the soft-stop position. The oscillation appeared to be an excitation of a local "accordion mode" such that adjacent panels almost slapped one another at the peak of the excitation. The crew reported a similar oscillation shortly after starting to retract from the 70-percent position. Evaluation of the video tapes showing the oscillation near the end of retraction indicates that the frequency of oscillation was approximately 0.75 hertz. This estimate is confirmed by PSDs of the tip accelerometers and the motor current during the retraction events which show a frequency at 0.70 to 0.73 hertz. The frequency was further confirmed by directing a video camera at the base of the mast canister during the postflight extension and retraction test. The conditions for this test are not identical to flight: in the test setup, the blanket centerline is constrained to a straight line and the mast canister is free to pivot, but, in flight, the canister is fixed to the orbiter and the blanket is unrestrained. Nevertheless, the "nodding" frequency of the canister was measured at 0.69 hertz in the tests, and this motion almost certainly caused the oscillation observed in flight.

To further understand the oscillation, the frequency of the first three modes of the partially deployed mast were computed by ignoring the mass of the deployed mast and blanket. This computation results in a model that is basically a massless beam with the tip mass and inertia of the containment box cover. The results of this evaluation are shown in Fig. 2-1. As seen in this figure, both the in-plane and out-of-plane modes have frequencies near the observed oscillation

frequency when the deployed length is 20 feet. If the calculations were refined to include the mass of the deployed mast and a portion of the deployed blanket mass, the frequency curves would all be slightly lowered in this figure.

The most likely source of the disturbance causing the observed oscillation is the motion of the rotating nut assembly. One might expect the frequency at which the longeron rollers exit the rotating nut to match the frequency of oscillation. This match seems likely since a very small amount of mast deformation accompanies the release of a longeron roller. However, this disturbance frequency is 0.17 hertz, and, therefore, not close to the frequency of the observed oscillation. Since it takes four turns of the rotating nut to release each set of longeron rollers, the rotational frequency of the rotating nut is 0.68 hertz, which matches closely the frequency of the observed oscillation. Thus, the panel oscillation seems to be caused by a resonance, occurring during the last 20 feet of retraction, between the rotational frequency of the rotating nut and the cantilevered mast modes. The disturbances in the mast excited the several most outboard panels of the array causing the observed panel oscillation.

The fact that this oscillation was greatly diminished during extension may be due to differences in panel groupings between extension and retraction. Another difference between the extension and retraction events is that, during retraction, strain energy is being stored in the mast as it enters the canister, whereas, during extension, strain energy is being released from the mast as it exits the canister. The oscillation observed shortly after starting retraction from the 70-percent position occurred most likely at another resonance position. For instance, the frequency of the cantilevered mast is approximately 0.17 hertz at a deployed length of 56 feet, which does match the frequency at which longeron rollers exit the canister.

The times required for the motors to extend and retract the mast during the flight are shown in Table 2-2, as are the times as measured in the preflight and postflight tests. The time required to go back and forth from the fully stowed position to the soft-stop position is not listed in the comparison since the allowable range of soft-stop positions is a significant part of the total mast travel for these events. The results that are listed in this figure show that the mast extension and retraction rate during flight was somewhat faster than the pre- and postflight ground tests. This difference is due to the fact that

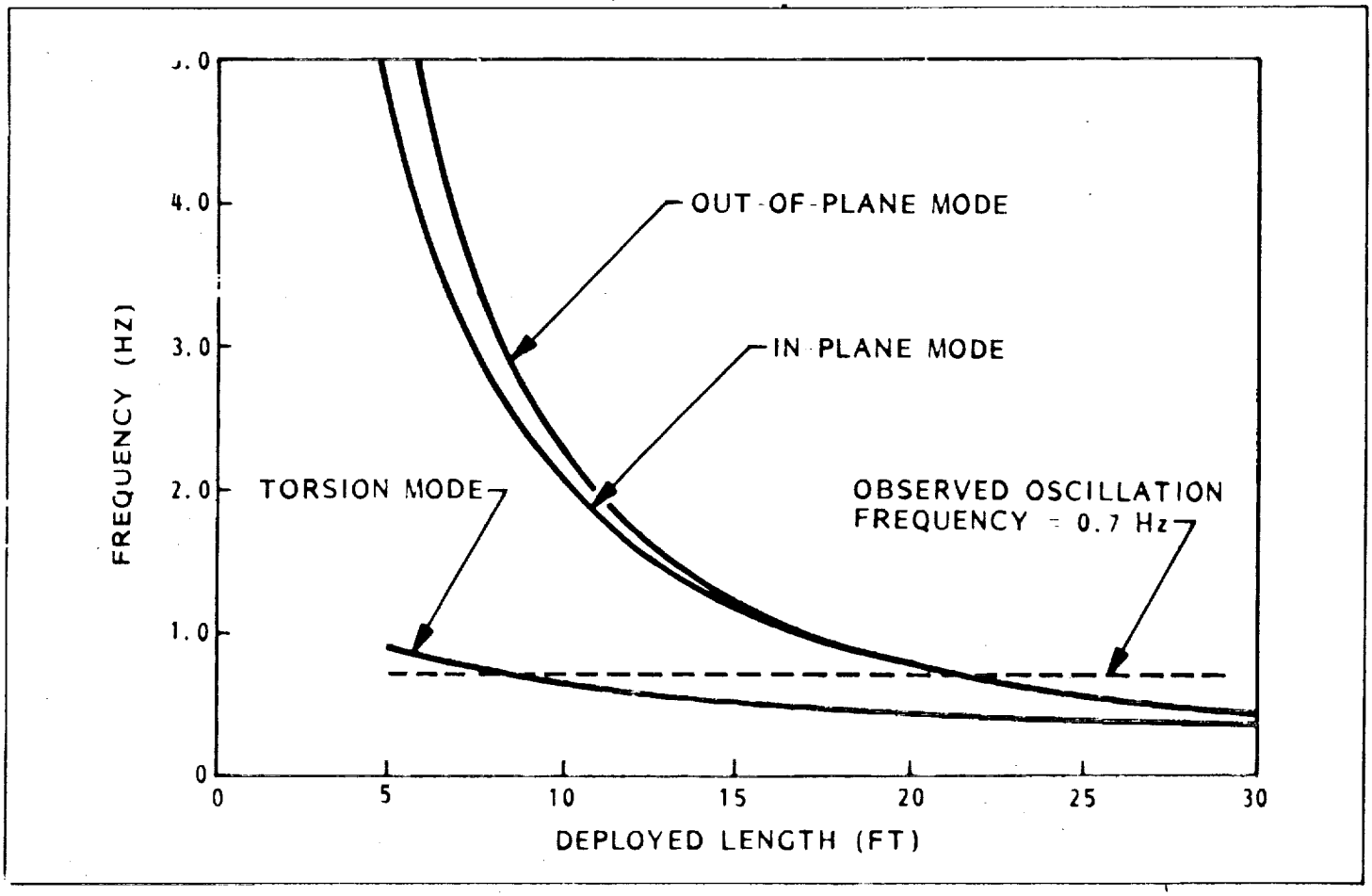

Fig. 2-1 Mast Frequencies During Final Position of Retraction Event

orbiter voltage during flight averaged 30.6 volts, whereas all round tests were conducted at 28.0 volts. Acceptance tests performed on the mast alone showed that the extension and retraction rate is nearly linear with voltage. It is interesting to note that both the extension and retraction rates increased throughout the flight, almost as if the drive system were "wearing in." No explanation for this behavior is known.

The motor current used by the two motors that extend and retract the mast is summarized in Table 2-3. The current profiles for the mast nut unlock and mast nut lock events are

Table 2-2 SUMMARY OF EXTENSION/RETRACTION TIME

	Average Times (seconds)		
	Flight	Preflight	Postflight
Extension from Soft Stop to 70%	533	582	596
Extension from 70% to 100%	221	226	236
Retraction from 100% to 70%	199	221	222
Retraction from 70% to Soft Stop	523	569	567

Table 2-3 SUMMARY OF MOTOR CURRENT USAGE

Operation Number	Event Description	Number	Average/Peak Motor Current	Average Voltage
1	Mast Nut Unlock	2	4.9/7.3*	31.0
2	First Extension, 70%	2	5.5	30.7
3	First Retraction	1	4.7	30.8
4	Second Extension, 70%	2	4.7	30.7
7	Second Retraction	1	4.1	30.7
8	Third Extension, 70%	2	4.2	30.7
16	Extend to 100%	2	6.5	30.9
18	Retract to 70%	1	3.7	30.7
19	Extend to 100%	2	5.9	30.8
21	Retract to 70%	1	3.4	30.4
22	Retract	1	3.2	30.3
23	Extend to 70%	2	3.8	30.2
30	Retract	1	3.8	30.4
31	Mast Nut Lock	1	6.5/11.9*	-

	Flight Current (A)	Preflight Current (A)	Postflight Current (A)
Motor 2, Avg/Peak, Stowed to Soft Stop	4.9/7.3	4.8/7.1	4.7/6.0
Motor 2, Avg, Stowed to 70%	4.6	3.3	3.2
Motor 2, Avg, 70% to 100%	6.2	3.5	3.4
Motor 1, Avg, 100% to 70%	3.6	3.2	3.1
Motor 1, Avg, 70% to Soft Stop	4.0	3.0	3.2
Motor 1, Avg/Peak, Soft Stop to Stowed	6.5/11.9	7.3/11.5	7.2/11.4

*See Figures 2 2 and 2 3 for current profile.

shown in Fig. 2-2 and 2-3, respectively. For these two events, the current usage during flight and that during ground test match closely. For the remainder of the extensions and retractions, the current usage in flight is slightly higher than in ground test. The most likely cause for the current increase relative to ground tests is the higher operating voltage, as discussed in the previous paragraph. Also, the blanket tension loads are reacted differently in flight than in ground test. In flight, the moment in the mast due to the offset tension loads causes the mast to bend and produces reaction loads on the longeron pivot fittings where the mast enters the canister. These loads increase the motor current required to drive the mast. During ground test, the mast support system reacts a portion of the moment loads so that the full moment load is not reacted by the longeron pivot fittings. Thus, the moment at the mast base during ground test is reduced from the flight condition. The net current usage depends not only on the bending moment at the base of the mast but also on the work being done by the motors on the tension system during extension and by the tension system on the motors during retraction. Therefore, the current values vary among the extensions to the 70-percent position, the extensions from the 70-percent to the 100-percent position, and the retractions over these same intervals. Considering the fact that the stall current

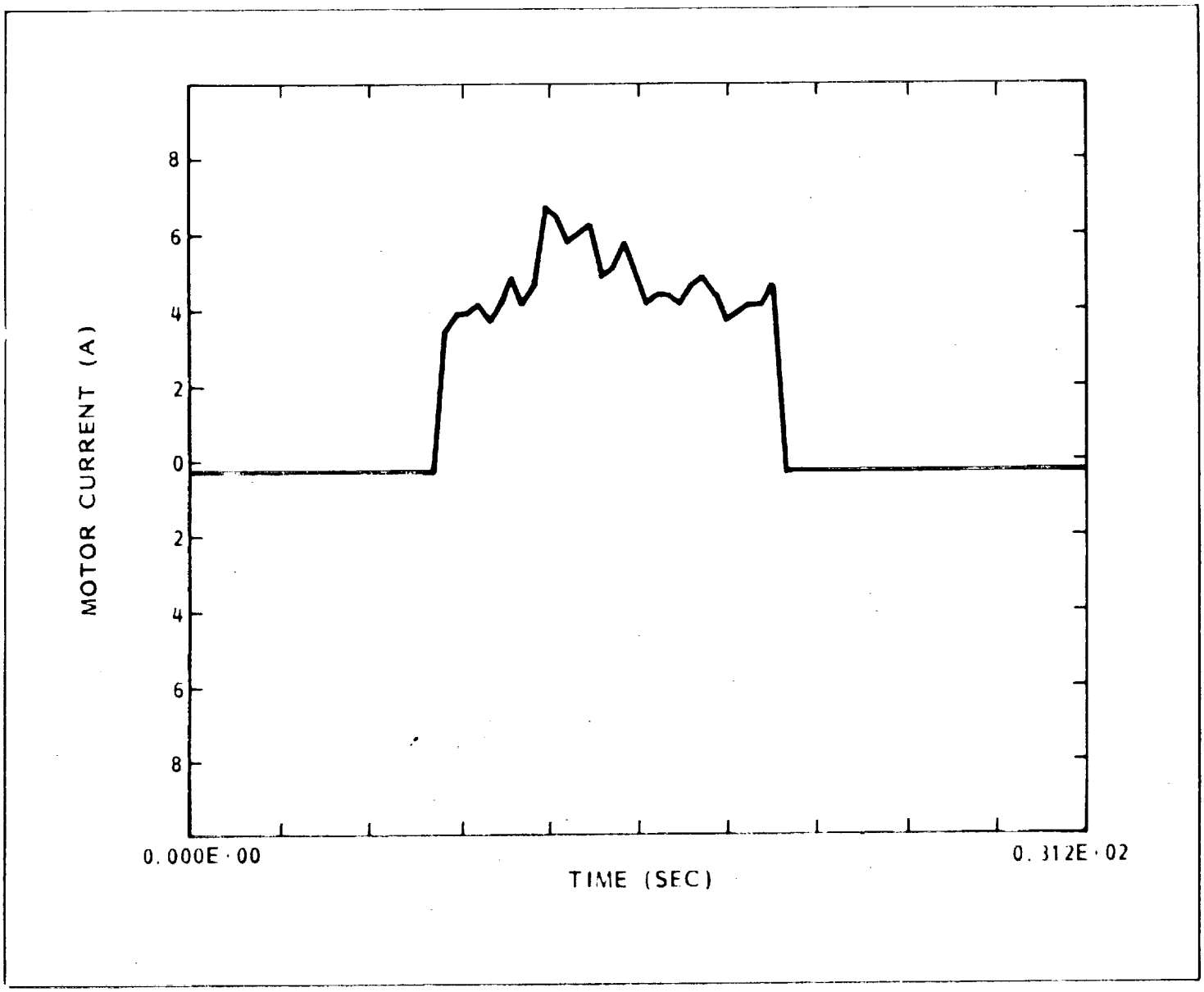

Fig. 2-2 Motor Current Usage During Mast Nut Unlock (Event 1)

e for each motor is 25 amperes, the current variations between flight and ground test are well within acceptable levels.

2.4.2 Wing Twist Evaluation

While deployed on orbit, the SAFE wing exhibited a visually detectable twist over its length. The twist was constant for the duration of the flight, and, because the twist had previously been observed in ground test, it is believed to be of manufacturing rather than environmental origin.

The twist in the array is caused by a twist in the mast, and the twist in the mast is caused by unequal lengths of crossing diagonal wires. When first constructed, the mast shape was measured on a water table where the manufactured twist was measured to be approximately four to six degrees. This twist was reduced to less than one degree by selectively replacing diagonals with others of slightly different length. The success of this effort demonstrated the sensitivity of mast twist to diagonal length differences. Much later during electromagnetic interference testing of the mast motors and drive electronics, the diagonals in the outermost bays of the mast were damaged by overcycling that part of the mast. Following a thorough inspection, all diagonals in the outermost 16 feet of the mast were replaced (126 diagonals), in addition to 11 diagonals distributed throughout the remainder of the mast. Due to cost and schedule considerations, measurement of the mast twist was not repeated on a water table at this time.

Later when the mast and canister were attached to the con-

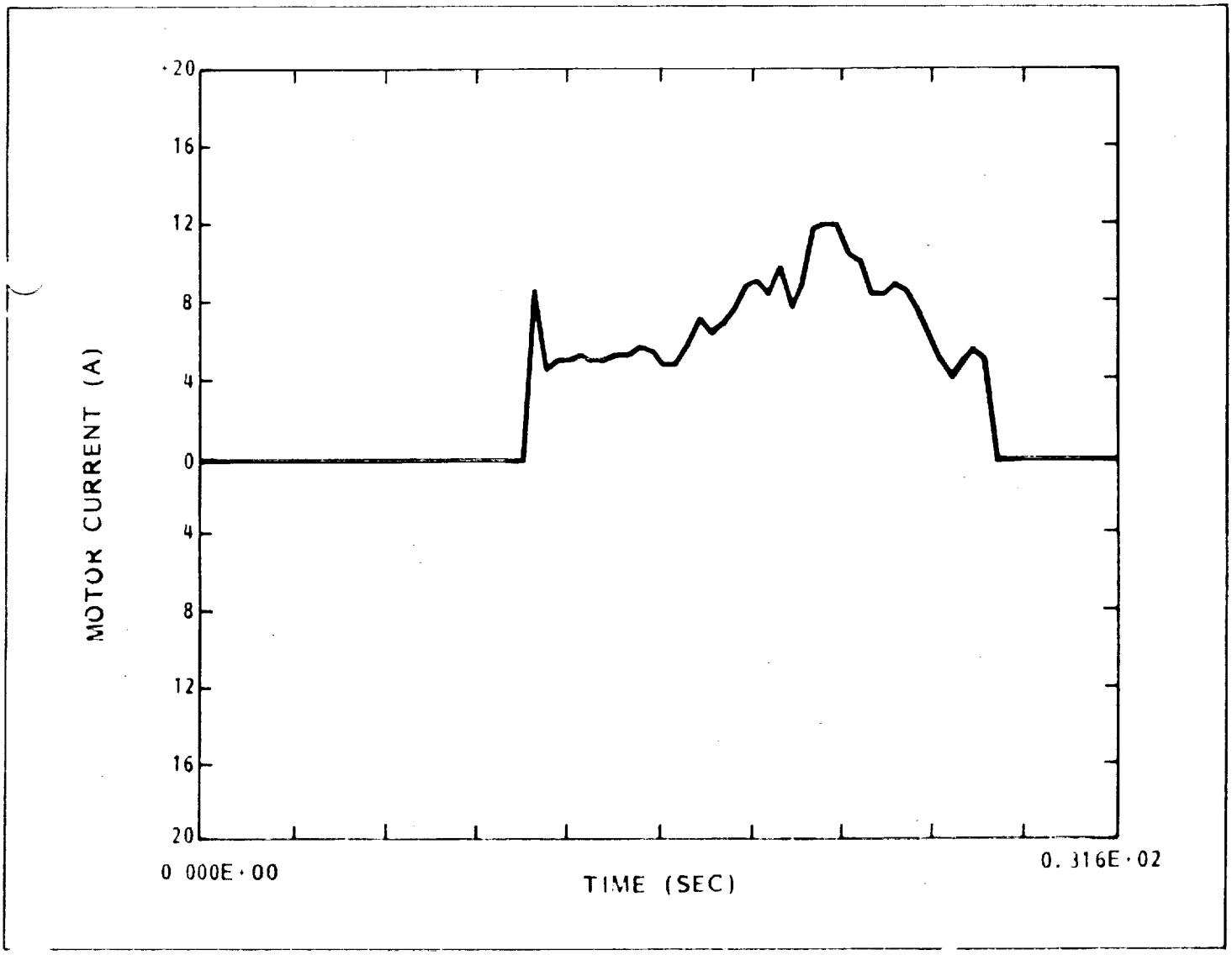

Fig. 2-3 Motor Current Usage During Mast Hard Retract (Event 31)

tainment box and installed in the horizontal deployment fixture, a small amount of twist was evident in the outer bays of the mast. Since this test fixture constrains the mast in torsion, measurements of twist in the fixture are not meaningful. The direction of twist was, however, the same as that in flight. Calculations at that time predicted the mast twist to be 6.9 degrees or less. Since the Contract End Item Specifications for the mast permits ten degrees of mast twist, the apparent mast twist was considered acceptable.

The array twist on orbit was measured with the DAE and the photogrammetry measurement systems. The DAE measurements were all taken at 70-percent extension at the stations shown in Fig. 2-4. Section AA represents the containment box cover; thus, the displacement of targets at this station defines the twist of the array tip relative to the base. The measurements for this station are shown in Fig. 2-5. By scaling from this figure, the array twist is determined to be 7.4 degrees. MSFC has reported the twist to be 7.8 degrees, and the photogrammetry data show similar results. Since no DAE tests were conducted at 100-percent extension, the only source of twist measurement at this position will be the photogrammetry data system. At this time, the data for these twist measurements have not been processed.

2.4.3 Panel Curvature Evaluation

As discussed in Section 2.2, the crew observed the array blanket to be curved about the mast during the dark portion of the $+X_{LV,\ 30\ roll}$ attitude (Fig. 2-27). After approximately ten minutes in the daylight portion of an orbit in this attitude, the blanket flattened out. This behavior was repeated for each orbit in this attitude. Additionally, the blanket was curved during the entire daylight portion of the $+X_{SI}$ attitude when the solar cell performance test was being conducted. A photograph of the curved panel is shown in Fig. 2-6. The panel curvature, as measured with the DAE for the center section of the blanket, is shown in Fig. 2-7. This measurement shows the panel edges to be approximately ten inches closer to the crew cabin than the panel center. The panel curvature was greatest near the midpoint of the blanket length (section CC in Fig. 2-4) and tapered off toward the blanket tip and base (sections BB and DD, respectively).

The observed panel curvature did not impair the electrical power-generating capability of the deployed array or the panel folding behavior during extension and retraction. Nevertheless, considerable effort has been expended to understand the cause of the panel curvature. The desire for understanding the panel curvature is to predict its occurrence and evaluate its effects on future designs for large solar arrays. Since the panels curved during the dark portion of the tail-to-Earth attitude and flattened out during the daylight portion of the orbit, the possibility of relative thermal growth between different materials in the blanket is certainly a likely cause of the panel curvature. However, this cause does not explain the curvature observed during the entire daylight portion of the solar inertial attitude. Nevertheless, a knowledge of the blanket materials and construction is necessary to understand the panel curvature.

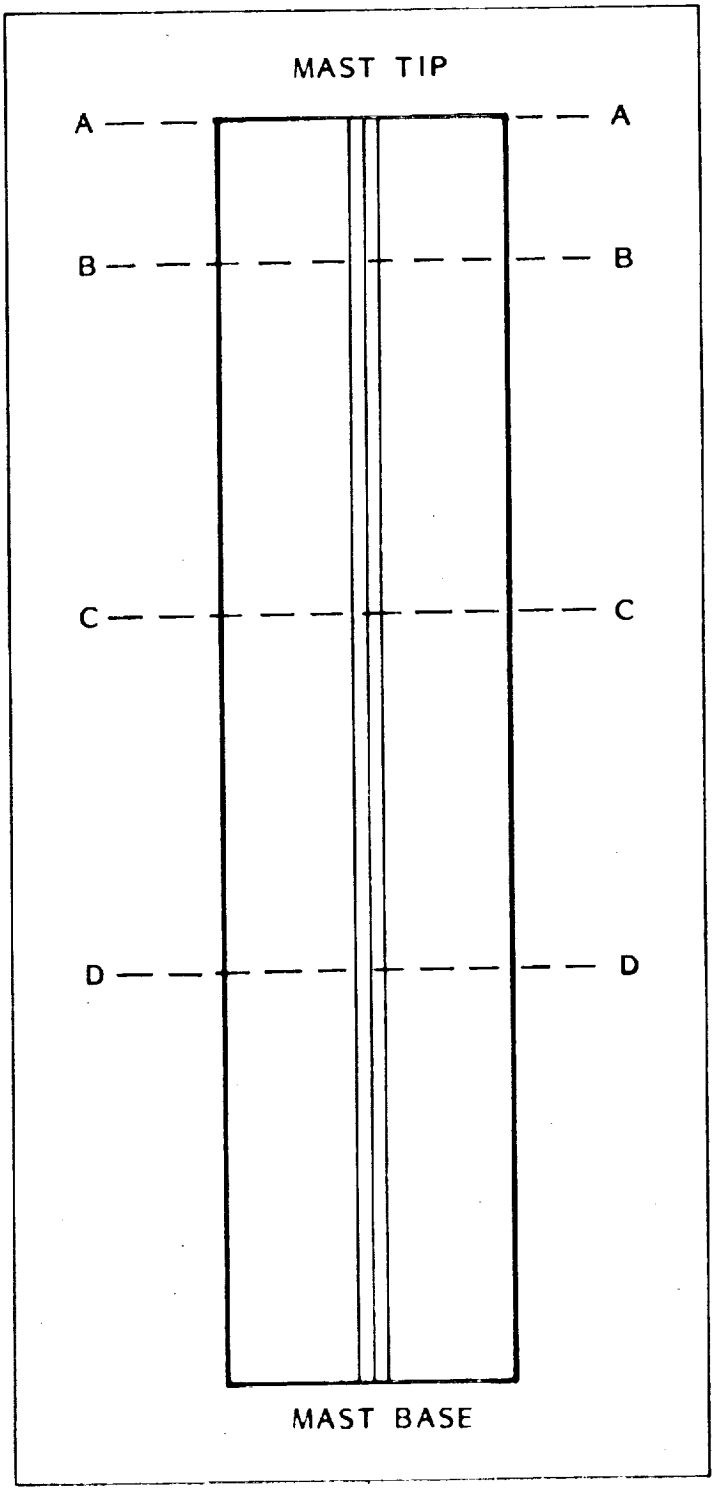

Fig. 2-4 Stations for DAE Measurements

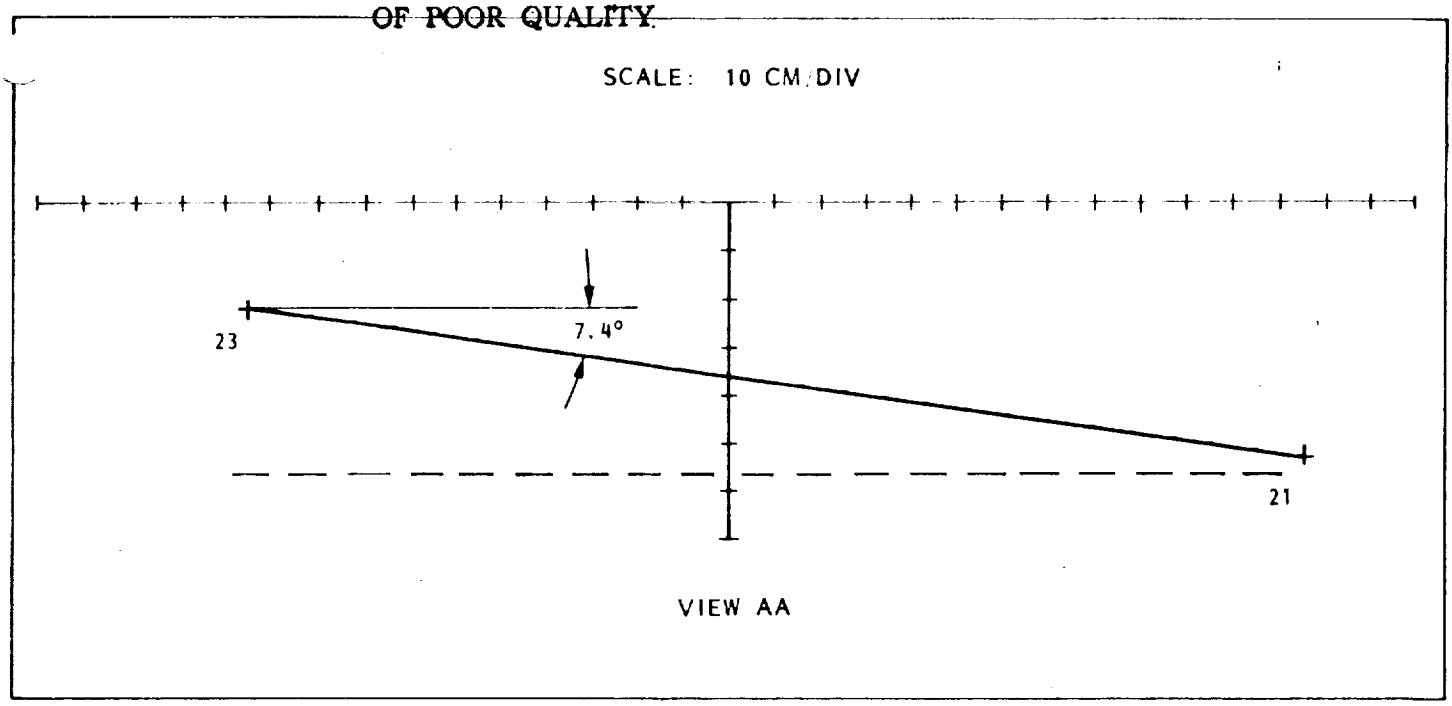

Fig. 2-5 DAE Measurement of Array Twist

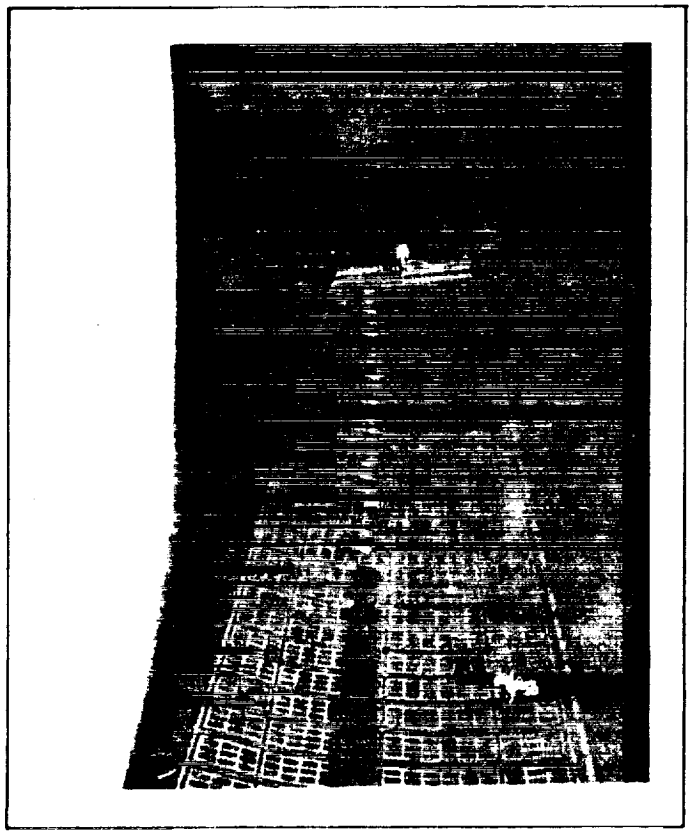

Fig. 2-6 Panel Curvature

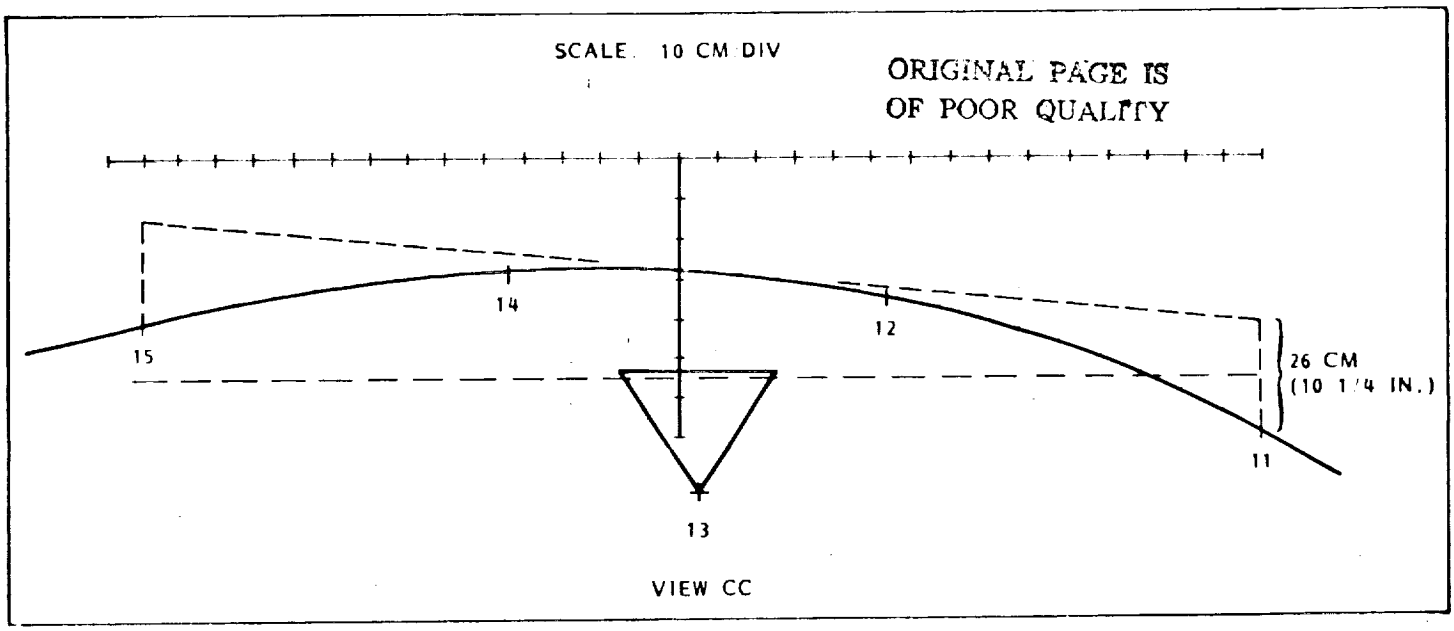

Fig. 2-7 DAE Measurements of Panel Curvature

Blanket Construction Details. Each panel contains a lightweight frame member that disciplines the motion of the panels during the extension and retraction events. The discipline is most important during retraction when all the panels must fold in an accordion fashion if they are to stow neatly within the containment box. To ensure that the panels all fold in the proper direction, leaf springs at the panel hinge lines apply a small torque to the frame members of adjacent panels. The panel hinges are of the "piano hinge" type. The alternate hinge loops from each panel are produced by notching the Kapton substrate every one inch, folding each tab over on itself, and bonding it down. A small-diameter rod of S-Glass epoxy is threaded through the alternate hinge loops from each panel to join them and complete the piano hinge.

Graphite epoxy is used for the panel frame members because its high modulus of elasticity permits the desired frame stiffness to be achieved with relatively small frame members. However, due to the high cost of fabricating graphite epoxy frame members, only the outermost five panels on the blanket were fitted with frames made from graphite epoxy. The remaining 79 panels were fitted with frames made from aluminum with dimensions that produce the same bending stiffness as the graphite epoxy frames. For this reason, the aluminum frames are considerably wider than the graphite frames.

Relative thermal growth between the S-glass epoxy hinge rods and the Kapton hinge loops is accommodated because the hinge rods are free to slide through the hinge loops in the cross panel direction. Relative thermal growth between the panel frames and the Kapton panels is accommodated by attaching the frames to the panels with Kapton sleeves A sketch of this concept is shown in Fig. 2-8.

Dimensions for the cross-panel frame members and sleeves are shown in Fig. 2-9. For both types of frames, the sleeves were oversized enough so that frame-to-sleeve clearance would exist over the temperature range from $-240°$ to $+240°$F. Since aluminum and Kapton have similar coefficients of thermal expansion, only 0.050 inch of clearance is required between the Kapton sleeve and the aluminum frame. Since Kapton and graphite epoxy have considerably different coefficients of thermal expansion, a clearance of 0.265 inch is required to accommodate the relative thermal growth.

Loss of Clearance Between Aluminum Frame Members and Kapton Sleeves. Investigation of the panel curvature has revealed a number of reasons to suggest that its probable cause was loss of the nominal 0.050-inch gap between the aluminum frames and Kapton sleeves.

The first reason is that, while the design was sized for relatively large bulk temperature changes, it was not sized for temperature differences between the aluminum and Kapton. Frequently, conservative bulk temperature assumptions will accommodate the growth caused by relative temperature differences. This is not the case, however, when the coefficients of thermal expansion of the two materials are nearly equal. There is reason to believe that the aluminum frames actually ran hotter than the Kapton sleeving material. Evidence of this

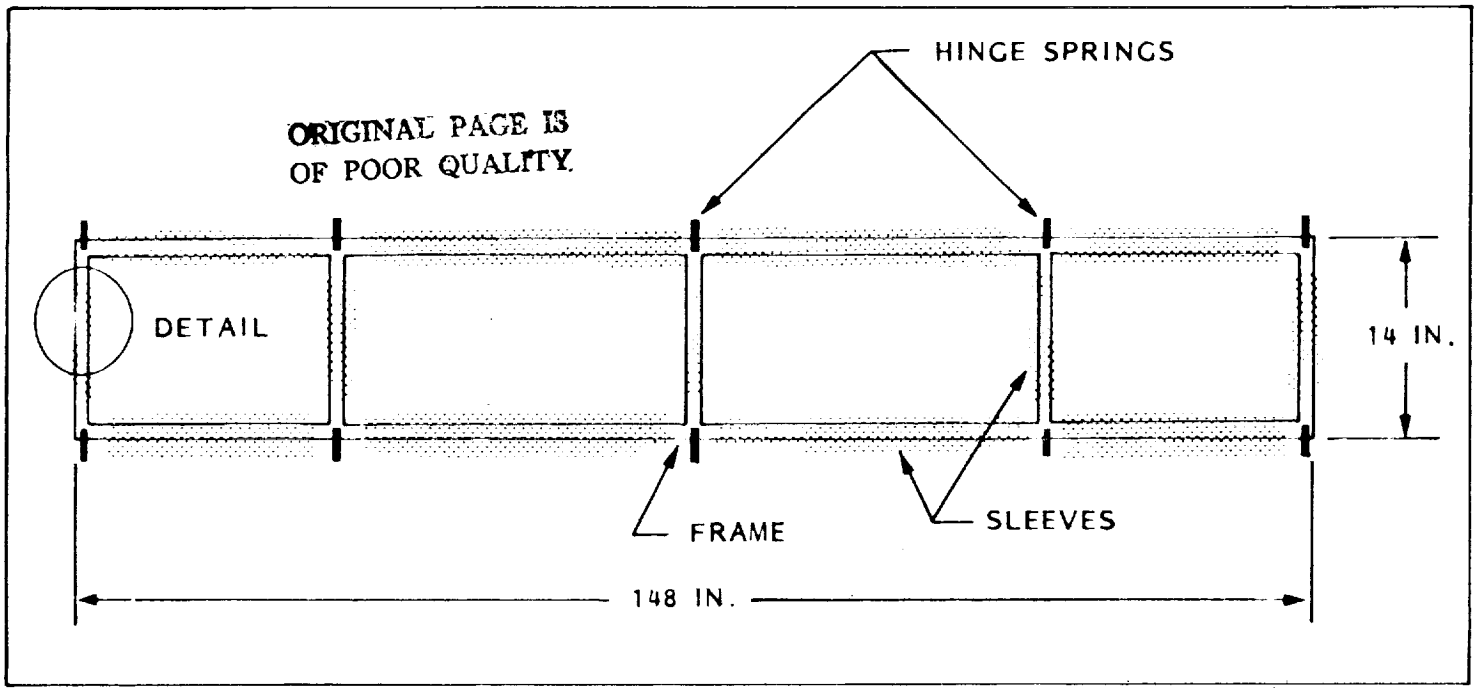

Fig. 2-8 Sleeve Construction for Panel Frames

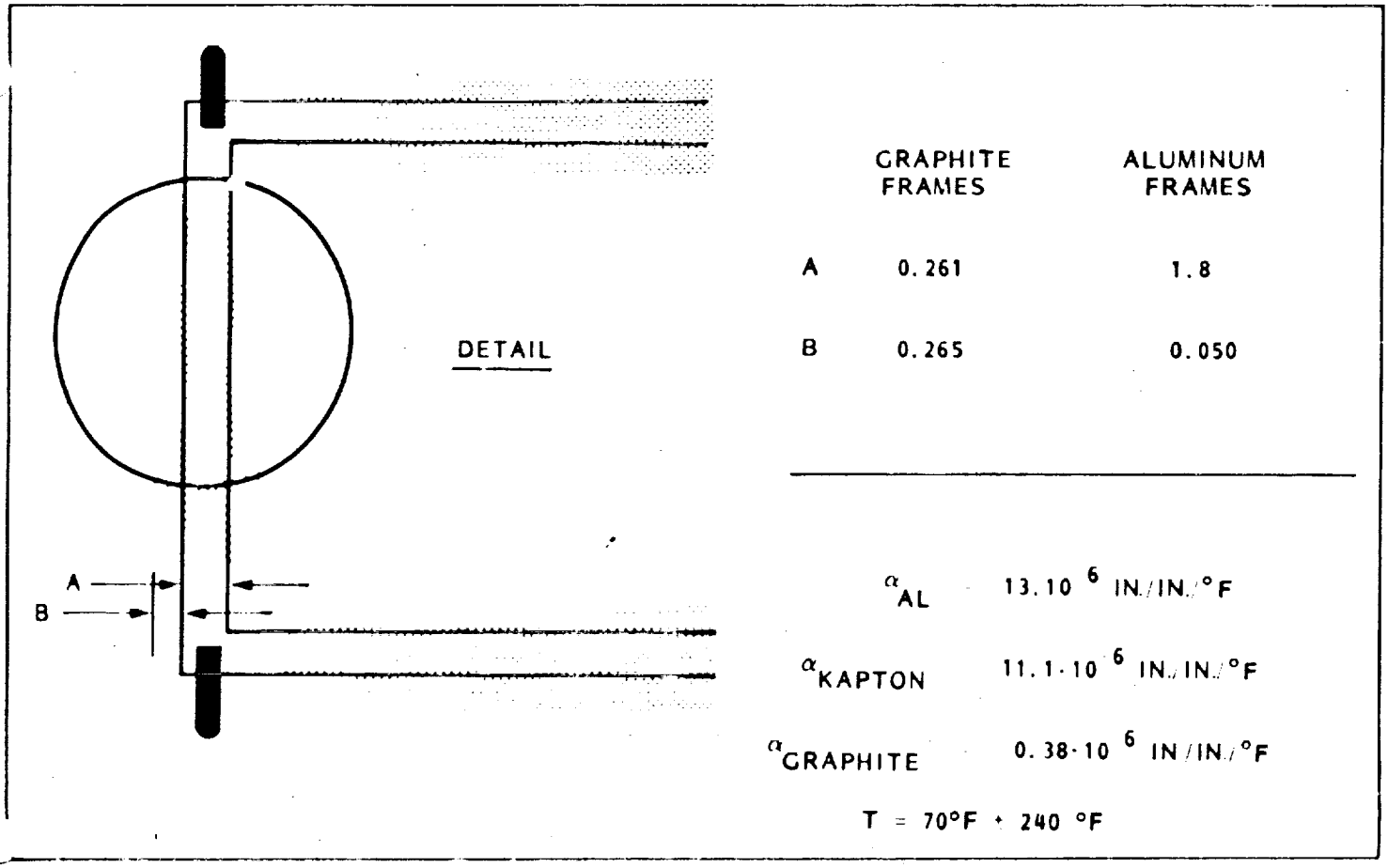

Fig. 2-9 Panel Frame and Sleeve Dimensions

phenomenum was demonstrated in the panel-curvature tests to be discussed in a subsequent paragraph.

Another reason for the inadequacy of the 0.050-inch gap is that Kapton increases dimension significantly with water absorption. If a panel is manufactured in a humid environment and then placed into the vacuum of space, the Kapton will contract as the moisture is released. Using a contraction coefficient of 2.2×10^{-5} in./in. per percent change in relative humidity, the half-panel contraction for a panel assembled in a 50-percent relative humidity environment would be 0.0825 inches. This contraction would eliminate the nominal clearance of 0.050 inch between the cross-panel frame member and the Kapton sleeve.

Kapton will also shrink as the residual stresses, caused when the material is wound on rolls during manufacturing, relax. These stresses are relieved the first time the material is heated in a condition under which it is free to contract. In the case of the SAFE panels, the "machine direction" is the 13.5-foot dimension of the panel, so that any shrinkage would contribute to a reduction in the frame-to-sleeve clearance. This shrinkage should be approximately 0.040 inch over the half-panel width.

An uncertain value for the coefficient of thermal expansion for Kapton might also cause the 0.050-inch frame-to-sleeve clearance to be inadequate. The value of 11×10^{-6} in./°F shown in Fig. 2-8 was supplied by Dupont; however, a considerable range of values has been documented in the literature.

Finally, the 0.050-inch gap between the aluminum frames and Kapton sleeves may have been inadequate because of the difficulty in maintaining this tolerance over a 13.5-foot span with bonded construction techniques. Any tension in the panel at the time of bonding or any misalignment in the sleeve segments would effectively reduce the intended gap at one location or another.

In conclusion, the gap between the aluminum frames and the Kapton sleeves was probably inadequate due to temperature uncertainties, shrinkage factors that were not realized as significant, material property variations, and manufacturing considerations. Because the aluminum frames are offset on one side of the Kapton panel (the cell side), shrinkage of the Kapton would cause the panel assembly to bend in a direction that gives the frame members a larger radius of curvature than the Kapton panel. This is exactly the direction of panel curvature observed at all times during the flight test of the experiment. Additional evidence that the panel curvature was caused by inadequate gap between the aluminum frames and Kapton sleeves was observed in the postflight curvature tests performed on five of the flight panels.

Panel Curvature Test. A panel-curvature test was performed on flight panels 3 through 7 (as measured from the array tip) by removing the panels from the blanket after the postflight extension and retraction tests. Panels 3, 4, and 5 have graphite epoxy frames, and panels 6 and 7 have aluminum frames. The panels were oriented in a test fixture as shown in Fig. 2-10. By selecting five panels, the panel weight produced a tension at the upper hinge line nearly equal to the uniform flight tension. Because the tests were to be exploratory, they were performed in room ambient conditions where test variables could be easily changed. The intent of the tests was not necessarily to reproduce the magnitude of flight curvature but to produce some curvature and to determine the source of it. Radiant lamps were used to heat the panels from the cell side, from the back side, or from both sides simultaneously. The lamps could be raised or lowered so that the heat could be directed at the panels with aluminum frames or at the panels with graphite epoxy frames. The frame temperatures were monitored with thermocouples, and the upper temperature limit was chosen as 176°F. This is the maximum solar cell temperature observed during the flight.

A particularly sensitive panel-support system was chosen for the tests since extremely small external forces can produce panel curvature and mask the intended curvature measurements. The selected support method consisted of seven pairs of styrofoam floats in two overhead water tanks as shown in Fig. 2-11. The float pairs were connected by aluminum cross beams, and a vertical rod from each cross beam picked up the panel. A test in progress with the lamps lowered to illuminate the panels with graphite epoxy frames is shown in Fig. 2-12.

Tests were first performed with all five panels hinged together in the test fixture. The panels with aluminum frames were heated from the cell side, from the back side, and from both sides simultaneously. The same was done for the panels with the graphite epoxy frames. Next, the panels with the graphite epoxy frames were separated from the panels with the aluminum frames, and each group of panels was tested separately.

In general, the curvature produced in the tests was considerably less than the curvature observed in flight. At most three or four inches of curvature were measured as opposed to ten inches observed in flight. Nevertheless, some important curvature trends were observed. Perhaps even more important, close inspection of the panels showed that the most outboard cross-panel frame members were no longer centered in the Kapton sleeves even under ambient conditions. This was true for both the panels with the aluminum frames and the panels with the graphite epoxy frames. For the panels with the aluminum frames, the 0.050-inch gap on the outboard side was completely eliminated, and the frame members were

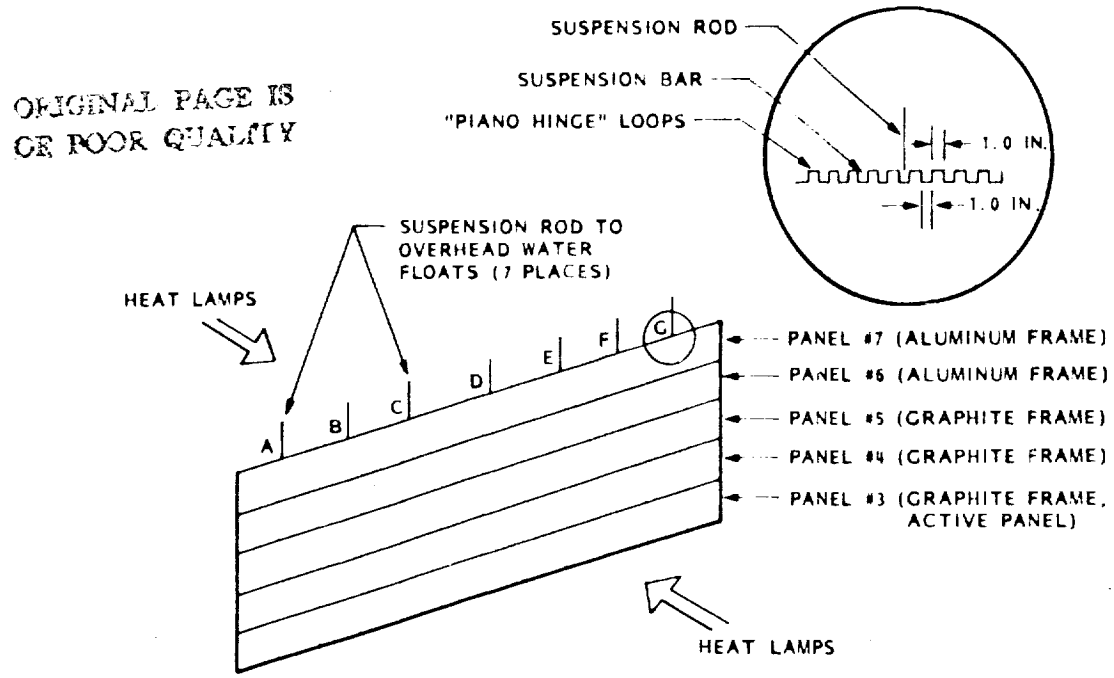

Fig. 2-10 Panel Curvature Test Method

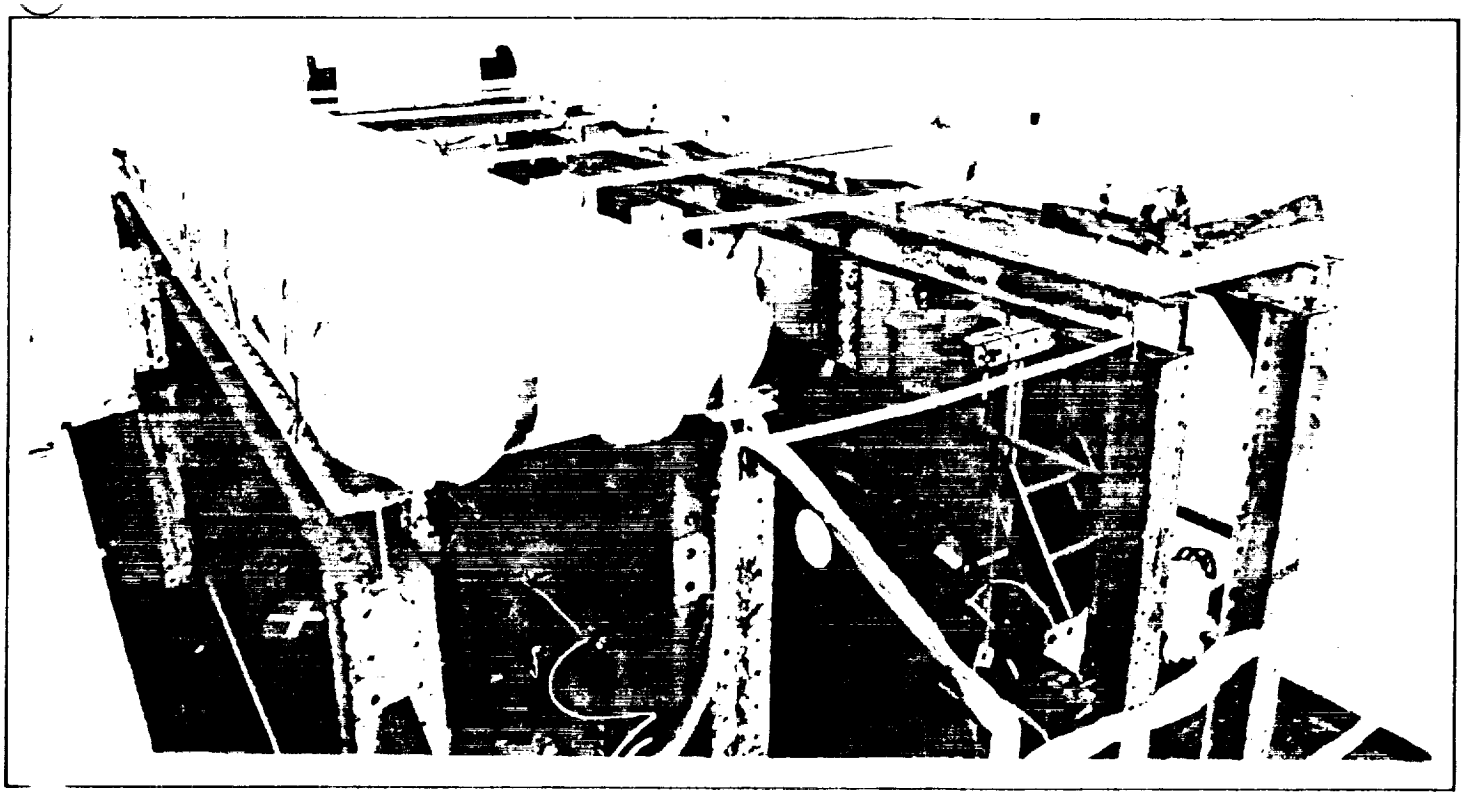

Fig. 2-11 Water Tanks and Float System for Panel Curvature Test

"hard up" against the sleeves. For the panels with the graphite epoxy frames, the gap on the inboard side was increased, and the gap on the outboard side was reduced but not to the point of elimination. This observation is consistent with Kapton's tendency to shrink upon relief of manufacturing stresses and/or humidity change. In all cases when the panels with the aluminum frames were heated, the panels curved in the same direction as in flight. This was true whether the panels were heated from the cell side, the backside, or both sides. Relative growth of the aluminum frames in the outboard direction relative to the Kapton panel was visually evident in these tests. If convective heat transfer effects are ignored, this observation indicates that the aluminum frame members operated at a higher temperature than the Kapton substrate. When frame insulation in the form of silverized fiberglass cloth was used to block the direct radiative heat transfer from the lamps to the frames, the panels curved in the same direction but with reduced magnitude.

To gain additional evidence that the panel curvature was the result of interference between the aluminum frames and the Kapton panel, 0.003-inch copper shims were slipped over the outermost cross panel frame members. The shims effectively increased the frame length, thereby worsening the situation caused by the Kapton shrinkage. When the panels were heated in this configuration, the resulting curvature was of a magnitude larger than previously measured.

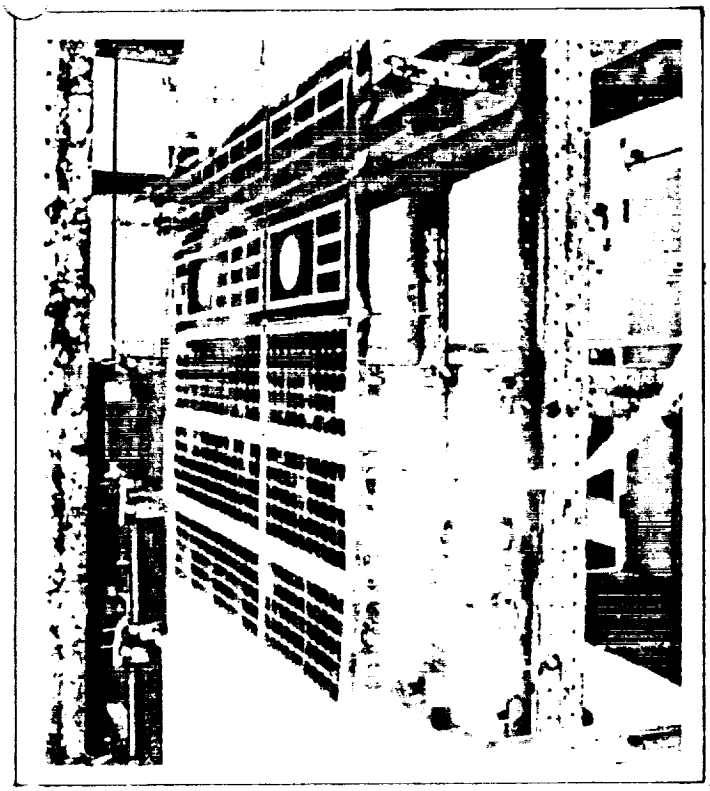

Fig. 2-12 Panel Curvature Test in Progress

In summary, the panel curvature observed on orbit seems to have been caused by an inadequate gap between the aluminum frames and Kapton sleeves. The major factors contributing to the inadequacy of the gap are Kapton shrinkage factors not considered in the design and temperature differences between the aluminum frames and the Kapton. The elevated frame temperature relative to the Kapton, when combined with inadequate gap due to Kapton shrinkage, caused the panels to curve in the direction observed in flight.

As a result of this investigation and set of tests, a list of measures to be considered in future designs to eliminate panel curvature has been formulated. These considerations are listed in Fig. 2-13. In addition, the final design for future applications should be subjected to a panel curvature test performed in a thermal vacuum chamber to verify the design adequacy.

- BE AWARE OF CURVATURE SENSITIVITY
- AVOID MATERIAL MISMATCH IN FRAMES
- DESIGN FOR FRAME TO KAPTON TEMPERATURE DIFFERENCES
- DESIGN FOR ALL KAPTON SHRINKAGE COEFFICIENTS AND/OR PRE-PROCESS KAPTON
- LUBRICATE OR COAT FRAME MEMBERS
- INCREASE SLEEVE OVERLAP AT ADHESIVE STRIP
- LUBRICATE OR COAT HINGE PINS, CONSIDER ALUMINUM HINGE PINS
- ELIMINATE OUTER CROSS PANEL SLEEVE. CONSIDER SLEEVE REDUCTION IN GENERAL
- INSPECT COMPLETED PANEL ASSEMBLIES FOR FRAME FREEDOM

Fig. 2-13 Potential Design Improvements to Eliminate Panel Curvature

2.4.4 Wing Dynamics Evaluation

While the SAFE demonstrated the readiness of advanced solar array technology, it was also important as a test bed for large space structures. Motion data resulting from planned firings of the orbiter thrusters have been collected, and these flight data are compared with preflight analytical predictions in the following paragraphs.

Data Sources. The principal instrumentation for the solar-array dynamic response are six accelerometers, located as shown in Fig. 2-14, providing acceleration time histories. The output of these accelerometers was recorded each time the thrusters of the VRCS were fired for a dynamics test. Data recording continued throughout the free response period.

A secondary source of data on mast-tip motion are photographs of the mast tip taken from the crew cabin with a 35-mm Nikon camera and 500-mm lens. This system allowed the crew to monitor the mast-tip motion in realtime by way of grid lines on the eye piece of the camera. The system functioned well, and the photographs taken at regular intervals provided additional data at little expense.

These photographs were taken only during the first daylight dynamics test at 70-percent extension and the first daylight dynamics test at 100-percent extension. Sixty-four frames of film were exposed in each case. The interval between frames was two seconds at 70-percent extension and four seconds at 100-percent extension. Typical frames from

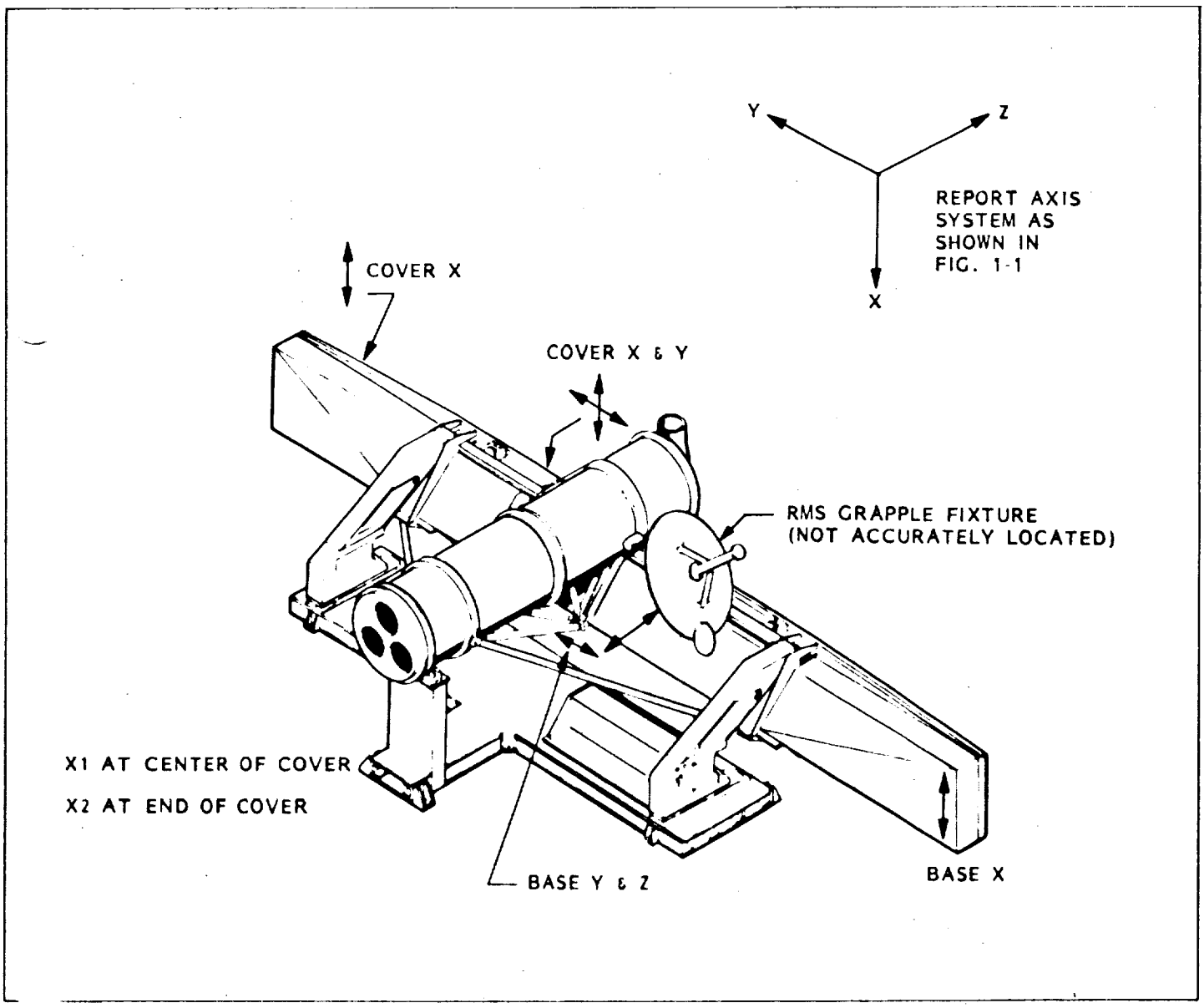

Fig. 2-14 Accelerometer Locations

the Nikon camera are shown in Figs. 2-15 and 2-16 for the mast extended to the 70-percent and 100-percent positions, respectively.

Although the camera was incorrectly focused at the 100-percent position, the data can still be used by measuring motion to the apparent center of the mast-tip target. The motion of the mast tip versus time is an independent piece of data that can be compared with the mast-tip time histories derived from the second integral of the accelerometer data.

Orbiter Thruster Performance. The four VRCS thrusters that produced the planned experiment disturbances are shown in Fig. 2-17. The theoretical orbiter accelerations produced at the base of the experiment by firing each of the thrusters are shown in Table 2-4. When more than one thruster is firing, the accelerations must be superimposed to arrive at the net accelerations at the base of the mast. These accelerations, combined with a knowledge of the thruster firing-time histories, determine the base motion accelerations for input into the dynamic model of the array. The planned thruster firing-time histories are listed in Table 2-5. In all cases, it was intended that the firing be preceded by a quiescent period to allow the displacement and velocity of the experiment to null out before each test. During the quiescent period, VRCS firings for station-keeping were inhibited and crew motion was minimized in order to limit disturbances to the experiment. These practices were also enforced following the planned firings so that data on experiment motion could be gathered during a true "free response" period.

In two cases, a deviation occurred from the plan to produce a quiescent period, perform the intended firings, and then monitor experiment motion. During the intended quiescent period preceding event 11, there is evidence of VRCS activity before the planned firings. Therefore, the initial conditions for this test may not be as near zero as for other tests. The other deviation occurred in event 27 in which the first of the intended thruster firings did not occur. In all other cases, the thruster firings were basically the intended ones as shown in Table 2-5. Since the times at which the thrusters were fired were manually controlled, the actual firings differ slightly from the intended firings in all cases. The actual thruster firing-time histories are shown in Appendix A. These time histories were compiled from orbiter instrumentation. These thruster firing histories, when combined with the acceleration levels shown in Table 2-4, result in acceleration-time histories at the experiment base as contained in Appendix B.

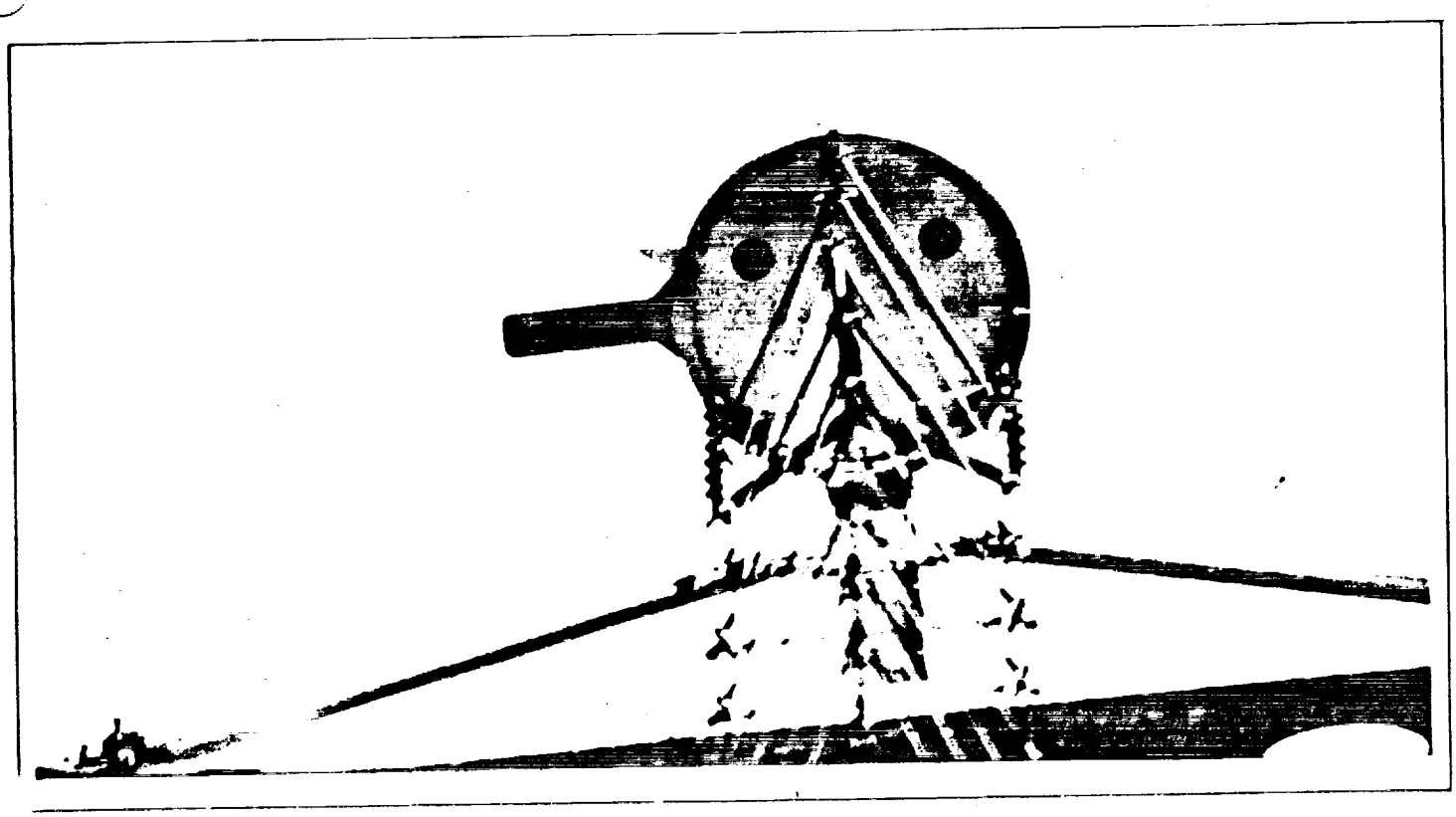

Fig. 2-15 Typical Image of Mast Tip at 70-Percent Extension as Seen by the Nikon Camera

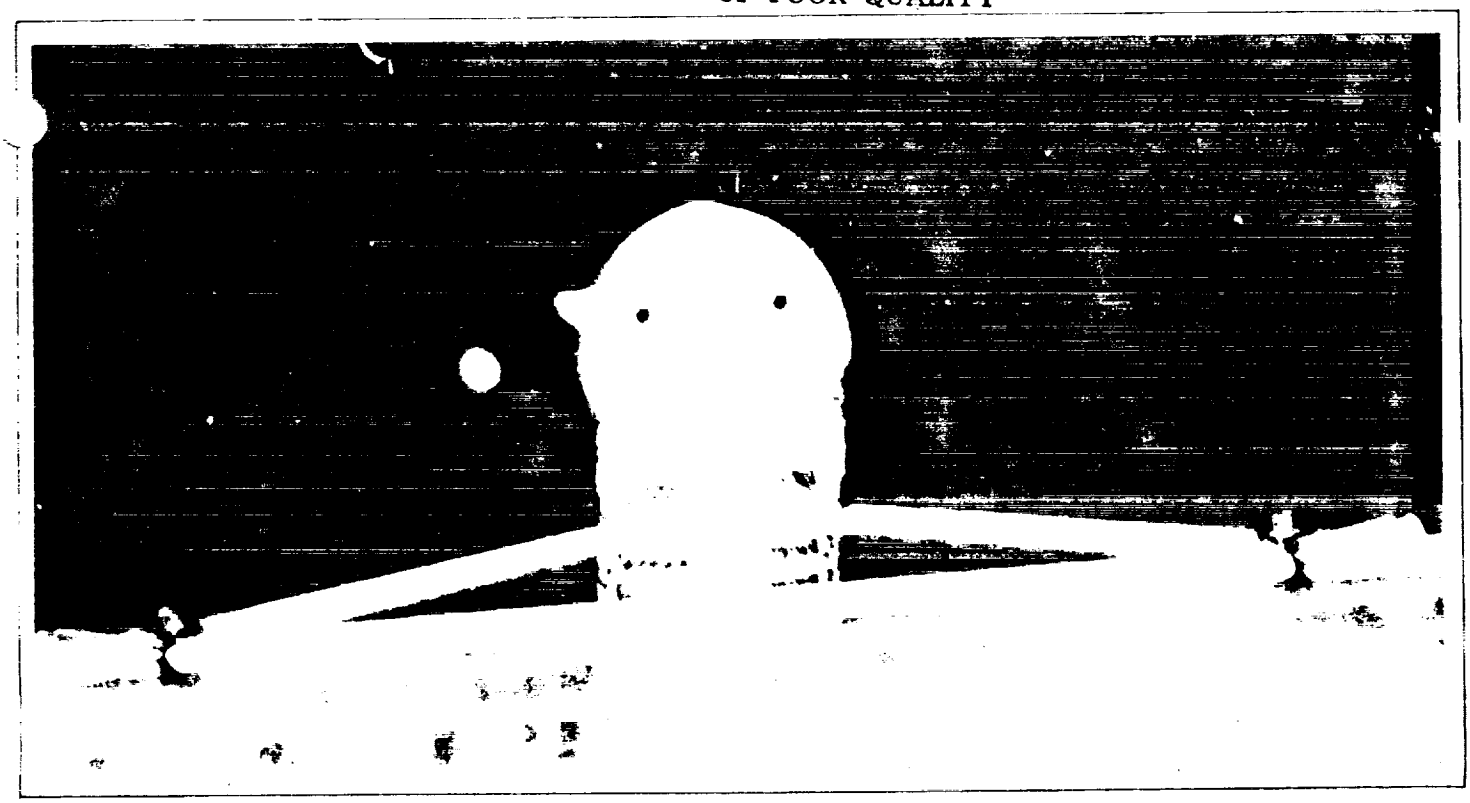

Fig. 2-16 Typical Image of Mast Tip at 100-Percent Extension as Seen by the Nikon Camera

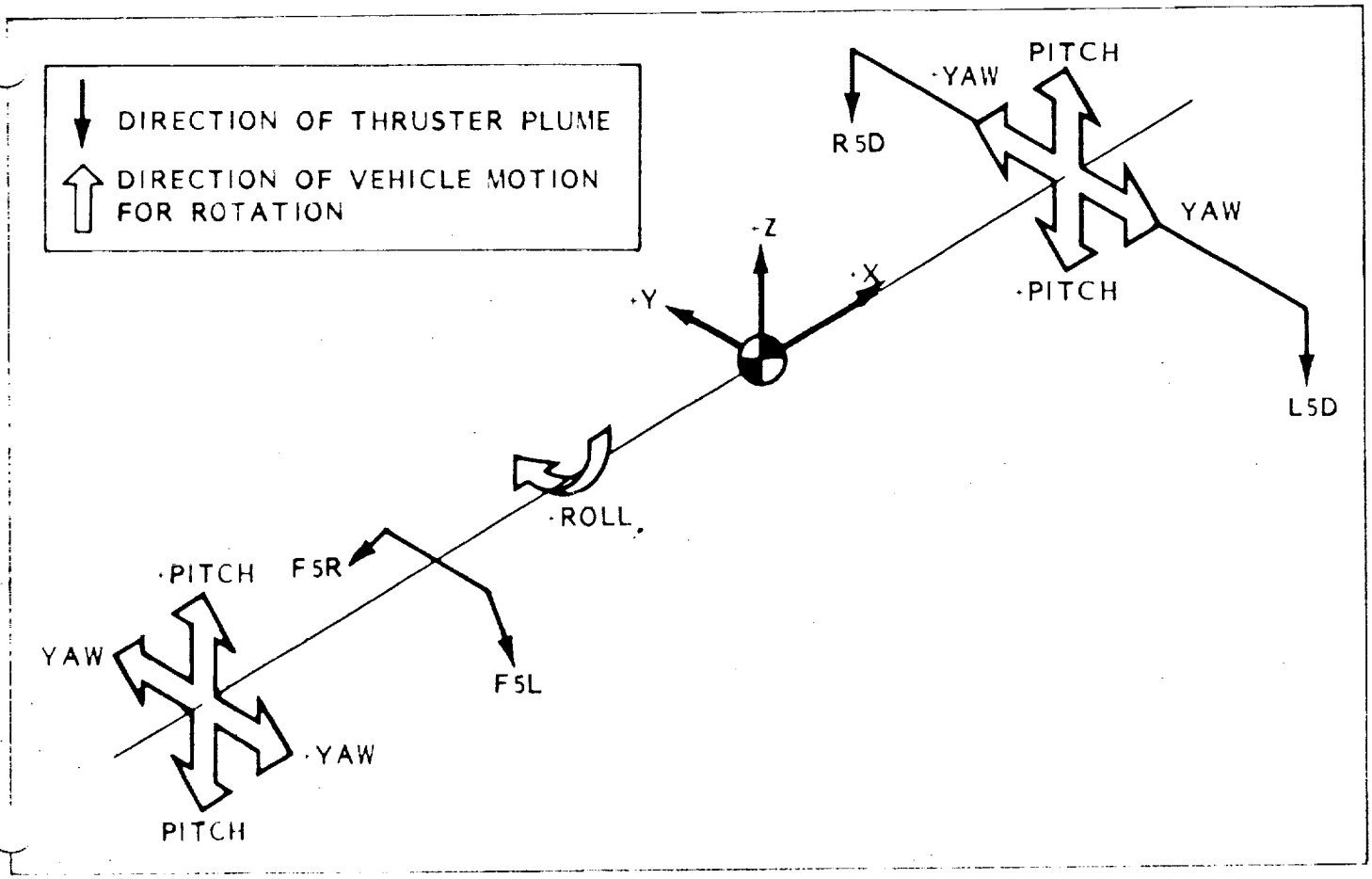

Fig. 2-17 Orbiter Thruster Locations

Table 2-4 SAFE BASE ACCELERATIONS DUE TO VRCS THRUSTER FIRINGS

All units are in./sec^2 and rad/sec^2

F5R	F5L
$\ddot{x} = 0.0$ $\ddot{y} = -0.07771$ $\ddot{z} = 0.07654$ $\ddot{\theta}x = 0.5337 \times 10^{-4}$ $\ddot{\theta}y = 0.1515 \times 10^{-3}$ $\ddot{\theta}y = 0.1448 \times 10^{-3}$	$\ddot{x} = 0.0$ $\ddot{y} = 0.07771$ $\ddot{z} = 0.07654$ $\ddot{\theta}x = 0.5337 \times 10^{-4}$ $\ddot{\theta}y = -0.1515 \times 10^{-3}$ $\ddot{\theta}z = -0.1448 \times 10^{-3}$
R5D	**L5D**
$\ddot{x} = 0.0$ $\ddot{y} = 0.0$ $\ddot{z} = 0.002182$ $\ddot{\theta}x = 0.13407 \times 10^{-3}$ $\ddot{\theta}y = -0.69924 \times 10^{-4}$ $\ddot{\theta}y = 0.0$	$\ddot{x} = 0.0$ $\ddot{y} = 0.0$ $\ddot{z} = 0.002182$ $\ddot{\theta}x = -0.13407 \times 10^{-3}$ $\ddot{\theta}y = -0.69924 \times 10^{-4}$ $\ddot{\theta}z = 0.0$

Table 2-5 THRUSTER FIRING-TIME HISTORIES

70% Out-of-Plane

t = 0, F5L +F5R for 3.6 sec
t = 8.4, L5D + R5D for 8.0 sec
t = 16.88, F5L + F5R for 3.6 sec
t = 25.28, L5D + R5D for 8.0 sec

70% In-Plane

t = 0, F5L for 3.36 sec and L5D for 7.36 sec
t = 7.52, F5R for 3.36 sec and R5D for 7.36 sec

70% Multi-Modal

t = 0, F5L for 4.0 sec
t = 4.96, R5D for 8.8 sec
t = 32.72, F5R for 4.0 sec
t = 40.72, L5D for 8.8 sec

100% Out-of-Plane

t = 0, F5L + F5R for 4.32 sec
t = 15.04, L5D + R5D for 9.52 sec

100% Multi Modal

t = 0, F5L +F5R for 4.0 sec and R5D for 5.52 sec
t = 10, L5D for 8.8 sec and R5D for 3.28 sec

(1.5) 70% Out of Plane

t = 0, F5L for 2.0 sec and L5D for 4.4 sec
t = 7.52, F5R for 2.0 sec and R5D for 4.4 sec
t = 14.96, F5L for 2.0 sec and L5D for 4.4 sec
t = 22.48, F5R for 2.0 sec and R5D for 4.4 sec

(1.5) 70% Multi Modal

t = 0, F5L for 2.48 sec
t = 32.72, F5R for 2.48 sec
t = 56.0, L5D for 5.44 sec
t = 100.0, F5L for 2.48 sec
t = 4.96, R5D for 5.44 sec
t = 40.72, L5D for 5.44 sec
t = 65.04, F5R for 2.48 sec
t = 108.0, R5D for 5.44 sec

Accelerometer Data. Data from the three accelerometers located on the support structure at the base of the experiment were used very little in evaluating the experiment dynamic performance. Because very low signal levels were being recorded, the effects of noise-level accelerations and signal shifts due to temperature changes significantly degraded the data. As an example of the data quality from this instrumentation source, the base acceleration-time histories from event 5 are shown in the first three pages of Appendix C.

The data from the three accelerometers on the containment box cover at the tip of the experiment were of much better quality. The superior quality results primarily because orbiter noise-level accelerations are not transmitted to the box cover by the mast/blanket structure and because accelerometers with low sensitivity to temperature were chosen for this location.

Before transmitting this data to LMSC, the accelerations were filtered and zero-adjusted by MSFC. The filtering eliminated useless high-frequency response content, and the zero-shift compensated for small dc signal shifts due to temperature change. Without the zero-adjustment, the acceleration signals have would produced erroneous velocity and displacement values when integrated. The adjusted acceleration-time histories are contained in Appendix C. PSDs of each of these acceleration histories are contained in Appendix D. Displacement-time histories, obtained by taking the second integral of the acceleration, are contained in Appendix E. The labeling of the accelerometer sensitive axes corresponds with the convention shown in Fig. 2-4. Shown in Table 2-6 are the dominant frequencies for each test record and the associated modal damping values. These were calculated from the accelerometer PSDs by MSFC, using the half-power method.

Quality of Accelerometer Data. Since much of the dynamics evaluation is based on the accelerometer data, the quality of the data is important. As mentioned earlier, the mast-tip motion as measured with the Nikon camera is independent data that can be compared with the second integral of the accelerometer data. The displacement-time history from the Nikon data for the 70-percent extension is shown in Fig. 2-18. For convenience, the corresponding data from the second integral of the accelerometer contained in Appendix E has been reproduced and included as Fig. 2-19. The mast-tip displacement from the Nikon data at 100-percent extension and from the accelerometer data for the same event are shown as Figs. 2-20 and 2-21, respectively. In each case, the integration of the acceleration data began 15 or 20 seconds before the start of the test event, so a shift of the time axis is needed to compare the data. When this shift is done, the time histories from the two

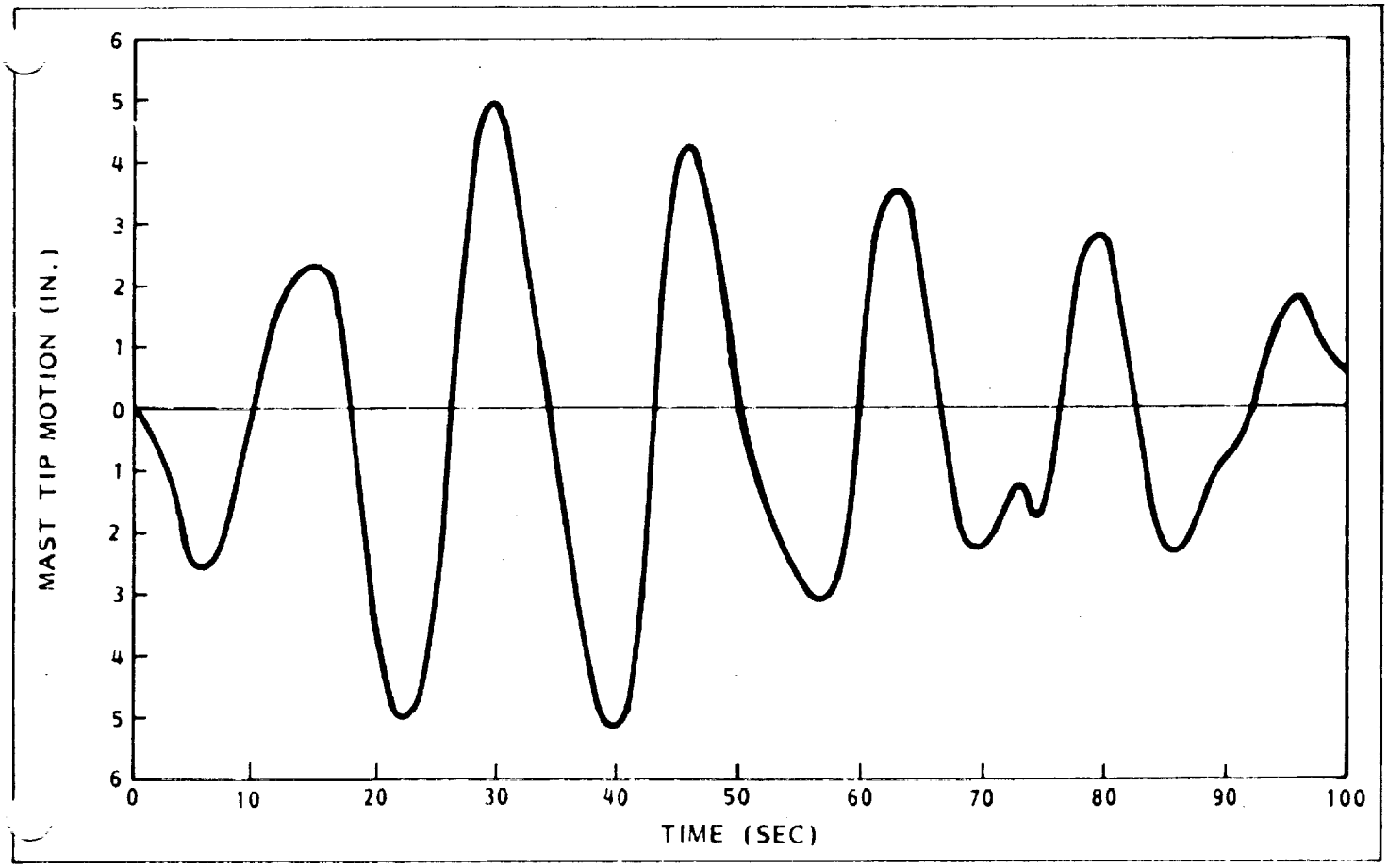

Fig. 2-18 Mast-Tip Motion From Nikon Data for First Out-of-Plane Test at 70-Percent Extension—File 5

Table 2-6

DOMINANT FREQUENCIES AND MODAL DAMPING VALUES
SUPPLIED BY MSFC

Event	Modal Frequency (Hz)	Modal Damping (% of Critical)
5	0.056	7.0
	0.103	0.9 or 2.6 in Y
	0.11	0.8
	0.165	1.8
6	0.058	11.0
	0.125	3.7
10	0.058	6.0
	0.075	3.6
11	0.062	10.0
12	0.056	8.6
	0.099	3.7
	0.157	1.8
13	0.065	1.4
	0.071	3.8
14	0.059	4.5
	0.075	2.4
15	0.064	1.4
	0.068	1.3
17	0.0375	6.9
	0.152	1.5
20	0.0375	7.2
	0.0577	7.0 in Y
	0.144	1.6
26	0.061	6.7
	0.076	3.01
	0.135	2.07
27	0.060	4.5
28	0.066	1.4
	0.093	3.3
29	0.063	4.4
	0.108	2.0

data sources show remarkable agreement, particularly true of the data comparison at 70-percent extension where the Nikon camera was properly focused. Note, for instance, the "warp-," of the otherwise sinusoidal trace during the period from 50 to 60 seconds after the start of the test. Note also the first full-blown appearance of a second mode in the period of 70 to 75 seconds after the start of the test. Also, the amplitudes from the two time histories match closely.

It is important to remember that the accelerometer data is an electronic signal that has been filtered, zero- adjusted, and double integrated, while the Nikon data is a photographic record that has been processed by some simple scaling techniques. The close match between these two independent sources of the data lends credence to both of them, but particularly to the accelerometer data as the basis for evaluation of the flight dynamic behavior.

Quiescence Before Testing. In the previous section, displacement histories were shown which were acquired by performing a double integration on the accelerometer signals. The integration of the acceleration was started 15 or 20 seconds before the start of the test, and the velocity and displacement at this time were assumed to be zero. This assumption was believed to be justified because of the long quiescent period preceding each test. If true quiescence had been achieved, the integration could have been started at any point within the 15- or 20-second period, and the integration would show no buildup of velocity or displacement before the start of the test. That this is not the case in Figs. 2-19 and 2-21 indicates that true quiescence was not achieved. The magnitude of the velocity and displacements that result from integration are indicative (but not accurate measures) of the experiment tip motion before test. Evaluation of the photogrammetric data by NASA LaRC confirms the presence of residual motion before each test. While the residual motion is a small part of the overall response in the first in-plane or out-of-plane mode of the experiment, it is sizable compared to the response in the

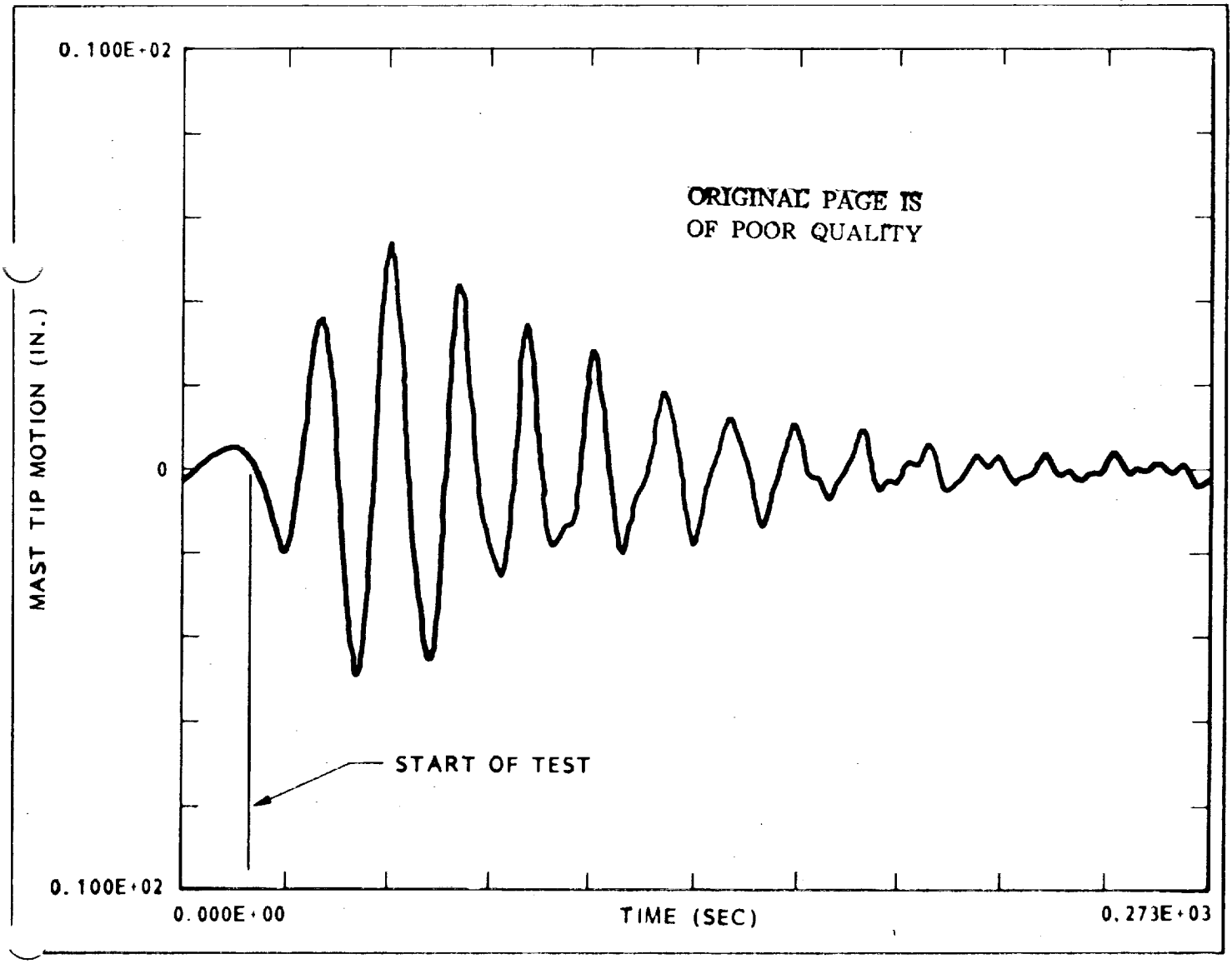

Fig. 2-19 Mast-Tip Motion From Accelerometer Data for First Out-of-Plane Test at 70-Percent Extension—File 5

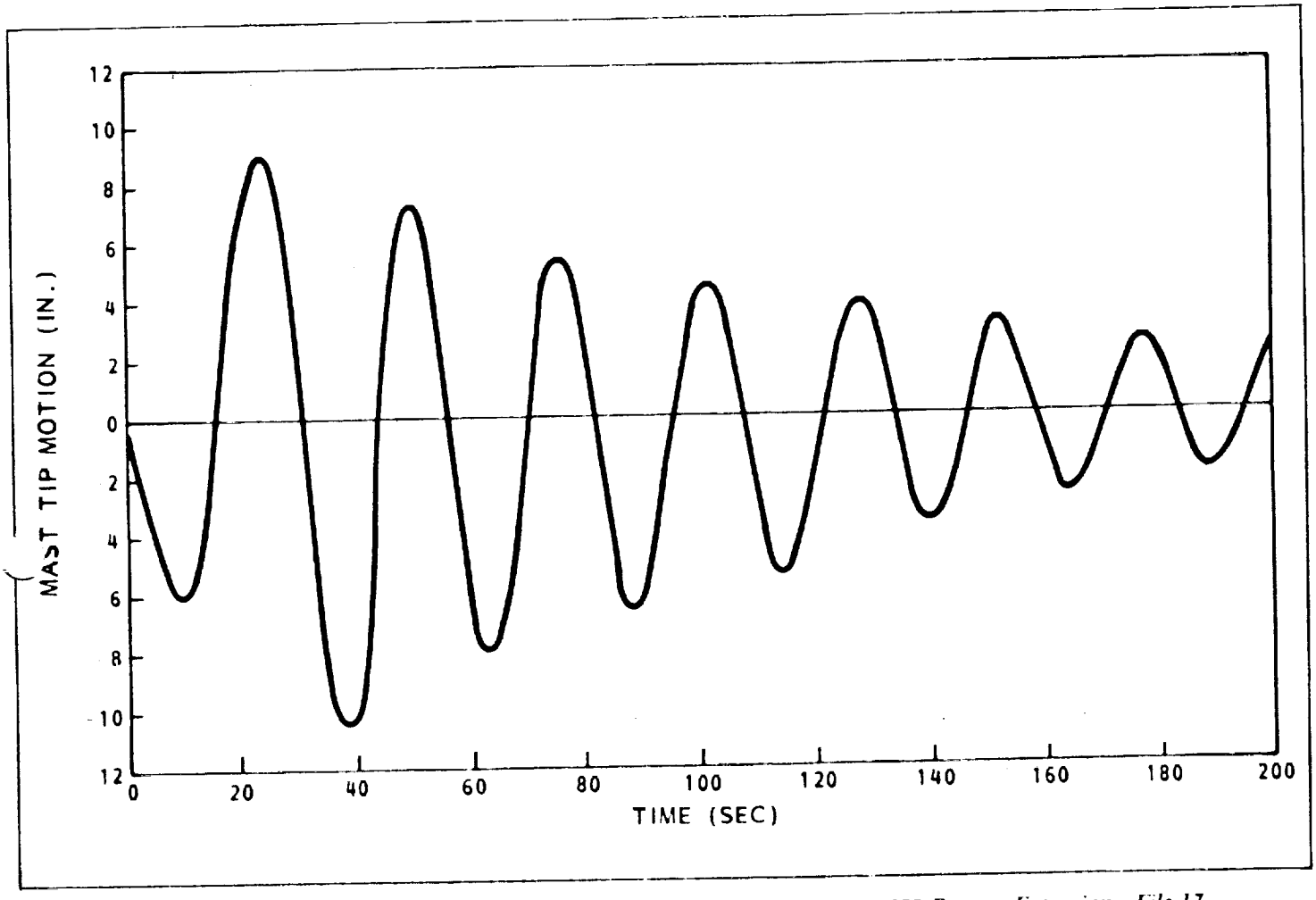

Fig. 2-20 Mast-Tip Motion From Nikon Data for First Out-of-Plane Test at 100-Percent Extension—File 17

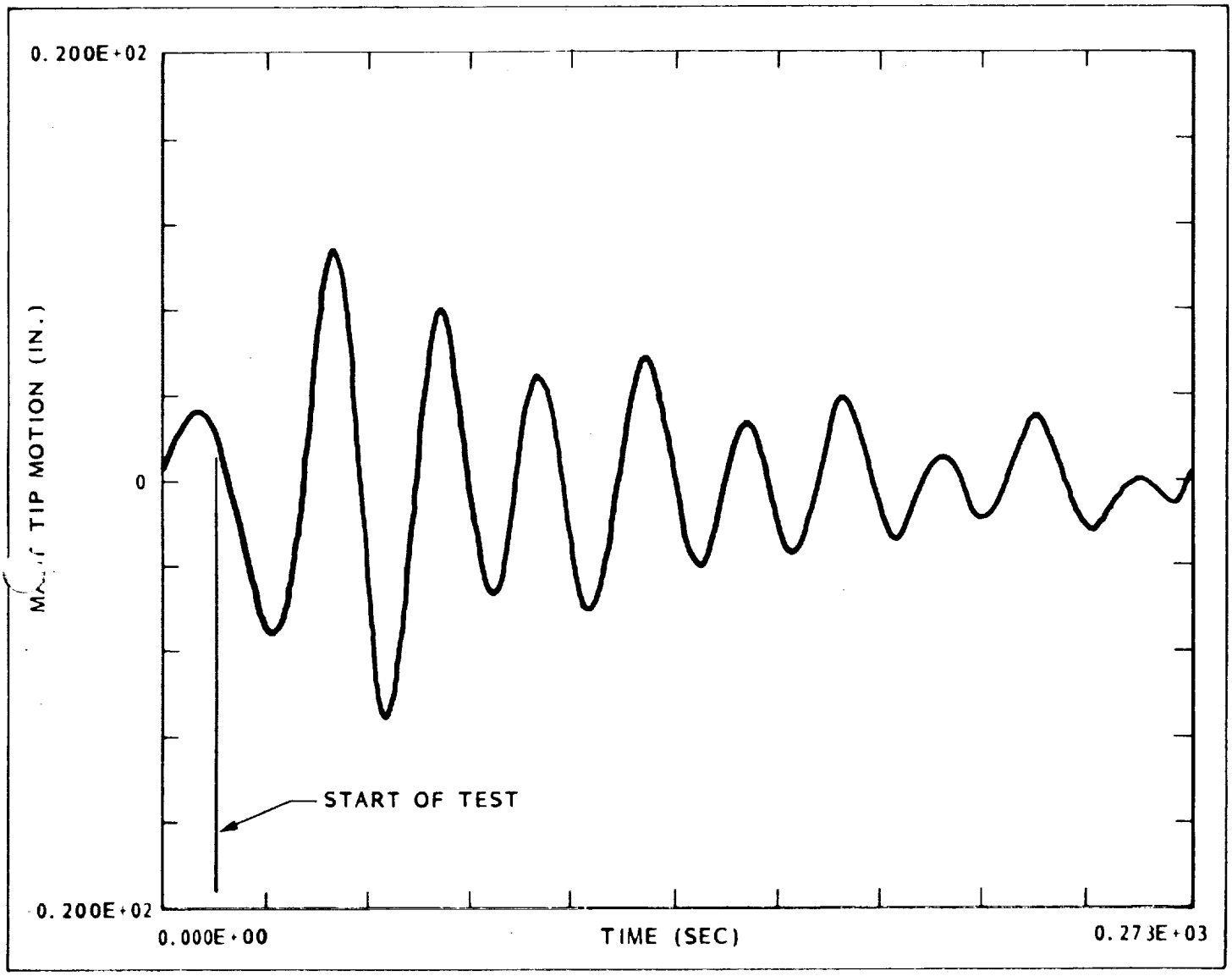

Fig. 2-21 Mast-Tip Motion From Accelerometer Data for First Out-of-Plane Test at 100-Percent Extension—File 17

second and higher structural modes. As will be discussed later, this fact makes evaluation of the structural response, and particularly of the structural damping, very difficult in any but the fundamental modes of the experiment.

Comparison of Measured and Predicted Frequencies. Before flight, the characteristic frequencies of the experiment were predicted for the 70-percent-extended and 100-percent-extended positions. These predictions can be compared with the frequencies that come from the PSDs of the accelerometer signals produced by MSFC and listed in Table 2-6. Since the frequencies coming from the PSDs contain no mode-shape information, the comparison is difficult when the predicted frequencies are closely spaced. Still, it is possible to compare many of the predicted and measured frequencies in this fashion. The comparison does, however, involve some educated guessing.

A supporting comparison based on mode-shape information comes from the evaluation of experiment blanket motion performed by LaRC. Since this evaluation involved the tracking of targets distributed on the blanket, modes with closely spaced frequencies can be distinguished by their shape. A summary of the frequency comparisons is contained in Table 2-7. This table shows an excellent correlation of predicted and measured frequencies. Further evidence of the preflight modeling accuracy is gained from the close match between measured and computed mode shapes for each of these frequencies.

It is worth noting that, in the evaluation performed by LaRC, the array in-plane mode was not evident in the response of the event selected for analysis. This fact is consistent with evidence that the in-plane mode of the experiment is very highly damped. As a result, any participation by this mode should quickly disappear after the VRCS firings are complete. This consideration will be discussed further in a subsequent section.

Modifications to the Dynamic Model. As discussed in the previous paragraphs, the frequencies predicted by the preflight

Table 2-7 COMPARISON OF PREFLIGHT FREQUENCY PREDICTIONS WITH MEASURED FREQUENCIES

70% Extension Mode	Preflight Prediction (Hz)	MSFC Measurements Day (Hz)	MSFC Measurements Night (Hz)	LaRC Measurements Day Only (Hz)
Out-of-Plane Bending	0.0593	0.058	0.061	0.059
In-Plane Bending	0.0662	0.063	0.064	–
Torsion	0.0764	0.075	0.072	0.076
Out-of-Plane Bending	0.119	0.105	0.093	0.114
Torsion	0.145	–	0.130	0.148
Out-of-Plane Bending & Torsion	0.196	0.161	–	0.160
100% Extension Mode	**Preflight Prediction (Hz)**	**MSFC Measurements Day Only (Hz)**		**LaRC Measurements Day Only (Hz)**
Out-of-Plane Bending	0.0344	0.0375		0.037
In-Plane Bending	0.0365	–		–
Torsion	0.0576	0.0577		0.057
Out-of-Plane Bending	0.0966	–		0.098
Torsion	0.112	–		–
Out-of-Plane Bending & Torsion	0.153	0.144		

dynamic model match quite closely the frequencies measured in flight. However, several refinements were implemented to better match the flight frequency measurements.

First, a five-pound mass was added at the edge of the containment box cover to account for the CG offset produced by the mast twist of 7.8 degrees. This modification causes a small amount of torsion to occur whenever thrusters are fired to excite the out-of-plane mode. Second, the mast bending stiffness in the 100-percent-deployed model was changed to more closely match the first out-of-plane bending mode at this position. Variations in blanket tension and mast-base compliance were considered as means for improving the frequency match; however, it is not possible for changes in either of these variables to increase the frequency as necessary. The true cause for the frequency mismatch may not be mast bending stiffness, but this is a convenient variable to adjust to improve the simulation. The predicted frequencies before and after these modifications are shown in Table 2-8.

A second modification was necessary to account for twist in the experiment because the twist causes the sensitive axes of the tip accelerometers to be misaligned with the orbiter axes. Thus, pure X-motion (fore and aft) of the array tip shows up on both the X and Y accelerometer signals. A simple coordinate transformation was performed on the predicted accelerations in order to compare them with the measurements from the accelerometers.

The dynamic model was not modified to account for blanket curvature; however, this exercise was performed by MSFC. The curvature is suspected to have caused the frequency measurement for the out-of-plane mode to be higher in the nighttime than in the daytime. MSFC has shown that the curvature could indeed have shifted the frequency by the amount shown in Table 2-7. Since the model without curvature considerations predicts a frequency that lies between the day and night frequency measurements, it was not modified for the response analyses contained herein.

Response Period Selected for Damping Evaluation. The method for evaluating the structural damping of the experiment was to apply the base motion disturbance to the dynamic model and adjust the damping in each mode until the best match between the predicted and measured response at the mast tip was obtained. A little study of the measured responses, particularly those from the in-plane tests, will

Table 2-8 FREQUENCY PREDICTIONS BEFORE AND AFTER MODEL MODIFICATION

Mode	70% Deployment	
	Preflight Frequency Prediction (Hz)	Frequency After Model Modification (Hz)
1 Out-of-Plane Bending	0.0593	0.0587
2 In-Plane Bending	0.0664	0.0653
3 Torsion	0.0764	0.0759
4 2nd Out-of-Plane Bending	0.1191	0.1178
5 2nd Torsion	0.1454	0.1413
6 Bending and Torsion	0.1961	0.1956

Mode	100% Deployment	
	Preflight Frequency Prediction (Hz)	Frequency After Model Modification (Hz)
1 Out-of-Plane Bending	0.0344	0.0375
2 In-Plane Bending	0.0371	0.0405
3 Torsion	0.0576	0.0596
4 2nd Out of-Plane Bending	0.0966	0.0965
5 2nd Torsion	0.1119	0.114
6 Bending and Torsion	0.1528	0.152

show that no single value of damping will characterize all iods of the response.

The experiment response during the period of the forcing function and shortly thereafter was chosen for evaluating the structural damping. There are three reasons for this decision. First, MSFC and LaRC are evaluating the portion of the response downstream from the forcing function. The approach selected by LMSC thereby provides damping information in a different time period. Secondly, the structural damping during the period of the forcing function is important from the standpoint of design loads. This is the period of maximum structural displacements and loads, and the damping values may be significantly larger than later in the response during low-level displacements. Finally, a comparison of responses during the later portion of the data gathering period would not be appropriate for a numerical integration exercise. The most appropriate period for comparison is early in the response when the contribution of the fundamental modes dominate the response and errors due to small frequency inaccuracies have not had a chance to accumulate.

Structural Damping Evaluation. The method selected for evaluation of the structural damping was to adjust the damping values in each of the modes used in the dynamic response analysis to obtain the best match with the measured acceleration-time histories of the array tip. This approach is ssible since only several of the structural modes actively participate in the responses.

The first events chosen for evaluation were the out-of-plane tests at 70-percent extension. Considerable time was spent on the first case in order to become familiar with the sensitivity of the response to the input damping values. It was obvious that the response was dominated by the first mode and that a relatively high damping value (five percent of critical) was needed to match the test data. In order to match a small contribution from the second out-of-plane mode, reducing the input damping value to 0.25 percent of critical for this mode was necessary. Since the displacements for the second mode are much smaller than for the first mode, it is not surprising that the damping value is also smaller. At such low values of displacement, however, the non-zero displacement and velocity at the start of the test are of the same magnitude as the response in the second mode. This fact "muddies the water" and makes accurate prediction of the damping in the second mode impossible without accurate knowledge of the initial conditions. Attempts were made to estimate the initial conditions; however, the combination of variable damping values and variable initial conditions greatly complicates the task of matching the test data. For this reason, initial conditions were not treated in subsequent cases.

A typical set of acceleration time histories, obtained by integrating the flight data from an out-of-plane test and by adjusting input values to the dynamic model, is shown in Fig. 2-22. As the figure shows, the comparison is quite close at the start of the test when the VRCS thrusters are active and during the period peak displacements. Later in the response period, the damping appears to be of reduced value.

Next, the in-plane tests at the 70-percent-extended position were evaluated. For these cases, the damping in the first in-plane mode averaged nearly ten percent of critical during VRCS thruster activity. Because of this high damping value, the response decayed quickly in the free response period. This result can be seen by comparing the measured and predicted acceleration time histories for an in-plane test shown in Fig. 2-23. Again, the damping value for the second in-plane mode that produces the best match is much lower and cannot be accurately determined due to the small response in this mode and the non-zero initial values of displacement and velocity.

Following evaluation of the in-plane and out-of-plane tests at the 70-percent-extended position, the only out-of-plane test at the 100-percent position was evaluated. Finally, the multi-modal tests at 70 percent and 100 percent were evaluated. In general, the damping values were lower for the 100-percent position, but the damping for the in-plane mode was still nearly double that of the out-of-plane mode. The confidence in the damping values for the 100-percent tests is not as high as for the 70-percent tests because only two tests were performed at the fully extended position.

The modal damping values that produce the best match between the analytical model and the test data are presented in Table 2-9. The response acceleration and displacement time histories that result from these values are contained in Appendixes F and G. A summary of the best-fit damping values is contained in Table 2-10. Only values for the fundamental in-plane and out-of-plane modes are listed here since the participation of the higher modes is so small. Small excitation of the fundamental torsion mode is most likely due to the VRCS thrusters selected for firing and the high yaw-axis inertia of the orbiter. The damping values are generally higher for the night tests than for the day tests, lower for the 100-percent position than for the 70-percent position, and higher for the in-plane mode than for the out-of-plane mode. The increased damping for the night tests is apparently a temperature phenomenon and is a fairly significant effect. The increased damping for the in-plane mode as opposed to the out-of-plane mode is even more dramatic, and, therefore, a small test program to explain this effect was implemented.

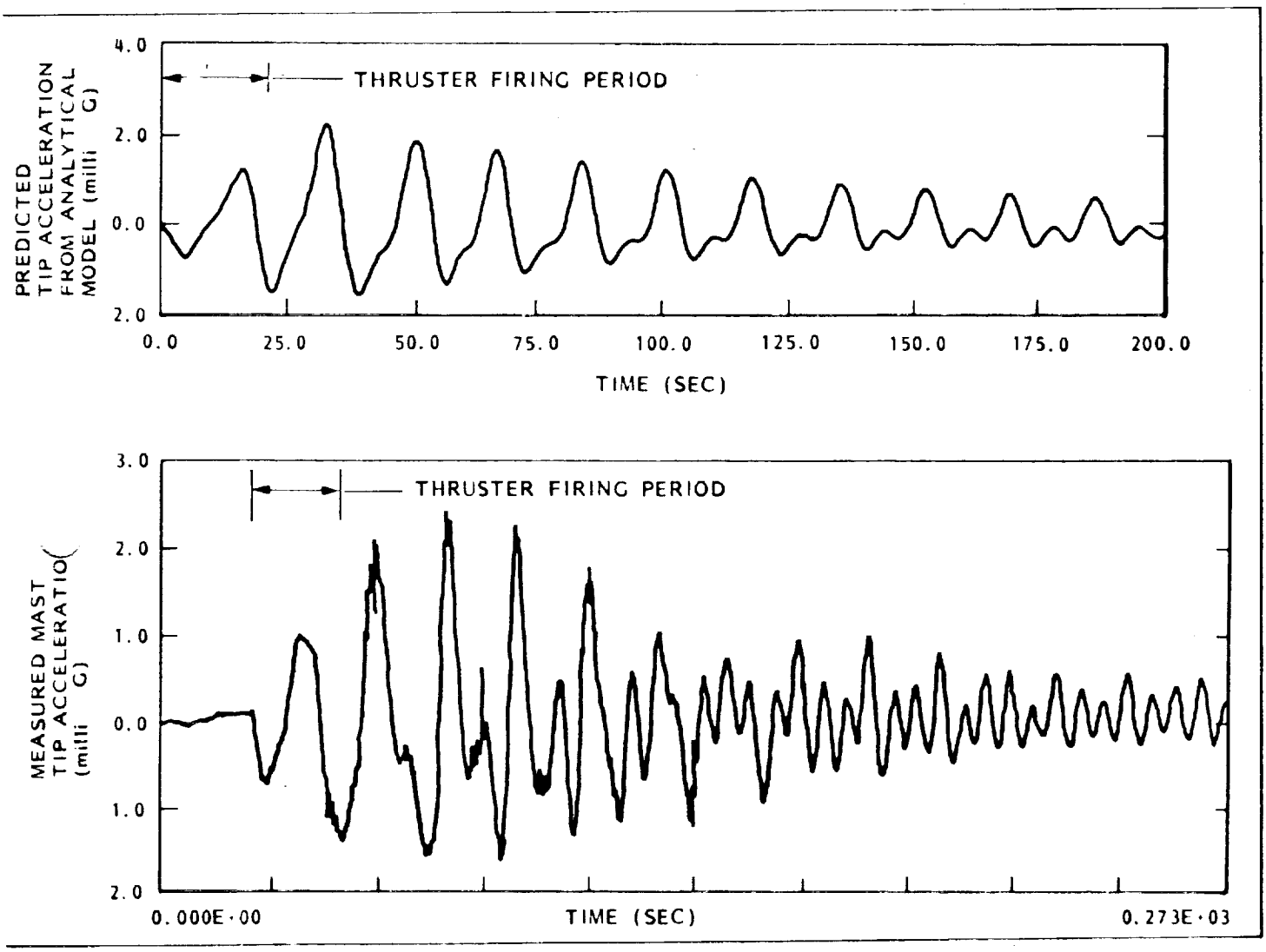

Fig. 2-22 Comparison of Out-of-Plane Mast-Tip Acceleration From Test Data and Analytical Model

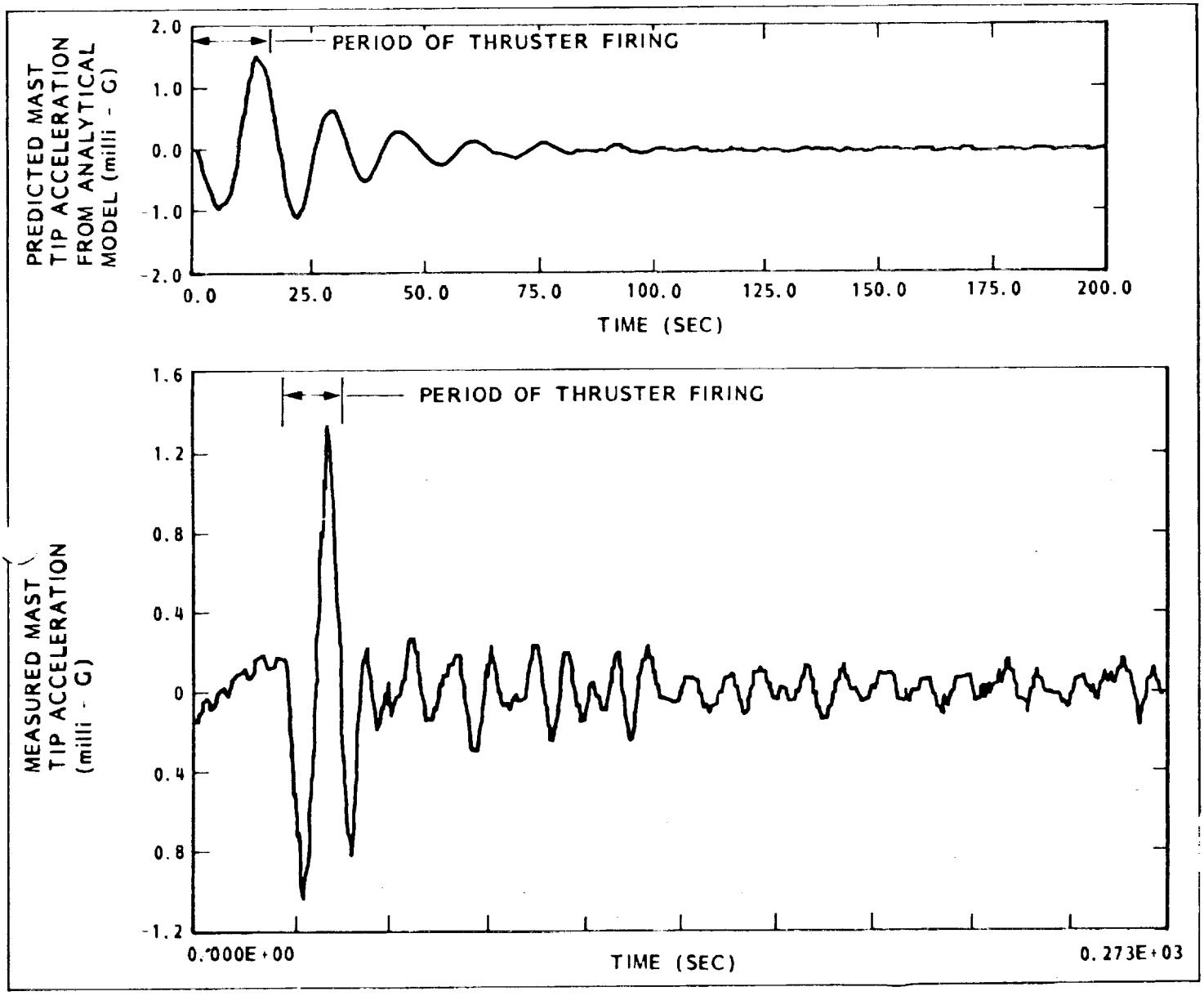

Fig. 2-23 Comparison of In-Plane Mast-Tip Acceleration From Test Data and Analytical Model

Table 2-9 DAMPING VALUES FOR BEST MATCH BETWEEN MODEL AND TEST DATA

Event	Damping for Out-of-Plane Mode (% Critical)	Damping for In-Plane Mode (% Critical)
5	3	–
6	6	–
10	7	8
11	3	11
12	4.5	–
13	–	11
14	4.5	11
15	4.5	11
17	2	–
20	2	4
26	6	11
27	3	9
28	6	15
29	–	11

Table 2-10 SUMMARY OF BEST-MATCH DAMPING VALUES

Mode	% of Critical		
	70% Day	70% Night	100% Day
Out-of-Plane Bending	4.4	5.1	2
In-Plane Bending	9.8	11.8	4

Guide Wire Negator Tests. One fundamental difference between the in-plane and the out-of-plane bending mode is that the two out-board tension wires must reel in and out a considerably larger amount for the in-plane mode. This difference is shown in Fig. 2-24, which compares the predicted tension-wire motion for a typical in-plane and out-of-plane test. Although the motion for the in-plane case is only about 0.2 inches, the peak kinetic energy of the experiment during this event is only about 0.4 in.-lb. Simple approximations show that if the tension-wire reel-out force were greater than the reel-in force by as little as 1.0 pound, then the entire experiment kinetic energy would be dissipated in one-half cycle of motion in the free response period. Because a difference between reel-out and reel-in force is likely in a mechanism such as the negator assemblies that tension the wires, a small test was performed to measure the negator force characteristics.

Since the negator mechanisms for the tension wires are not readily accessible, the test was performed on a negator mechanism for one of the guide wires. To perform this test, a small cover was removed from the experiment containment box to access one of the outboard guide wires. This guide wire is normally routed under a pulley and up through the floor of the containment box, through the grommets on every other panel hinge line, and finally attached to the containment box cover. The wire was cut and rerouted so that it passed over the pully, out through the access hole, and down to a small load cell and motor-driven actuator. An overall view of the test setup is shown in Fig. 2-25. The actuation motor and series load cell are shown in Fig. 2-26. The motor speed and stroke of the crank were selected to approximate the frequency and stroke of the wire during a dynamics test. The difference in the reel-in and reel-out force was measured with the guide wire at the 0-percent-, 35-percent-, 70-percent-, and 100-percent-extended positions at room ambient conditions. The test results are shown in Table 2-11. These results clearly show that the force difference between the reel-out and reel-in motion of the guide wire (and thus of the tension wire) is significant. This difference is probably the cause of the high structural damping for the in-plane mode of the experiment.

2.4.5 Experiment Thermal Evaluation

An integrated thermal model of the SAFE electrical equipment was developed by Teledyne Brown Engineering (TBE). The TBE model of the equipment includes only external surfaces that are linked by external radiation heat transfer. No conductive heat transfer, no internal power dissipation, and no radiation heat transfer within the equipment are included. The design cases were derived by assuming the orbiter to be in one of its several attitudes for many orbits rather than addressing planned attitude changes as shown on the flight time line. From this integrated thermal analysis resulted a set of environments for the SAFE components that were supplied to LMSC for each design case. The environments for each component consist of the incoming heat flux, the boundary temperature, and the boundary radiation conductance for each surface of the SAFE equipment. LMSC used the external environments combined with component internal modeling to determine more realistic equipment temperatures. The component internal models include a conduction network, internal power dissipation, and internal radiation heat transfer.

The orbiter attitudes of interest are shown in Fig. 2-27. To describe these attitudes, the nomenclature is consistent with the axis system shown in Fig. 1-1. The subscript "LV" refers to "Local Vertical," and the subscript "SI" refers to "Solar Inertial." The $+X_{LV,\ 30^\circ\ roll}$ attitude is a stable gravity gradient attitude in which most array extensions and retractions and all dynamics tests occurred. The $+X_{SI}$ attitude was used for the two solar cell performance tests. The $+Z_{SI}$ attitude was used for tests on the Solar Cell Calibration Facility, another experiment on the OAST-1 (Office of Aeronautics and Space Technology) payload. This attitude produces a relatively hot environment for equipment in the cargo bay. The final attitude shown in this figure is the $+Z_{LV}$, or Earth-oriented, attitude. This is a relatively benign thermal attitude. The $+Z_{LV}$ attitude is essentially the "home base" attitude for the orbiter with excursions to the $+X_{LV,\ 30^\circ\ roll}$ attitude for dynamics tests, the $+X_{SI}$ attitude for solar cell performance tests, and the $+Z_{SI}$ attitude for Solar Cell Calibration Facility tests. Because the orbiter spends most of its time in a benign thermal attitude with excursions to the hot and cold attitudes, the analysis that assumes the orbiter to be in a single attitude for many orbits is a conservative approach. Only in case of a flight anomaly leading to a hold in a specific attitude would the temperatures predicted from the thermal design cases be realized. Since the orbiter was not forced to hold in any of the hot or cold attitudes shown in Fig. 2-27, the SAFE component temperatures during the flight were all well within the design extremes.

A noteworthy example of an unplanned attitude hold did occur on the third day of the flight when the orbiter was oriented with the port wing facing the sun ($-Y_{SI}$) for ten hours in an attempt to melt an ice formation. Although experiment equipment heaters did cycle on during this period, all equipment temperatures remained within the design limits.

Temperatures during the flight were monitored by ten thermistors. Five of these thermistors were dedicated to measuring the operating temperatures of the active solar cells, and the remaining five were distributed on the experiment electrical equipment and containment box cover. Table 2-12 shows the locations of these ten thermistors. Table 2-13 summarizes component temperatures for the containment box cover and experiment electrical equipment. Figures 2-28 through 2-30 plot the temperatures over time. The figures show that the electrical equipment, which is all located on structure that remains within the cargo bay, remained mostly within the range of 0°F to +40°F throughout the flight. The heaters for the motors

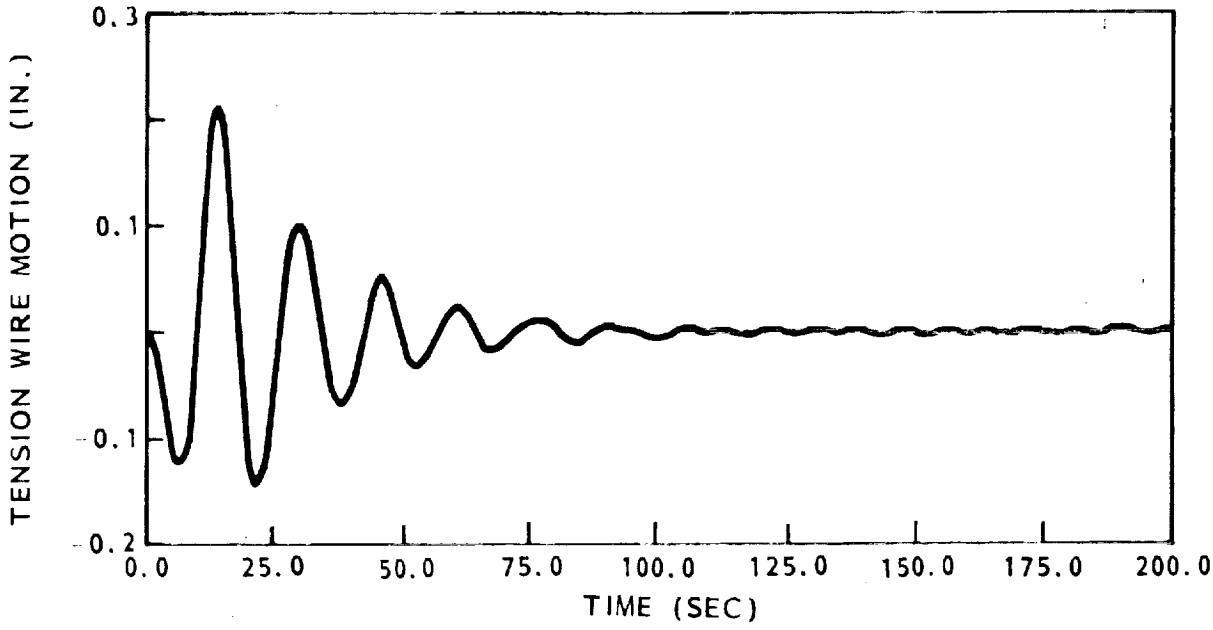

A. IN-PLANE CASE

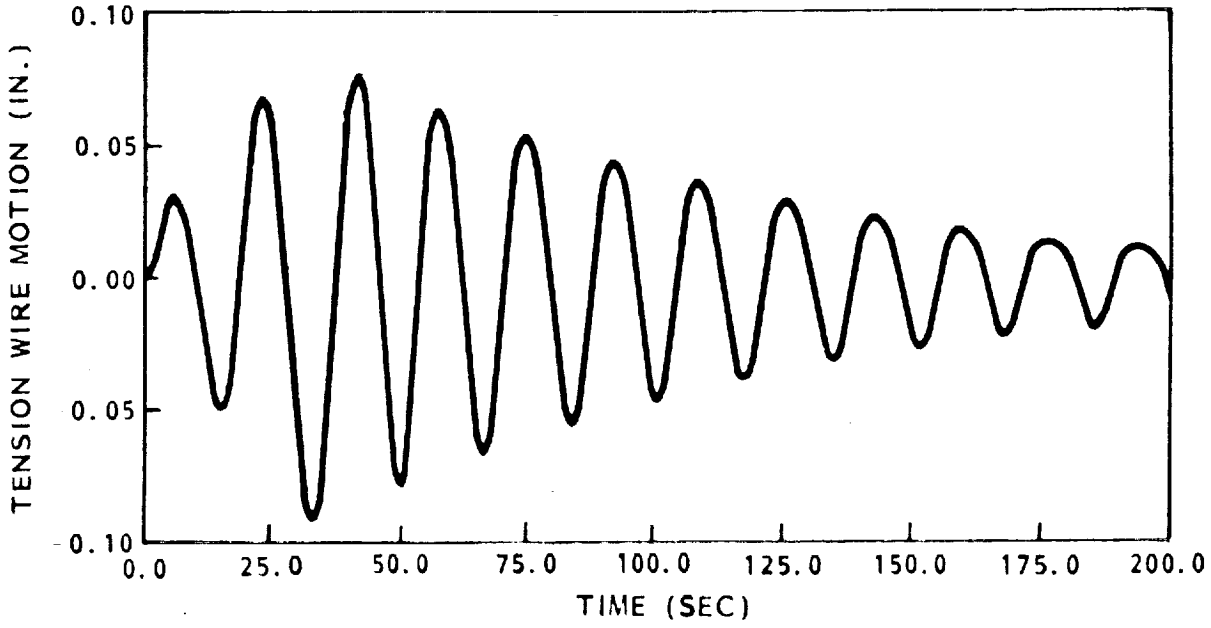

B. OUT OF PLANE CASE

Fig. 2-24 Comparison of Tension Wire Motion for an In-Plane and Out-of-Plane Test

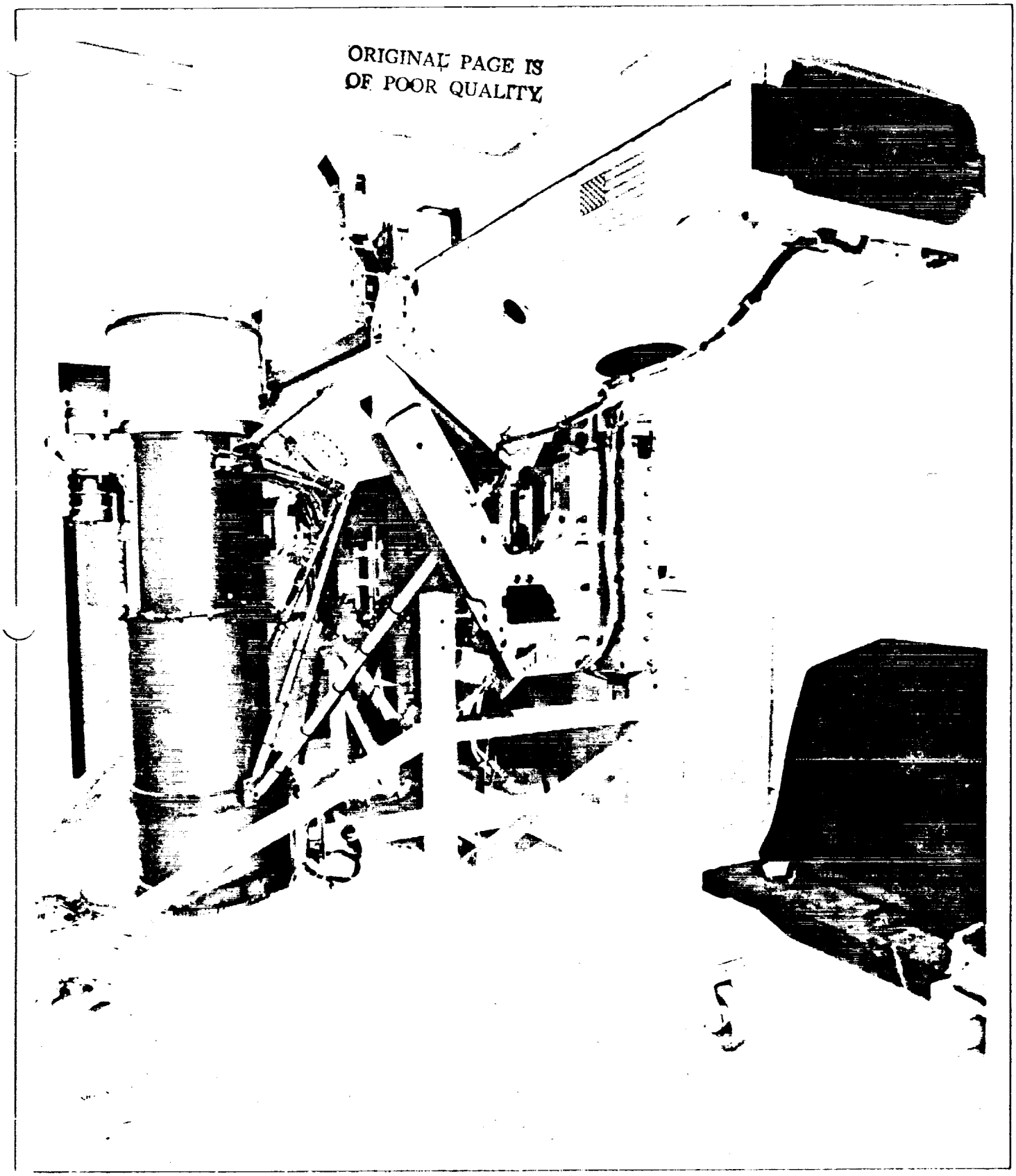

Fig. 2-25 Test Setup for Negator Hysteresis Tests

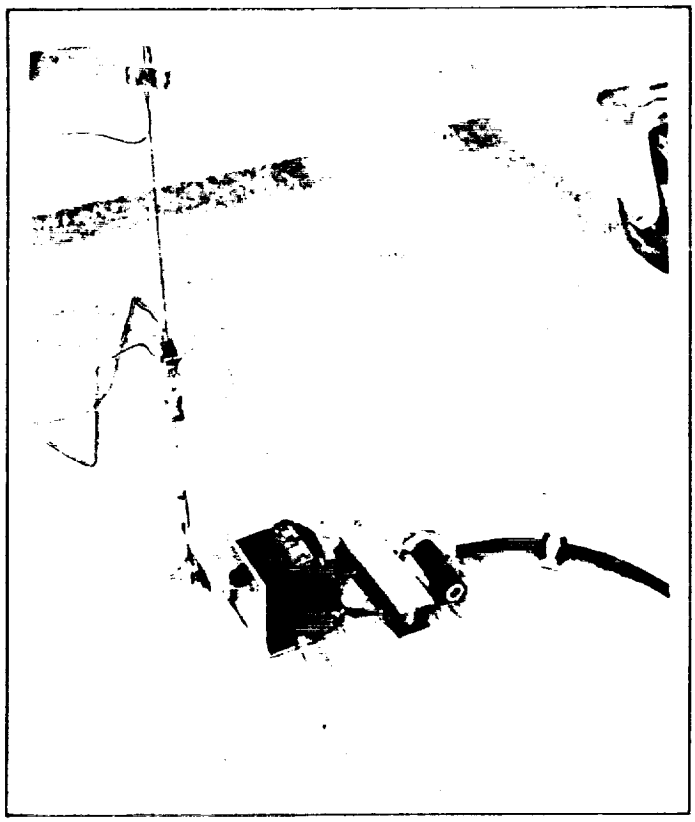

Fig. 2-26 Load Cell and Motor Actuator for Negator Hysteresis Tests

Table 2-11 RESULTS OF NEGATOR HYSTERESIS TESTS

Tension Cable Position (% Extension)	Force During Reel-Out of Tension Wire (lb)	Force During Reel-In of Tension Wiere (lb)	Force Difference (lb)
0%	1.50	0.88	0.62
35%	1.54	0.92	0.62
70%	1.62	0.96	0.66
100%	1.74	1.06	0.68

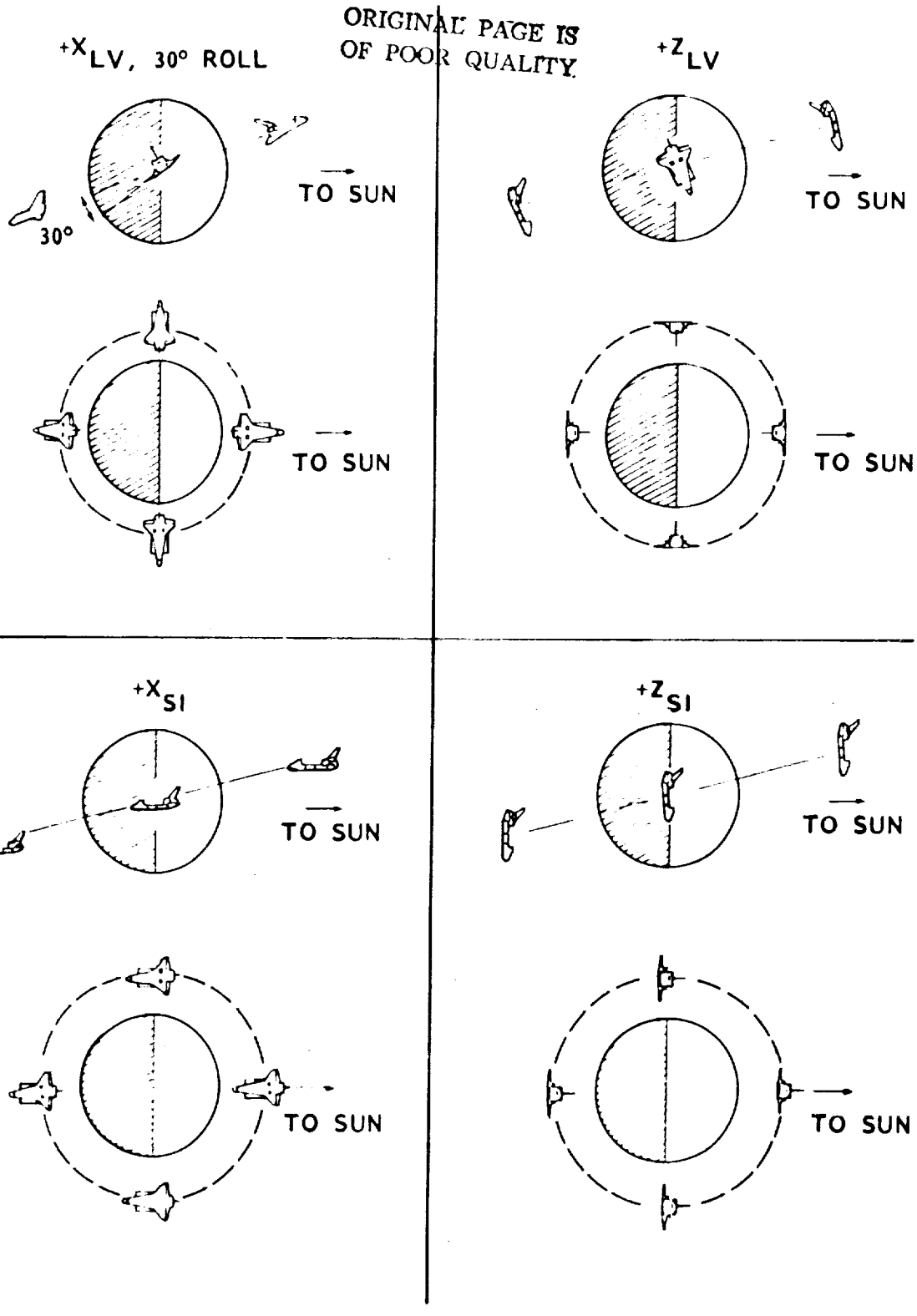

Fig. 2-27 Orbiter Attitudes During SAFE Operation

Table 2-12 THERMISTOR LOCATIONS

Thermistor Number	Drawing & Sheet Number	Location
1	1244386 No. 2, 3, 7	Back side of 2 x 4 (cm) cells
2	1244386 No. 2, 3, 7	Back side of Kapton on 2 x 4 (cm) cells
3	1244396 No. 1, 2	Back side of Kapton on thin cell module
4	1244386 No. 2, 3, 7	Back side of 5.9 x 5.9 (cm) cells
5	1244386 No. 2, 3, 7	Back side of Kapton on 5.9 x 5.9 (cm) cells
6	1239941 No. 6	On container cover at center on accelerometer mount
7	SEP 154	Motor No. 1 - on motor housing under heater clamp (bottom motor)
8	SEP 154	Motor No. 2 - on motor housing under heater clamp (top motor)
9	SEP 153	Tape Recorder Heater Support
10	1243174 No. 1, 1243156 No. 1	DAS Box - inside

Table 2-13 SUMMARY OF FLIGHT TEMPERATURE DATA

LOW AND HIGH TEMPERATURE (°F)

File No.	No. 6 Wing Cover		No. 7 Motor No. 1		No. 8 Motor No. 2		No. 9 Tape Recorder		No. 10 DAS Box	
1	32	32	25	25	25	25	26	26	42	42
2	1	4	17	17	16	24	18	22	39	39
3	6	18	16	34	20	28	18	30	38	38
4	4	4	27	27	26	34	21	21	40	40
5	5	10	26	26	29	29	20	20	38	38
6	15	5	29	29	26	32	23	23	40	40
7	27	18	26	36	28	28	19	19	38	38
8	3	8	24	24	24	30	26	26	44	44
9	38	27	10	18	10	20	16	20	36	40
10	42	24	5	7	2	2	8	8	28	28
11	15	6	11	14	9	12	13	13	30	30
12	15	9	10	16	3	3	7	10	28	28
13	12	4	18	18	15	18	16	18	32	32
14	16	8	4	6	3	3	8	8	30	30
15	15	10	15	15	3	16	15	15	32	34
16	25	20	8	8	8	13	11	11	32	32
17	13	6	8	11	11	13	11	16	32	32
18	6	13	18	25	20	25	23	23	32	32
19	28	28	16	16	15	18	13	13	35	35
20	18	13	13	13	15	15	11	13	34	34
21	4	16	20	27	23	25	20	20	34	34
22	27	41	32	44	30	34	23	23	38	38
23	16	23	34	34	34	39	26	26	44	44
24	4	13	32	32	32	37	22	25	43	43
25	1	9	27	27	25	27	23	23	43	43
26	22	25	18	20	18	18	18	18	41	41
27	13	6	10	10	11	11	13	15	36	36
28	16	11	20	22	20	22	18	20	41	41
29	18	10	18	18	15	18	13	17	39	39
30	1	20	20	37	18	30	20	27	39	39
31	60	60	54	54	54	54	44	44	53	53

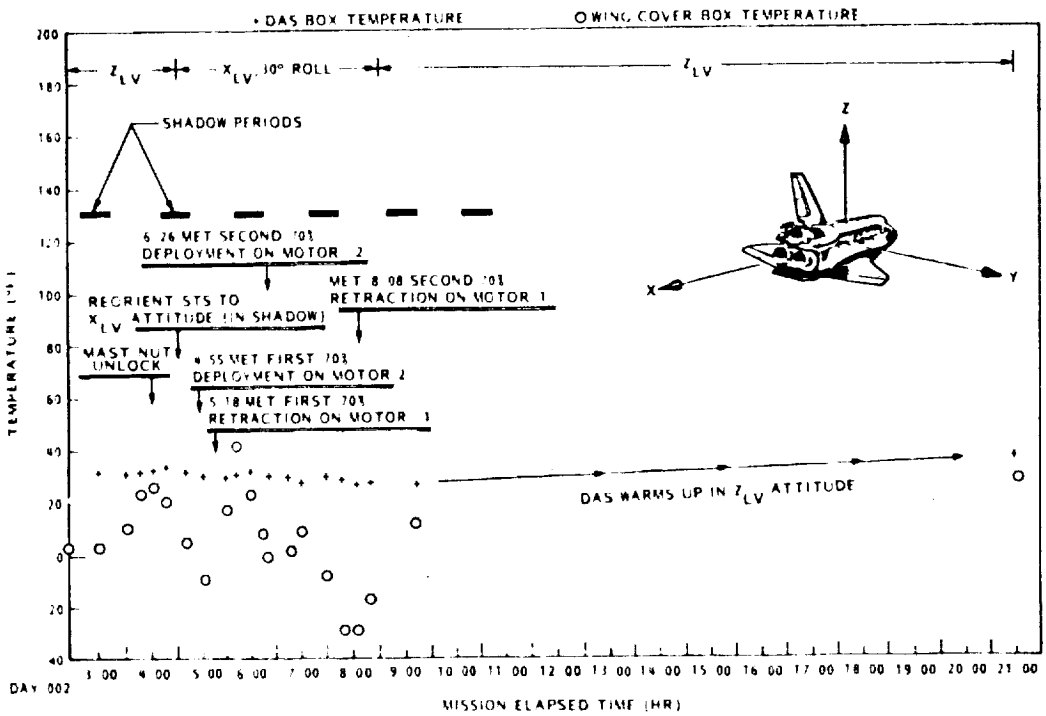

Fig. 2-28a DAS Box and Containment Box Cover Temperature Versus Time

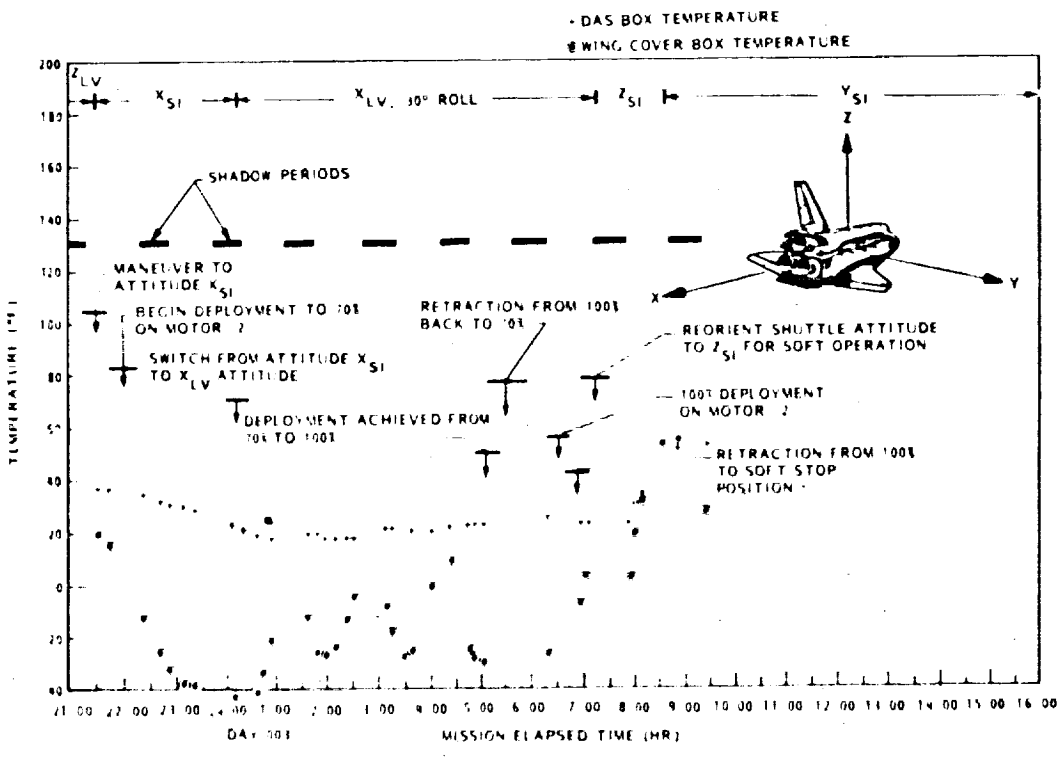

Fig. 2-28b DAS Box and Containment Box Cover Temperature Versus Time

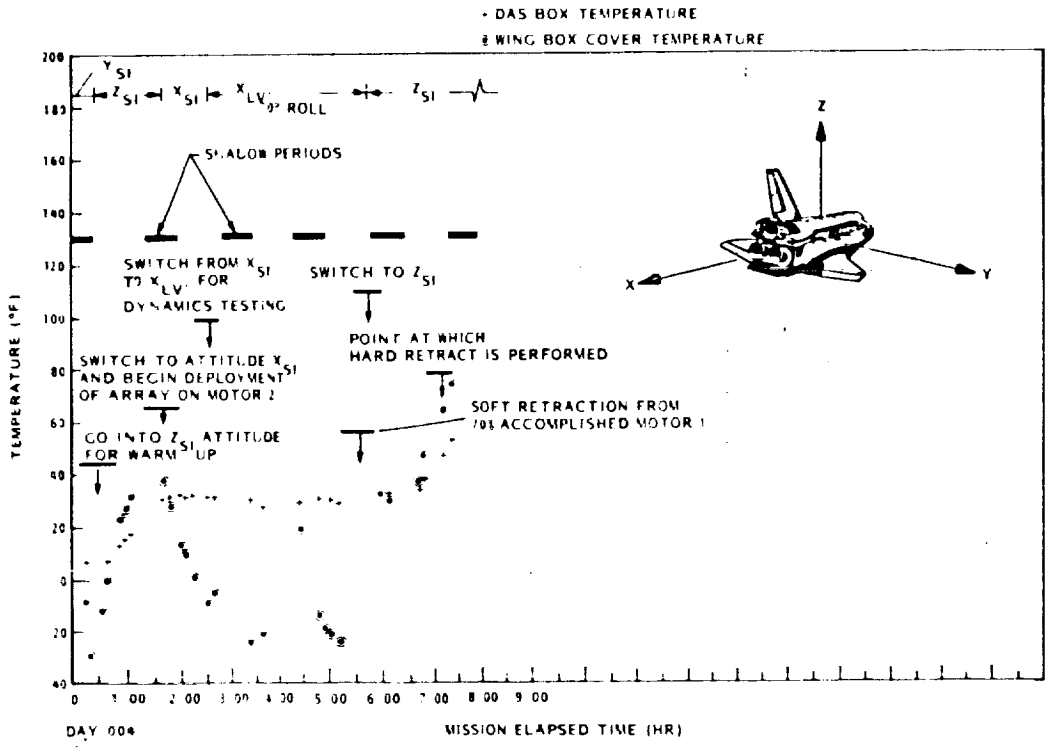

Fig. 2-28c DAS Box and Containment Box Cover Temperature Versus Time

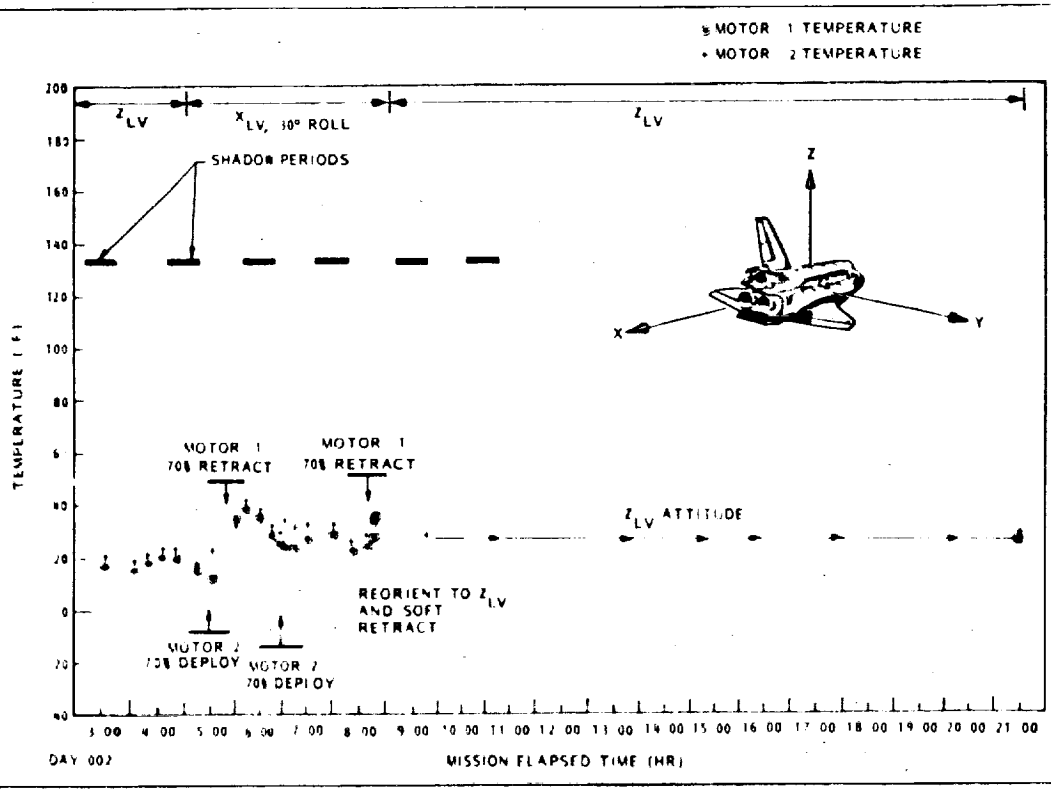

Fig. 2-29a Mast Motor Temperatures Versus Time

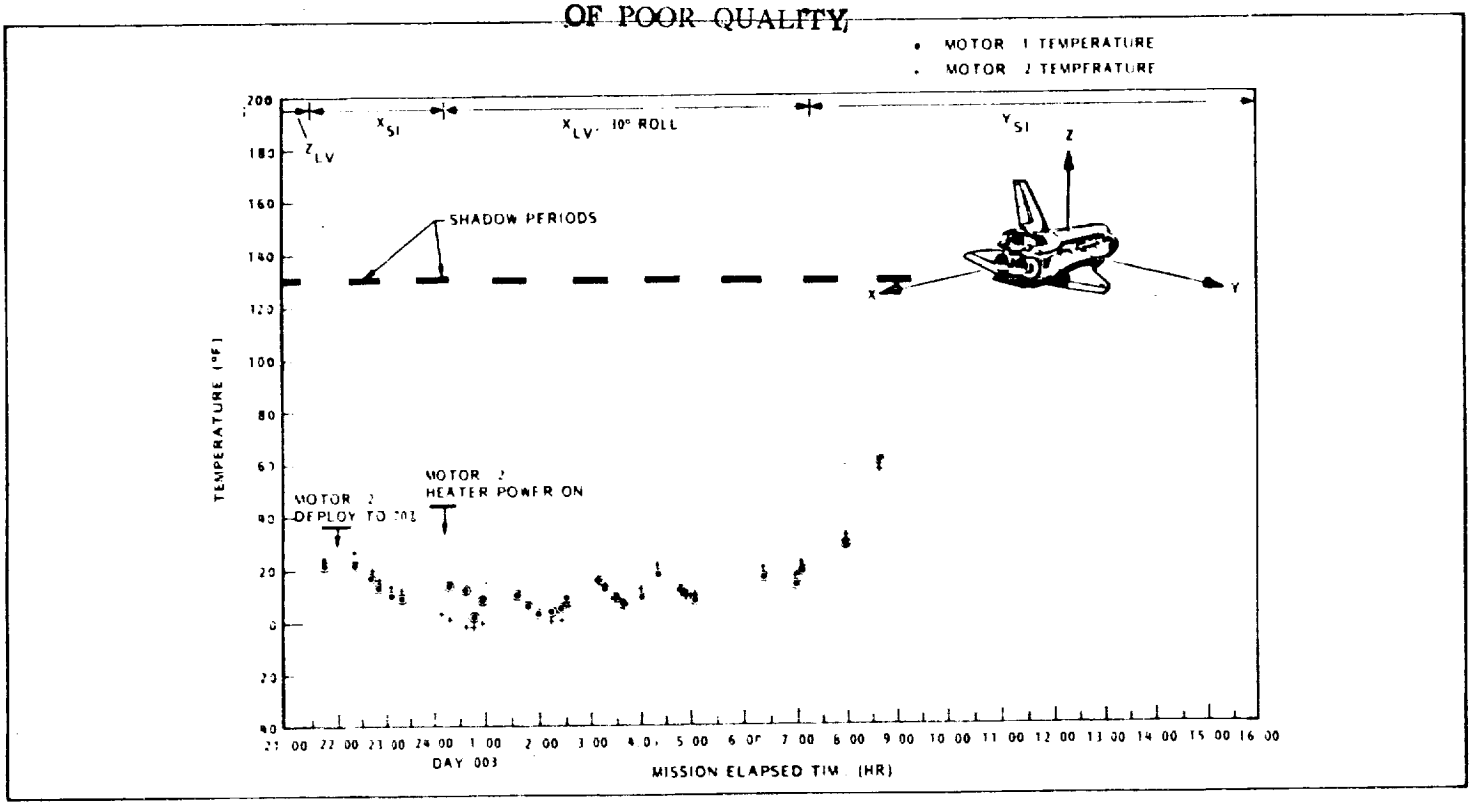

Fig. 2-29b Mast Motor Temperatures Versus Time

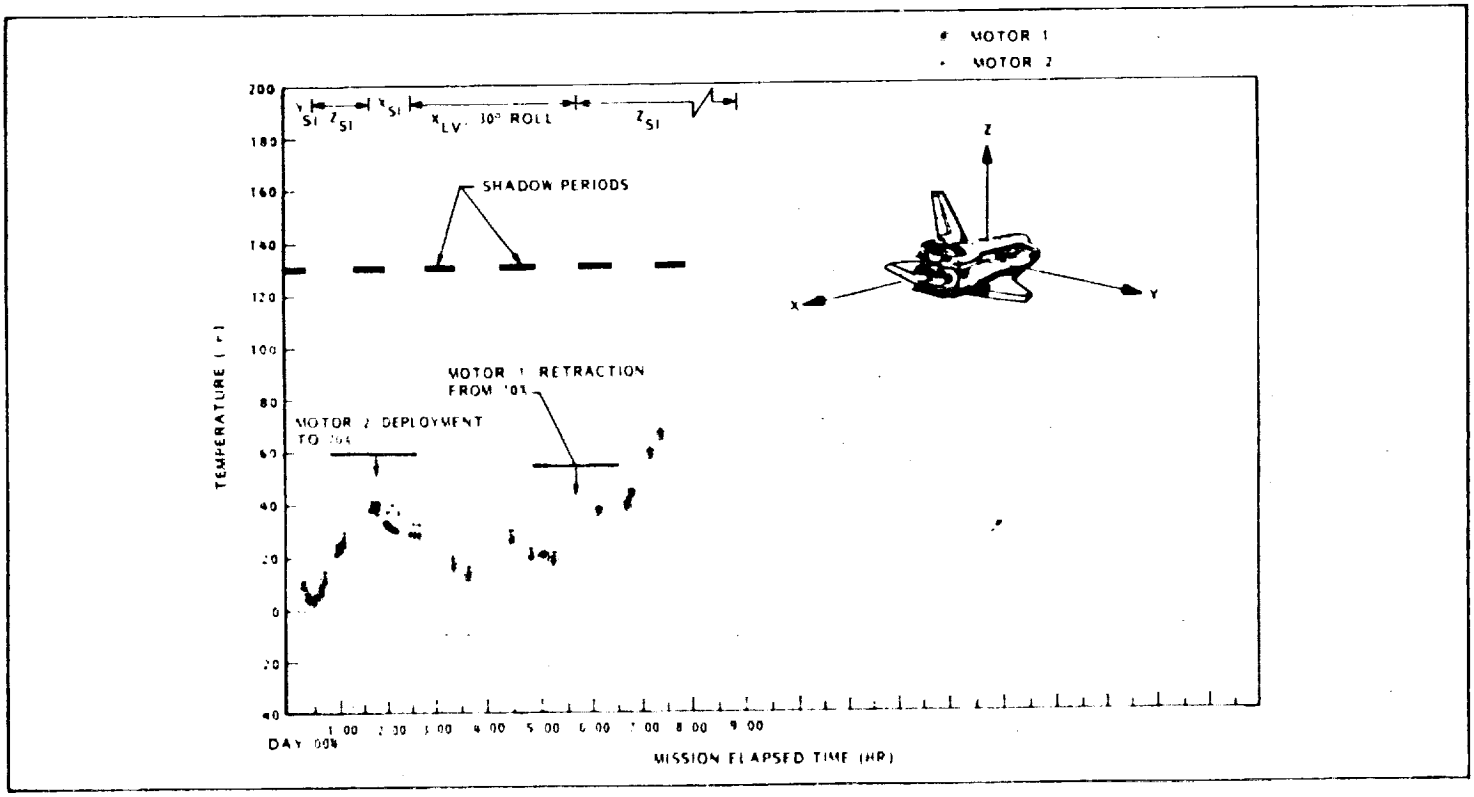

Fig. 2-29c Mast Motor Temperatures Versus Time

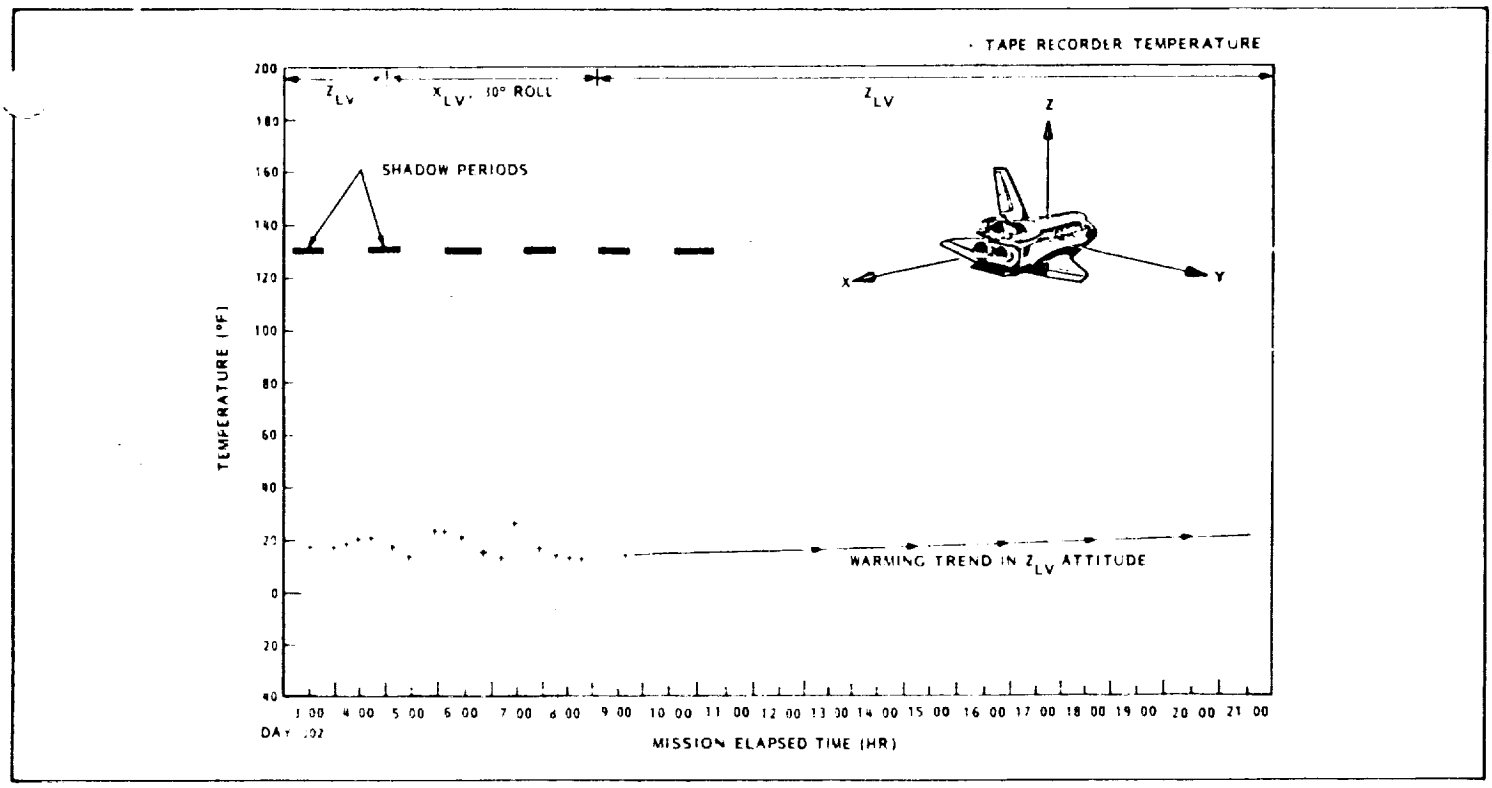

Fig. 2-30a Tape Recorder Temperature Versus Time

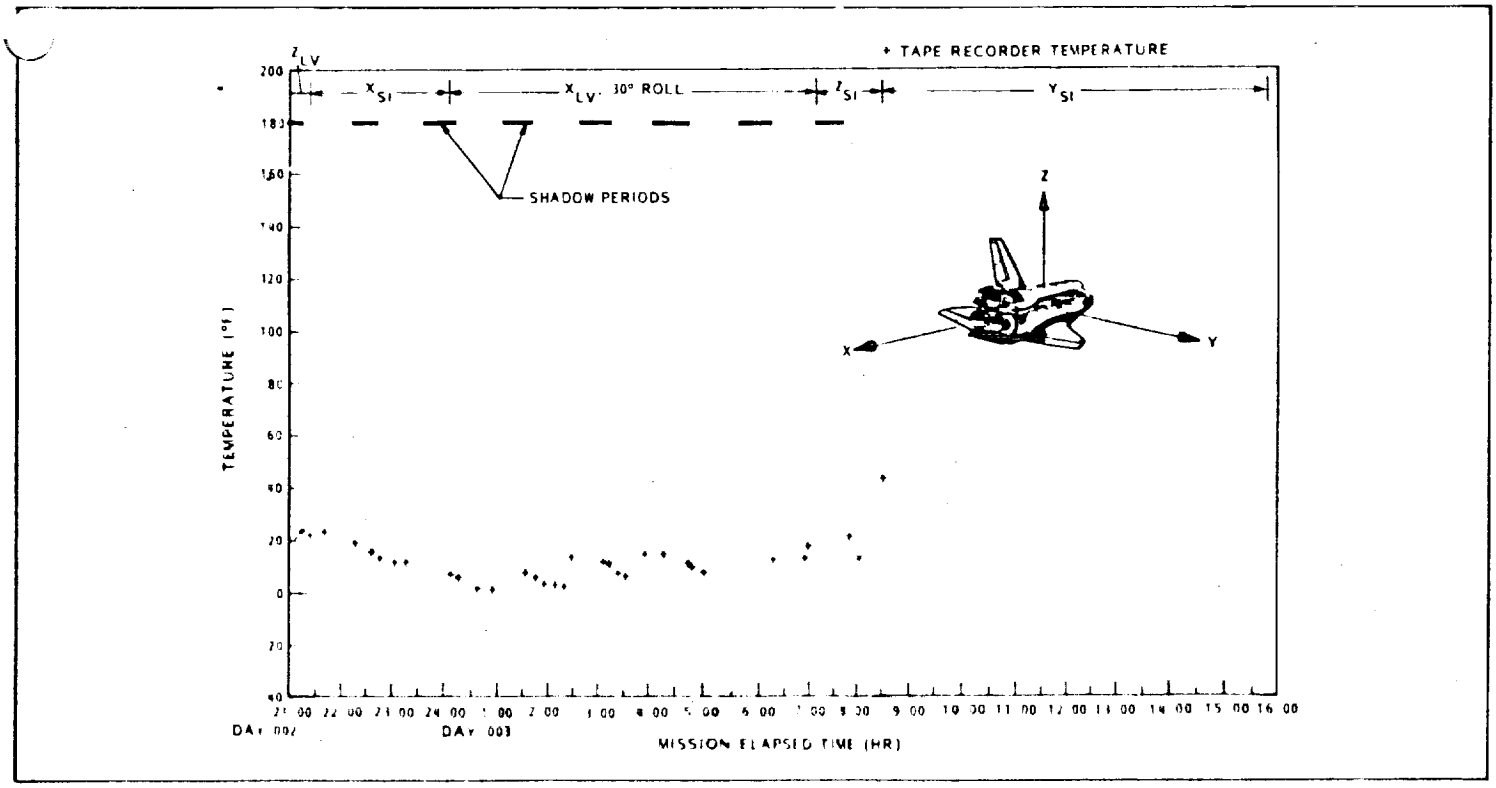

Fig. 2-30b Tape Recorder Temperature Versus Time

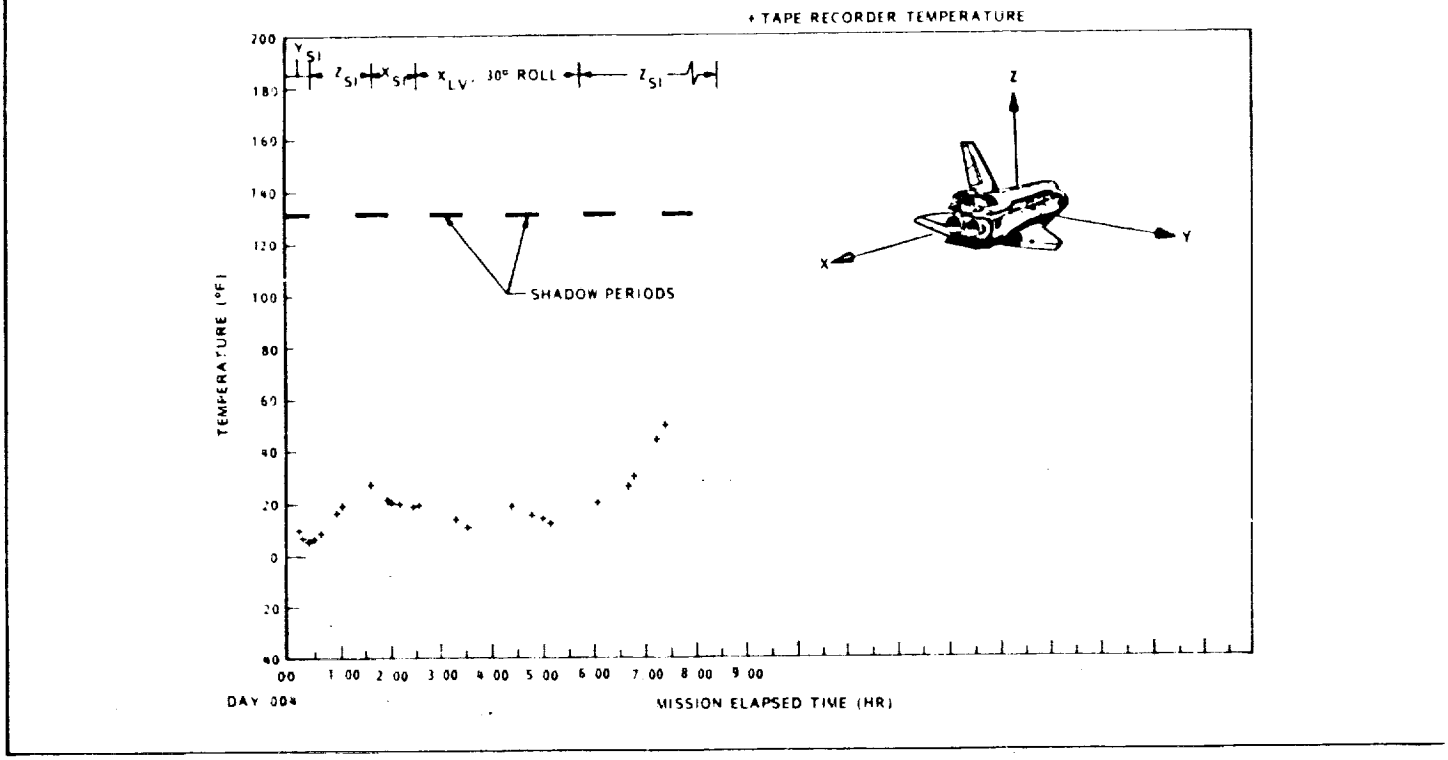

Fig. 2-30c Tape Recorder Temperature Versus Time

and tape recorder did activate on several occasions, but the heaters for the DAS box were never required. The containment box cover temperature readings were generally colder than the electrical equipment temperatures. These differences occurred because the thermistor for this measurement was mounted on one of the cover accelerometers that was often shaded by the sides of the containment box cover and by the locking-lever hardware during the daylight portion of the $+X_{LV,\ 30^\circ\ roll}$ attitude. The accelerometer has little thermal mass compared to the electrical equipment; it cooled off during the nighttime portion of the orbit and never really warmed up during the daylight. Because this reading is not indicative of the box cover temperature, the thermistor probably could have been mounted at a more useful location.

The LMSC thermal evaluation of the SAFE electrical components (DAS box, motors, and tape recorder) was published as Reference 1 in March 1984 in anticipation of a June launch date. Last-second problems with the June launch caused the launch date to slip to August 30. The resulting change in orbital beta angle caused the primary operational attitude ($+X_{LV,\ 30^\circ\ roll}$) to change from the hottest expected operational attitude to a cold operational attitude. Only the pre-launch thermal analysis relative to the solar inertial attitude remained valid. New environments were generated by TBI but were not received until August 27. With limited tim remaining before SAFE on-orbit operation, several compo nent analyses were selected for evaluation with the ne environments. These cases are presented in Table 2-14.

The DAS box temperature predictions for case 1 and case are shown in Figs. 2-31 and 2-32, respectively. Case 1 can b compared with the DAS box temperatures measured durin hours 4.5 through 8.6 of Flight Day 2 as shown in Fig. 2-28a The predicted and measured temperatures center around 30° and show a gradual decay with time. Case 2 temperature pre dictions can be compared with the measurements taken o Flight Day 3, hours 7.9 through 8.7, as shown in Fig. 2-28b Both the measurements and predictions show a sharp rise i temperature in going to the hot $+Z_{SI}$ attitude. Since th orbiter only stayed in this attitude for a short time, the mea sured temperatures did not reach those predicted for a extended stay in the attitude.

The motor-assembly temperature predictions for cases 3 an 4 are shown in Figs. 2-33 and 2-34, respectively. It is difficult t compare these predicted temperatures with the measure

Table 2-14 COMPONENT ANALYSIS AND ENVIRONMENTS

Case	Component	Environment
1	DAS Box	3 orbits of transient analysis starting from orbit average conditions with power on in attitude $+X_{LV}$, 30° roll
2	DAS Box	Transient analysis starting from attitude $+X_{LV}$, 30° roll and maneuvering to $+Z_{SI}$ attitude with power on
3	Mast Motor Assemblies	3 orbits of transient analysis starting from 0°F in attitude $+X_{LV}$, 30° roll with simulated solar array extension
4	Mast Motor Assemblies	Transient analysis starting from 0°F in attitude $+X_{LV}$, 30° roll and maneuvering to $+Z_{SI}$ attitude
5	Tape Recorder	5 orbits of transient analysis starting from 0°F in attitude $+X_{LV}$, 30° roll, no power dissipation in recorder

values shown in Fig. 2-29. This difficulty occurs because the predicted motor temperatures are for the armature mass at the center of the motor windings, whereas the measured values are from thermistors located at the outer surface of the motor casing underneath the heater band. Therefore, it is not surprising that the predicted motor temperature rise for an extension event is 18°F, whereas the measured values (Table 2-13) average only 7°F for extensions on motor 2. Retractions on motor 1 produced an average temperature rise of 14°F. Since motor 1 actually drew less current on the average than did motor 2, the higher indicated temperature rise from motor 1 was probably caused by variations in the conductive path from the motor casing through the thermal grease and into the thermistor/heater band.

The tape recorder temperature predictions for case 5 are shown in Fig. 2-35. The predictions for the heater support plate are the ones most comparable to the measurements from the thermistors shown in Fig. 2-30. The temperature variations from the shadow periods to the sunlight periods are about 10°F in each case. The predicted temperatures are a little lower than the measured values since the predictions are a cold case with a nonoperational recorder.

The temperature measurements for solar cells and for the Kapton behind the solar cells during the first solar cell performance test are shown in Figs. 2-36 through 2-40. These figures show that all three groups of cells operated at similar temperatures. Additionally, the Kapton behind the cells operated at essentially the same temperature as the cells. The Kapton temperature measurements may not be accurate, however, because of the problems inherent in using thermistors to measure the temperature of a transparent material.

The temperature predictions for the solar cells during the orbit of performance testing are shown in Figs. 2-41 and 2-42. The pertinent data used for predicting the solar cell temperatures are presented in Table 2-15. The cell efficiencies are taken as zero for these analyses since resistances for measuring current and voltage values were connected across the cells for only a small percentage of the time. The temperature predictions are somewhat higher than the measured values, particularly for the 5.9 × 5.9 cm cells. The differences, however, are well within the differences between the temperature predictions and test measurements made in the past. The possibility that the actual cell temperatures were higher than the measurements indicate is discussed in the following section.

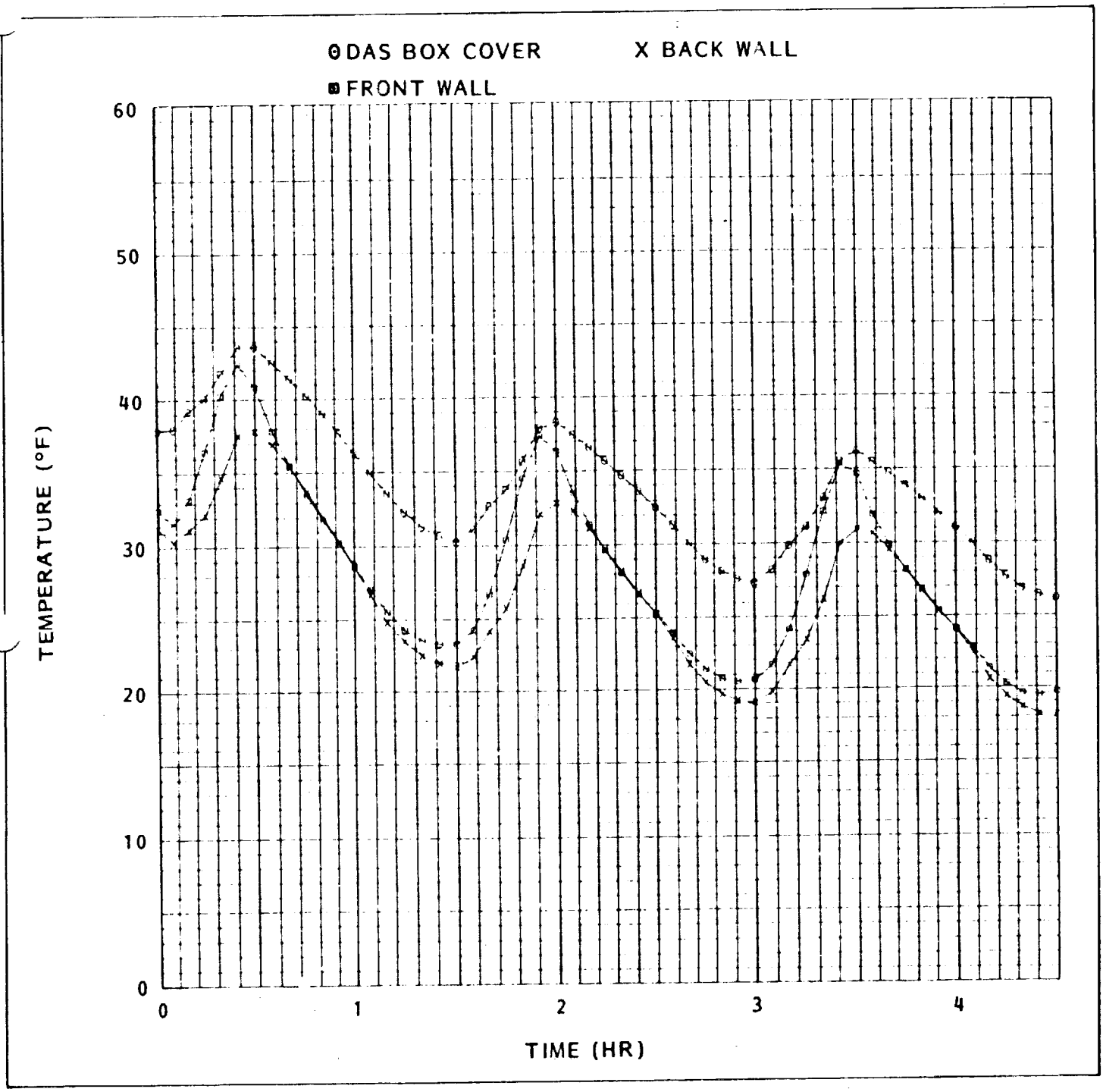

Fig. 2-31 DAS Box Temperature Predictions for Extended Stays in $+X_{LV,\ 30^\circ\ Roll}$ Attitude (Case 1)

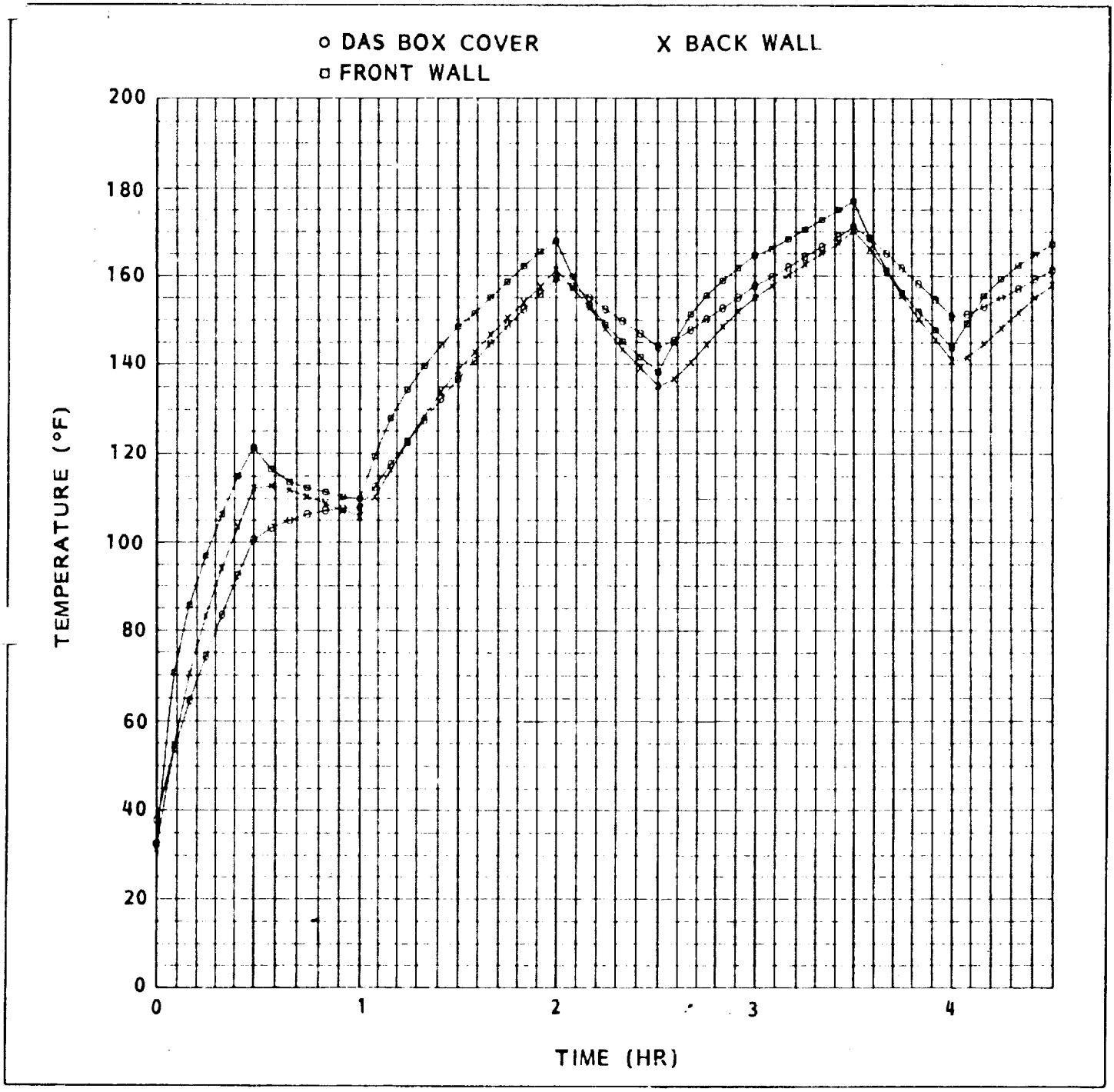

Fig. 2-32 DAS Box Temperature Predictions Following Maneuvers from $+X_{LV,\ 30^\circ\ Roll}$ Attitude to Z_{SI} Attitude (Case 2)

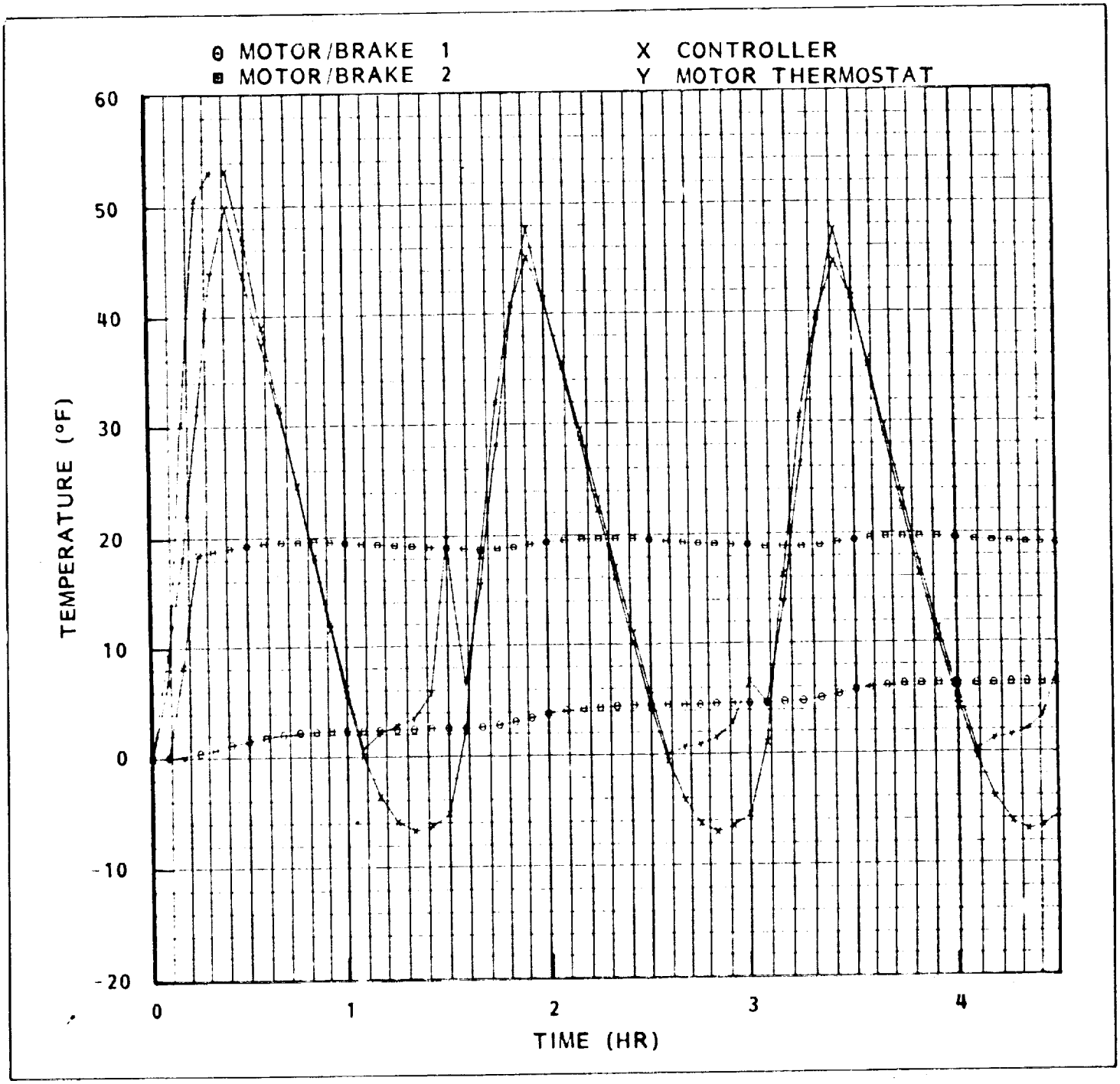

Fig. 2-33 Mast Motor Assembly Predicted Temperatures for Extended Stay in Attitude + $X_{IV,30^\circ\ Roll}$ Attitude (Case 3)

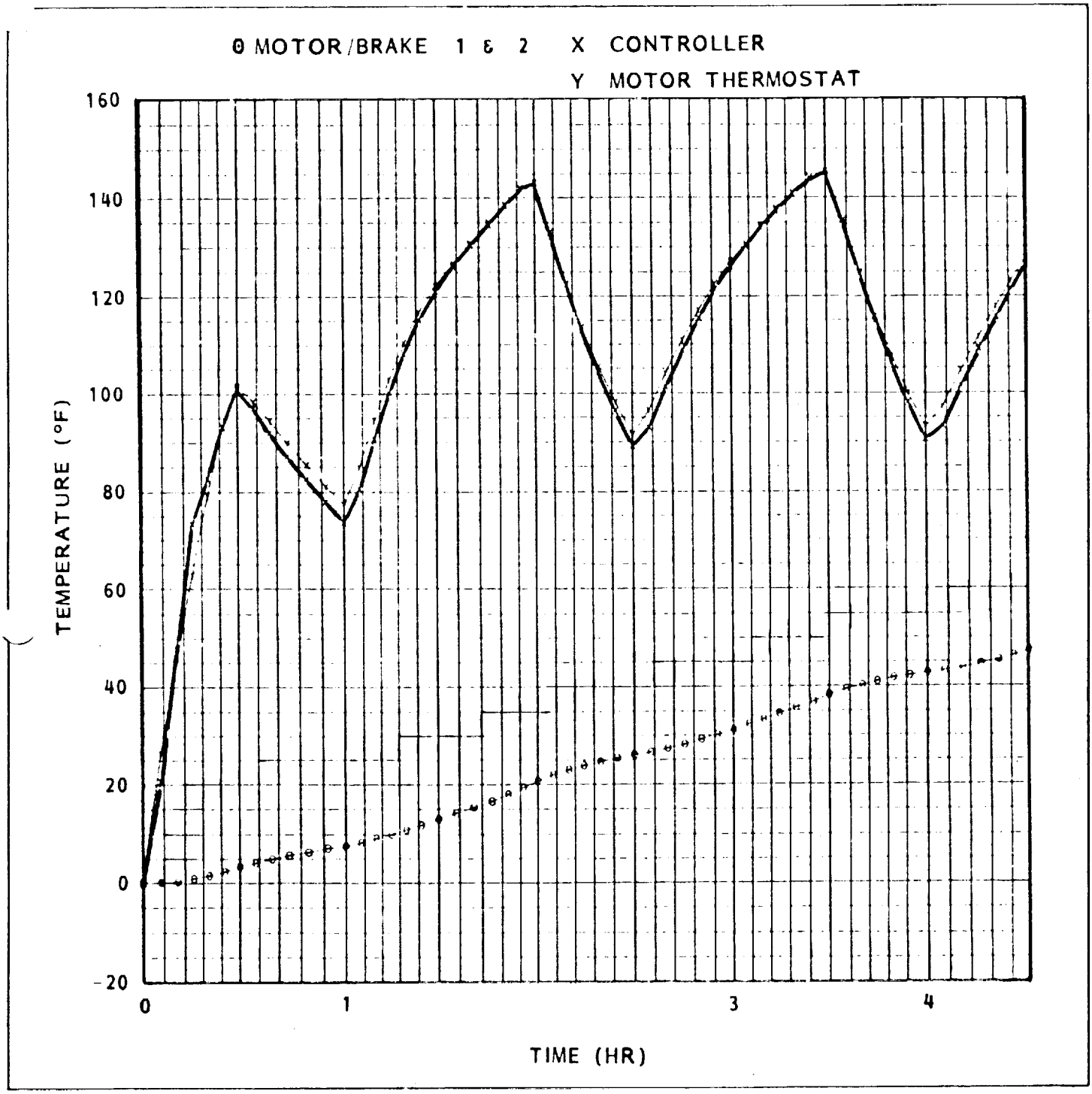

Fig. 2-34 Mast Motor Assembly Predicted Temperatures Following Maneuver from $+X_{LV,30\ Roll}$ Attitude to Z_{SI} Attitude (Case 4)

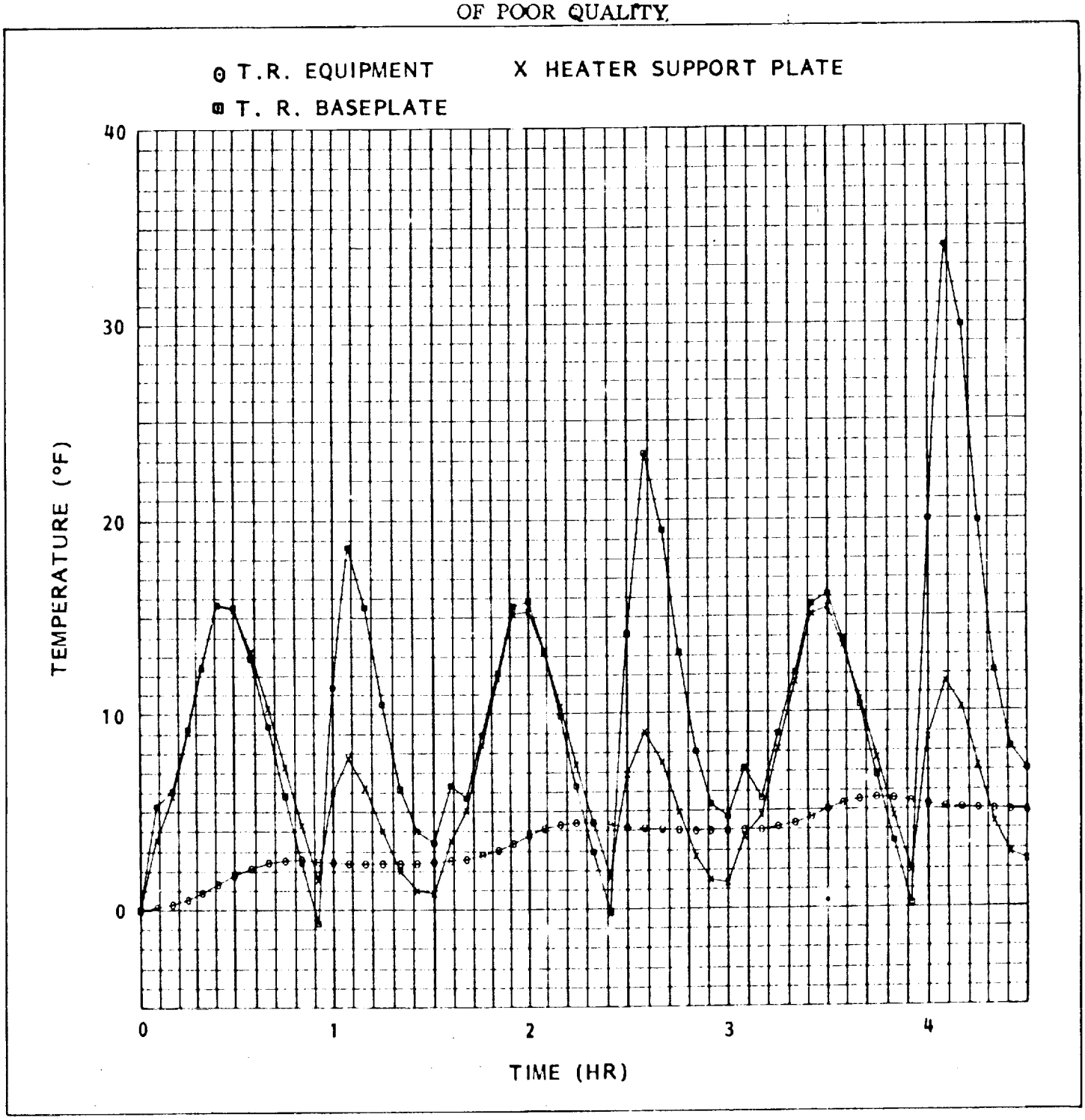

Fig. 2-35 Tape Recorder Temperature Predictions for Extended Stay in X_{LV}, 30 Roll Attitude (Case 5)

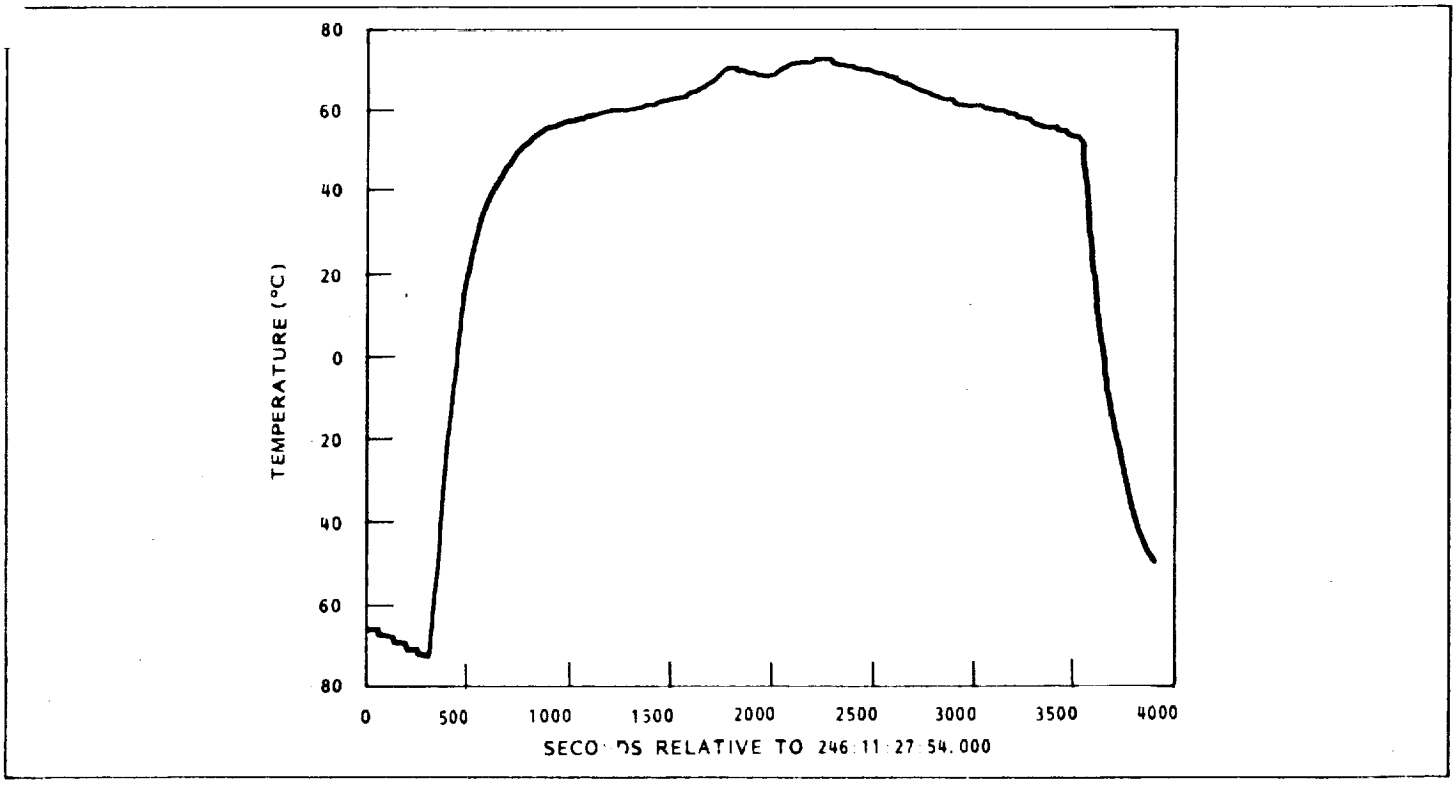

Fig. 2-36 Temperature of Back Side of 2 × 4 cm Cell During Solar Cell Performance Test (Event 9)

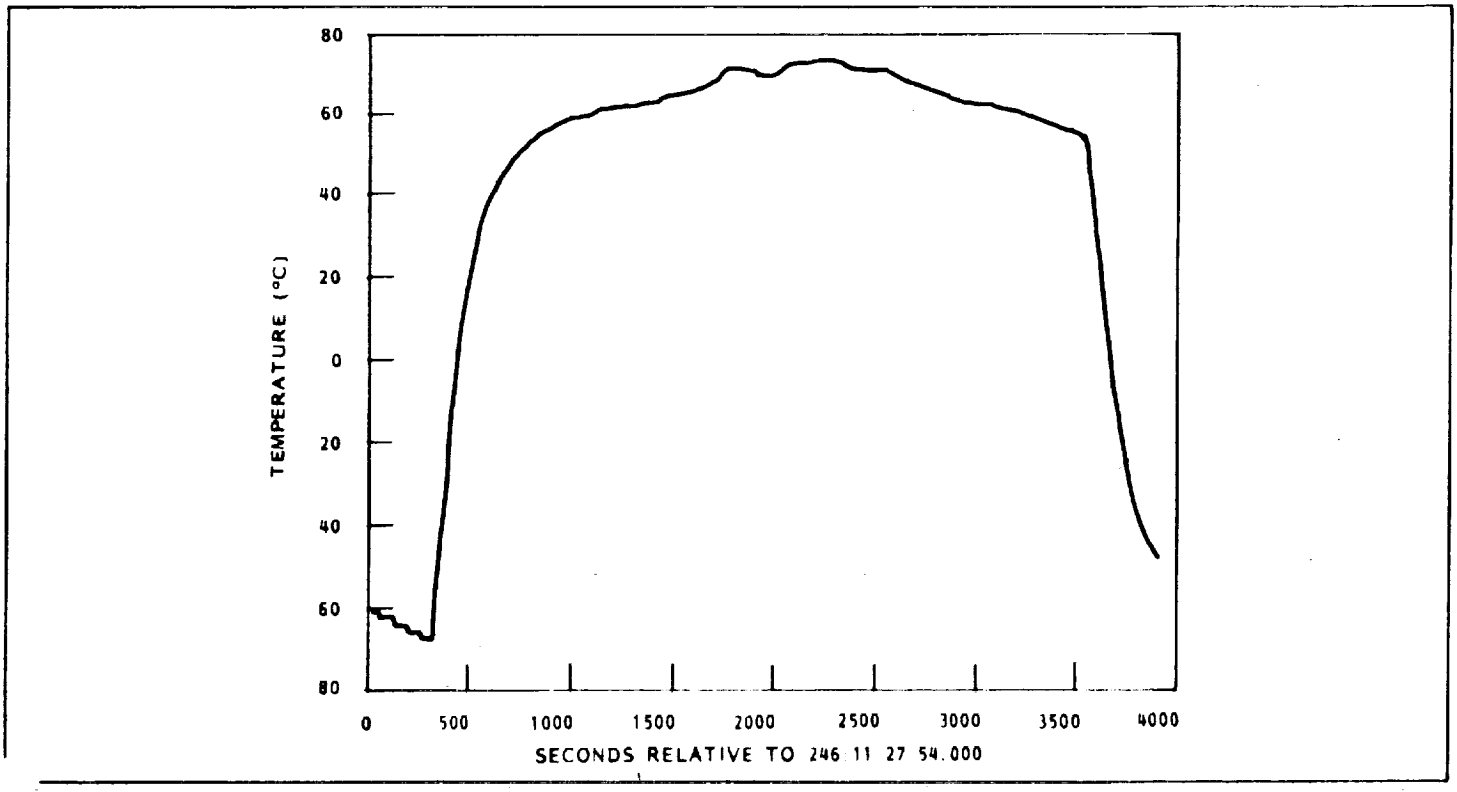

Fig. 2-37 Temperature of Kapton on Back Side of 2 × 4 cm Cell During Solar Cell Performance Test (Event 9)

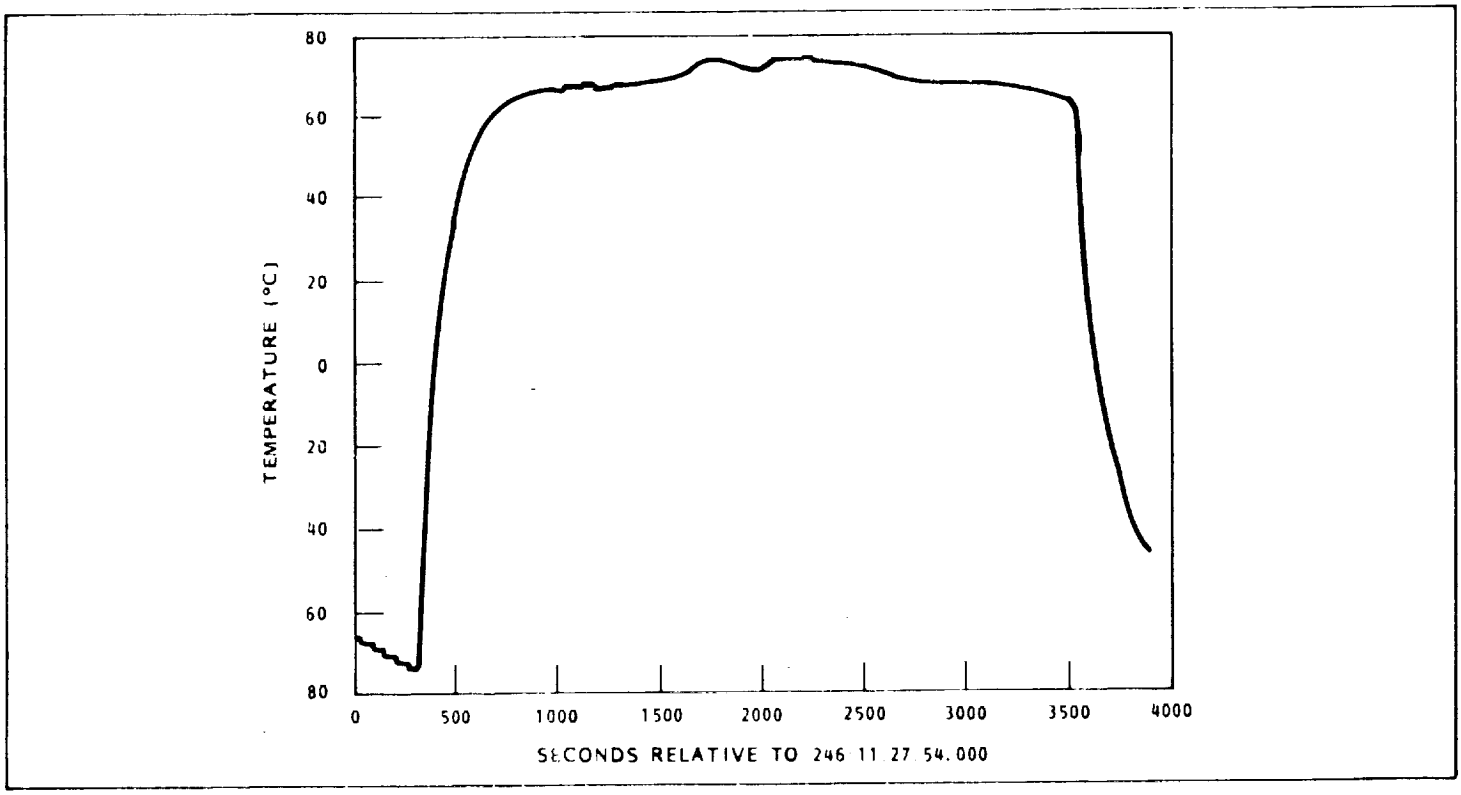

Fig. 2-38 Temperature of Kapton on Back Side of Thin Cell (2 mil) During Solar Performance Test (Event 9)

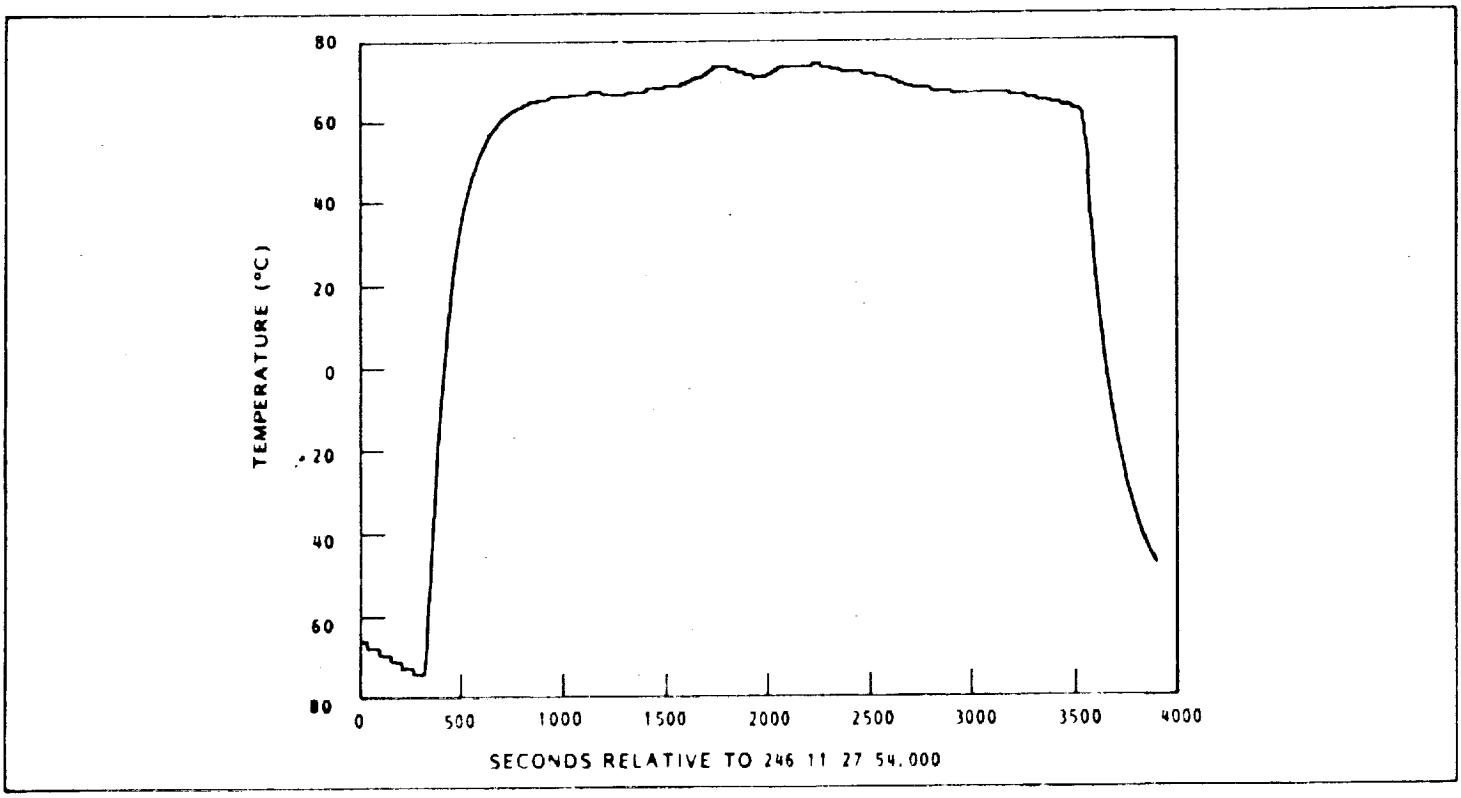

Fig. 2-39 Temperature on Back Side of 5.9 × 5.9 cm Cell During Solar Cell Performance Test (Event 9)

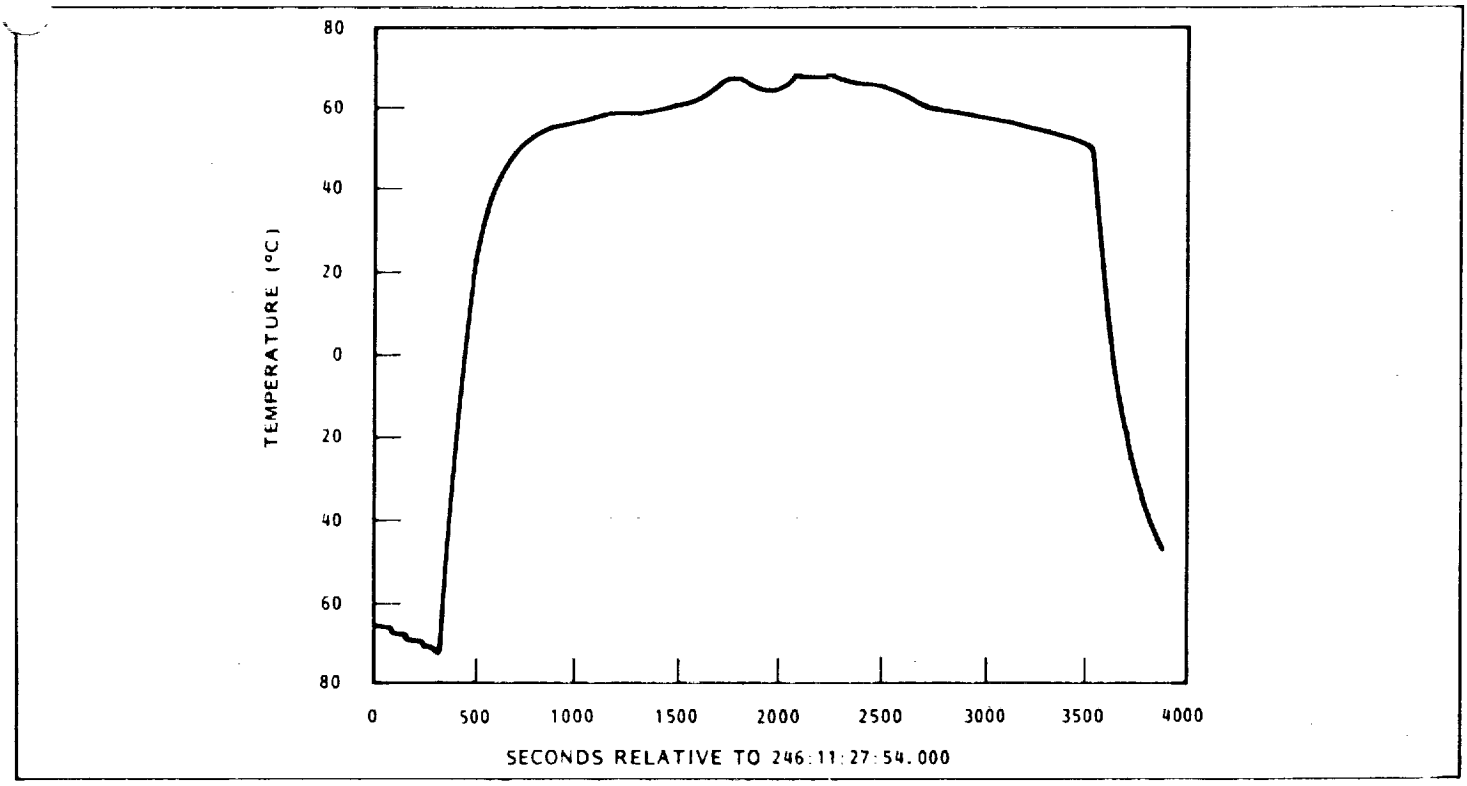

Fig. 2-40 Temperature of Kapton on Back Side of 5.9 × 5.9 cm Cell During Solar Cell Performance Test (Event 9)

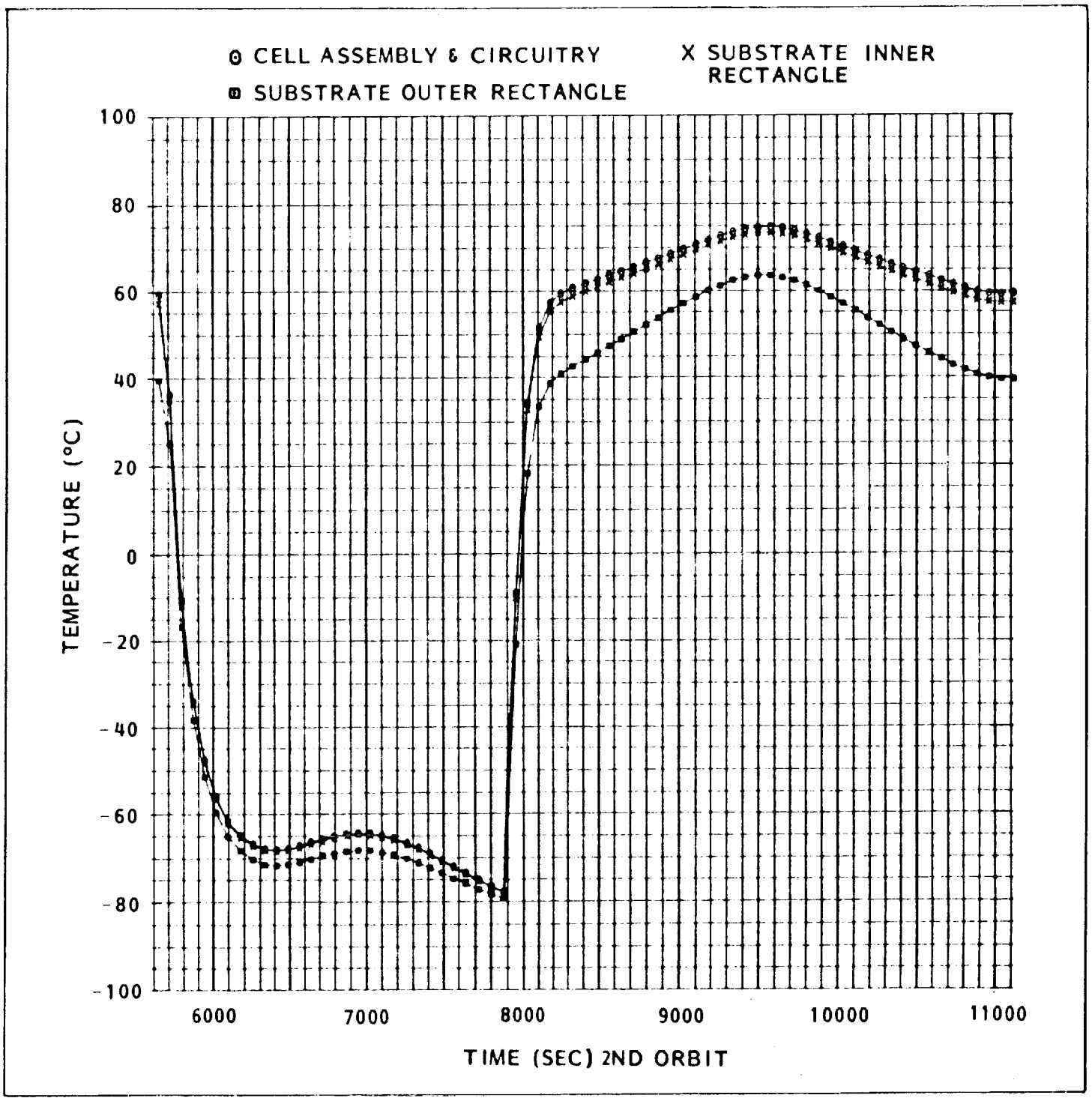

Fig. 2-41 Predicted Temperatures for 2 × 4 cm Cells

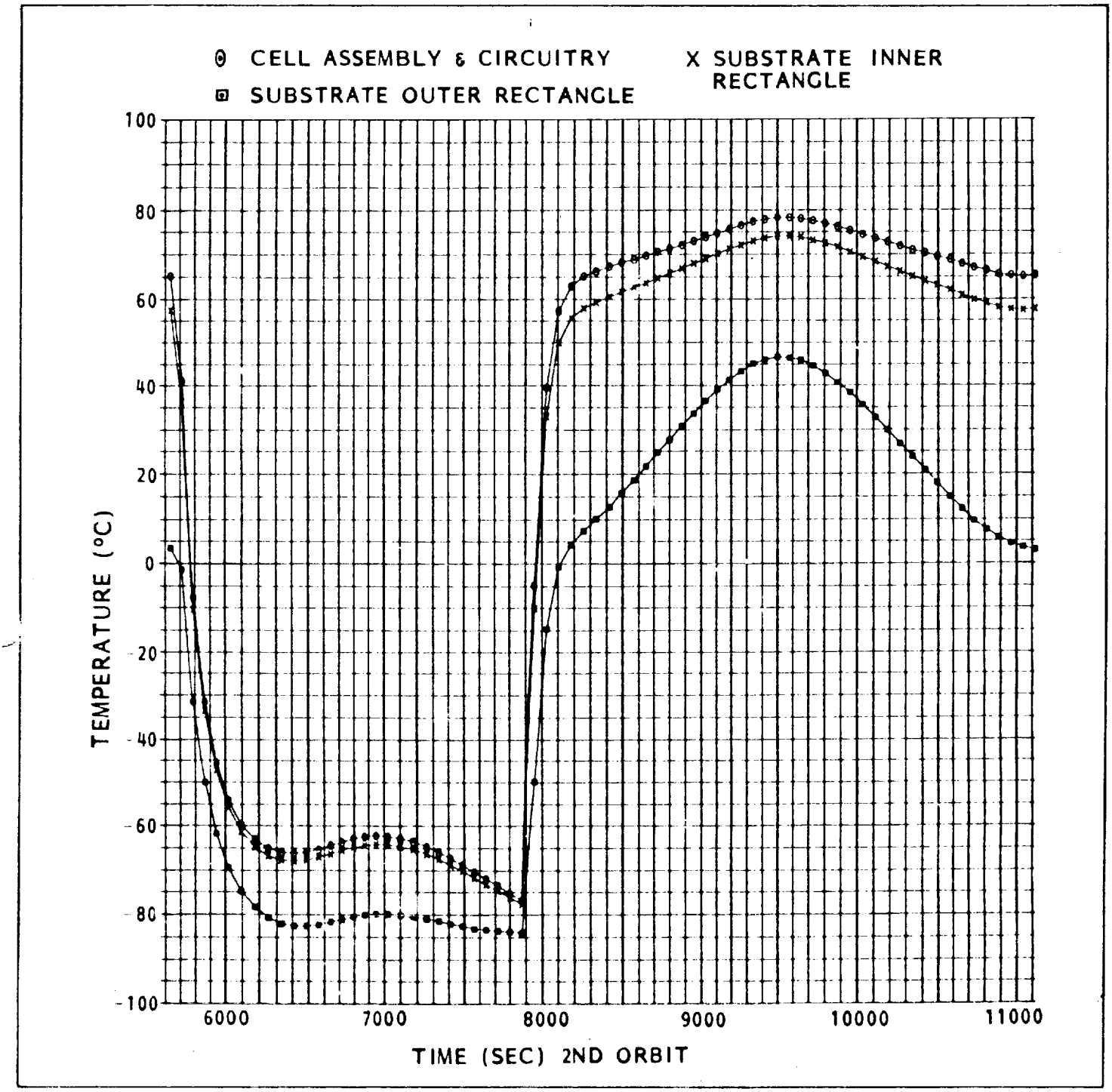

Fig. 2-42 Predicted Temperatures for 5.9 × 5.9 cm Cells

Table 2-15 PERTINENT DATA FOR SOLAR CELL TEMPERATURE PREDICTIONS

Surface Optical Properties

Parameter	Value
Frontface Solar Absorptivity	0.70
Frontface Emissivity (IR)	0.84
Circuitry Solar Absorptivity	0.37
Circuitry Emissivity (IR)	0.74
Space Side Solar Absorptivity of Substrate	0.28
Cell Side Solar Absorptivity of Substrate	0.28
Space Side Emissivity (IR) of Substrate	0.66
Cell Side Emissivity (IR) of Substrate	0.66
Solar Transmissivity of Substrate	0.35
Solar Absorptivity of Cell Backface	0.18
Emissivity (IR) of Cell Backface	0.09

Orbital Data

Parameter	Value
Orbital Altitude	163 NM
Orbital Beta Angle	6.8°

Cell Geometry and Performance Data

Parameter	Value for 2 cm x 4 cm Cells	Value for 5.9 cm x 5.9 cm Cells
Total Cell Area	8.1 cm^2	34.8 cm^2
Circuitry Length Under Cell	13.4 cm	28.3 cm
Circuitry Percentage of Area	57.1%	50.3%
Cell Efficiency Constant	0%	0%

.4.6 Solar Cell Performance

Solar cell performance was measured on two occasions during the SAFE flight. These performance tests are identified as events 9 and events 24 and 25 in Table 2-1. In each case, the orbiter was maneuvered to the $+X_{SI}$ attitude as shown in Fig. 2-27. In this attitude, the array blanket is positioned at 90 degrees to the solar vector with the active solar cells facing the sun. Only in event 9 was this attitude maintained for the entire daylight portion of the orbit. Events 24 and 25 were a mini-solar-cell-performance test, and the $+X_{SI}$ attitude was not maintained long enough for the solar cells to reach thermal equilibrium. Therefore, evaluation of the solar cell performance is limited to the data collected during event 9.

Solar cell performance data were collected for three separate electrical modules. One module was a half-panel populated with solar cells measuring 2 × 4 cm. The second electrical module was the other half of this panel, populated by solar cells measuring 5.9 × 5.9 cm. The third electrical module was a smaller grouping of much thinner solar cells measuring approximately 2 × 2 cm. Detail specifications of the solar cells and their grouping in the electrical module are contained in Table 2-16.

The solar performance was recorded by measuring the current and voltage produced by each of the solar cell modules at six different load resistances and at the short circuit current and open circuit voltage. These measurements provide eight data pairs for generating current versus voltage (IV) curves. A schematic of the circuit used to make the measurements is shown in Fig. 2-43. The three resistors shown in the diagram were switched into the circuit in the combinations shown to produce the six load resistance values. This measurement system outputs the current and voltage for each of the load points versus time. This data must be cross-plotted to obtain IV curves. The open circuit voltage versus time and short circuit current versus time are shown in Figs. 2-44 through 2-49. The rise in short circuit current at sunrise and sunset is due to albedo illumination on the front surface of the cells as well as to the direct solar illumination.

To compare predicted solar cell performance with the measured performance, it is desirable to stay away from orbital sunrise and sunset, when temperature changes in the cells cause variations in cell performance. Therefore, IV curve comparison was performed at 2250 seconds past the GMT reference time of 246:11:27:54 used for this event. Figures 2-36 through 2-49 show that this is a time near orbital noon when all three electrical panels are operating at near maximum temperature. A second time of 1000 seconds past the reference time was selected for a comparison at a different temperature yet at a time when cell performance was not changing rapidly. The two times selected for IV curve comparison correspond to GMTs of 246:11:44:34 and 246:12:05:24.

Preliminary evaluation of the flight IV curves showed a dip in the current from the electrical modules near the short circuit current end of the curve. The dip was most pronounced in the data from the electrical modules of 2 × 4 cm cells and 5.9 × 5.9 cm cells. A typical set of data depicting the current dip is shown in Fig. 2-50. This figure shows that load point 3 is below the fitted curve and load point 2 is lower yet. Because of this current dip, investigative tests were performed on the DAS box. The investigation concluded that the current dip in the flight IV curves resulted from current leaks in the bases of the transistors used in the measurement circuit shown in Fig. 2-43. For each transistor that is closed to complete a load circuit, a small amount of current from the solar cells is shunted around the current sensing resistor. Thus, for load point 4, current is lost through only one transistor while, for load point 3, current is lost through two transistors and, for load point 2, current is lost through three transistors. Because of these facts, the flight data were corrected by increasing the measured current values by the theoretical transistor leakage of 11 milliamperes per transistor used for that load point. These current corrections are presented in Table 2-17. The corrections were not applied to the measurements from the thin cell electrical module since the shunted current was negligible for this load circuit design.

The flight data for the 2 × 4 cm cells are shown in Figs. 2-51 and 2-52. The data described as "flight conditions" in these figures are the raw flight data plus the current correction due to current shunting in the DAS box.

The data, which is corrected to 28°C, 1 AU, include correction factors to account for the seasonal variation in solar intensity, the reduced solar flux due to array twist, and the variation in voltage and current with cell temperature. These correction factors are also given in Table 2-17.

In these curves, a very slight dip in current can still be observed in the horizontal portion of the curve. After these curves were prepared, the DAS box was disassembled and the current leak in the transistors determined to be 17 milliamperes rather than 11 milliamperes. If the curves were redrawn with this latest input, the slight dip would be eliminated.

The IV curves measured in preflight and postflight flash tests on these cells are shown in Figs. 2-53 and 2-54. All of these results are combined for comparison at 28°C in Fig. 2-55. Similar results are shown for the module of 5.9 × 5.9 cm cells and for the module of thin cells in Figs. 2-56 through 2-60 and Figs. 2-61 through 2-65, respectively. An overview of all this data can be gained by looking at Figs. 2-55, 2-60, and 2-65.

These figures show that the flight performance of the solar cells was diminished on open circuit voltage and elevated on closed circuit current compared to the flash test performance for all three modules. Near the peak power point, the performance is nearly identical.

This variation in performance could be caused by an error in the temperature measurements for the solar cells. If the actual cell temperatures in flight were hotter than the temperature measurements indicate, then the voltage correction made to the flight data to reach the 28°C performance is too small. A temperature error of 9.8°C on the modules of 2 × 4 cm cells, 9.9°C on the module of 5.9 × 5.9 cm cells, and 7.3°C on the module of thin cells will cause the open circuit voltages from flight to match the flash test data at 28°C. This type of error would also improve the match of the short circuit current values from test to flight and the match of the predicted cell temperatures to those measured in flight.

Table 2-16 SOLAR CELL AND ELECTRICAL MODULE CHARACTERISTICS

Electrical Module with 5.9 cm x 5.9 cm Solar Cells	
Contact Design	Wrap Around
Cell Size	5.9 cm x 5.9 cm
Cell Thickness	0.008 inches
Number of Cells in Module	150
Cell Interconnect	Single String of 150 Cells in Series
Cover Slide	0.006 inches micro sheet
Cover Slide Adhesive	0.002 inches DC 93-500
Front Surface Coating	UV and anti-reflective
Back Surface Coating	BSR
Base Resistivity	2 ohm-cm

Electrical Module with 2 cm x 4 cm Solar Cells	
Contact Design	Wrap Around
Cell Size	2 cm x 4 cm
Cell Thickness	0.008 inches
Number of Cells in Module	704
Cell Interconnect	4 Parallel Strings of 176 Cells in Series
Cover Slide	0.006 inches fused silica
Cover Slide Adhesive	0.002 inches DC 93-500
Front Surface Coating	UV and anti-reflective
Back Surface Coating	BSR
Base Resistivity	2 ohm-cm

Electrical Module with 2 cm x 2 cm Thin Solar Cells	
Contact Design	Top/Bottom
Cell Size	2 cm x 2 cm
Cell Thickness	0.002 inches
Number of Cells in Module	80
Cell Interconnect	4 Parallel Strings of 20 Cells in Series
Cover Slide	0.002 inches micro sheet
Cover Slide Adhesive	DC 93-500
Front Surface Coating	None
Back Surface Coating	BSF
Base Resistivity	2 ohm-cm

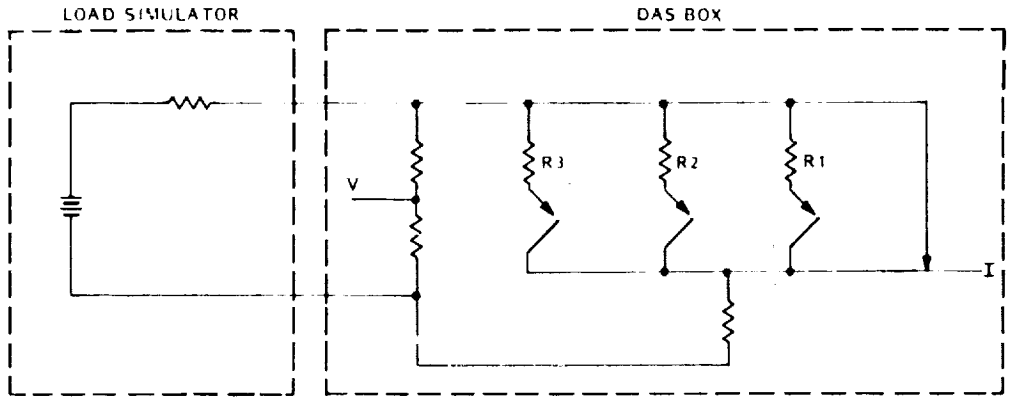

MEASUREMENT	CIRCUIT CONDITION
I_0	SHORT
I_1	R1, R2, R3
I_2	R1, R3
I_3	R1
I_4	R1, R2
I_5	R2
I_6	R3
I_7	OPEN

Fig. 2-43 Schematic of Circuits Used to Make IV Curve Measurements

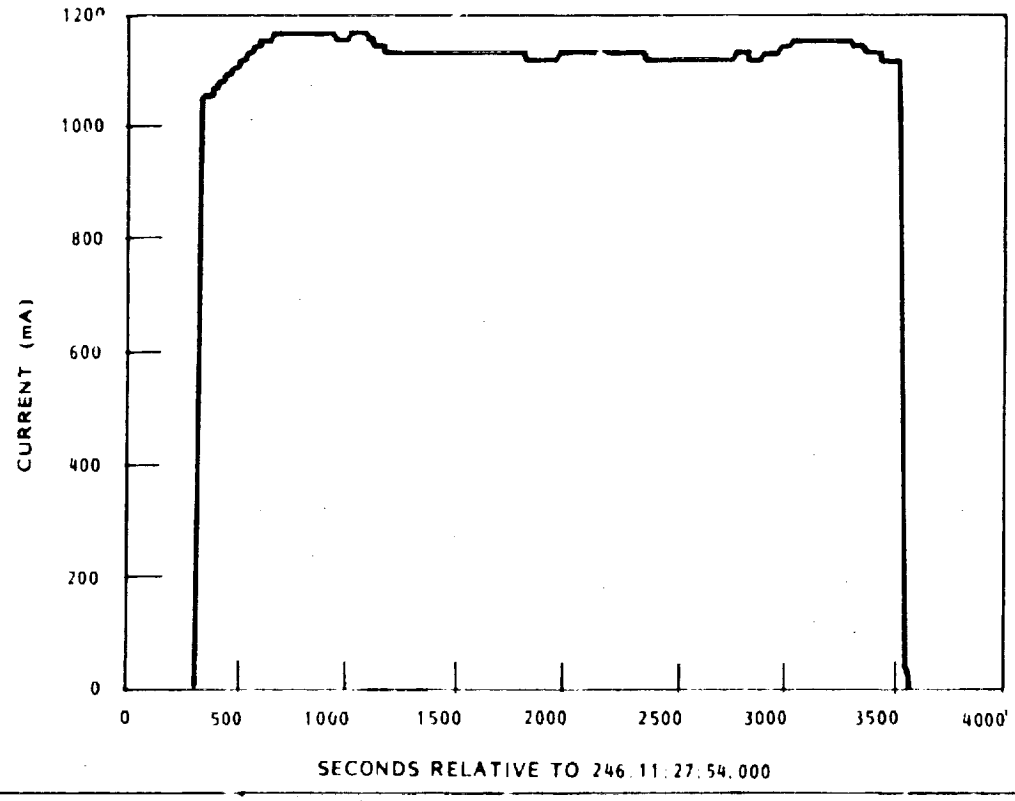

Fig. 2-44 Short Circuit Current for Module of 2 × 4 cm Solar Cells During Solar Cell Performance Test (Event 9)

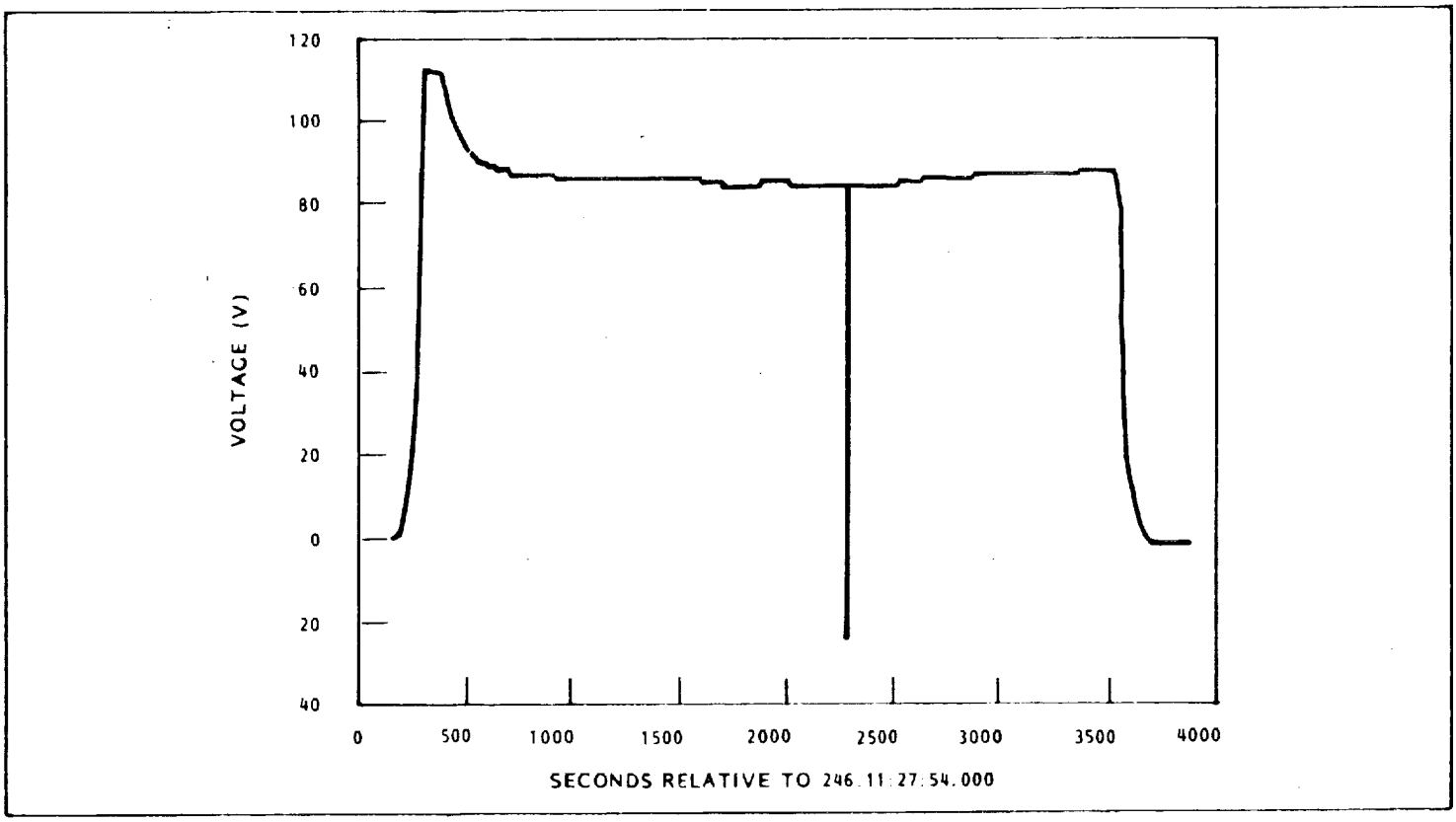

Fig. 2-45 Open Circuit Voltage for the Module of 2 × 4 cm Solar Cells During Solar Cell Performance Test (Event 9)

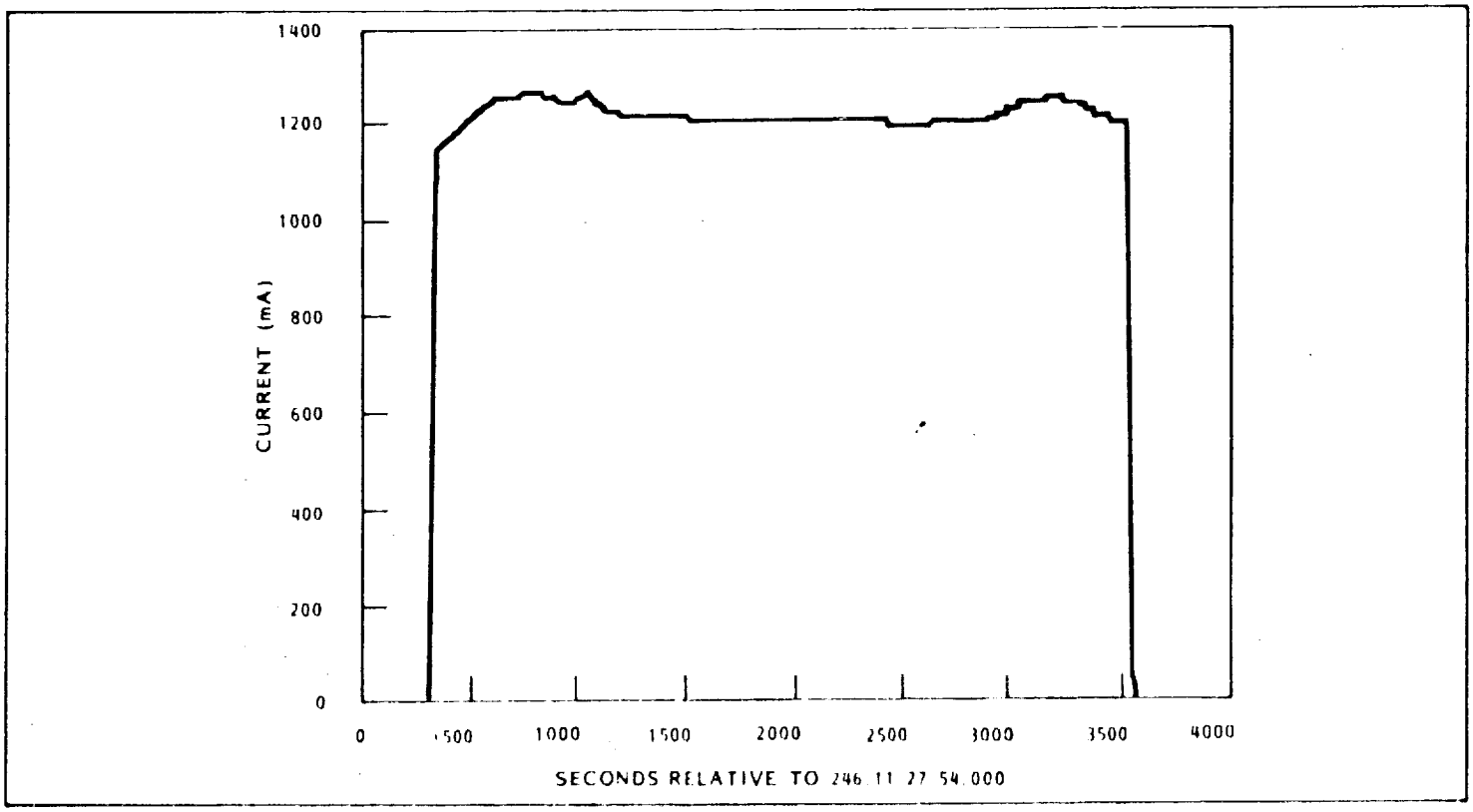

Fig. 2-46 Short Circuit Current for the Module of 5.9 × 5.9 cm Solar Cells During Solar Cell Performance Test (Event 9)

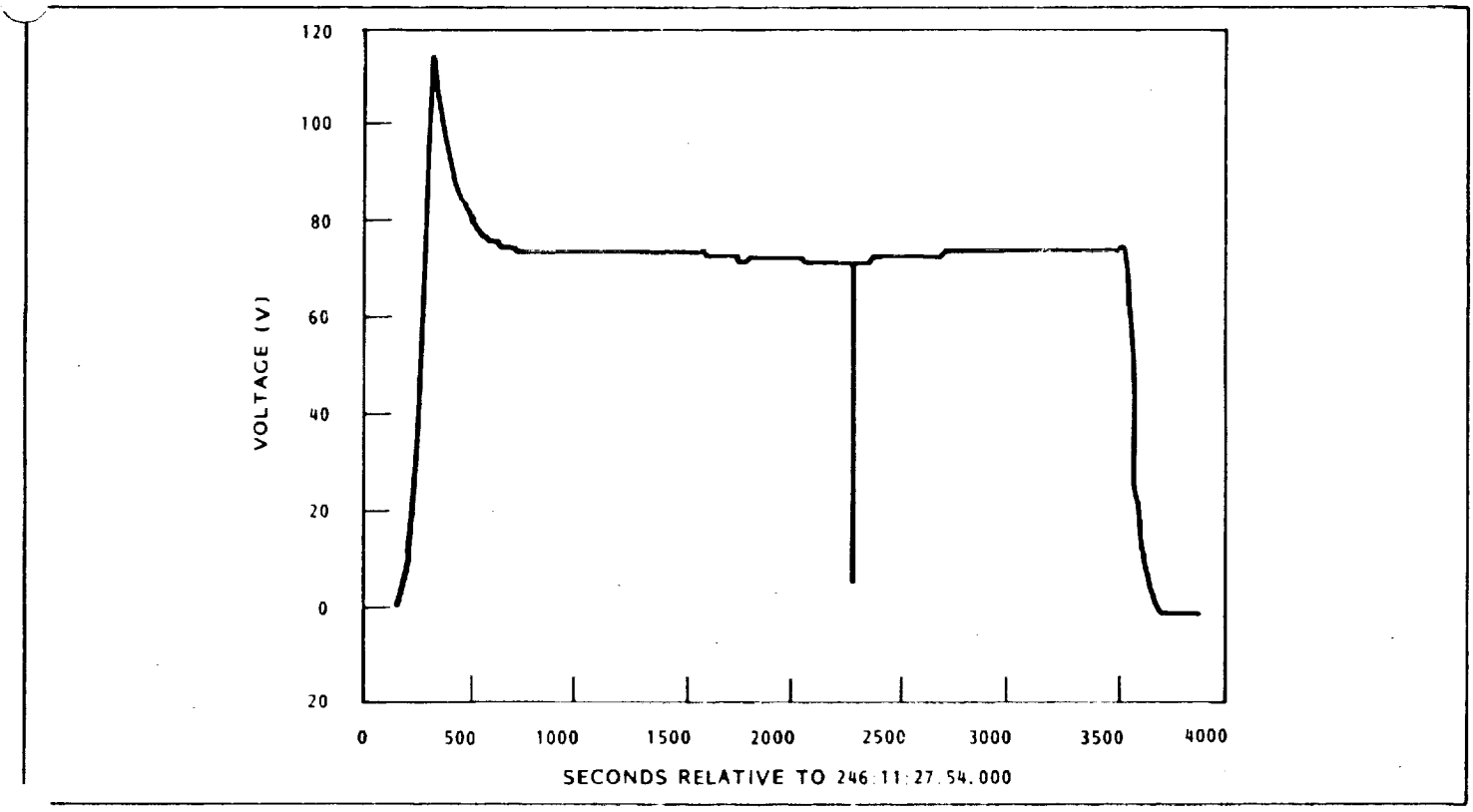

Fig. 2-47 Open Circuit Voltage for the Module of 5.9 × 5.9 cm Solar Cells During Solar Cell Performance Test (Event 9)

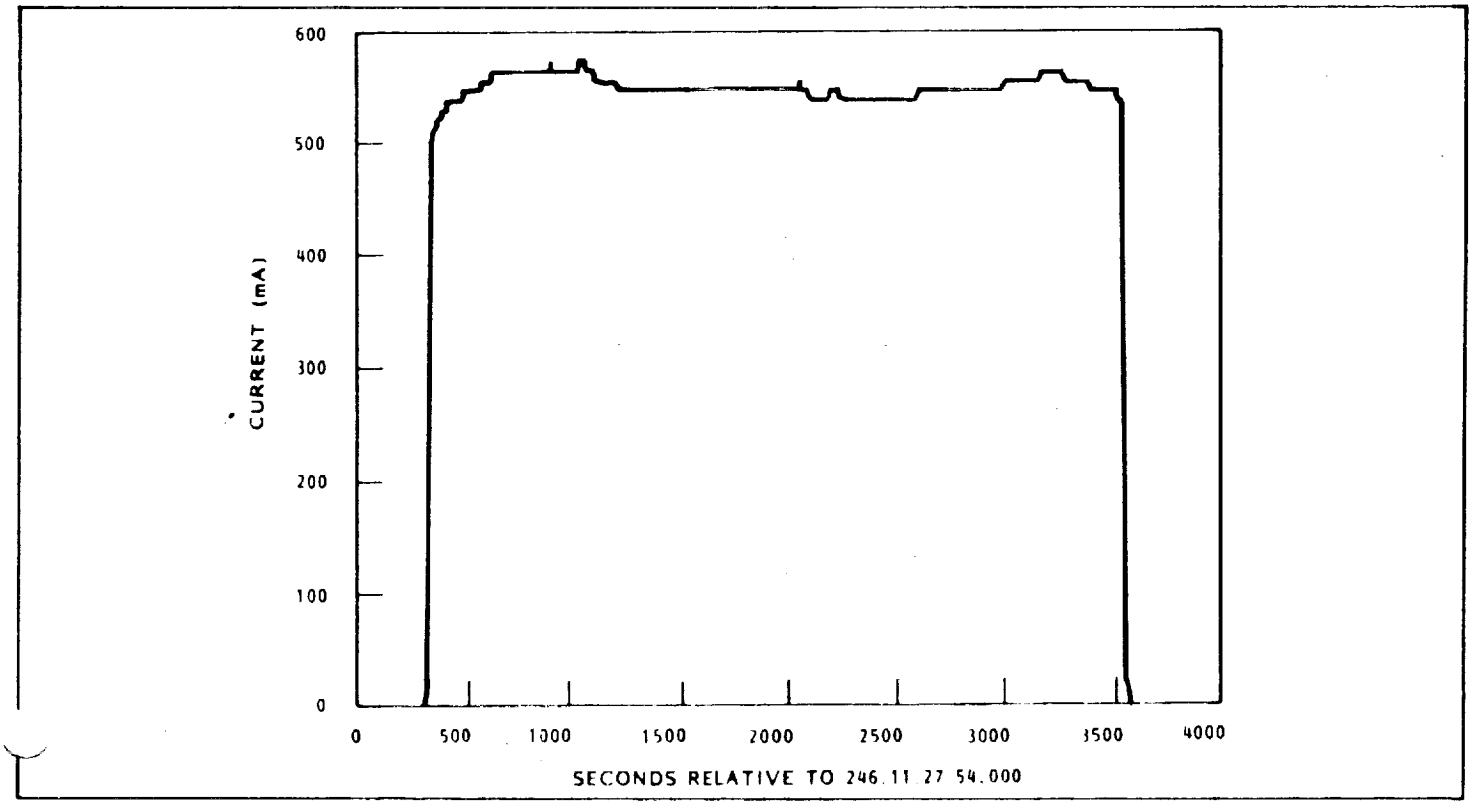

Fig. 2-48 Short Circuit Current for the Module of Thin Cells During Solar Cell Performance Test (Event 9)

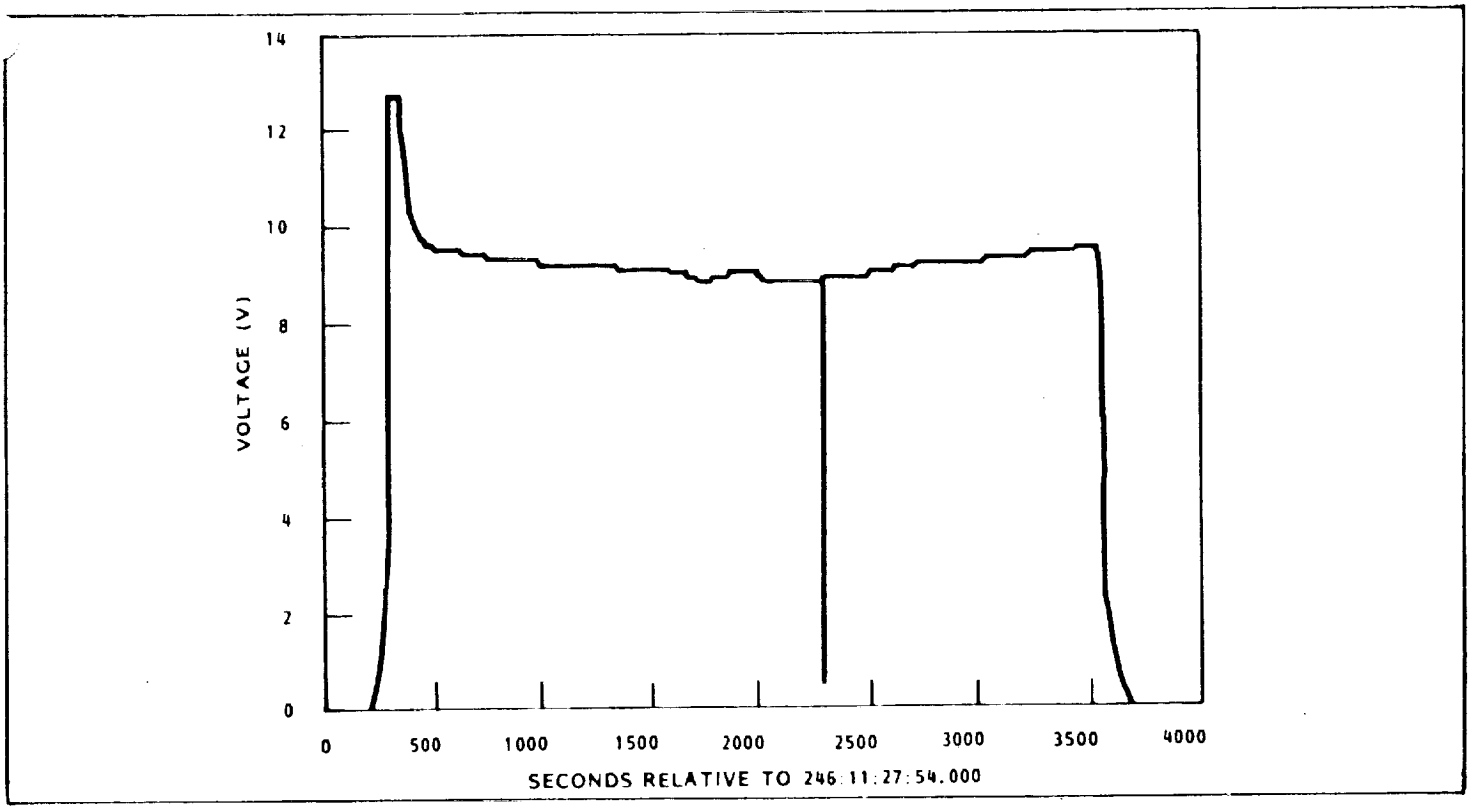

Fig. 2-49 Open Circuit Voltage for the Module of Thin Cells During Solar Cell Performance Test (Event 9)

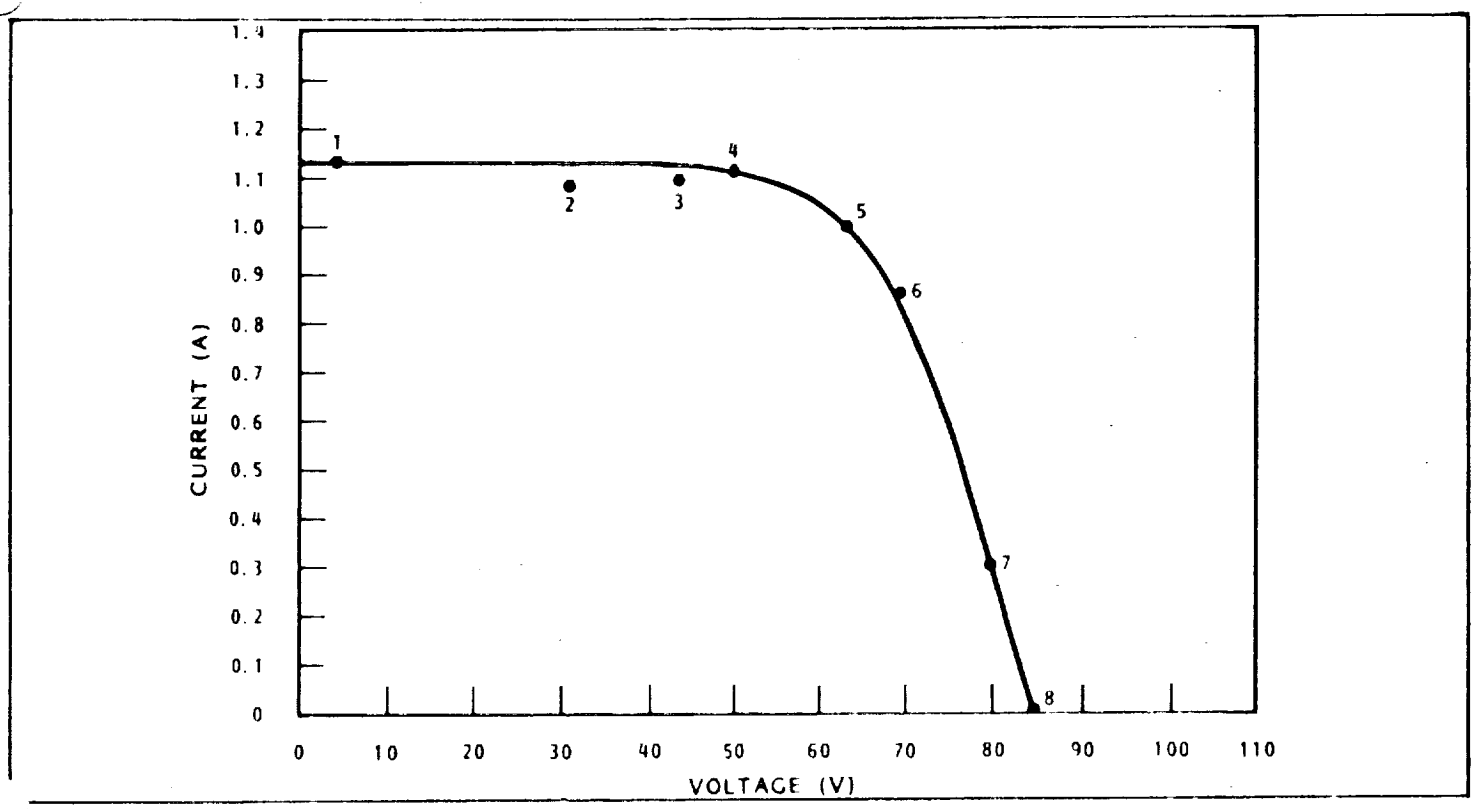

Fig. 2-50 Typical Flight IV Curve Before Correction of Measurement System Error

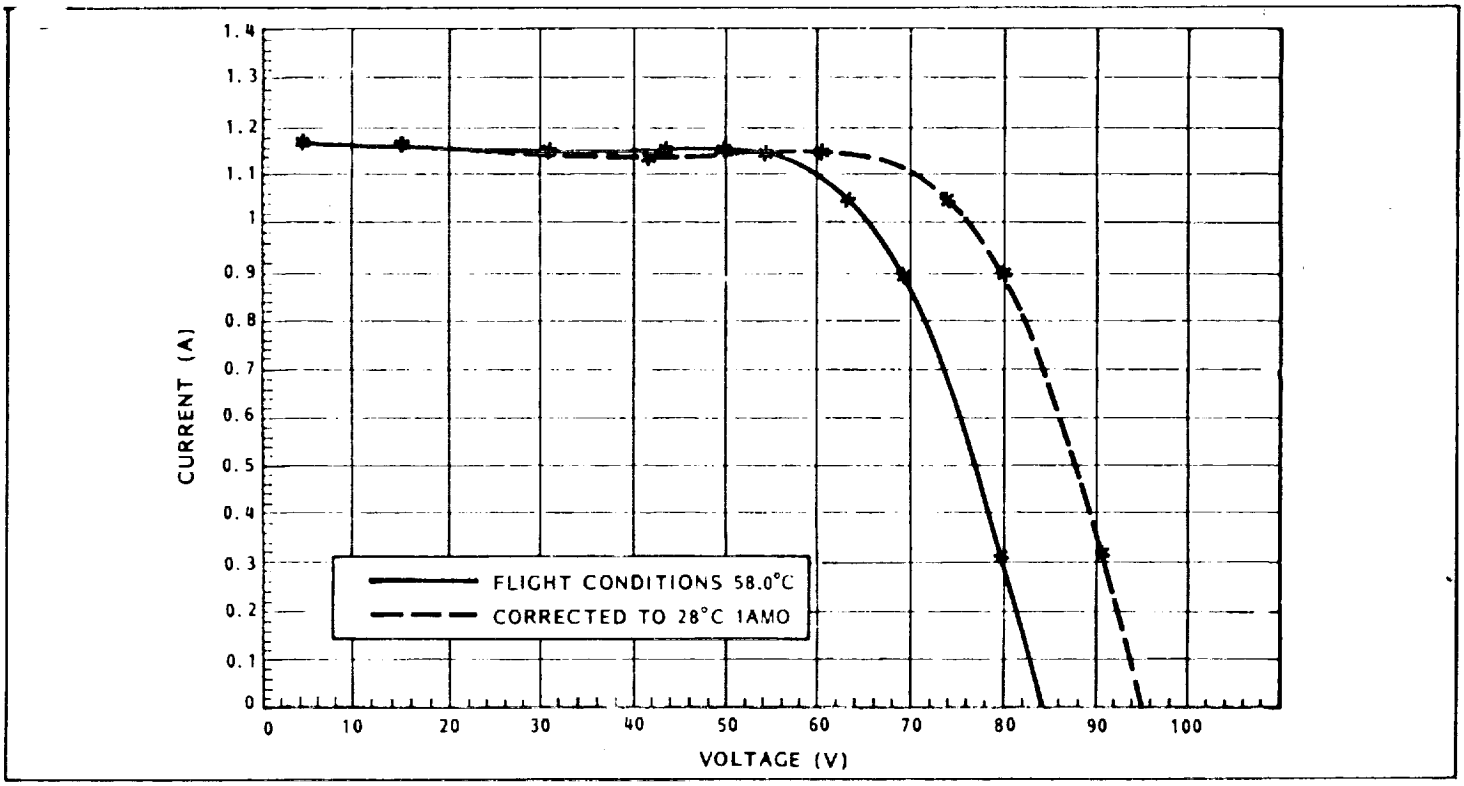

Fig. 2-51 IV Curve from Module of 2 × 4 cm Cells—GMT 246:11:44:34

Table 2-17 CURRENT AND VOLTAGE CORRECTION FACTORS

DAS Box Current Correction Factors for Electrical Module of 2 cm x 4 cm Cells and Electrical Module of 5.9 cm x 5.9 cm Cells

	I_1	I_2	I_3	I_4	I_5	I_6	I_7	I_8
Current Correction (mA)	+11	+33	+22	+11	+22	+11	+11	0

Current Correction Due to Array Twist of 7.8°

$$I_{corrected} = 1.0093\ I_{measured}$$

Current Correction Due to Seasonal Solar Flux Variation

$$I_{corrected} = 1.0178\ I_{measured}$$

Current and Voltage Temperature Coefficients

	Property Change per °C		
Property	2 cm x 4 cm	5.9 cm x 5.9 cm	Thin Cell
Isc (mA/series string)	0.112	0.0484	0.083
Voc (mV/cell)	2.023	2.023	2.07
Imp (mA/series string)	0.0409	0.177	0.0036
Vmp (mV/cell)	-1.998	-1.998	2.11

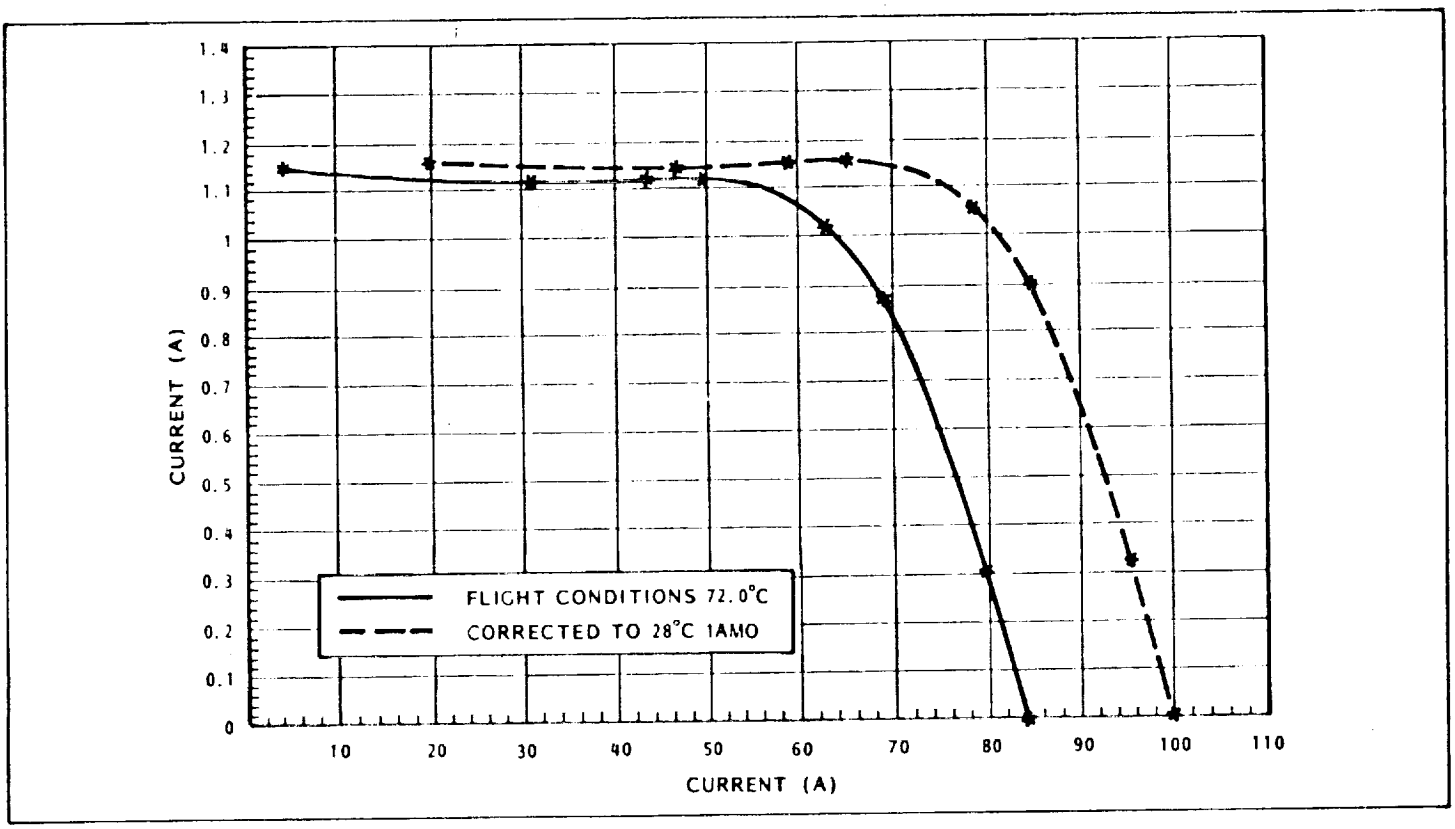

Fig. 2-52 IV Curve from Module of 2 × 4 cm Cells—GMT 246:12:05:24

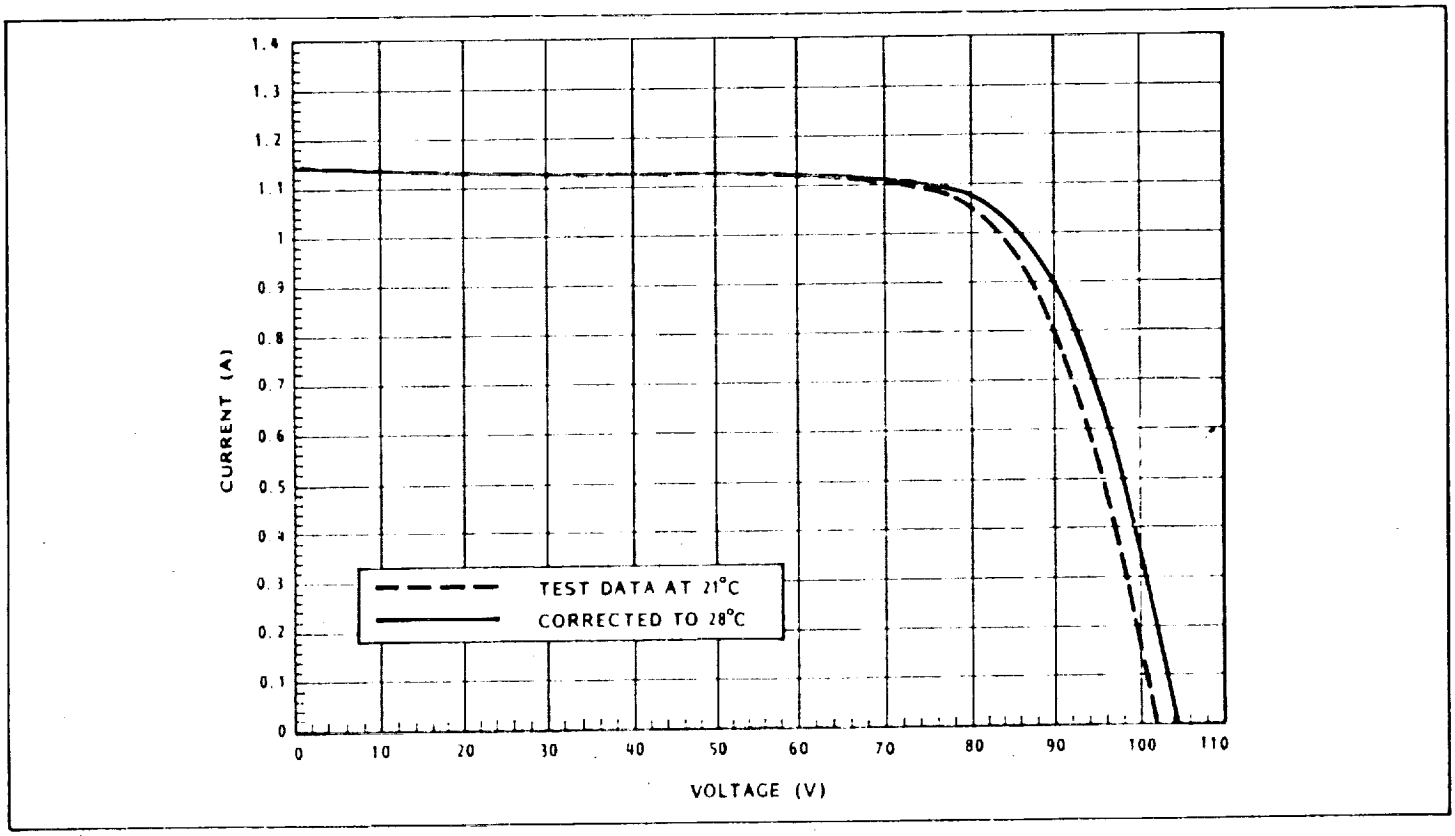

Fig. 2-53 IV Curve From Module of 2 × 4 cm Cells—Preflight Flash Test

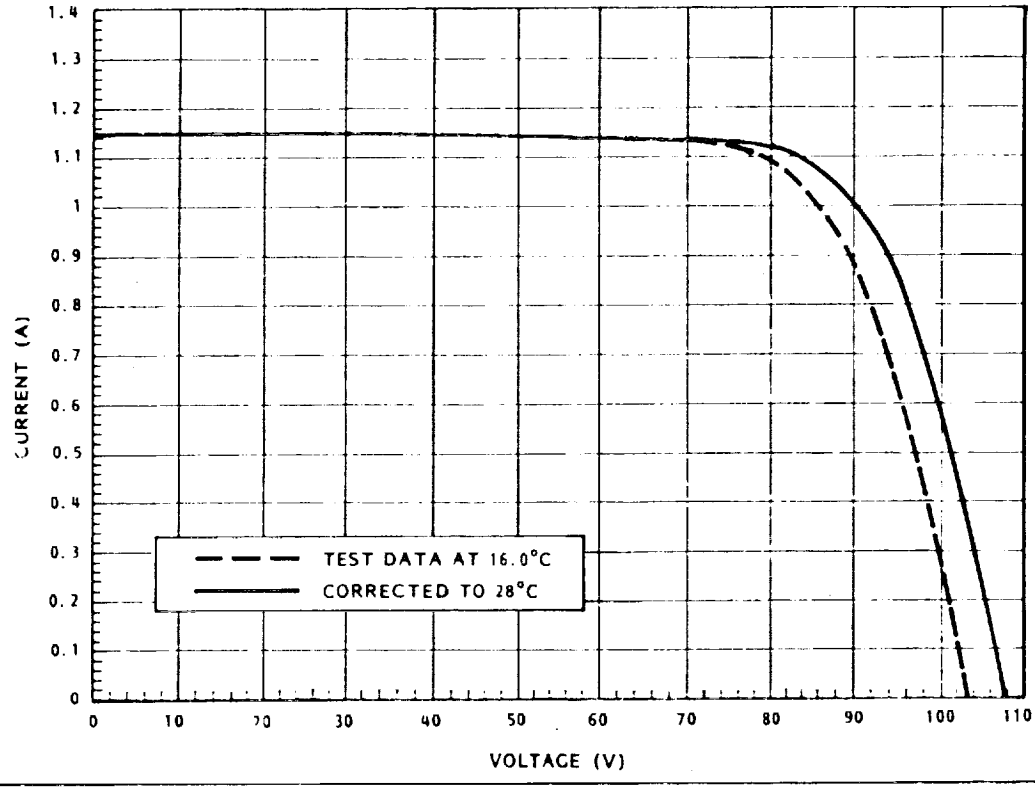

Fig. 2-54 IV Curve From Module of 2 × 4 cm Cells—Postflight Flash Test

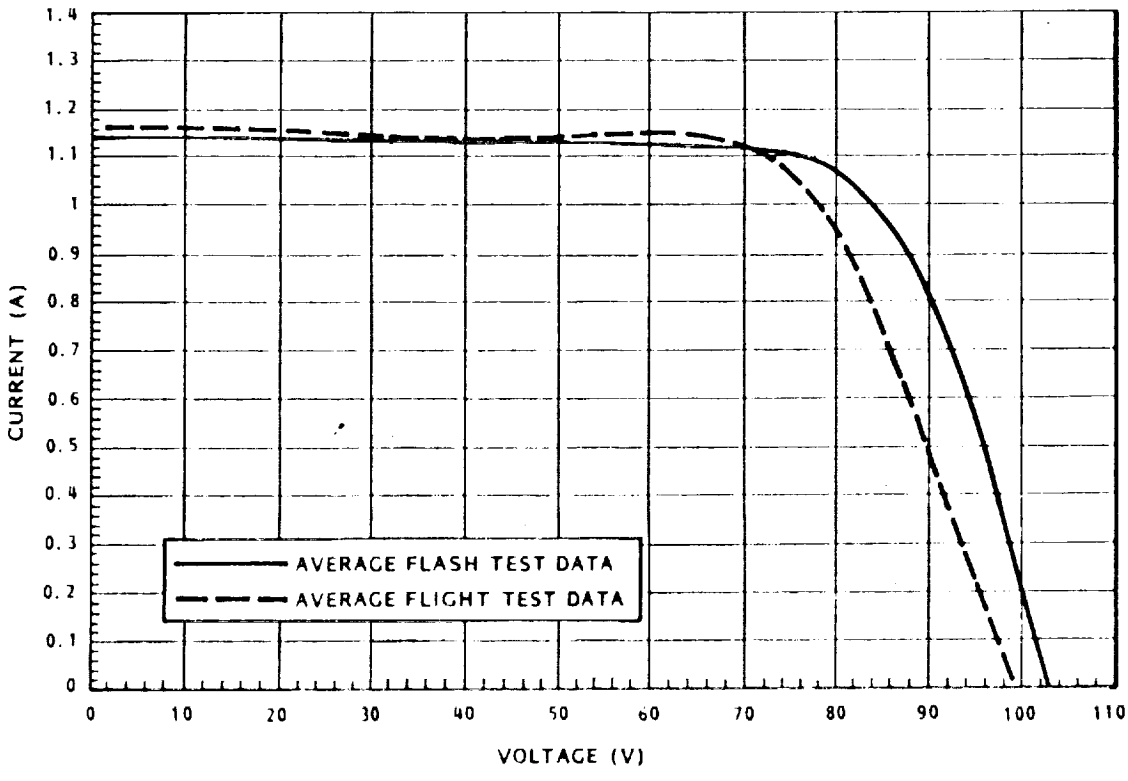

Fig. 2-55 Comparison of IV Curves From Flight and Ground Test for Modules of 2 × 4 cm Cells

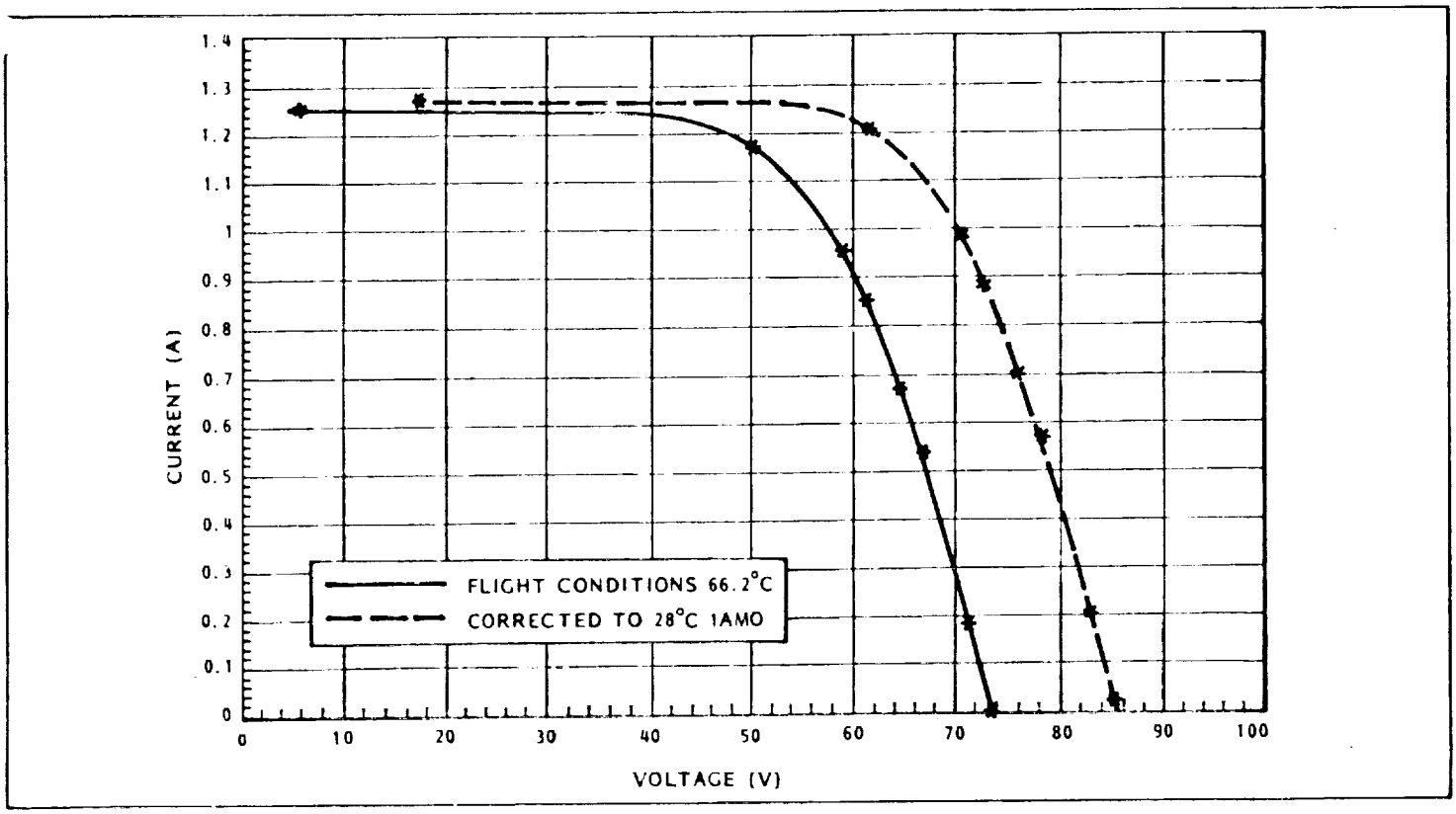

Fig. 2-56 IV Curve From Module of 5.9 × 5.9 cm Cells—GMT 246:11:44:34

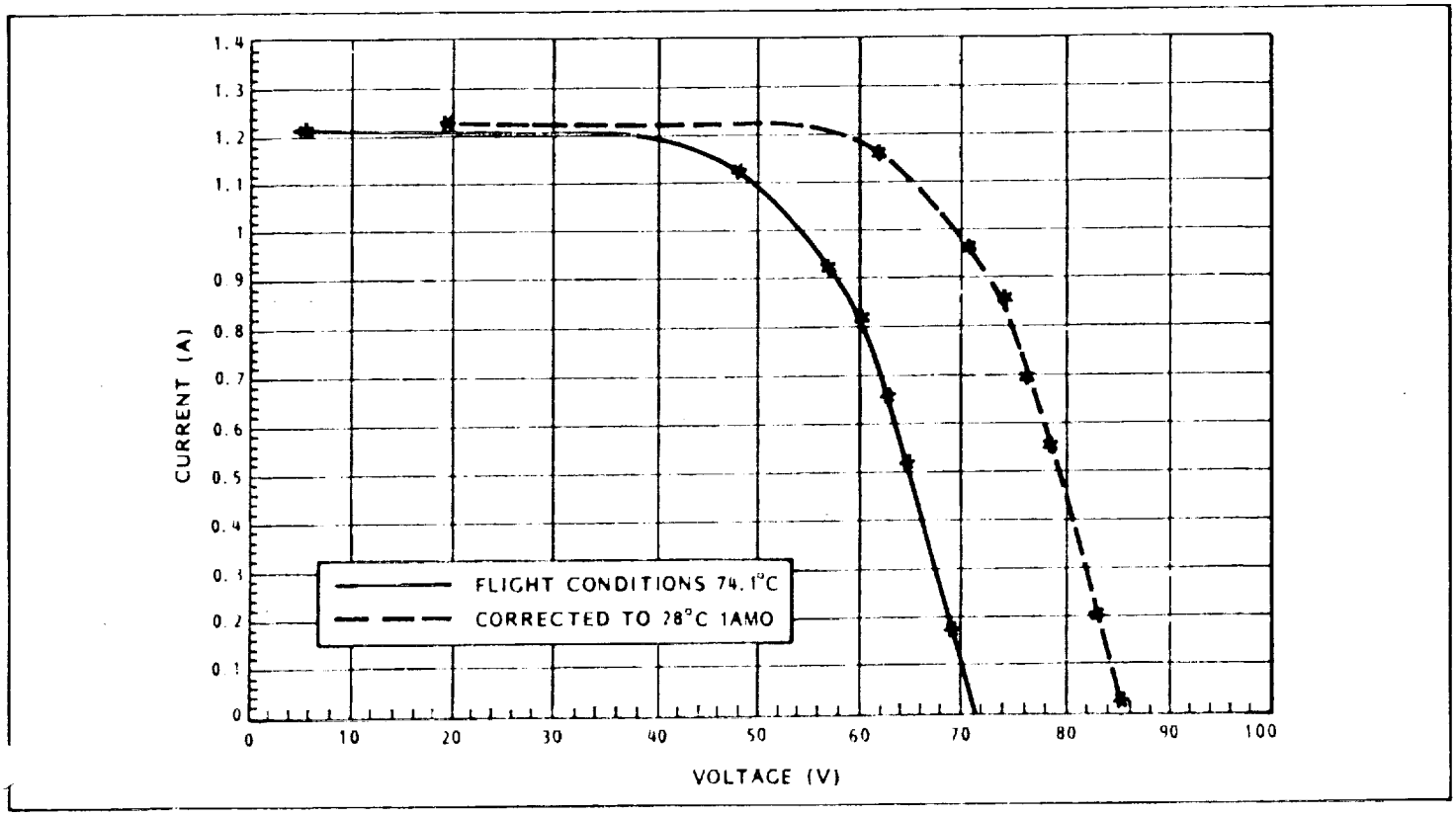

Fig. 2-57 IV Curve From Module of 5.9 × 5.9 cm Cells—GMT 246:12:05:24

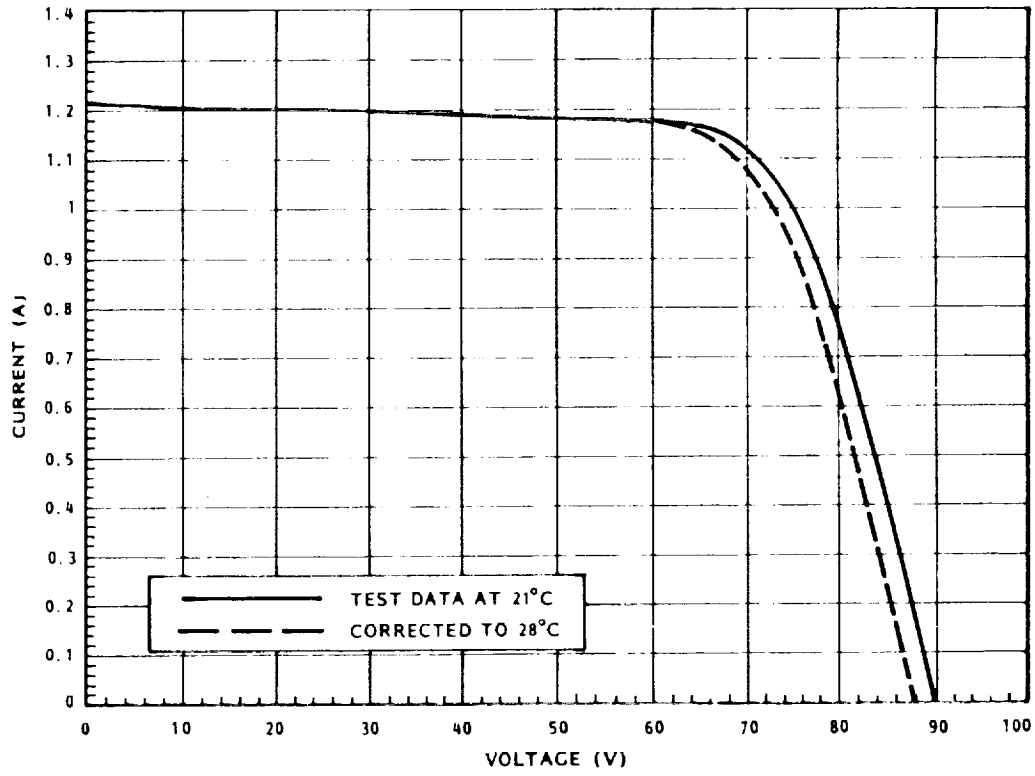

Fig. 2-58 IV Curve From Module of 5.9 × 5.9 cm Cells—Preflight Flash Test

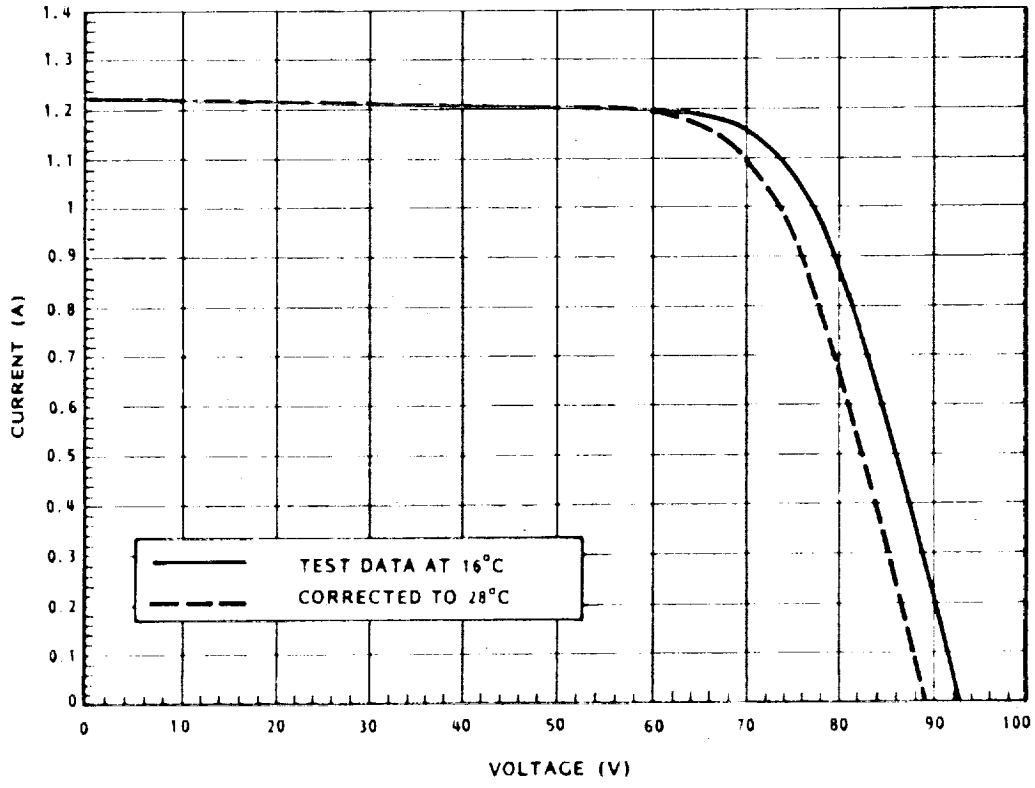

Fig. 2-59 IV Curve From Module of 5.9 × 5.9 cm Cells—Postflight Flash Test

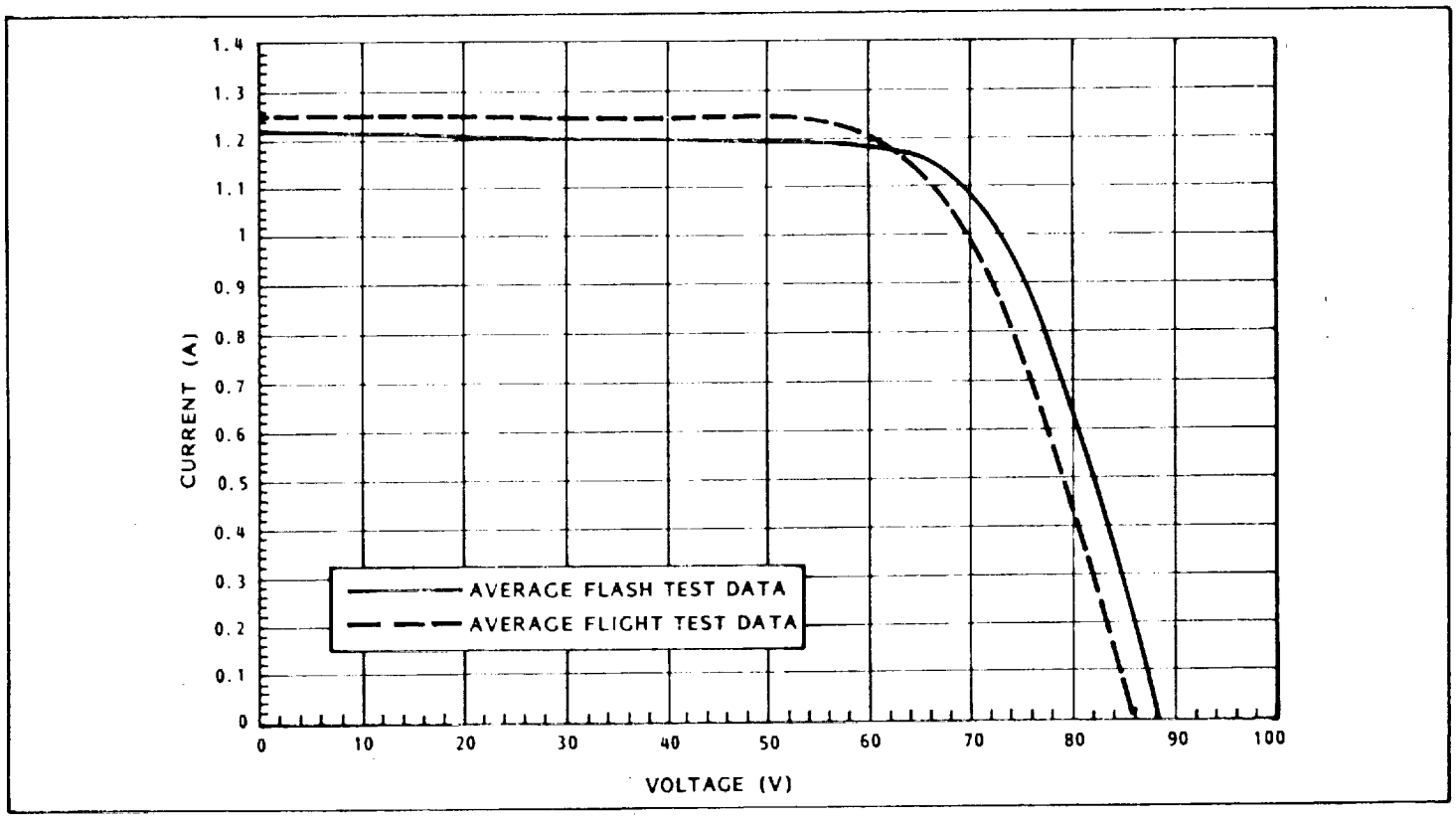

Fig. 2-60 Comparison of IV Curves From Flight and Ground Test for Module of 5.9 × 5.9 cm Cells

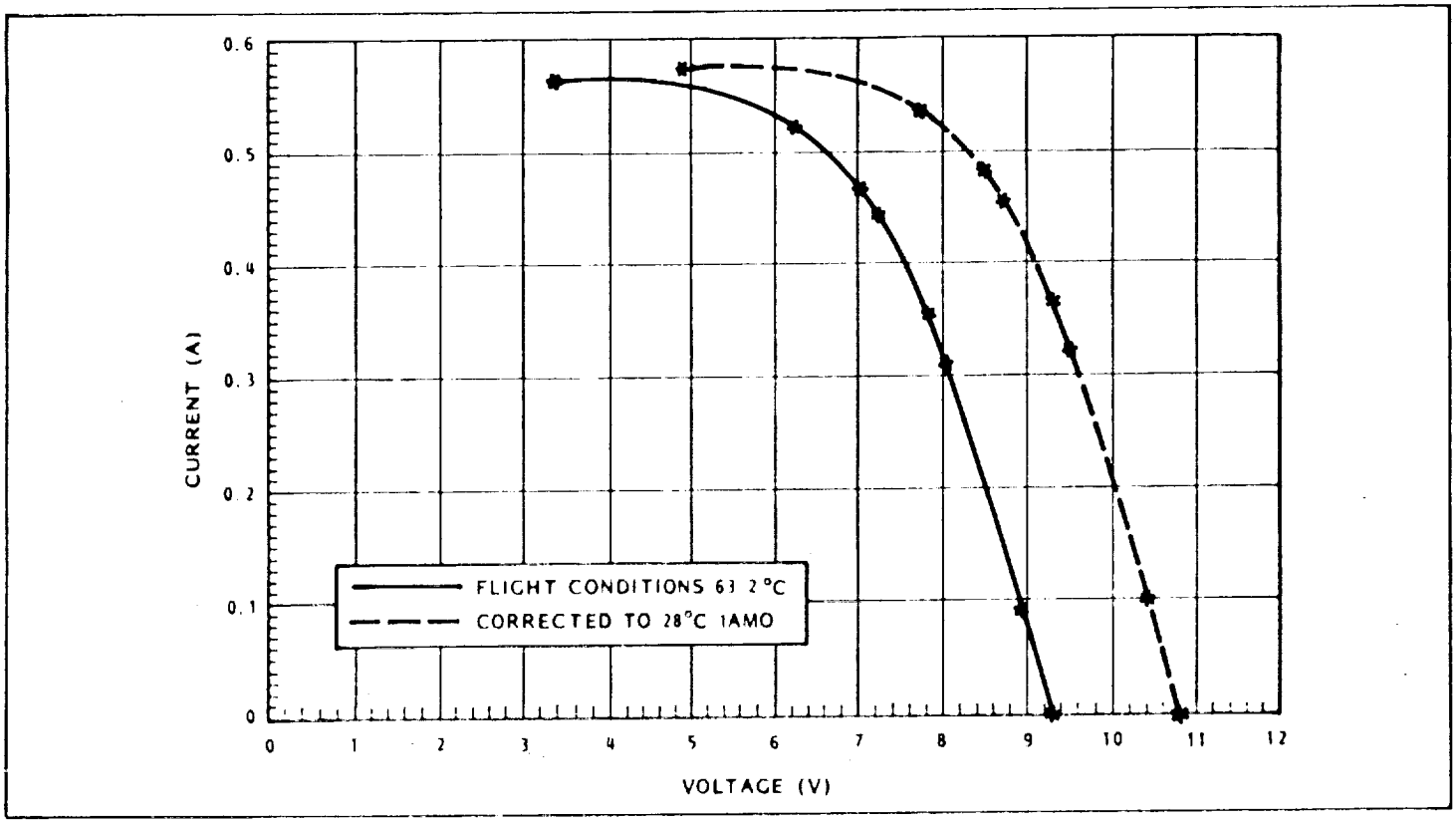

Fig. 2-61 IV Curve From Module of Thin Cells—GMT 246:11:44:34

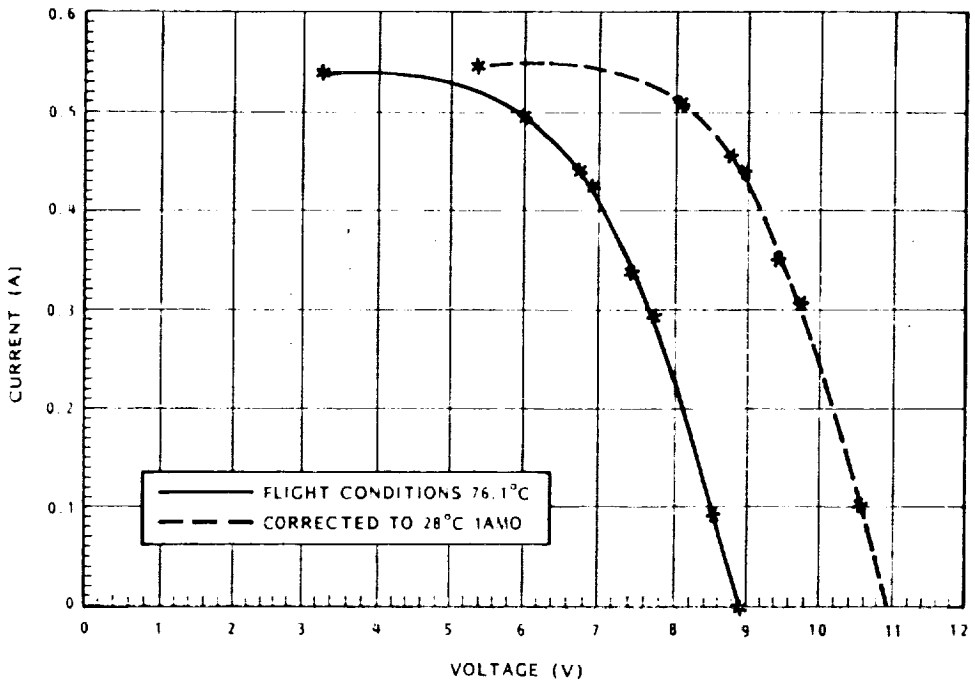

Fig. 2-62 IV Curve From Module of Thin Cells—GMT 246:12:05:24

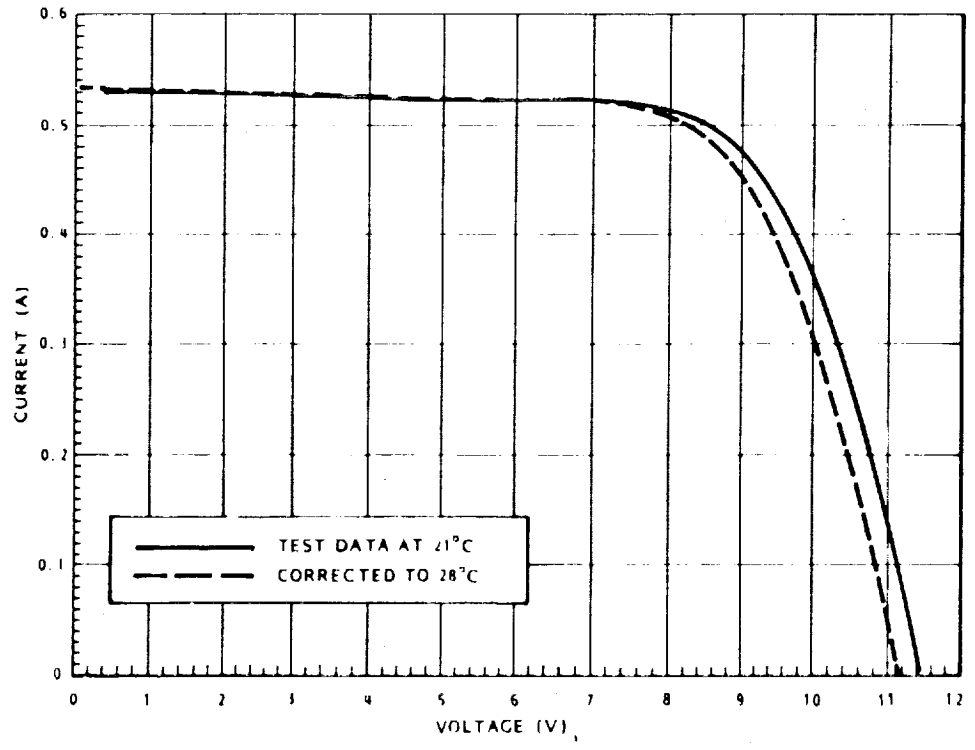

Fig. 2-63 IV Curve From Module of Thin Cells—Preflight Flash Test

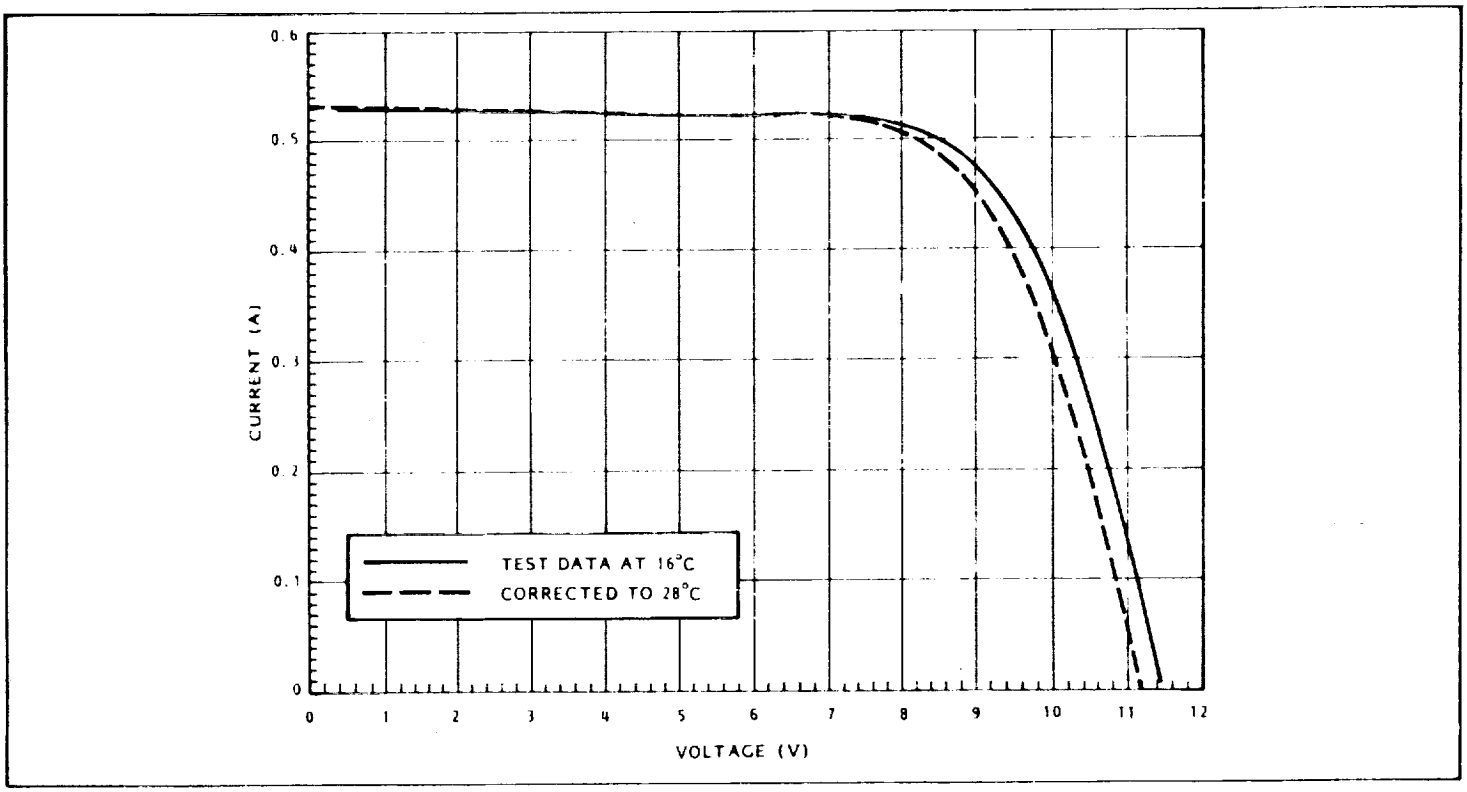

Fig. 2-64 IV Curve From Module of Thin Cells—Postflight Flash Test

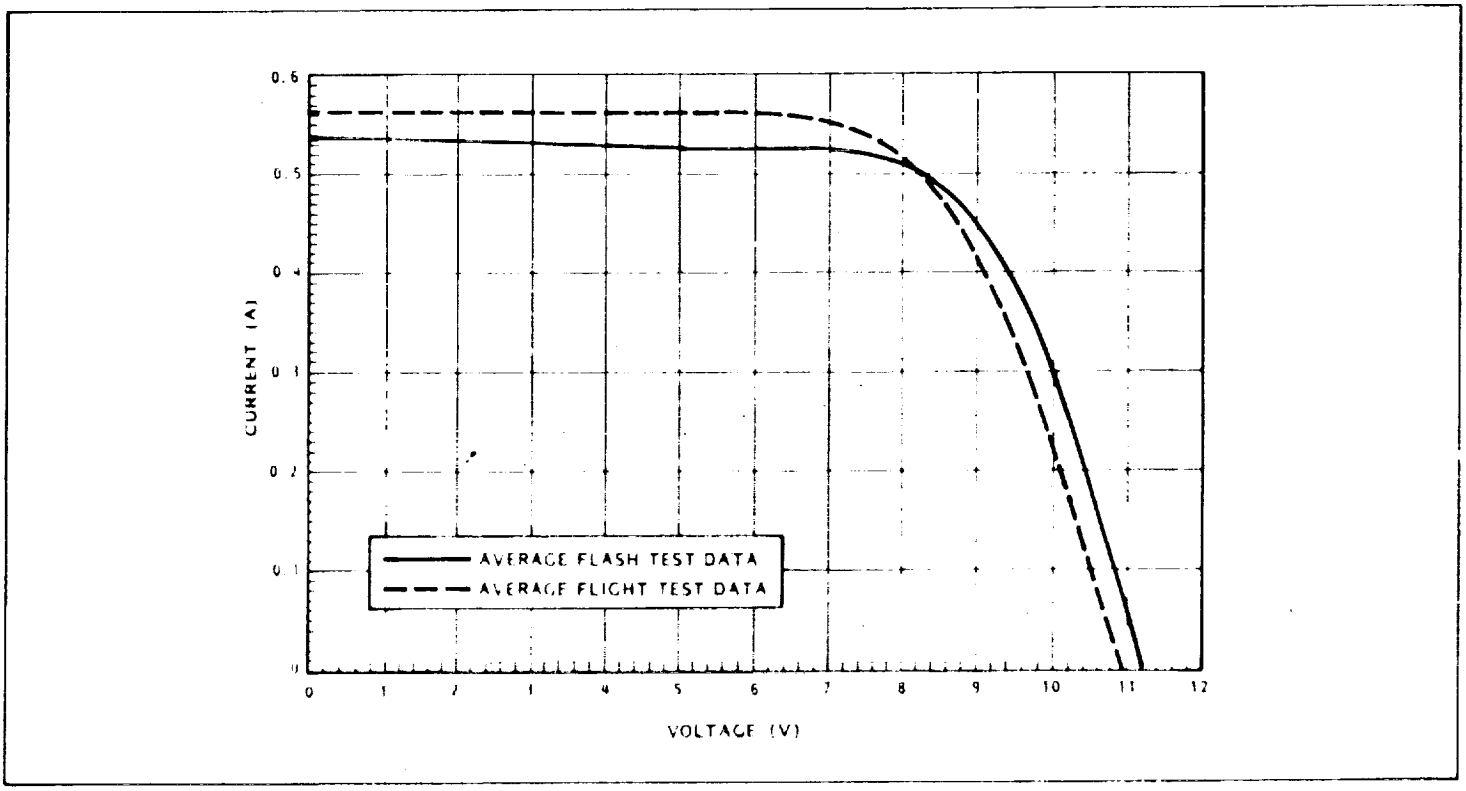

Fig. 2-65 Comparison of IV Curves From Flight and Ground Test for Module of Thin Cells

Final Report

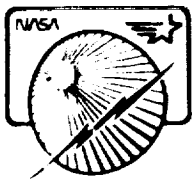

Section 3
Postflight Tests and Inspections

Section 3
POSTFLIGHT TESTS AND INSPECTIONS

Following the return of the orbiter to Kennedy Space Center, the SAFE was removed from the Mission Peculiar Equipment Support Structure and installed on the ground handling dolly. At this time, the wing assembly was visually inspected, and the tape recorder was removed to MSFC for evaluation of the flight data tape. The SAFE was then packaged and shipped to LMSC. Upon arrival at LMSC, the hardware was stored for approximately 2-1/2 months until construction could be completed on the facility that houses the horizontal deployment fixture.

In December 1984, the SAFE was removed from the shipping container and installed in the horizontal deployment fixture. In this fixture, the mast and blanket were extended first to the 70-percent position and then to the 100-percent position. At this time, all hardware was thoroughly inspected. This inspection included the mast and canister, the blanket, and the active solar cells. The mast was then retracted to the 70-percent position and then to a position with the mast extended approximately 15 feet. In this position, a postflight flash test was performed. The mast was then retracted to the fully stowed position and removed from the test fixture. Since its removal from the test fixture, the hardware has undergone three component-level tests. These include the DAS box tests described in Section 2.4.6, the panel-curvature tests described in Section 2.4.3, and the guide-wire negator tests described in Section 2.4.4.

3.1 INSPECTION RESULTS AT THE KENNEDY SPACE CENTER

Visual inspection of the hardware after removal from the orbiter revealed little or no change from its preflight condition. All components were intact, and the panels were neatly stowed in the containment box with the proper preload applied. There was no evidence of distortion or deterioration of any painted or annodized exterior surface.

The only anomalous conditions identified were some score marks on two of the jostle plates and one guide wire that was extended approximately two inches through its attachment hole in the containment box cover. These conditions are shown in Figs. 3-1 and 3-2, respectively.

The jostle plates with the score marks were located diagonally on opposite corners of the experiment. The marks were probably caused by rubbing of the locking lever assemblies on the jostle plates as the wing was retracted with a small amount of twist present. Since the purpose of the jostle plates is to guide the locking-lever assemblies into the proper stowed position, it is concluded that the plates effectively performed this task.

The condition in which a guide wire is not pulled completely through its attachment hole in the cover had been

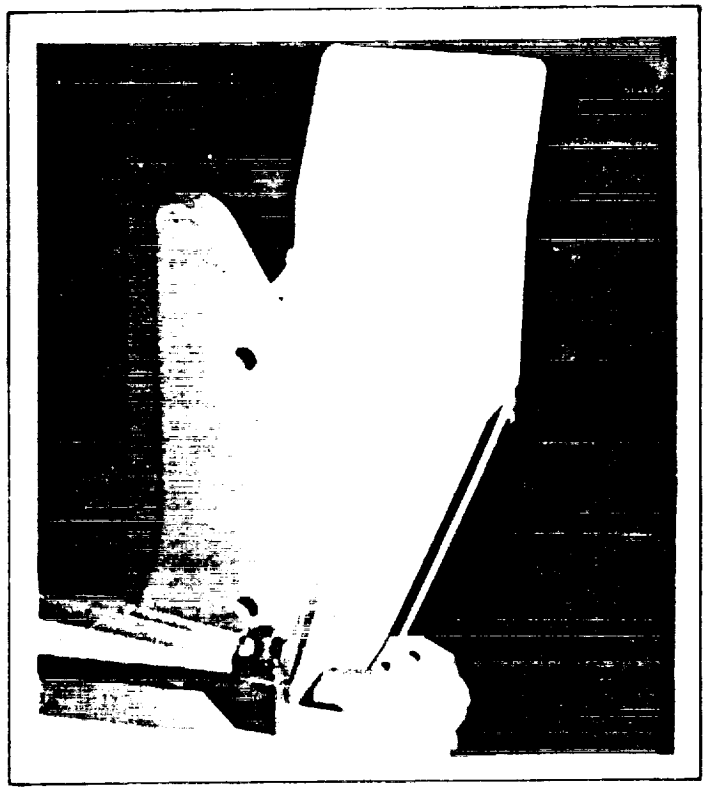

Fig. 3-1 Score Marks on Jostle Plate

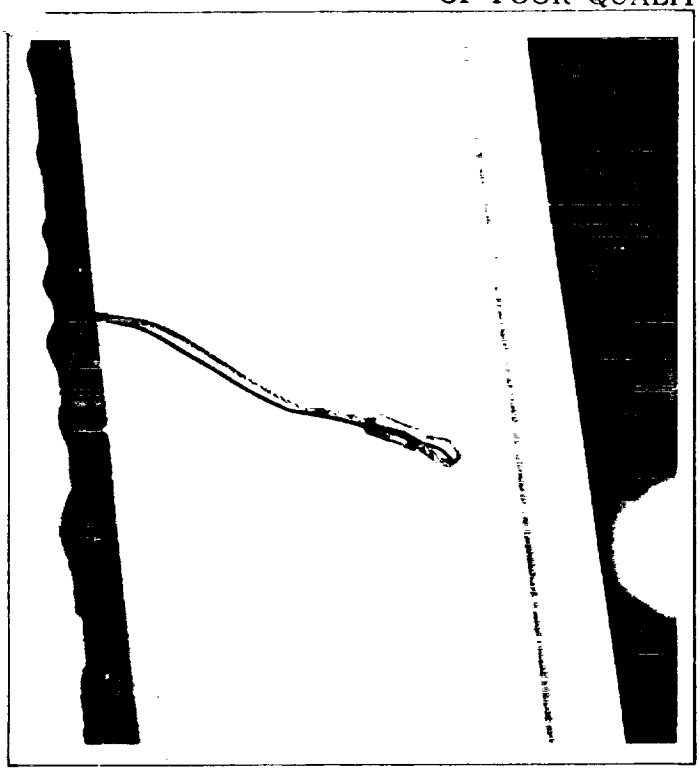

3-2 Guide Wire Extending Through Attachment Hole

observed on many previous occasions during ground tests. The condition occurs because, as the panels begin to acquire preload force, the guide wire grommets at the hinge lines of alternating panels are no longer able to shift laterally. Small misalignments in the stack of panels and, therefore, in the stack of grommets prevent the small reel-in force from the negator (less than 1.0 pounds) from pulling the wire through the stack of grommets. Thus, a small amount of wire is left protruding through the attachment hole in the containment box cover. The small amount of slack wire causes no operational problems because it is immediately pulled taut at the start of a subsequent extension. This was the case in the postflight extension tests performed at LMSC.

3.2 POSTFLIGHT TESTS AND INSPECTIONS AT LMSC

3.2.1 Extension Reaction Performance

The postflight extension and retraction performance of the SAFE wing was essentially unchanged from the preflight performance. Motor current was nominal during extension, retraction, and preloading of the panels. Some panel sticking was apparent, but it had been observed both in the preflight testing and during the first extension in flight. At one point in the extension from 70 percent to 100 percent, the panels moved erratically, but this movement was traced to formation of rust in the track of the deployment fixture. The microswitches controlling the automatic shutoff of the mast performed properly at all positions, as did the microswitches which signal that the locking levers and positive mast lock are properly configured when the wing is fully stowed.

3.2.2 Surface Examinations

At the 100-percent-deployed position of the postflight extension/retraction tests, the SAFE received a thorough visual examination. The hardware was scrutinized not only by the test director and quality assurance representatives but also by a host of interested NASA and LMSC personnel. Of particular interest to many was any evidence of atomic oxygen degradation. Evidence of atomic oxygen degradation to the SAFE panels is not easily detected since the Kapton surfaces were abraided during manufacturing in order to increase the holding power of adhesives used in the construction of the panels. Furthermore, any such degradation would be expected to be slight since (1) the array was only extended for several days, (2) the flight occurred during a period of low solar activity, and (3) the blanket was oriented with its edge aligned with the velocity vector for most of the flight. Consequently, no atomic oxygen degradation was visually detectable. In addition, no micrometeorite damage was visually detectable.

In fact, the only contamination discovered on any of the experiment surface was a small amount of black material on the outermost photogrammetric targets. Chemical evaluation of this material showed it to be BRAYCO grease, which had been applied in excess to the axles of the rollers on the longeron pivot fittings. The black color of the grease came from particles of hard annodizing from the rollers and interior surfaces of the rotating nut. In addition, the chemical analysis revealed the presence of a waxy substance in the contamination. The source of the wax was traced to the strands of stainless steel wire used for the diagonal cables.

3.2.3 Mechanical Condition

Although the SAFE was found to be in basically excellent condition, the postflight examinations did reveal several small anomalies. The most obvious of these was a stretching beyond its elastic limit of one of the small springs on the final tension bar. A photograph of the subject spring is shown in Fig. 3-3. No specific cause for the spring's condition could be identified. However, the final tension bar and the springs that attach to it must nest compactly into the container along side the panels; thus, there is a large amount of hardware near the spring on which it could snag. Because many such springs are distributed across the final tension bar, the damage to one of

them did not impair the performance of the blanket tensioning system.

Another small anomaly was detected on two of the small leaf springs located at the panel hinge lines. On one of these springs, the Kapton tape that secures the two leaves of the spring had debonded. At another location, the tape had debonded and the two leaves had flipped by one another. Photographs of these conditions are shown in Figs. 3-4 and 3-5. The cause of the failure was probably poor surface preparation. The loss of spring torque at the location where the leaves flipped by each other caused no panel folding problems; the remaining springs at the hinge line provided the necessary folding torque.

A less easily detected anomaly was a wrinkling of the flat conductor cable at one point on the blanket. This condition is shown in Fig. 3-6. No cause for the wrinkling can be identified. It is possible that the condition existed before flight but was only discovered during the detailed postflight inspection.

One final imperfection observed in the postflight inspection was a small amount of peeling paint on the mid tension bar. The bar was also slightly curved. Preflight photographs, however, show a similar degree of curvature and, in fact, evaluation of the tension loads on the bar indicate that it should be curved. Therefore, the only anomalous condition was the peeled paint, probably caused by poor surface preparation.

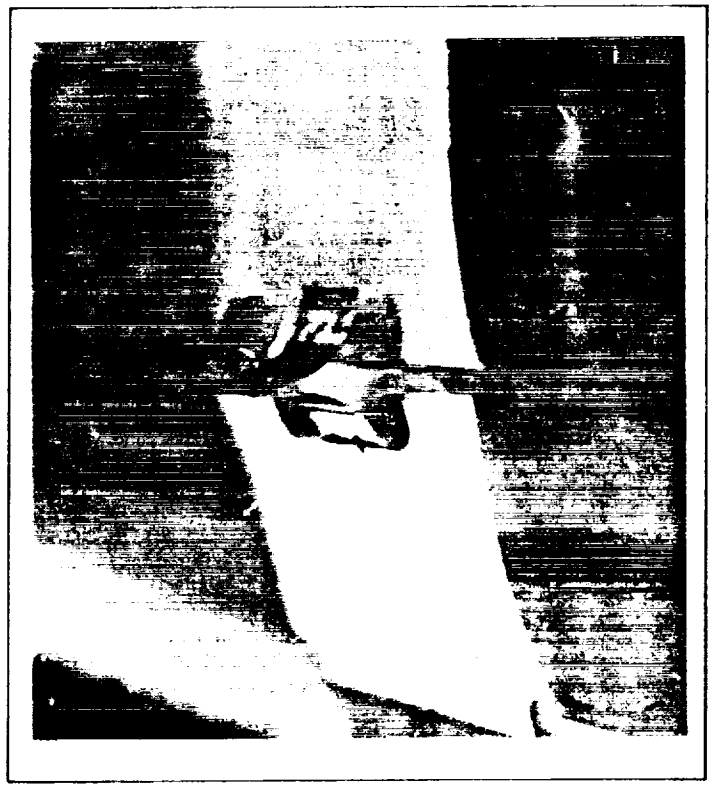

Fig. 3-4 Debonded Tape on Hinge Spring

Fig. 3-3 Overstretched Spring on Final Tension Bar

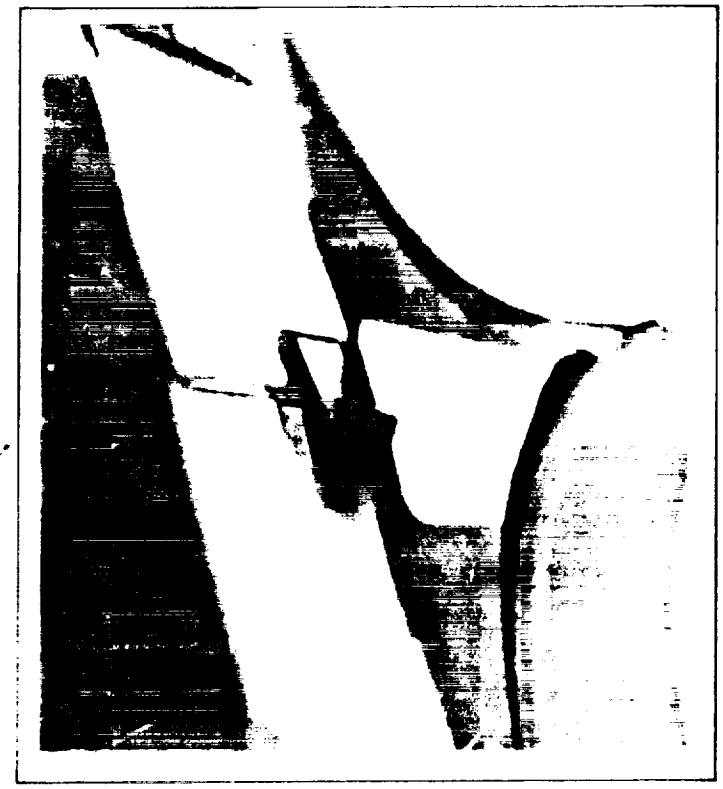

Fig. 3-5 Hinge Spring Anomaly

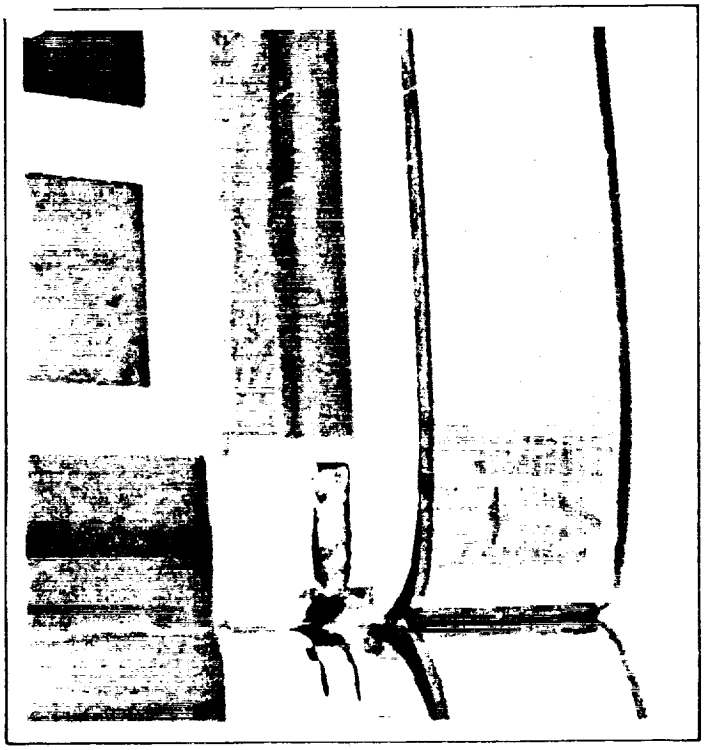

Fig. 3-6 Wrinkled Flat Conductor Cable

3.2.4 Active Solar Cell Examination

In the postflight examination of the SAFE, the active solar cells were inspected to determine if any damage had resulted from the flight activities. This inspection is particularly difficult because access to the panels is restricted and lighting conditions are hard to control when the panels are suspended from the deployment test fixture. These conditions make it difficult to distinguish between hairline cracks in the cell cover slides and actual damage to a cell. Therefore, the postflight inspection was performed by the same individual who performed all of the preflight inspections.

The inspection revealed that no cell damage occurred from the flight activities. These activities include the exposure to ascent vibration and acoustic environments, the multiple extensions and retractions of the array, the on-orbit thermal cycling, the stowage and preloading of the panels for landing, and the landing environments. Consistent with the inspection results, the postflight flash tests provided additional evidence that no cell damage occurred during flight. The postflight flash test results are discussed in Section 2.4.6. These tests showed that the active solar cells produced essentially the same power after the flight as they did before the flight.

Final Report

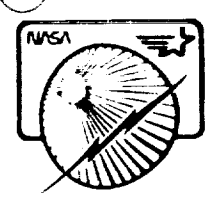

Section 4
Results and Conclusions

Section 4
RESULTS AND CONCLUSIONS

The SAFE mission had three primary objectives:

a. To demonstrate the deployment, retraction, and restowage of the array
b. To measure the dynamic behavior of a large, flexible space structure
c. To measure the on-orbit electrical and thermal performance of the array

Each of these objectives was accomplished. The results of the flight data analysis are summarized in the following sections, according to the mission objective to which they pertain.

4.1 DEPLOYMENT, RETRACTION, AND RESTOWAGE

During three days of on-orbit testing, the SAFE wing was successfully extended to the 70-percent position and retracted four times. On two occasions while at the 70-percent position, it was extended to the 100-percent position and then retracted. On all but the final retraction, the mast motion was manually stopped just short of the point where a significant preload was applied to the panels. On the final retraction, the mast motion was allowed to continue until the panels were properly preloaded to survive the landing environments.

The time required for the mast to extend and retract the array was well within the operational requirements. The extension and retraction rate was somewhat higher than observed in ground test since the voltage supplied by the orbiter was nearly 31 volts, while ground tests were performed at the nominal 28 volts. Interestingly, the extension and retraction rate increased throughout the flight as if the drive system were "wearing in."

Current drawn by the motors was also nominal during the extension and retraction operations. Small variations from the current measured during extension and retraction in ground test can be explained by the voltage variation noted in the previous paragraph and by limitations of the ground support structure. During stowage of the array, when current draw is the highest, the flight current usage closely matched that measured in ground test.

On the first extension from the stowed position to the 70-percent position and during the first extension from the 70-percent position to the 100-percent position, some sticking occurred between adjacent panels. The sticking caused the panels to unfold non-uniformly on these occasions. In all other extension and retraction operations, the panels folded and unfolded in a uniform, accordion-like fashion. The panel sticking behavior had been previously observed in ground testing and was caused by trace amounts of stray adhesive used in construction of the blanket. Only when the panels are preloaded in the container is there enough pressure on them to cause the adhesive to stick adjacent panels together.

During the retraction events, an oscillation in the panels was observed during the last 15 to 20 feet of retraction. The oscillation appeared to be excitation of a local accordion mode with adjacent panels nearly slapping one another at the peak of the excitation. The panel oscillation was caused by a resonance between the rotational frequency of the rotating nut and frequency of the cantilevered mast modes during the last part of the retraction event. The resonant frequency, approximately 0.7 hertz, was apparent from the video tape and accelerometer data.

In all of the extension and retraction events, the microswitches that automatically stop the mast performed properly. On the final restowage of the array, the limit switches on the locking levers and the positive mast lock also performed properly. On no occasion was there any anomaly in the extension, retraction, or restowage performance that required manual intervention.

Upon return to Earth, the solar array panels were found to be neatly stowed in the containment box with the proper preload applied. One of the panel guide wires was protruding through its attachment hole, as had been the condition in previous ground tests. At the start of wing extension in the ground test fixture, the tension from the negator assembly properly positioned the wire.

Close inspection of the extended wing assembly showed it to be in remarkably good condition. Only four significant anomalies in the experiment condition were detected. These consisted of score marks on the jostle plates of the preload mechanism, an overstretched spring on the final tension distribution bar, a tape bond failure at two hinge spring locations, and a small amount of contamination visible on the photogrammetric targets of the outermost panels.

The score marks on the jostle plates were probably caused by rubbing of the locking lever assemblies on the jostle plates as the experiment was retracted with a small amount of twist present. The purpose of the jostle plates is to guide the locking lever assemblies into position, and it appears that they effectively performed this task.

The overstretched spring on the final tension bar was one of many that distribute the tension load from the tension bar into the blanket. Because there are many of these springs and only one was overstretched, operation was not compromised.

Damage to the spring was probably caused by its snagging on nearby hardware. While no specific snag point could be identified, the tension bar and springs are required to rest compactly beside the panels within the container. Therefore, snagging on adjacent hardware during exit from or entrance to the container is a likely cause of the damage.

The tape bond failures at the two hinge spring locations were probably caused by inadequate surface preparation. In one case, the leaf spring halves functioned properly even without the discipline provided by the tape. In the other case, the leaf spring halves flipped by each other causing a loss of spring torque at that location. No panel folding problems resulted since the remaining springs at the panel hinge line provided necessary folding torque.

The contamination discovered on the outermost photogrammetric targets was determined to be BRAYCO grease which had been applied in excess to the axles of the rollers on the longeron pivot fittings. The black color of the grease came from particles of hard annodizing from the pivot fitting rollers and the interior surfaces of the rotating nut.

4.2 DYNAMIC BEHAVIOR

The dynamic behavior of the SAFE was tested on 14 occasions during which the structure responded to planned firings of the orbiter VRCS thrusters. Twelve of these tests were performed with the wing extended to the 70-percent position, and two were performed with it extended to the 100-percent position. Each dynamic test was preceded by a quiescent period during which crew and orbiter activities were restricted so that the initial displacement and velocity of the experiment would be near zero. The thruster firings were followed by a second quiescent period so that data could be taken on a freely responding structure. During the daytime tests, the experiment motion was recorded by the photogrammetry data system; during the nighttime tests, data was recorded with the DAE. Accelerations of the mast tip were recorded during all tests by accelerometers mounted on the containment box cover. Mast-tip motion during the first daylight test at 70-percent extension and at 100-percent extension was monitored by the crew in real time with a 35-mm Nikon camera with a 500-mm lens. Photographs taken at regular intervals with this camera recorded the motion.

Characteristic frequencies and mode shapes of the deployed wing assembly were obtained from an evaluation of the photogrammetry data by LaRC. This information was supplemented with frequency estimates obtained from PSDs of the accelerometer traces processed by MSFC. In both cases, the correlation is excellent between the flight frequency measurements and those predicted in preflight analysis. The mode shape information from LaRC also correlates closely with analytical predictions. The correlation is particularly good at the 70-percent-extended position where frequencies of the first six elastic modes match closely. At 100-percent extension, the predicted frequency for the first out-of-plane bending mode is about ten percent lower than measured. Parametric studies with the analytical model show that the frequency shift cannot be attributed to variations in blanket tension or mast-base compliance. Only when the mast bending stiffness was adjusted could a ten percent frequency shift be achieved. Although variation in mast stiffness may not be the physical cause of the frequency shift, mast stiffness was the analytical parameter that was varied to more closely match the experiment dynamics in subsequent analyses to evaluate the structural damping.

Estimates for structural damping were obtained by adjusting damping values for each of the modes in the structural model until a best match was obtained between the predicted mast-tip accelerations and those obtained from the accelerometers mounted on the containment box cover. This technique is possible because only several modes actively participate in the experiment response to the disturbances caused by the thruster firings. The accelerometer data is believed to be of good quality because the displacement-versus-time data acquired by a double integration of the signal agrees closely with similar data obtained by scaling the mast-tip motion from the photographs taken at regular intervals with the Nikon camera.

The portion of the response that includes the period of thruster firings and shortly thereafter was chosen for damping evaluation. This is the period of maximum structural displacement and maximum loads within the experiment. Damping evaluations performed later in the free response period, when displacements are smaller, might be expected to result in smaller damping estimates. Estimates for damping values are limited to the fundamental modes of the experiment because the participation in the response by higher order modes was negligible; it was impossible to distinguish between a response in these modes and the initial noise level conditions that exist even after a period of quiescence.

Mast-tip motion during most dynamics tests was less than computed in preflight analyses. This difference occurred because the preflight analyses were directed toward producing conservative load estimates for the mast longerons. Therefore, only 0.5-percent model damping was used in the analyses. Damping values considerably higher than this were measured in flight. The measured values at the 70-percent-extended position are approximately five percent for the out-of-plane bending mode and ten percent for the in-plane bending mode. Slightly higher damping values were measured during the nighttime tests than during the daytime tests. The measured values at the 100-percent-extended position are two percent for the out-of-plane bending mode and four percent for the in-plane bending mode. Only daylight tests were performed at this extended position.

The difference between the damping values at 70-percent and 100-percent extension is not understood, but the data for 70 percent are probably more accurate due to the larger number of tests performed at this position. The higher damping for the in-plane bending mode than for the out-of-plane bending mode is believed to be caused by energy losses in the tension-wire negators. These devices are much more active during experiment in-plane motion than during out-of-plane motion. Component tests on the devices have shown that a hysteresis loop in the mechanism could easily have produced the higher damping values measured for the in-plane mode.

4.3 ON-ORBIT THERMAL AND ELECTRICAL PERFORMANCE

The performance of the active solar cells on the SAFE was measured on two occasions while on orbit. During these measurements, the orbiter attitude was controlled so that the plane of the blanket was nominally perpendicular to the solar vector. Only in the first performance test was the attitude maintained for a period that allowed the active cells to reach thermal equilibrium. The perpendicularity of the blanket to the solar vector was less than perfect during the solar cell performance tests due to a 7.8-degree twist in the mast assembly. Additionally, the blanket assumed a curvature about the extension mast during these tests with the edges of the blanket approximately ten inches nearer the crew cabin than the blanket center. These deformations reduced the solar-cell power output by less than one percent.

Before flight, the power output of the active solar cells was periodically measured by performing a flash test on the panel. Since the circuits in the DAS box that measure the solar cell performance in flight cannot be synchronized with the high speed flash, current and voltage measurements in the flash tests were taken directly from the separation connector at the base of the flat conductor cables. Due to the size of the panel and the limitations of the facilities, the flash tests were necessarily performed with the blanket installed in the horizontal deployment fixture. In addition, a visual inspection of the cells was performed with each flash test to record any cell damage due to ground handling. Following the flight, the flash tests and cell inspections were repeated.

The conclusion from comparing the preflight, flight, and postflight solar-cell electrical performance is that the flight environments did not degrade solar cell performance. While the preflight cell inspections regularly revealed cracks in the cell cover slides due to ground handling activities, the postflight inspection revealed no incremental damage over the last preflight inspection. This result means that the solar cell/panel assembly survived transportation to Kennedy Space Center, eight months of preloaded storage before flight, the ascent accoustic and vibration environments, the on-orbit environments (extensions, retractions, dynamics tests, thermal cycling, and restowage), the landing vibration environments, and transportation back to LMSC without performance degradation. This achievement demonstrates the readiness of large-area, lightweight, solar array technology.

LMSC-F087173

Final Report

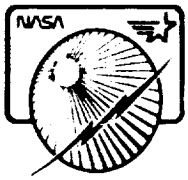

Appendix A
Thruster Firing Time Histories

ORIGINAL PAGE IS
OF POOR QUALITY

THRUSTER FIRING HISTORIES

REFERENCE GMT = 245:19:25:44.6 - FILE 5

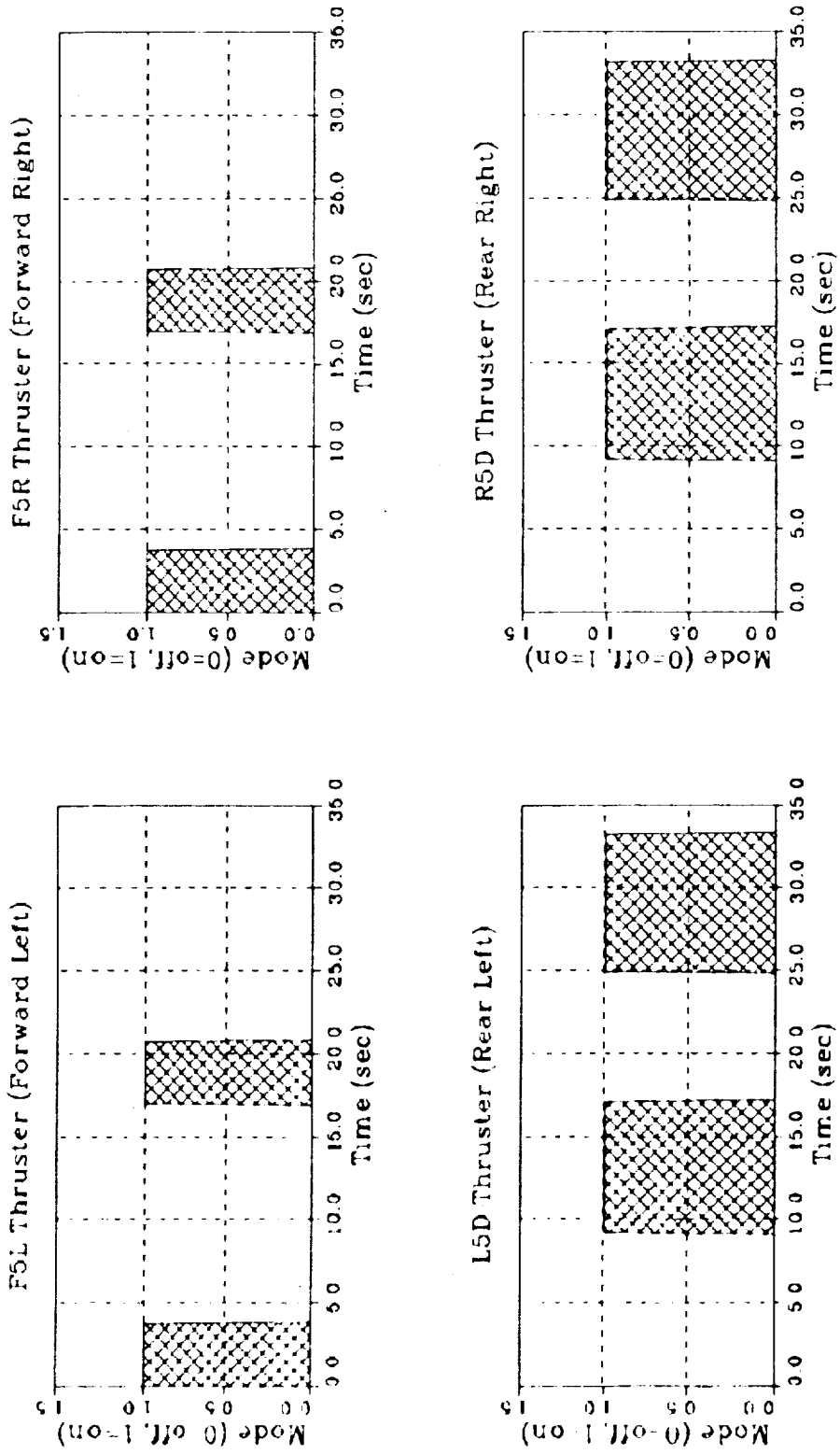

ORIGINAL PAGE IS
OF POOR QUALITY

THRUSTER FIRING HISTORIES

REFERENCE GMT = 245:20:13:45.9 – FILE 6

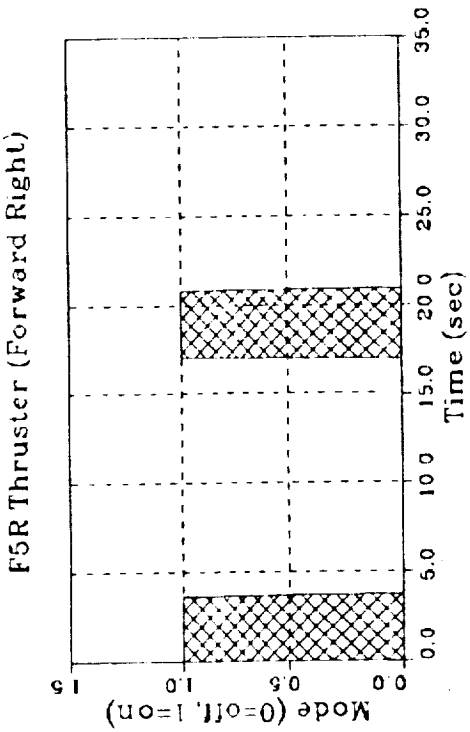

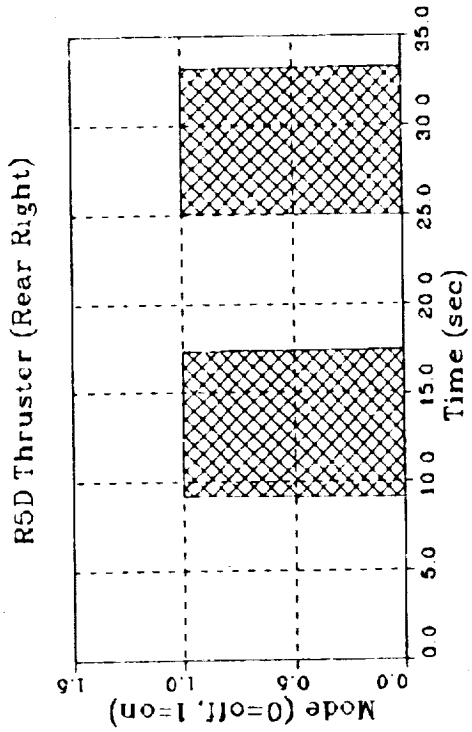

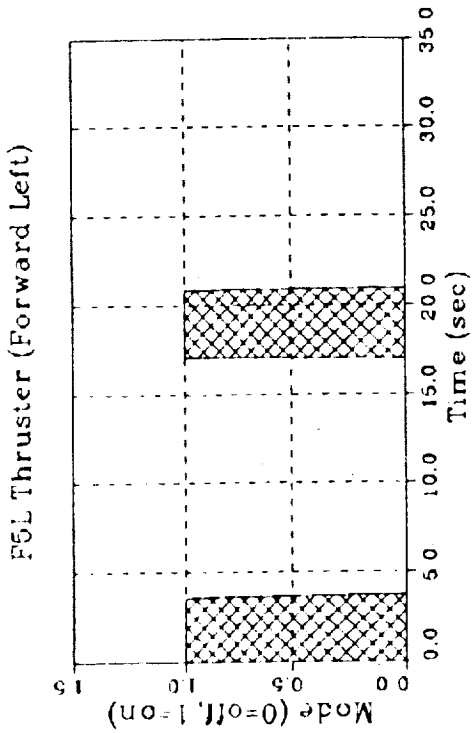

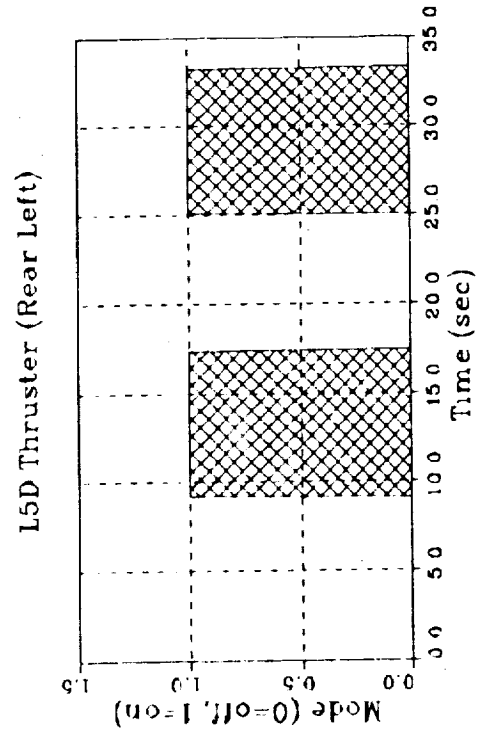

THRUSTER FIRING HISTORIES

REFERENCE GMT = 246:13:29:43.7 – FILE 10

F5L Thruster (Forward Left)

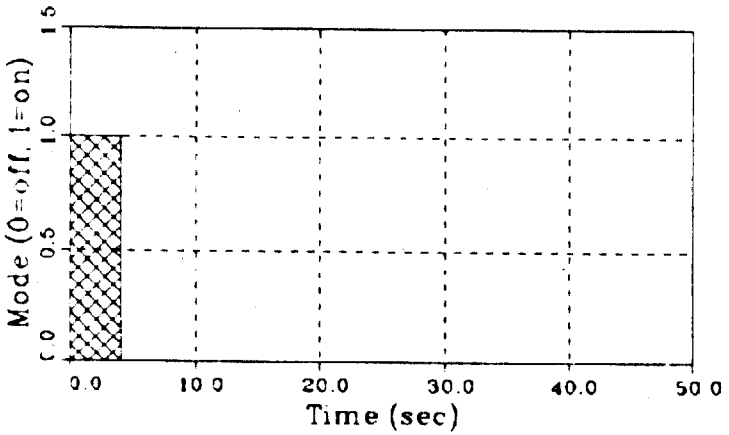

F5R Thruster (Forward Right)

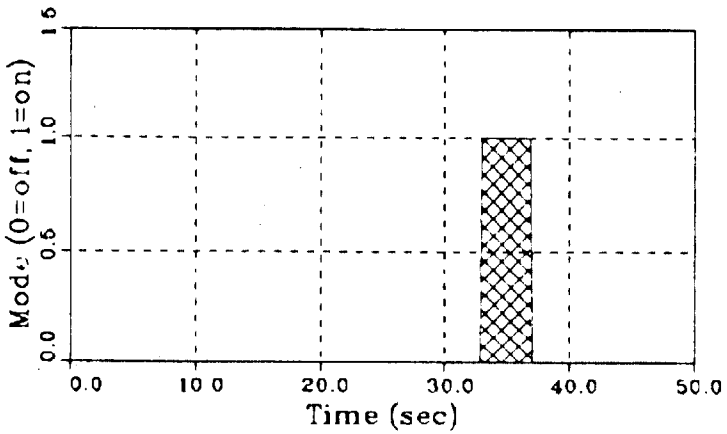

L5D Thruster (Rear Left)

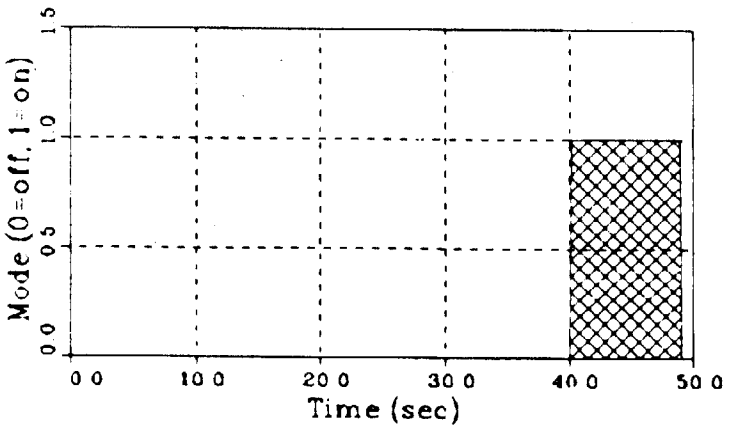

R5D Thruster (Rear Right)

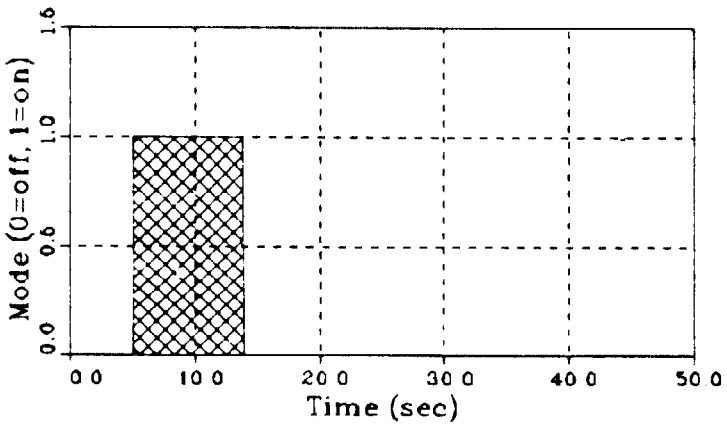

ORIGINAL PAGE IS
OF POOR QUALITY

ORIGINAL PAGE IS
OF POOR QUALITY

THRUSTER FIRING HISTORIES

REFERENCE GMT = 246:14:22: 9.9 – FILE 11

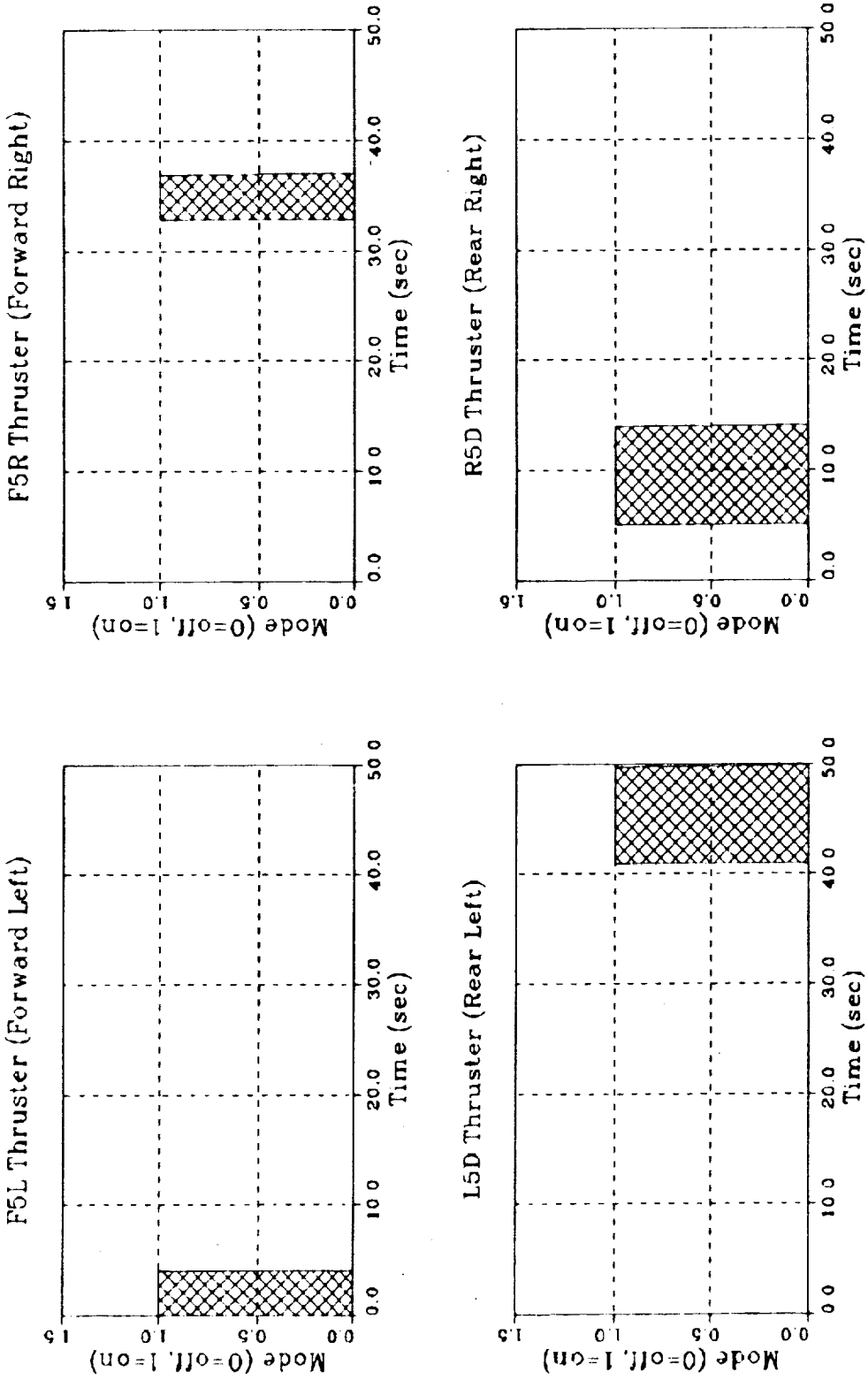

THRUSTER FIRING HISTORIES

REFERENCE GMT = 246 15: 0:42.4 – FILE 12

F5L Thruster (Forward Left)

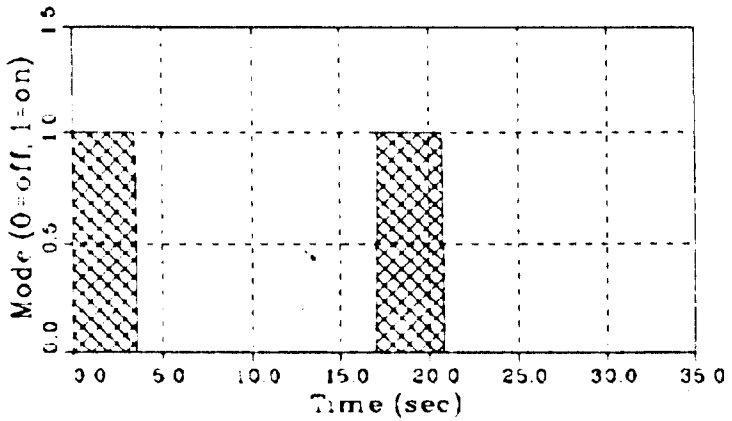

F5R Thruster (Forward Right)

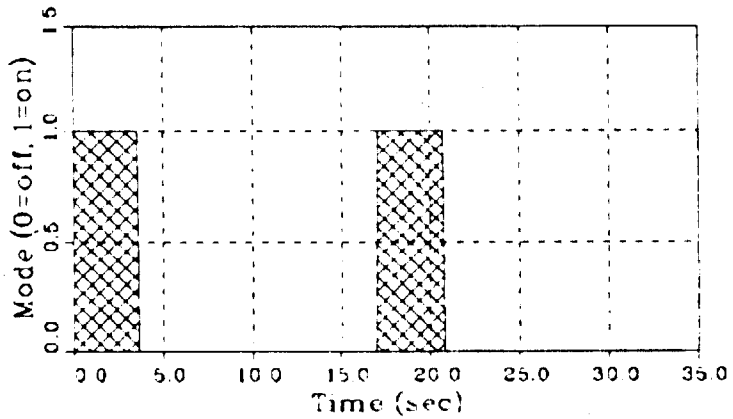

L5D Thruster (Rear Left)

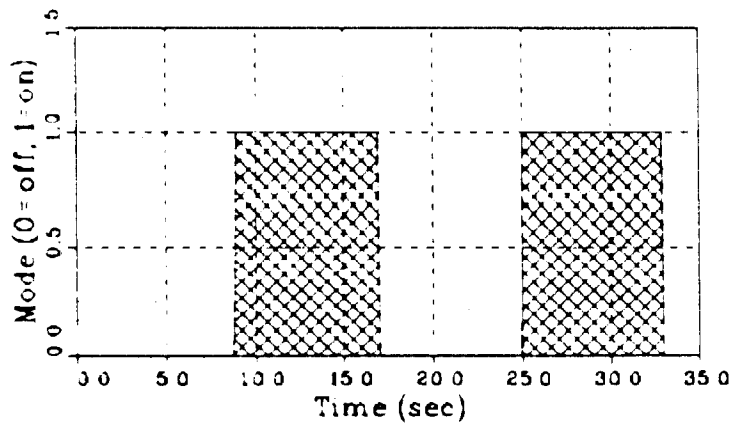

R5D Thruster (Rear Right)

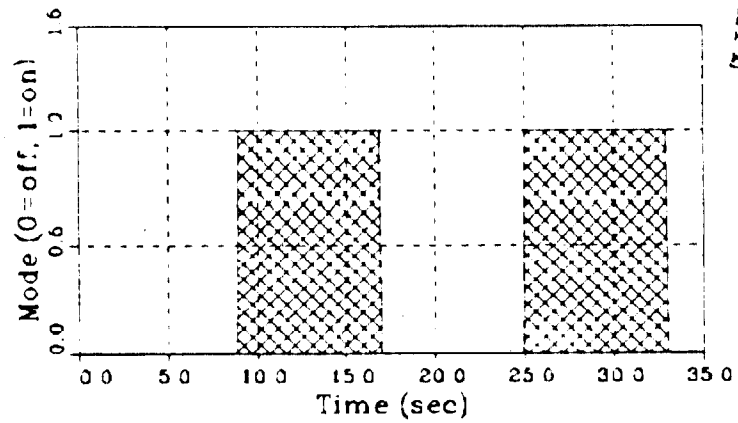

ORIGINAL PAGE IS
OF POOR QUALITY

THRUSTER FIRING HISTORIES

REFERENCE GMT = 246:15:52:50.1 – FILE 13

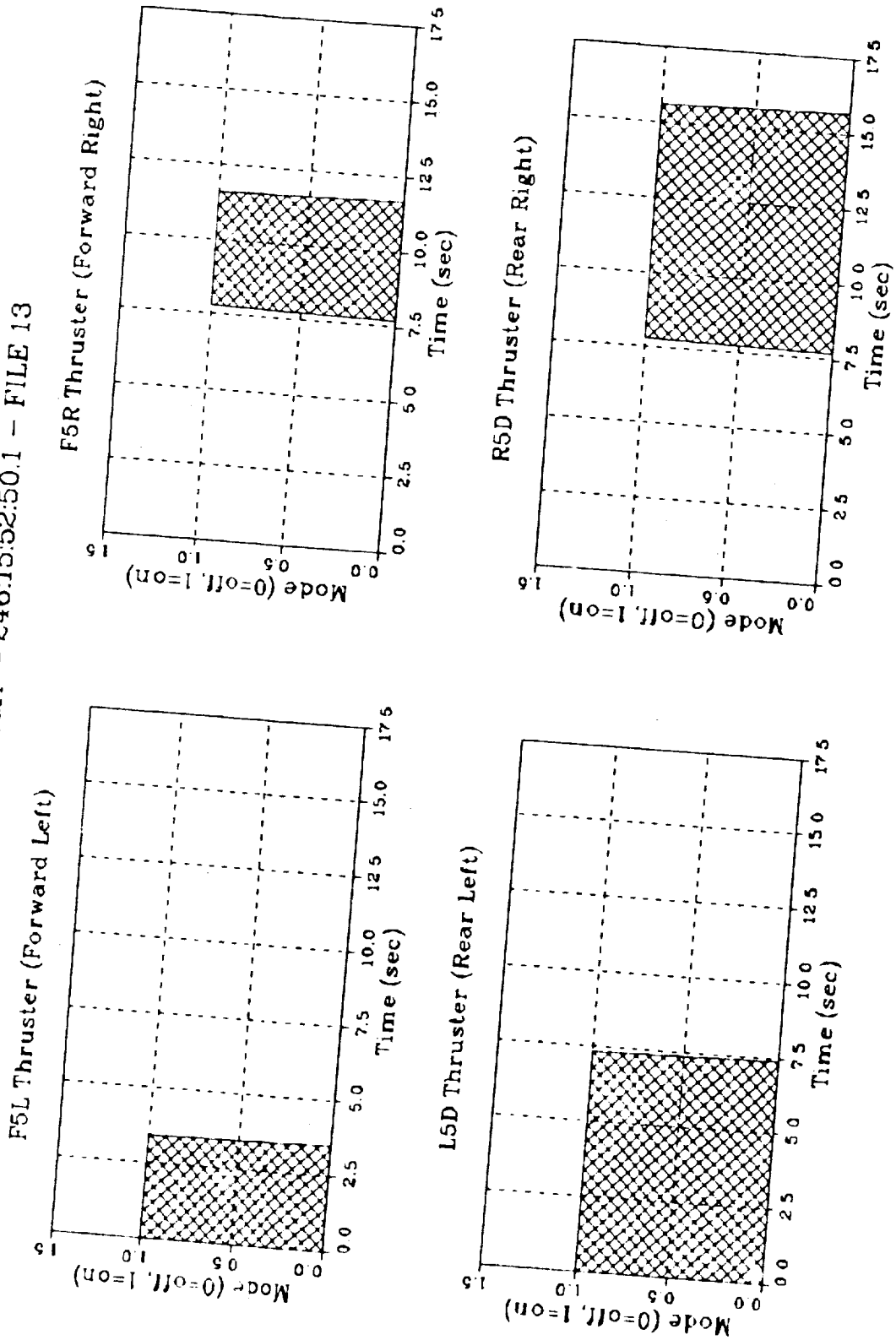

C-2

THRUSTER FIRING HISTORIES

REFERENCE GMT = 246:16:30:43.8 – FILE 14

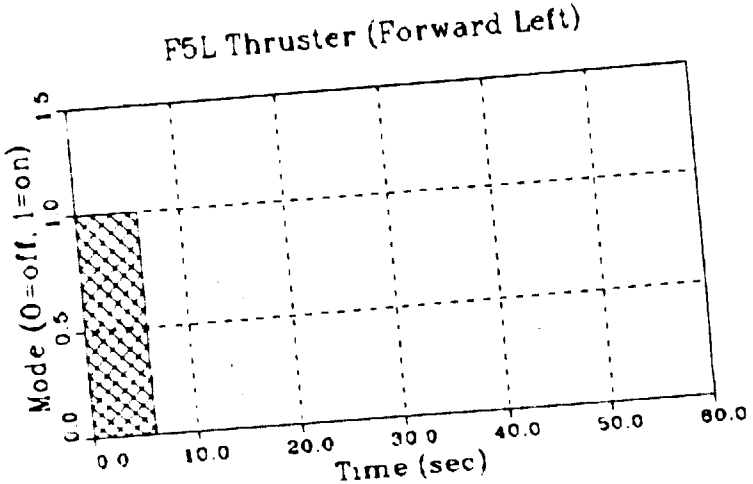

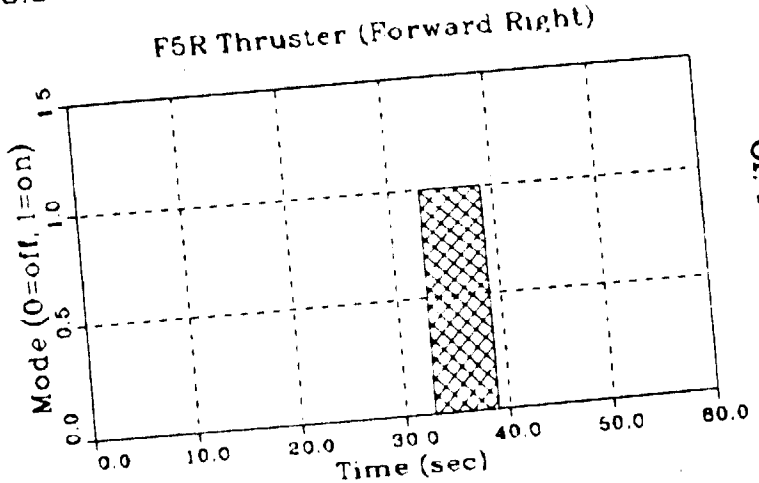

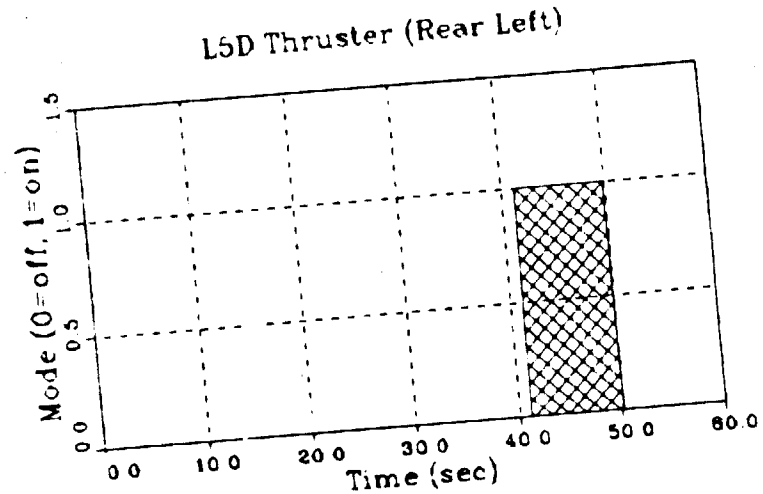

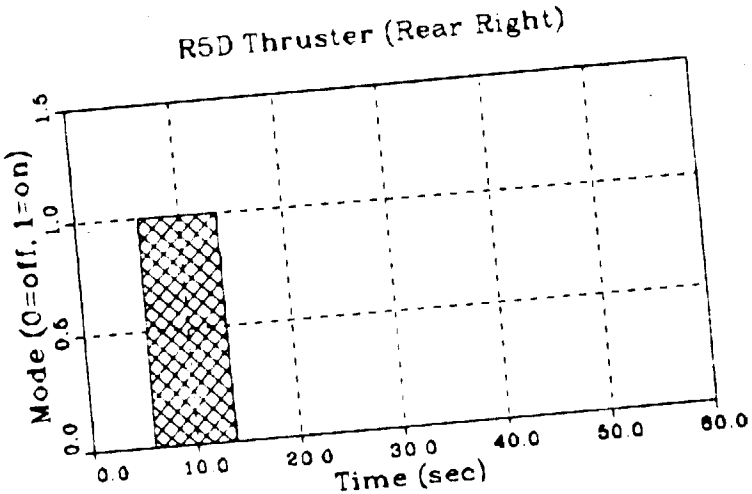

ORIGINAL PAGE IS
OF POOR QUALITY

B-V

THRUSTER FIRING HISTORIES

REFERENCE GMT = 246:17:23:23.6 – FILE 15

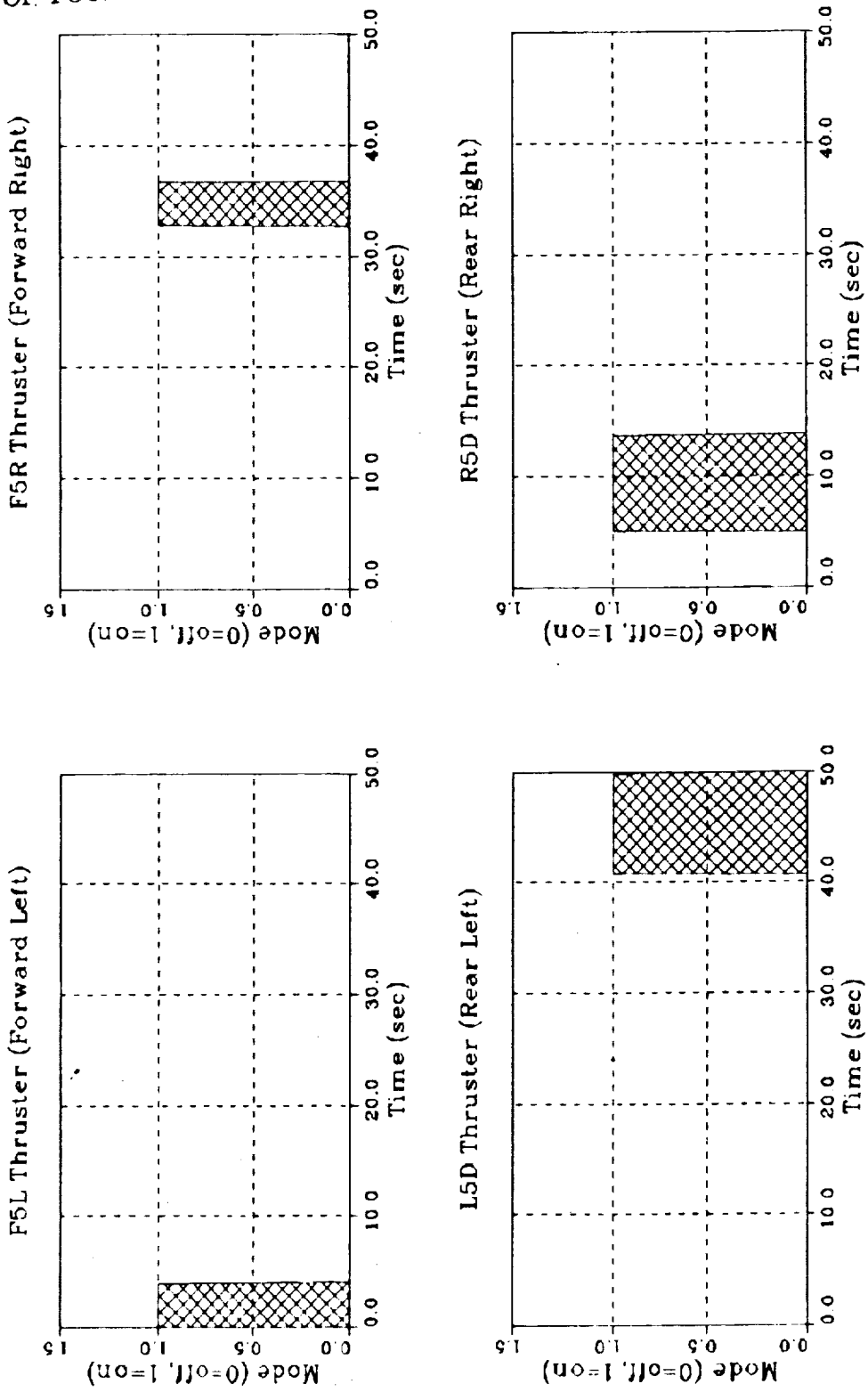

THRUSTER FIRING HISTORIES

REFERENCE GMT = 246:18: 6:44.3 – FILE 17

F5L Thruster (Forward Left)

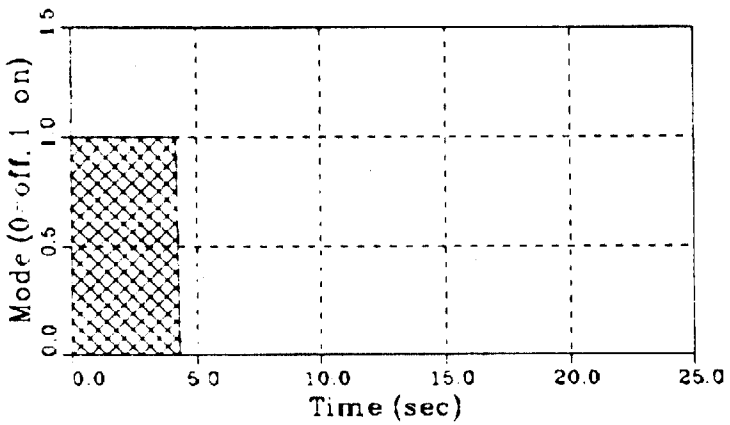

F5R Thruster (Forward Right)

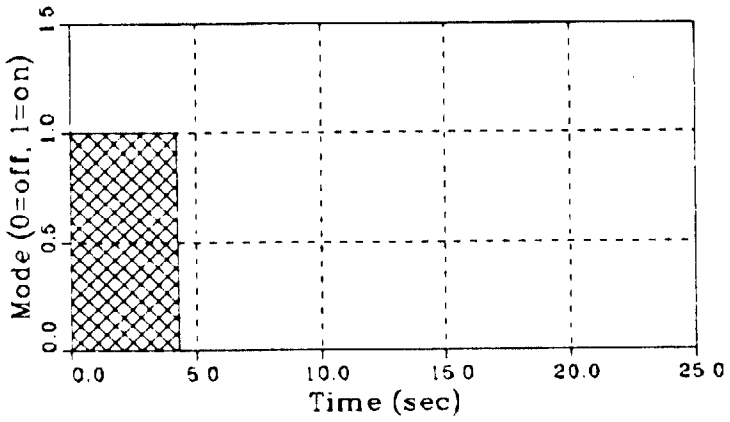

L5D Thruster (Rear Left)

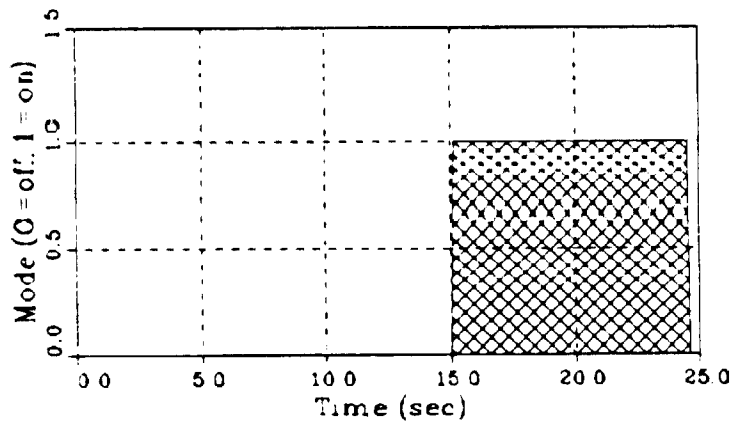

R5D Thruster (Rear Right)

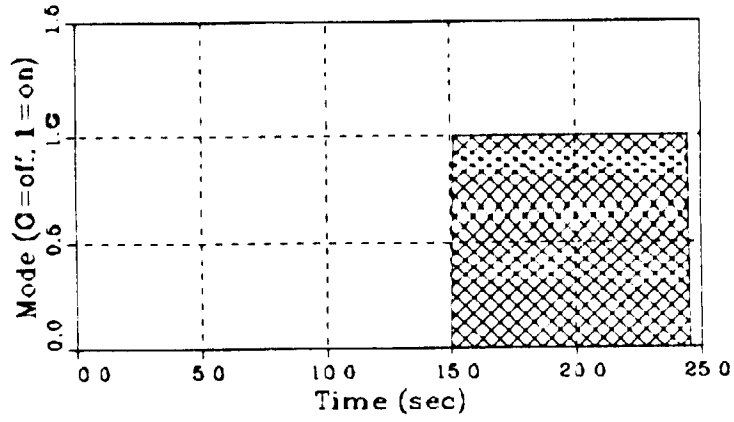

ORIGINAL PAGE IS
OF POOR QUALITY

ORIGINAL PAGE IS
OF POOR QUALITY

THRUSTER FIRING HISTORIES

REFERENCE GMT = 246:19:31:47.4 – FILE 20

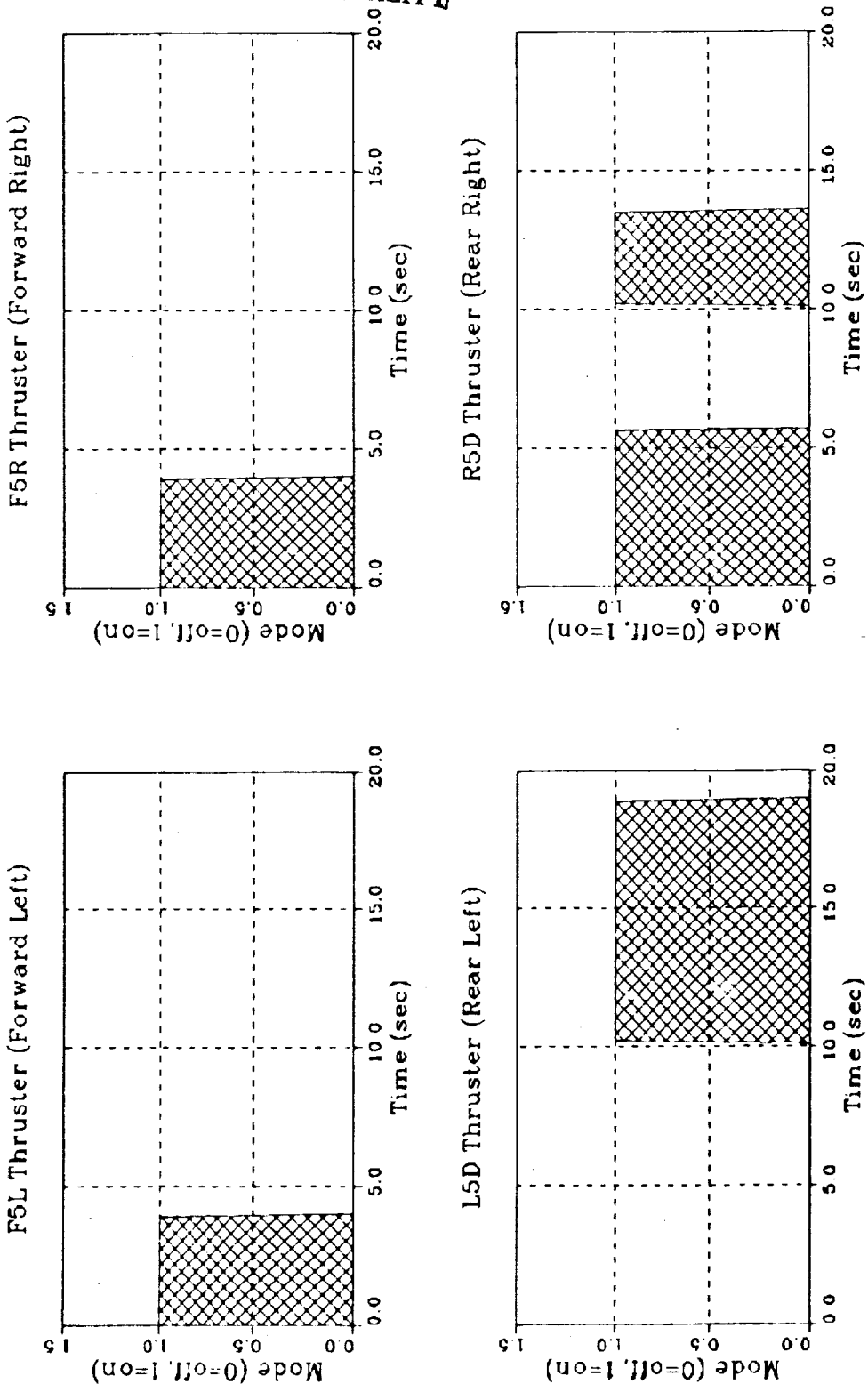

ORIGINAL PAGE IS
OF POOR QUALITY

THRUSTER FIRING HISTORIES

REFERENCE GMT = 247 17 32.58 + FILE 28

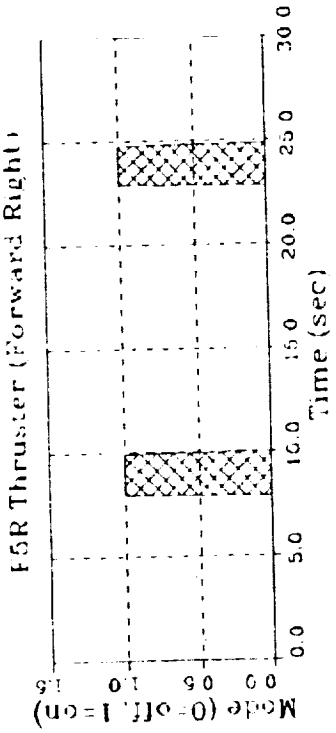

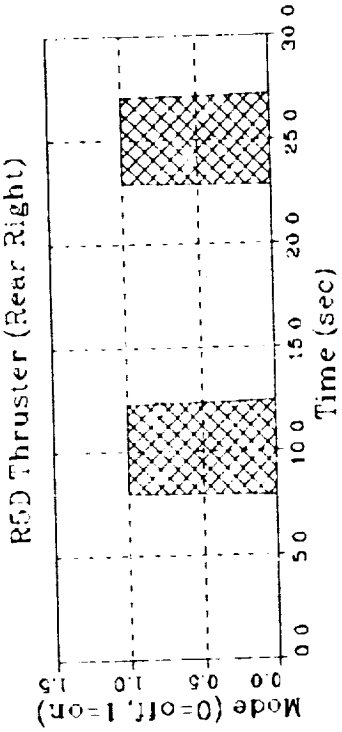

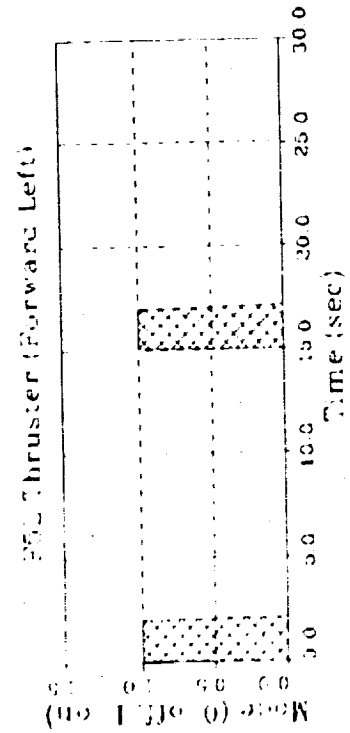

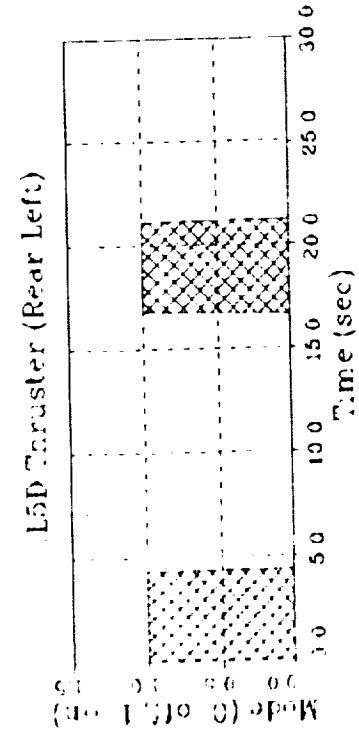

PRECEDING PAGE BLANK NOT FILMED

A-12
A-13

ORIGINAL PAGE IS
OF POOR QUALITY

THRUSTER FIRING HISTORIES

REFERENCE GMT = 247:18: 7:45.6 – FILE 29

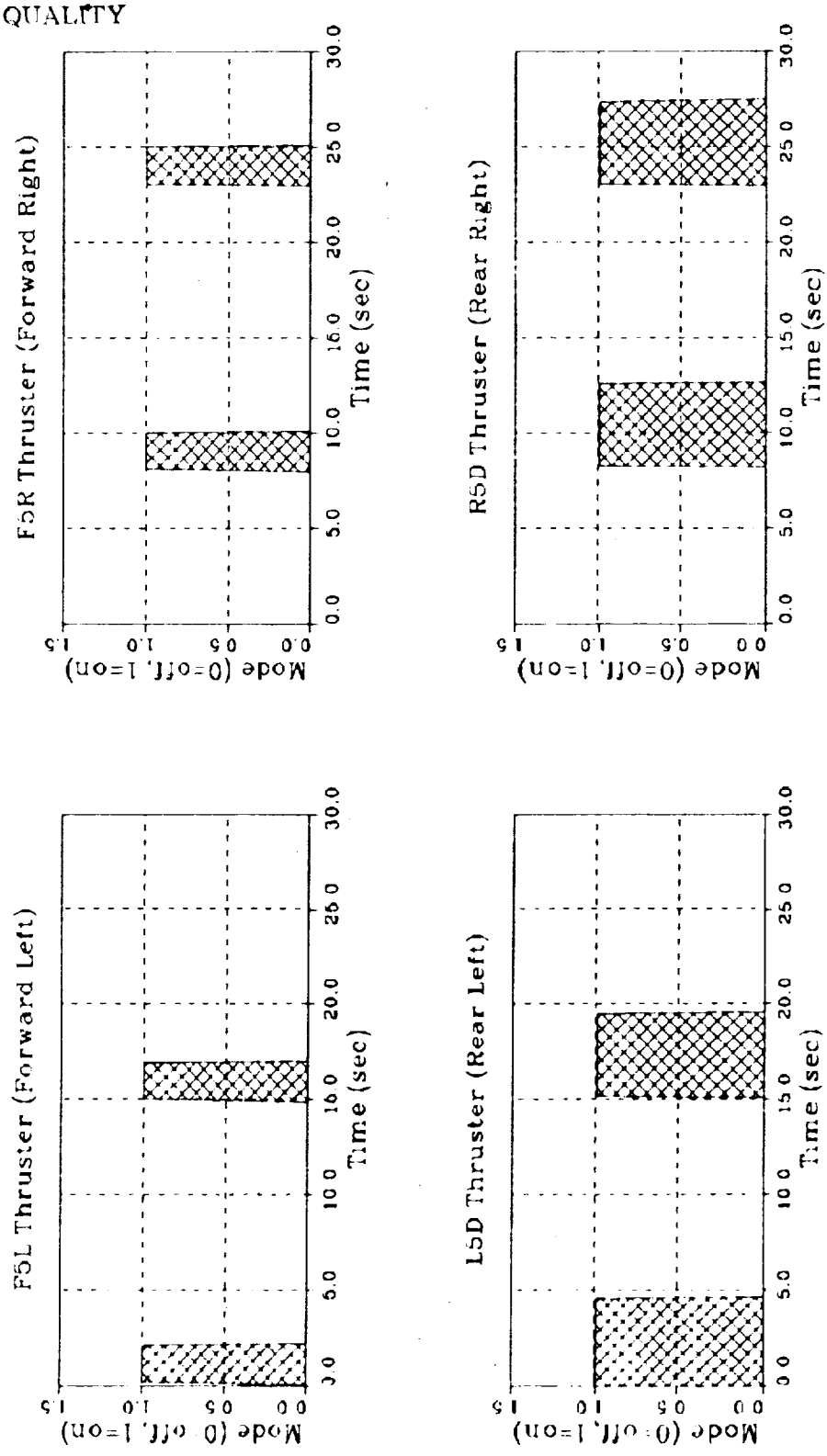

Final Report

LMSC-F037173

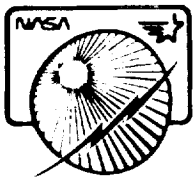

Appendix B
Computed Accelerations at Experiment Base

ORIGINAL PAGE IS
OF POOR QUALITY

BASE ACCELERATION HISTORY IN STS COORDINATES

REFERNECE GMT = 245:19:25:44.6 – FILE 5

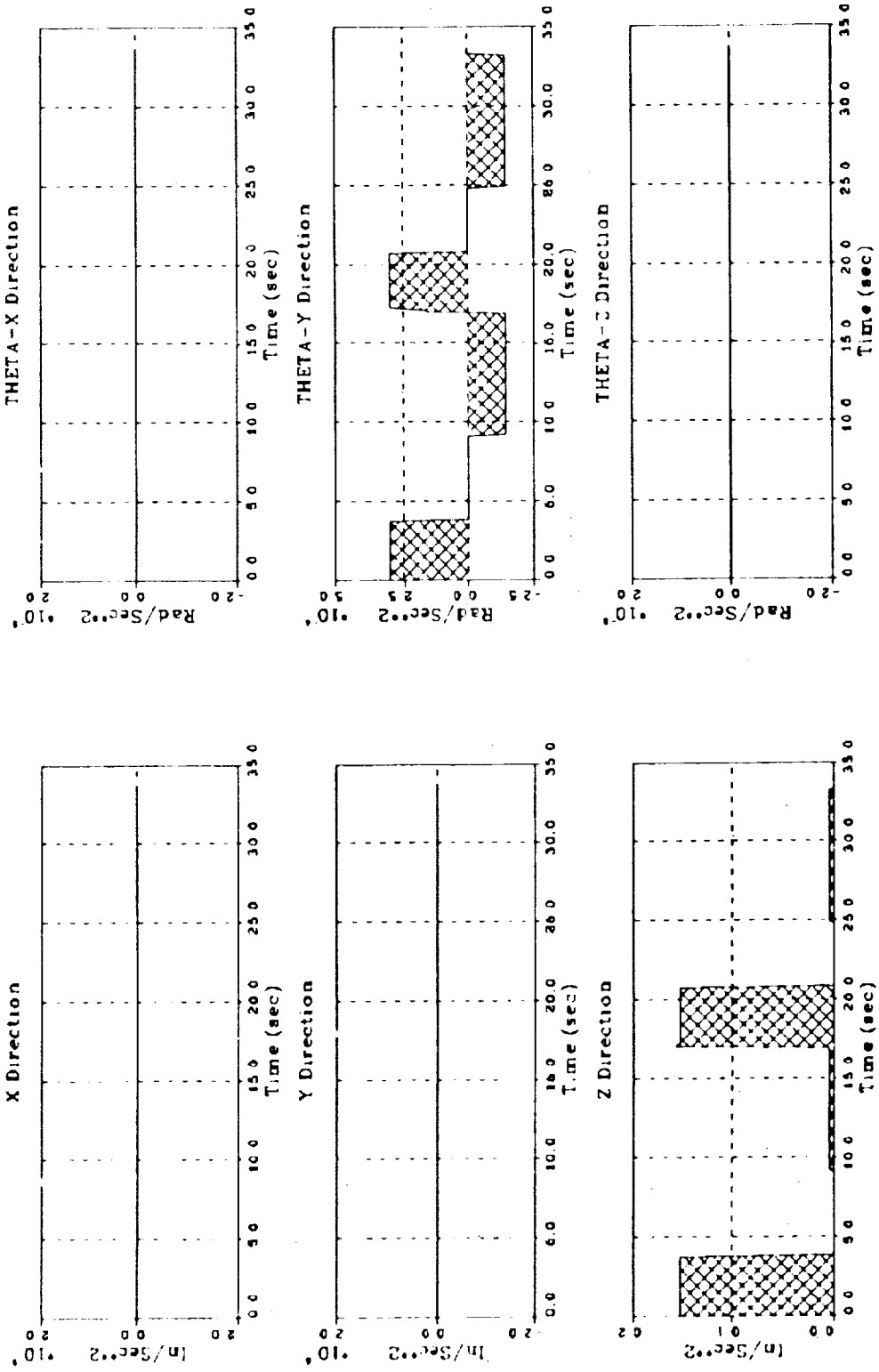

ORIGINAL PAGE IS
OF POOR QUALITY

BASE ACCELERATION HISTORY IN STS COORDINATES

REFERNECE GMT = 245:20:13:45.9 – FILE 6

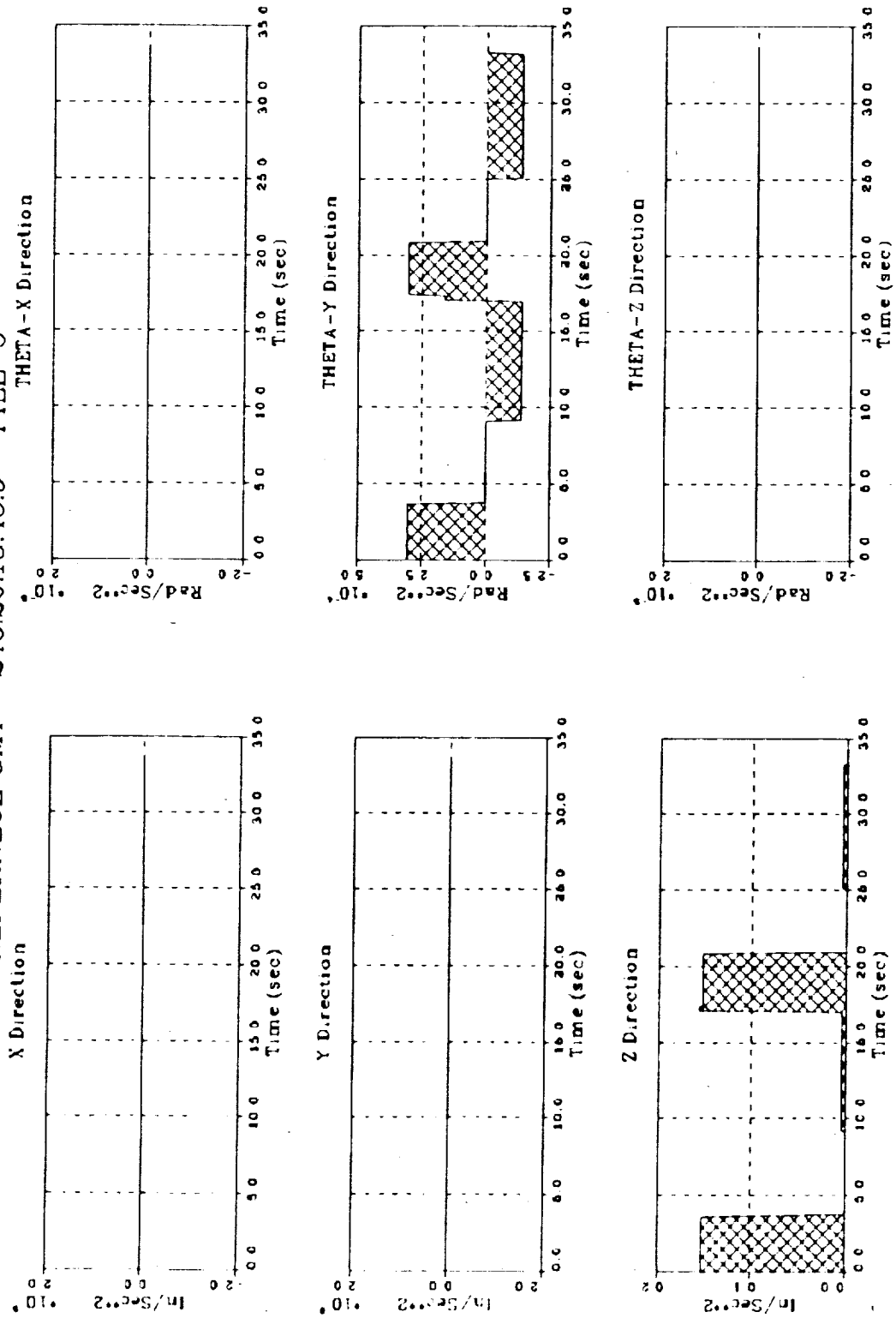

BASE ACCELERATION HISTORY IN STS COORDINATES

REFERNECE GMT = 246:13:29:43.7 – FILE 10

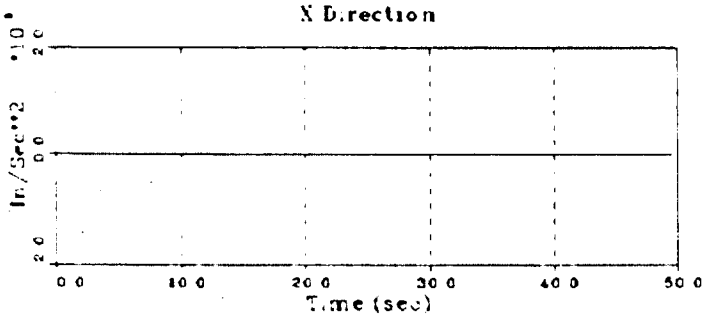

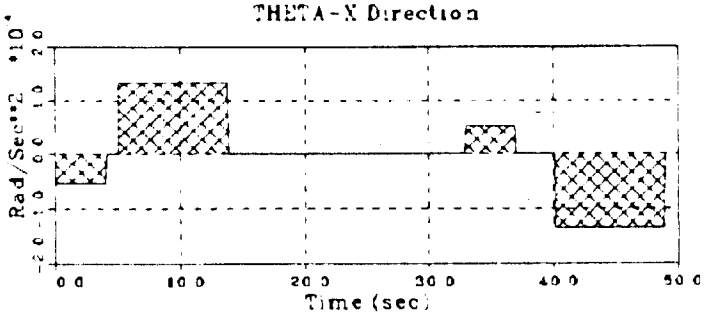

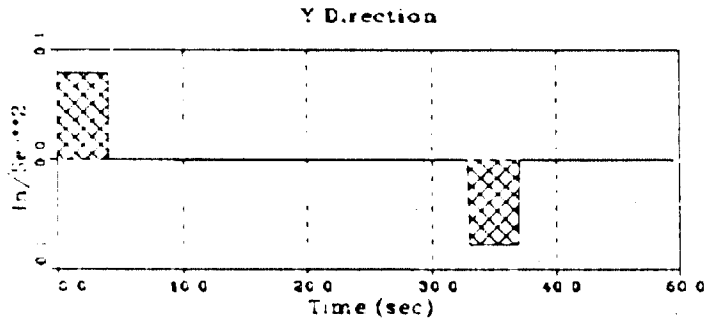

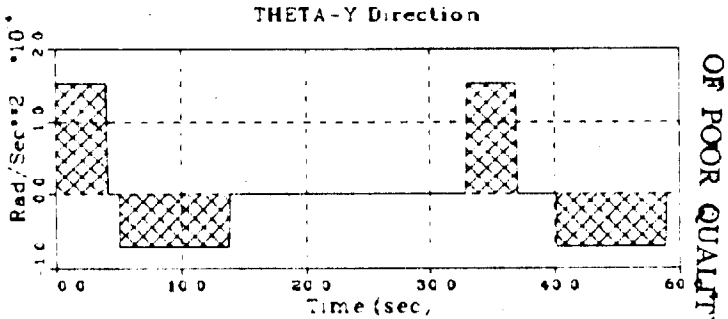

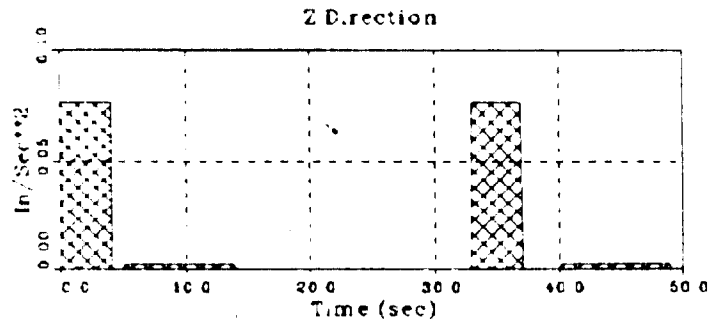

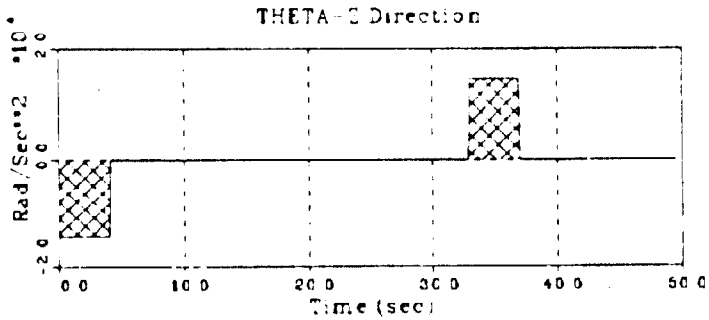

ORIGINAL PAGE IS
OF POOR QUALITY

ORIGINAL PAGE IS
OF POOR QUALITY

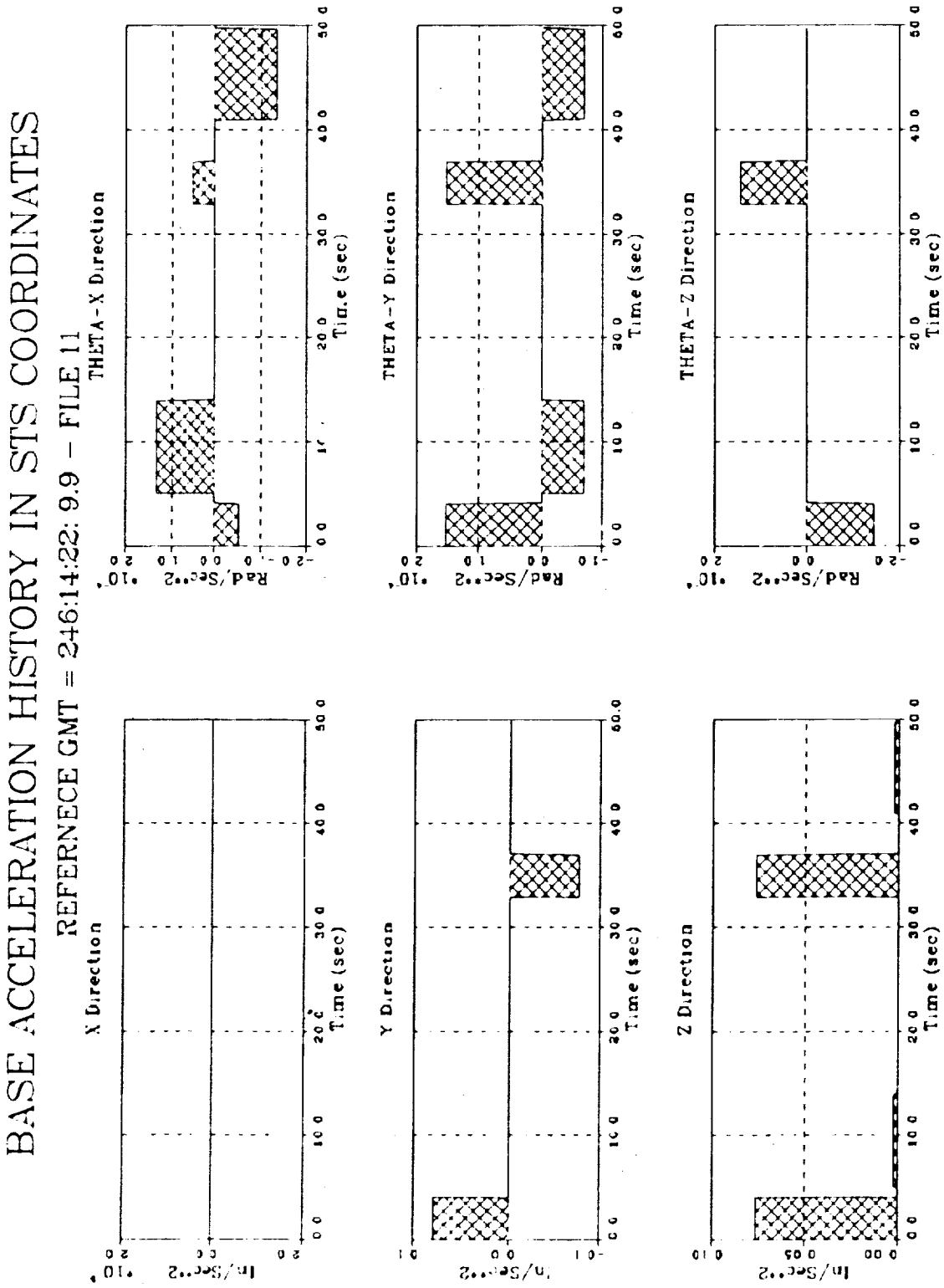

ORIGINAL PAGE IS
OF POOR QUALITY

BASE ACCELERATION HISTORY IN STS COORDINATES

REFERNECE GMT = 246:15: 0:42.4 – FILE 12

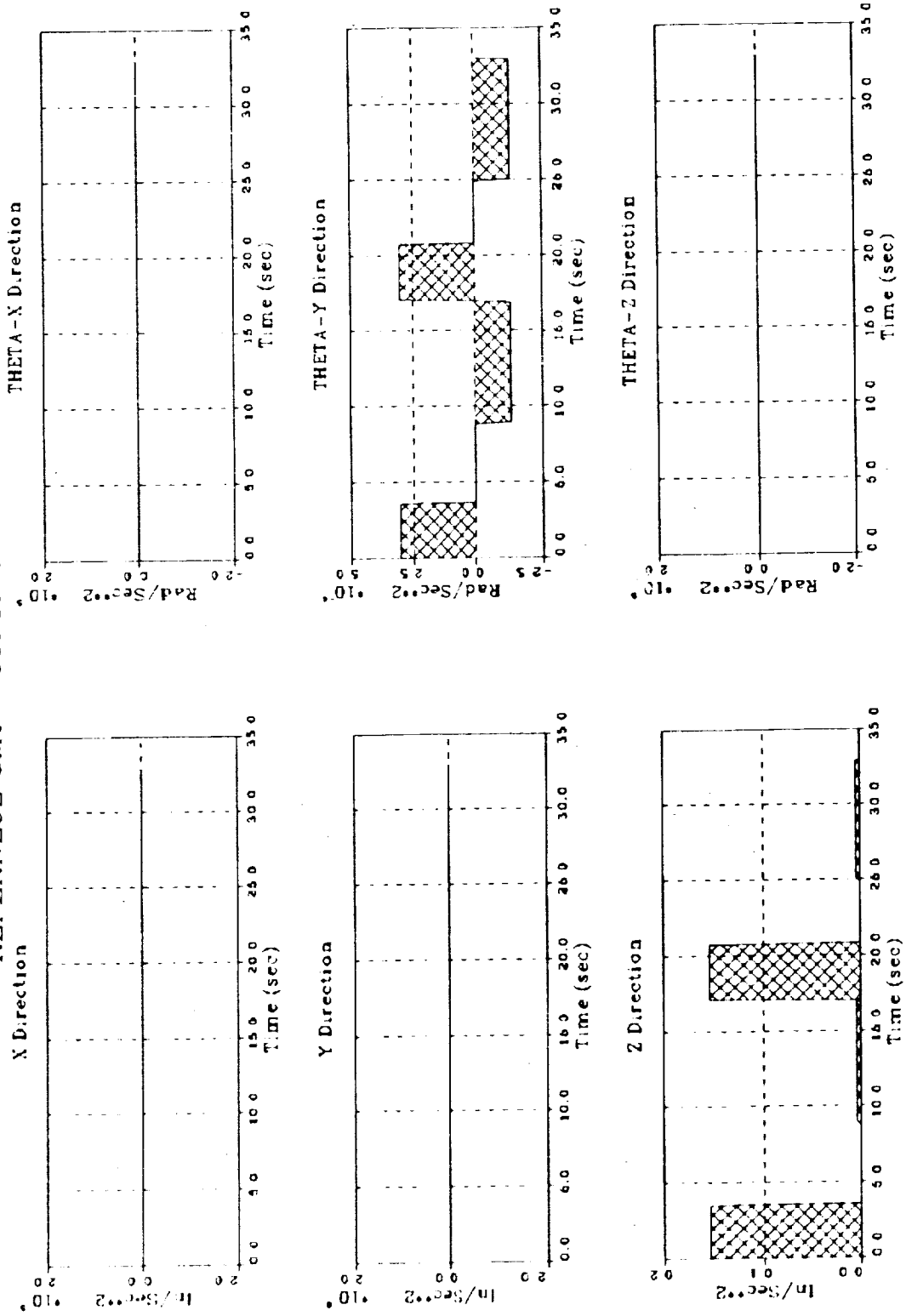

ORIGINAL PAGE IS
OF POOR QUALITY

BASE ACCELERATION HISTORY IN STS COORDINATES

REFERNECE GMT = 246:15:52:50.1 – FILE 13

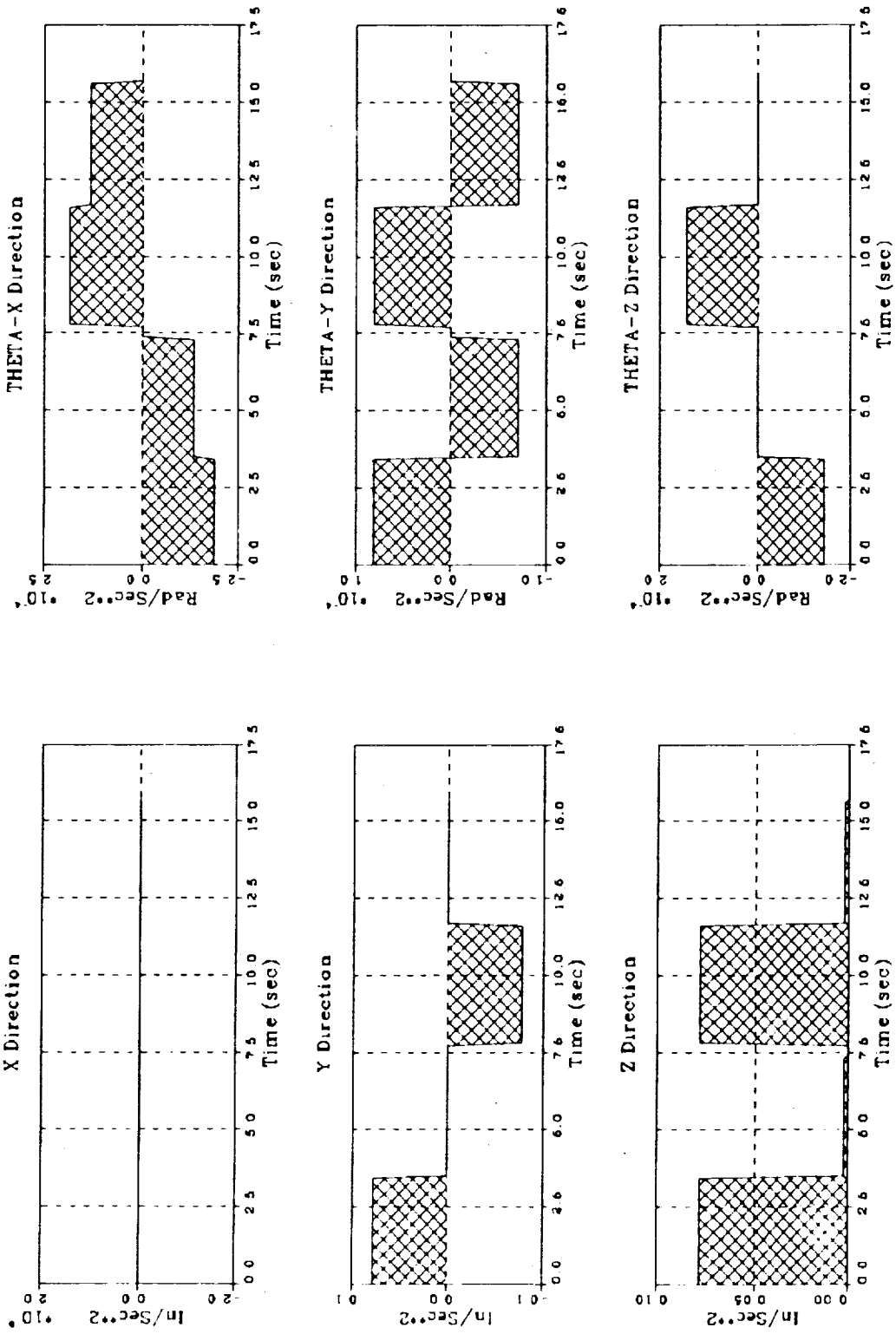

ORIGINAL PAGE IS
OF POOR QUALITY

BASE ACCELERATION HISTORY IN STS COORDINATES

REFERNECE GMT = 246:16:30:43.8 – FILE 14

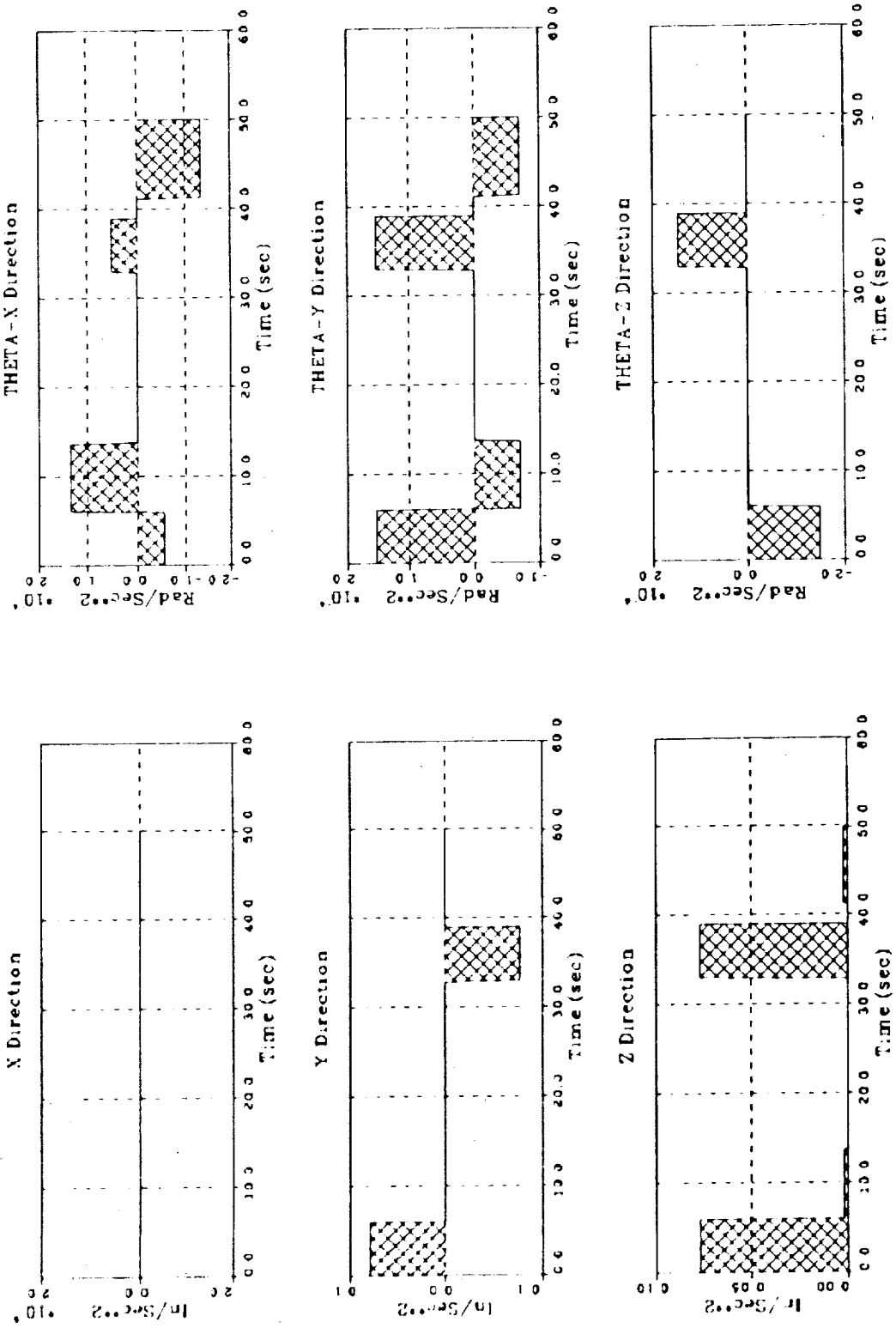

ORIGINAL PAGE IS
OF POOR QUALITY

BASE ACCELERATION HISTORY IN STS COORDINATES

REFERNECE GMT = 246:17:23:23.6 – FILE 15

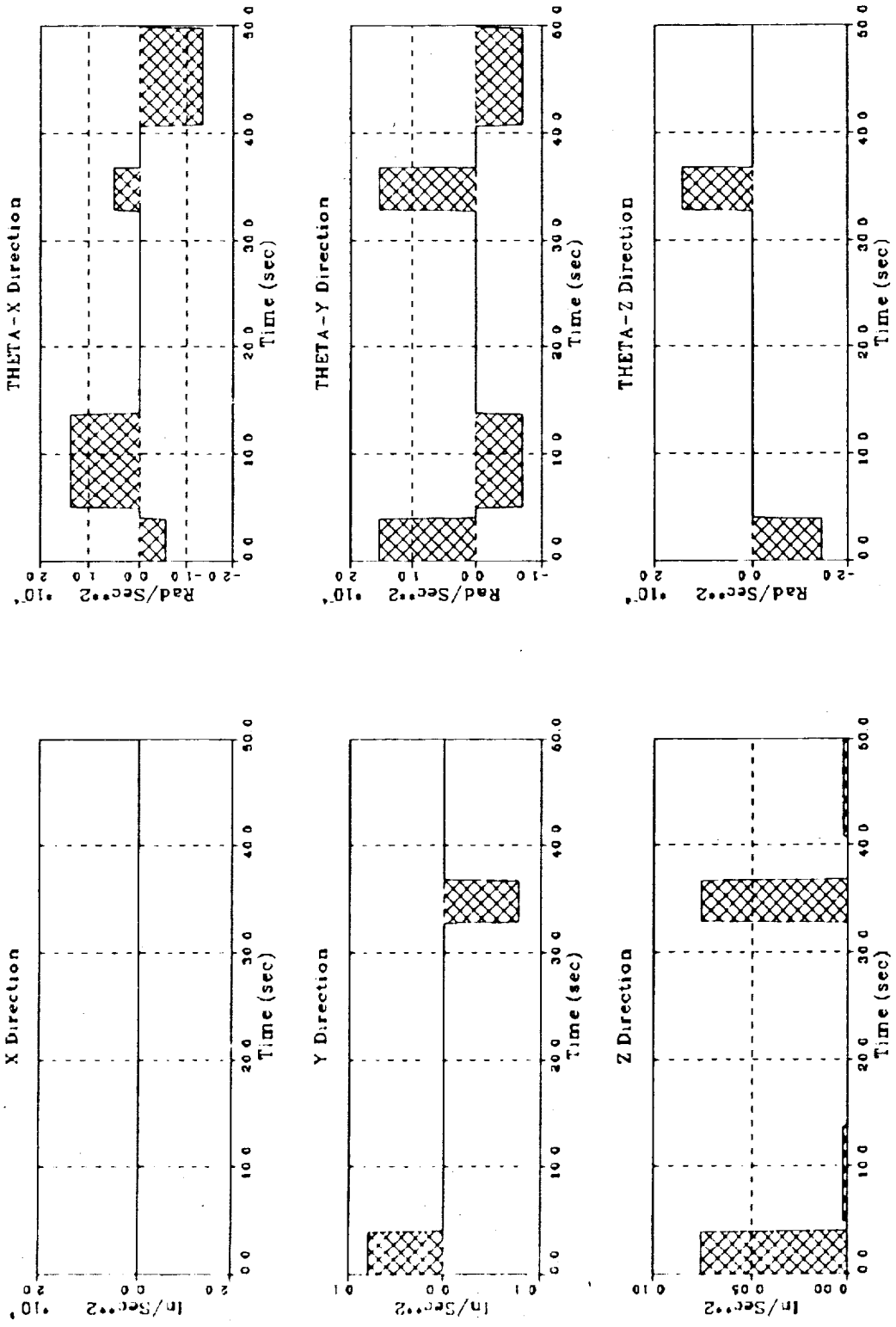

ORIGINAL PAGE IS
OF POOR QUALITY

BASE ACCELERATION HISTORY IN STS COORDINATES

REFERNECE GMT = 246:18: 6:44.3 – FILE 17

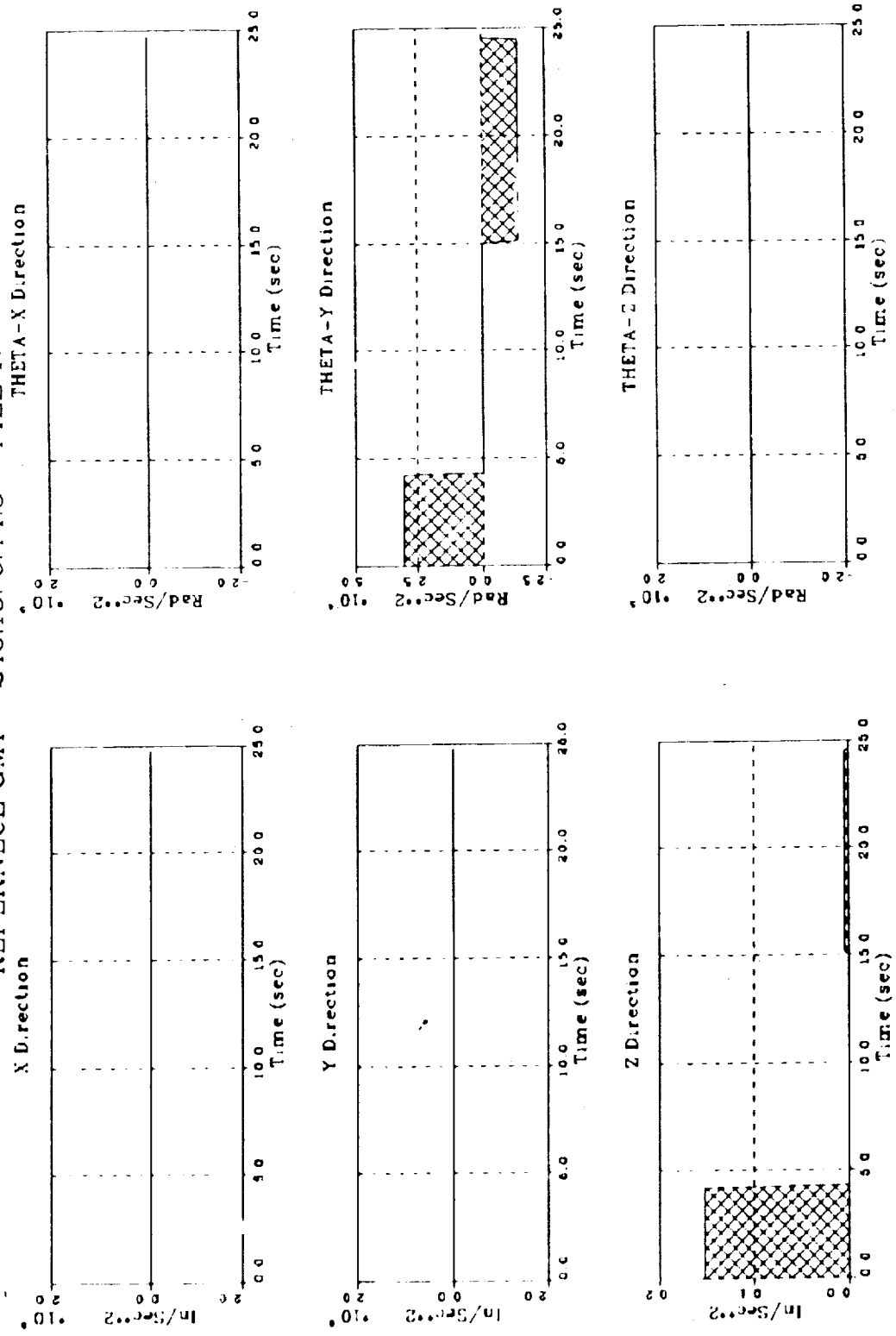

ORIGINAL PAGE IS
OF POOR QUALITY

BASE ACCELERATION HISTORY IN STS COORDINATES

REFERNECE GMT = 246:19:31:47.4 – FILE 20

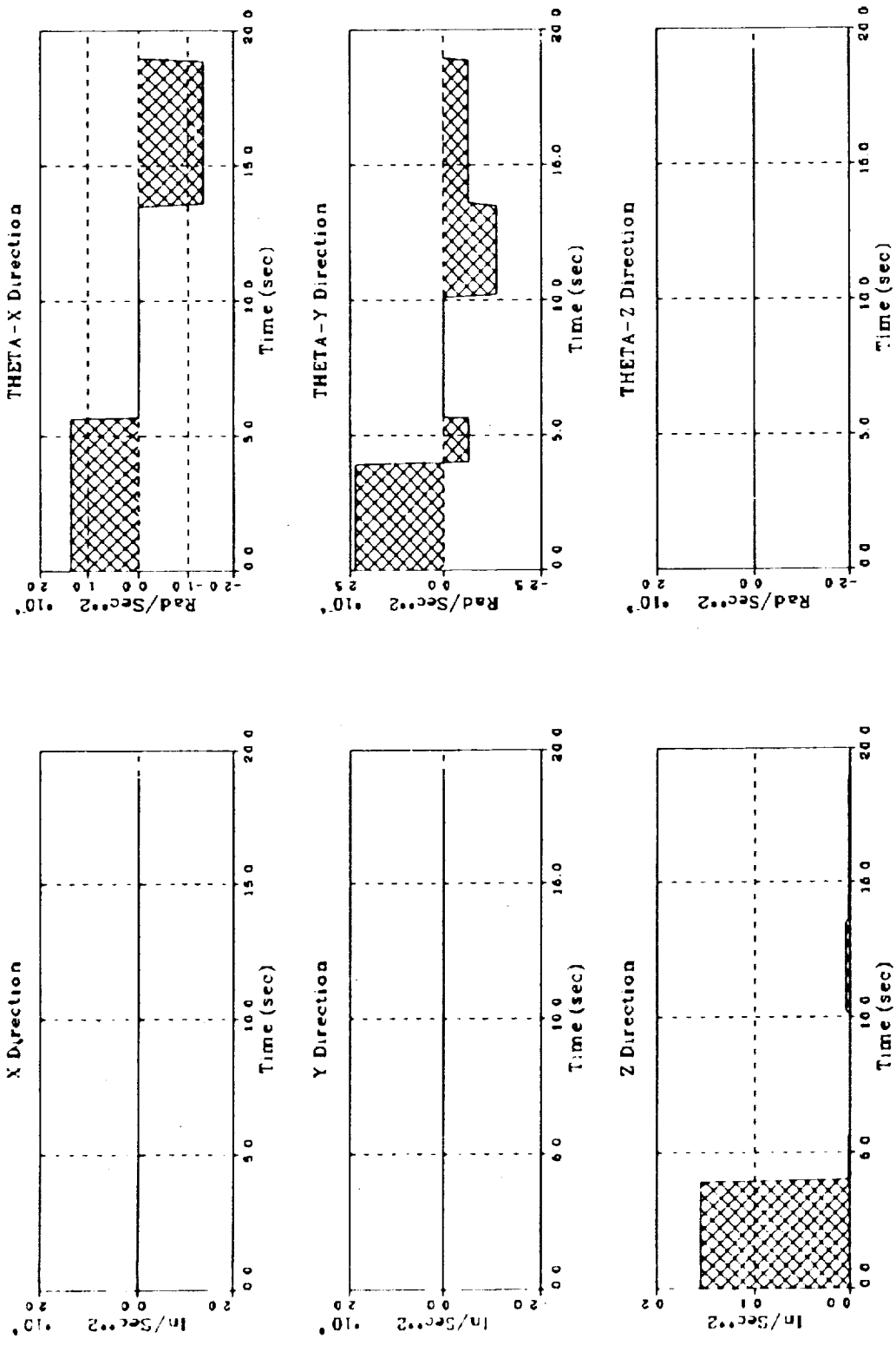

ORIGINAL PAGE IS
OF POOR QUALITY

BASE ACCELERATION HISTORY IN STS COORDINATES

REFERENCE GMT = 247:16:22:20.7 – FILE 26

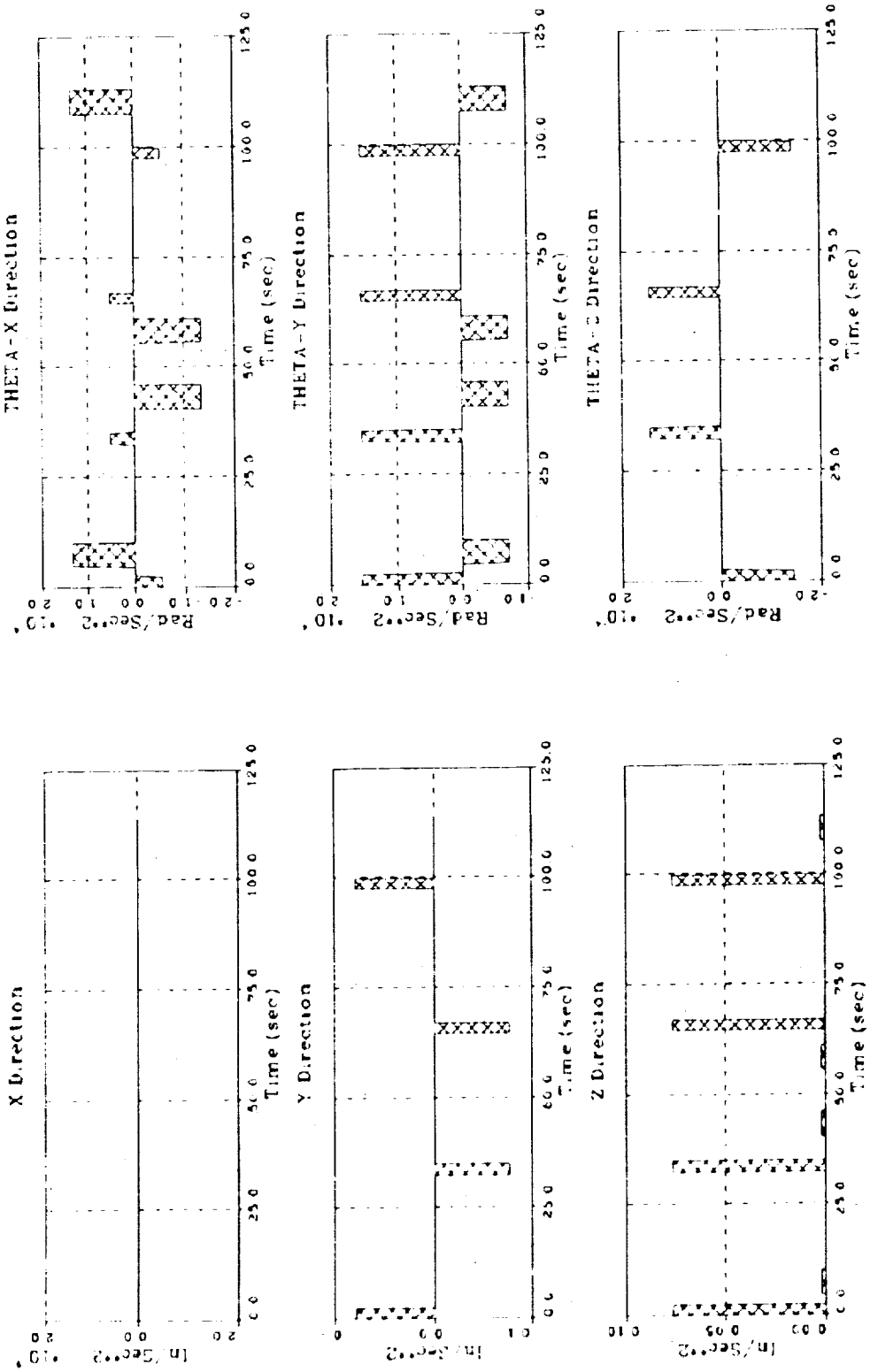

ORIGINAL PAGE IS
OF POOR QUALITY

BASE ACCELERATION HISTORY IN STS COORDINATES

REFERENCE GMT = 247 16:37:49 + - FILE 27

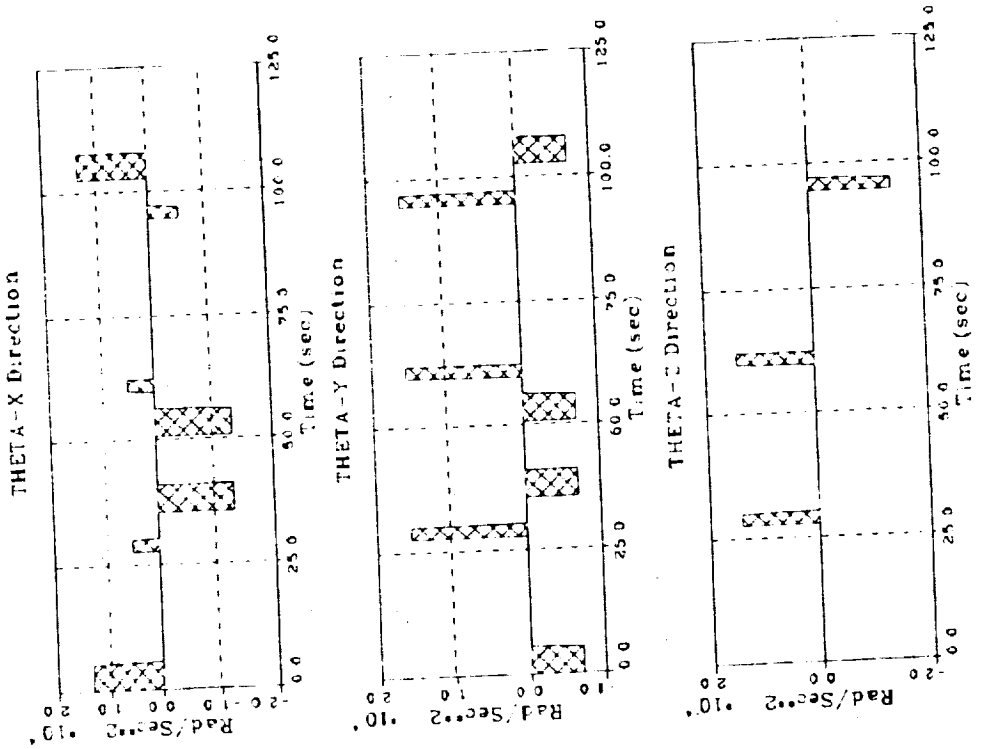

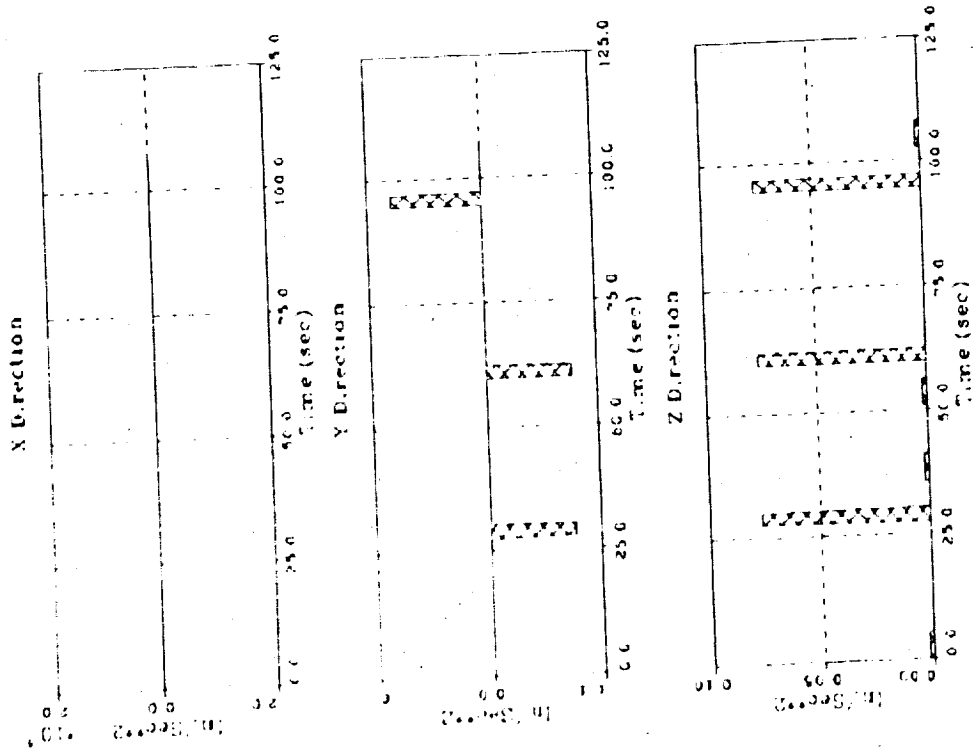

ORIGINAL PAGE IS
OF POOR QUALITY

BASE ACCELERATION HISTORY IN STS COORDINATES

REFERENCE GMT = 247:17:32:58.4 – FILE 28

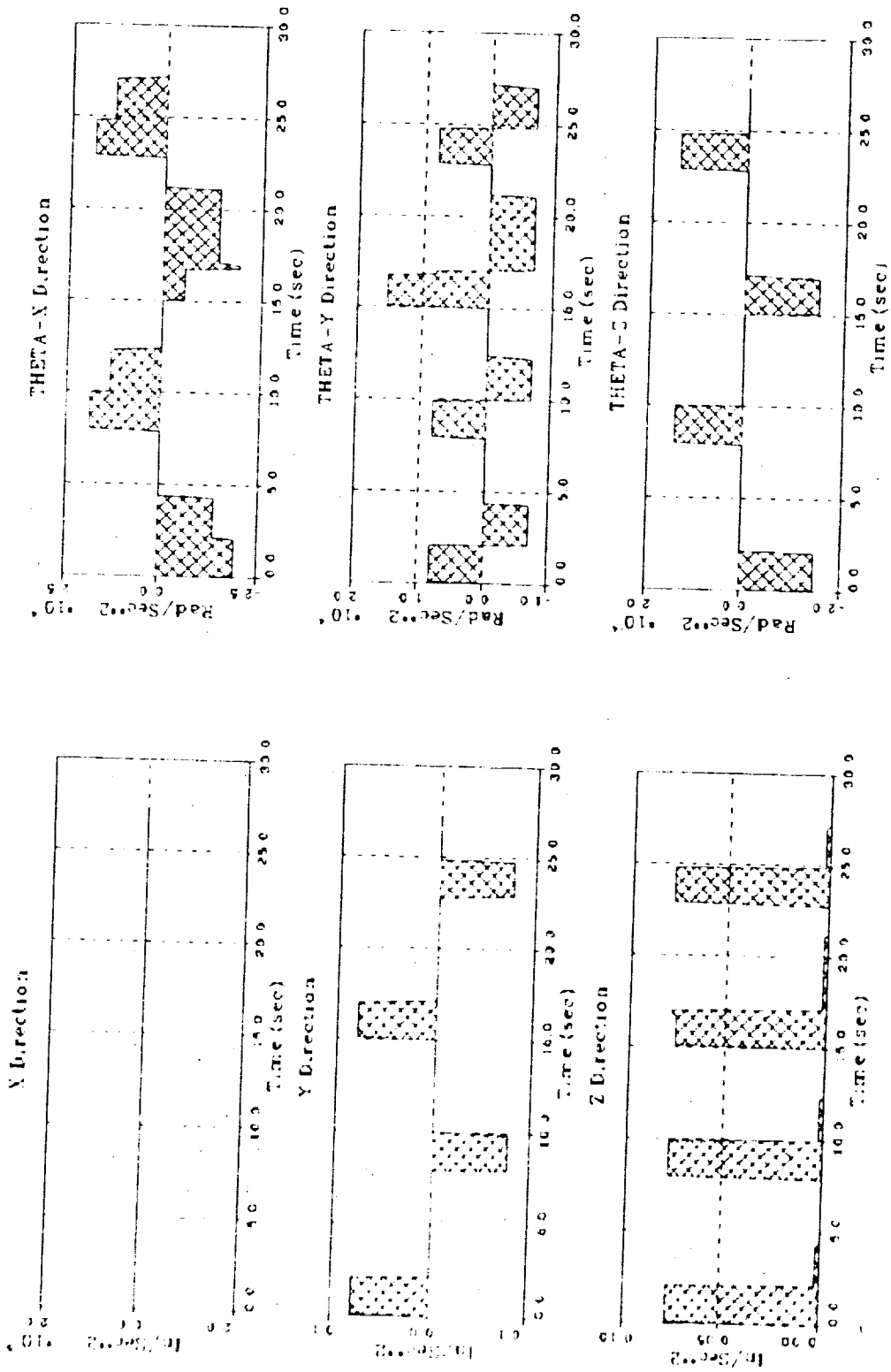

ORIGINAL PAGE IS
OF POOR QUALITY

BASE ACCELERATION HISTORY IN STS COORDINATES

REFERNECE GMT = 247:18: 7:45.6 – FILE 29

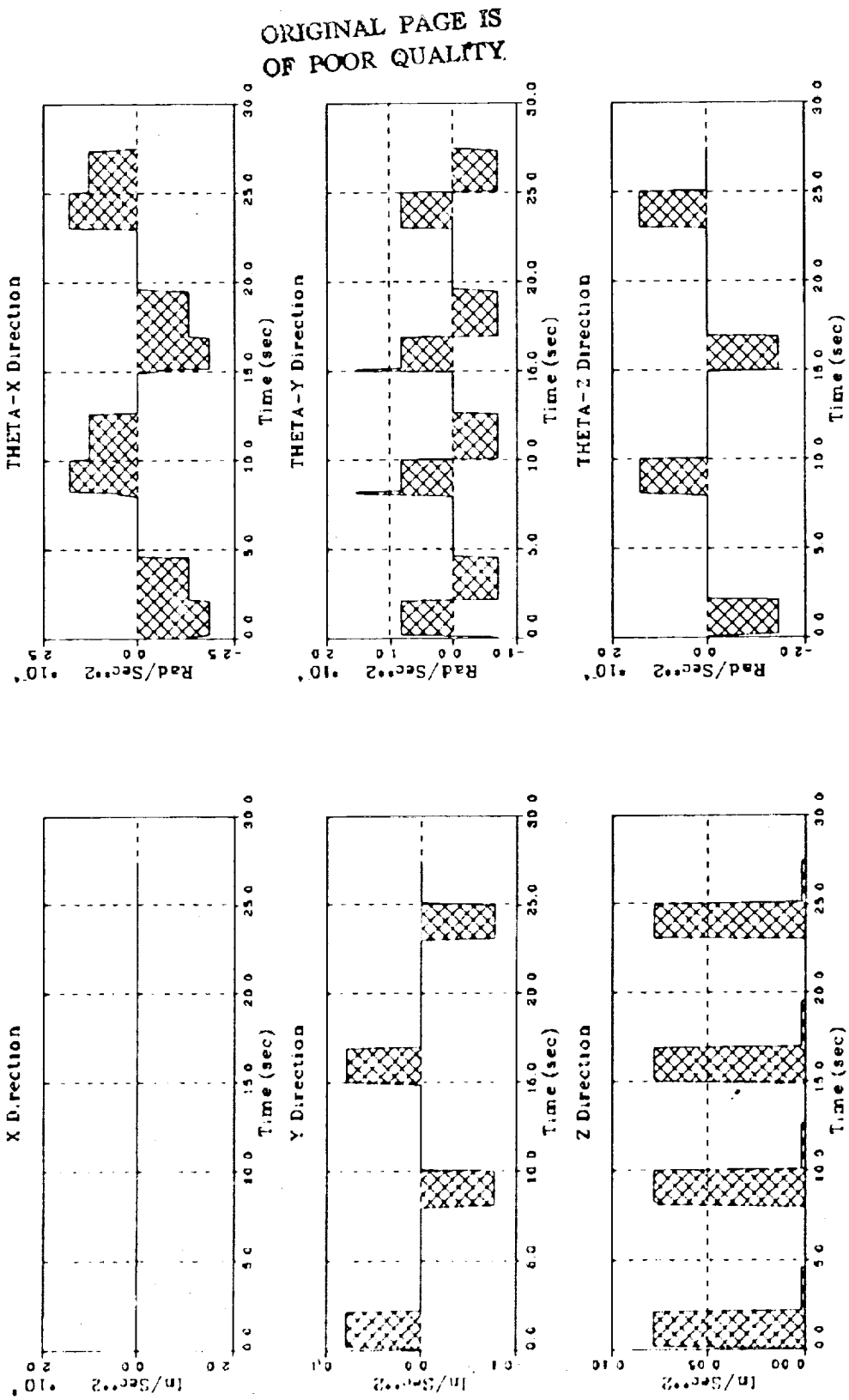

LMSC-F087173

Final Report

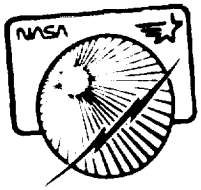

Appendix C
Mast Tip Acceleration Data

NTI

TEST NAME=SAE ACC MSTDS
MEASUREMENT= . COVER X1
REFF TIME = 245 19 25 27. 0
TIME OFFSET= 1.001
TOTAL TIME= 273.100

NNOFFT = 1
FFTBW-HZ= 0.00000E+00
FFTERR = 0.00
FFTTIM = 0.0
FFTLIN = 0

UNITS= (MIL-C)
MEAN=-0.12005330E-06
S.D. = 0.64088860E+00
SAMPLE RATE= 0.3750E+01

D: 2-12-85
T: 14- 6-18

0.500E+01

RAW DATA

DOMINANT TIME

TIME	MAGNITUDE
0.725E+02	0.2409E+01
0.731E+02	0.2311E+01
0.733E+02	0.2301E+01
0.728E+02	0.2297E+01
0.909E+02	0.2236E+01
0.723E+02	0.2177E+01
0.912E+02	0.2128E+01
0.917E+02	0.2096E+01
0.544E+02	0.2079E+01
0.915E+02	0.2077E+01

-0.500E+01

0.000E+00

TIME IN SECONDS

0.273E+03

ORIGINAL PAGE IS
OF POOR QUALITY

ORIGINAL PAGE IS
OF POOR QUALITY

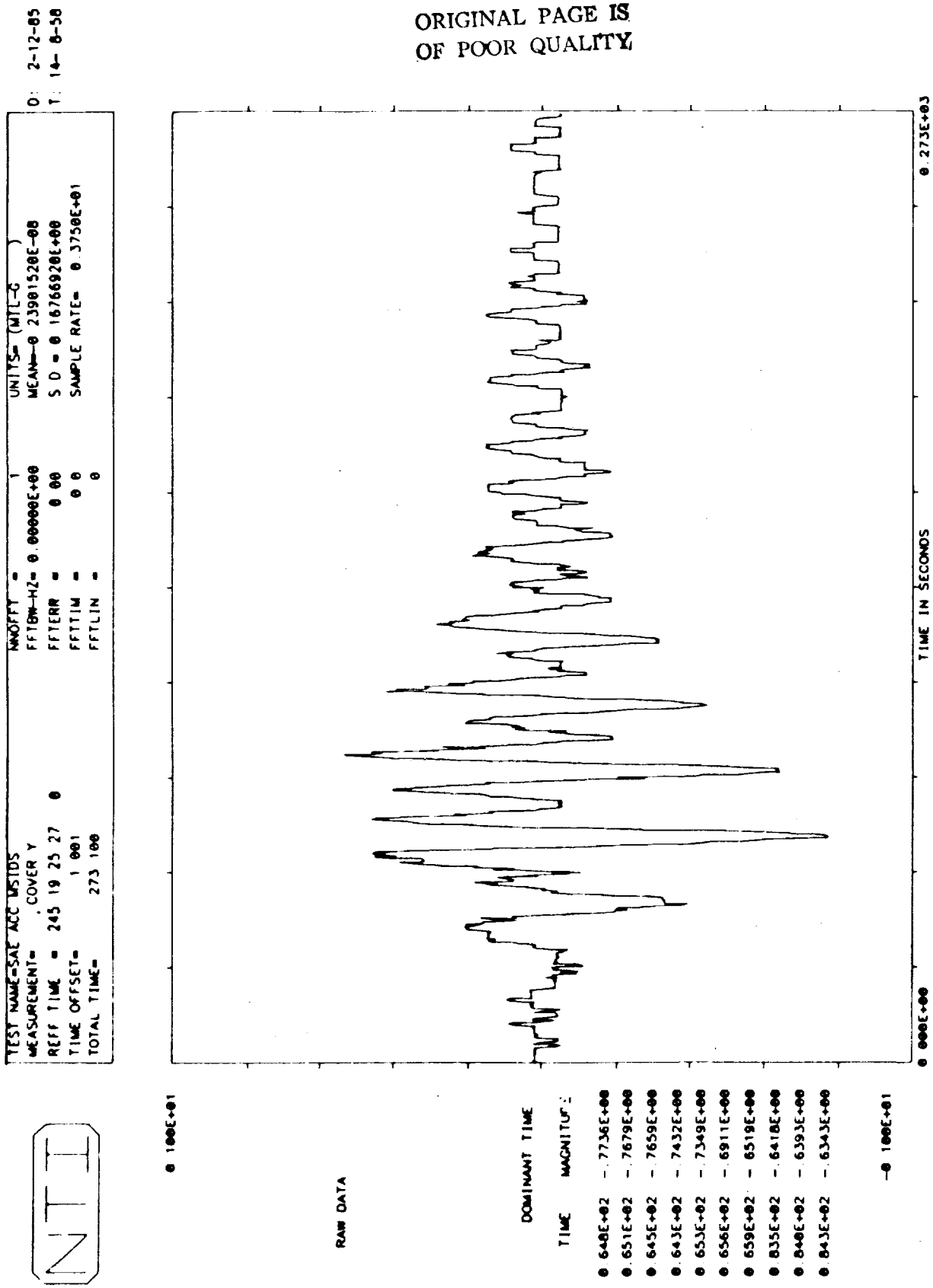

TEST NAME=SAE ACC MSIDS		NNOFFT =	1	UNITS= (MIL-G)	
MEASUREMENT=	COVER X2	FFTBW-HZ=	0.00000E+00	MEAN= 0.23719620E-08	D: 2-12-85
REFF TIME =	245 19 25 27. 0	FFTERR =	0 00	S D = 0 79632310E+00	T: 14- 7-37
TIME OFFSET=	1 001	FFTTIM =	0 0	SAMPLE RATE= 0.3750E+01	
TOTAL TIME=	273 100	FFTLIN =	0		

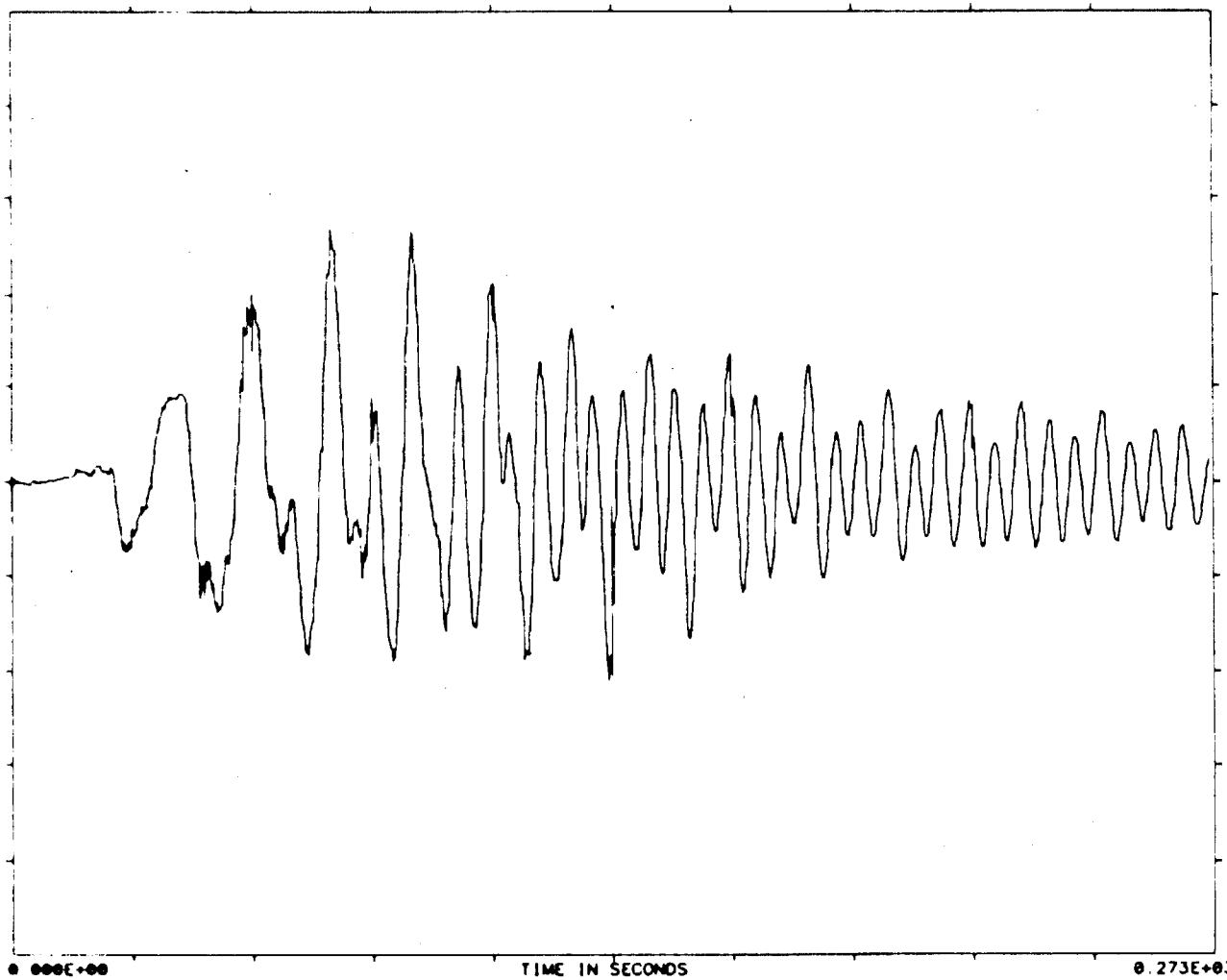

DOMINANT TIME

TIME	MAGNITUDE
0 725E+02	0 2703E+01
0 909E+02	0 2679E+01
0 728E+02	0 2555E+01
0 912E+02	0 2506E+01
0 731E+02	0 2489E+01
0 733E+02	0 2475E+01
0 904E+02	0 2409E+01
0 915E+02	0 2382E+01
0 723E+02	0 2357E+01
0 907E+02	0 2349E+01

ORIGINAL PAGE IS
OF POOR QUALITY

ORIGINAL PAGE IS
OF POOR QUALITY

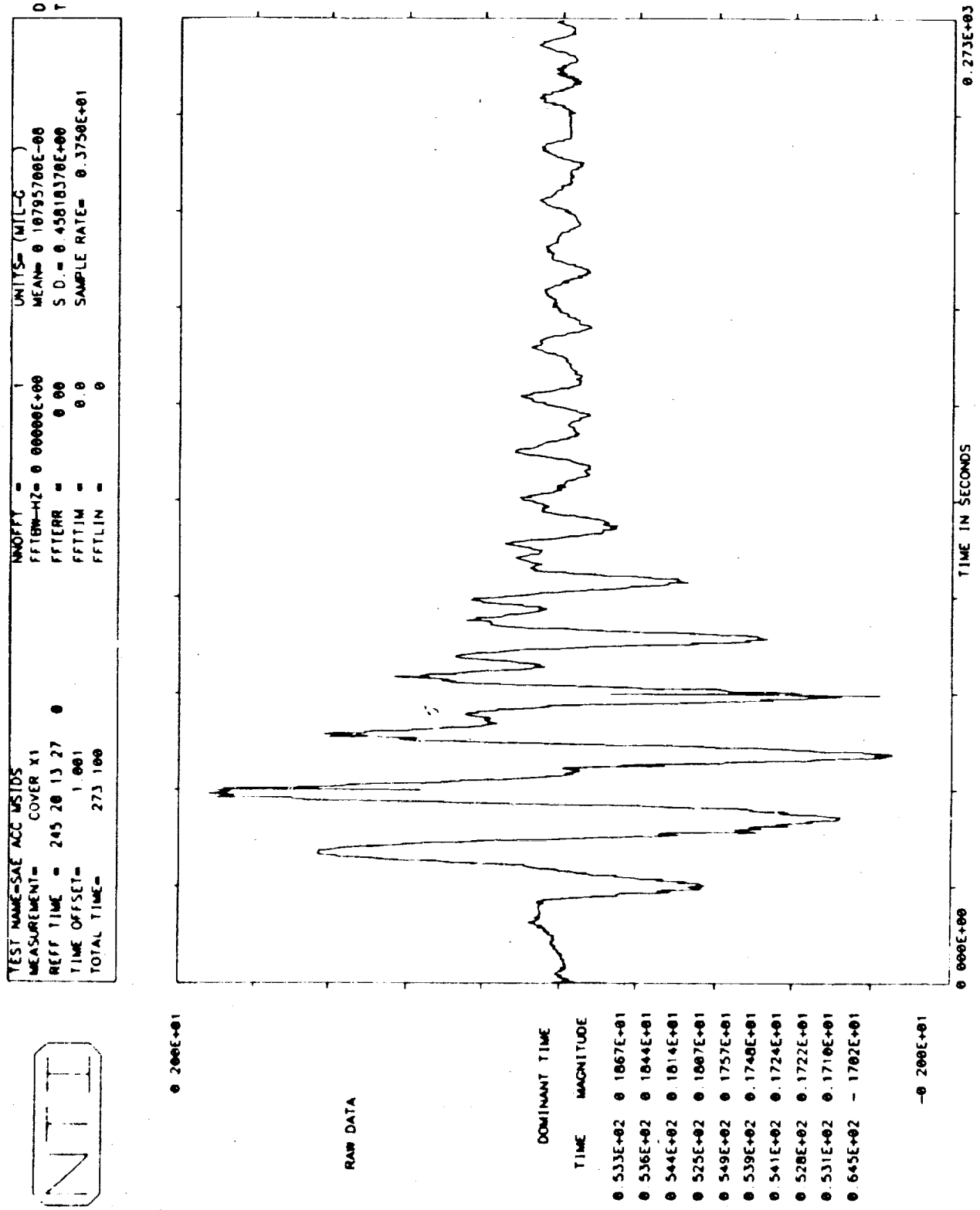

NTI

TEST NAME=SAE ACC MSIDS	NNOFFT = 1	UNITS= (MIL-G)	D: 2-12-85
MEASUREMENT= COVER Y	FFTBW-HZ= 0.00000E+00	MEAN=-0.17898860E-08	T: 14- 4-57
REFF TIME = 245.20:13:27. 0	FFTERR = 0.00	S.D.= 0.14093390E+00	
TIME OFFSET= 1.001	FFTTIM = 0.0	SAMPLE RATE= 0.3750E+01	
TOTAL TIME= 273.100	FFTLIN = 0		

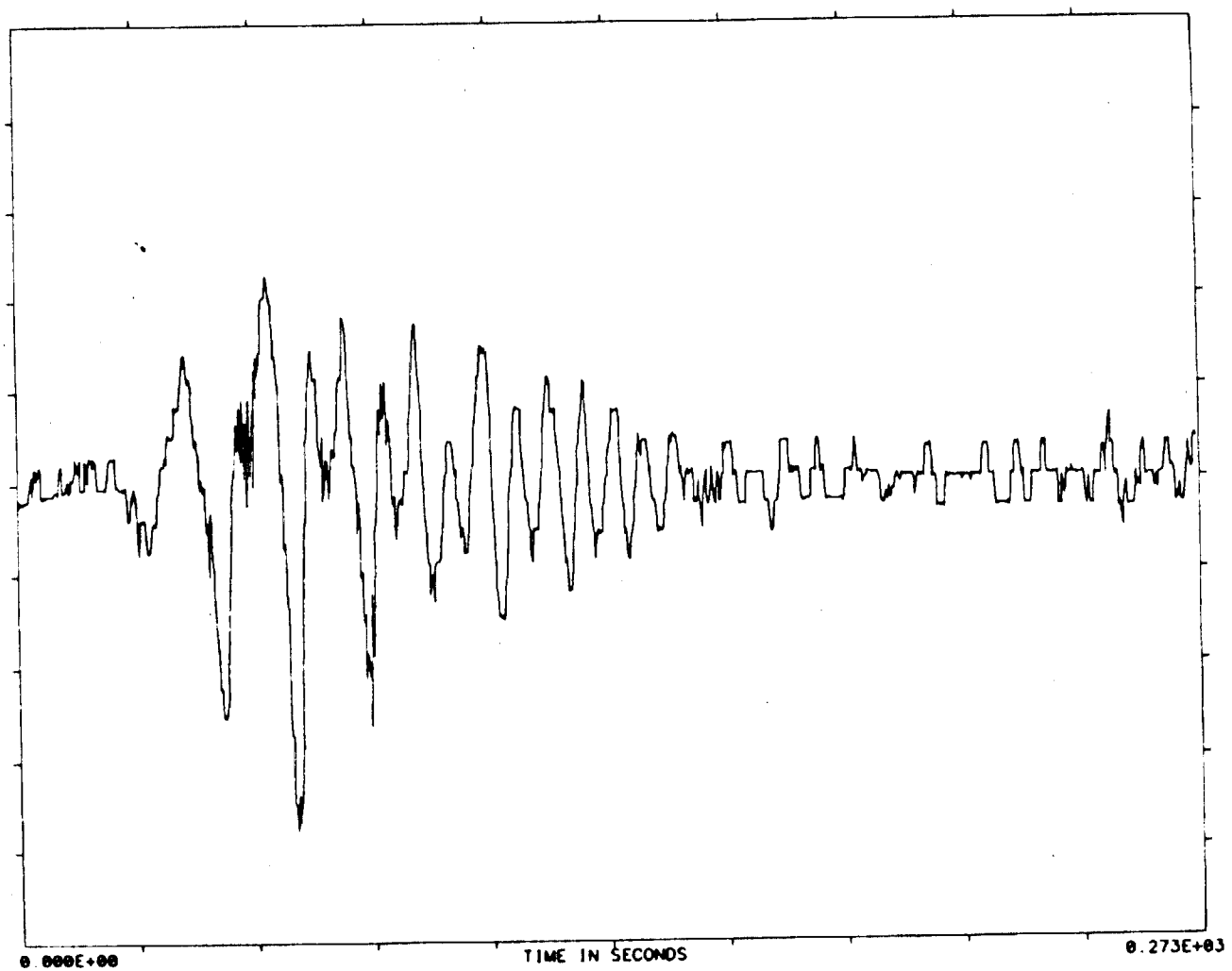

DOMINANT TIME

TIME	MAGNITUDE
0.640E+02	-.7558E+00
0.645E+02	-.7379E+00
0.648E+02	-.7167E+00
0.637E+02	-.6957E+00
0.635E+02	-.6903E+00
0.643E+02	-.6732E+00
0.651E+02	-.6674E+00
0.653E+02	-.5517E+00
0.629E+02	-.5436E+00
0.632E+02	-.5419E+00

ORIGINAL PAGE IS
OF POOR QUALITY

TEST NAME=SAE ACC MSIDS		NWOFFT =	1	UNITS= (MIL-G)	D: 2-12-85
MEASUREMENT=	COVER X2	FFTBW-HZ=	0.00000E+00	MEAN= 0.62718760E-08	T: 14- 3-19
REFF TIME =	245.20 13.27. 0	FFTERR =	0.00	S D = 0.48462778E+00	
TIME OFFSET=	1.001	FFTTIM =	0.0	SAMPLE RATE= 0.3750E+01	
TOTAL TIME=	273.100	FFTLIN =	0		

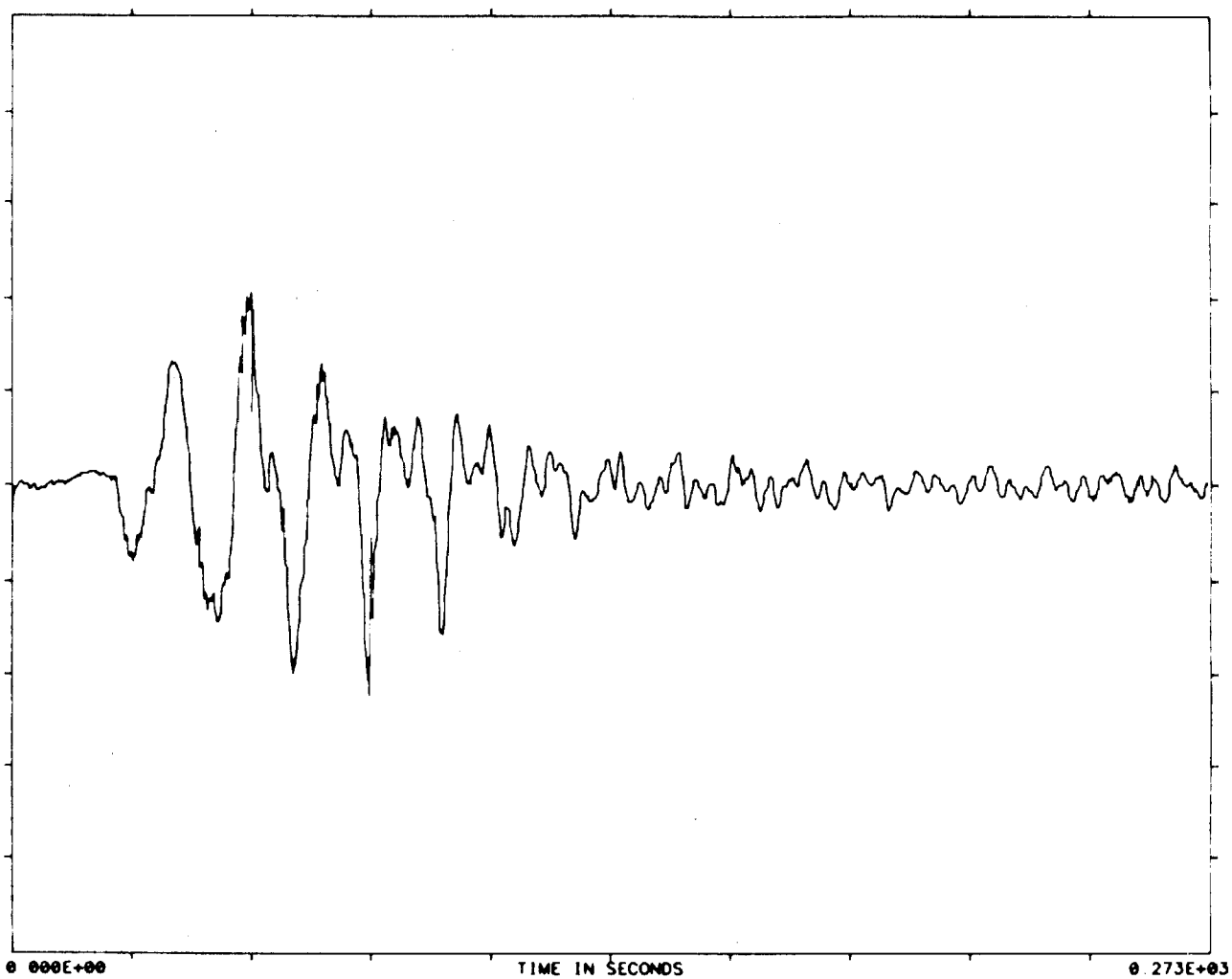

RAW DATA

DOMINANT TIME

TIME	MAGNITUDE
0.816E+02	- 2227E+01
0.544E+02	0.2082E+01
0.811E+02	-.2072E+01
0.533E+02	0.2052E+01
0.536E+02	0.2009E+01
0.640E+02	-.1994E+01
0.541E+02	0.1985E+01
0.645E+02	-.1916E+01
0.549E+02	0.1878E+01
0.539E+02	0.1865E+01

ORIGINAL PAGE IS
OF POOR QUALITY

NTI

TEST NAME=SAE ACC MSIDS		NNOFFT =	1	UNITS= (MIL-G)	
MEASUREMENT=	COVER X1	FFTBW-HZ=	0.00000E+00	MEAN=-0 27648640E-09	D: 2-12-85
REFF TIME =	246 13 29 27 0	FFTERR =	0 00	S D = 0 19808230E+00	T: 14-10-17
TIME OFFSET=	1 001	FFTTIM =	0.0	SAMPLE RATE= 0.3750E+01	
TOTAL TIME=	273 100	FFTLIN =	0		

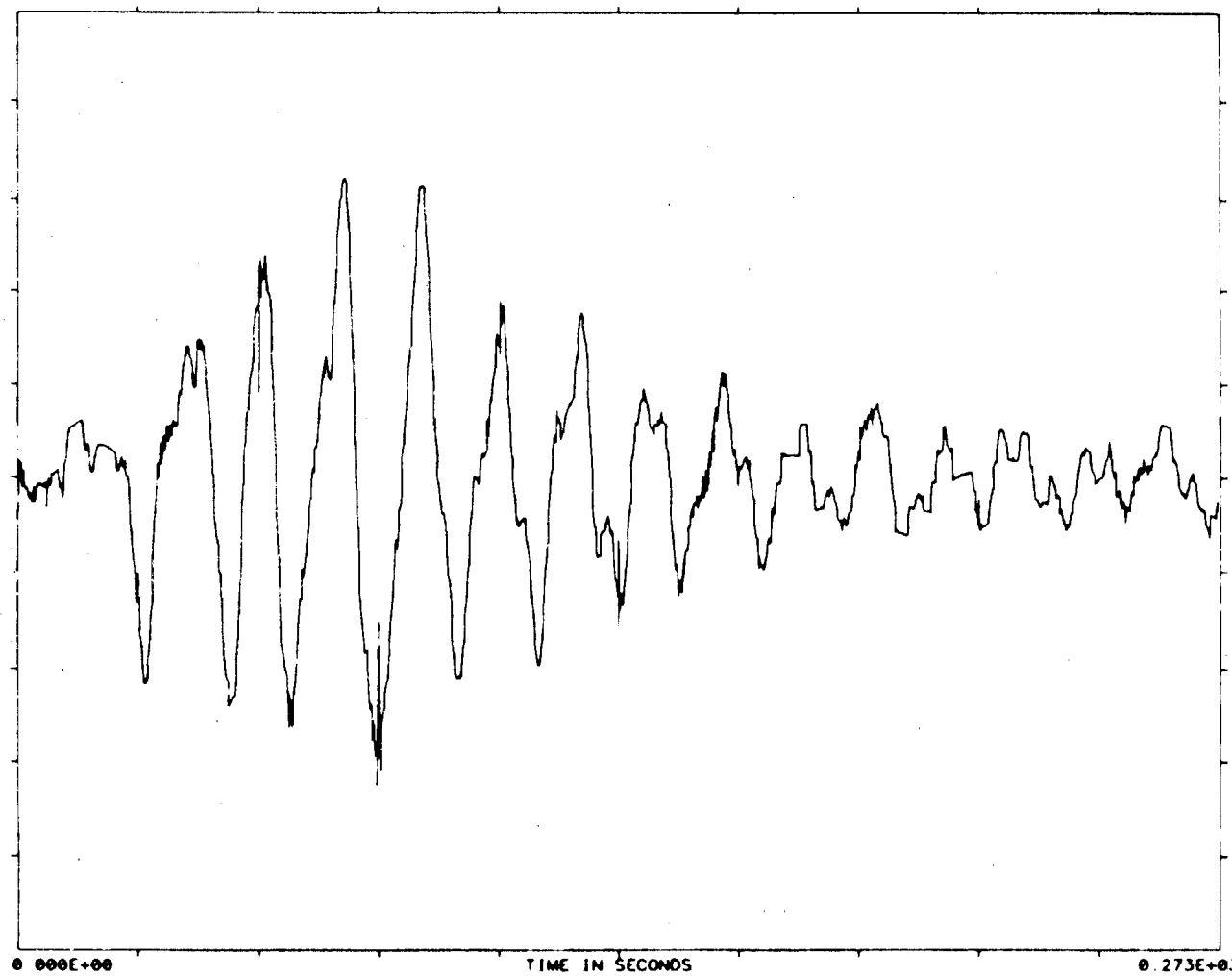

DOMINANT TIME

TIME	MAGNITUDE
0 816E+02	-.6489E+00
0 741E+02	0.6453E+00
0 739E+02	0 6423E+00
0.744E+02	0 6326E+00
0 920E+02	0.6293E+00
0.915E+02	0.6256E+00
0 821E+02	- 6247E+00
0 917E+02	0.6227E+00
0 923E+02	0.6222E+00
0 912E+02	0.6206E+00

TEST NAME=SAE ACC MSIDS		NNOFFT =	1	UNITS= (MIL-G)	D: 2-12-85
MEASUREMENT=	COVER Y	FFTBW-HZ=	0 00000E+00	MEAN=-0 14533730E-00	T: 14-12-55
REFF TIME =	246 13 29 27 0	FFTERR =	0 00	S.D.= 0 19405130E+00	
TIME OFFSET=	1 001	FFTTIM =	0 0	SAMPLE RATE= 0.3750E+01	
TOTAL TIME=	273 100	FFTLIN =	0		

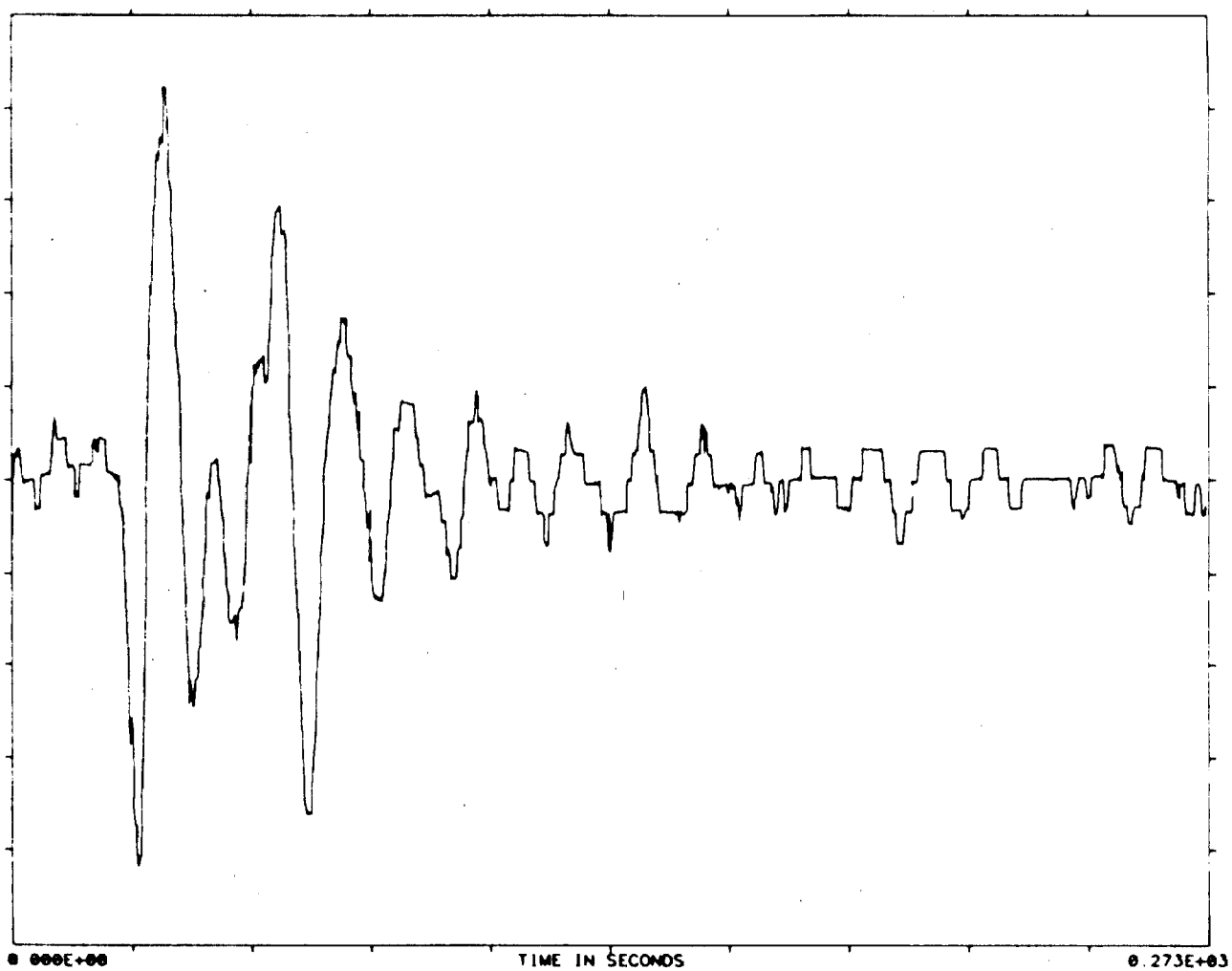

DOMINANT TIME

TIME	MAGNITUDE
0 349E+02	0 8501E+00
0 347E+02	0 8470E+00
0 288E+02	- 8396E+00
0 352E+02	0 8172E+00
0 291E+02	- 8153E+00
0 293E+02	- 8106E+00
0 285E+02	- 7855E+00
0 283E+02	- 7577E+00
0 344E+02	0 7514E+00
0 280E+02	- 7424E+00

ORIGINAL PAGE IS
OF POOR QUALITY

NTI

TEST NAME=SAE ACC MSTDS		NNOFFT =	1	UNITS= (MIL-G)	D: 2-12-85
MEASUREMENT=	COVER X2	FFTBW-HZ=	0.00000E+00	MEAN=-0 12514650E-08	T: 14-11-35
REFF TIME =	246 13 29 27 0	FFTERR =	0 00	S D = 0 24247970E+00	
TIME OFFSET=	1 001	FFTTIM =	0 0	SAMPLE RATE= 0 3750E+01	
TOTAL TIME=	273 100	FFTLIN =	0		

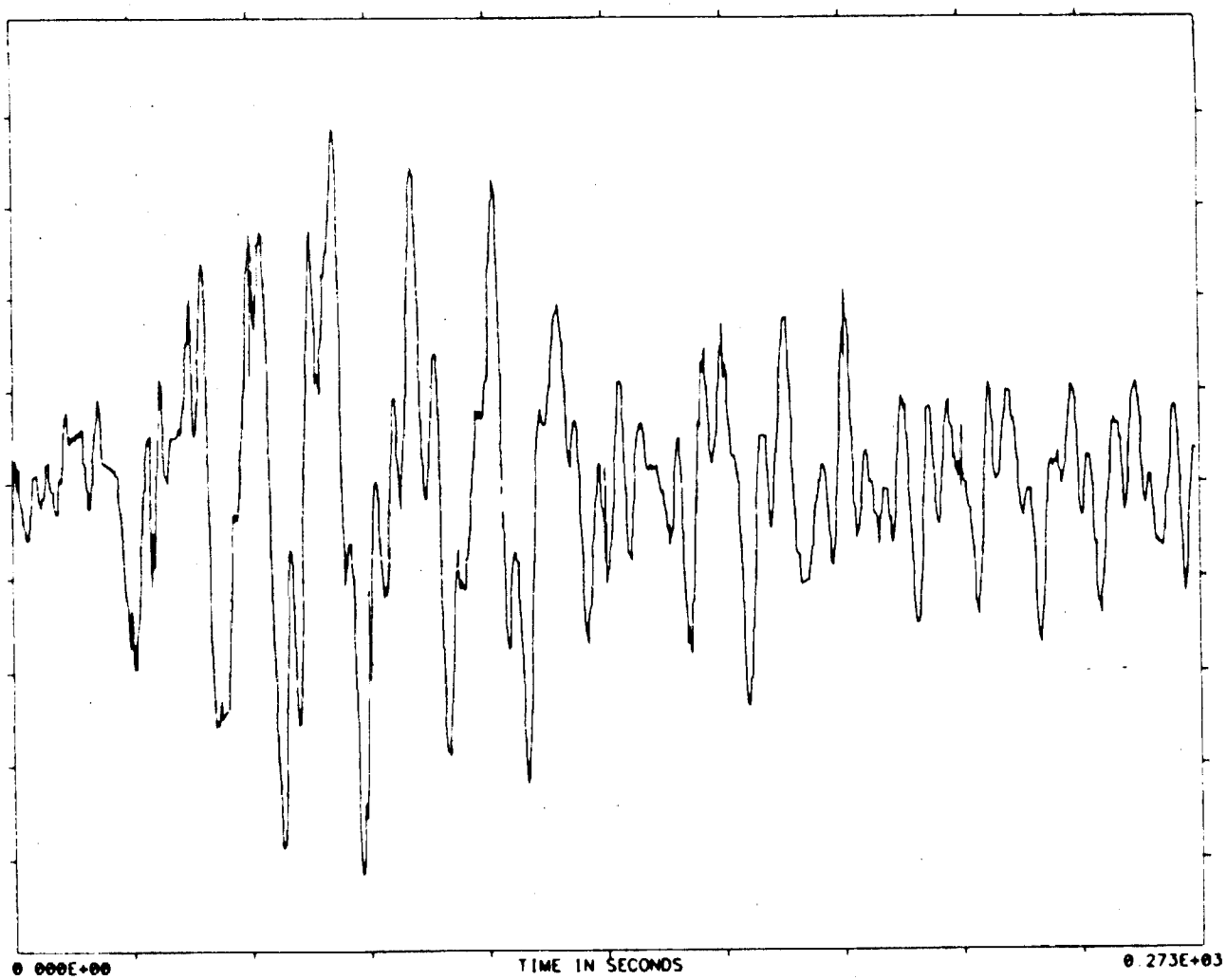

DOMINANT TIME

TIME	MAGNITUDE
0 800E+02	- 8355E+00
0 805E+02	- 8150E+00
0 803E+02	- 8086E+00
0 797E+02	- 7958E+00
0 739E+02	0 7759E+00
0 613E+02	- 7733E+00
0 619E+02	- 7724E+00
0 616E+02	- 7665E+00
0 621E+02	- 7521E+00
0 741E+02	0 7485E+00

ORIGINAL PAGE IS
OF POOR QUALITY

NTI

TEST NAME=SAE ACC MSIDS
MEASUREMENT= COVER X1
REFF TIME = 246 14 21 55. 0
TIME OFFSET= 1 001
TOTAL TIME= 273 100

NNOFFT = 1
FFTBW-HZ= 0 00000E+00
FFTERR = 0 00
FFTTIM = 0 0
FFTLIN = 0

UNITS= (MTL-G)
MEAN= 0 23610480E-08
S D = 0 25347540E+00
SAMPLE RATE= 0 3750E+01

D: 2-12-85
T: 14-14-17

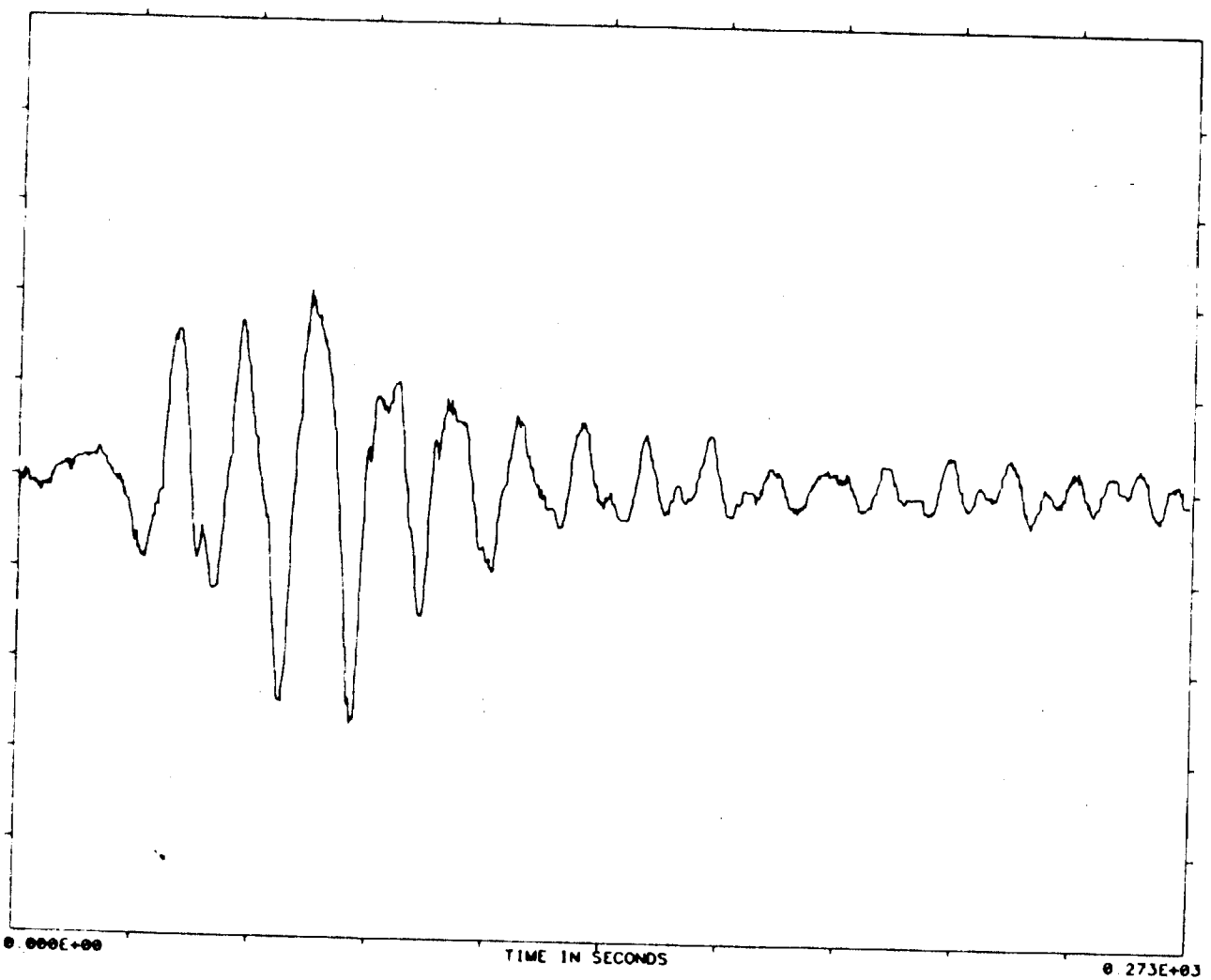

DOMINANT TIME

TIME	MAGNITUDE
0 776E+02	- 1083E+01
0 773E+02	- 1075E+01
0 781E+02	- 1061E+01
0 779E+02	- 1044E+01
0 768E+02	- 9943E+00
0 613E+02	- 9872E+00
0 608E+02	- 9806E+00
0 611E+02	- 9786E+00
0 784E+02	- 9571E+00
0 771E+02	- 9571E+00

NTI

TEST NAME=SAE ACC MSIDS
MEASUREMENT= COVER Y
REFF TIME = 248 14 21 55. 0
TIME OFFSET= 1 001
TOTAL TIME= 273 100

NNOFFT = 1
FFTBW-HZ= 0 00000E+00
FFTERR = 0.00
FFTTIM = 0.0
FFTLIN = 0

UNITS= (MIL-G)
MEAN= 0 20736480E-08
S D = 0 15536560E+00
SAMPLE RATE= 0 3750E+01

D: 2-12-85
T: 14-17-41

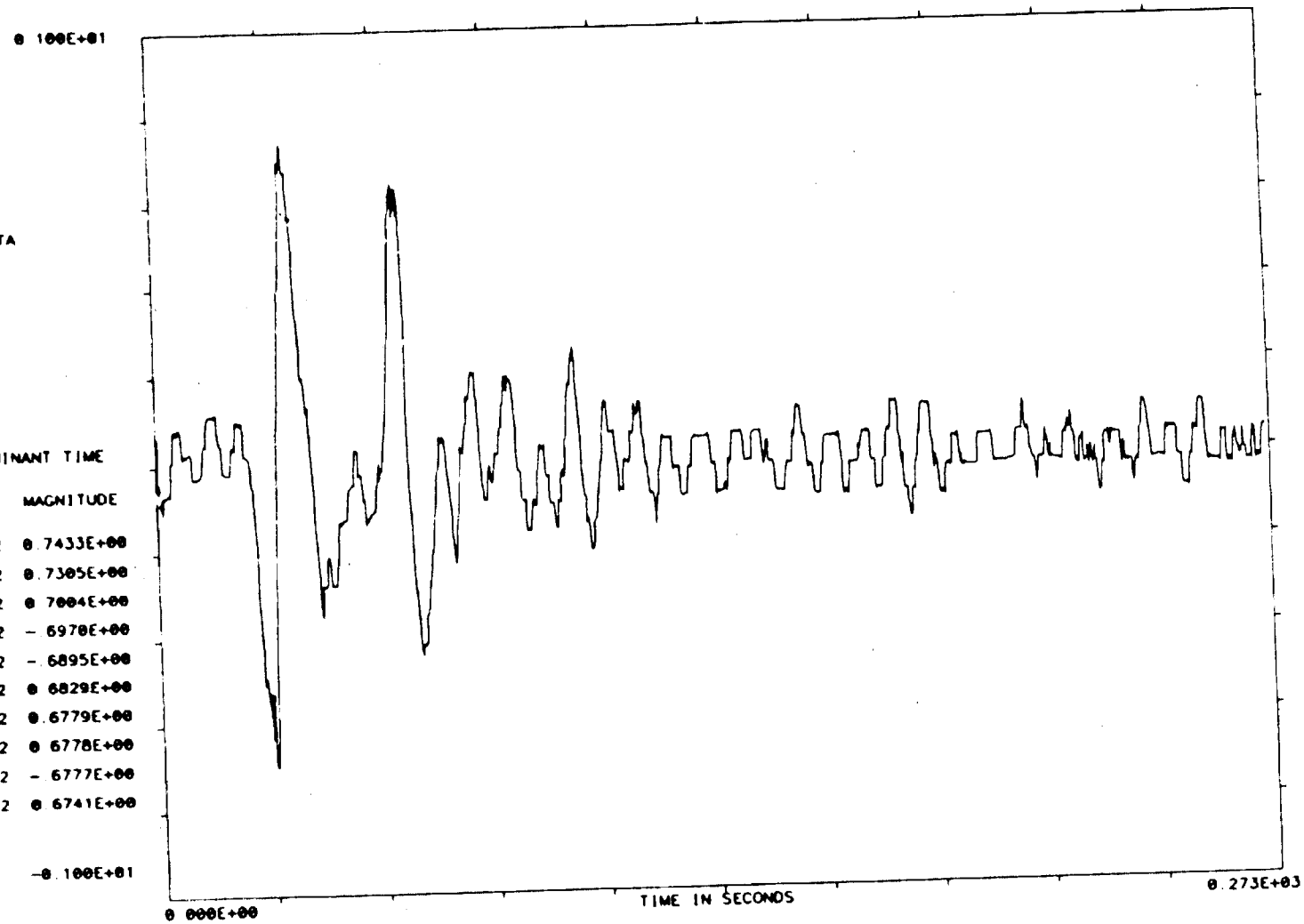

DOMINANT TIME

TIME	MAGNITUDE
0 325E+02	0 7433E+00
0 323E+02	0 7305E+00
0 317E+02	0 7004E+00
0 280E+02	- 6970E+00
0 277E+02	- 6895E+00
0 328E+02	0 6829E+00
0 333E+02	0 6779E+00
0 320E+02	0 6778E+00
0 275E+02	- 6777E+00
0 331E+02	0 6741E+00

ORIGINAL PAGE IS
OF POOR QUALITY

ORIGINAL PAGE IS
OF POOR QUALITY

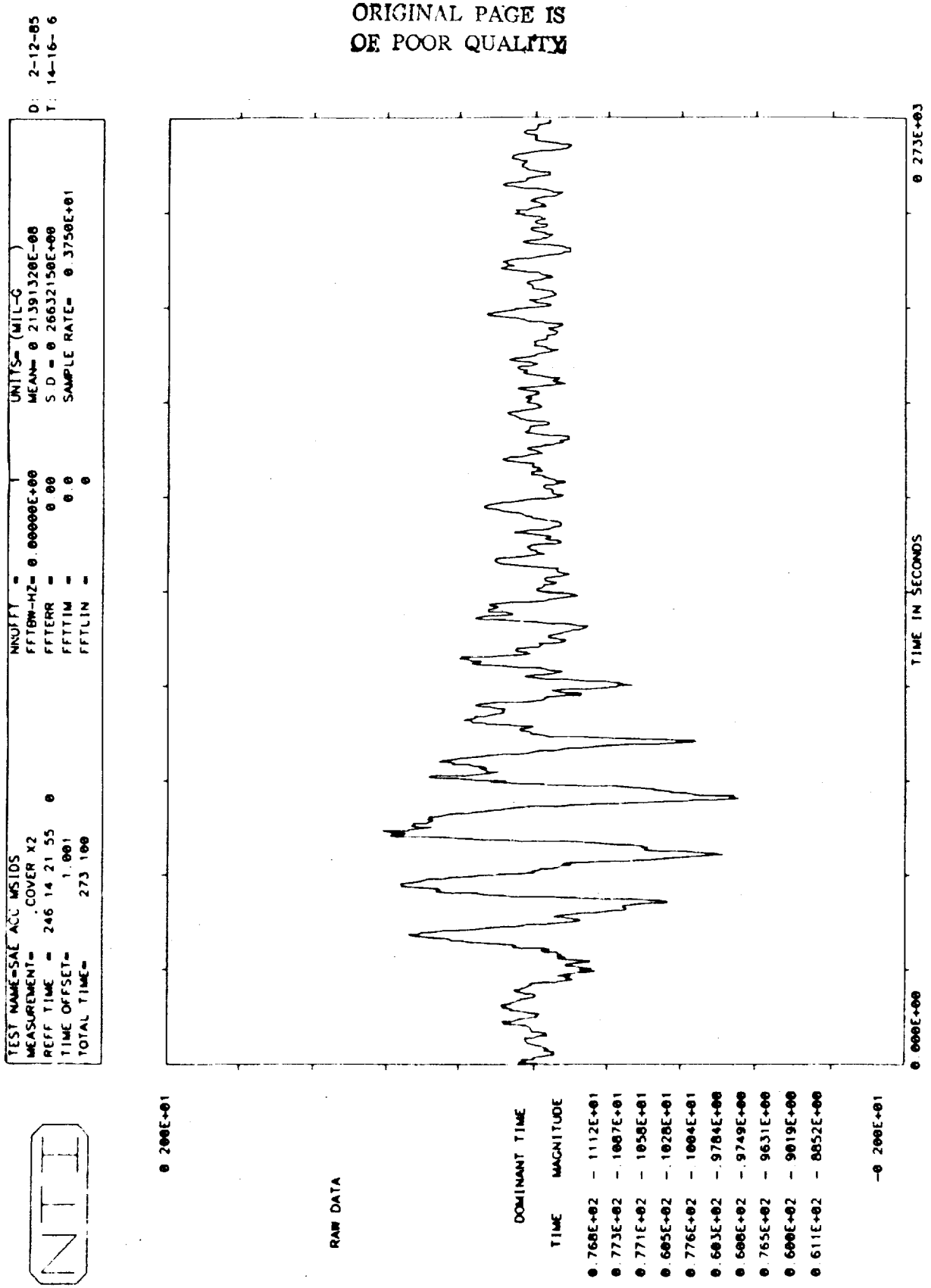

TEST NAME-SAE ACC MSIDS		NNOFFT =	1	UNITS= (MIL-G)	D: 2-12-85
MEASUREMENT=	COVER X1	FFTBW-HZ=	0.00000E+00	MEAN=-0.50786190E-08	T: 14-20-16
REFF TIME =	246.15 0.26. 0	FFTERR =	0.00	S.D. = 0.54256680E+00	
TIME OFFSET=	1.001	FFTTIM =	0.0	SAMPLE RATE= 0.3750E+01	
TOTAL TIME=	273.100	FFTLIN =	0		

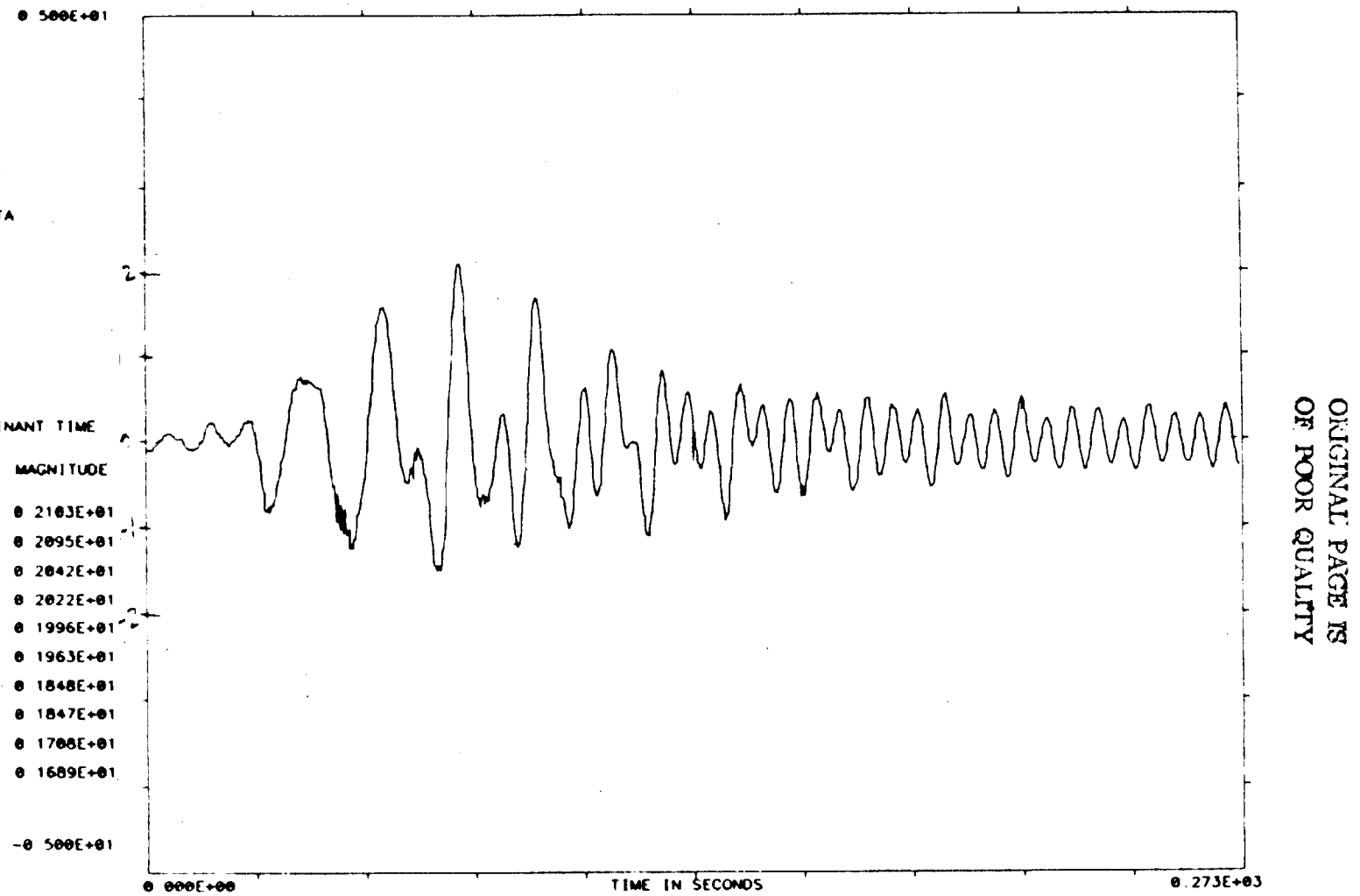

ORIGINAL PAGE IS
OF POOR QUALITY

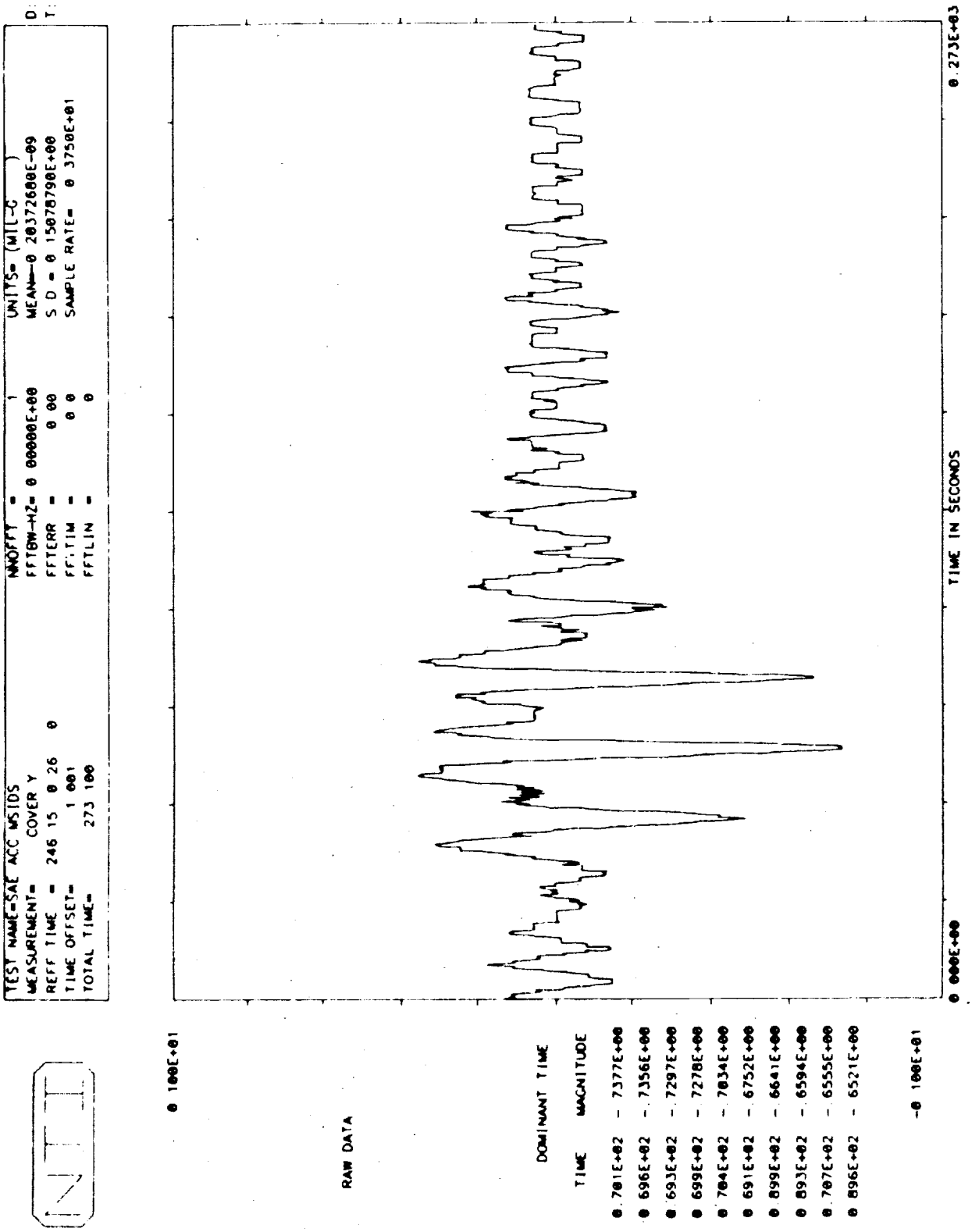

TEST NAME=SAE ACC MSIDS
MEASUREMENT= COVER X2
REF TIME = 246 15 0 26 0
TIME OFFSET= 1 001
TOTAL TIME= 273 100

NNOFFT = 1
FFTRW-HZ= 0 00000E+00
FFTERR = 0 00
FFTTIM = 0 0
FFTLIN = 0

UNITS= (MIL-G)
MEAN= 0 15570550E-00
S D = 0 61850320E+00
SAMPLE RATE= 0 3750E+01

D 2-12-85
T 14-21-53

0 500E+01

RAW DATA

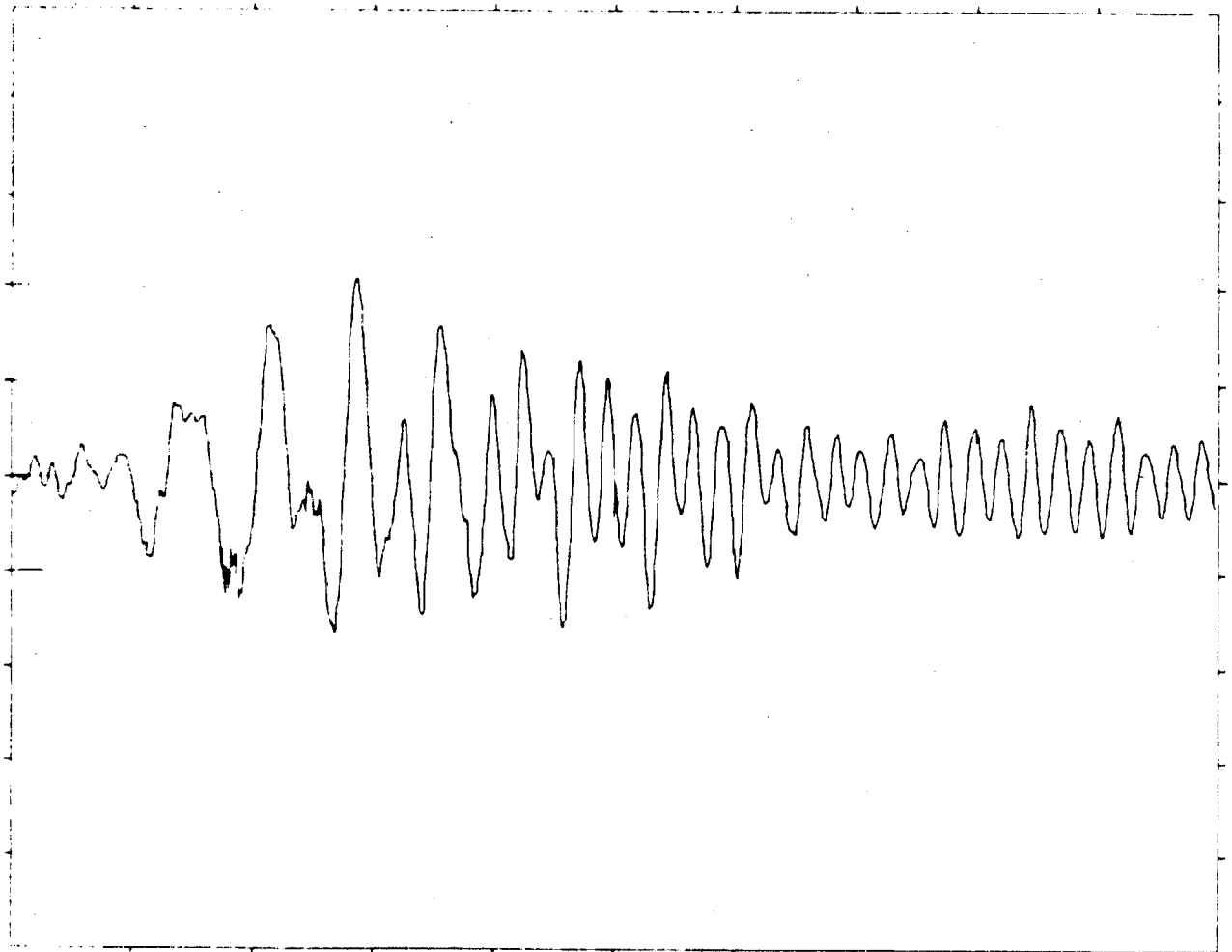

DOMINANT TIME

TIME	MAGNITUDE
0 781E+02	0 2103E+01
0 779E+02	0 2091E+01
0 784E+02	0 2028E+01
0 773E+02	0 2003E+01
0 787E+02	0 1990E+01
0 776E+02	0 1986E+01
0 789E+02	0 1869E+01
0 771E+02	0 1836E+01
0 792E+02	0 1762E+01
0 731E+02	- 1650E+01

-0 500E+01

0 000E+00 TIME IN SECONDS 0 273E+03

ORIGINAL PAGE IS
OF POOR QUALITY

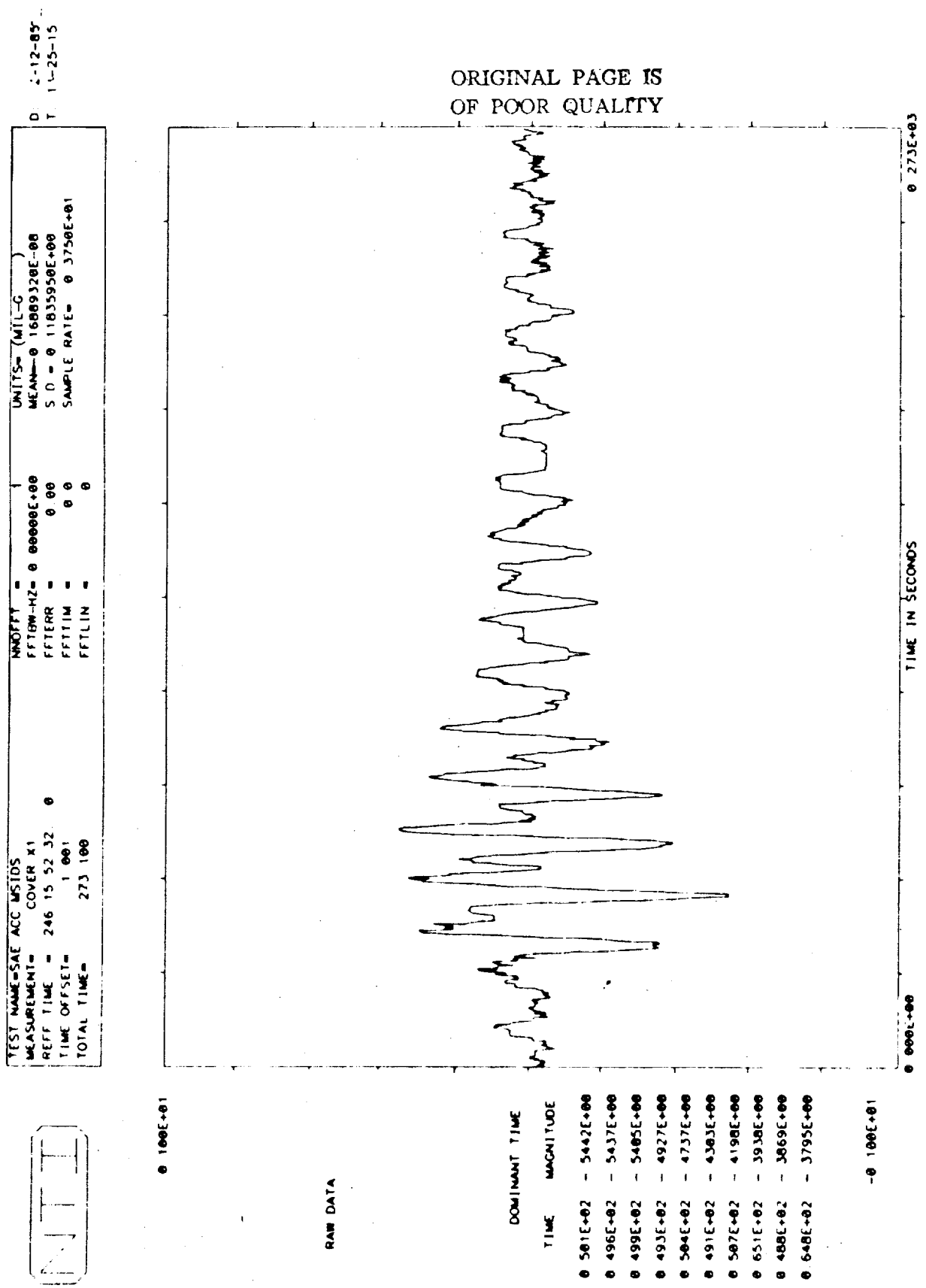
ORIGINAL PAGE IS
OF POOR QUALITY
TEST NAME=SAE ACC MSIDS
MEASUREMENT= COVER X1
REFF TIME = 246 15 52 32 0
TIME OFFSET= 1 001
TOTAL TIME= 273 100
NAOFFT = 1
FFTBW-HZ= 0 00000E+00
FFTERR = 0 00
FFTTIM = 0 0
FFTLIN = 0
UNITS= (MIL-G)
MEAN= 0 16089320E-00
S D = 0 11835950E+00
SAMPLE RATE= 0 3750E+01
D 2-12-85
T 15-25-15
0 100E+01
-0 100E+01
0 000E+00
0 273E+03
TIME IN SECONDS
RAW DATA
DOMINANT TIME
TIME MAGNITUDE
0 501E+02 - 5442E+00
0 496E+02 - 5437E+00
0 499E+02 - 5405E+00
0 493E+02 - 4927E+00
0 504E+02 - 4737E+00
0 491E+02 - 4383E+00
0 507E+02 - 4198E+00
0 651E+02 - 3938E+00
0 488E+02 - 3869E+00
0 648E+02 - 3795E+00

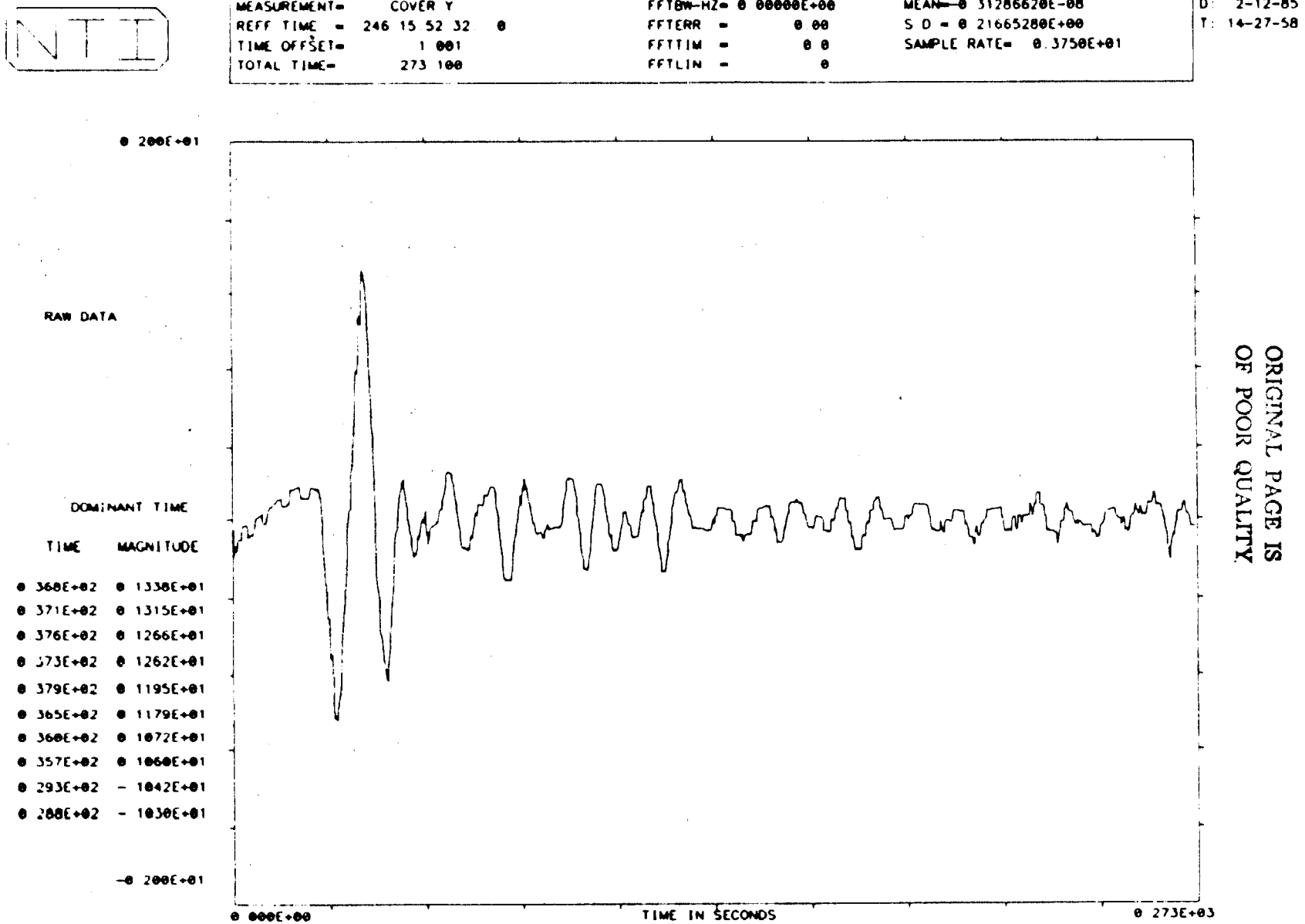

ORIGINAL PAGE IS
OF POOR QUALITY

ORIGINAL PAGE IS
OF POOR QUALITY

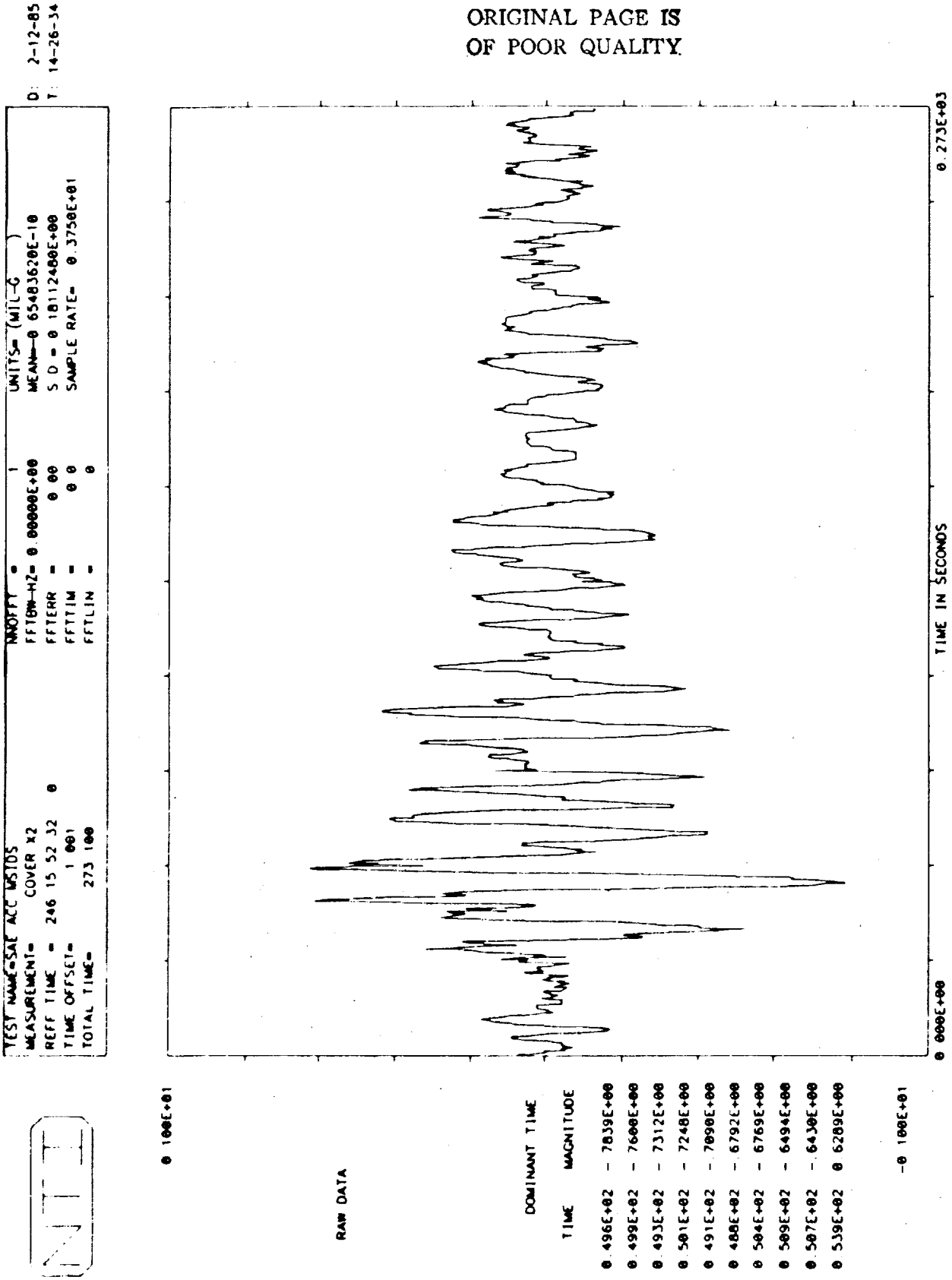

NTI

TEST NAME=SAE ACC MSIDS	NNOFFT = 1	UNITS= (MIL-G)
MEASUREMENT= COVER X1	FFTBW-HZ= 0.00000E+00	MEAN= 0.84492060E-09
REFF TIME = 246 16 30 22. 0	FFTERR = 0.00	S.D. = 0.26332400E+00
TIME OFFSET= 1.001	FFTTIM = 0 0	SAMPLE RATE= 0.3750E+01
TOTAL TIME= 273.100	FFTLIN = 0	

D: 2-12-85
T: 14-29-18

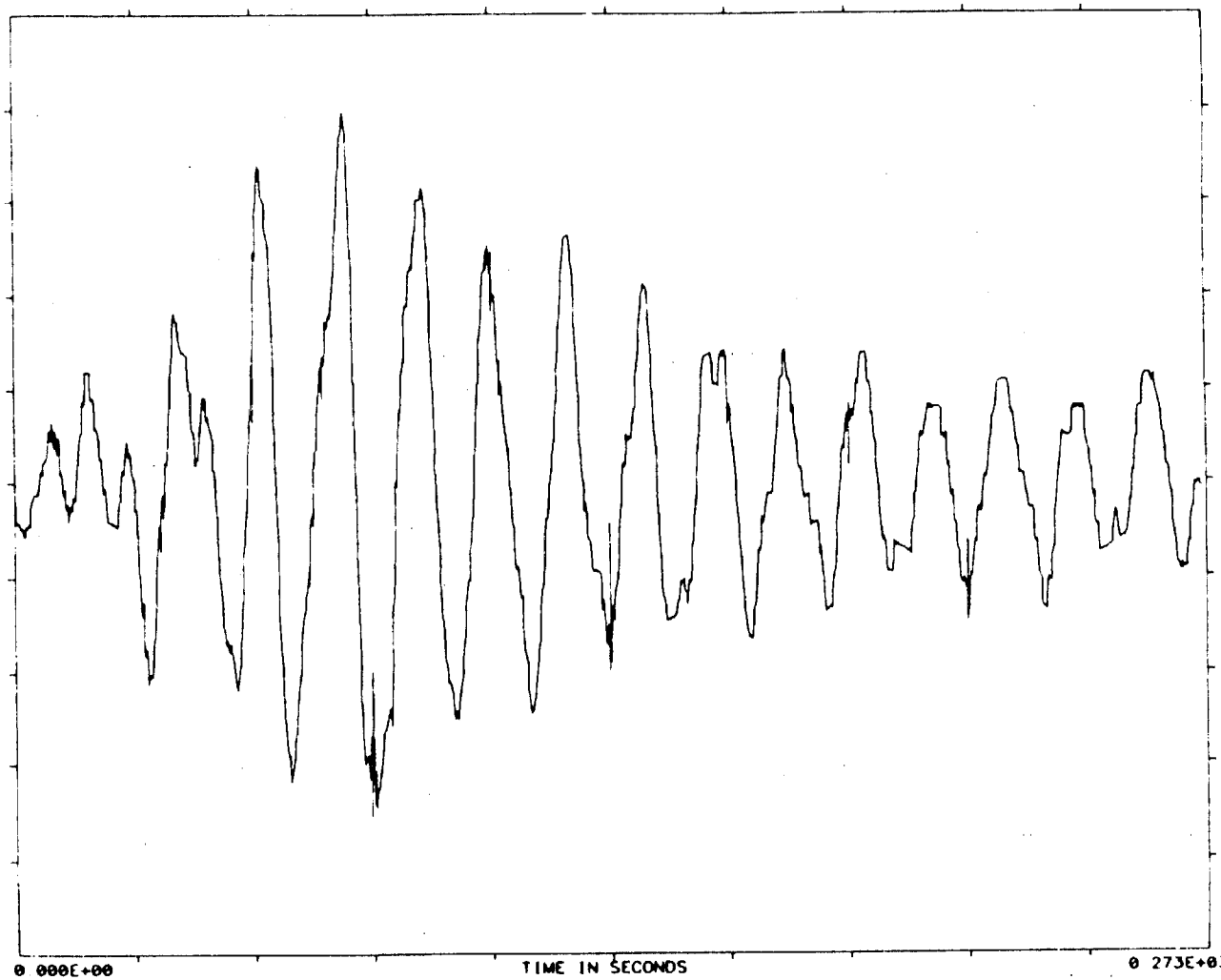

RAW DATA

DOMINANT TIME

TIME	MAGNITUDE
0.757E+02	0.7979E+00
0.760E+02	0.7639E+00
0.763E+02	0.7531E+00
0.752E+02	0.7512E+00
0.755E+02	0.7507E+00
0.749E+02	0.7417E+00
0.816E+02	-.7106E+00
0.747E+02	0.6958E+00
0.765E+02	0.6948E+00
0.827E+02	-.6945E+00

ORIGINAL PAGE IS
OF POOR QUALITY

NTI

TEST NAME=SAE ACC MSIDS	NNOFFT = 1	UNITS= (MIL-G)
MEASUREMENT= COVER Y	FFTBW-HZ= 0 00000E+00	MEAN=-0 10786610E-08
REFF TIME = 246 16 30 22 0	FFTERR = 0 00	S D.= 0 19704790E+00
TIME OFFSET= 1 001	FFTTIM = 0 0	SAMPLE RATE= 0 3750E+01
TOTAL TIME= 273 100	FFTLIN = 0	

D: 2-12-85
T: 14-32- 5

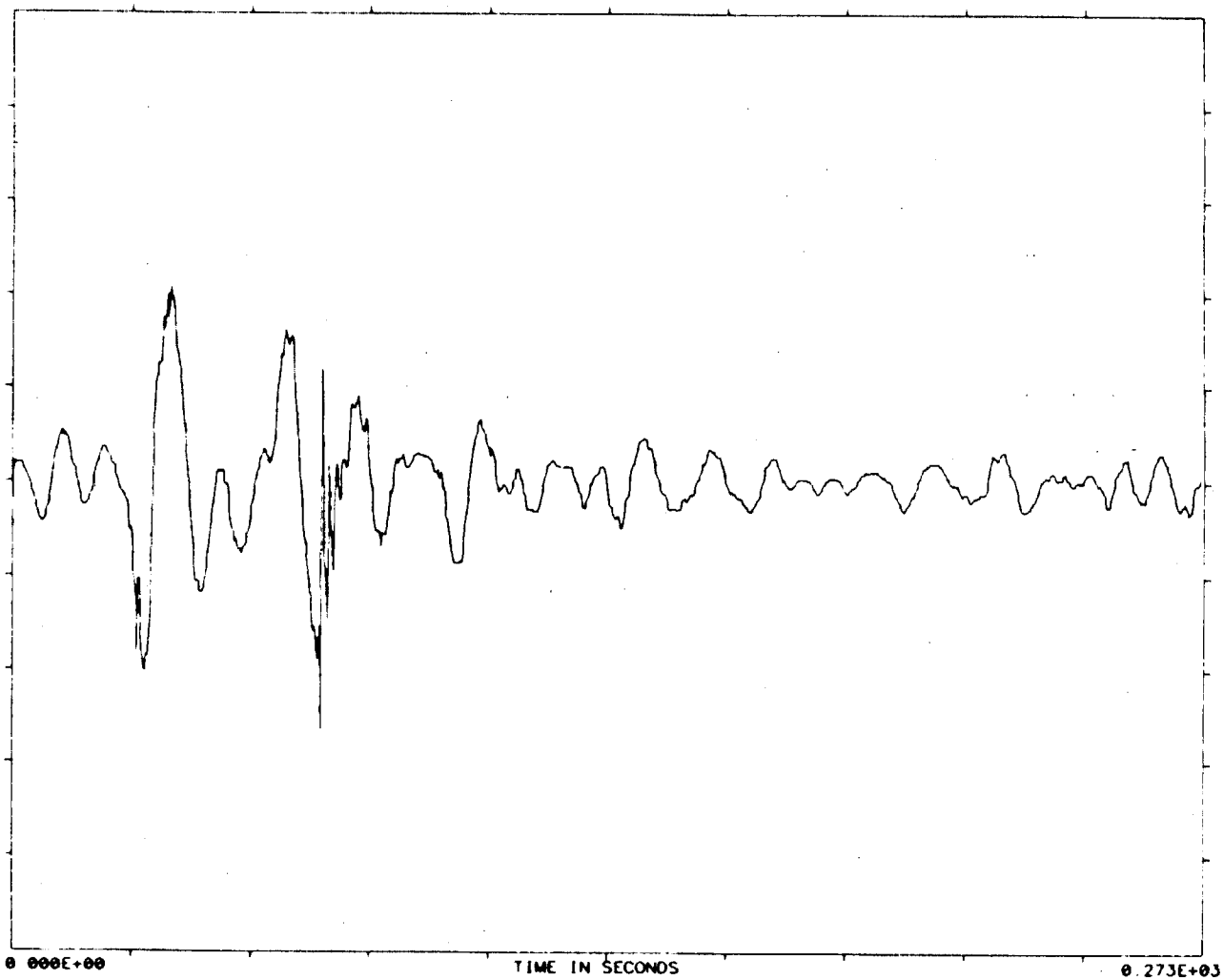

DOMINANT TIME

TIME	MAGNITUDE
0 704E+02	- 1067E+01
0 363E+02	0 8357E+00
0 301E+02	- 8083E+00
0 355E+02	0 8066E+00
0 365E+02	0 8013E+00
0 368E+02	0 7884E+00
0 360E+02	0 7579E+00
0 699E+02	- 7553E+00
0 299E+02	- 7551E+00
0 352E+02	0 7503E+00

NTI

TEST NAME=SAE ACC MSIDS		NNOFFT =	1	UNITS= (MIL-G)	D: 2-12-85
MEASUREMENT=	COVER X2	FFTBW-HZ=	0 00000E+00	MEAN= 0 55479180E-09	T: 14-30-41
REFF TIME =	246 16 30 22 0	FFTERR =	0 00	S D = 0 28967550E+00	
TIME OFFSET=	1 001	FFTTIM =	0 0	SAMPLE RATE= 0 3750E+01	
TOTAL TIME=	273 100	FFTLIN =	0		

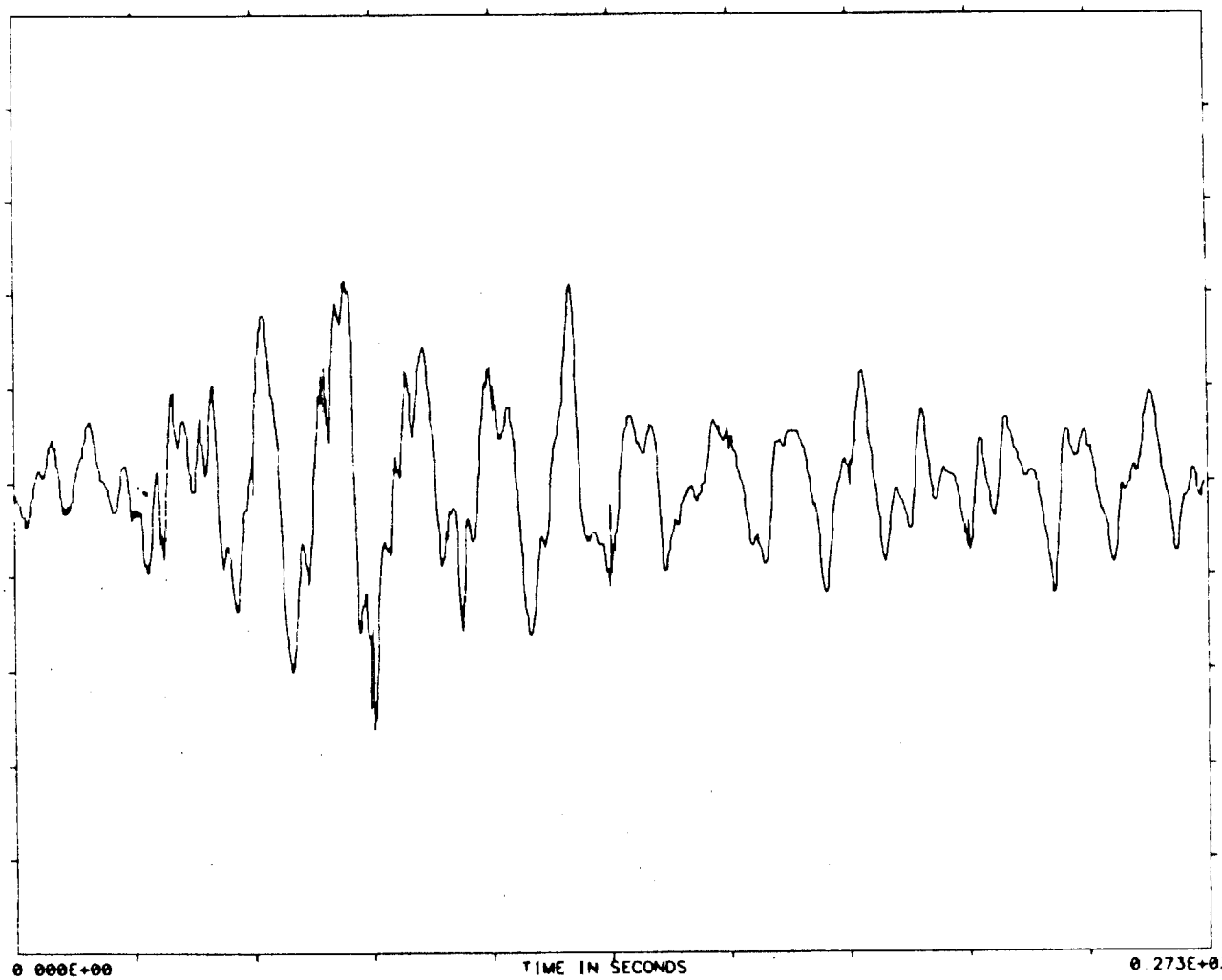

DOMINANT TIME

TIME	MAGNITUDE
0.821E+02	- 1055E+01
0 827E+02	- 1007E+01
0 824E+02	- 9637E+00
0 816E+02	- 9608E+00
0 757E+02	0 8688E+00
0 755E+02	0 8491E+00
0 127E+03	0 8458E+00
0 127E+03	0 8456E+00
0 829E+02	- 8256E+00
0 127E+03	0 8231E+00

ORIGINAL PAGE IS
OF POOR QUALITY

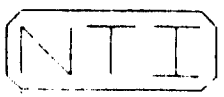

TEST NAME=SAE ACC MSIDS		NNOFFT =	1	UNITS= (MIL-G)	D: 2-12-85
MEASUREMENT=	COVER X1	FFTBW-HZ=	0 00000E+00	MEAN= 0 87311490E-09	T: 14-33-36
REFF TIME =	246 17 23 4 0	FFTERR =	0 00	S D = 0 28511730E+00	
TIME OFFSET=	1 001	FFTTIM =	0.0	SAMPLE RATE= 0 3750E+01	
TOTAL TIME=	273.100	FFTLIN =	0		

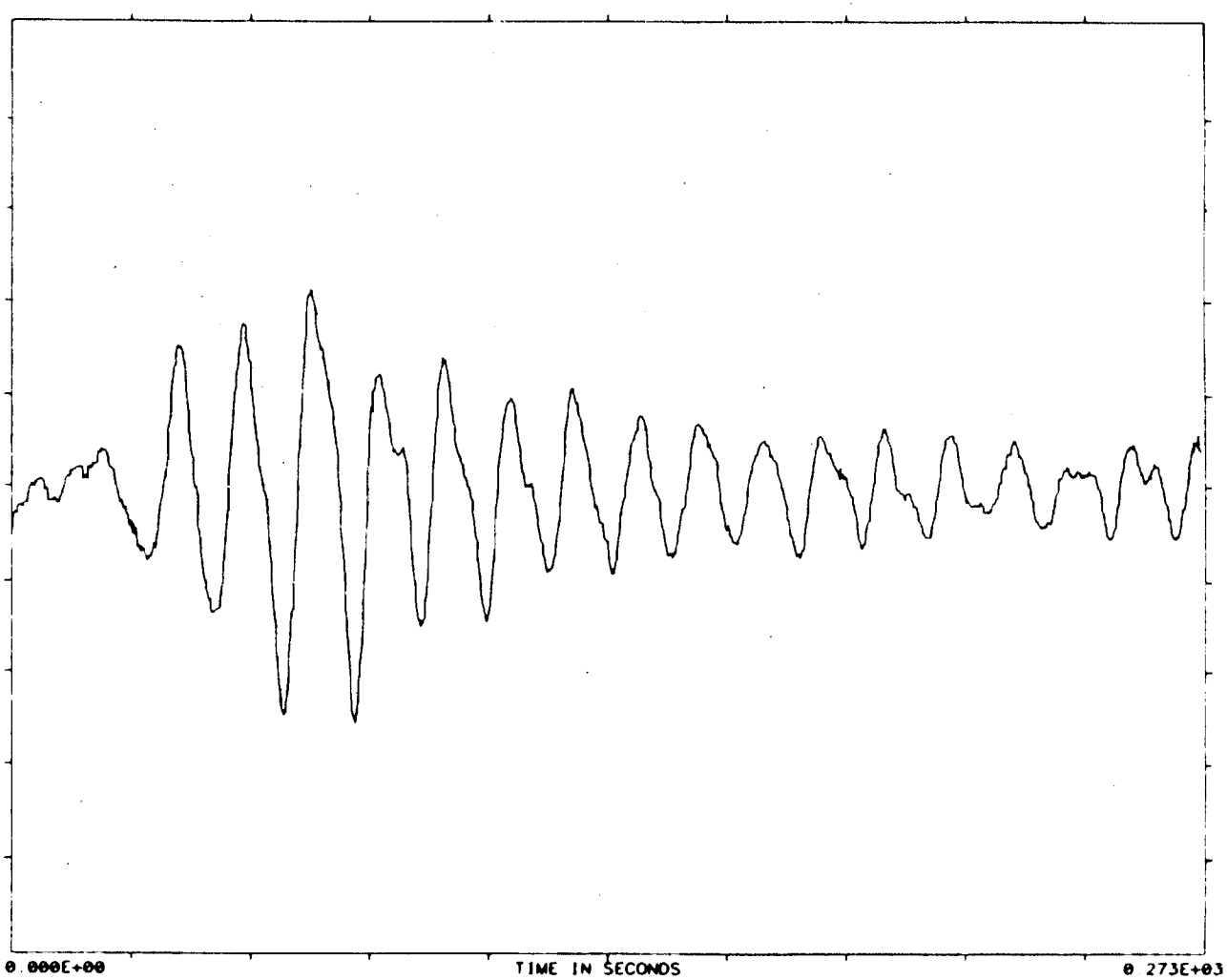

DOMINANT TIME

TIME	MAGNITUDE
0 787E+02	- 1025E+01
0.784E+02	- 1012E+01
0.781E+02	- 9964E+00
0 621E+02	- 9925E+00
0.789E+02	- 9769E+00
0 619E+02	- 9715E+00
0.624E+02	- 9667E+00
0 779E+02	- 9634E+00
0 627E+02	- 9498E+00
0 616E+02	- 9411E+00

ORIGINAL PAGE IS
OF POOR QUALITY

TEST NAME=SAE ACC MSTDS		NNOFFT =	1	UNITS= (MIL-G)	
MEASUREMENT=	COVER Y	FFTBW-HZ=	0.00000E+00	MEAN= 0.74578570E-09	D: 2-12-85
REFF TIME =	246 17 23 4 0	FFTERR =	0.00	S.D.= 0.16622690E+00	T: 14-37-12
TIME OFFSET=	1.001	FFTTIM =	0 0	SAMPLE RATE= 0.3750E+01	
TOTAL TIME=	273.100	FFTLIN =	0		

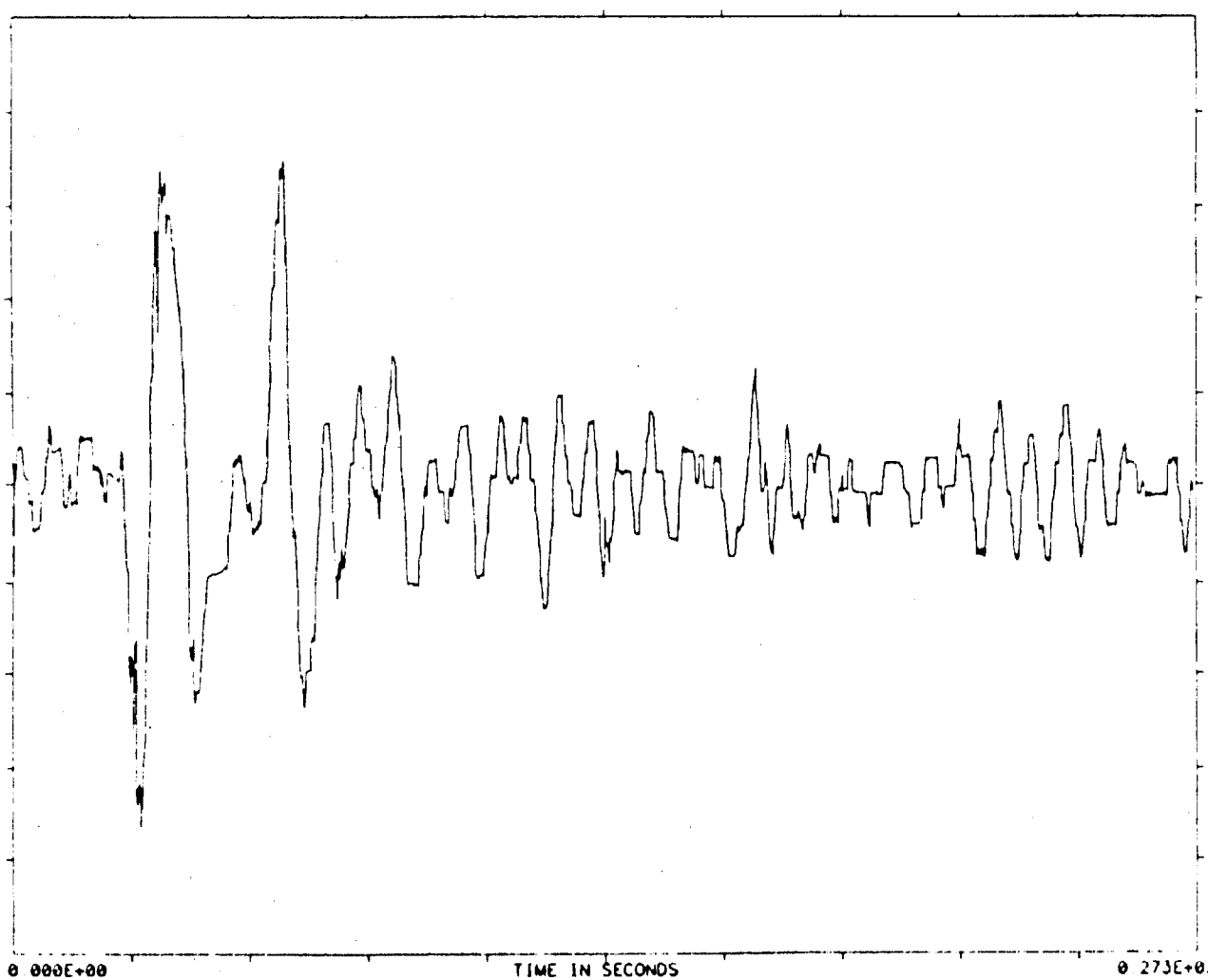

DOMINANT TIME

TIME	MAGNITUDE
0.296E+02	- 7310E+00
0.624E+02	0 7019E+00
0.627E+02	0 6938E+00
0.341E+02	0 6887E+00
0.619E+02	0 6863E+00
0.288E+02	-.6831E+00
0.621E+02	0 6590E+00
0.352E+02	0 6568E+00
0.293E+02	-.6534E+00
0.299E+02	- 6460E+00

ORIGINAL PAGE IS
OF POOR QUALITY

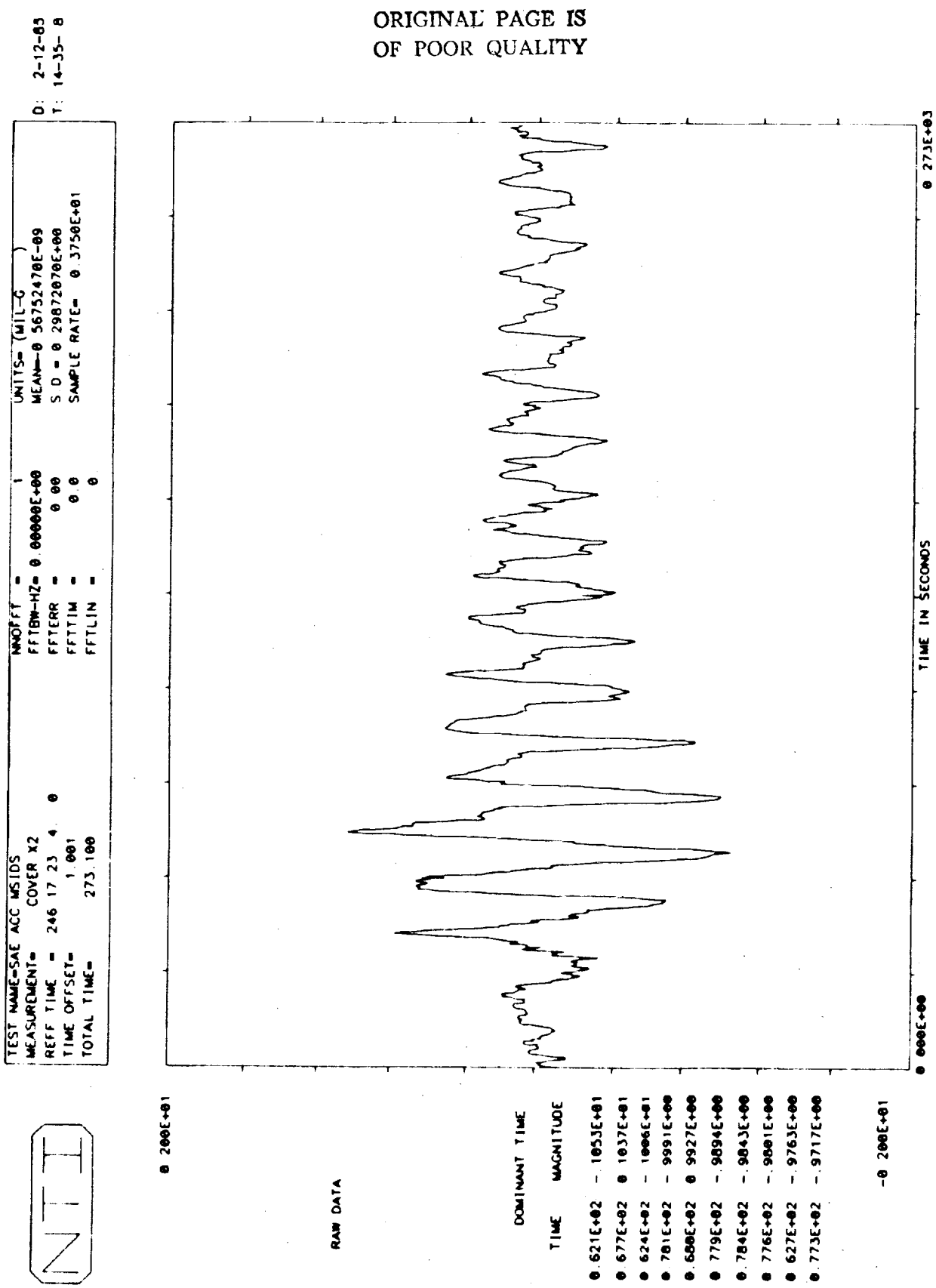

TEST NAME=SAE ACC WSTDS	NNOFFT = 1	UNITS= (MIL-G)
MEASUREMENT= COVER X1	FFTBW-HZ= 0 00000E+00	MEAN=-0 11012160E-07
REFF TIME = 246 18 6 29 0	FFTERR = 0 00	S D = 0 51032360E+00
TIME OFFSET= 1 001	FFTTIM = 0 0	SAMPLE RATE= 0 3750E+01
TOTAL TIME= 273 100	FFTLIN = 0	

D 12-85
T 14-38-48

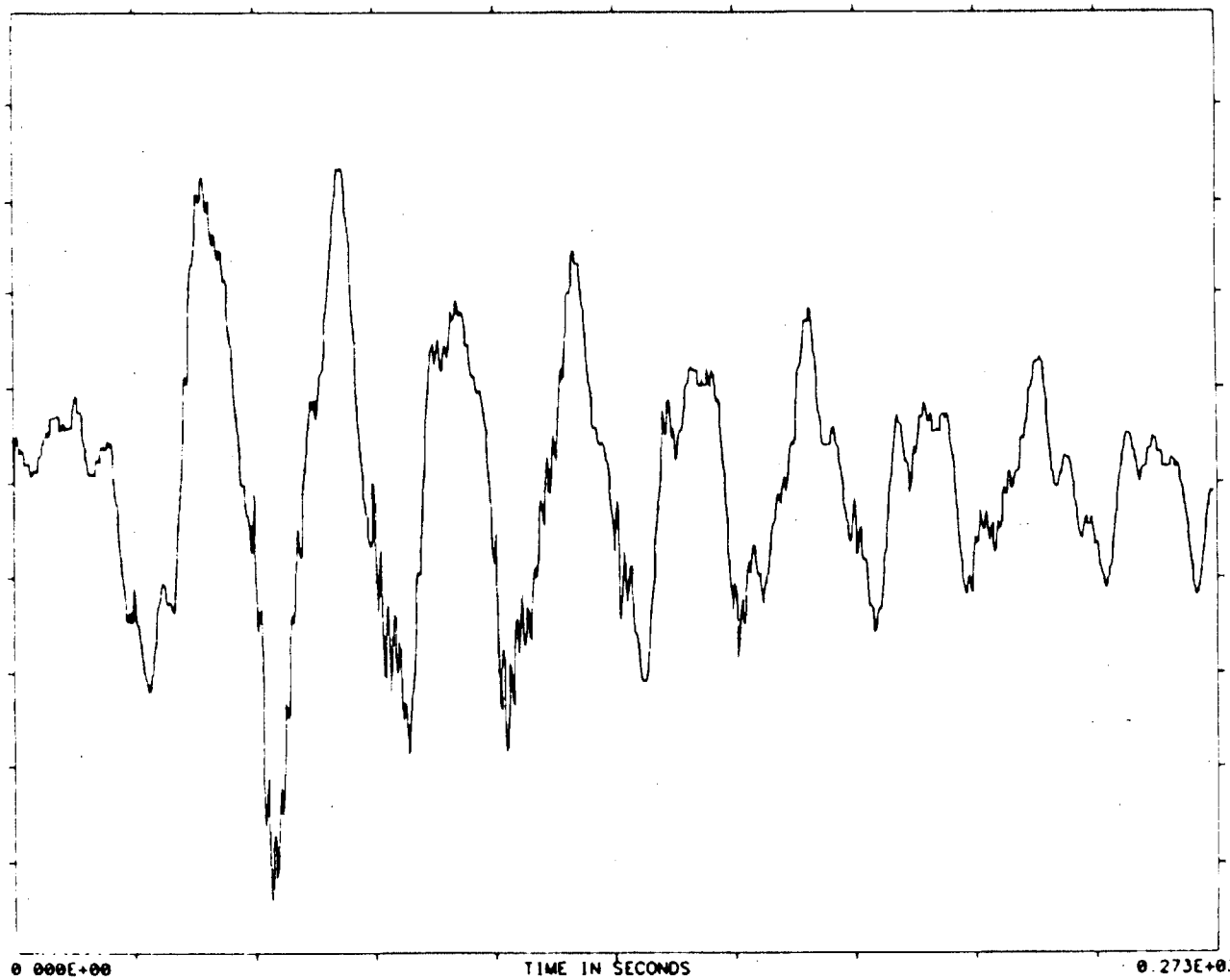

DOMINANT TIME

TIME	MAGNITUDE
0 581E+02	- 1773E+01
0 584E+02	- 1704E+01
0 595E+02	- 1672E+01
0 597E+02	- 1618E+01
0 579E+02	- 1588E+01
0 592E+02	- 1568E+01
0 587E+02	- 1547E+01
0 589E+02	- 1467E+01
0 568E+02	- 1447E+01
0 600E+02	- 1415E+01

C-26

ORIGINAL PAGE IS
OF POOR QUALITY

NTI

TEST NAME=SAE ACC MSIDS		NNOFFT =	1	UNITS= (MIL-G)	D: 2-12-85
MEASUREMENT=	COVER Y	FFTBW-HZ=	0 00000E+00	MEAN=-0 15425030E-08	T: 14-42-11
REFF TIME =	246 18 6 29 0	FFTERR =	0 00	S D = 0 76232910E-01	
TIME OFFSET=	1 001	FFTTIM =	0 0	SAMPLE RATE= 0 3750E+01	
TOTAL TIME=	273 100	FFTLIN =	0		

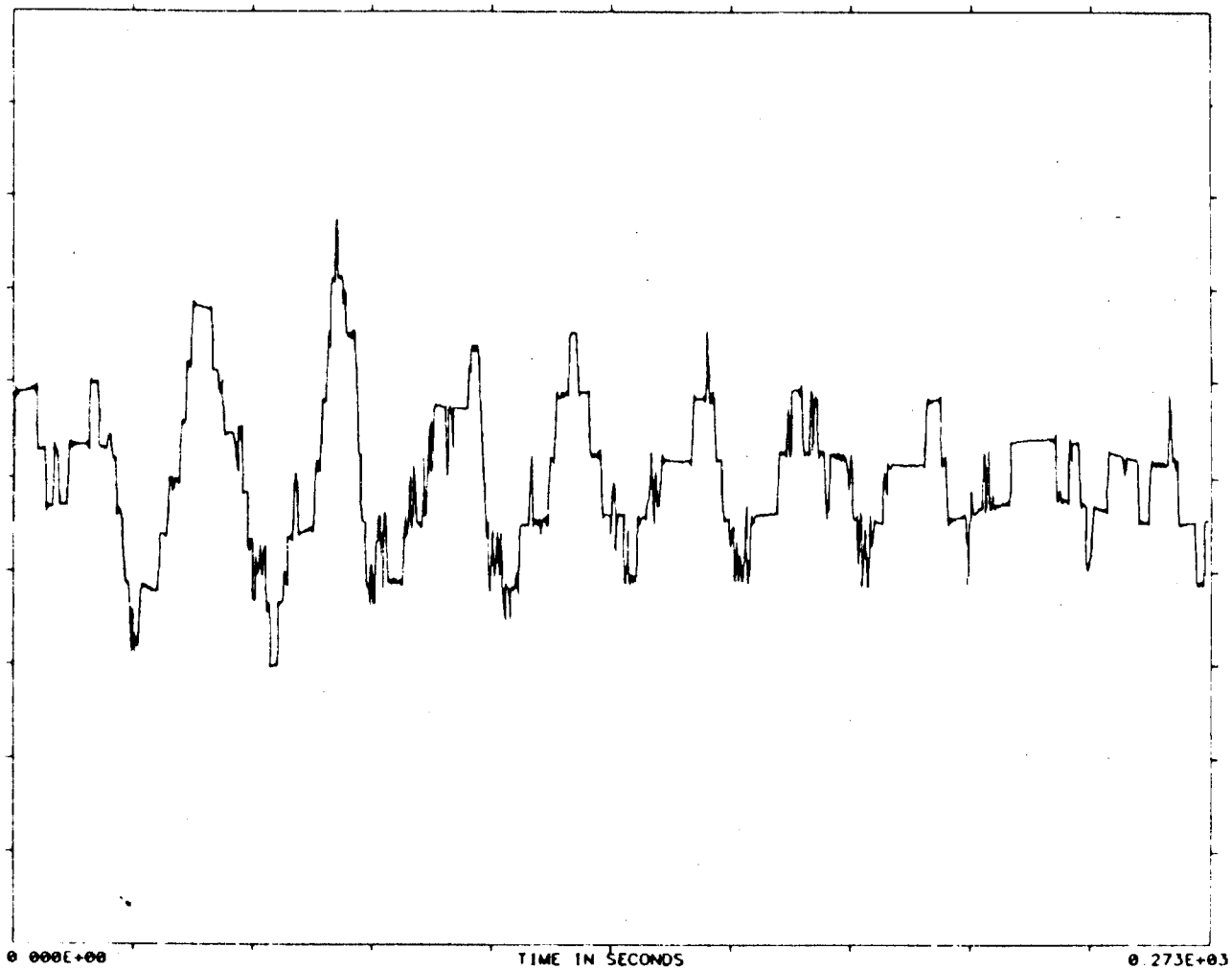

DOMINANT TIME

TIME	MAGNITUDE
0 739E+02	0 2761E+00
0 736E+02	0 2444E+00
0 749E+02	0 2158E+00
0 744E+02	0 2155E+00
0 731E+02	0 2134E+00
0 728E+02	0 2134E+00
0 747E+02	0 2117E+00
0 741E+02	0 2111E+00
0 752E+02	0 2068E+00
0 733E+02	0 2065E+00

ORIGINAL PAGE IS
OF POOR QUALITY

NTI

TEST NAME=SAE ACC MSIDS	NNOFFT = 1	UNITS= (MIL-G)	D: 2-12-8
MEASUREMENT= COVER X2	FFTBW-HZ= 0 00000E+00	MEAN=-0 14311810E-07	T: 14-40-2
REFF TIME = 246 18 6 29 0	FFTERR = 0 00	S D = 0 53818800E+00	
TIME OFFSET= 1 001	FFTTIM = 0 0	SAMPLE RATE= 0 3750E+01	
TOTAL TIME= 273 100	FFTLIN = 0		

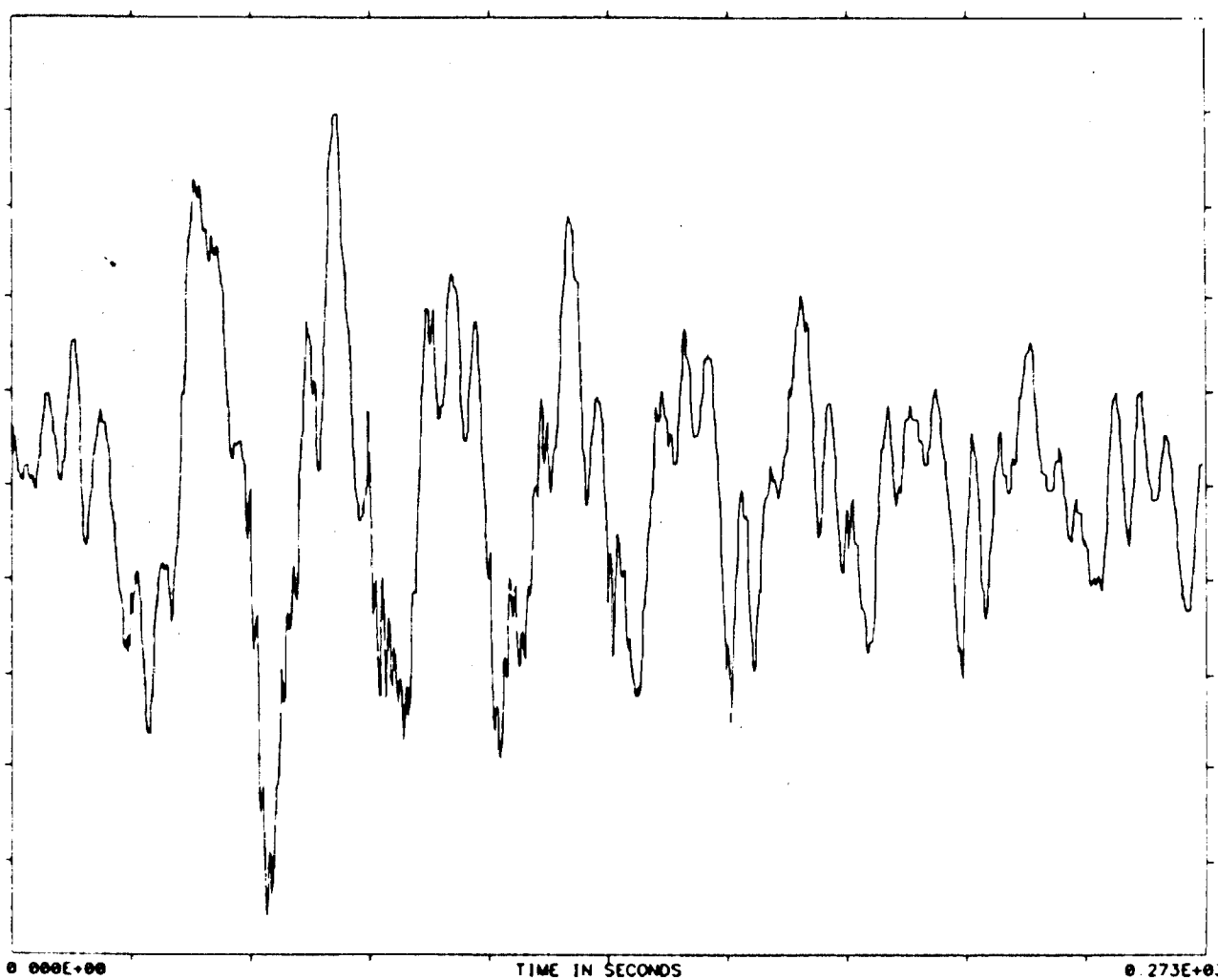

DOMINANT TIME

TIME	MAGNITUDE
0 581E+02	- 1842E+01
0 584E+02	- 1768E+01
0 595E+02	- 1748E+01
0 579E+02	- 1686E+01
0 597E+02	- 1673E+01
0 592E+02	- 1658E+01
0 587E+02	- 1640E+01
0 739E+02	0 1590E+01
0 744E+02	0 1589E+01
0 741E+02	0 1589E+01

ORIGINAL PAGE IS
OF POOR QUALITY

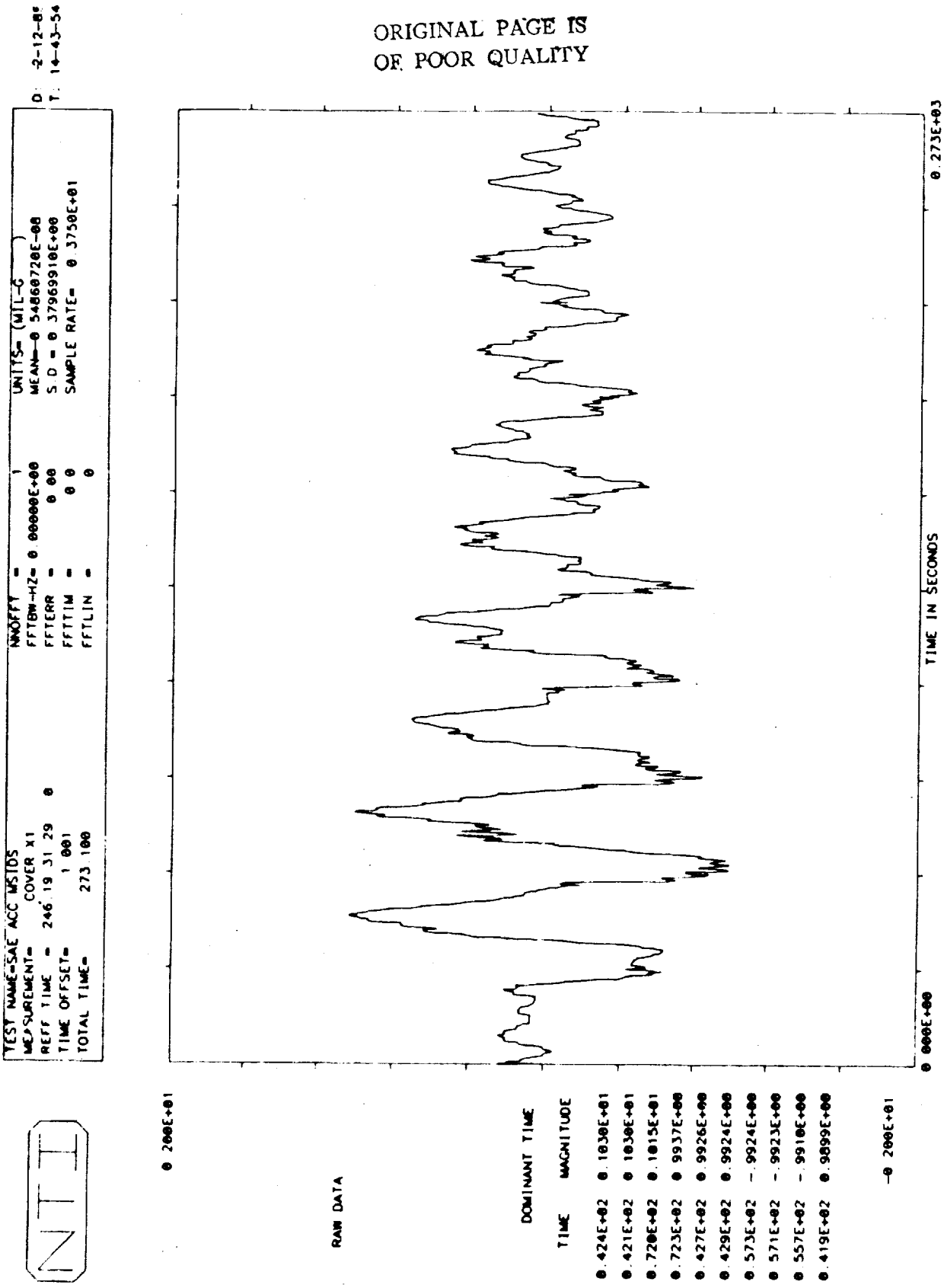

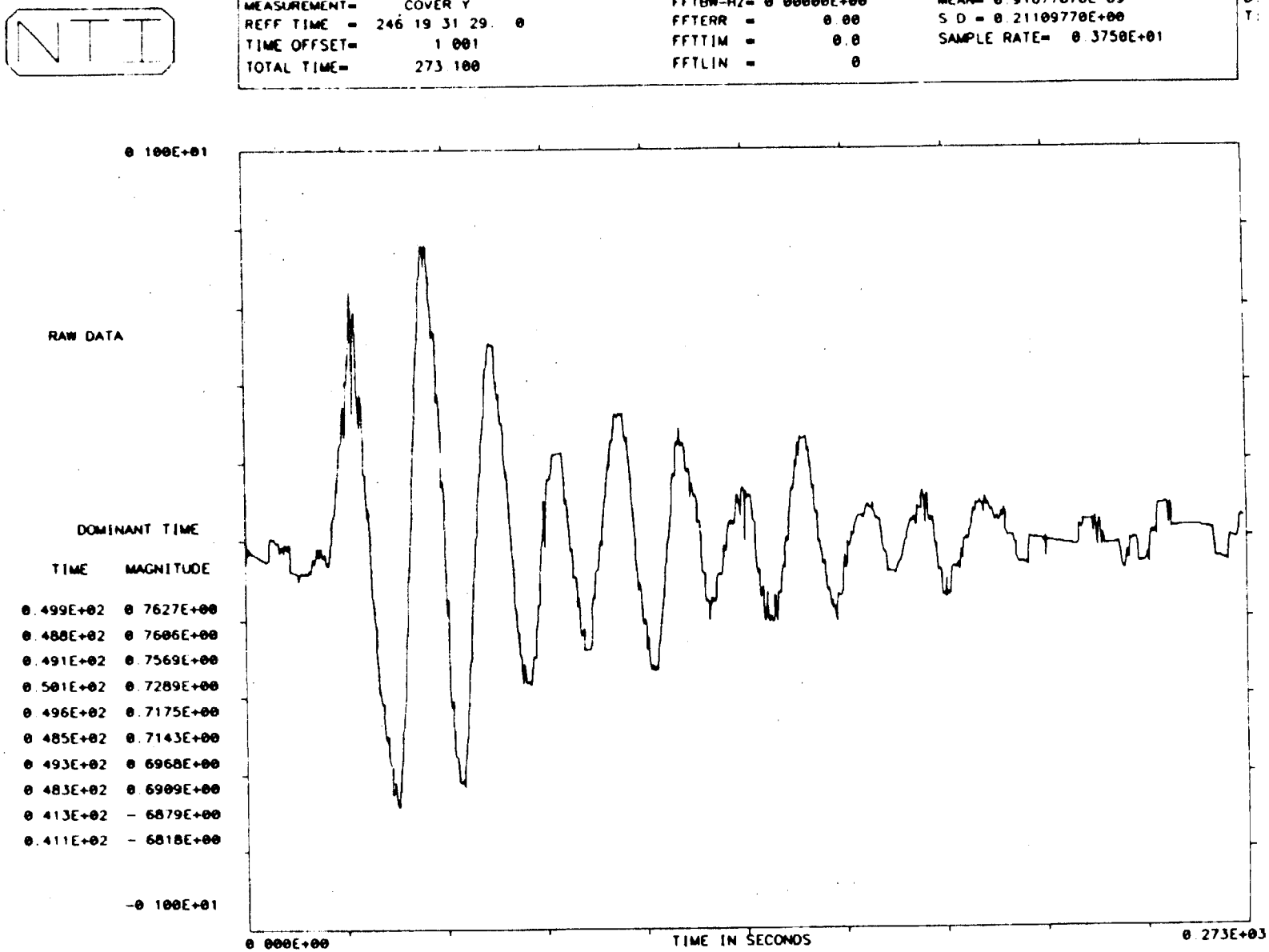

ORIGINAL PAGE IS
OF POOR QUALITY

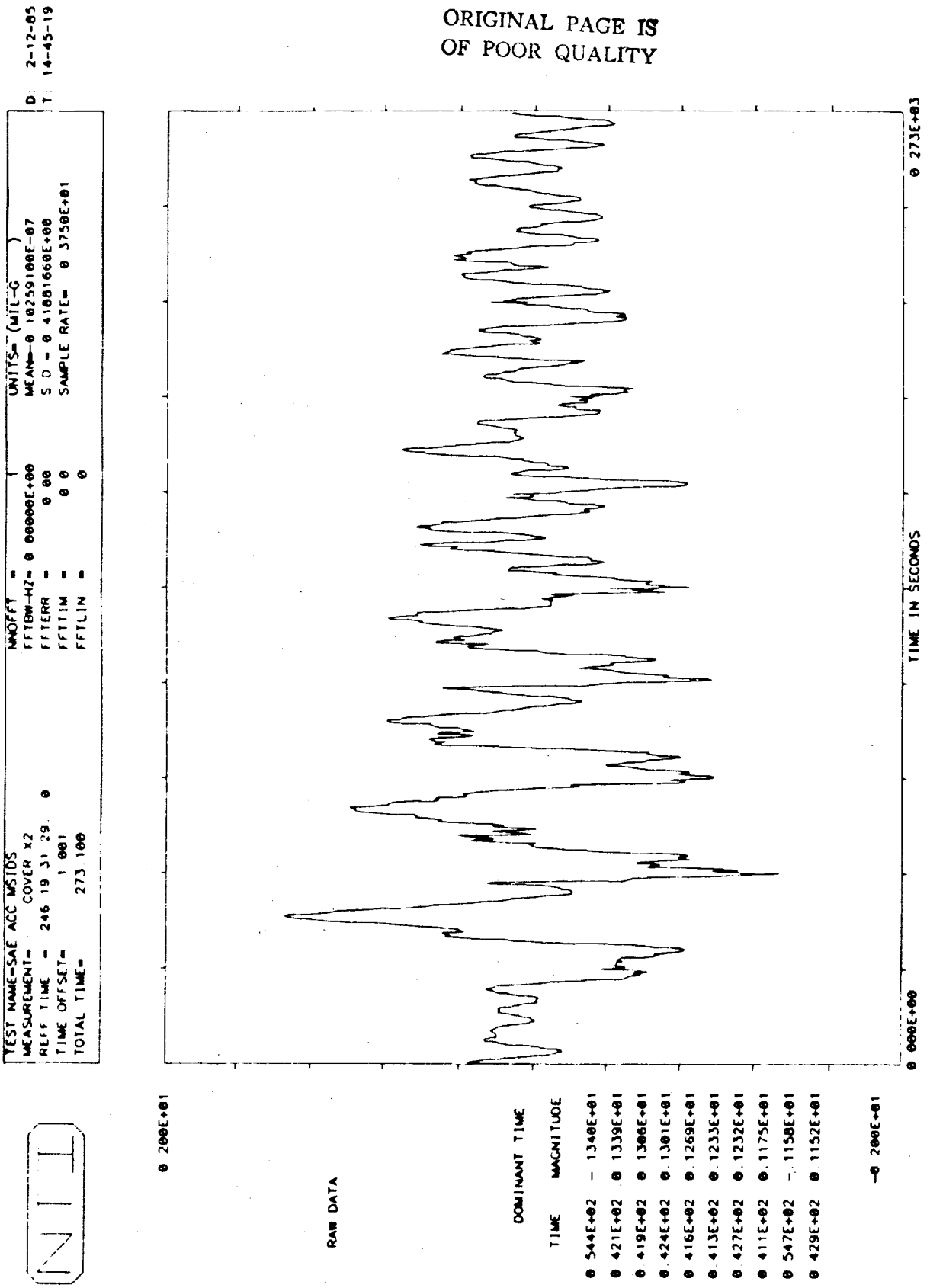

TEST NAME=SAE ACC MSIDS		NNOFFT =	1	UNITS= (MTL-G)	
MEASUREMENT=	COVER X1	FFTBW-HZ=	0 00000E+00	MEAN= 0 42018660E-09	D: 2-12-85
REFF TIME =	247 16 2 11. 0	FFTERR =	0 00	S D = 0 22344040E+00	T: 14-53-50
TIME OFFSET=	1 001	FFTTIM =	0 0	SAMPLE RATE= 0 3750E+01	
TOTAL TIME=	273 100	FFTLIN =	0		

0 100E+01

RAW DATA

DOMINANT TIME

TIME	MAGNITUDE
0 797E+02	0 6187E+00
0 800E+02	0 6113E+00
0 792E+02	0 6110E+00
0 795E+02	0 6102E+00
0 103E+03	- 6098E+00
0 103E+03	- 6066E+00
0 103E+03	- 6062E+00
0 787E+02	0 6062E+00
0 102E+03	- 6061E+00
0 936E+02	0 6041E+00

-0 100E+01

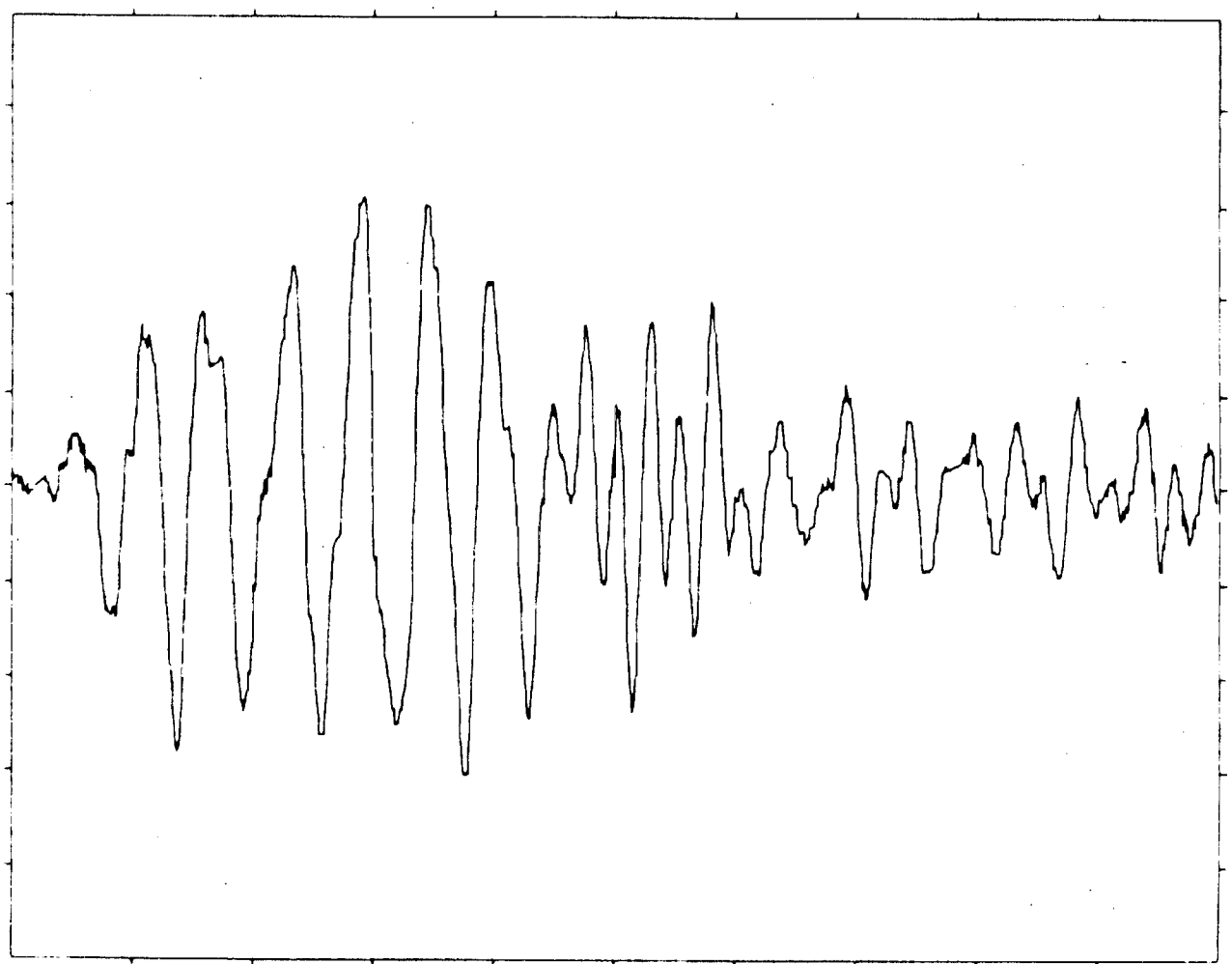

0 000E+00 TIME IN SECONDS 0 273E+03

ORIGINAL PAGE IS
OF POOR QUALITY

ORIGINAL PAGE IS
OF POOR QUALITY

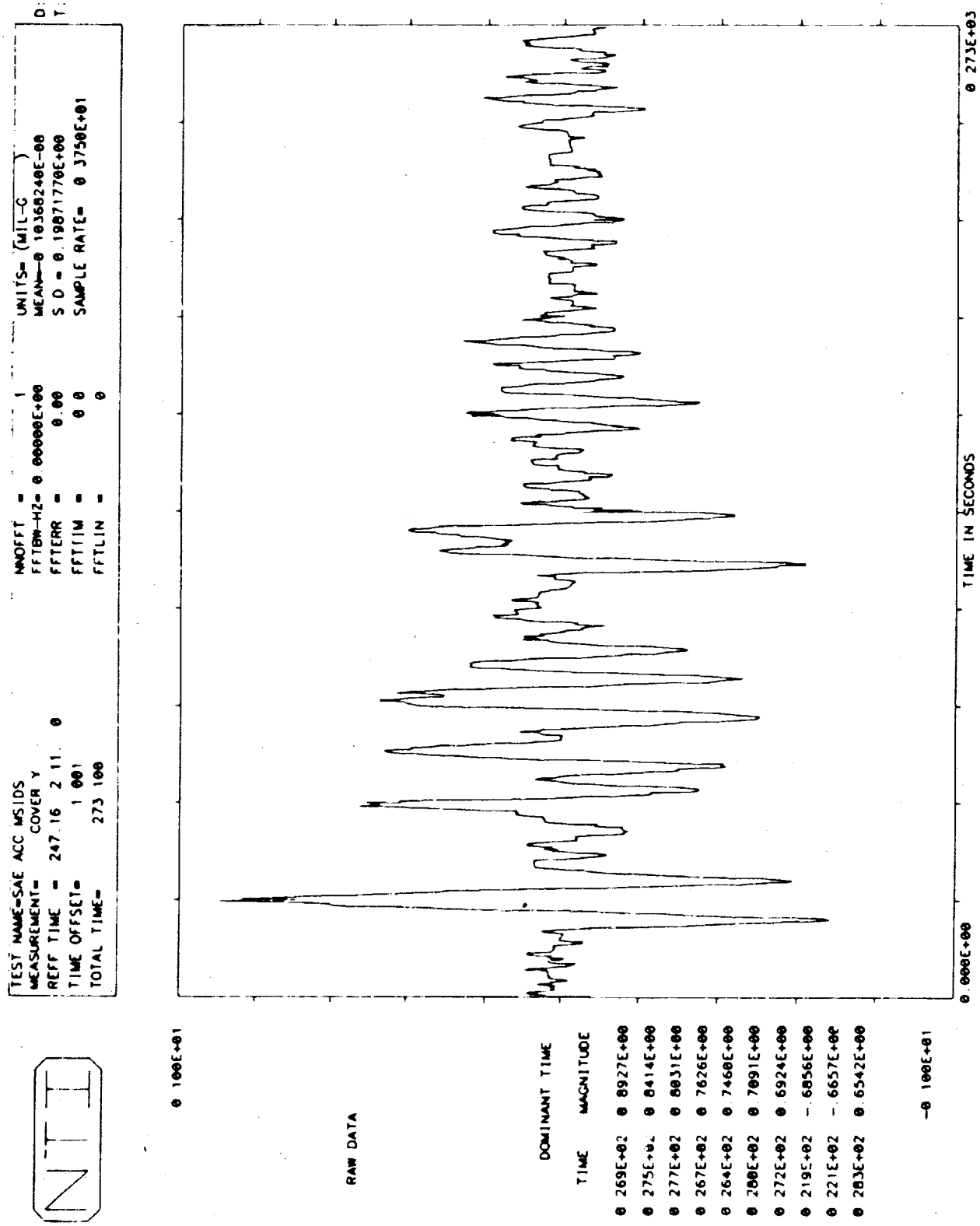

NTI

TEST NAME=SAE ACC MSIDS		NNOFFT =	1	UNITS= (MIL-G)	
MEASUREMENT=	COVER X2	FFTBW-HZ=	0.00000E+00	MEAN= 0.80035540E-09	D: 2-12-85
REFF TIME =	247 16 2 11. 0	FFTERR =	0.00	S D = 0.26401210E+00	T: 14-55- 9
TIME OFFSET=	1.001	FFTTIM =	0.0	SAMPLE RATE= 0.3750E+01	
TOTAL TIME=	273.100	FFTLIN =	0		

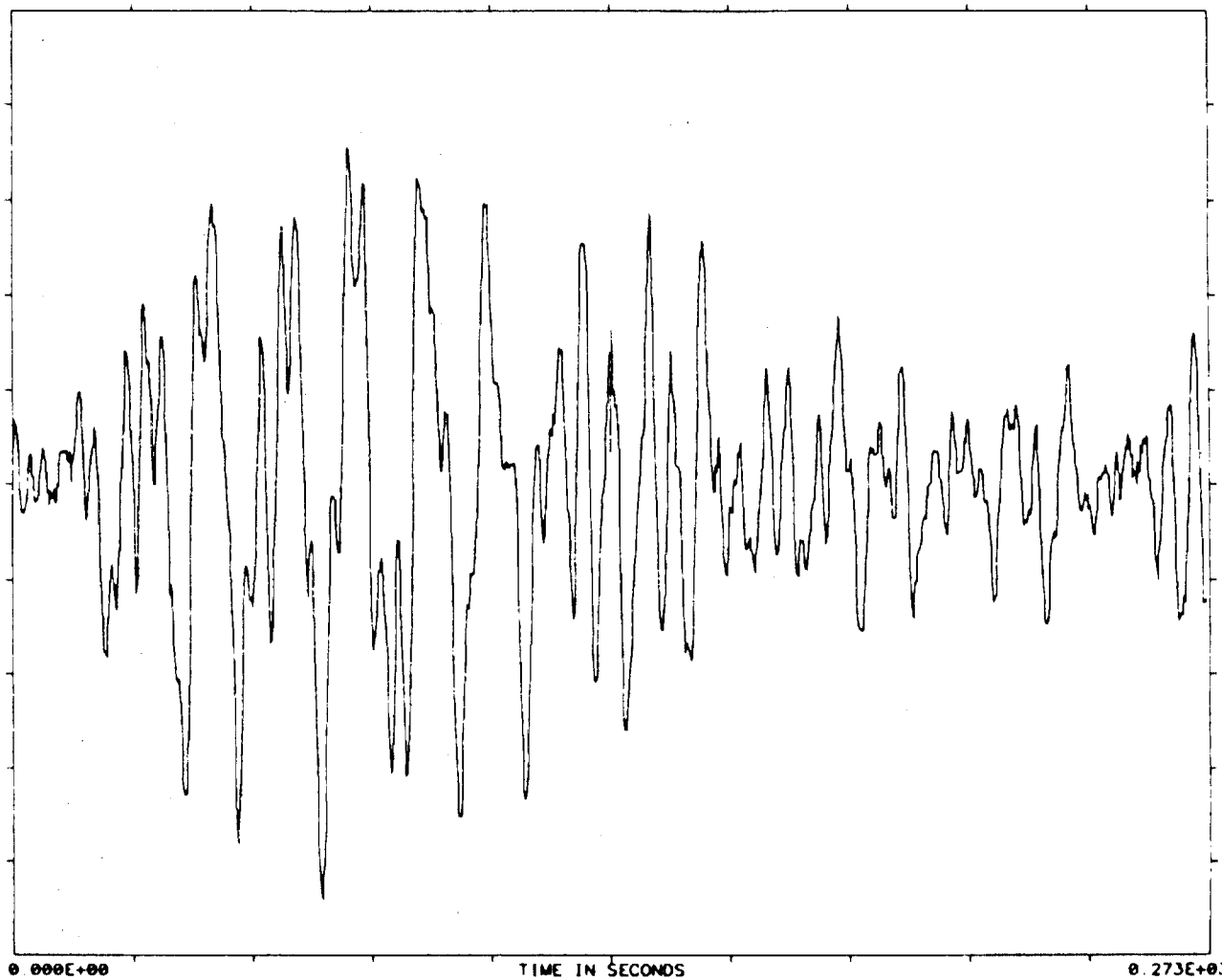

DOMINANT TIME

TIME	MAGNITUDE
0.704E+02	-.8840E+00
0.701E+02	-.8730E+00
0.707E+02	-.8334E+00
0.699E+02	-.8147E+00
0.709E+02	-.8044E+00
0.512E+02	-.7627E+00
0.696E+02	-.7574E+00
0.509E+02	-.7425E+00
0.712E+02	-.7191E+00
0.515E+02	-.7178E+00

ORIGINAL PAGE IS
OF POOR QUALITY

NTI

TEST NAME=SAE ACC MSIDS		NNOFFT =	1	UNITS= (MIL-G)	D: 12-12-85
MEASUREMENT=	COVER X1	FFTBW-HZ=	0.00000E+00	MEAN=-0.41036400E-08	T: 14-57-56
REFF TIME =	247 16 37 24. 0	FFTERR =	0.00	S.D. = 0.38237610E+00	
TIME OFFSET=	1 001	FFTTIM =	0 0	SAMPLE RATE= 0.3750E+01	
TOTAL TIME=	273 100	FFTLIN =	0		

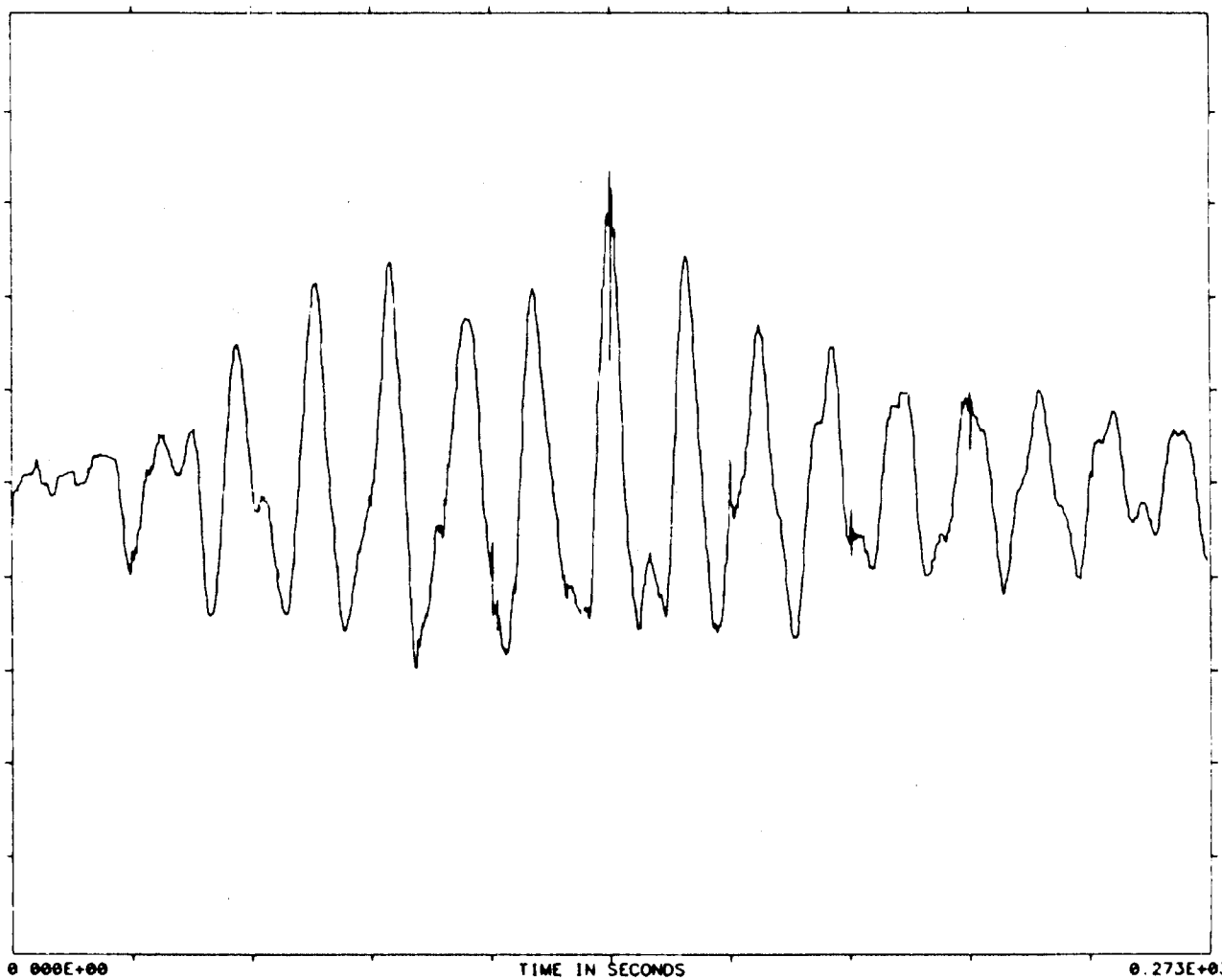

DOMINANT TIME

TIME	MAGNITUDE
0.136E+03	0.1346E+01
0.137E+03	0.1265E+01
0.136E+03	0.1155E+0.
0.136E+03	0.1102E+01
0.137E+03	0.1085E+01
0.137E+03	0.1050E+01
0.135E+03	0.1044E+01
0.135E+03	0.1006E+01
0.154E+03	0.9766E+00
0.153E+03	0.9681E+00

ORIGINAL PAGE IS
OF POOR QUALITY

NTI

TEST NAME=SAE ACC MSIDS		NNOFFT =	1	UNITS= (MIL-G)	
MEASUREMENT= COVER Y		FFTBW-HZ=	0.00000E+00	MEAN= 0.67666410E-09	D: 2-12-85
REFF TIME = 247.16.37.24. 0		FFTERR =	0.00	S.D = 0.23295560E+00	T: 15- 1- 6
TIME OFFSET= 1.001		FFTTIM =	0.0	SAMPLE RATE= 0.3750E+01	
TOTAL TIME= 273.100		FFTLIN =	0		

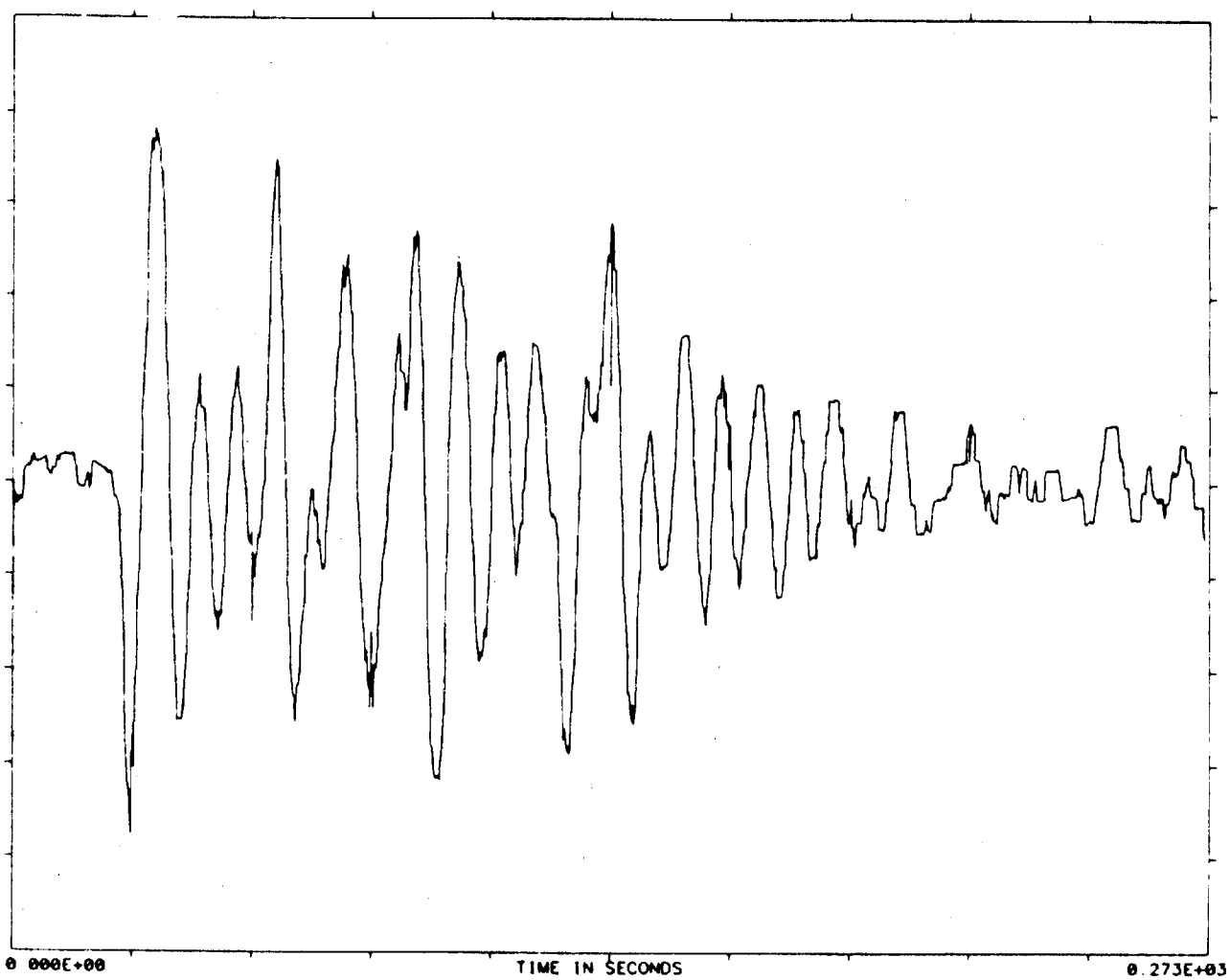

DOMINANT TIME

TIME	MAGNITUDE
0.325E+02	0.7665E+00
0.269E+02	-.7527E+00
0.328E+02	0.7497E+00
0.315E+02	0.7434E+00
0.320E+02	0.73[illegible]E+00
0.323E+02	0.7340E+00
0.331E+02	0.7261E+00
0.333E+02	0.7208E+00
0.317E+02	0.7093E+00
0.312E+02	0.7080E+00

ORIGINAL PAGE IS
OF POOR QUALITY

ORIGINAL PAGE IS
OF POOR QUALITY

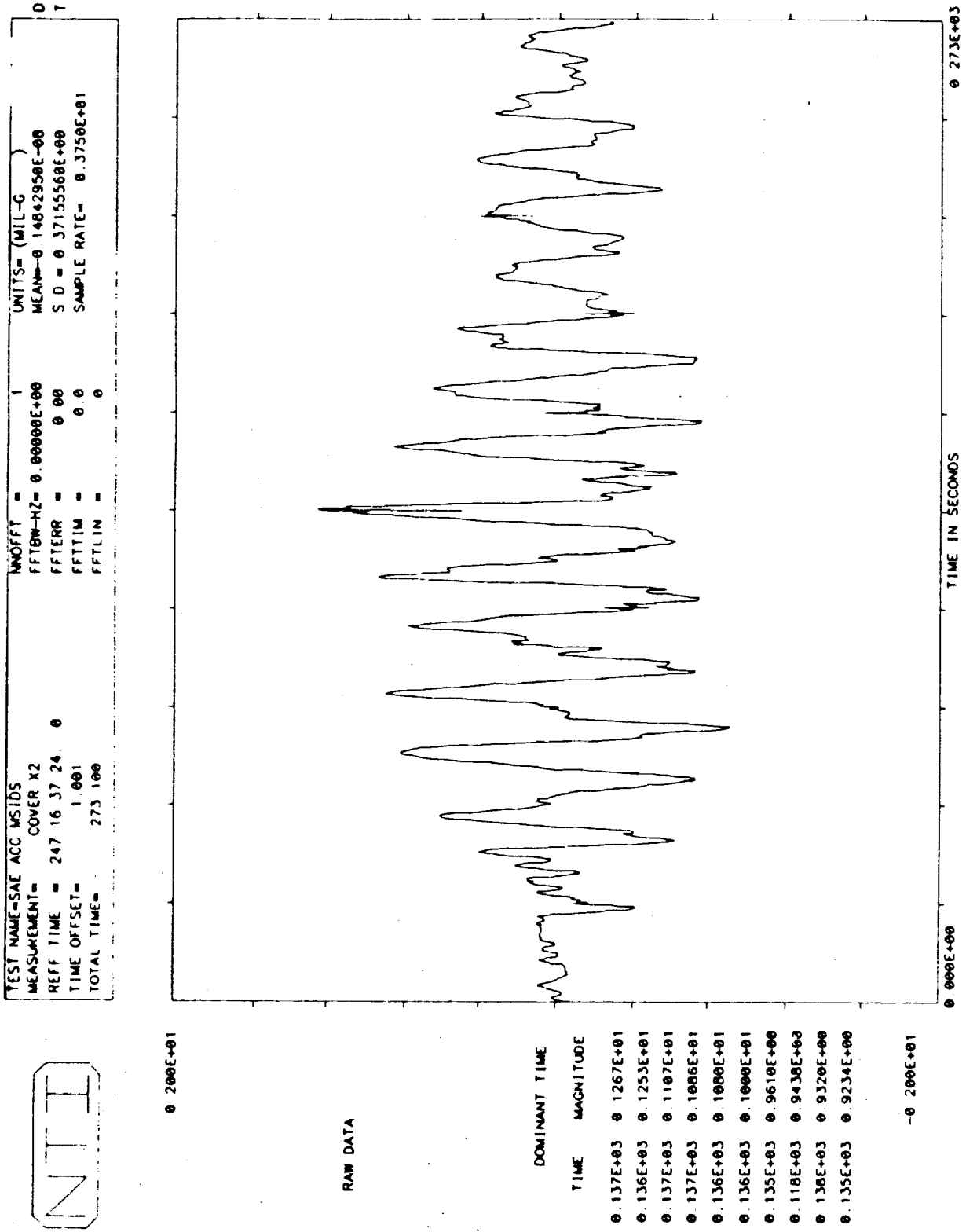

NTI

TEST NAME=SAE ACC MSIDS		NAVOFFT =	1	UNITS= (MIL-G)	
MEASUREMENT=	COVER X1	FFTBW-HZ=	0.00000E+00	MEAN= 0.49112710E-10	D: 2-13-85
REFF TIME =	247.17 32 39. 0	FFTERR =	0.00	S.D.= 0.14472160E+00	T: 7-26-31
TIME OFFSET=	1.001	FFTTIM =	0.0	SAMPLE RATE= 0.3750E+01	
TOTAL TIME=	273.100	FFTLIN =	0		

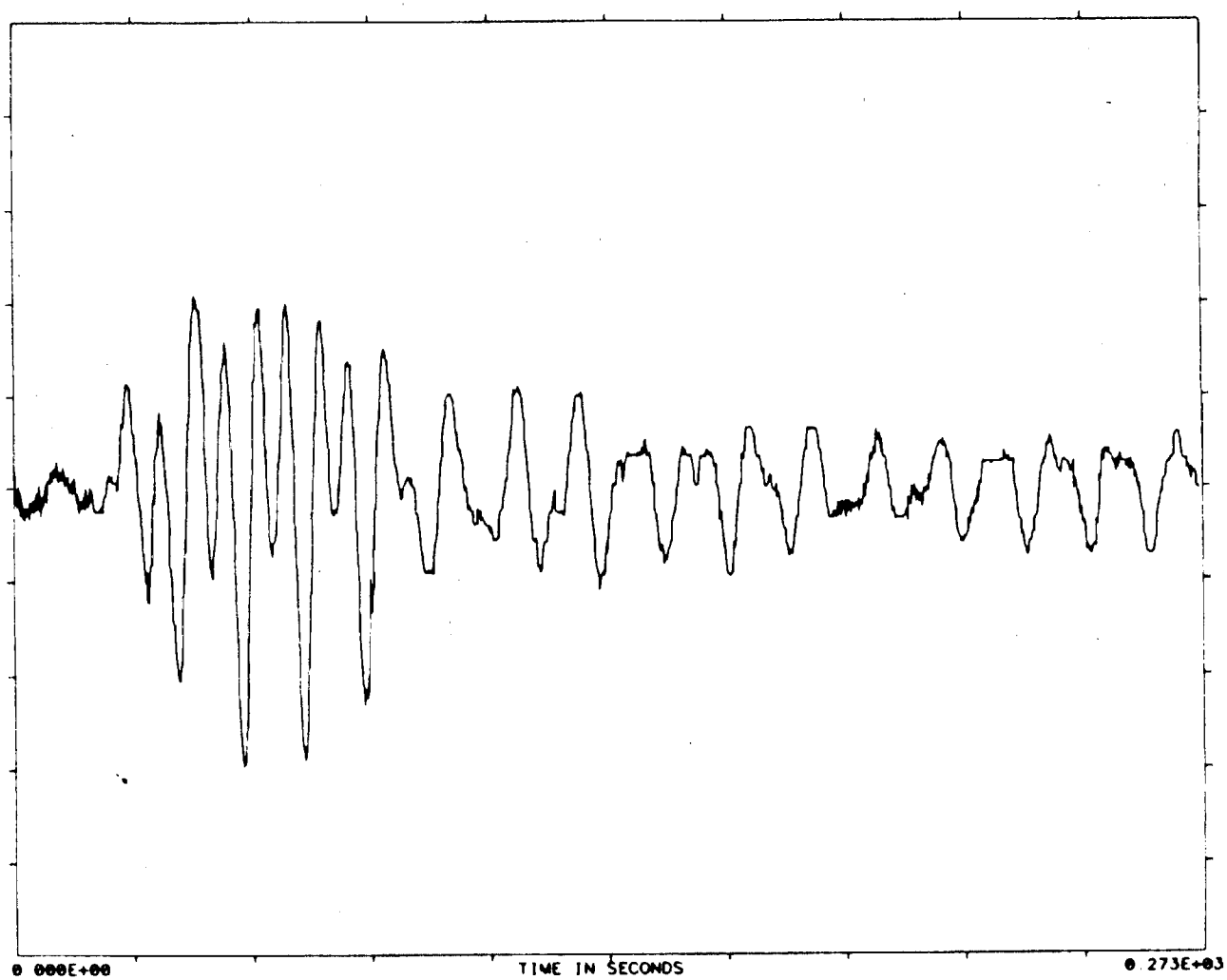

RAW DATA

DOMINANT TIME

TIME	MAGNITUDE
0.523E+02	-.5978E+00
0.525E+02	-.5903E+00
0.528E+02	-.5902E+00
0.667E+02	-.5832E+00
0.664E+02	-.5674E+00
0.669E+02	-.5581E+00
0.661E+02	-.5570E+00
0.520E+02	-.5566E+00
0.531E+02	-.5342E+00
0.659E+02	-.5078E+00

ORIGINAL PAGE IS
OF POOR QUALITY

TEST NAME=SAE ACC MSIDS		NNOFFT =	1	UNITS= (MIL-G)	
MEASUREMENT=	COVER Y	FFTBW-HZ=	0.00000E+00	MEAN= 0.15861590E-06	D: 2-13-85
REFF TIME =	247 17:32 39. 0	FFTERR =	0.00	S.D.= 0.22810240E+00	T: 7-29-38
TIME OFFSET=	1.001	FFTTIM =	0.0	SAMPLE RATE= 0.3750E+01	
TOTAL TIME=	273.100	FFTLIN =	0		

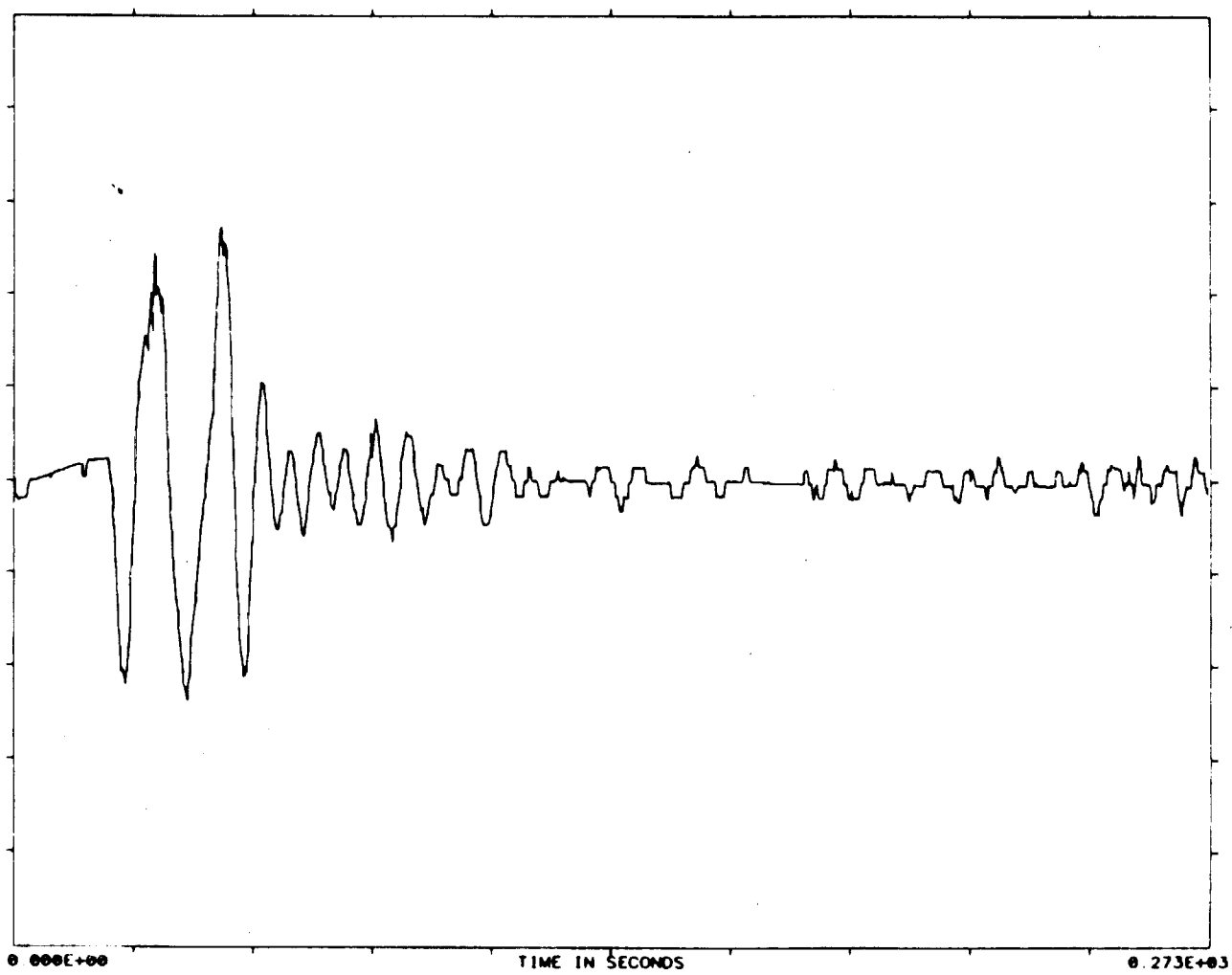

DOMINANT TIME

TIME	MAGNITUDE
0.472E+02	0.1092E+01
0.469E+02	0.1054E+01
0.480E+02	0.1025E+01
0.475E+02	0.9947E+00
0.483E+02	0.9939E+00
0.320E+02	0.9797E+00
0.477E+02	0.9627E+00
0.395E+02	-.9590E+00
0.467E+02	0.9276E+00
0.392E+02	-.9224E+00

ORIGINAL PAGE IS
OF POOR QUALITY.

TEST NAME=SAE ACC MSTDS		NNOFFT =	1	UNITS= (MIL-G)	
MEASUREMENT=	COVER X2	FFTBW-HZ=	0.00000E+00	MEAN= 0.86674850E-09	D: 2-13-85
REFF TIME =	247:17 32:39. 0	FFTERR =	0.00	S.D = 0.16731890E+00	T: 7-28-19
TIME OFFSET=	1.001	FFTTIM =	0.0	SAMPLE RATE= 0.3750E+01	
TOTAL TIME=	273.100	FFTLIN =	0		

0.100E+01

RAW DATA

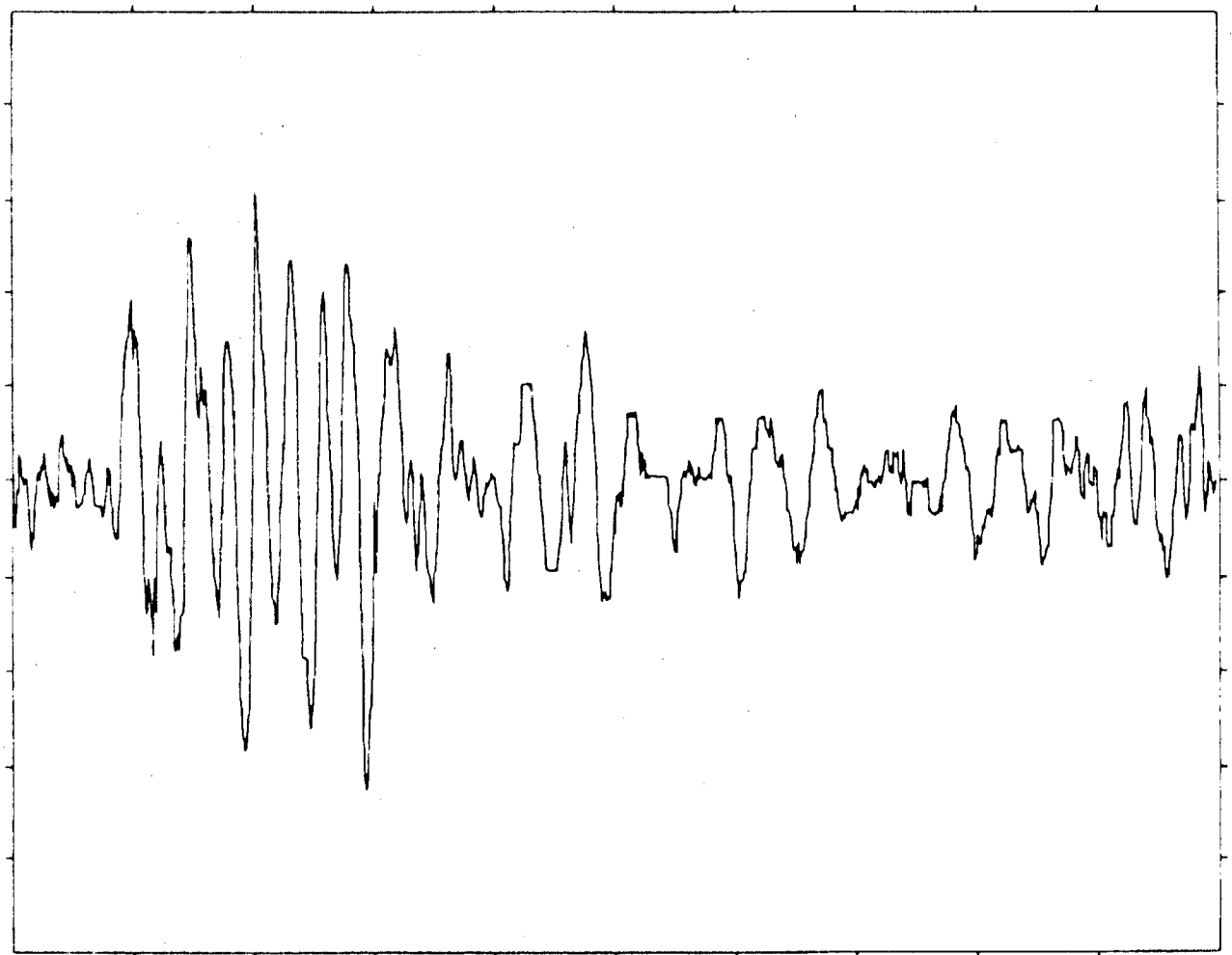

-0.100E+01

0.000E+00 TIME IN SECONDS 0.273E+03

DOMINANT TIME

TIME	MAGNITUDE
0.800E+02	- 6493E+00
0.549E+02	0.6247E+00
0.797E+02	- 6183E+00
0.803E+02	- 6075E+00
0.805E+02	- 5795E+00
0.555E+02	0.5706E+00
0.525E+02	- 5687E+00
0.552E+02	0.5655E+00
0.528E+02	- 5617E+00
0.520E+02	- 5437E+00

ORIGINAL PAGE IS
OF POOR QUALITY

ORIGINAL PAGE IS
OF POOR QUALITY

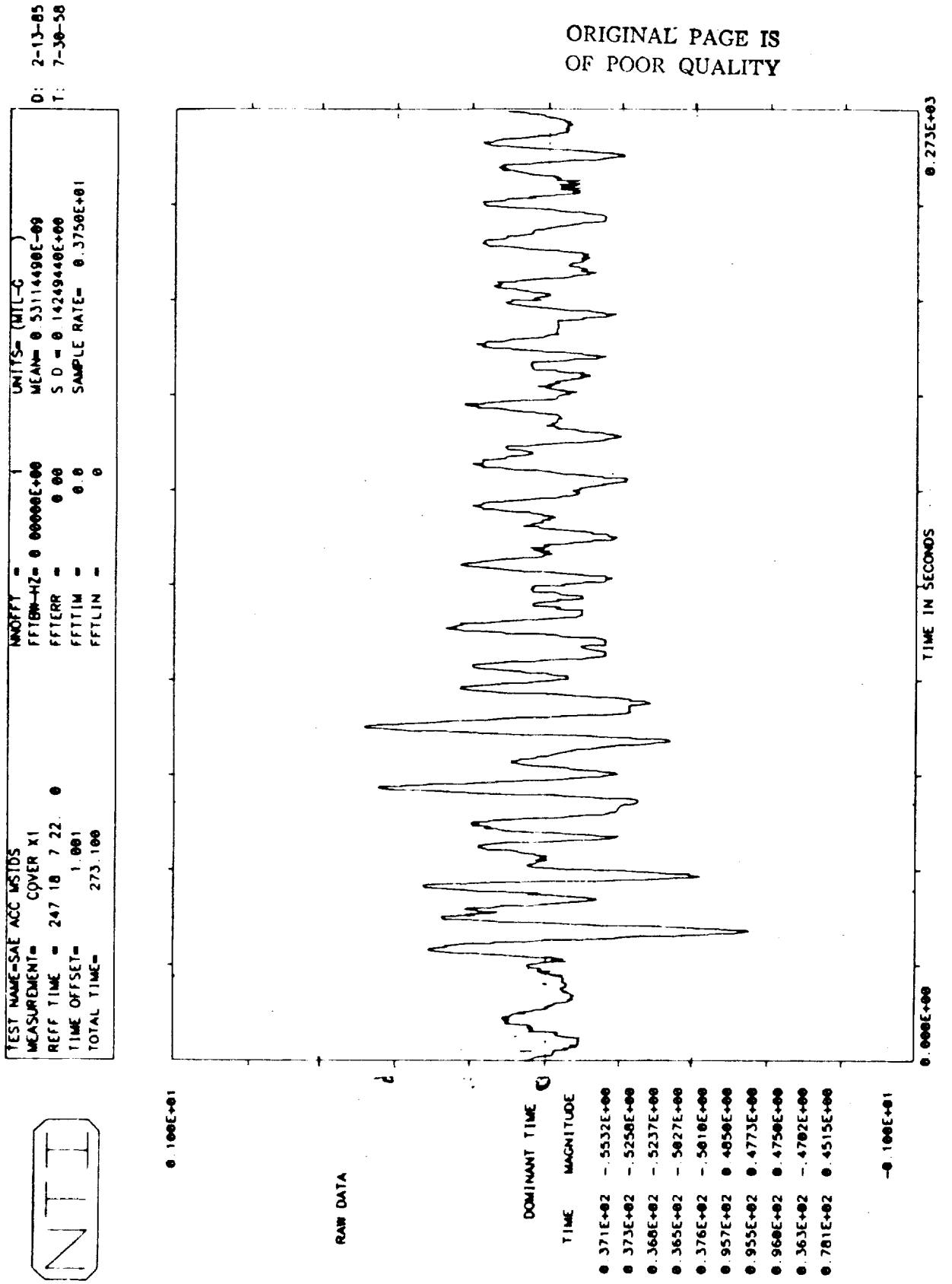

NTI

TEST NAME=SAE ACC MSIDS		NNOFFT =	1	UNITS= (MIL-G)	
MEASUREMENT=	COVER X2	FFTBW-HZ=	0.00000E+00	MEAN= 0.11496010E-08	D: 2-13-85
REFF TIME =	247 18 7 22. 0	FFTERR =	0 00	S D = 0 27261610E+00	T: 7-32-20
TIME OFFSET=	1.001	FFTTIM =	0.0	SAMPLE RATE= 0.3750E+01	
TOTAL TIME=	273.100	FFTLIN =	0		

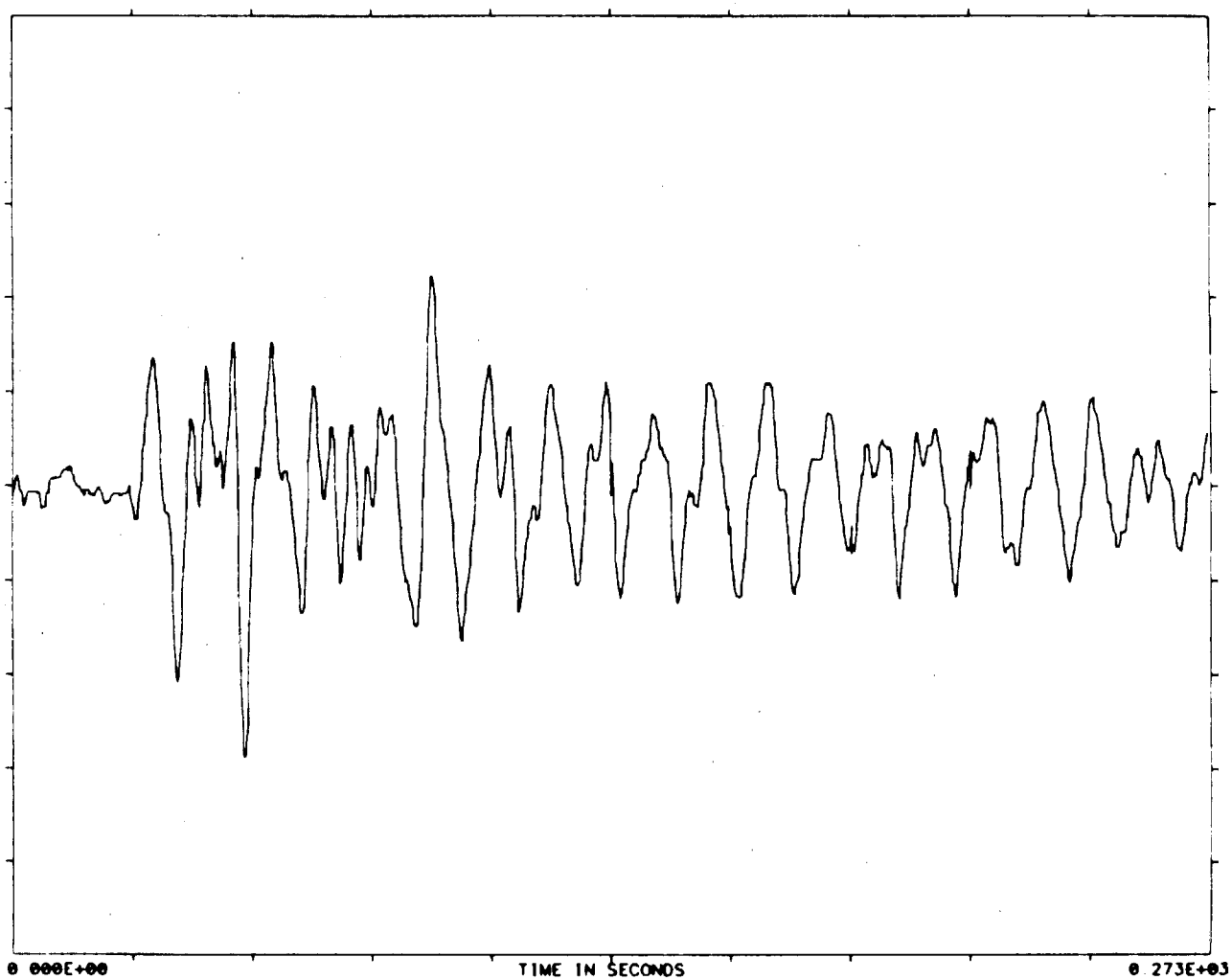

DOMINANT TIME

TIME	MAGNITUDE
0.528E+02	-.1161E+01
0.525E+02	-.1124E+01
0.531E+02	-.1101E+01
0.523E+02	-.1035E+01
0.533E+02	-.1005E+01
0.520E+02	-.8984E+00
0.955E+02	0.8952E+00
0.957E+02	0.8947E+00
0.960E+02	0.8653E+00
0.952E+02	0.8513E+00

ORIGINAL PAGE IS
OF POOR QUALITY

TEST NAME=SAE ACC MSIDS	NNOFFT = 1	UNITS= (MIL-G)
MEASUREMENT= COVER Y	FFTBW-HZ= 0.00000E+00	MEAN=-0.46020430E-08
REFF TIME = 247 18: 7 22. 0	FFTERR = 0.00	S.D = 0.28986190E+00
TIME OFFSET= 1.001	FFTTIM = 0.0	SAMPLE RATE= 0.3750E+01
TOTAL TIME= 273.100	FFTLIN = 0	

D: 2-13-85
T: 7-33-40

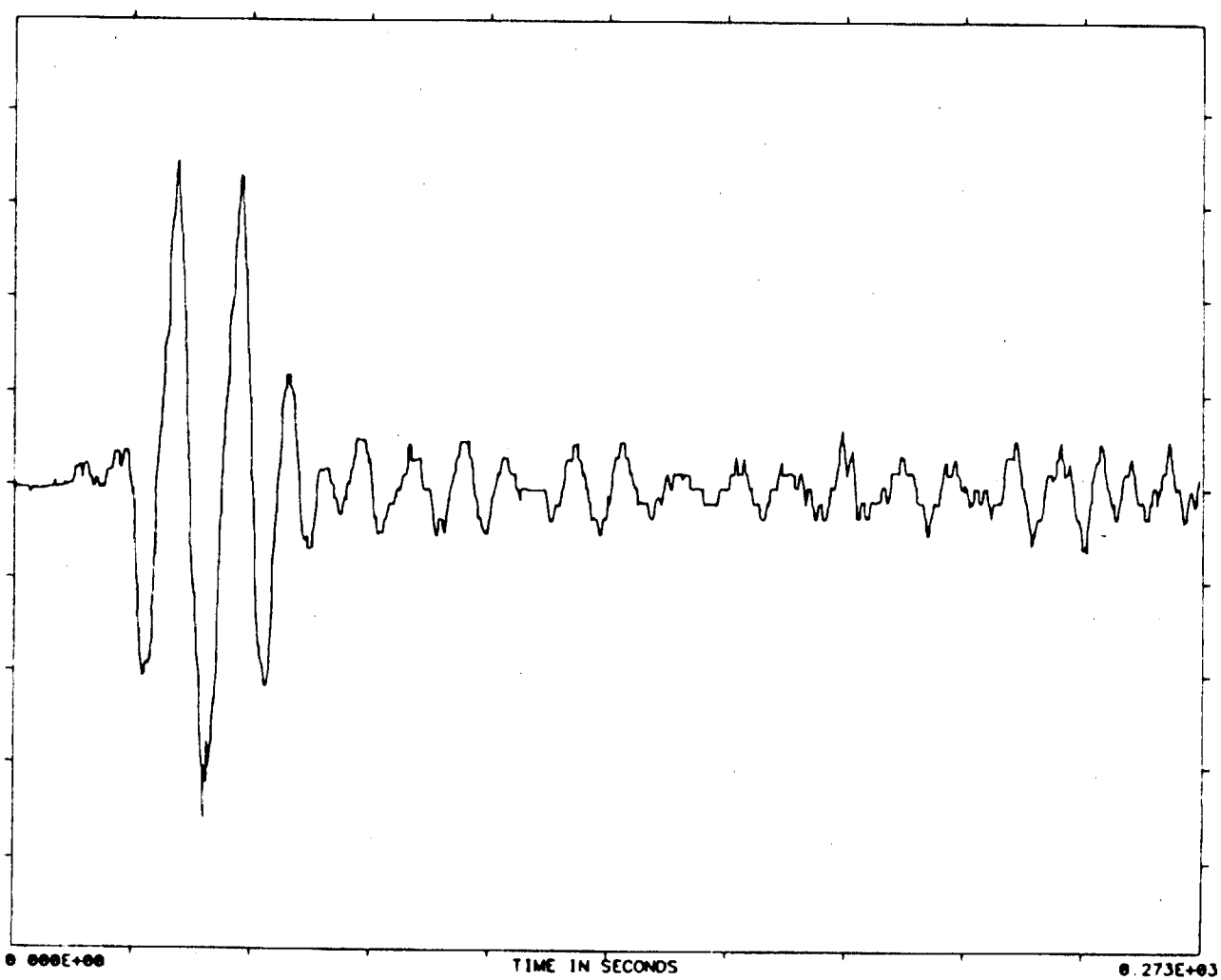

DOMINANT TIME

TIME	MAGNITUDE
0.435E+02	-.1433E+01
0.373E+02	0.1389E+01
0.376E+02	0.1336E+01
0.520E+02	0.1320E+01
0.371E+02	0.1315E+01
0.523E+02	0.1306E+01
0.443E+02	-.1289E+01
0.440E+02	-.1279E+01
0.525E+02	0.1229E+01
0.432E+02	-.1219E+01

ORIGINAL PAGE IS
OF POOR QUALITY

Final Report

LMSC-F087173

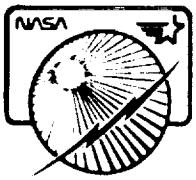

Appendix D
Power Spectral Densities of Mast Tip Acceleration Data

NTI

TEST NAME=SAE ACC MSIDS	NNOFFT = 1	UNITS=(MTL-G)**2/HZ	D: 2-12-85
MEASUREMENT= COVER X1	FFTBW-HZ= 0.91553E-03	MEAN=-0 12085330E-08	T 14- 6-24
REFF TIME = 245 19 25 27 0	FFTERR = 50 00	S D = 0 64088860E+00	
TIME OFFSET= 1 001	FFTTIM = 1092 2	SAMPLE RATE= 0 3750E+01	
TOTAL TIME= 273 100	FFTLIN = 4096		

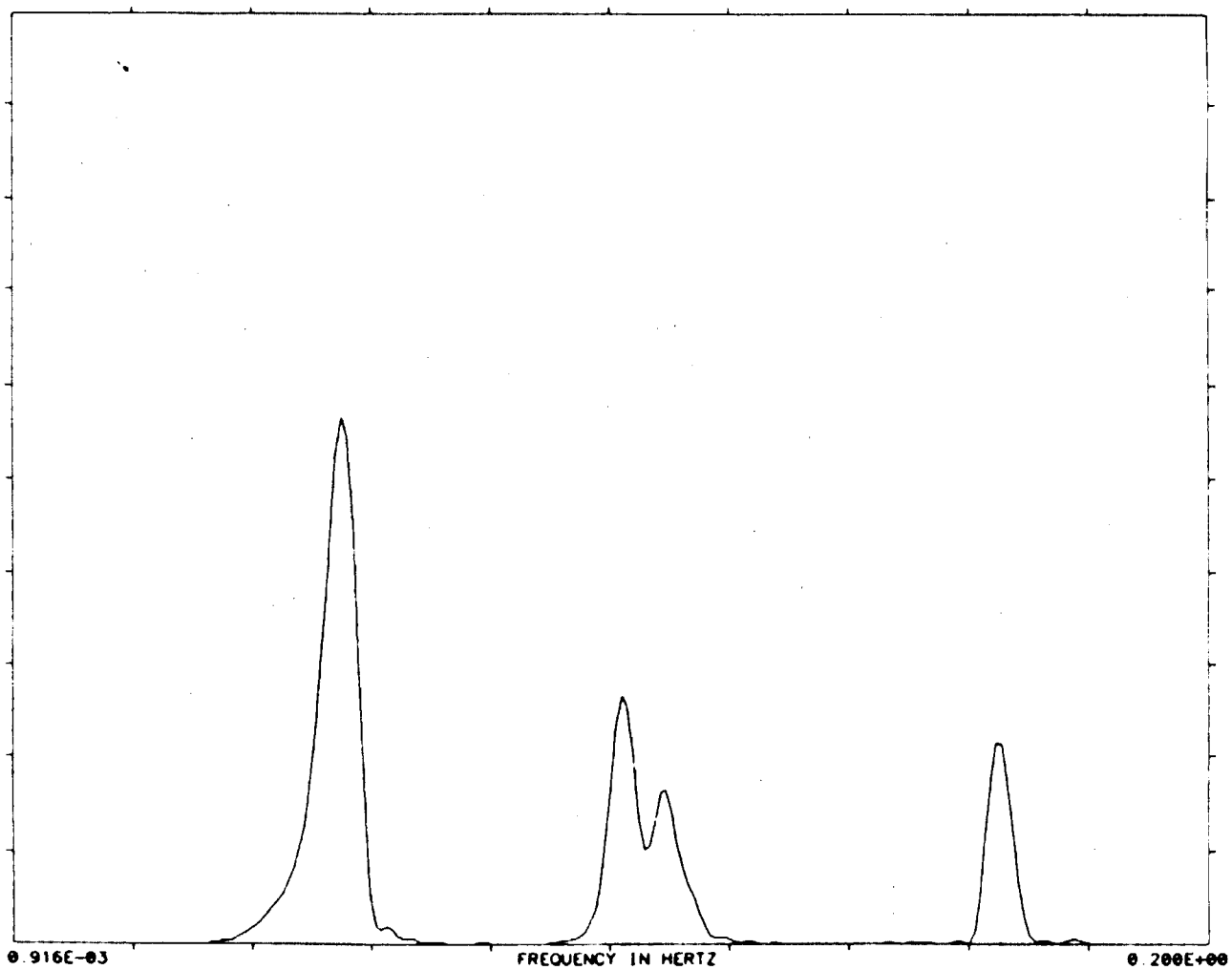

DOMINANT FREQ

FREQ	MAGNITUDE
0 5585E-01	0 113E+03
0 5676E-01	0 109E+03
0 5493E-01	0 106E+03
0 5402E-01	0 917E+02
0 5768E-01	0 902E+02
0 5310E-01	0 756E+02
0 5859E-01	0 609E+02
0 5219E-01	0 596E+02
0 1025E+00	0 529E+02
0 1035E+00	0 503E+02

ORIGINAL PAGE IS
OF POOR QUALITY

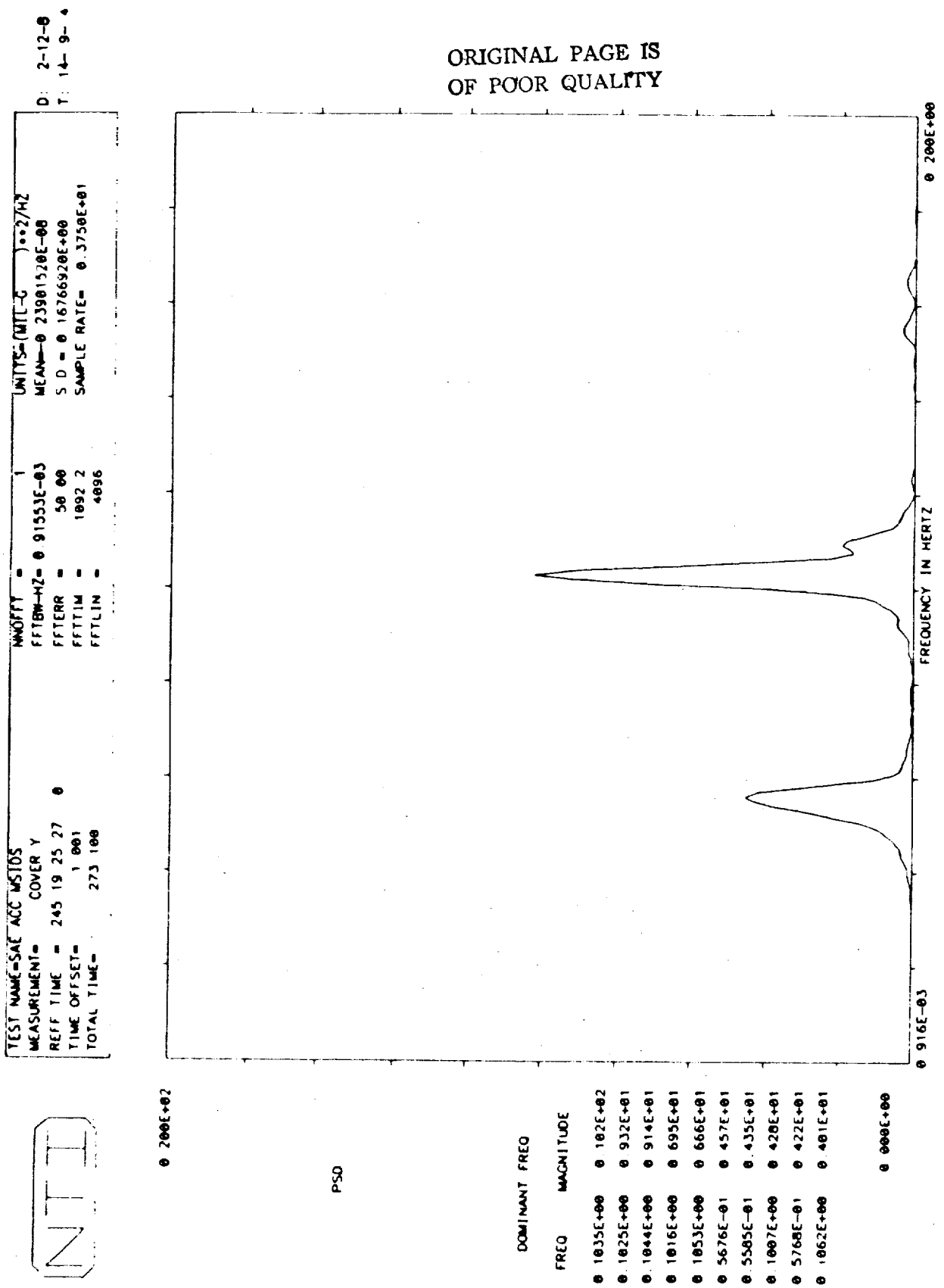

NTI

TEST NAME=SAE ACC MSIDS		NNOFFT =	1	UNITS=(MIL-G)**2/HZ	D: 2-12-85
MEASUREMENT=	COVER X2	FFTBW-HZ=	0.91553E-03	MEAN= 0 23719620E-08	T: 14: 7-43
REFF TIME =	245 19 25 27. 0	FFTERR =	50 00	S D = 0 79632310E+00	
TIME OFFSET=	1 001	FFTTIM =	1092 2	SAMPLE RATE= 0.3750E+01	
TOTAL TIME=	273.100	FFTLIN =	4096		

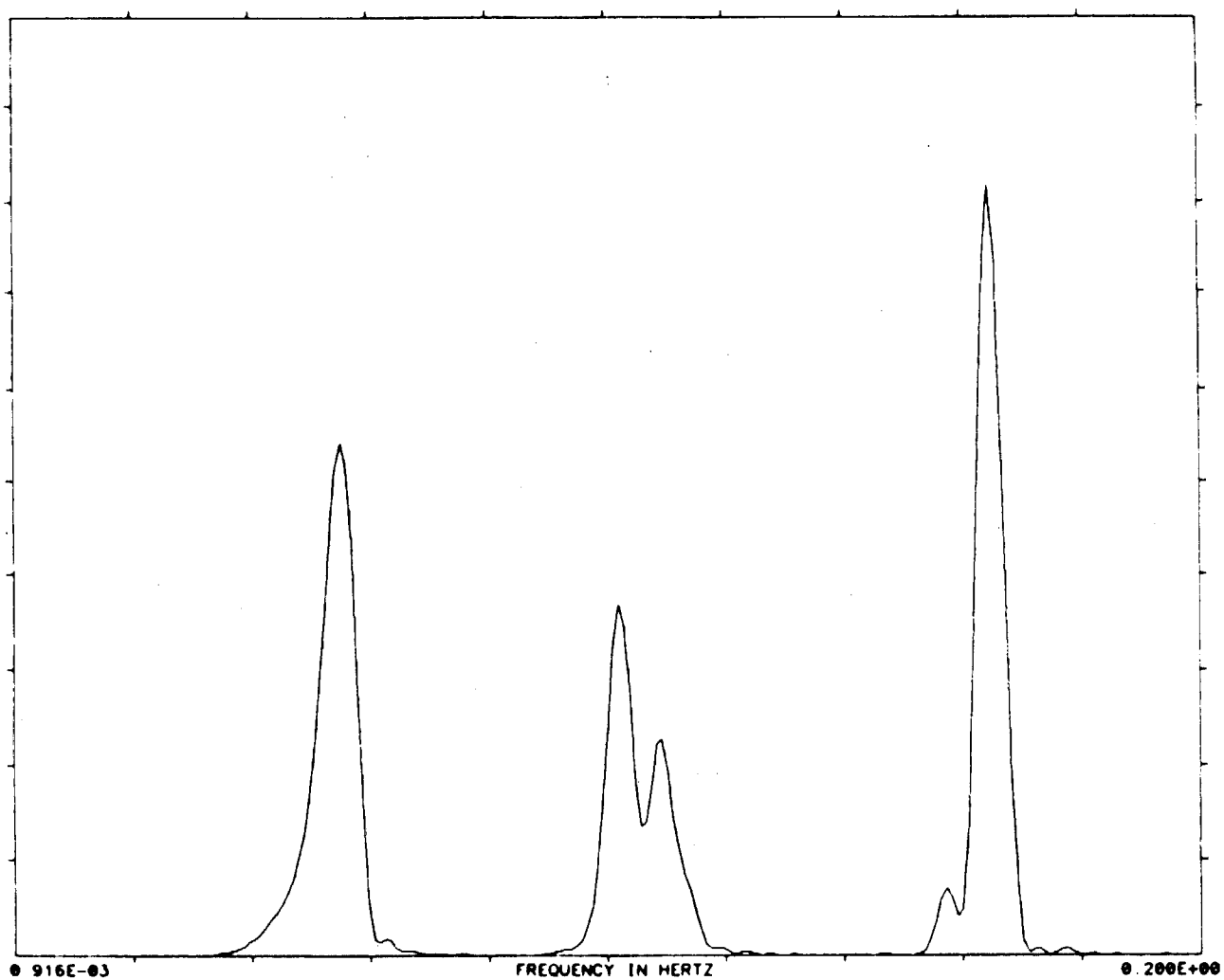

DOMINANT FREQ

FREQ	MAGNITUDE
0 1648E+00	0 163E+03
0 1639E+00	0.150E+03
0 1657E+00	0.148E+03
0.1666E+00	0.113E+03
0 1530E+00	0 112E+03
0 5585E-01	0.109E+03
0.5676E-01	0.104E+03
0 5493E-01	0.102E+03
0 5402E-01	0.891E+02
0.5768E-01	0.857E+02

NTI

TEST NAME=SAE ACC MSIDS	NNOFFT = 1	UNITS=(MIL-G)**2/HZ
MEASUREMENT= COVER X1	FFTBW-HZ= 0.91553E-03	MEAN= 0 10795700E-08
REFF TIME = 245 20 13 27 0	FFTERR = 50 00	S D = 0 45818370E+00
TIME OFFSET= 1 001	FFTTIM = 1092 2	SAMPLE RATE= 0 3750E+01
TOTAL TIME= 273 100	FFTLIN = 4096	

D 2-12-85
T 14- 2- 0

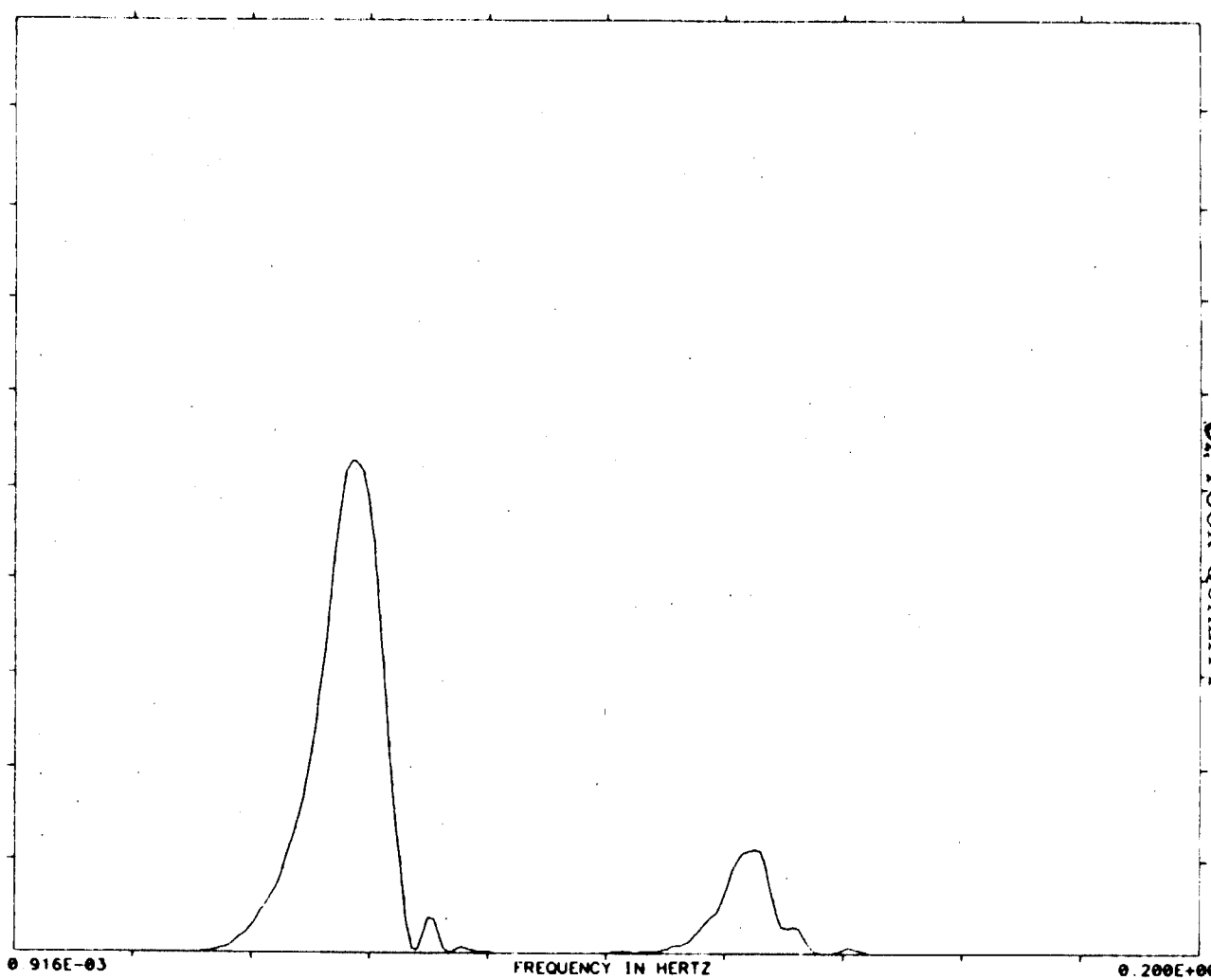

DOMINANT FREQ

FREQ	MAGNITUDE
0 5768E-01	0 528E+02
0 5859E-01	0 527E+02
0 5951E-01	0 518E+02
0 5676E-01	0 516E+02
0 6042E-01	0 493E+02
0 5585E-01	0 484E+02
0 6134E-01	0 441E+02
0 5493E-01	0 434E+02
0 5402E-01	0 378E+02
0 6226E-01	0 365E+02

ORIGINAL PAGE IS
OF POOR QUALITY

NTI

TEST NAME=SAE ACC MSIDS	NNOFFT = 1	UNITS=(MIL-G)**2/HZ	D: 2-12-85
MEASUREMENT= COVER Y	FFTBW-HZ= 0.91553E-03	MEAN=-0.17898860E-08	T: 14- 5- 4
REFF TIME = 245:20:13:27. 0	FFTERR = 50.00	S.D. = 0.14093390E+00	
TIME OFFSET= 1.001	FFTTIM = 1092.2	SAMPLE RATE= 0.3750E+01	
TOTAL TIME= 273.100	FFTLIN = 4096		

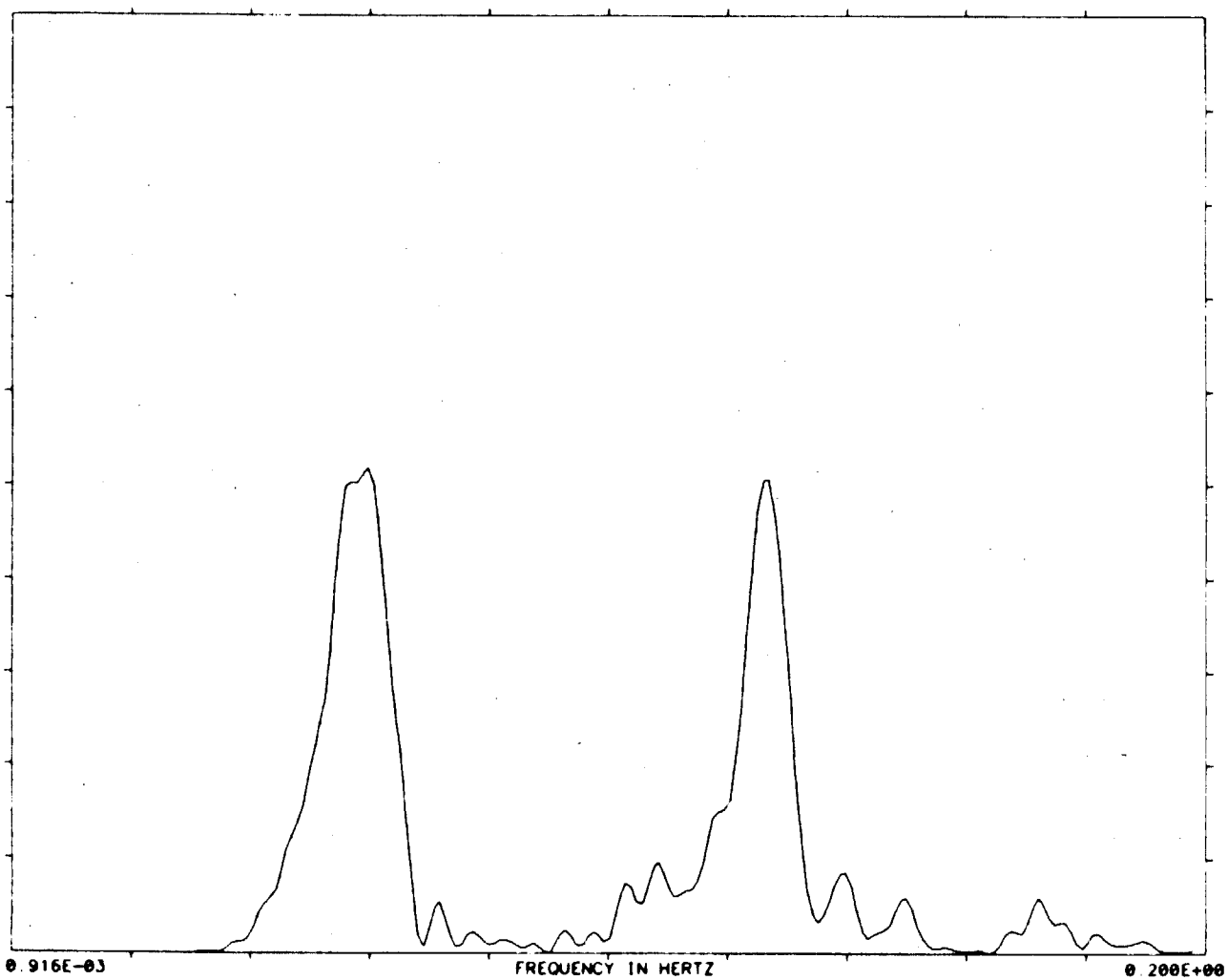

DOMINANT FREQ

FREQ	MAGNITUDE
0.6842E-01	0.259E+01
0.5951E-01	0.256E+01
0.1273E+00	0.253E+01
0.1263E+00	0.252E+01
0.5768E-01	0.251E+01
0.5859E-01	0.251E+01
0.6134E-01	0.250E+01
0.5676E-01	0.249E+01
0.1282E+00	0.240E+01
0.1254E+00	0.236E+01

0.000E+00

NTI

TEST NAME=SAE ACC MSIDS		NNOFFT =	1	UNITS=(MIL-G)**2/HZ	
MEASUREMENT=	COVER X2	FFTBW-HZ=	0.91553E-03	MEAN= 0.62718760E-08	D: 2-12-85
REFF TIME =	245:20 13 27 0	FFTERR =	50.00	S.D = 0.48462770E+00	T: 14- 3-26
TIME OFFSET=	1.001	FFTTIM =	1092.2	SAMPLE RATE= 0.3750E+01	
TOTAL TIME=	273.100	FFTLIN =	4096		

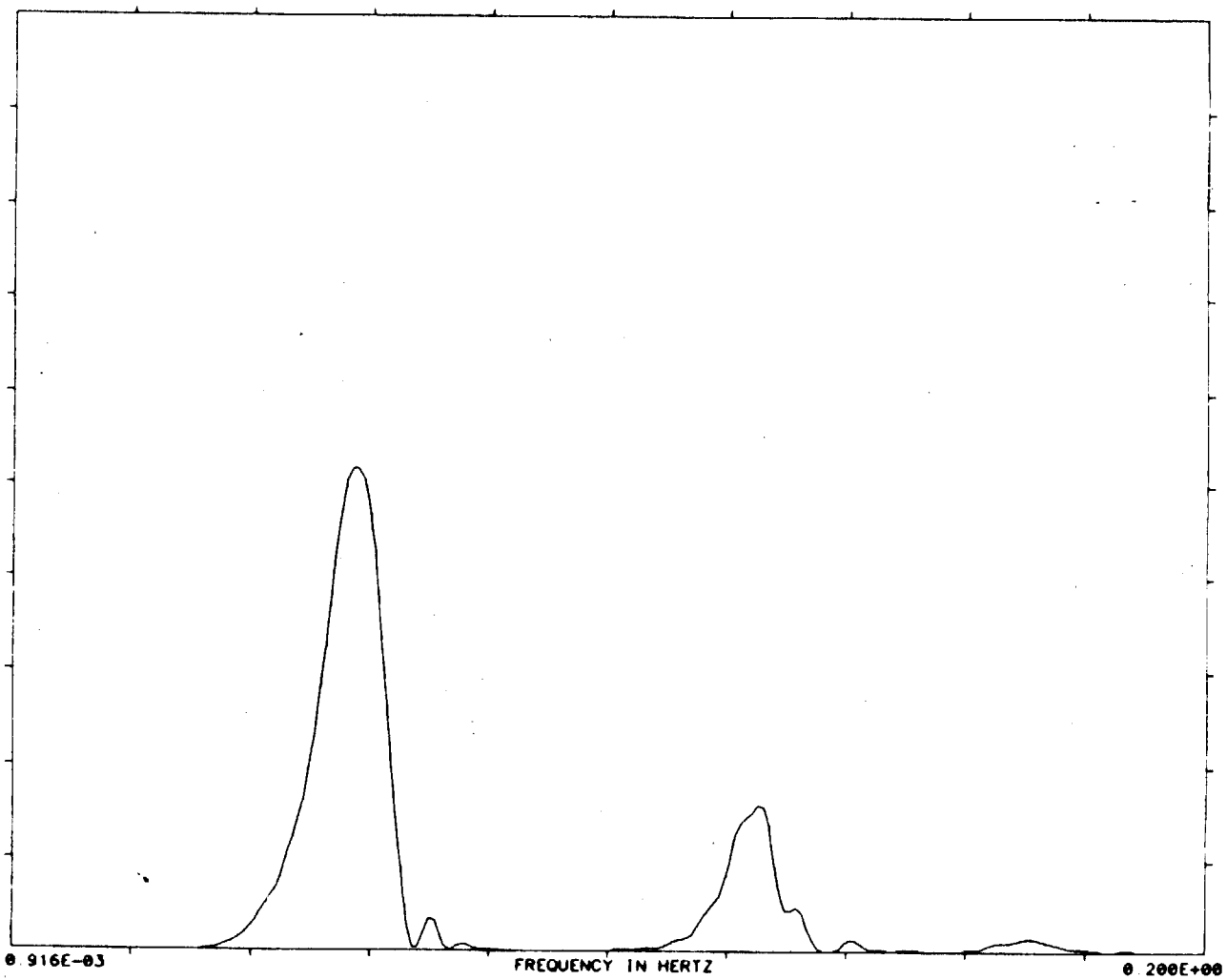

DOMINANT FREQ

FREQ	MAGNITUDE
0.5768E-01	0.518E+02
0.5859E-01	0.518E+02
0.5951E-01	0.507E+02
0.5676E-01	0.505E+02
0.6042E-01	0.478E+02
0.5585E-01	0.474E+02
0.5493E-01	0.428E+02
0.6134E-01	0.426E+02
0.5402E-01	0.376E+02
0.6226E-01	0.352E+02

ORIGINAL PAGE IS
OF POOR QUALITY

NTI

TEST NAME=SAE ACC MSIDS		NNOFFT =	1	UNITS=(MIL-G)**2/HZ	D: 2-12-85
MEASUREMENT=	COVER X1	FFTBW-HZ=	0.91553E-03	MEAN=-0.27648640E-09	T: 14-10-24
REFF TIME =	246 13 29 27 0	FFTERR =	50.00	S D = 0.19808230E+00	
TIME OFFSET=	1 001	FFTTIM =	1092 2	SAMPLE RATE= 0 3750E+01	
TOTAL TIME=	273 100	FFTLIN =	4096		

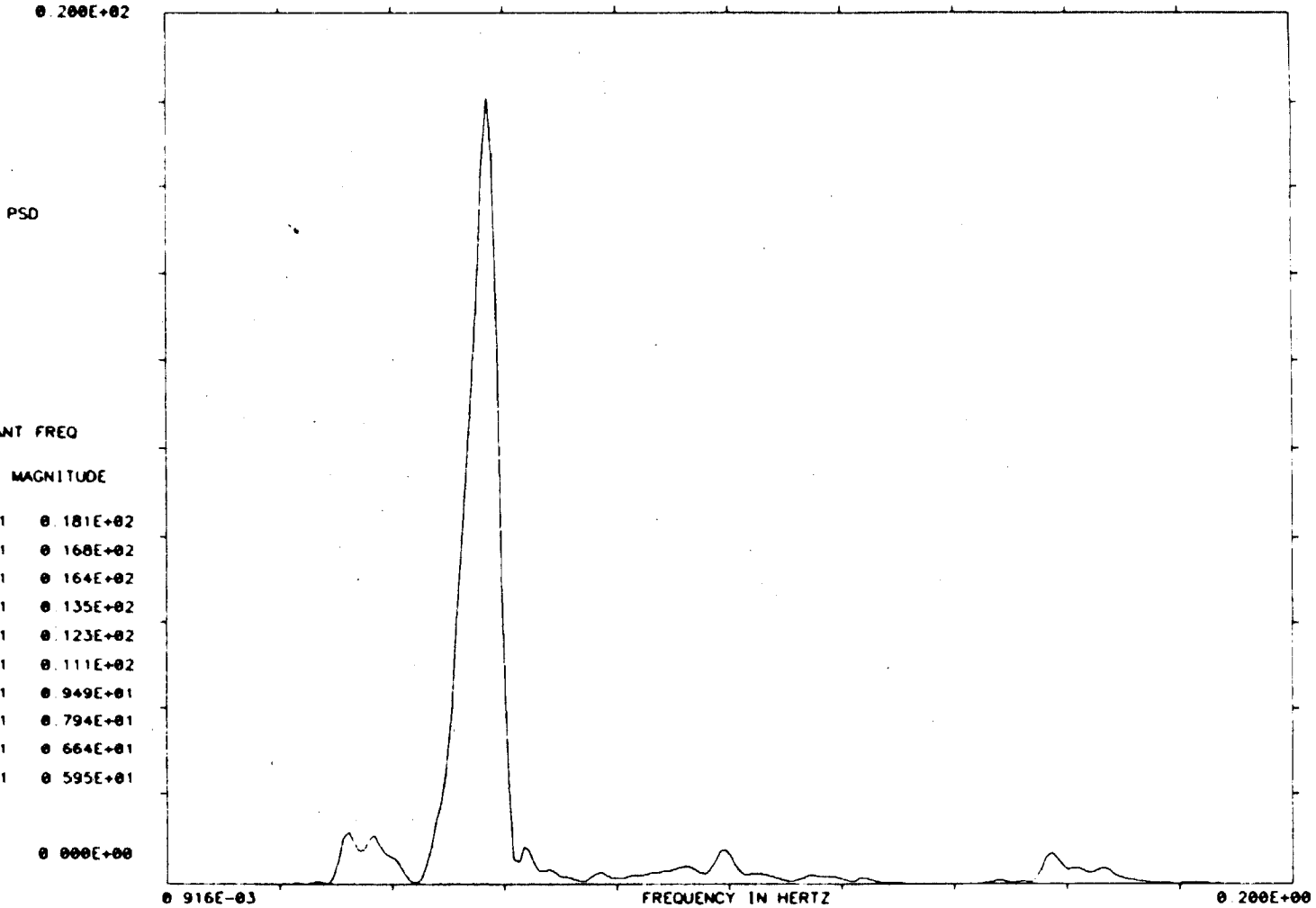

DOMINANT FREQ

FREQ	MAGNITUDE
0 5768E-01	0 181E+02
0 5859E-01	0 168E+02
0 5676E-01	0 164E+02
0 5585E-01	0 135E+02
0 5951E-01	0 123E+02
0 5493E-01	0 111E+02
0 5402E-01	0 949E+01
0 5310E-01	0 794E+01
0 6042E-01	0 664E+01
0 5219E-01	0 595E+01

0 000E+00

NTI

TEST NAME=SAE ACC MSIDS	NNOFFT = 1	UNITS=(MIL-G)**2/HZ
MEASUREMENT= COVER Y	FFTBW-HZ= 0.91553E-03	MEAN= 0 14533730E-08
REFF TIME = 246 13 29 27 0	FFTERR = 50 00	S D = 0 19405130E+00
TIME OFFSET= 1 001	FFTTIM = 1092 2	SAMPLE RATE= 0 3750E+01
TOTAL TIME= 273 100	FFTLIN = 4096	

D 2-12-85
T: 14-13- 1

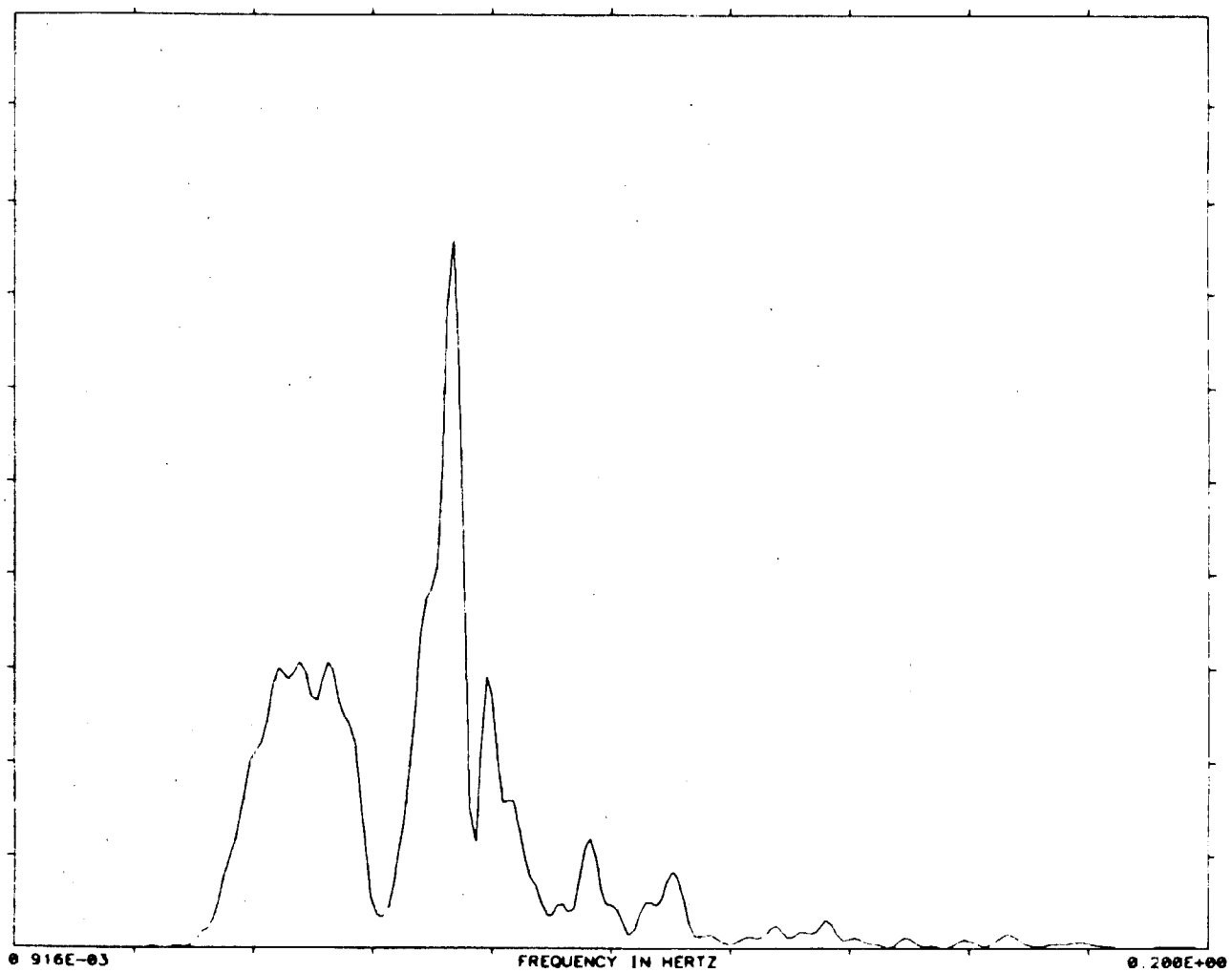

DOMINANT FREQ

FREQ	MAGNITUDE
0 7416E-01	0 760E+01
0 7324E-01	0 685E+01
0 7507E-01	0 637E+01
0 7233E-01	0 521E+01
0 7141E-01	0 410E+01
0 7050E-01	0 383E+01
0 6958E-01	0 375E+01
0 7599E-01	0 373E+01
0 6866E-01	0 331E+01
0 5310E-01	0 307E+01

NTI

TEST NAME=SAE ACC MSIDS		NNOFFT =	1	UNITS=(MIL-G)**2/HZ	D: 2-12-85
MEASUREMENT=	COVER X2	FFTBW-HZ=	0.91553E-03	MEAN=-0 12514650E-08	T: 14-11-42
REFF TIME =	246 13 29 27 0	FFTERR =	50 00	S D = 0 24247970E+00	
TIME OFFSET=	1 001	FFTTIM =	1092 2	SAMPLE RATE= 0 3750E+01	
TOTAL TIME=	273 100	FFTLIN =	4096		

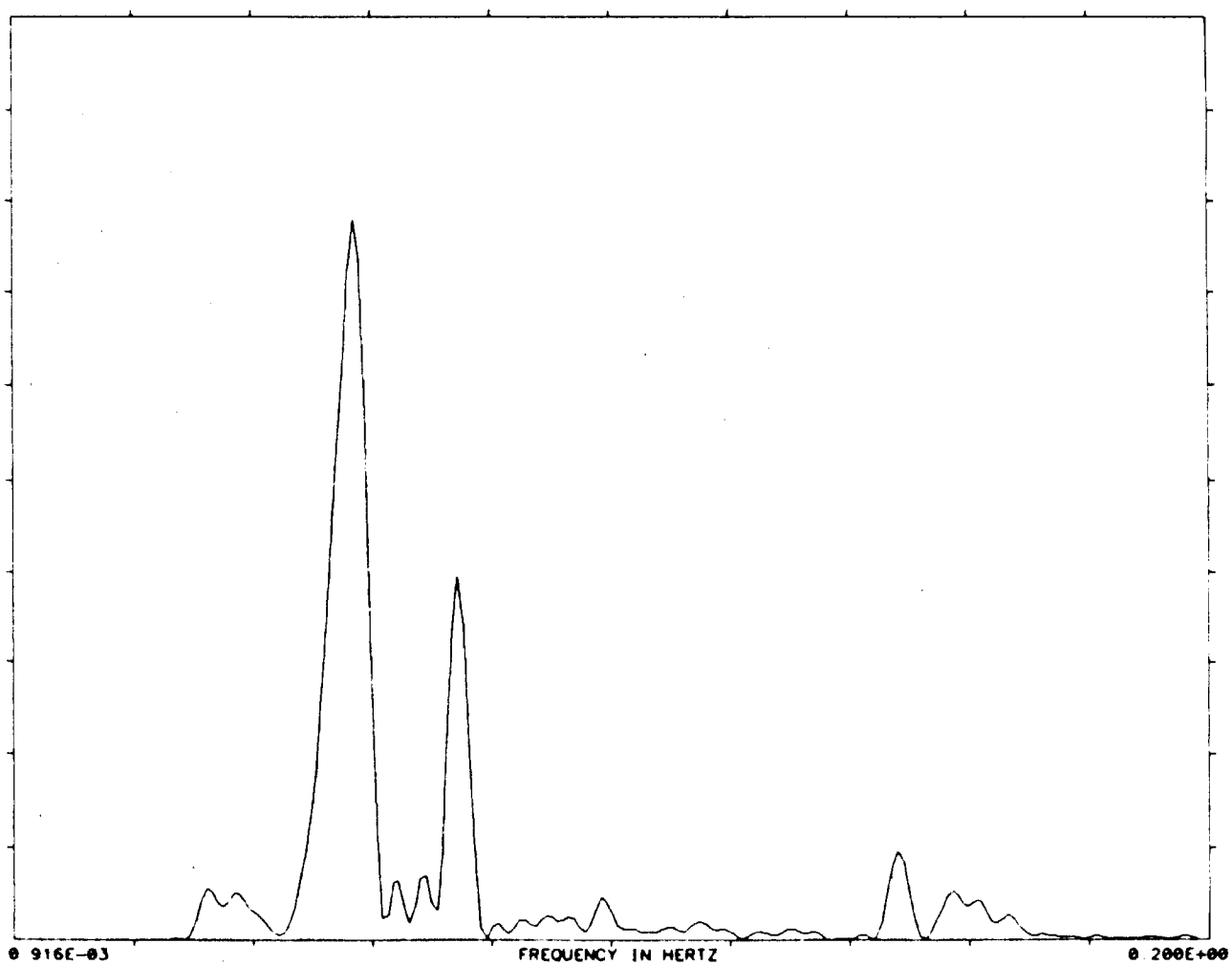

DOMINANT FREQ

FREQ	MAGNITUDE
0 5768E-01	0 156E+02
0 5859E-01	0 149E+02
0 5676E-01	0 144E+02
0 5585E-01	0 124E+02
0 5951E-01	0 115E+02
0 5493E-01	0 106E+02
0 5402E-01	0 893E+01
0 7507E-01	0 793E+01
0 5310E-01	0 711E+01
0 7416E-01	0 688E+01

ORIGINAL PAGE IS
OF POOR QUALITY

ORIGINAL PAGE IS
OF POOR QUALITY

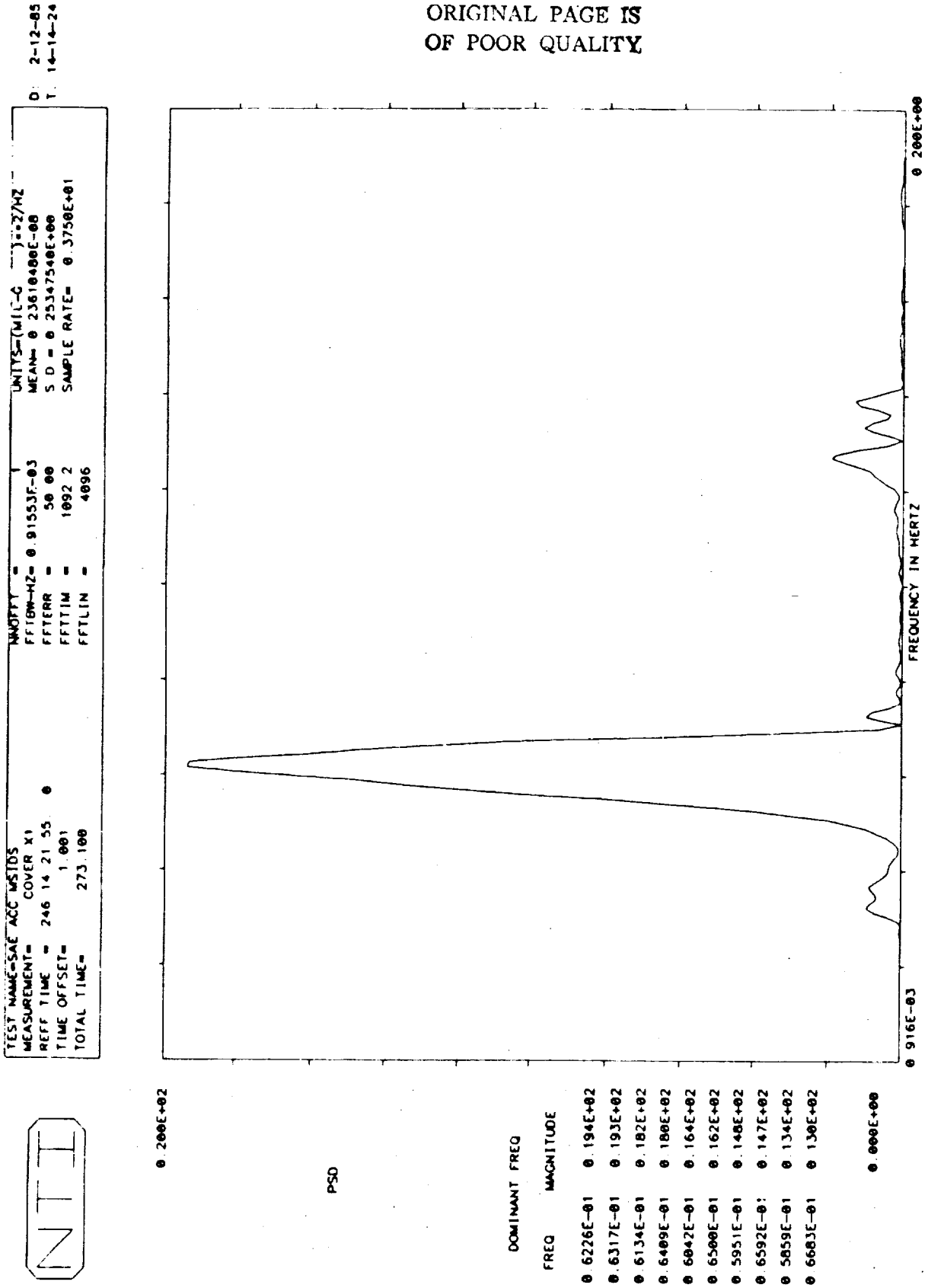

TEST NAME=SAE ACC MSTDS		NNOFFT = 1		UNITS=(MIL-G)**2/HZ	
MEASUREMENT= COVER Y		FFTBW-HZ= 0.91553E-03		MEAN= 0.20736480E-08	D: 2-13-85
REFF TIME = 246 14.21 55. 0		FFTERR = 50.00		S.D = 0.15536560E+00	T: 7-46-59
TIME OFFSET= 1.001		FFTTIM = 1092.2		SAMPLE RATE= 0.3750E+01	
TOTAL TIME= 273.100		FFTLIN = 4096			

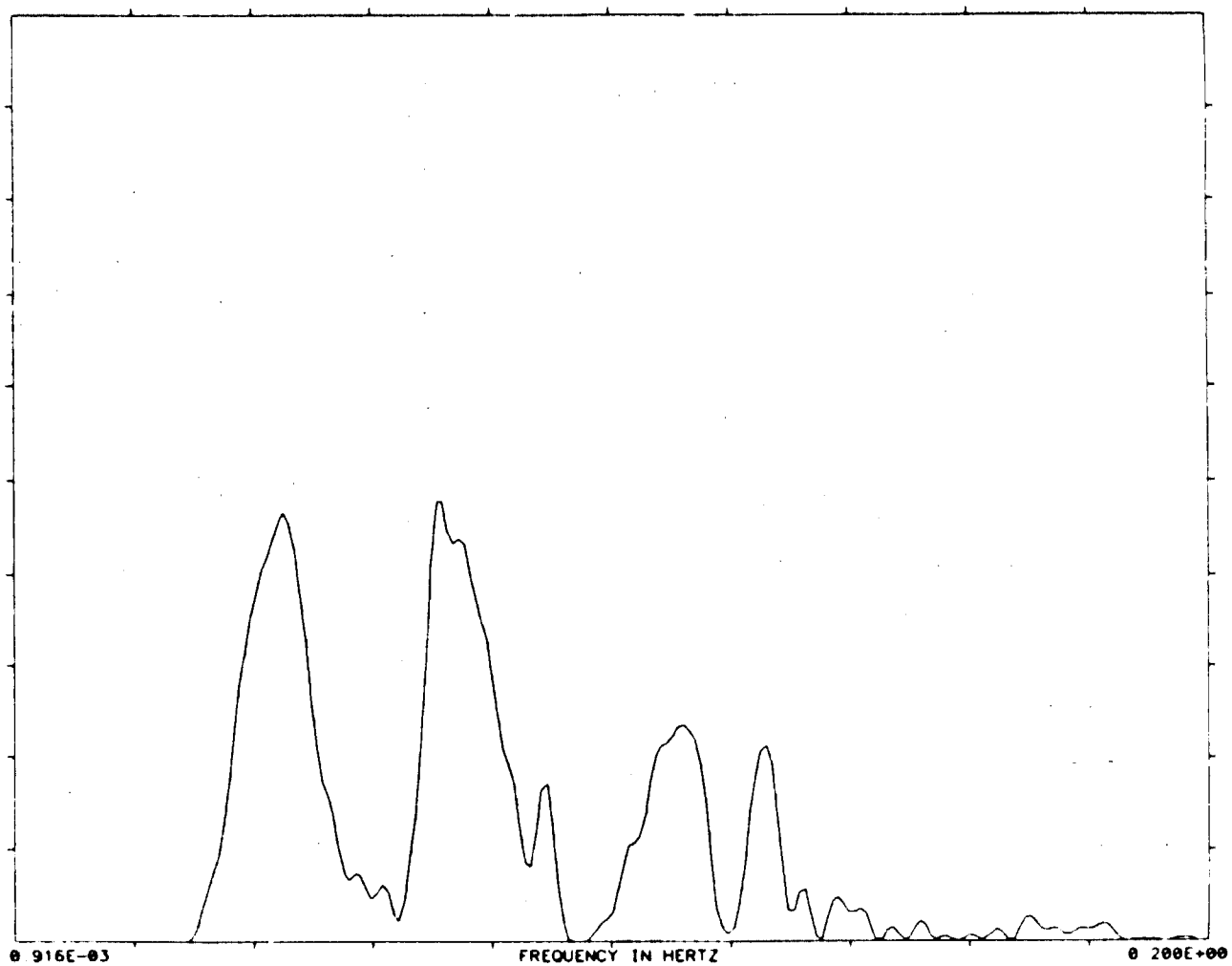

DOMINANT FREQ

FREQ	MAGNITUDE
0.7233E-01	0.239E+01
0.7141E-01	0.239E+01
0.4578E-01	0.233E+01
0.4486E-01	0.228E+01
0.4669E-01	0.228E+01
0.7324E-01	0.224E+01
0.7507E-01	0.219E+01
0.4395E-01	0.218E+01
0.7416E-01	0.217E+01
0.7599E-01	0.217E+01

0.000E+00

ORIGINAL PAGE IS
OF POOR QUALITY.

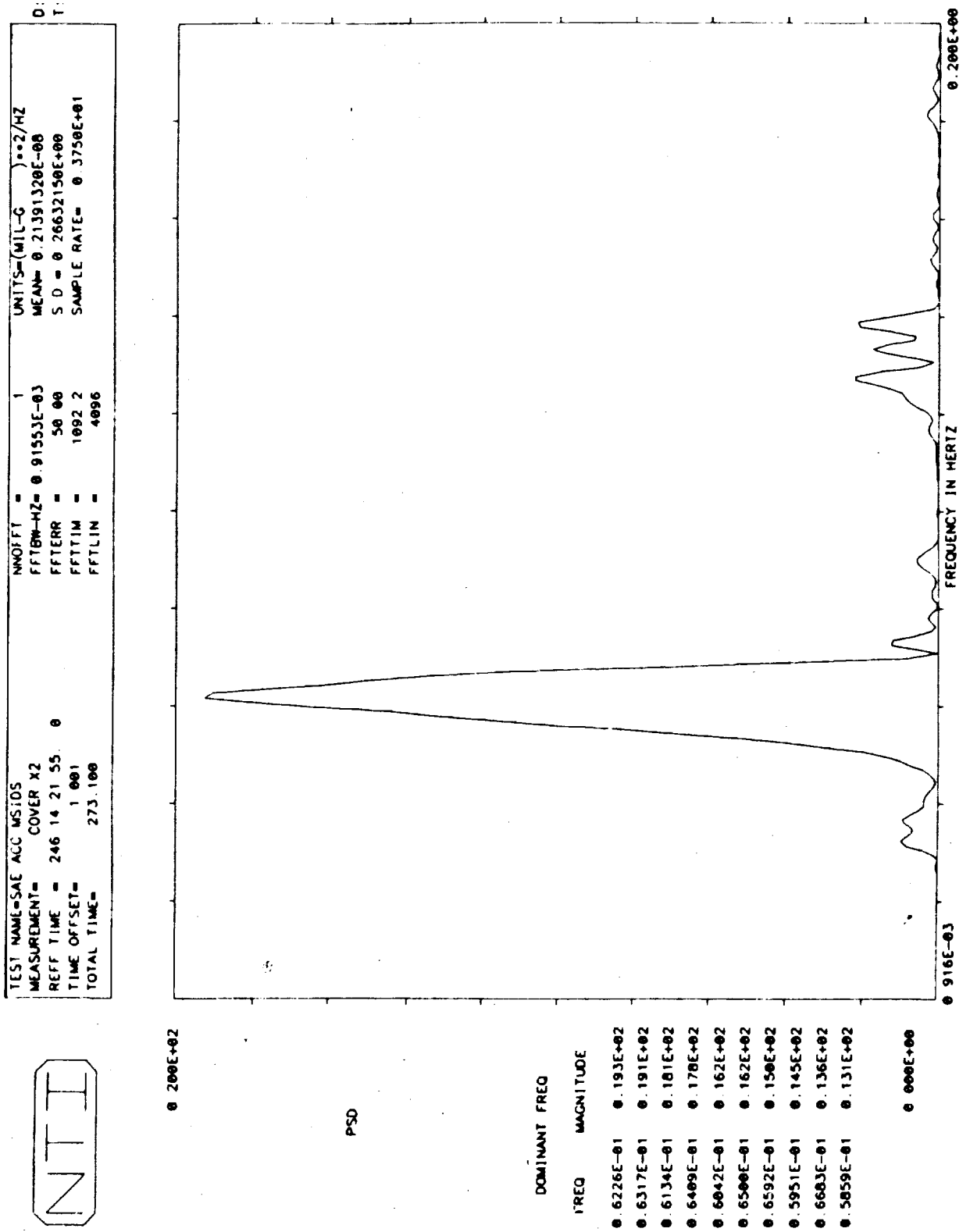

TEST NAME=SAE ACC MSIDS	NNOFFT = 1	UNITS=(MIL-G)**2/HZ	D: 2-12-85
MEASUREMENT= COVER X1	FFTBW-HZ= 0.91553E-03	MEAN=-0 50786190E-08	T: 14-20-24
REFF TIME = 246 15 0 26 0	FFTERR = 50 00	S D = 0.54256680E+00	
TIME OFFSET= 1 001	FFTTIM = 1092 2	SAMPLE RATE= 0 3750E+01	
TOTAL TIME= 273 100	FFTLIN = 4096		

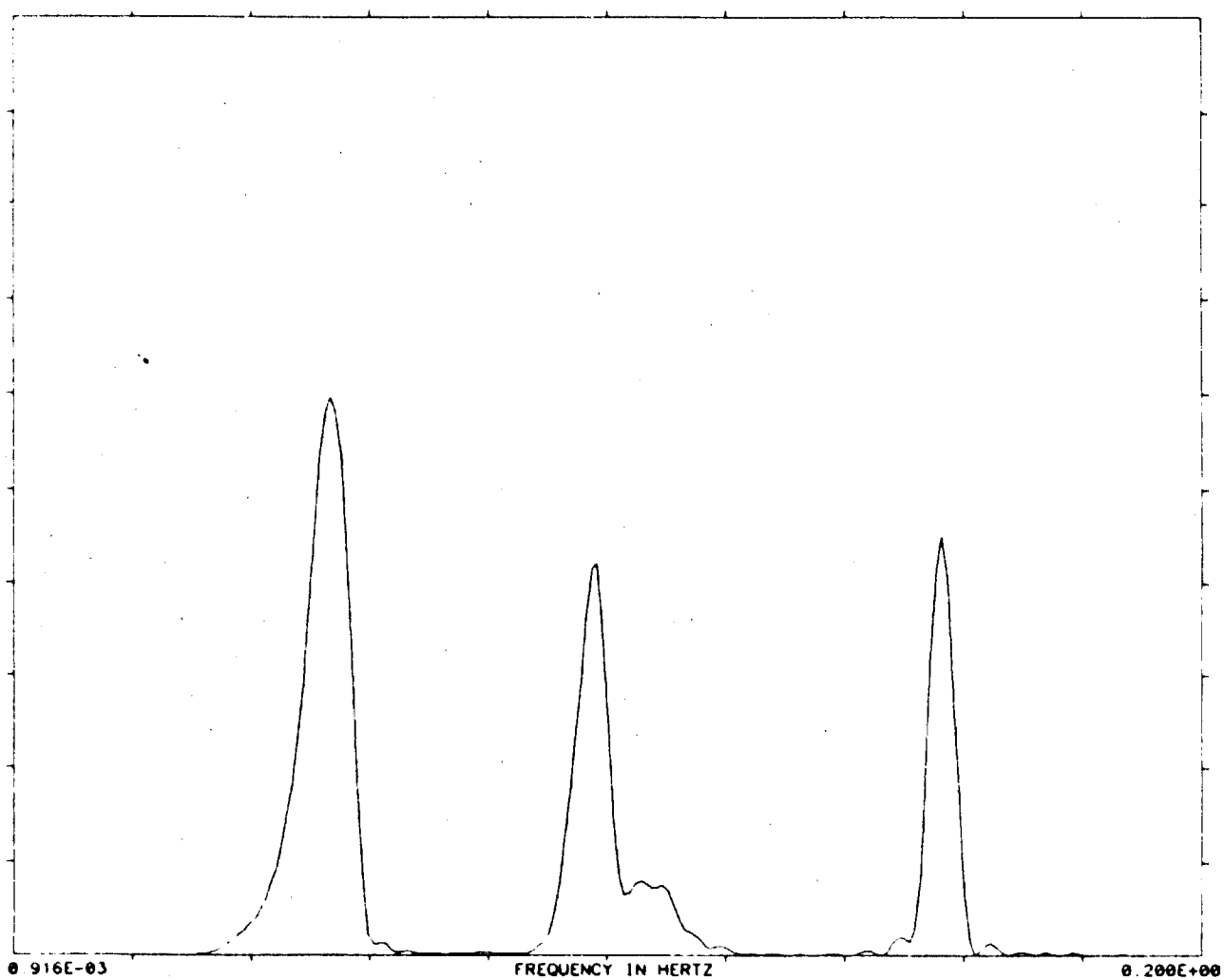

DOMINANT FREQ

FREQ	MAGNITUDE
5402E-01	0 597E+02
5493E-01	0 584E+02
5310E-01	0 581E+02
5585E-01	0 537E+02
5219E-01	0 531E+02
5127E-01	0 453E+02
1566E+00	0 451E+02
5676E-01	0 449E+02
9888E-01	0 421E+02
9796E-01	0 416E+02

0 000E+00

ORIGINAL PAGE IS
OF POOR QUALITY

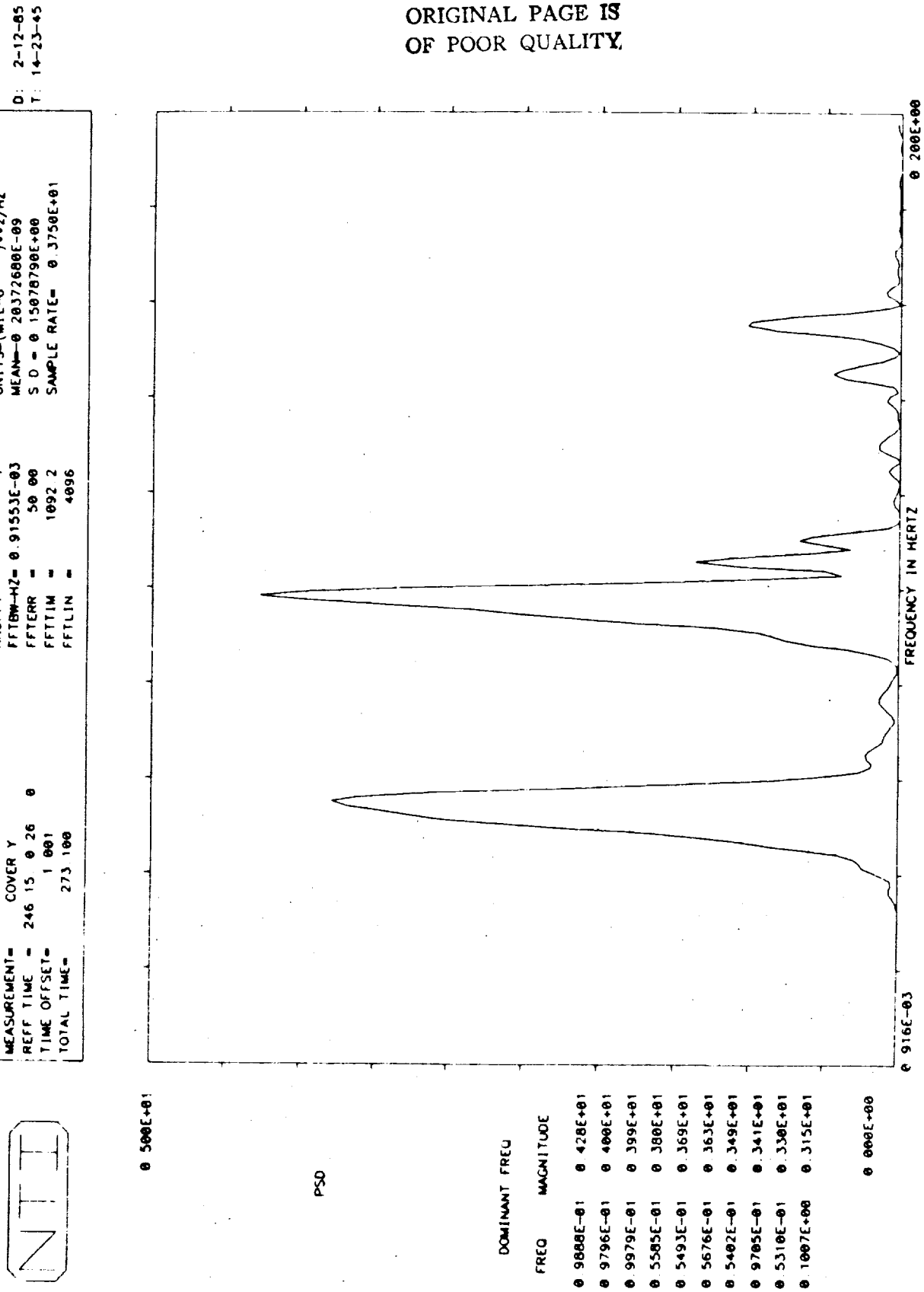

NTI

TEST NAME=SAE ACC MSIDS		NNOFFT =	1	UNITS=(MIL-G)**2/HZ	D: 2-12-85
MEASUREMENT=	COVER X2	FFTBW-HZ=	0.91553E-03	MEAN= 0.15570550E-08	T: 14-22- 1
REFF TIME =	246 15 0 26 0	FFTERR =	50.00	S D = 0.61850320E+00	
TIME OFFSET=	1.001	FFTTIM =	1092.2	SAMPLE RATE= 0.3750E+01	
TOTAL TIME=	273.100	FFTLIN =	4096		

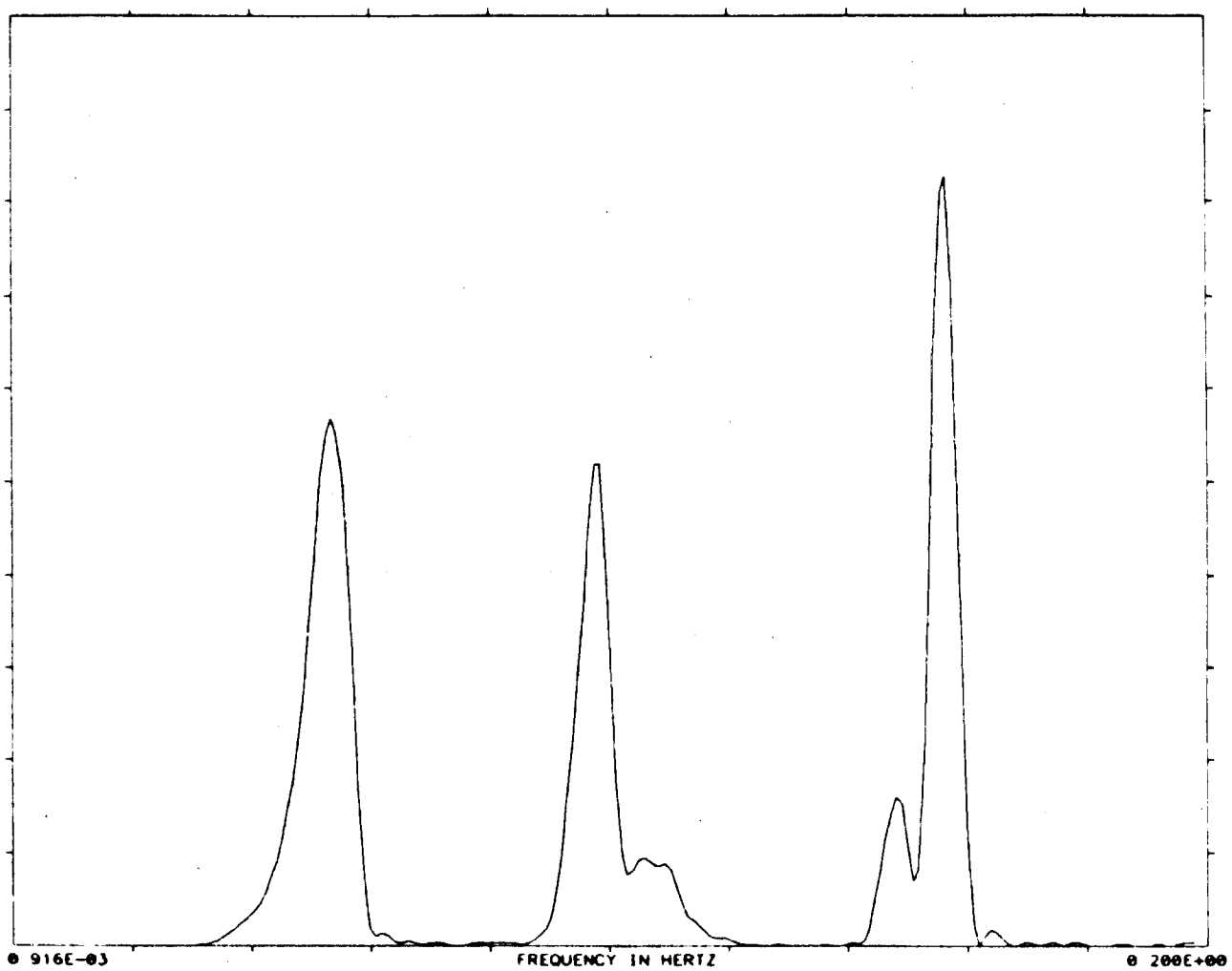

DOMINANT FREQ

FREQ	MAGNITUDE
0.1566E+00	0.826E+02
0.1556E+00	0.807E+02
0.1575E+00	0.712E+02
0.1547E+00	0.653E+02
0.5402E-01	0.569E+02
0.5310E-01	0.554E+02
0.5493E-01	0.553E+02
0.9888E-01	0.521E+02
0.9796E-01	0.521E+02
0.1584E+00	0.510E+02

0.000E+00

TEST NAME=SAE ACC MSTDS
MEASUREMENT= COVER X1
REFF TIME = 246 15 52 32 0
TIME OFFSET= 1.001
TOTAL TIME= 273.100

NNOFFT = 1
FFTBW-HZ= 0.91553E-03
FFTERR = 50.00
FFTTIM = 1092.2
FFTLIN = 4096

UNITS=(MIL-G)**2/HZ
MEAN=-0 16889320E-08
S D = 0 11835950E+00
SAMPLE RATE= 0 3750E+01

D: 2-12-85
T: 14-25-21

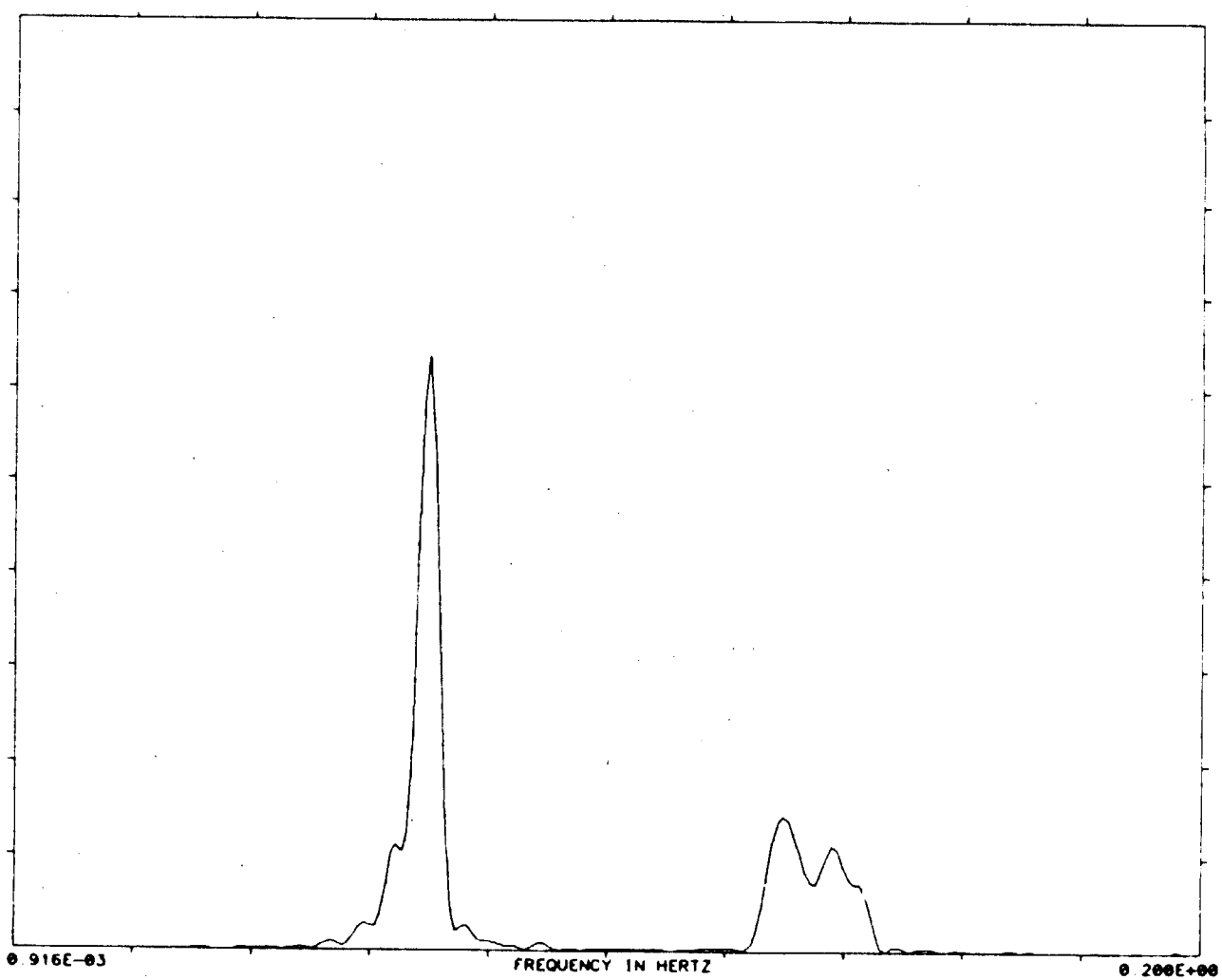

DOMINANT FREQ

FREQ	MAGNITUDE
0.7050E-01	0 637E+01
0.6958E-01	0.585E+01
0.7141E-01	0.528E+01
0.6866E-01	0.413E+01
0.7233E-01	0.326E+01
0.6775E-01	0.230E+01
0 1300E+00	0.144E+01
0.7324E-01	0.141E+01
0.1309E+00	0.138E+01
0 1291E+00	0.136E+01

ORIGINAL PAGE IS
OF POOR QUALITY

TEST NAME=SAE ACC MSTDS	NNOFFT = 1	UNITS=(MIL-G)**2/HZ	D: 2-12-85
MEASUREMENT= COVER Y	FFTBW-HZ= 0.91553E-03	MEAN=-0 31286620E-08	T: 14-28- 5
REFF TIME = 246 15 52 32 0	FFTERR = 50 00	S D = 0 21665280E+00	
TIME OFFSET= 1 001	FFTTIM = 1092 2	SAMPLE RATE= 0 3750E+01	
TOTAL TIME= 273 100	FFTLIN = 4096		

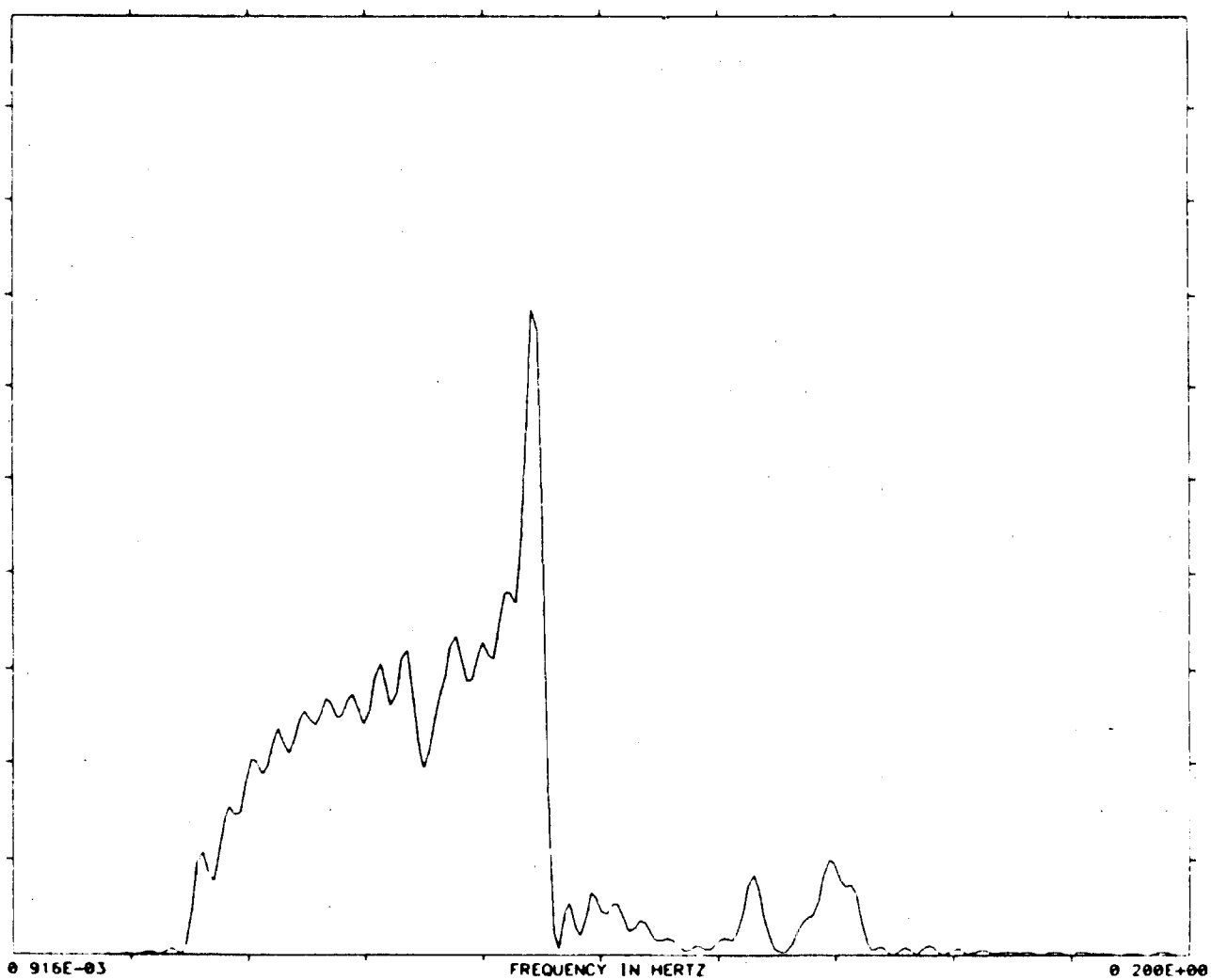

DOMINANT FREQ

FREQ	MAGNITUDE
0 8881E-01	0 684E+01
0 8972E-01	0 660E+01
0 8789E-01	0 557E+01
0 9064E-01	0 454E+01
0 8698E-01	0 419E+01
0 8514E-01	0 379E+01
0 8423E-01	0 378E+01
0 8606E-01	0 368E+01
0 8331E-01	0 342E+01
0 7599E-01	0 336E+01

ORIGINAL PAGE IS
OF POOR QUALITY

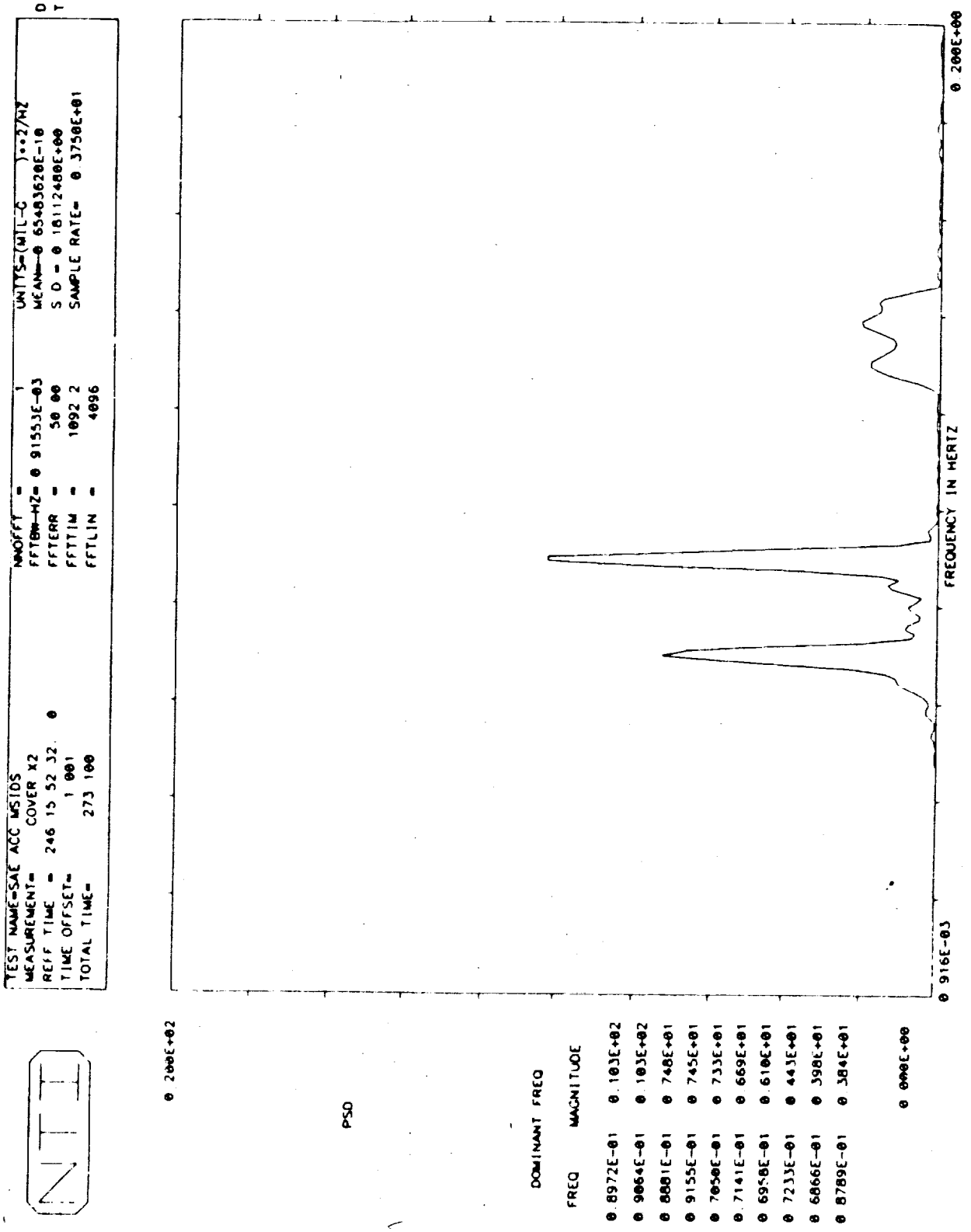

NTI

TEST NAME=SAE ACC MSIDS		NNOFFT =	1	UNITS=(MIL-G)**2/HZ	D: 2-12-85
MEASUREMENT=	COVER X1	FFTBW-HZ=	0.91553E-03	MEAN= 0 84492060E-09	T: 14-29-25
REFF TIME =	246 16 30 22 0	FFTERR =	50 00	S D = 0 26332400E+00	
TIME OFFSET=	1 001	FFTTIM =	1092 2	SAMPLE RATE= 0 3750E+01	
TOTAL TIME=	273 100	FFTLIN =	4096		

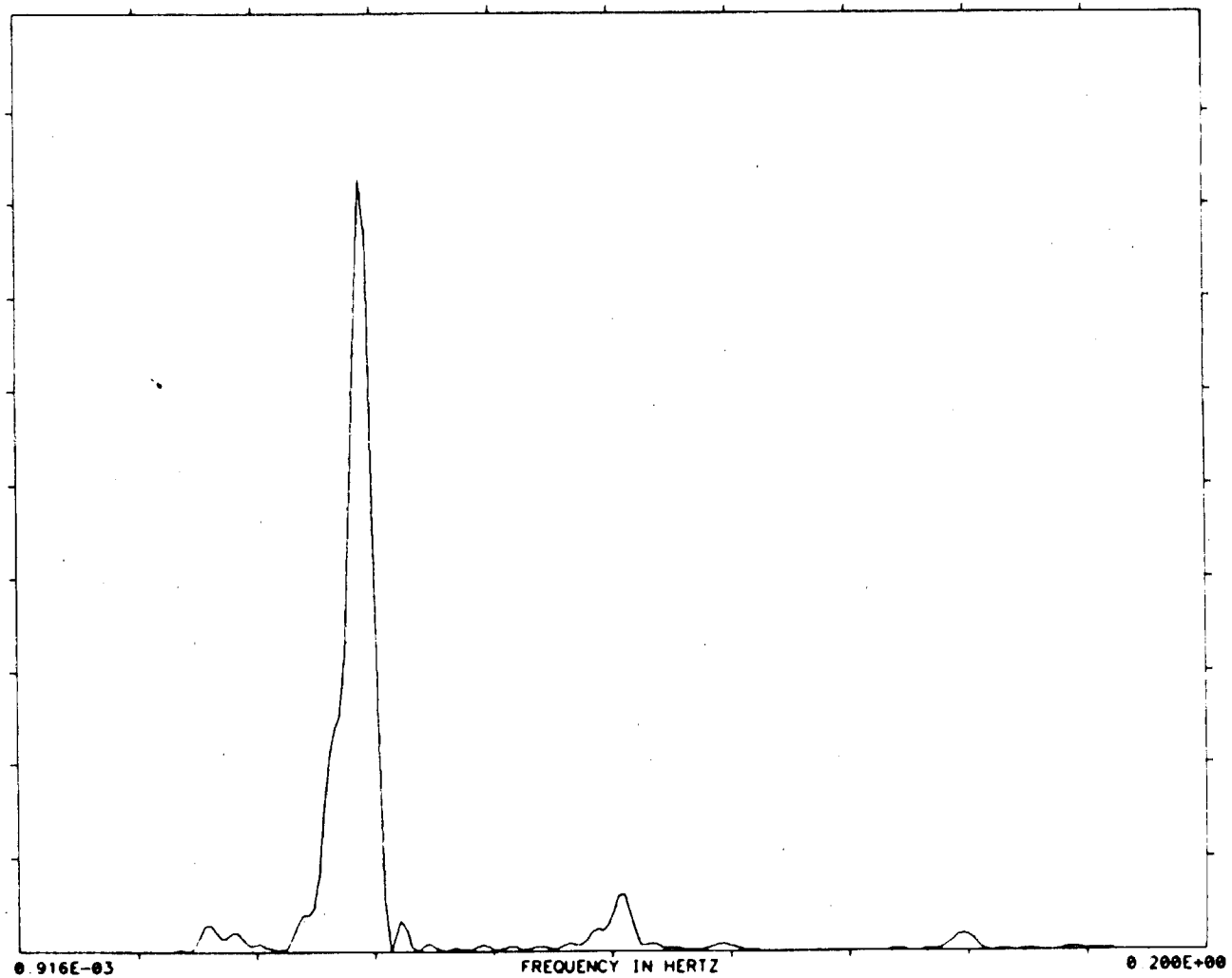

DOMINANT FREQ

FREQ	MAGNITUDE
0 5859E-01	0.414E+02
0.5951E-01	0 382E+02
0.5768E-01	0.351E+02
0.6042E-01	0.263E+02
0 5676E-01	0.244E+02
0 5585E-01	0.160E+02
0.5493E-01	0.125E+02
0.6134E-01	0.122E+02
0.5402E-01	0.119E+02
0 5310E-01	0.106E+02

0.000E+00

ORIGINAL PAGE IS
OF POOR QUALITY

NTI

TEST NAME=SAE ACC MSIDS		NNOFFT =	1	UNITS=(MIL-G)**2/HZ	
MEASUREMENT=	COVER Y	FFTBW-HZ=	0.91553E-03	MEAN=-0.10786610E-08	D: 2-12-85
REFF TIME =	246 16 30 22. 0	FFTERR =	50.00	S D = 0.19704790E+00	T: 14-32-13
TIME OFFSET=	1 001	FFTTIM =	1092.2	SAMPLE RATE= 0.3750E+01	
TOTAL TIME=	273 100	FFTLIN =	4096		

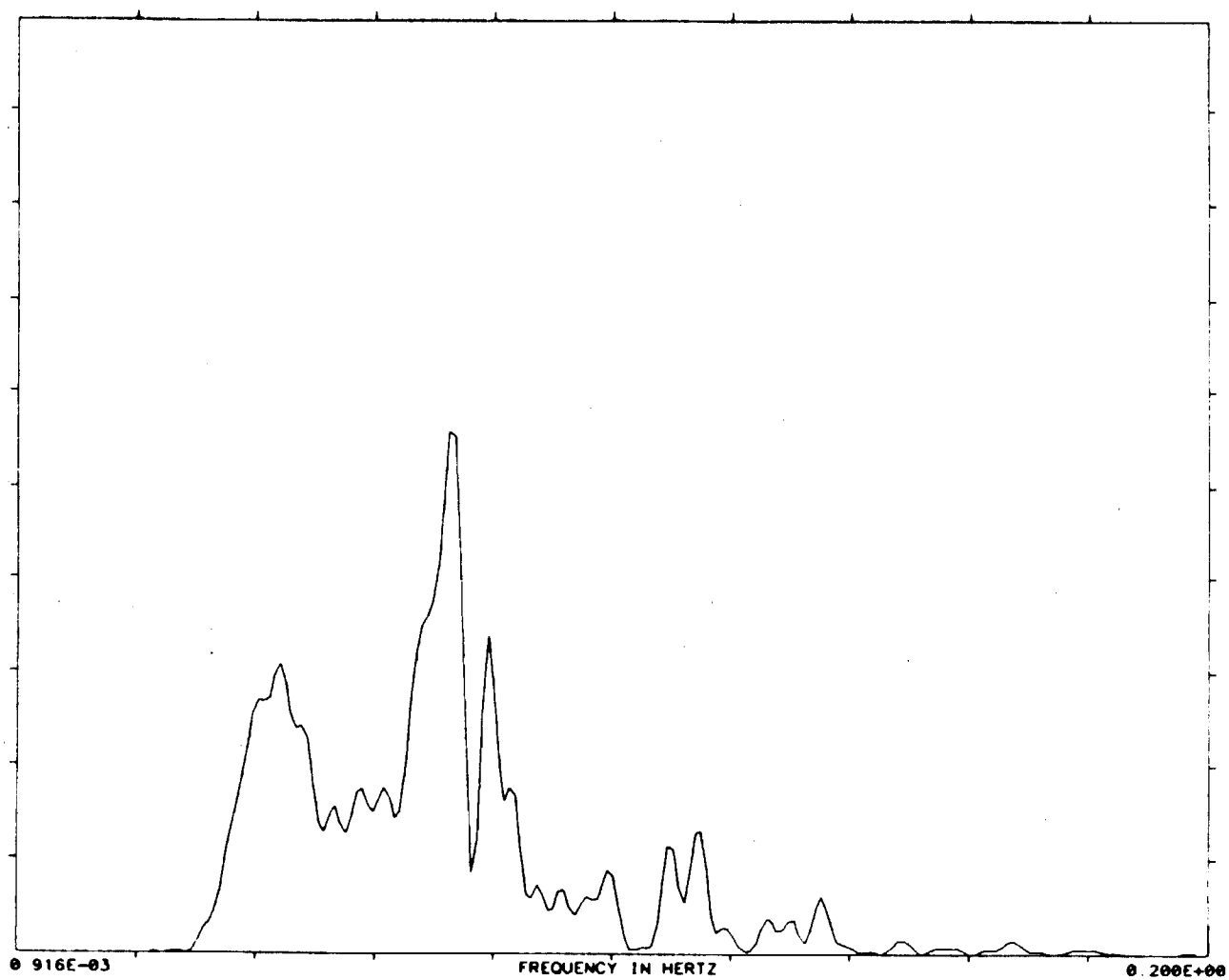

DOMINANT FREQ

FREQ	MAGNITUDE
0.7324E-01	0.559E+01
0.7416E-01	0.554E+01
0.7233E-01	0.487E+01
0.7507E-01	0.420E+01
0.7141E-01	0.415E+01
0.7050E-01	0.376E+01
0.6958E-01	0.360E+01
0.6866E-01	0.349E+01
0.7965E-01	0.338E+01
0.6775E-01	0.322E+01

ORIGINAL PAGE IS
OF POOR QUALITY

TEST NAME=SAE ACC MSIDS	NNOFFT = 1	UNITS=(MIL-G)**2/HZ	D: 2-12-85
MEASUREMENT= COVER X2	FFTBW-HZ= 0 91553E-03	MEAN= 0 55479180E-09	T: 14-30-48
REFF TIME = 246 16 30 22. 0	FFTERR = 50 00	S D = 0 2896550E+00	
TIME OFFSET= 1 001	FFTTIM = 1092 2	SAMPLE RATE= 0 3750E+01	
TOTAL TIME= 273 100	FFTLIN = 4096		

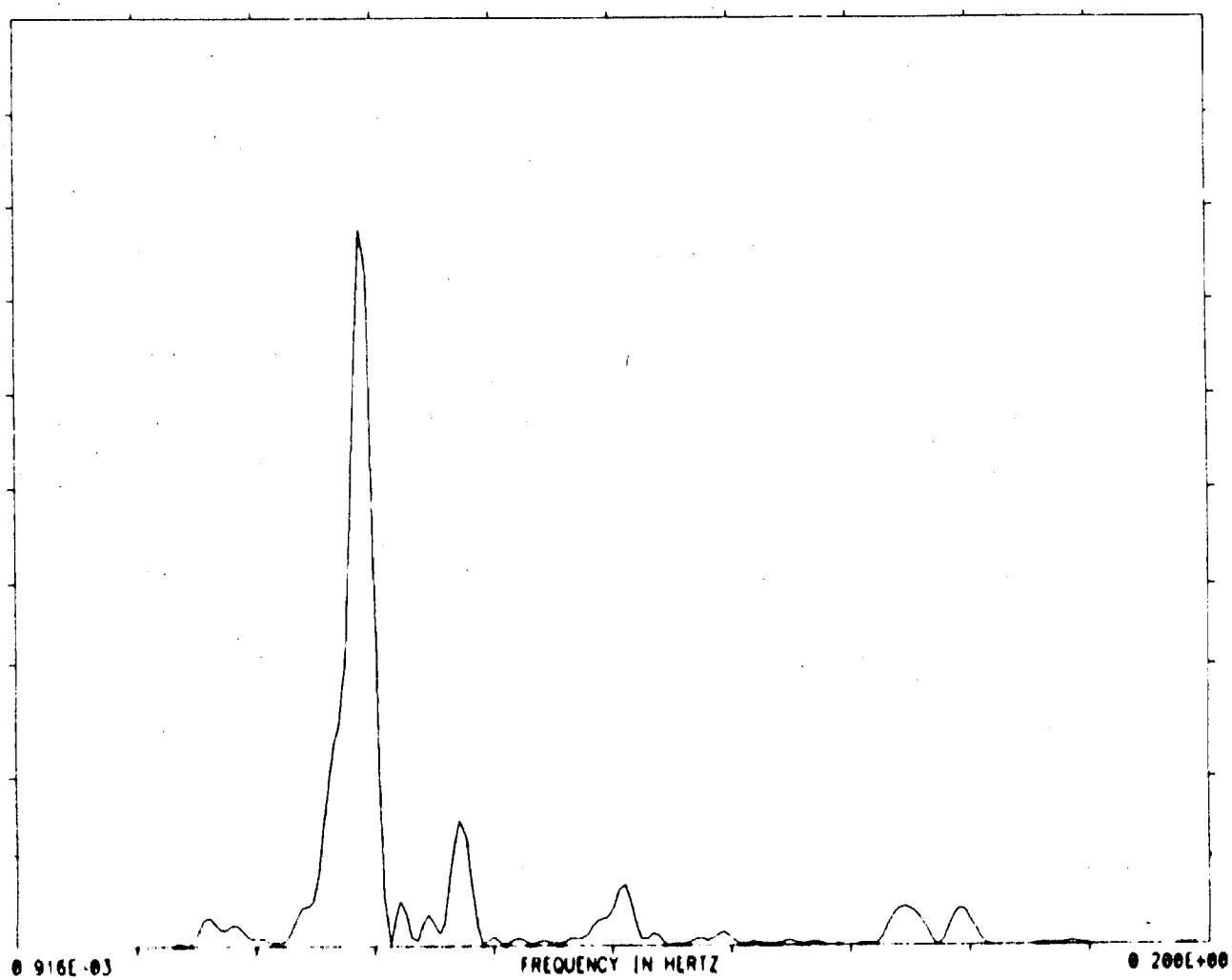

DOMINANT FREQ

FREQ	MAGNITUDE
0 5859E-01	0 388E+02
0 5951E-01	0 365E+02
0 5708E-01	0 323E+02
0 6042E-01	0 255E+02
0 5676E-01	0 224E+02
0 5585E-01	0 150E+02
0 5493E-01	0 122E+02
0 6134E-01	0 119E+02
0 5402E-01	0 119E+02
0 5310E-01	0 997E+01

0 000E+00

ORIGINAL PAGE IS
OF POOR QUALITY

ORIGINAL PAGE IS
OF POOR QUALITY

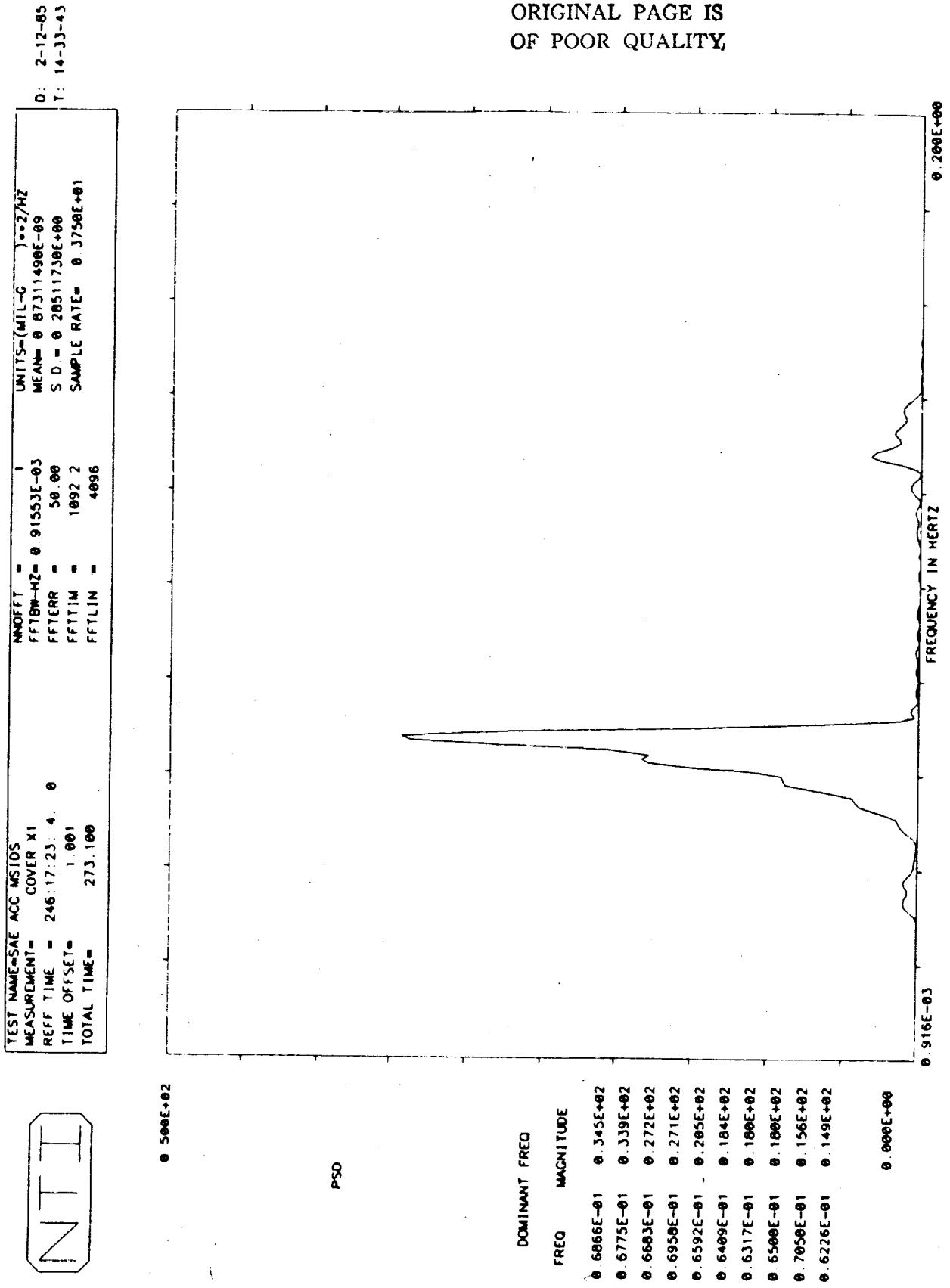

TEST NAME=SAE ACC MSIDS	NNOFFT = 1	UNITS=(MIL-G)**2/HZ	D: 2-12-85
MEASUREMENT= COVER Y	FFTBW-HZ= 0 91553E-03	MEAN= 0 74578570E-09	T: 14-37-23
REFF TIME = 246 17 23 4. 0	FFTERR = 50.00	S.D = 0 16622690E+00	
TIME OFFSET= 1 001	FFTTIM = 1092 2	SAMPLE RATE= 0.3750E+01	
TOTAL TIME= 273 100	FFTLIN = 4096		

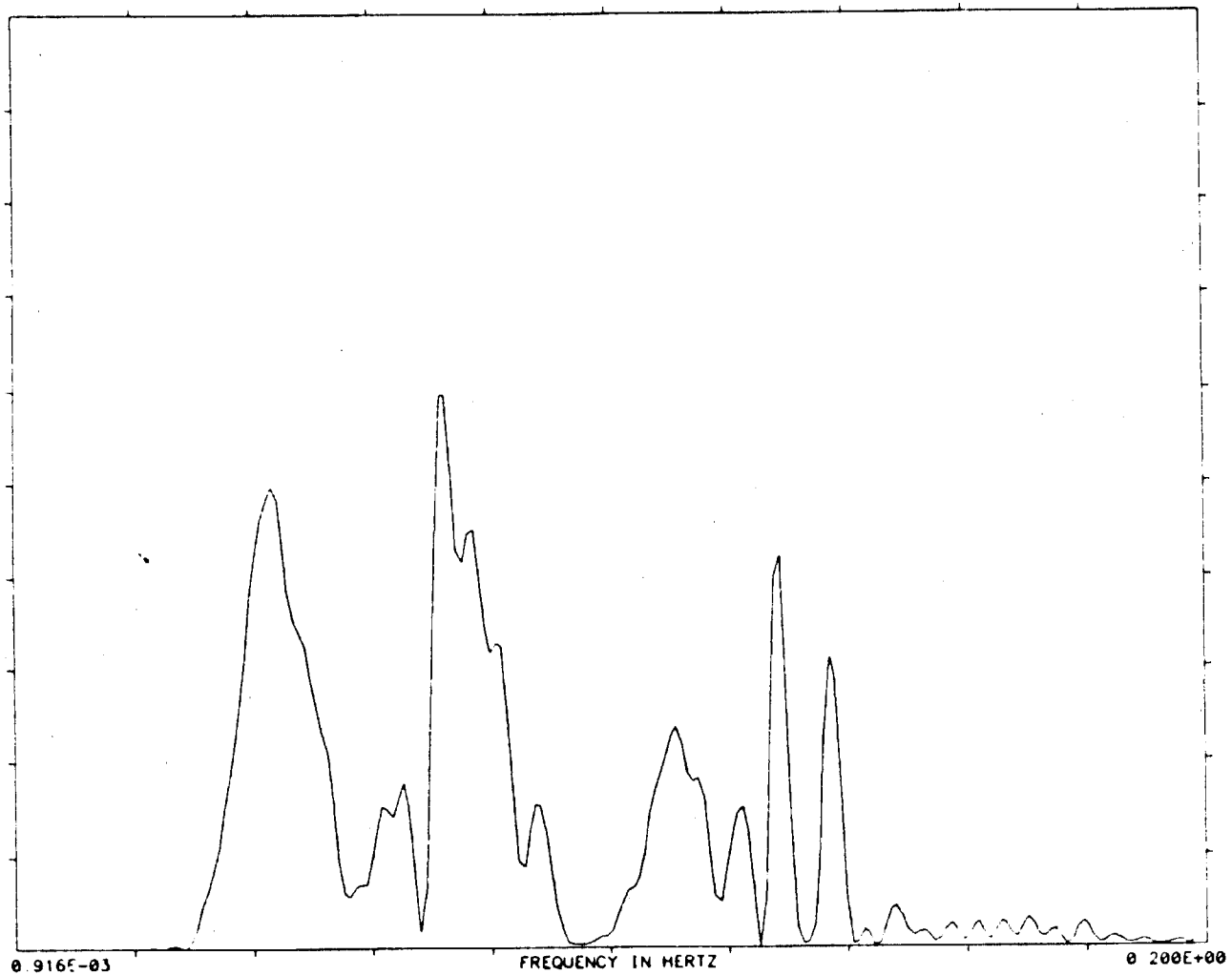

DOMINANT FREQ

FREQ	MAGNITUDE
0.7233E-01	0 297E+01
0.7324E-01	0.297E+01
0.7416E-01	0.254E+01
0.4395E-01	0.248E+01
0.4303E-01	0.242E+01
0.4486E-01	0.242E+01
0.4211E-01	0.231E+01
0.7141E-01	0.230E+01
0.7782E-01	0.226E+01
0.7690E-01	0.223E+01

ORIGINAL PAGE IS
OF POOR QUALITY

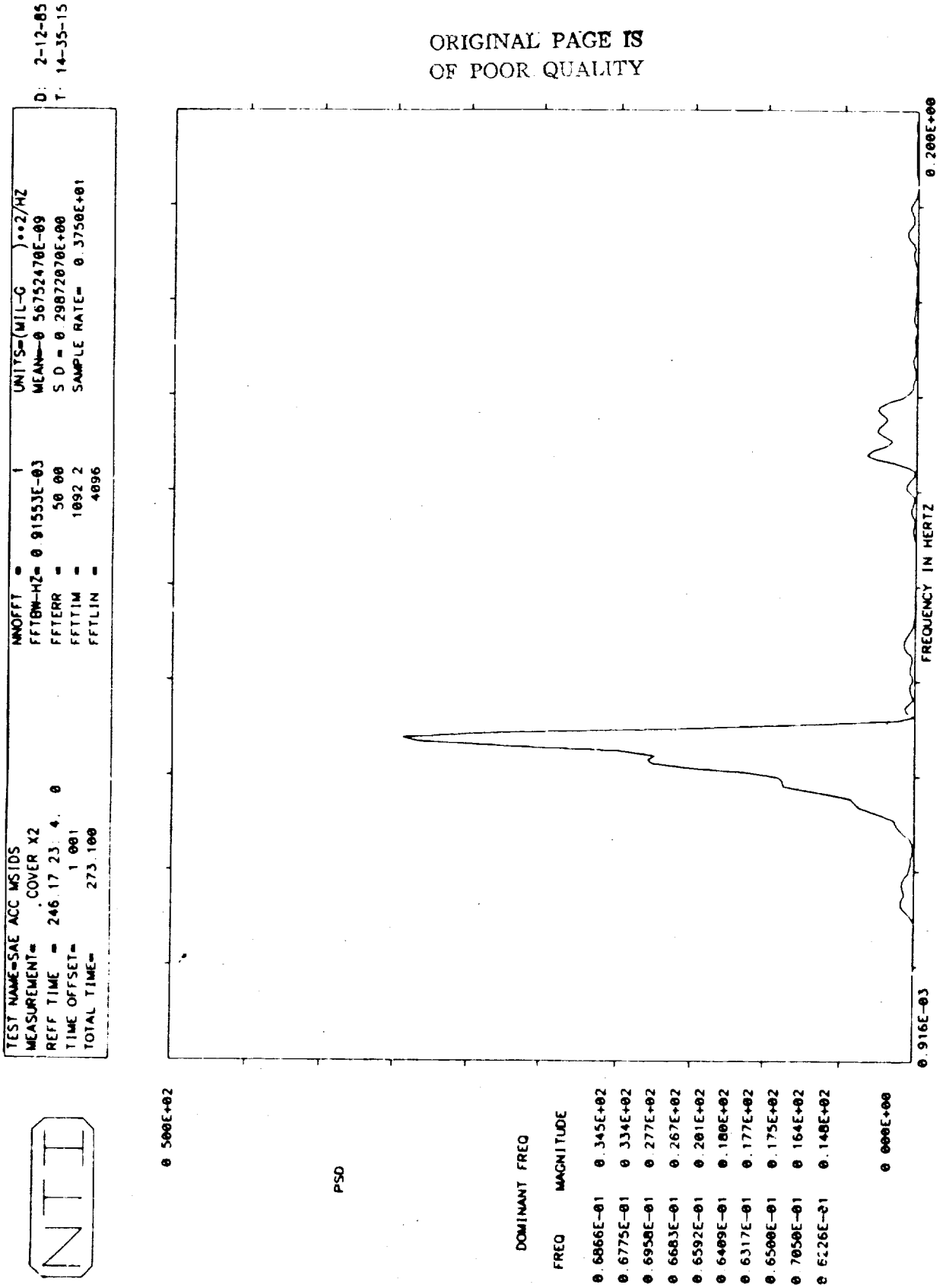

NTI

TEST NAME=SAE ACC MSIDS	NNOFFT = 1	UNITS=(MIL-G)**2/HZ	D: 2-12-85
MEASUREMENT= COVER X1	FFTBW-HZ= 0.91553E-03	MEAN= 0.11012160E-07	T: 14-38-56
REFF TIME = 246 18 6 29. 0	FFTERR = 50 00	S D = 0.51032360E+00	
TIME OFFSET= 1.001	FFTTIM = 1092 2	SAMPLE RATE= 0.3750E+01	
TOTAL TIME= 273 100	FFTLIN = 4096		

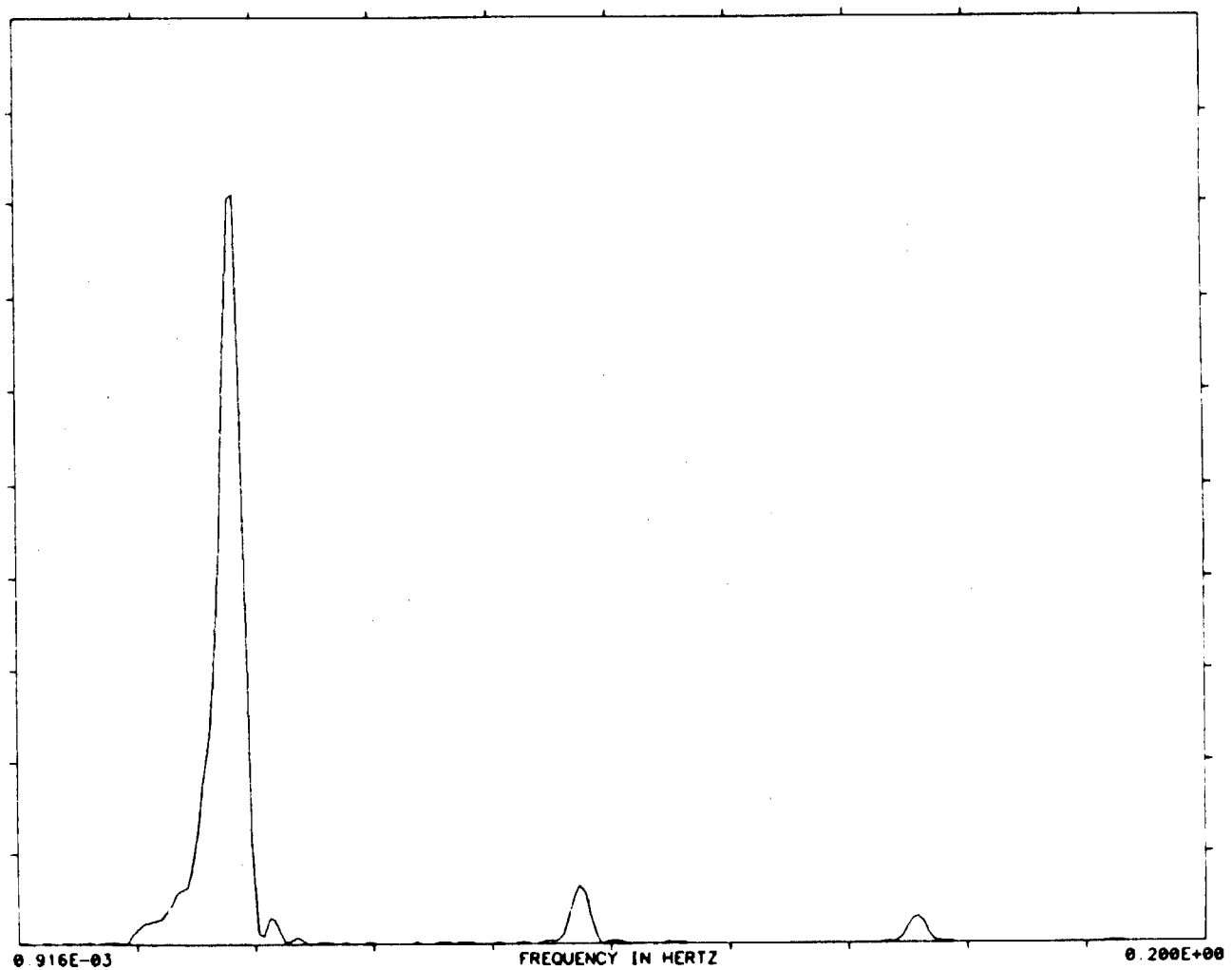

DOMINANT FREQ

FREQ	MAGNITUDE
0.3754E-01	0.162E+03
0.3662E-01	0.161E+03
0.3571E-01	0.128E+03
0.3845E-01	0.124E+03
0.3479E-01	0.870E+02
0.3937E-01	0.679E+02
0.3387E-01	0.586E+02
0.3296E-01	0.446E+02
0.3204E-01	0.356E+02
0.3113E-01	0.255E+02

ORIGINAL PAGE IS
OF POOR QUALITY

ORIGINAL PAGE IS
OF POOR QUALITY

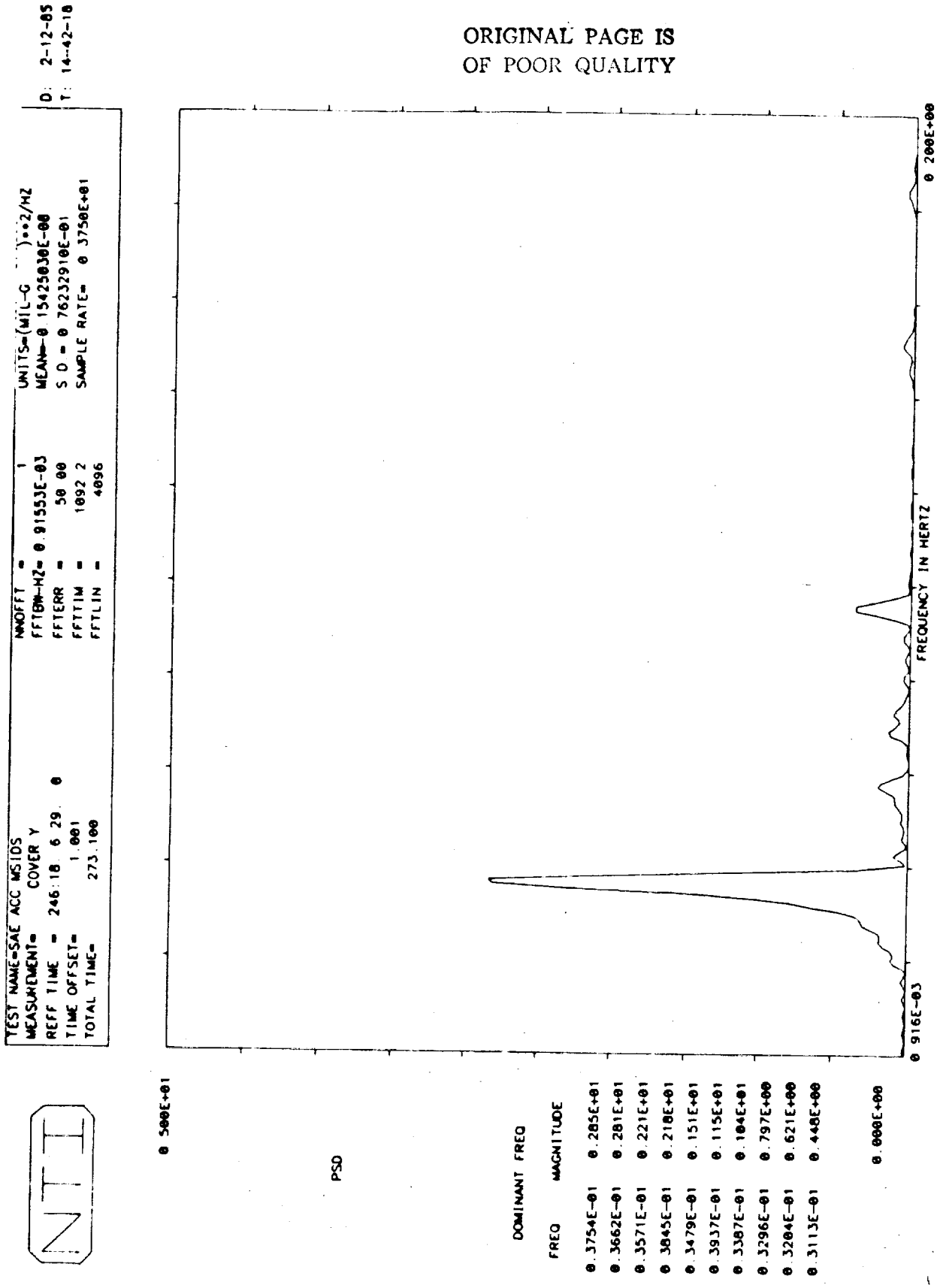

NTI

TEST NAME=SAE ACC MSIDS
MEASUREMENT= COVER X2
REFF TIME = 246:18: 6:29. 0
TIME OFFSET= 1.001
TOTAL TIME= 273.100

NNOFFT = 1
FFTBW-HZ= 0.91553E-03
FFTERR = 50.00
FFTTIM = 1092.2
FFTLIN = 4096

UNITS=(MIL-G)**2/HZ
MEAN=-0.14311810E-07
S.D.= 0.53818800E+00
SAMPLE RATE= 0.3750E+01

D: 2-12-85
T: 14-40-27

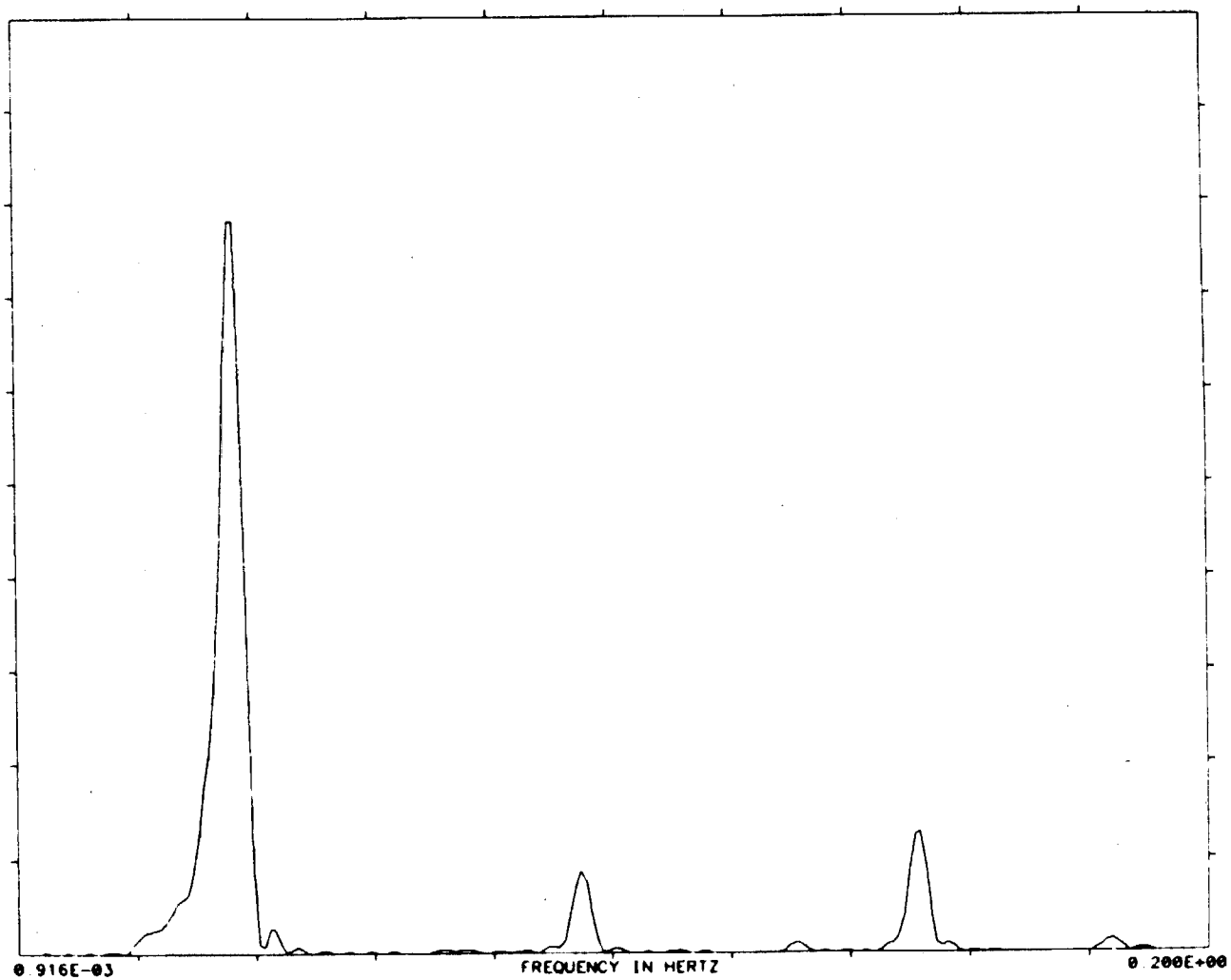

DOMINANT FREQ

FREQ	MAGNITUDE
0.3754E-01	0.156E+03
0.3662E-01	0.156E+03
0.3571E-01	0.125E+03
0.3845E-01	0.120E+03
0.3479E-01	0.851E+02
0.3937E-01	0.655E+02
0.3387E-01	0.574E+02
0.3296E-01	0.435E+02
0.3204E-01	0.347E+02
0.1520E+00	0.255E+02

ORIGINAL PAGE IS
OF POOR QUALITY

ORIGINAL PAGE IS
OF POOR QUALITY

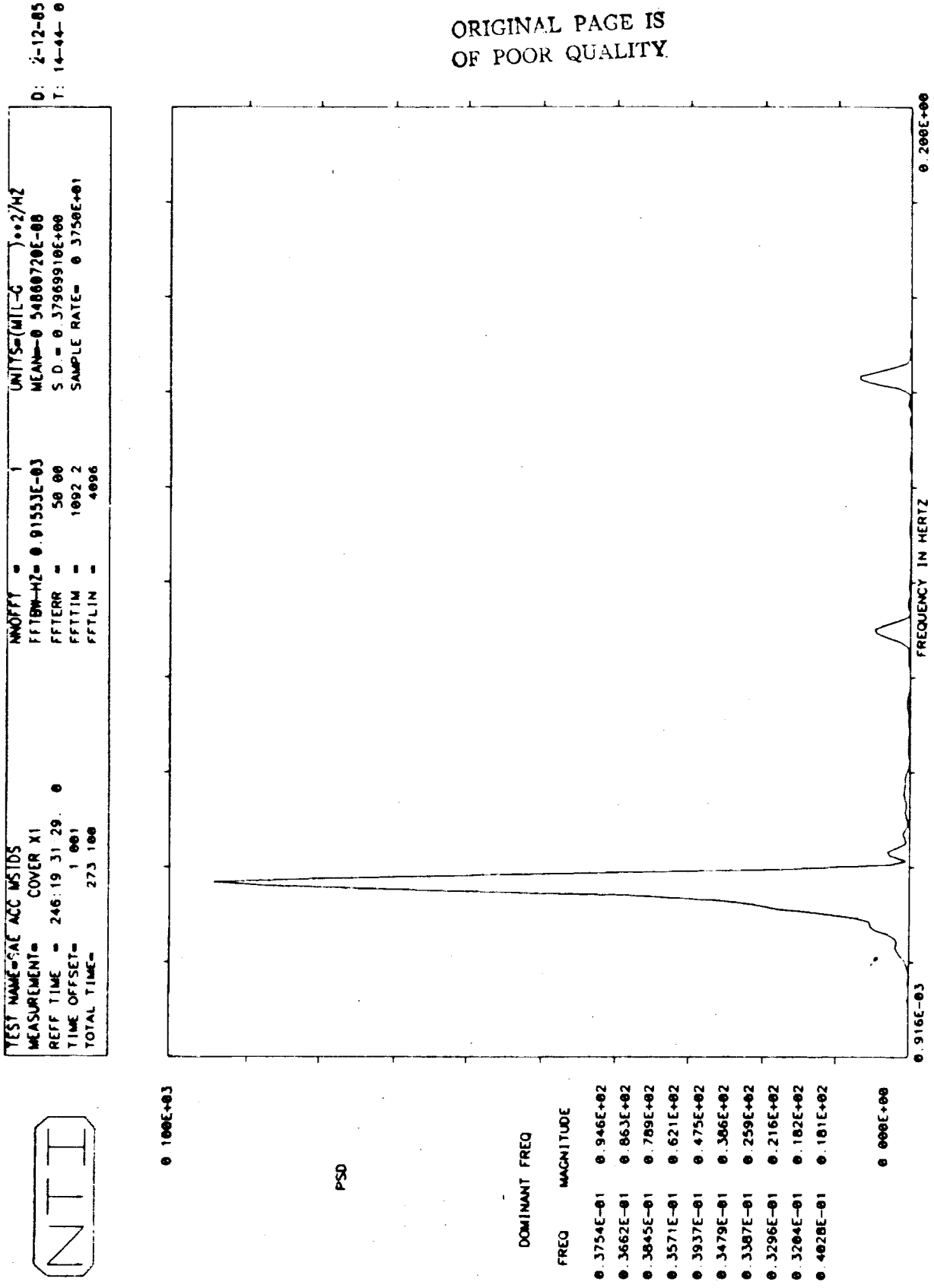

NTI

TEST NAME=SAE ACC MSIDS		NNOFFT =	1	UNITS=(MIL-G)**2/HZ	D: 2-12-85
MEASUREMENT=	COVER Y	FFTBW-HZ=	0.91553E-03	MEAN= 0 91677070E-09	T: 14-51-39
REFF TIME =	246:19 31 29. 0	FFTERR =	50 00	S D = 0 21109770E+00	
TIME OFFSET=	1 001	FFTTIM =	1092 2	SAMPLE RATE= 0 3750E+01	
TOTAL TIME=	273.100	FFTLIN =	4096		

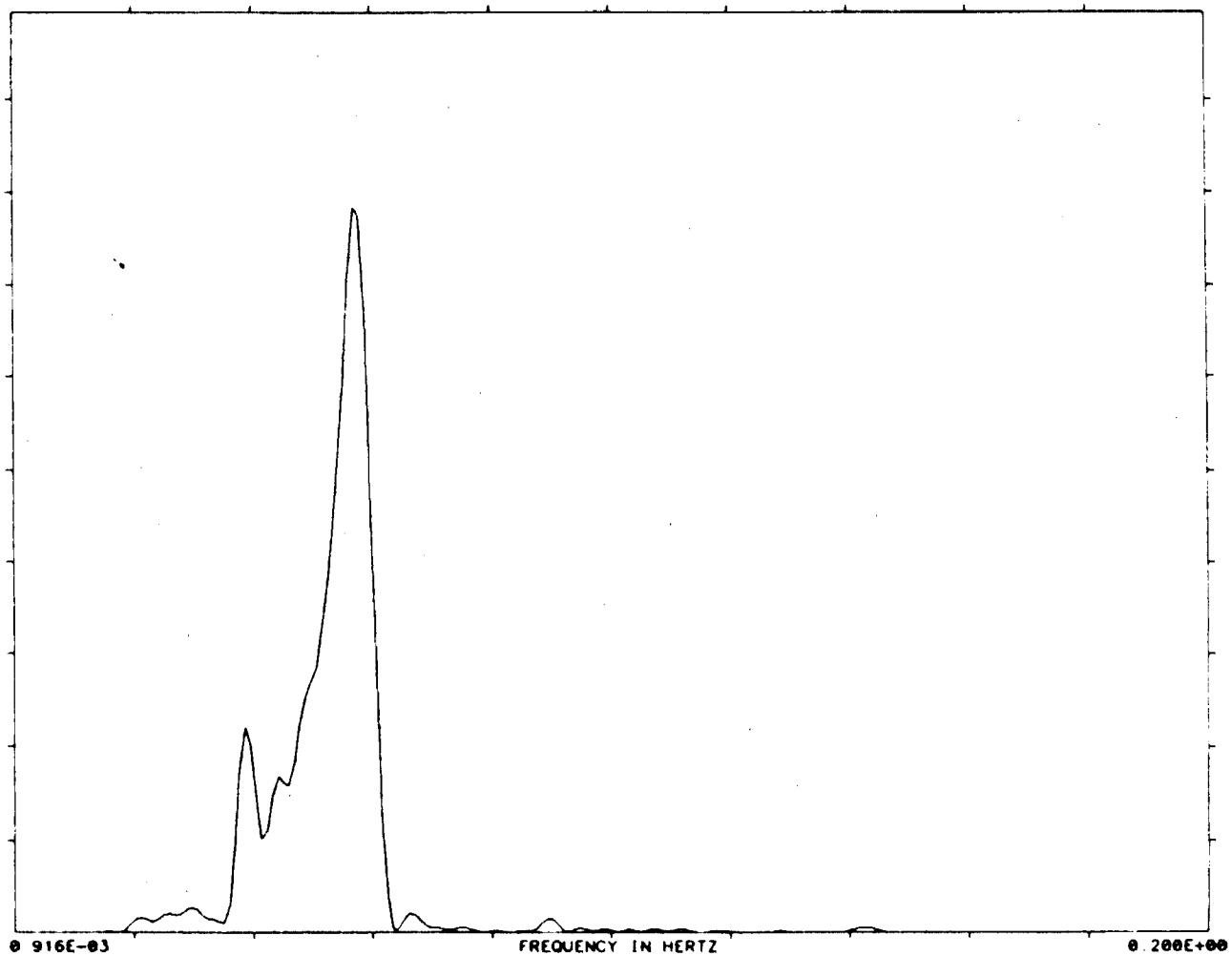

DOMINANT FREQ

FREQ	MAGNITUDE
0.5768E-01	0.157E+02
0.5859E-01	0.155E+02
0.5676E-01	0.141E+02
0.5951E-01	0.133E+02
0.5585E-01	0.119E+02
0.5493E-01	0.999E+01
0.6042E-01	0.958E+01
0.5402E-01	0.867E+01
0.5310E-01	0.755E+01
0.5219E-01	0.649E+01

ORIGINAL PAGE IS
OF POOR QUALITY

ORIGINAL PAGE IS
OF POOR QUALITY

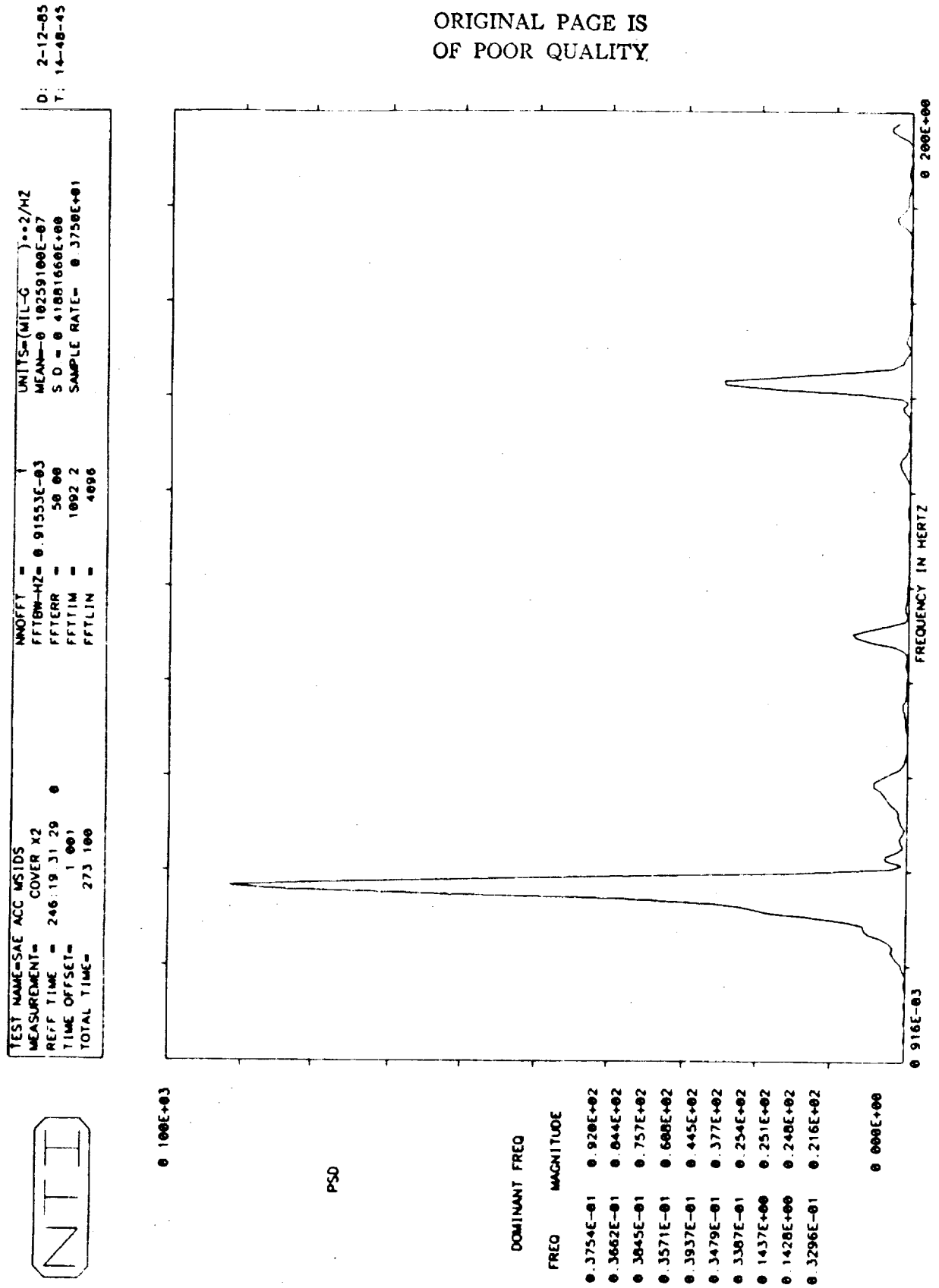

NTI

TEST NAME=SAE ACC MSIDS		NNOFFT =	1	UNITS=(MIL-G)**2/HZ	
MEASUREMENT=	COVER X1	FFTBW-HZ=	0.91553E-03	MEAN=-0.42018660E-09	D: 2-12-85
REFF TIME =	247 16 2 11 0	FFTERR =	50 00	S D = 0 22344040E+00	T: 14-53-56
TIME OFFSET=	1 001	FFTTIM =	1092 2	SAMPLE RATE= 0.3750E+01	
TOTAL TIME=	273 100	FFTLIN =	4096		

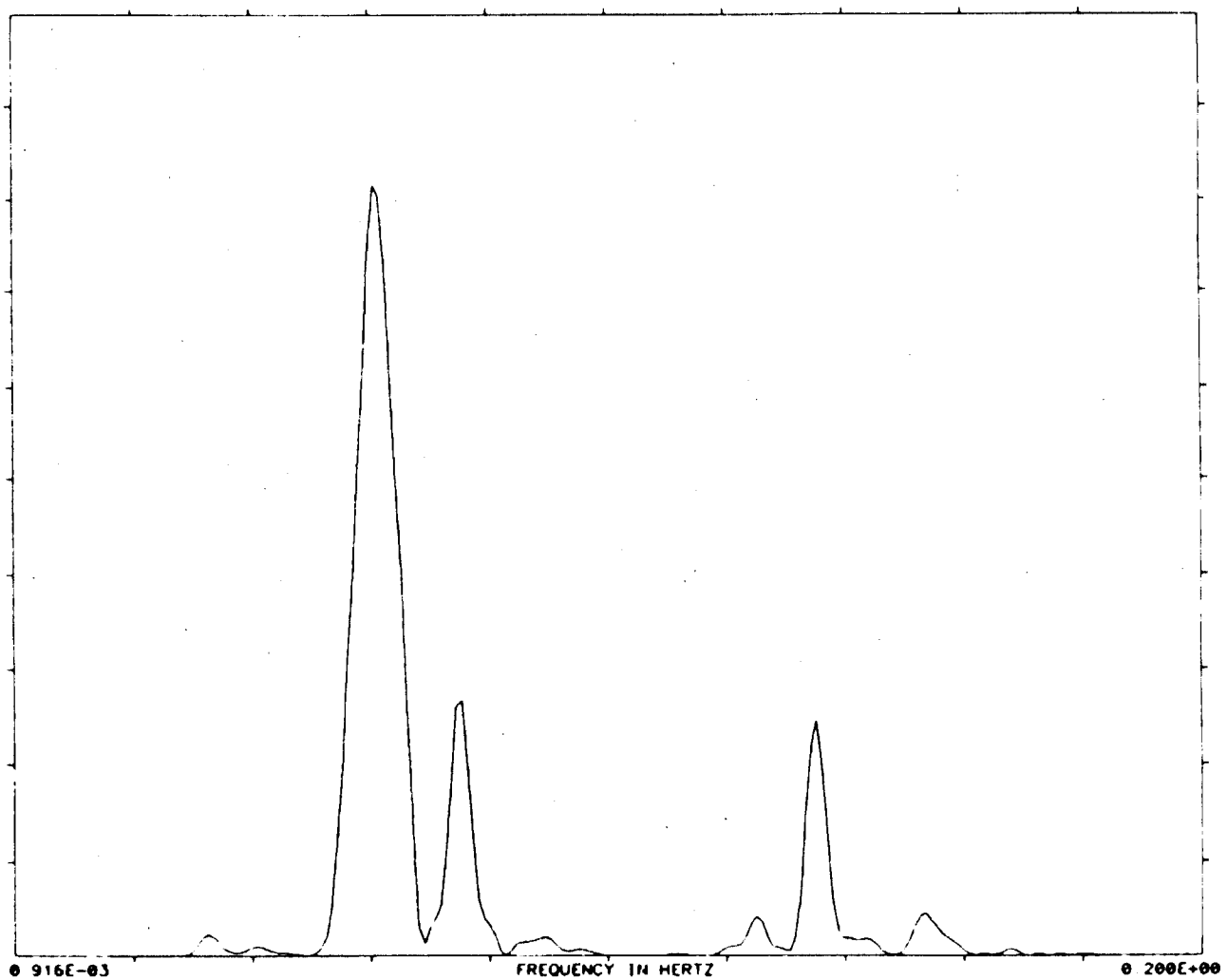

DOMINANT FREQ

FREQ	MAGNITUDE
0 6134E-01	0 163E+02
0 6226E-01	0 161E+02
0 6042E-01	0 148E+02
0 6317E-01	0 144E+02
0 5951E-01	0 123E+02
0 6409E-01	0 122E+02
0 6500E-01	0 101E+02
0 5859E-01	0 985E+01
0 6592E-01	0 793E+01
0 5768E-01	0 779E+01

ORIGINAL PAGE IS
OF POOR QUALITY

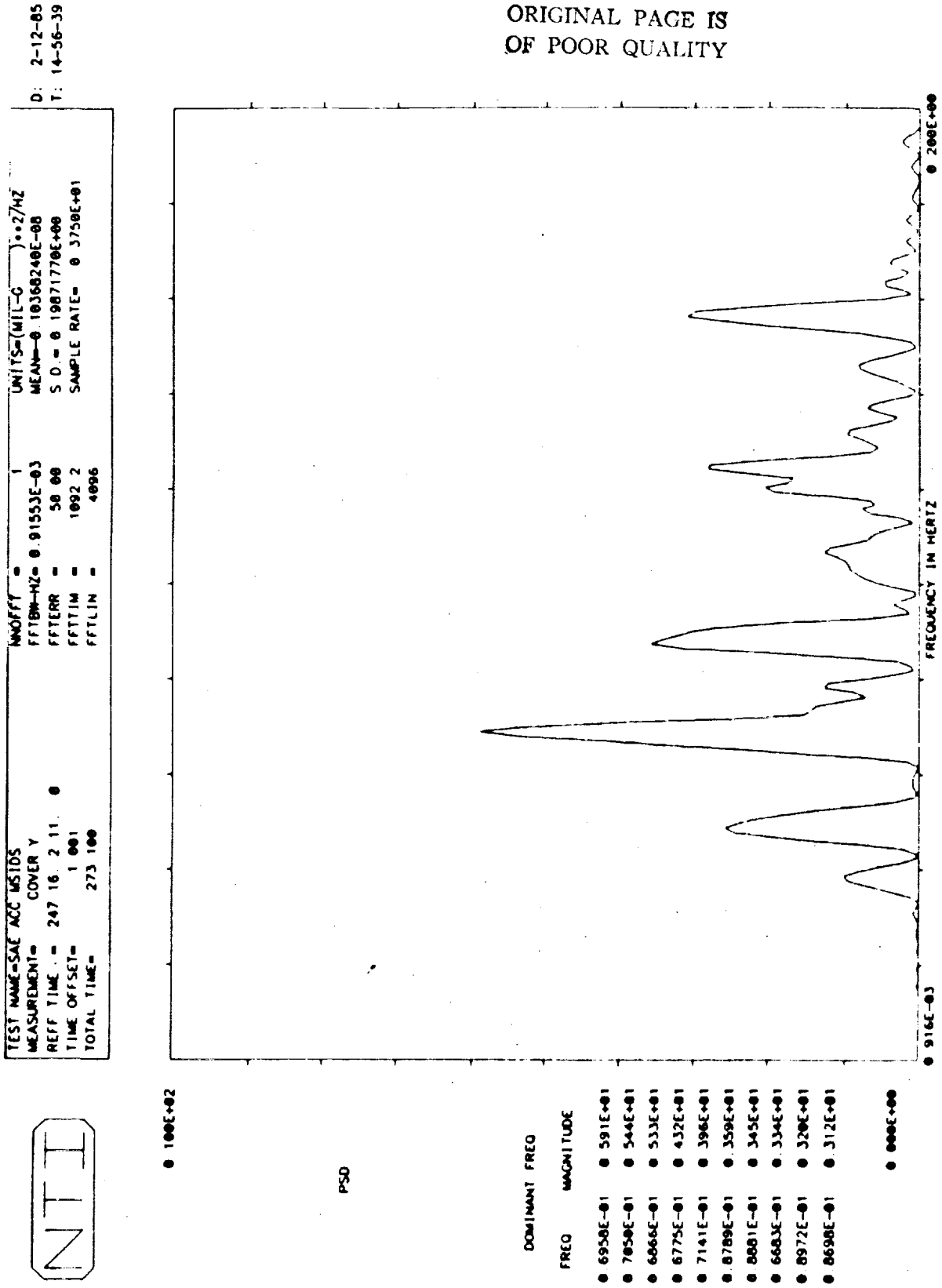

C-3

NTI

TEST NAME=SAE ACC MSIDS		NNOFFT =	1	UNITS=(MIL-G)**2/HZ	D: 2-12-85
MEASUREMENT=	COVER Y	FFTBW-HZ=	0.91553E-03	MEAN= 0.67666410E-09	T: 15: 1-12
REFF TIME =	247 16 37 24 0	FFTERR =	50 00	S D = 0.23295560E+00	
TIME OFFSET=	1.001	FFTTIM =	1092.2	SAMPLE RATE= 0.3750E+01	
TOTAL TIME=	273 100	FFTLIN =	4096		

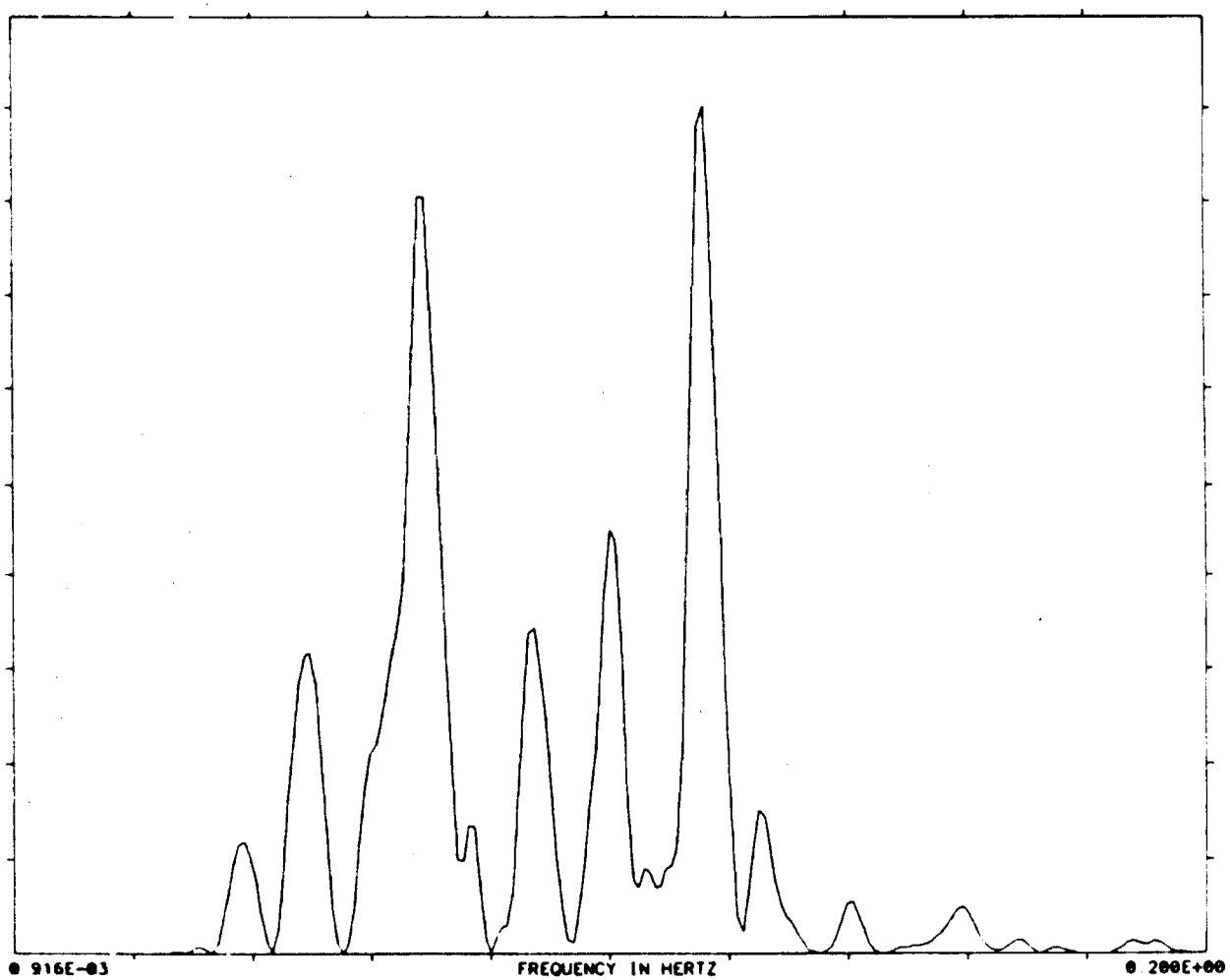

DOMINANT FREQ

FREQ	MAGNITUDE
0.1163E+00	0.903E+01
0.1154E+00	0.880E+01
0.6958E-01	0.804E+01
0.6866E-01	0.804E+01
0.1172E+00	0.799E+01
0.1144E+00	0.782E+01
0.7050E-01	0.700E+01
0.6775E-01	0.679E+01
0.1181E+00	0.637E+01
0.7141E-01	0.567E+01

0.000E+00

ORIGINAL PAGE IS
OF POOR QUALITY

ORIGINAL PAGE IS
OF POOR QUALITY

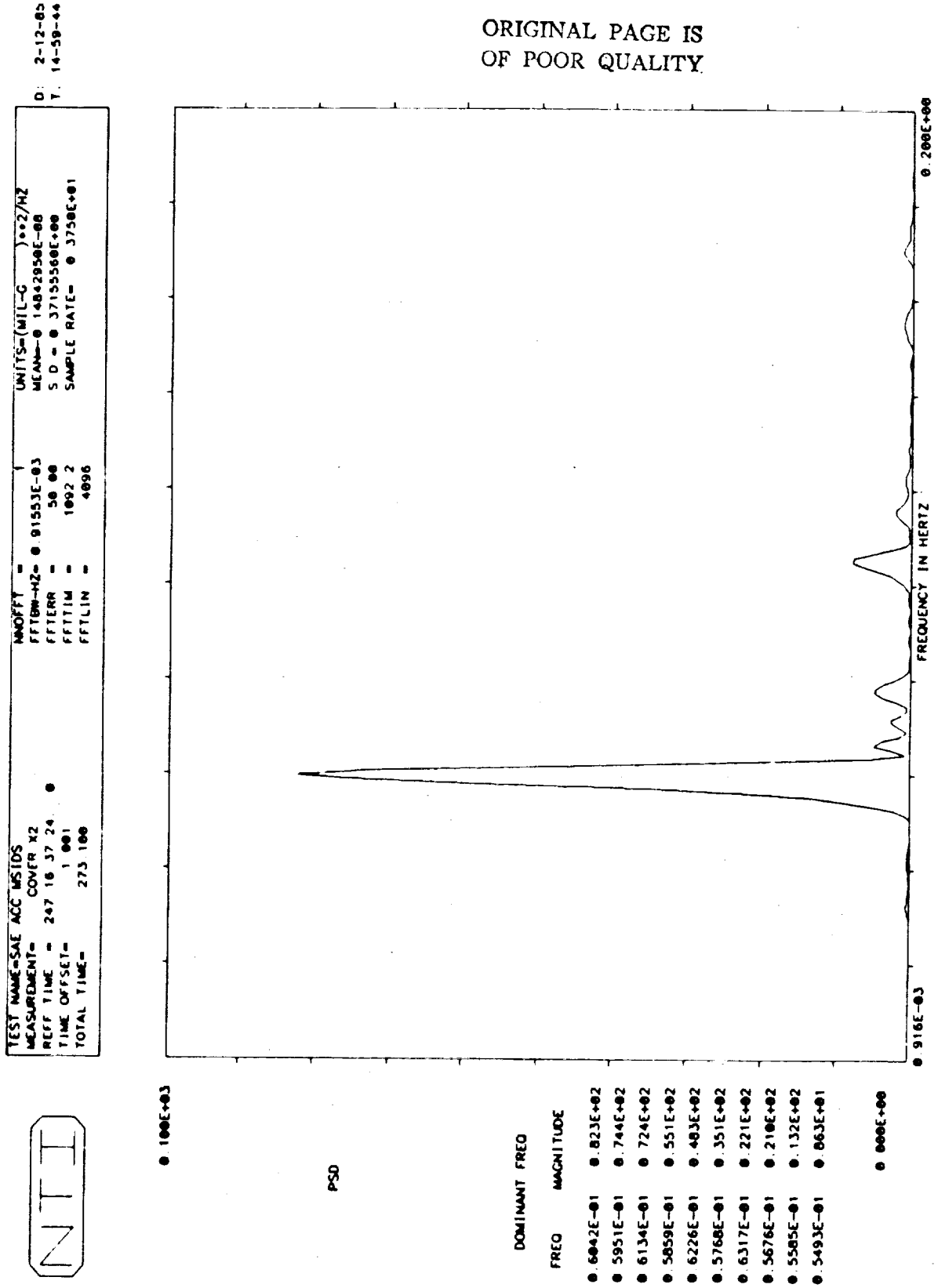

NTI

TEST NAME=SAE ACC MSTDS		NNOFFT = 1		UNITS=(MIL-G)**2/HZ	D: 2-13-85
MEASUREMENT= COVER X1		FFTBW-HZ= 0.91553E-03		MEAN= 0.49112710E-10	T: 7-26-38
REFF TIME = 247:17:32 39. 0		FFTERR = 50.00		S.D.= 0.14472160E+00	
TIME OFFSET= 1.001		FFTTIM = 1092.2		SAMPLE RATE= 0.3750E+01	
TOTAL TIME= 273.100		FFTLIN = 4096			

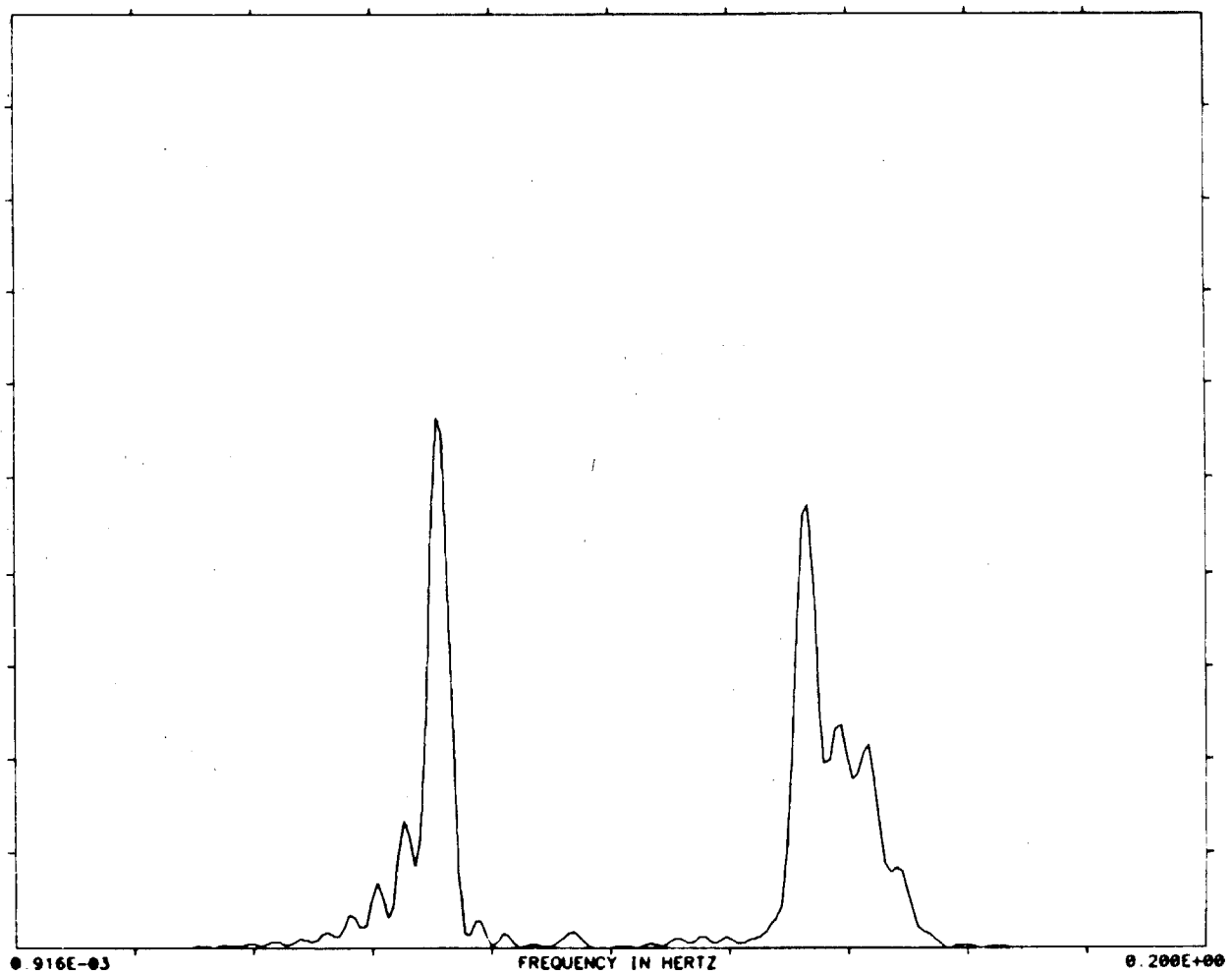

DOMINANT FREQ

FREQ	MAGNITUDE
0.7141E-01	0.564E+01
0.7233E-01	0.549E+01
0.1337E+00	0.470E+01
0.1328E+00	0.459E+01
0.7050E-01	0.442E+01
0.7324E-01	0.409E+01
0.1346E+00	0.381E+01
0.1318E+00	0.348E+01
0.1355E+00	0.262E+01
0.6958E-01	0.254E+01

0.000E+00

ORIGINAL PAGE IS
OF POOR QUALITY

NTI

TEST NAME=SAE ACC MSIDS		NNOFFT =	1	UNITS=(MIL-G)**2/HZ	D: 2-13-85
MEASUREMENT=	COVER Y	FFTBW-HZ=	0.91553E-03	MEAN=-0.15861590E-08	T: 7-29-44
REFF TIME =	247 17 32 39. 0	FFTERR =	50.00	S D = 0.22810240E+00	
TIME OFFSET=	1 001	FFTTIM =	1092.2	SAMPLE RATE= 0.3750E+01	
TOTAL TIME=	273 100	FFTLIN =	4096		

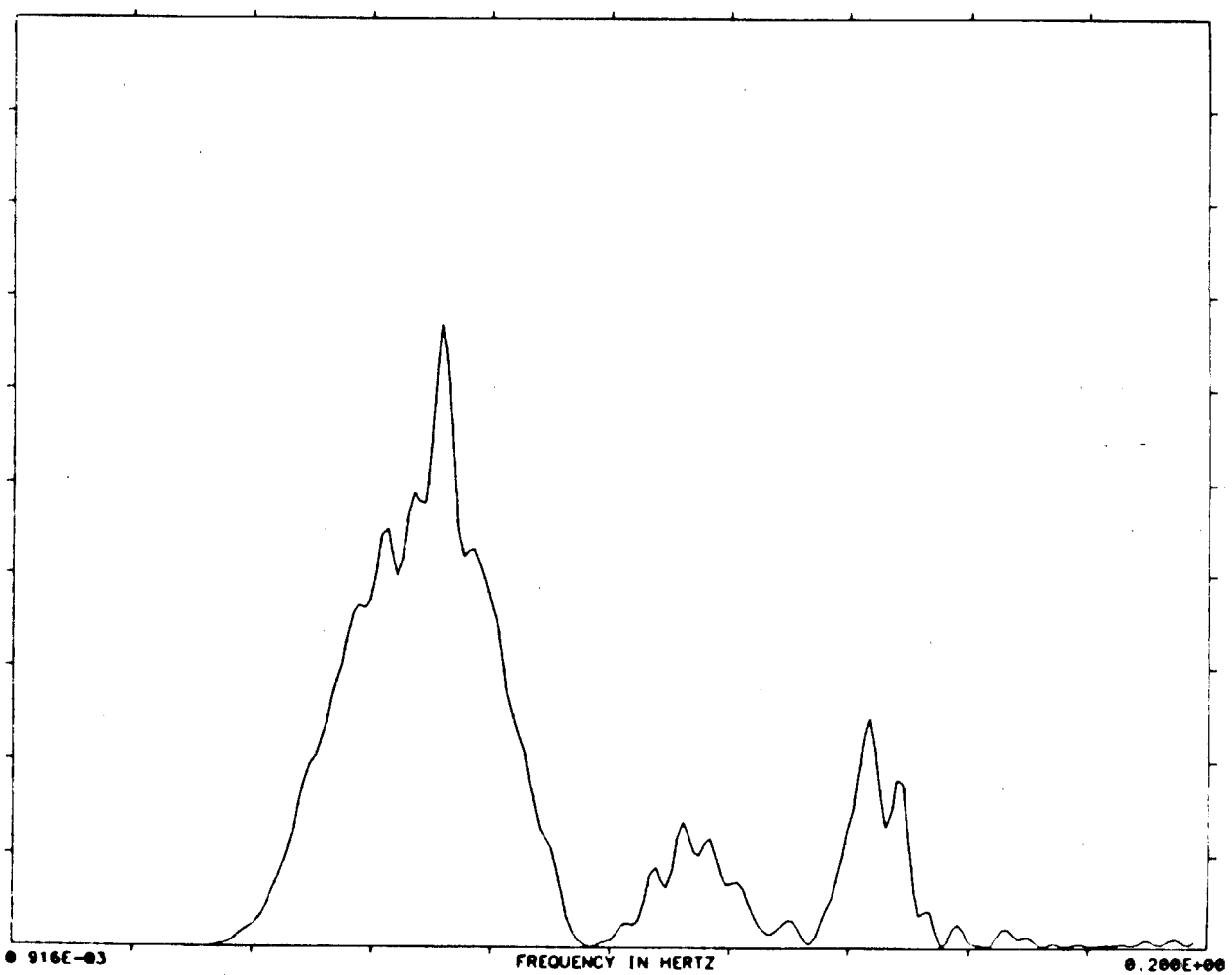

DOMINANT FREQ

FREQ	MAGNITUDE
0.7233E-01	0.671E+01
0.7324E-01	0.632E+01
0.7141E-01	0.621E+01
0.7416E-01	0.533E+01
0.7050E-01	0.531E+01
0.6775E-01	0.491E+01
0.6866E-01	0.480E+01
0.6958E-01	0.478E+01
0.6683E-01	0.465E+01
0.6317E-01	0.450E+01

NTI

TEST NAME=SAE ACC MSIDS		NNOFFT =	1	UNITS=(MIL-G)**2/HZ	
MEASUREMENT=	COVER X2	FFTBW-HZ=	0.91553E-03	MEAN= 0.86674850E-09	D: 2-13-85
REFF TIME =	247 17 32 39. 0	FFTERR =	50.00	S D = 0.16731890E+00	T: 7-28-26
TIME OFFSET=	1 001	FFTTIM =	1092.2	SAMPLE RATE= 0.3750E+01	
TOTAL TIME=	273 100	FFTLIN =	4096		

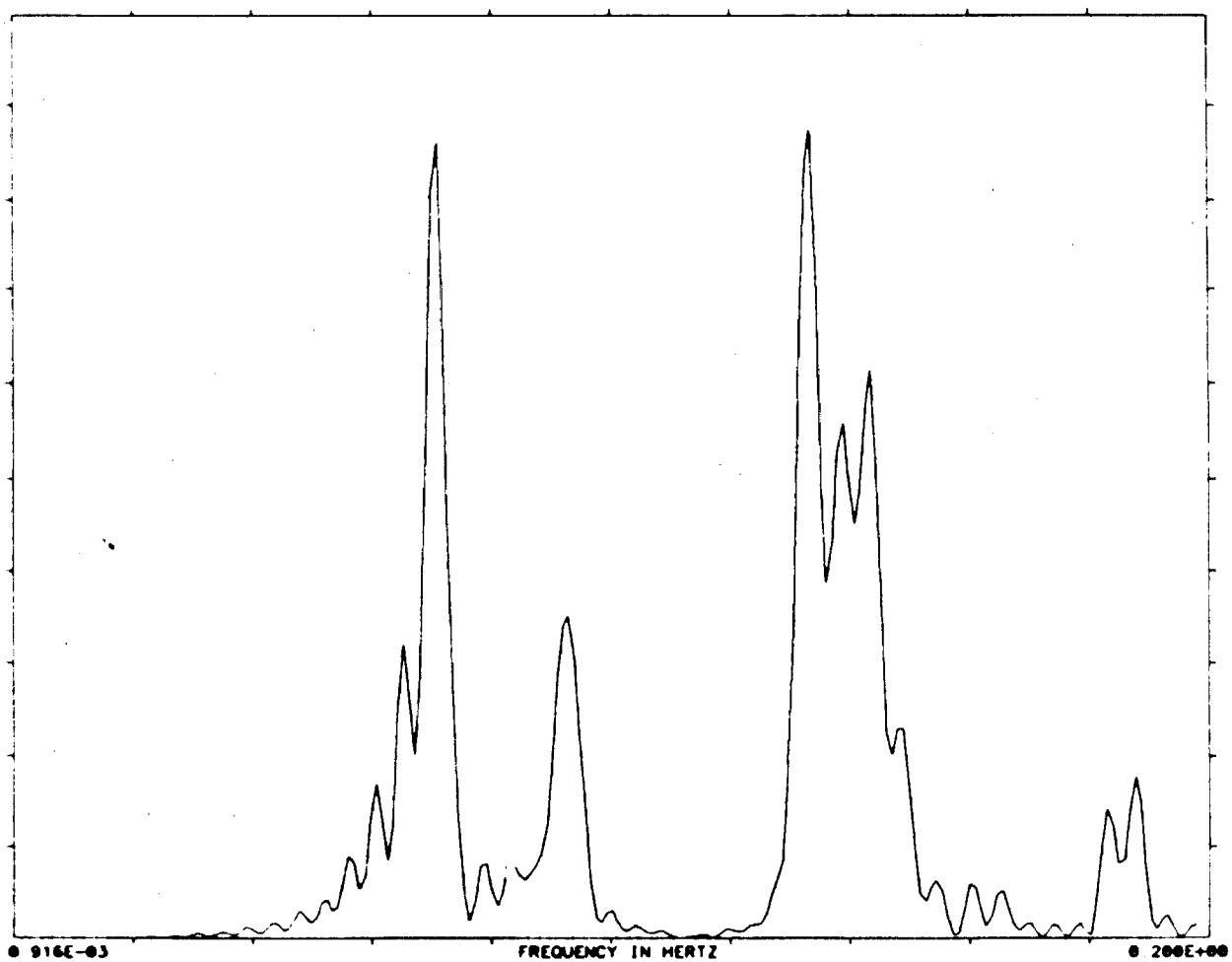

DOMINANT FREQ

FREQ	MAGNITUDE
0.1337E+00	0.437E+01
0.7141E-01	0.431E+01
0.1328E+00	0.419E+01
0.7050E-01	0.403E+01
0.1346E+00	0.357E+01
0.7233E-01	0.351E+01
0.1318E+00	0.310E+01
0.1437E+00	0.307E+01
0.1428E+00	0.290E+01
0.1392E+00	0.280E+01

0.000E+00

ORIGINAL PAGE IS
OF POOR QUALITY

NTI

TEST NAME=SAE ACC MSIDS
MEASUREMENT= COVER X1
REFF TIME = 247 18 7 22. 0
TIME OFFSET= 1 001
TOTAL TIME= 273 100

NNOFFT = 1
FFTBW-HZ= 0.91553E-03
FFTERR = 50 00
FFTTIM = 1092 2
FFTLIN = 4096

UNITS=(MIL-G)**2/HZ
MEAN= 0 53114490E-09
S D = 0 14249440E+00
SAMPLE RATE= 0.3750E+01

D: 2-13-85
T: 7-31- 6

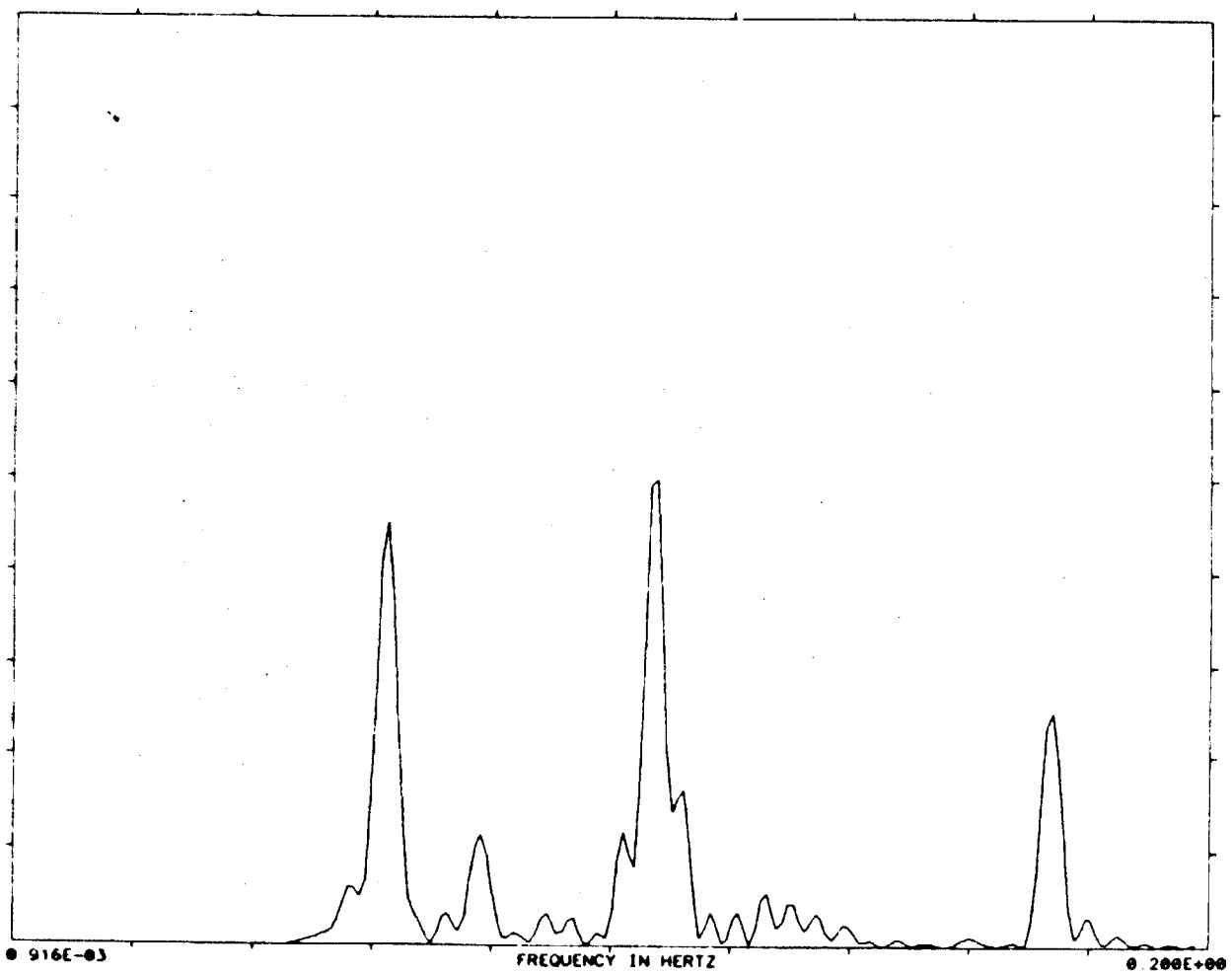

DOMINANT FREQ

FREQ	MAGNITUDE
0 1080E+00	0 500E+01
0 1071E+00	0 493E+01
0 6317E-01	0 452E+01
0 6226E-01	0 411E+01
0 6409E-01	0 380E+01
0 1089E+00	0 365E+01
0 1062E+00	0 340E+01
0 6134E-01	0 284E+01
0 1740E+00	0 252E+01
0 6500E-01	0 242E+01

TEST NAME=SAE ACC MSIDS		NNOFFT =	1	UNITS=(MTL-G)**2/HZ	
MEASUREMENT=	COVER Y	FFTBW-HZ=	0.91553E-03	MEAN=-0 46020430E-00	D: 2-13-85
REFF TIME =	247.18 / 22. 0	FFTERR =	50.00	S.D = 0 28986190E+00	T: 7-33-47
TIME OFFSET=	1 001	FFTTIM =	1092 2	SAMPLE RATE= 0 3750E+01	
TOTAL TIME=	273 100	FFTLIN =	4096		

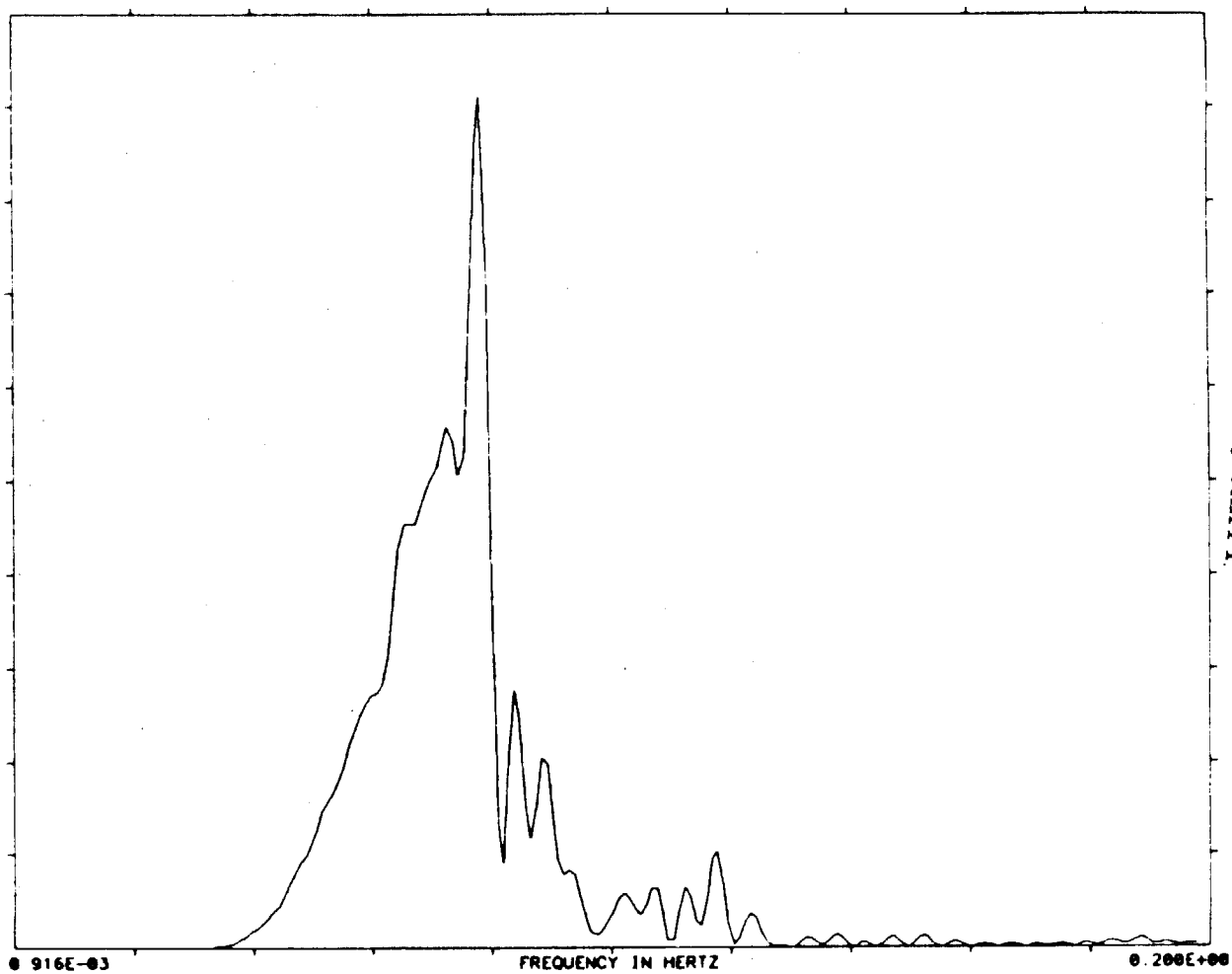

DOMINANT FREQ

FREQ	MAGNITUDE
0.7874E-01	0.182E+02
0.7782E-01	0.171E+02
0.7965E-01	0.146E+02
0.7690E-01	0.133E+02
0.7324E-01	0.112E+02
0.7416E-01	0.109E+02
0.7233E-01	0.108E+02
0.7599E-01	0.105E+02
0.7141E-01	0.103E+02
0.7507E-01	0.101E+02

0 000E+00

NTI

TEST NAME=SAE ACC MSIDS		NNOFFT = 1		UNITS=(MIL-G)**2/HZ	D: 2-13-85
MEASUREMENT= COVER X2		FFTBW-HZ= 0.91553E-03		MEAN= 0.11496010E-00	T: 7-32-27
REFF TIME = 247 18: 7 22. 0		FFTERR = 50.00		S D = 0.27261610E+00	
TIME OFFSET= 1.001		FFTTIM = 1092.2		SAMPLE RATE= 0.3750E+01	
TOTAL TIME= 273.100		FFTLIN = 4096			

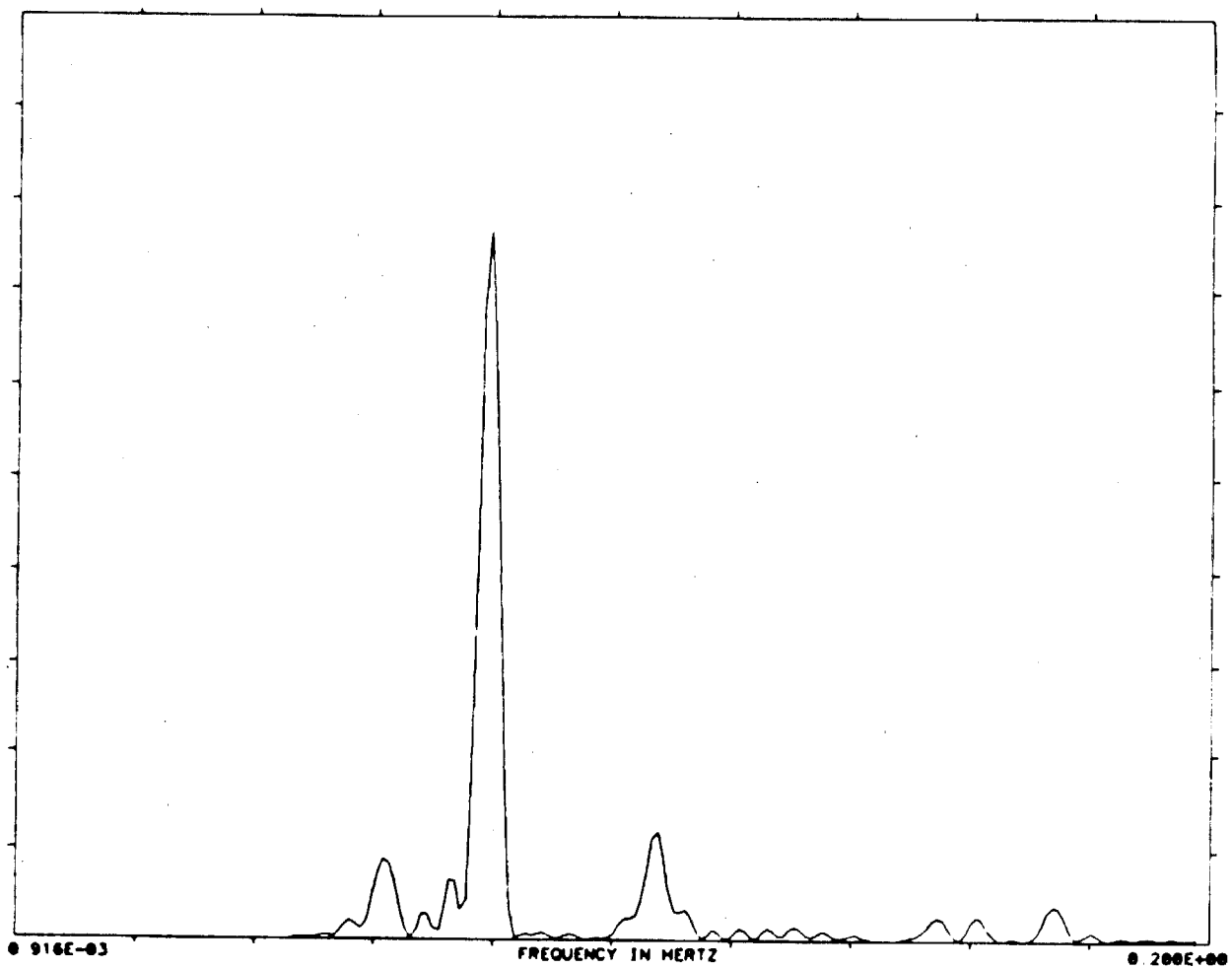

DOMINANT FREQ

FREQ	MAGNITUDE
0.7965E-01	0.383E+02
0.7874E-01	0.337E+02
0.8057E-01	0.324E+02
0.7782E-01	0.214E+02
0.8148E-01	0.201E+02
0.7690E-01	0.887E+01
0.8240E-01	0.846E+01
0.1000E+00	0.598E+01
0.1071E+00	0.555E+01
0.1089E+00	0.473E+01

0.000E+00

ORIGINAL PAGE IS
OF POOR QUALITY

TEST NAME=SAE ACC MSIDS		NNOFFT =	1	UNITS=(MIL-G)**2/HZ	D: 2-12-85
MEASUREMENT=	COVER X2	FFTBW-HZ=	0.91553E-03	MEAN=-0 00035540E-09	T: 14-55-16
REFF TIME =	247 16 2 11 0	FFTERR =	50 00	S D = 0 26401210E+00	
TIME OFFSET=	1 001	FFTTIM =	1092 2	SAMPLE RATE= 0 3750E+01	
TOTAL TIME=	273 100	FFTLIN =	4096		

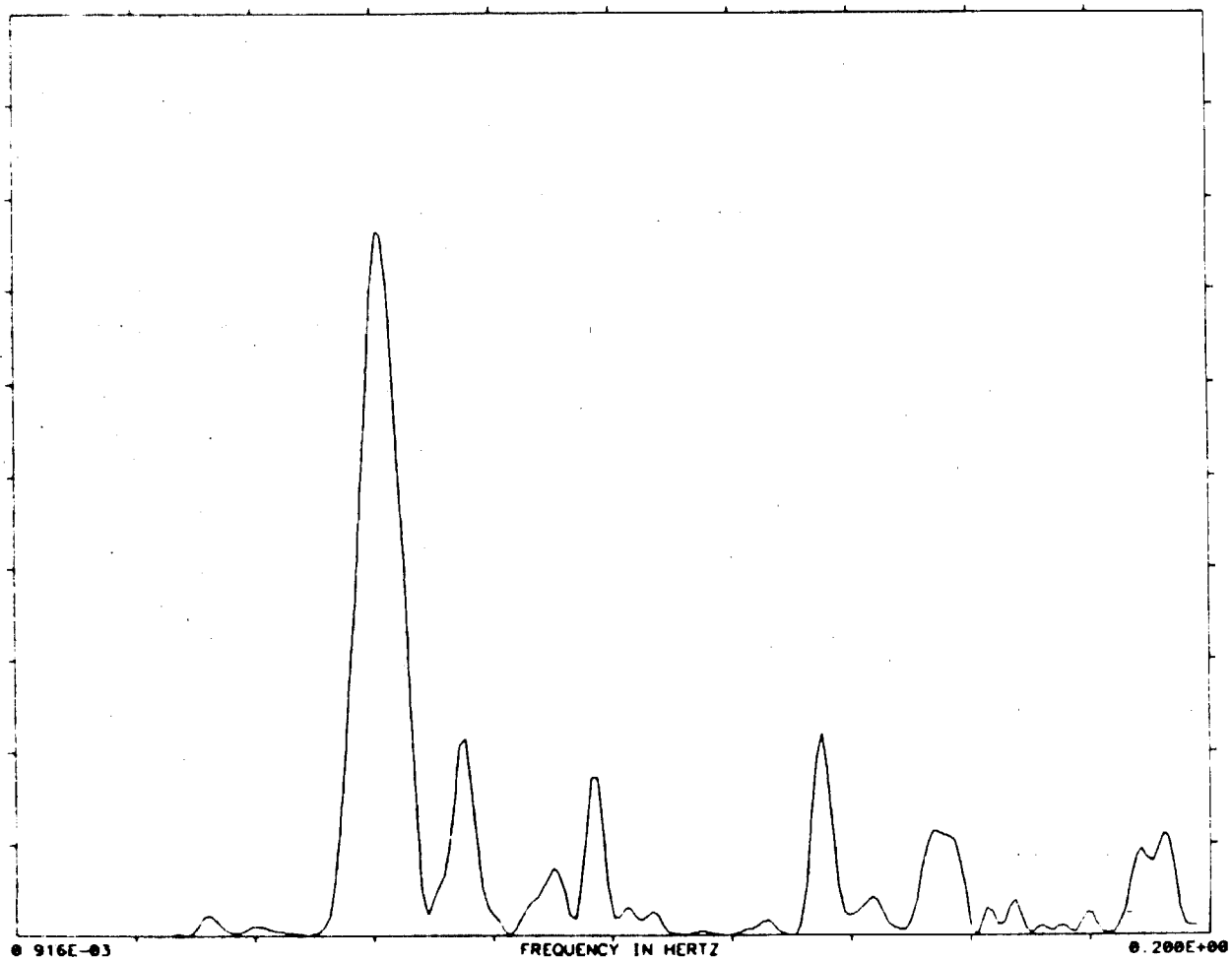

DOMINANT FREQ

FREQ	MAGNITUDE
0 6134E-01	0 153E+02
0 6226E-01	0 152E+02
0 6042E-01	0 140E+02
0 6317E-01	0 139E+02
0 6409E-01	0 121E+02
0 5951E-01	0 117E+02
0 6500E-01	0 102E+02
0 5859E-01	0 940E+01
0 6592E-01	0 814E+01
0 5768E-01	0 734E+01

Final Report

LMSC-F087173

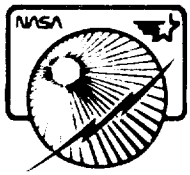

Appendix E
Mast Tip Displacement Data

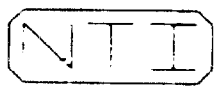

TEST NAME=SAE ACC WSIDS		NNOFFT =	1	UNITS= (INCHES)	
MEASUREMENT=	COVER X1	FFTBW-HZ=	0.00000E+00	MEAN= 0.16763818E-07	D. 2-12-85
REFF TIME =	245 15 25 27. 0	FFTERR =	0.00	S D = 0.15943978E+01	T. 14- 7- 4
TIME OFFSET=	1.001	FFTTIM =	0.0	SAMPLE RATE= 0.3750E+01	
TOTAL TIME=	273.100	FFTLIN =	.0		

0.100E+02

RAW DATA

DOMINANT TIME

TIME	MAGNITUDE
0.549E+02	0.5385E+01
0.547E+02	0.5375E+01
0.552E+02	0.5345E+01
0.544E+02	0.5327E+01
0.555E+02	0.5257E+01
0.541E+02	0.5229E+01
0.557E+02	0.5123E+01
0.539E+02	0.5082E+01
0.560E+02	0.4946E+01
0.536E+02	0.4890E+01

-0.100E+02

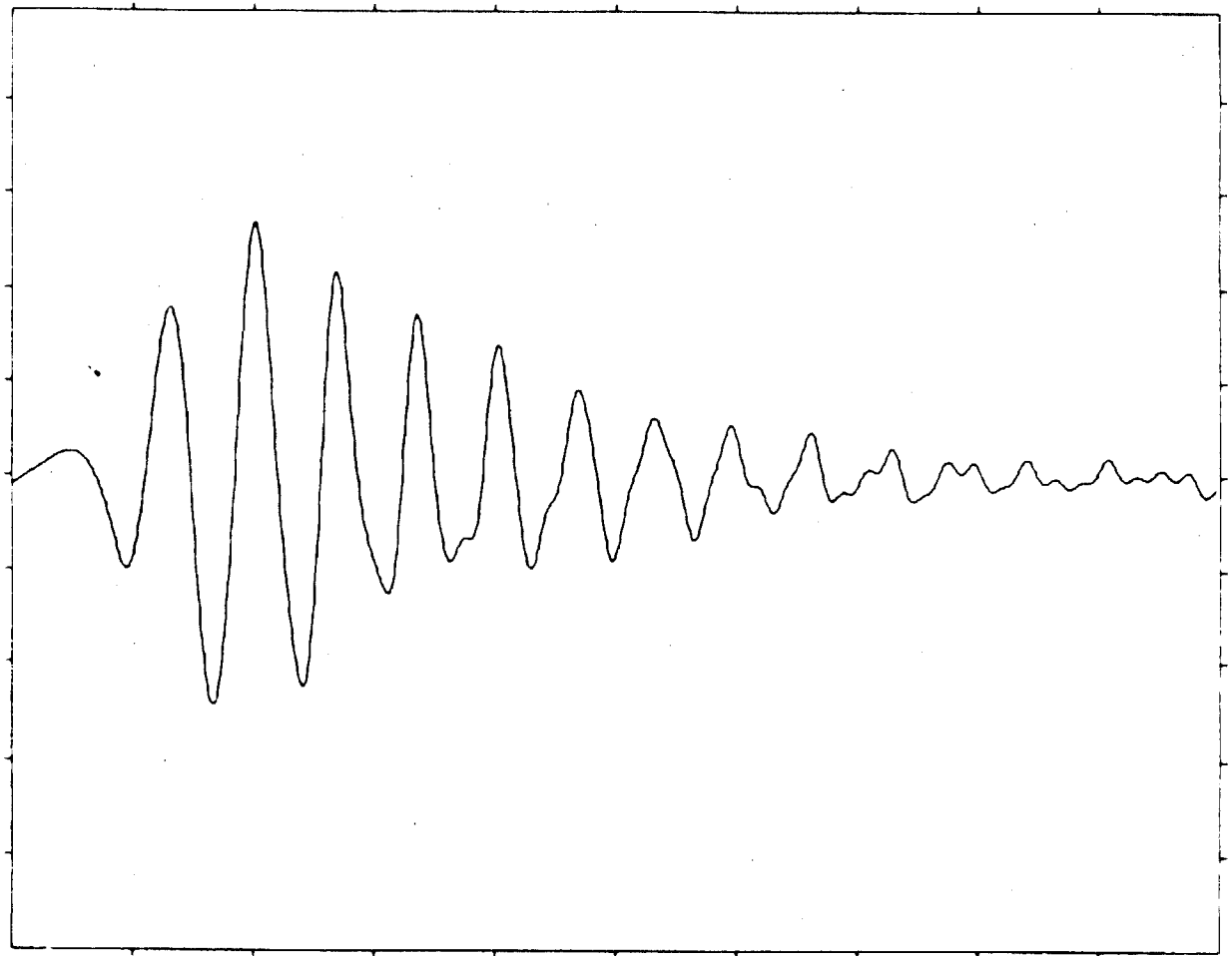

0.000E+00 TIME IN SECONDS 0.273E+03

ORIGINAL PAGE IS
OF POOR QUALITY

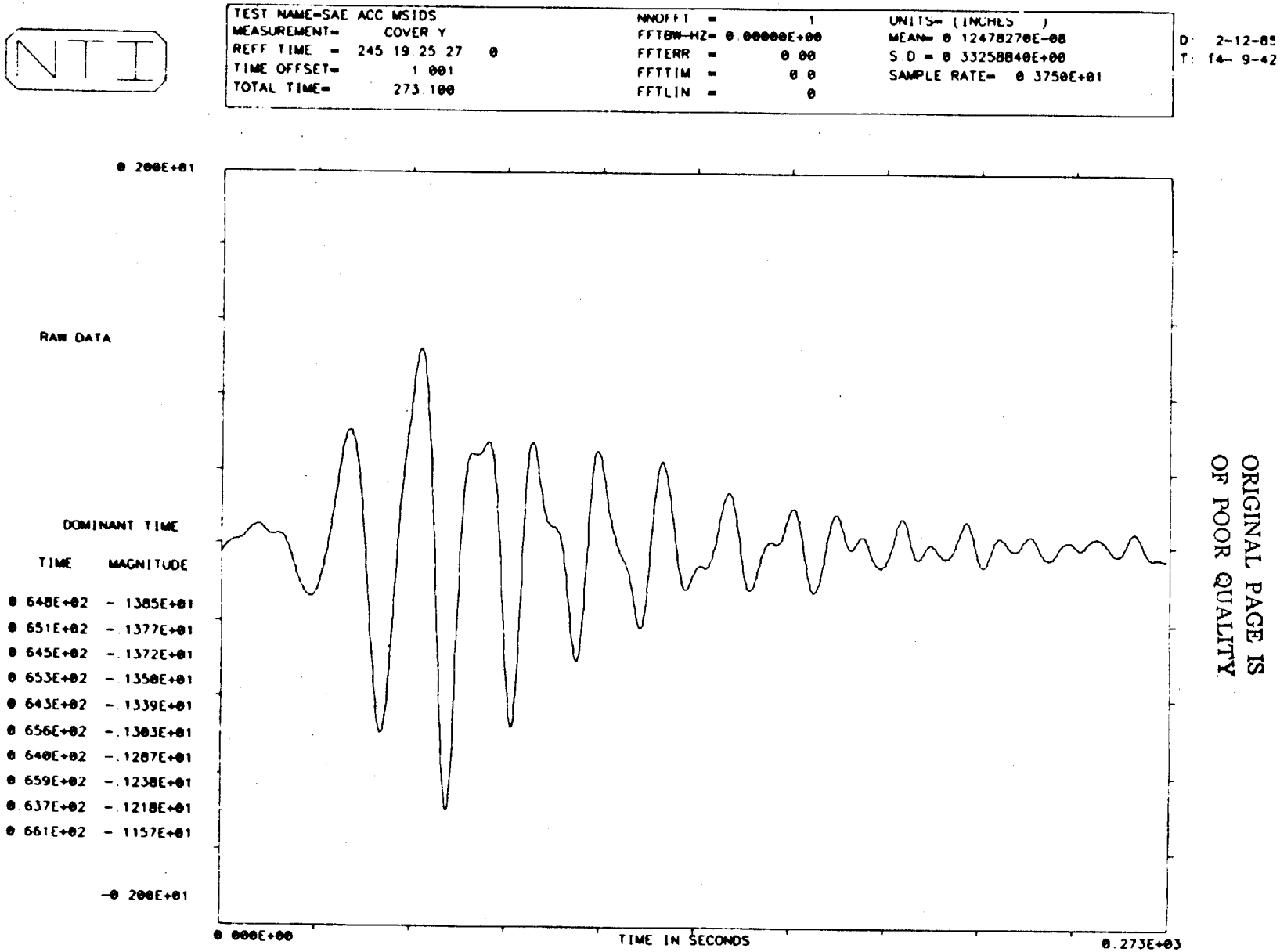

ORIGINAL PAGE IS
OF POOR QUALITY

NTI

TEST NAME=SAE ACC MSIDS		NNOFFT =	1	UNITS= (INCHES)	D: 2-12-85
MEASUREMENT=	COVER X2	FFTBW-HZ=	0.00000E+00	MEAN= 0.11175870E-07	T: 14- 8-24
REFF TIME =	245:19:25:27. 0	FFTERR =	0.00	S.D.= 0.15875360E+01	
TIME OFFSET=	1.001	FFTTIM =	0.0	SAMPLE RATE= 0.3750E+01	
TOTAL TIME=	273.100	FFTLIN =	0		

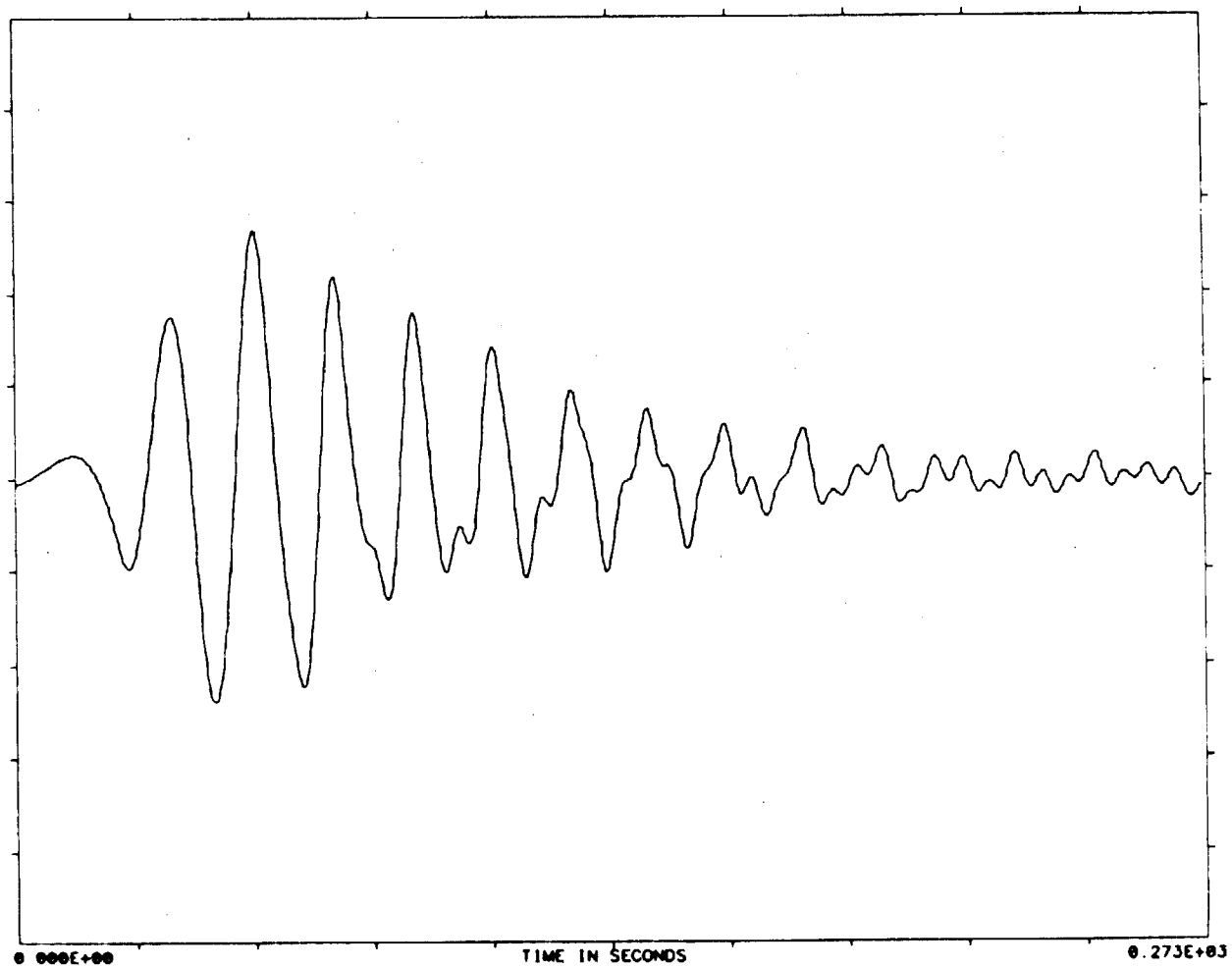

DOMINANT TIME

TIME	MAGNITUDE
0.549E+02	0.5372E+01
0.547E+02	0.5367E+01
0.552E+02	0.5329E+01
0.544E+02	0.5323E+01
0.555E+02	0.5237E+01
0.541E+02	0.5229E+01
0.557E+02	0.5098E+01
0.539E+02	0.5089E+01
0.560E+02	0.4915E+01
0.536E+02	0.4903E+01

ORIGINAL PAGE IS
OF POOR QUALITY

ORIGINAL PAGE IS
OF POOR QUALITY

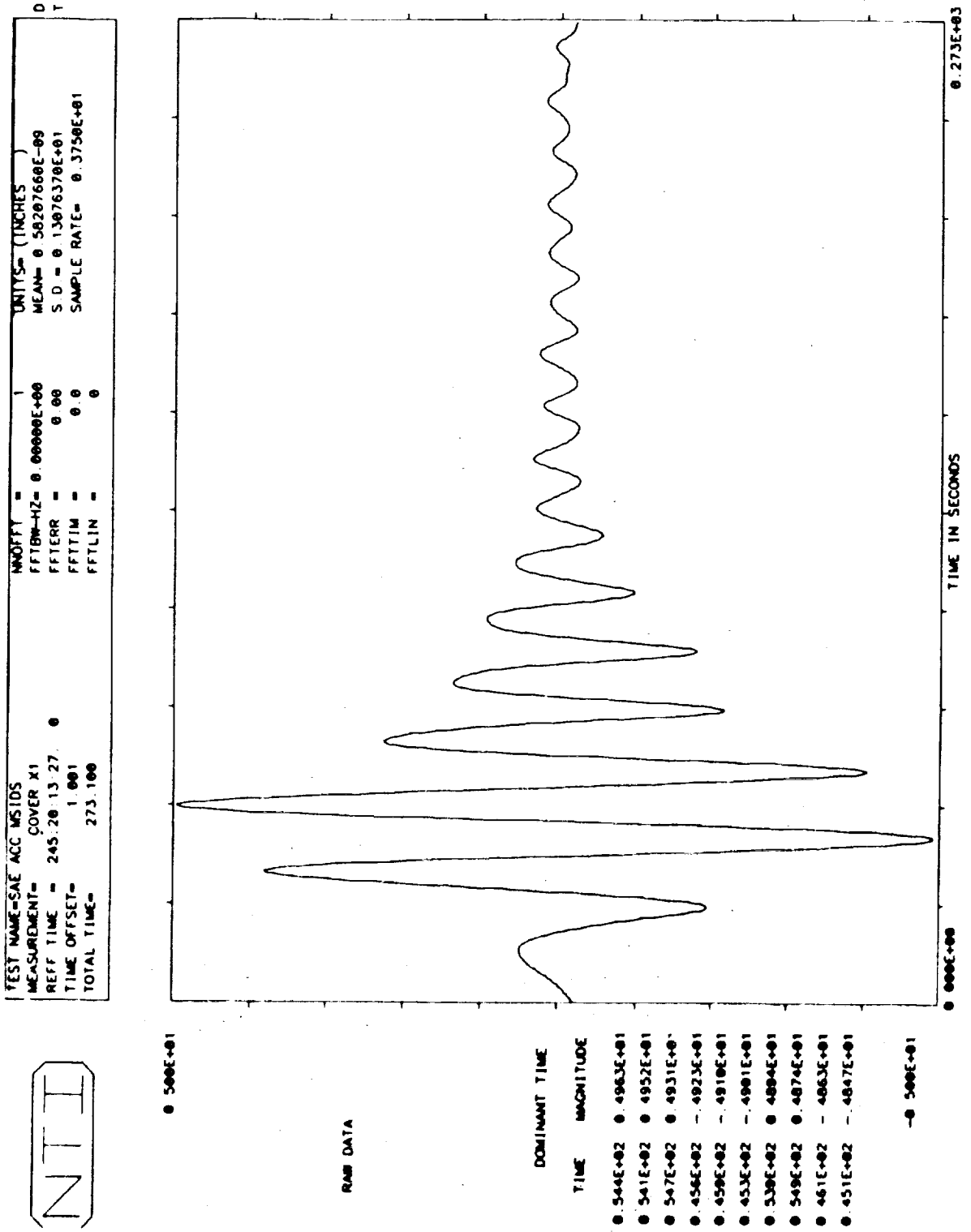

NTI

TEST NAME=SAE ACC MSIDS		NNOFFT =	1	UNITS= (INCHES)	D: 2-12-85
MEASUREMENT= COVER Y		FFTBW-HZ=	0.00000E+00	MEAN=-0.37471180E-09	T: 14- 5-43
REFF TIME = 245 20 13 27 0		FFTERR =	0 00	S D = 0 29581990E+00	
TIME OFFSET= 1.001		FFTTIM =	0.0	SAMPLE RATE= 0.3750E+01	
TOTAL TIME= 273.100		FFTLIN =	0		

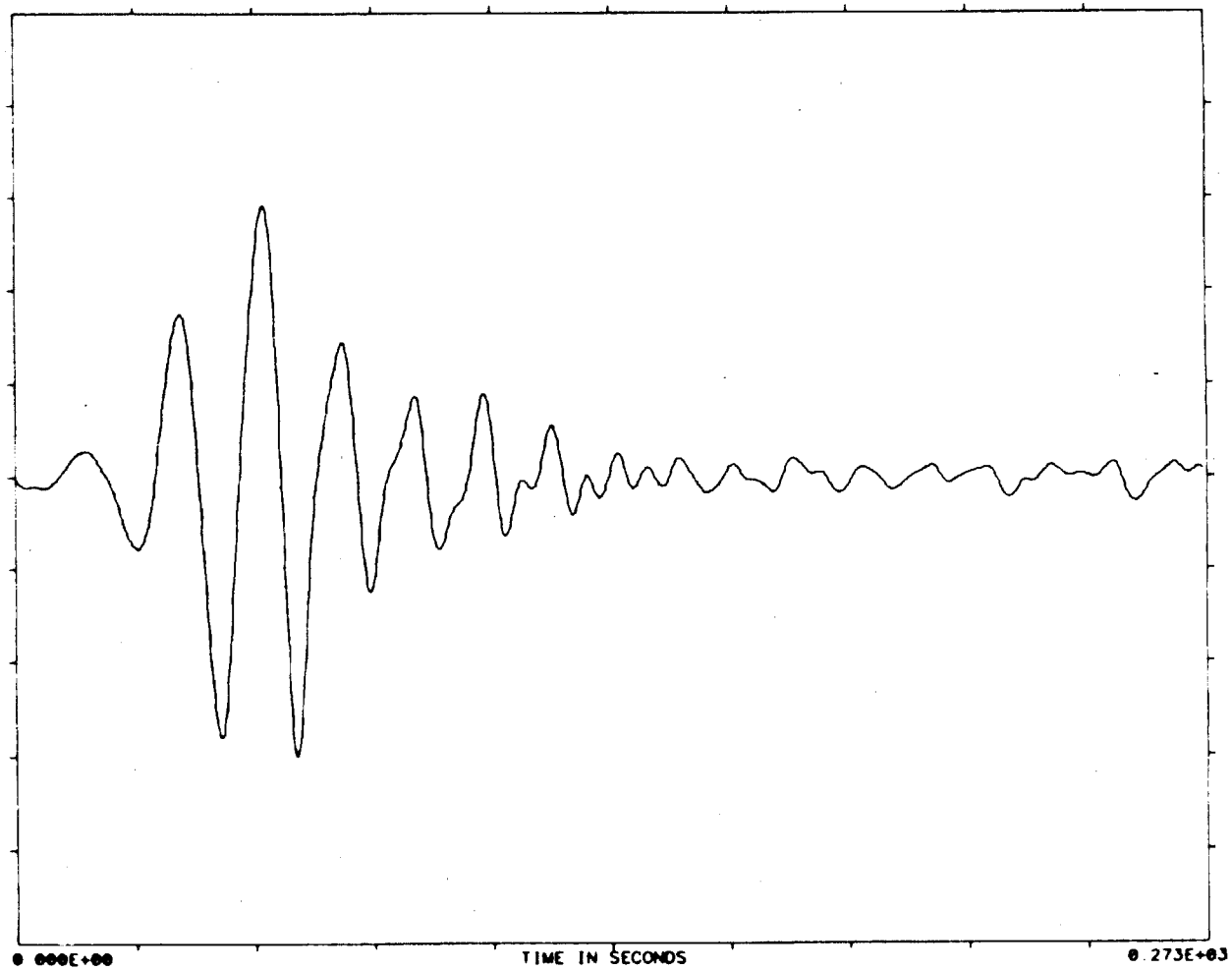

DOMINANT TIME

TIME	MAGNITUDE
0.643E+02	- 1203E+01
0.645E+02	- 1198E+01
0.640E+02	- 1190E+01
0.648E+02	- 1174E+01
0.568E+02	0.1165E+01
0.565E+02	0.1161E+01
0.637E+02	- 1158E+01
0.571E+02	0.1158E+01
0.563E+02	0.1147E+01
0.573E+02	0.1141E+01

ORIGINAL PAGE IS
OF POOR QUALITY

E-8

ORIGINAL PAGE IS
OF POOR QUALITY

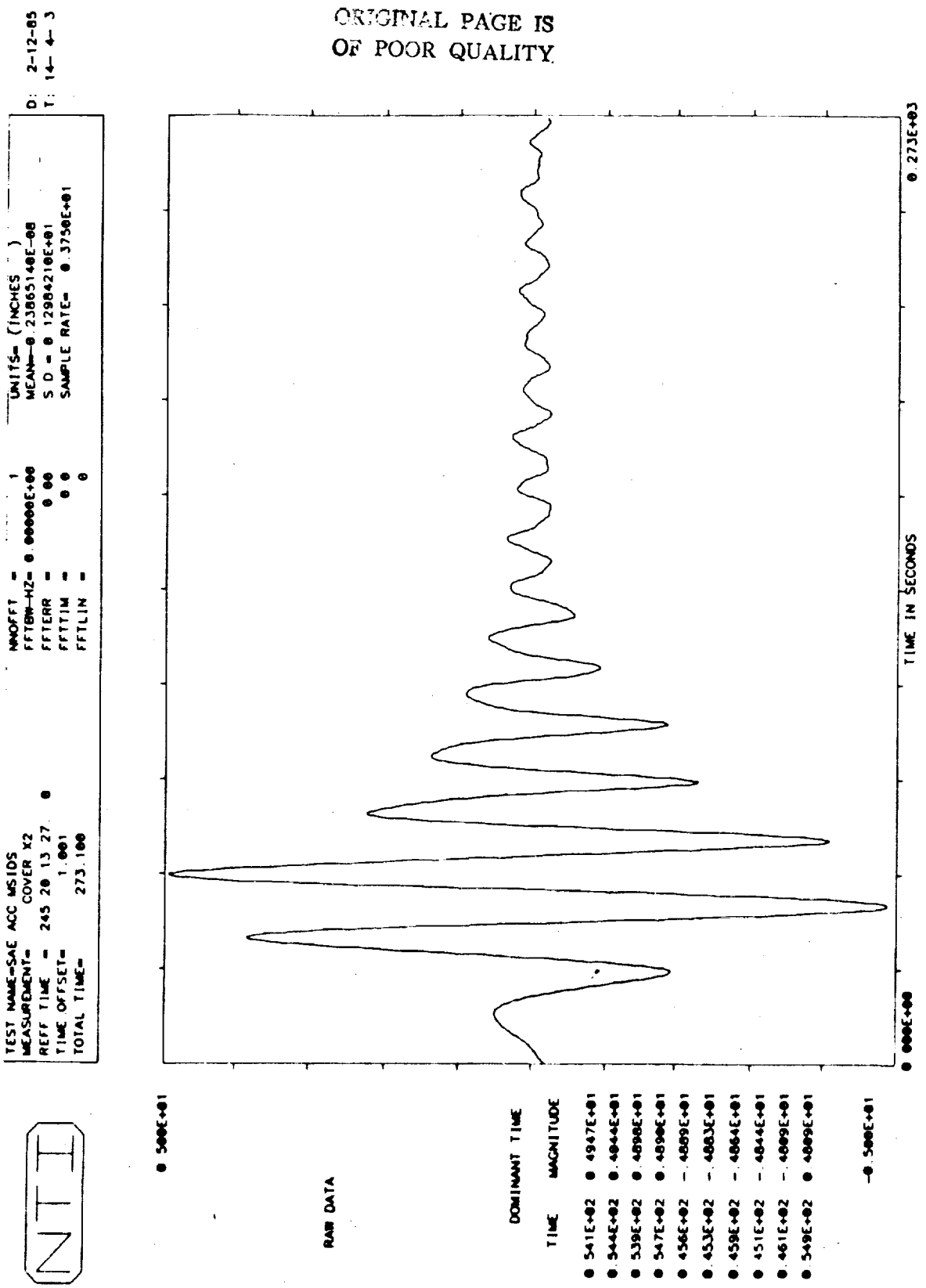

NTI

TEST NAME=SAE ACC MSIDS
MEASUREMENT= COVER X1
REFF TIME = 246 13 29 27 0
TIME OFFSET= 1.001
TOTAL TIME= 273.100

NNOFFT = 1
FFTBW-HZ= 0.00000E+00
FFTERR = 0.00
FFTTIM = 0.0
FFTLIN = 0

UNITS= (INCHES)
MEAN= -0.12048990E-07
S.D. = 0.65164670E+00
SAMPLE RATE= 0.3750E+01

D: 2-12-85
T: 14-11- 1

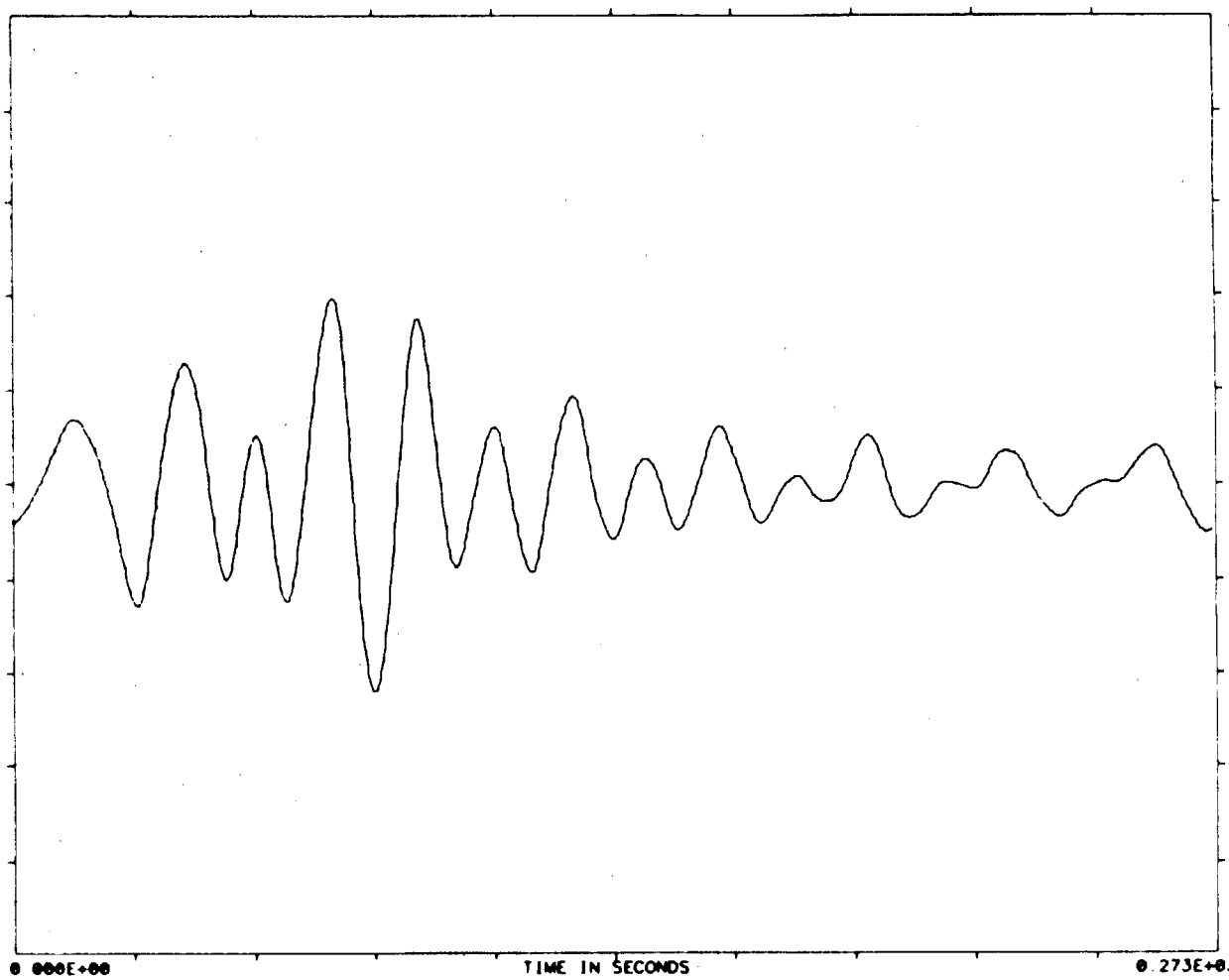

DOMINANT TIME

TIME	MAGNITUDE
0.819E+02	- 2202E+01
0.821E+02	- 2201E+01
0.816E+02	- 2193E+01
0.824E+02	- 2186E+01
0.813E+02	- 2168E+01
0.827E+02	- 2156E+01
0.811E+02	- 2128E+01
0.829E+02	- 2114E+01
0.808E+02	- 2072E+01
0.832E+02	- 2058E+01

ORIGINAL PAGE IS
OF POOR QUALITY

ORIGINAL PAGE IS
OF POOR QUALITY

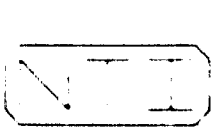

TEST NAME=SAE ACC MSIDS
MEASUREMENT= COVER X2
REFF TIME = 246 13 29 27 0
TIME OFFSET= 1 001
TOTAL TIME= 273 100

NNOFFT = 1
FFTBW-HZ= 0 00000E+00
FFTERR = 0 00
FFTTIM = 0 0
FFTLIN = 0

UNITS= (INCHES)
MEAN= 0 58207660E-09
S D = 0 64922660E+00
SAMPLE RATE= 0 3750E+01

D: 2-12-85
T: 14-12-22

0 500E+01

RAW DATA

DOMINANT TIME

TIME	MAGNITUDE
0 808E+02	- 2094E+01
0 811E+02	- 2093E+01
0 720E+02	0 2079E+01
0 805E+02	- 2076E+01
0 813E+02	- 2075E+01
0 723E+02	0 2073E+01
0 717E+02	0 2072E+01
0 725E+02	0 2054E+01
0 715E+02	0 2053E+01
0 816E+02	- 2040E+01

-0 500E+01

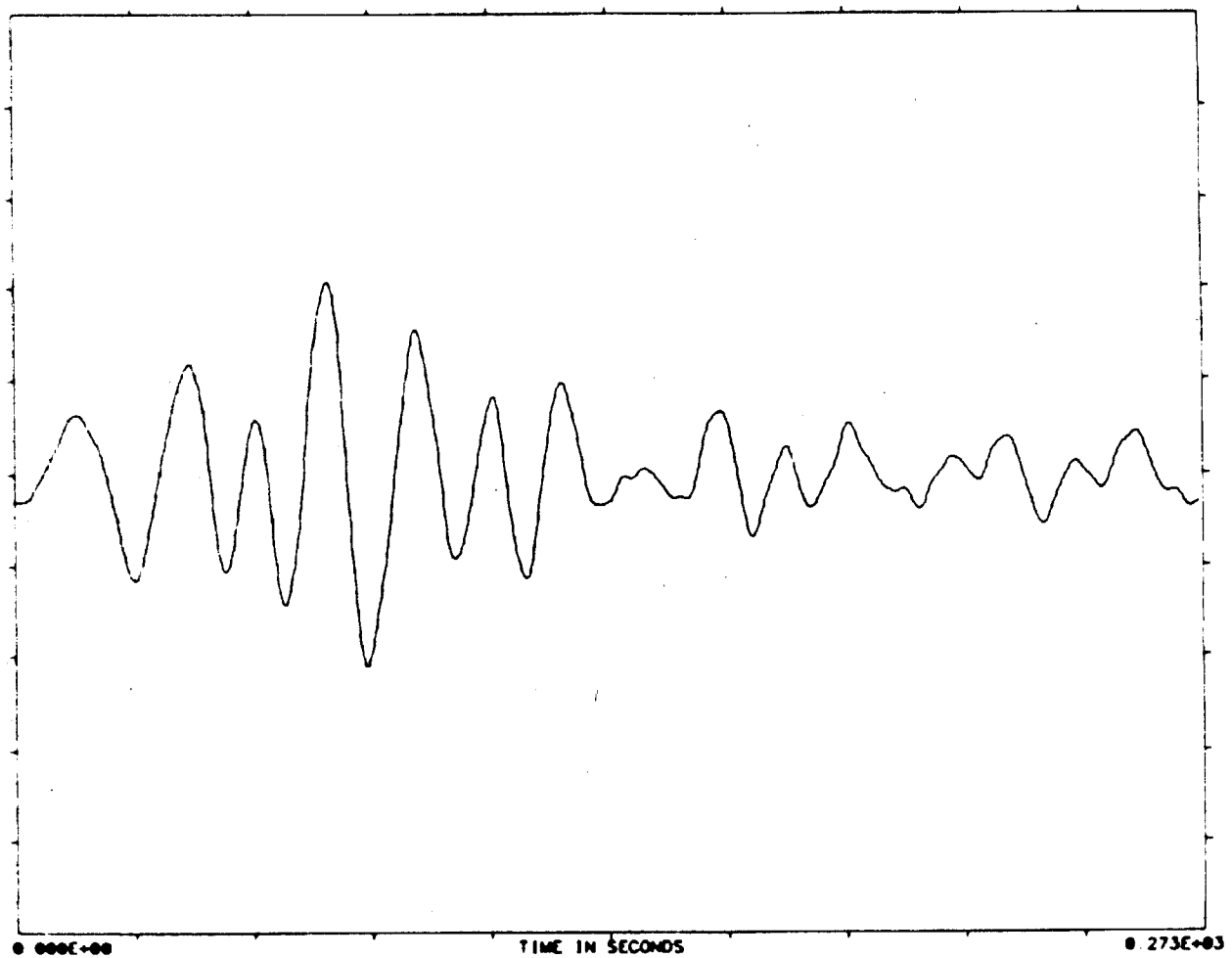

0 000E+00 TIME IN SECONDS 0 273E+03

ORIGINAL PAGE IS
OF POOR QUALITY

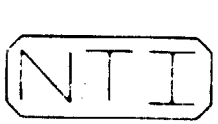

TEST NAME=SAE ALL MSIDS
MEASUREMENT= COVER X1
REFF TIME = 246 14 21 55. 0
TIME OFFSET= 1 001
TOTAL TIME= 273 100

NNOFFT = 1
FFTBW-HZ= 0 00000E+00
FFTERR = 0 00
FFTTIM = 0 0
FFTLIN = 0

UNITS= (INCHES)
MEAN=-0 35506670E-08
S D = 0 68762010E+00
SAMPLE RATE= 0 3750E+01

D: 2-12-85
T: 14-15- 8

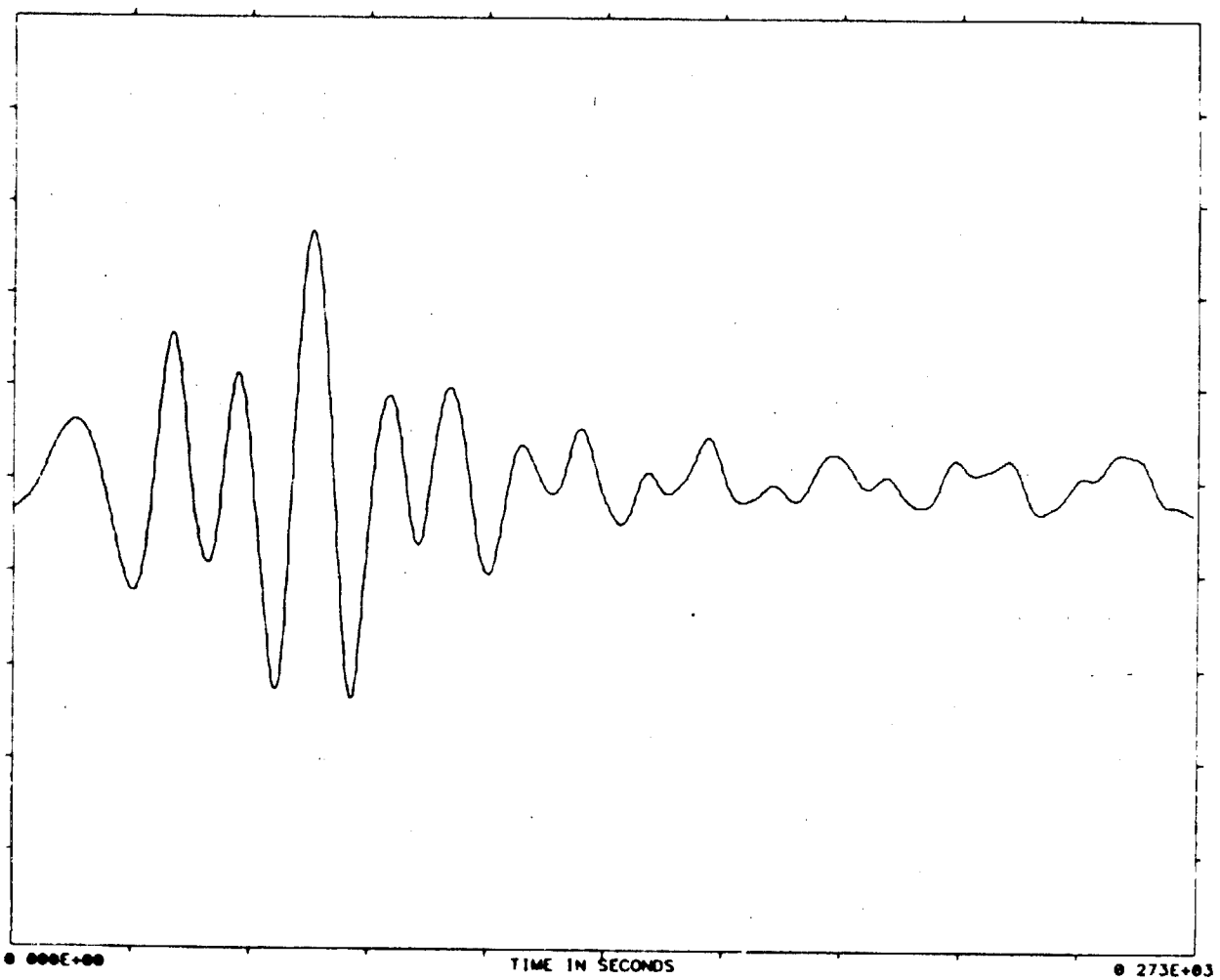

DOMINANT TIME

TIME	MAGNITUDE
0 688E+02	0 2682E+01
0 691E+02	0 2677E+01
0 685E+02	0 2668E+01
0 693E+02	0 2654E+01
0 683E+02	0 2636E+01
0 696E+02	0 2612E+01
0 680E+02	0 2584E+01
0 699E+02	0 2552E+01
0 677E+02	0 2513E+01
0 701E+02	0 2476E+01

ORIGINAL PAGE IS
OF POOR QUALITY

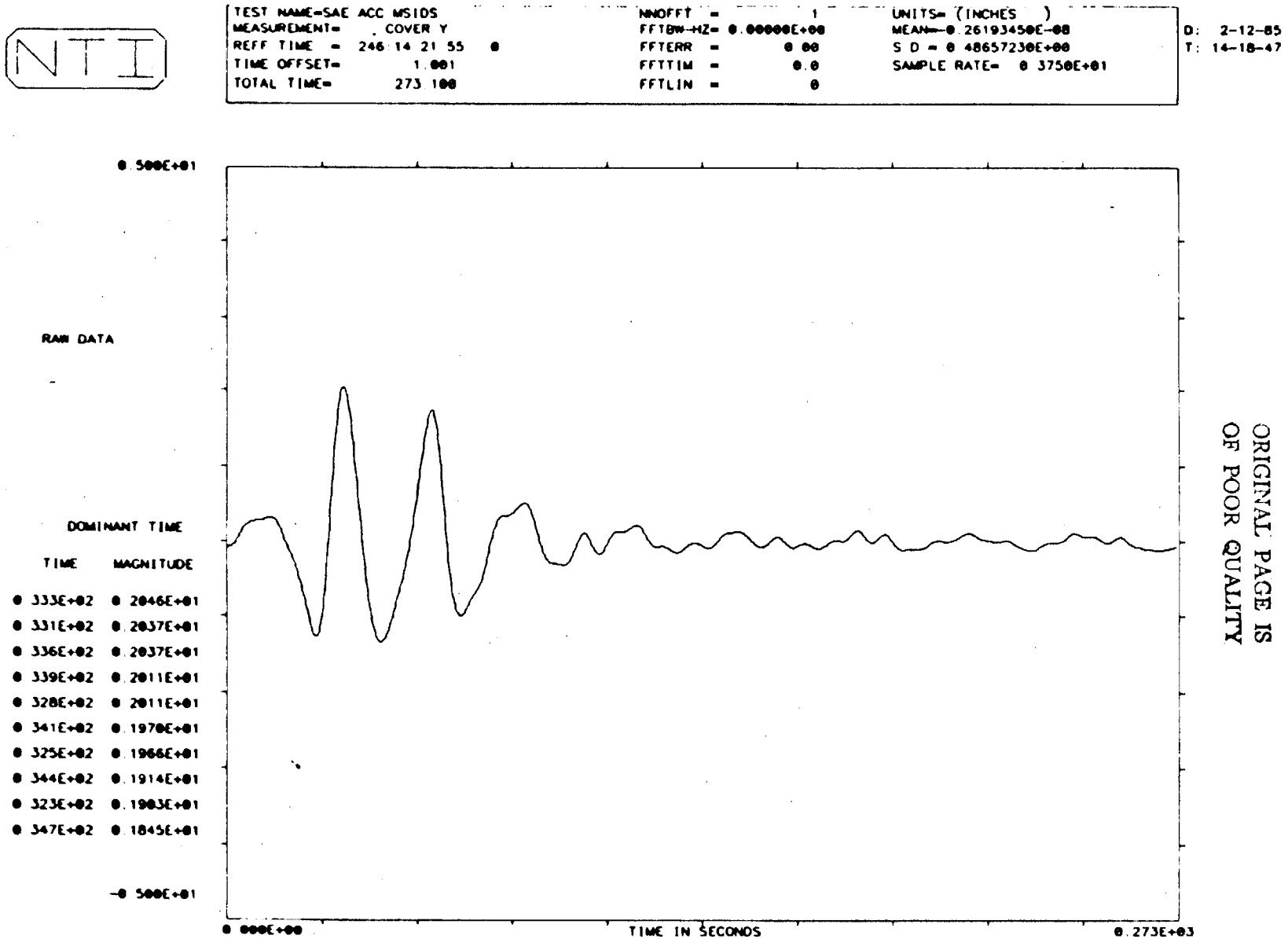

ORIGINAL PAGE IS
OF POOR QUALITY

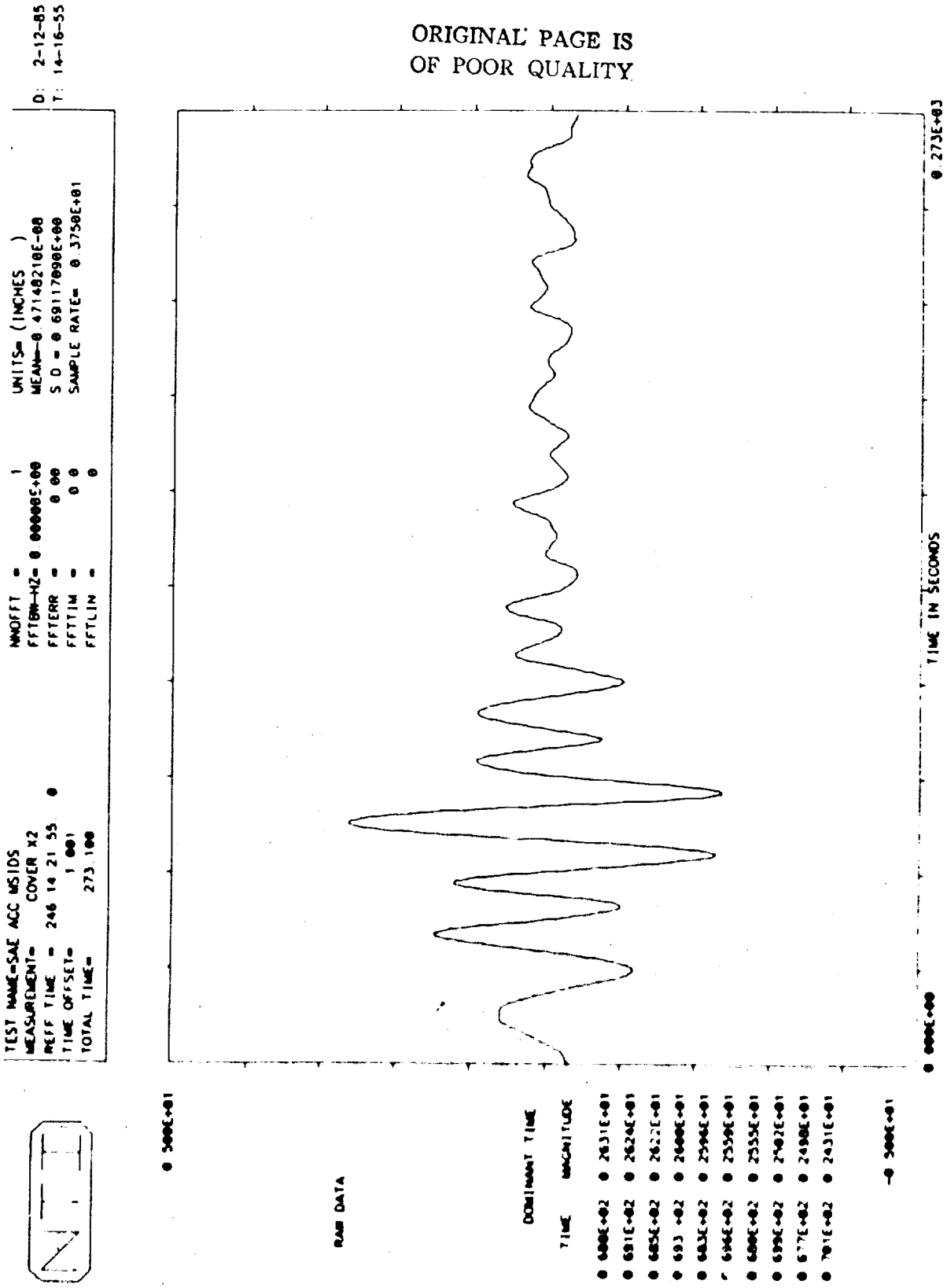

TEST NAME=SAE ACC MSIDS
MEASUREMENT= COVER X1
REFF TIME = 246 15 0 26 0
TIME OFFSET= 1 001
TOTAL TIME= 273 100

NNOFFT = 1
FFTBW-HZ= 0 00000E+00
FFTERR = 0 00
FFTTIM = 0 0
FFTLIN = 0

UNITS= (INCHES)
MEAN= 0 13475070E-07
S D = 0 13714150E+01
SAMPLE RATE= 0 3750E+01

D: 2-12-85
T: 14-21- 6

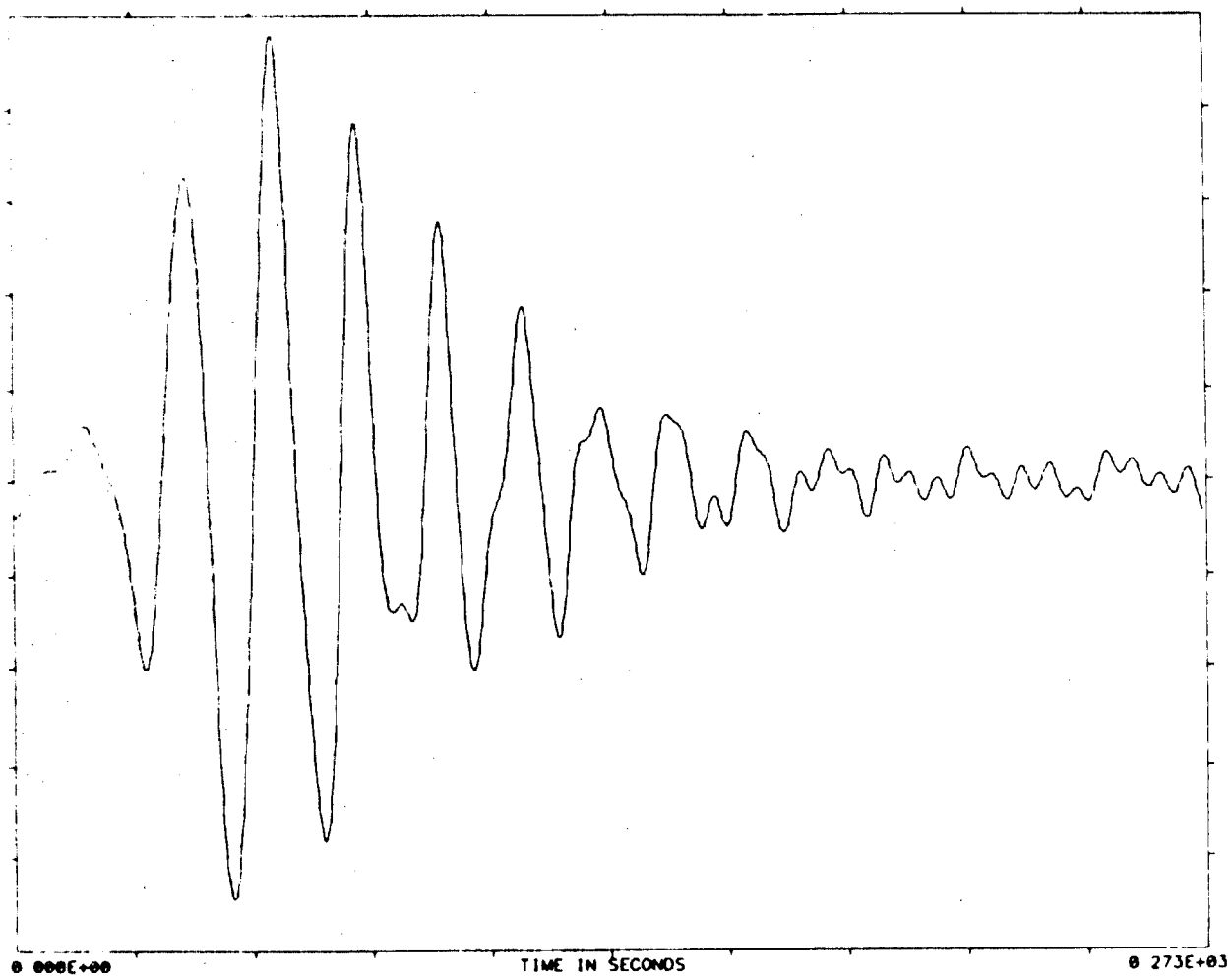

DOMINANT TIME

TIME	MAGNITUDE
0 592E+02	0 4788E+01
0 595E+02	0 4785E+01
0 589E+02	0 4750E+01
0 597E+02	0 4742E+01
0 587E+02	0 4670E+01
0 600E+02	0 4658E+01
0 584E+02	0 4549E+01
0 603E+02	0 4536E+01
0 501E+02	- 4428E+01
0 499E+02	- 4427E+01

ORIGINAL PAGE IS
OF POOR QUALITY

ORIGINAL PAGE IS
OF POOR QUALITY

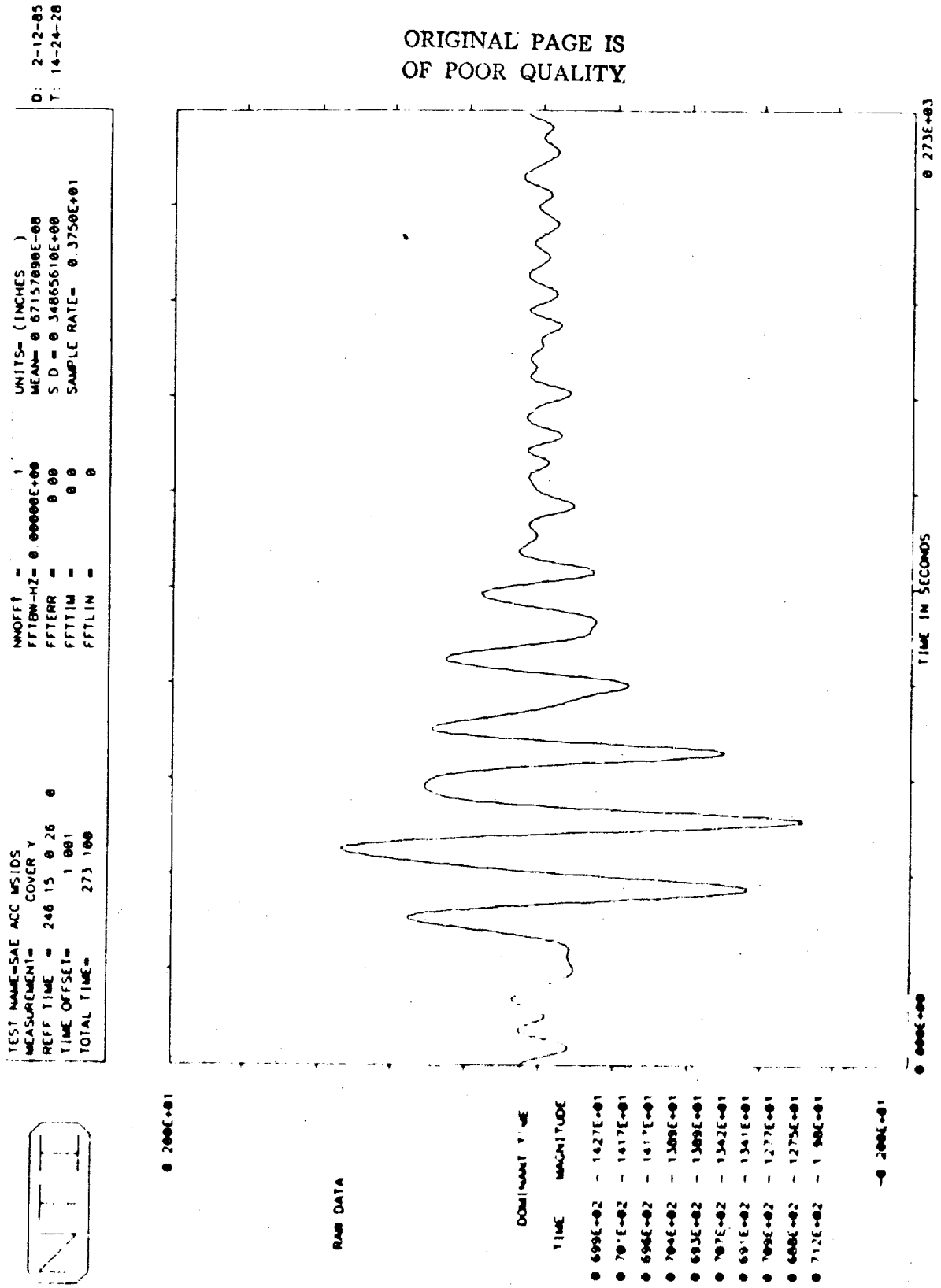

ORIGINAL PAGE IS
OF POOR QUALITY

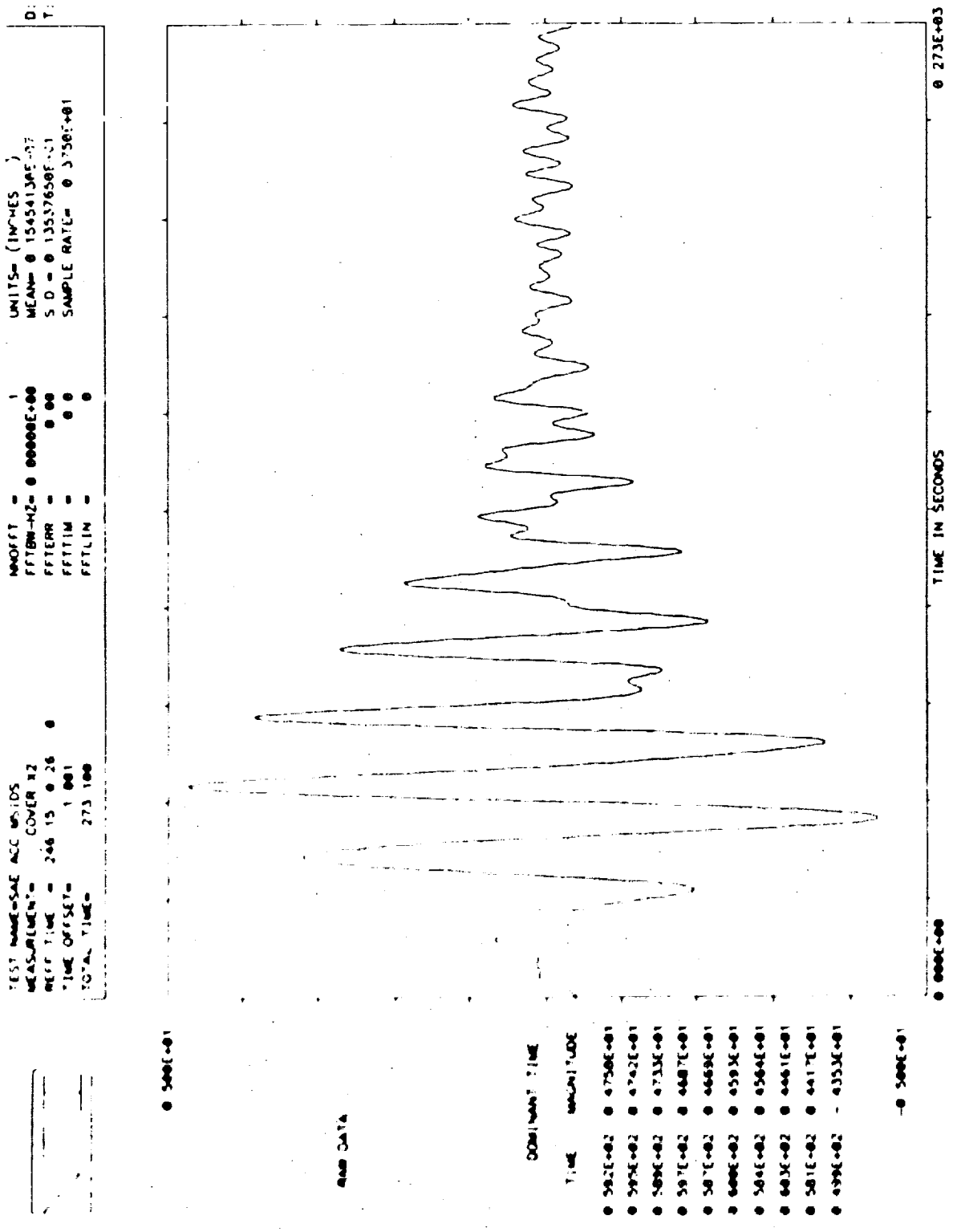

ORIGINAL PAGE IS
OF POOR QUALITY

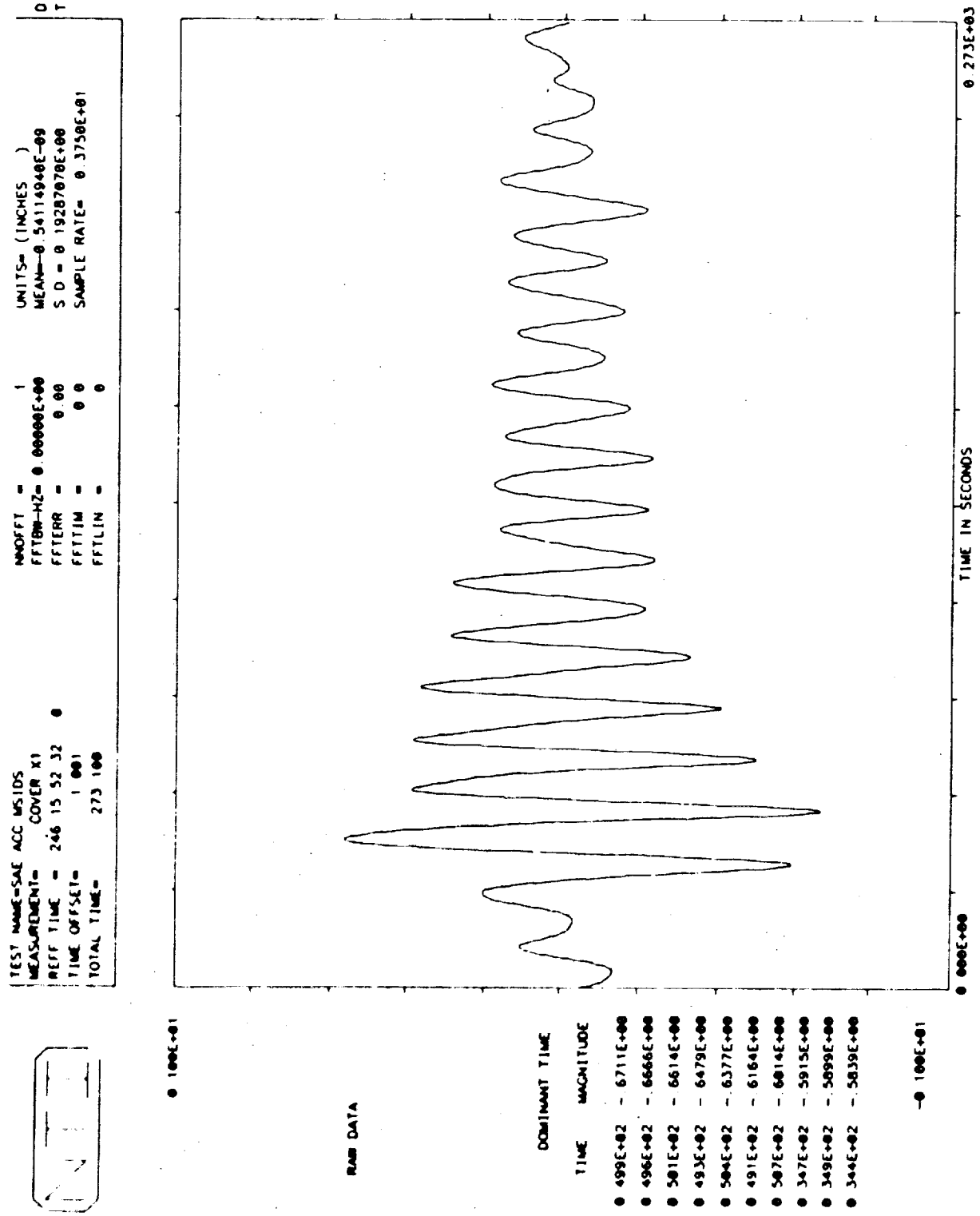

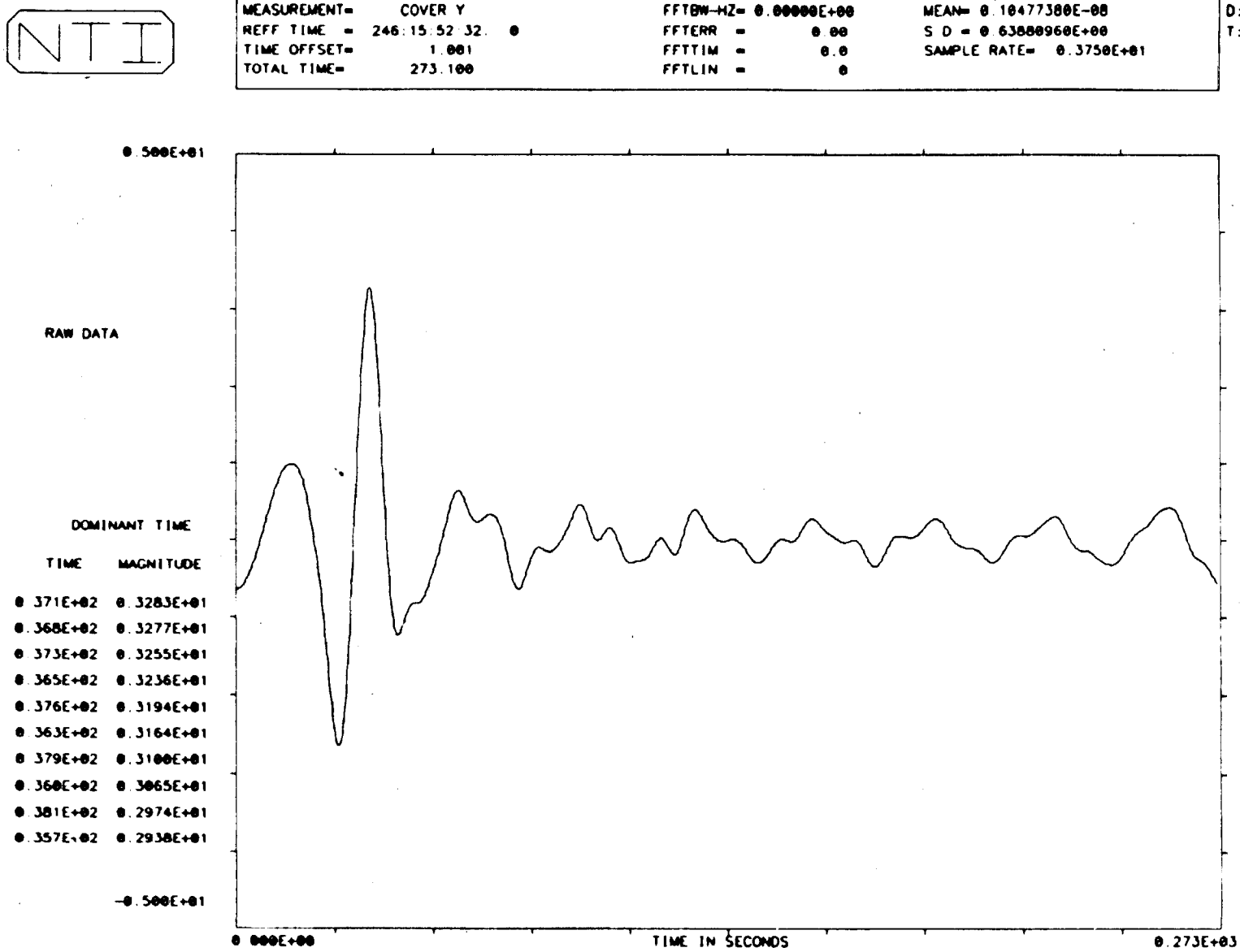

ORIGINAL PAGE IS
OF POOR QUALITY

ORIGINAL PAGE IS
OF POOR QUALITY

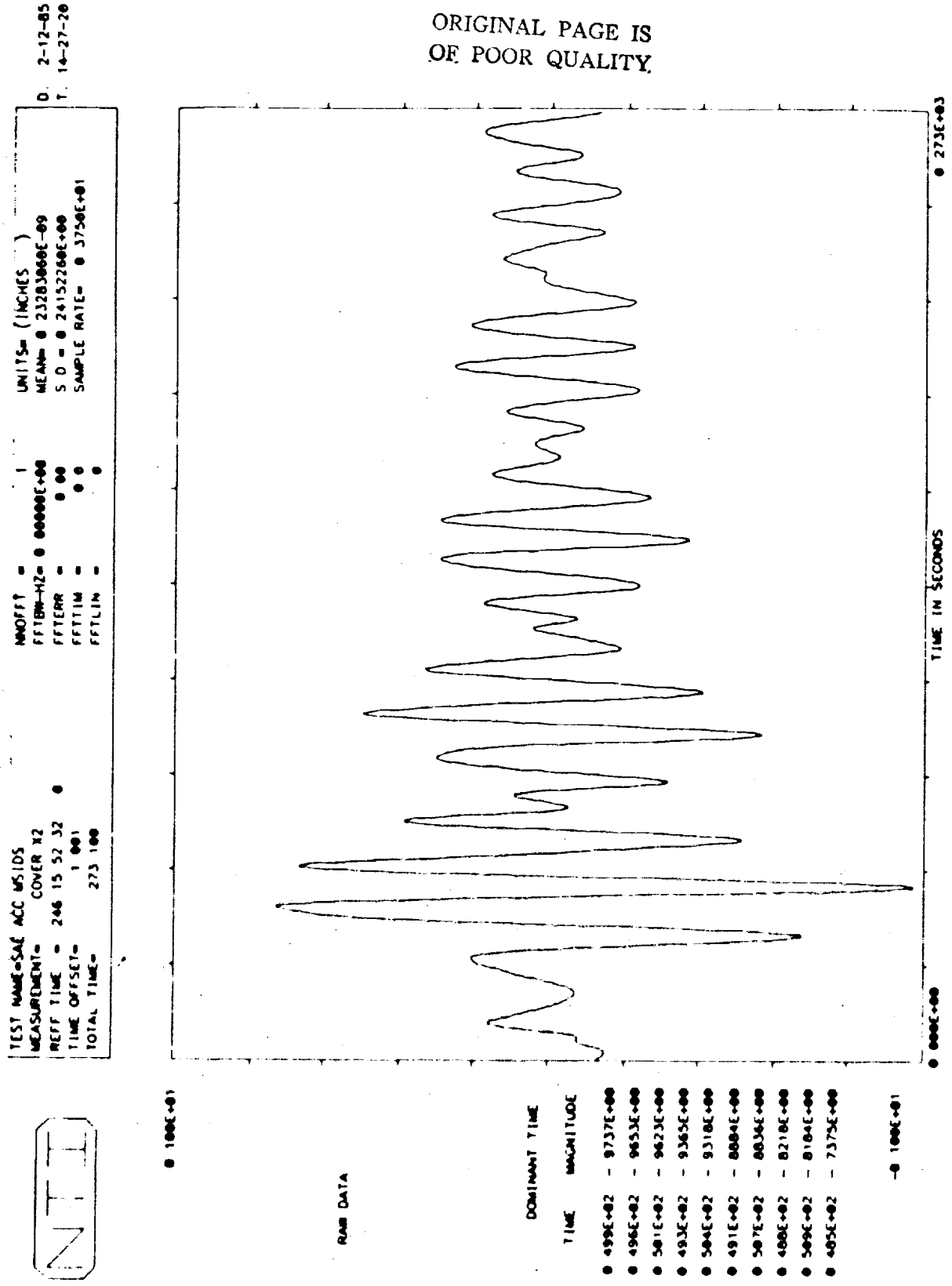

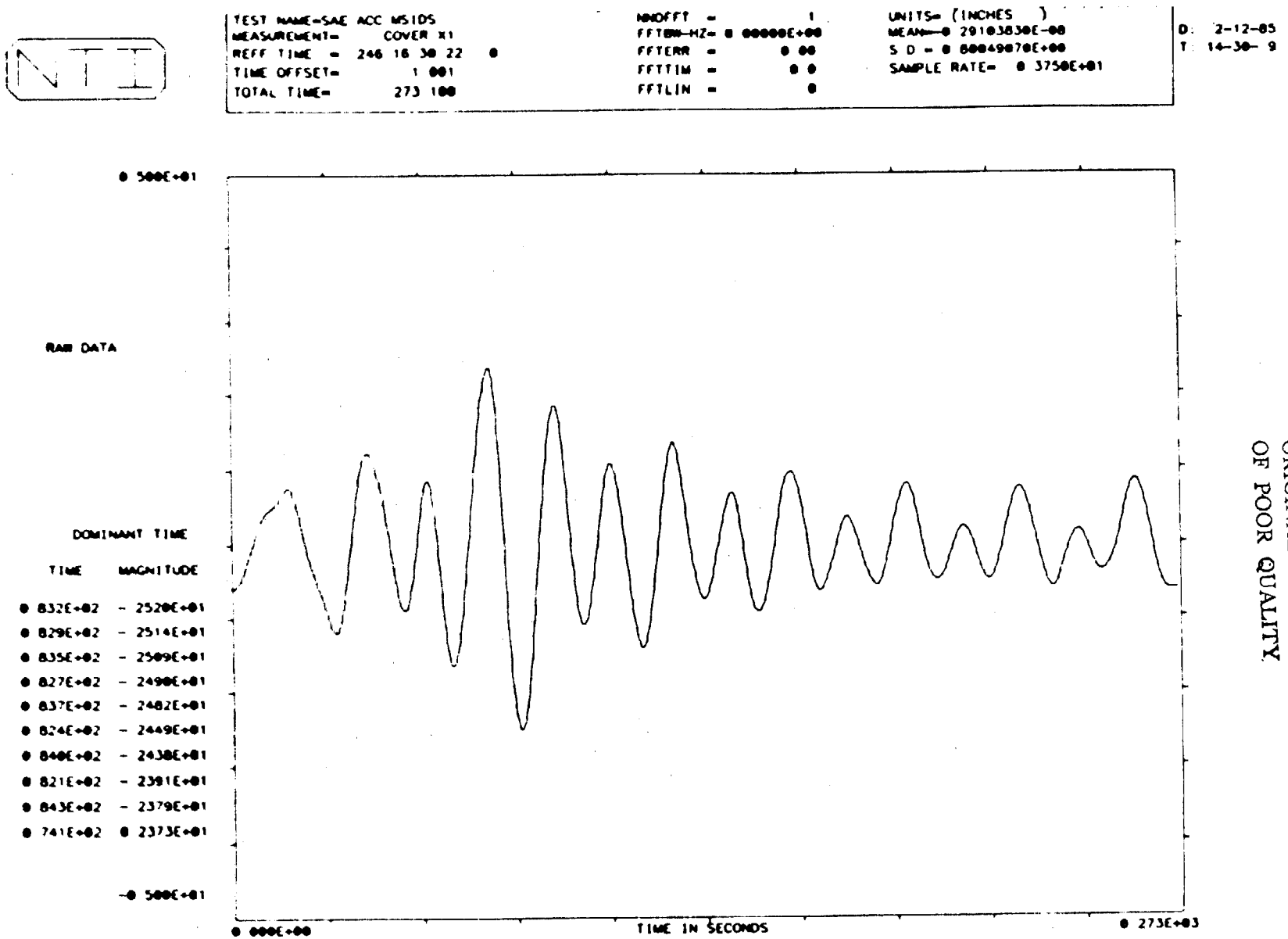

ORIGINAL PAGE IS
OF POOR QUALITY

ORIGINAL PAGE IS
OF POOR QUALITY.

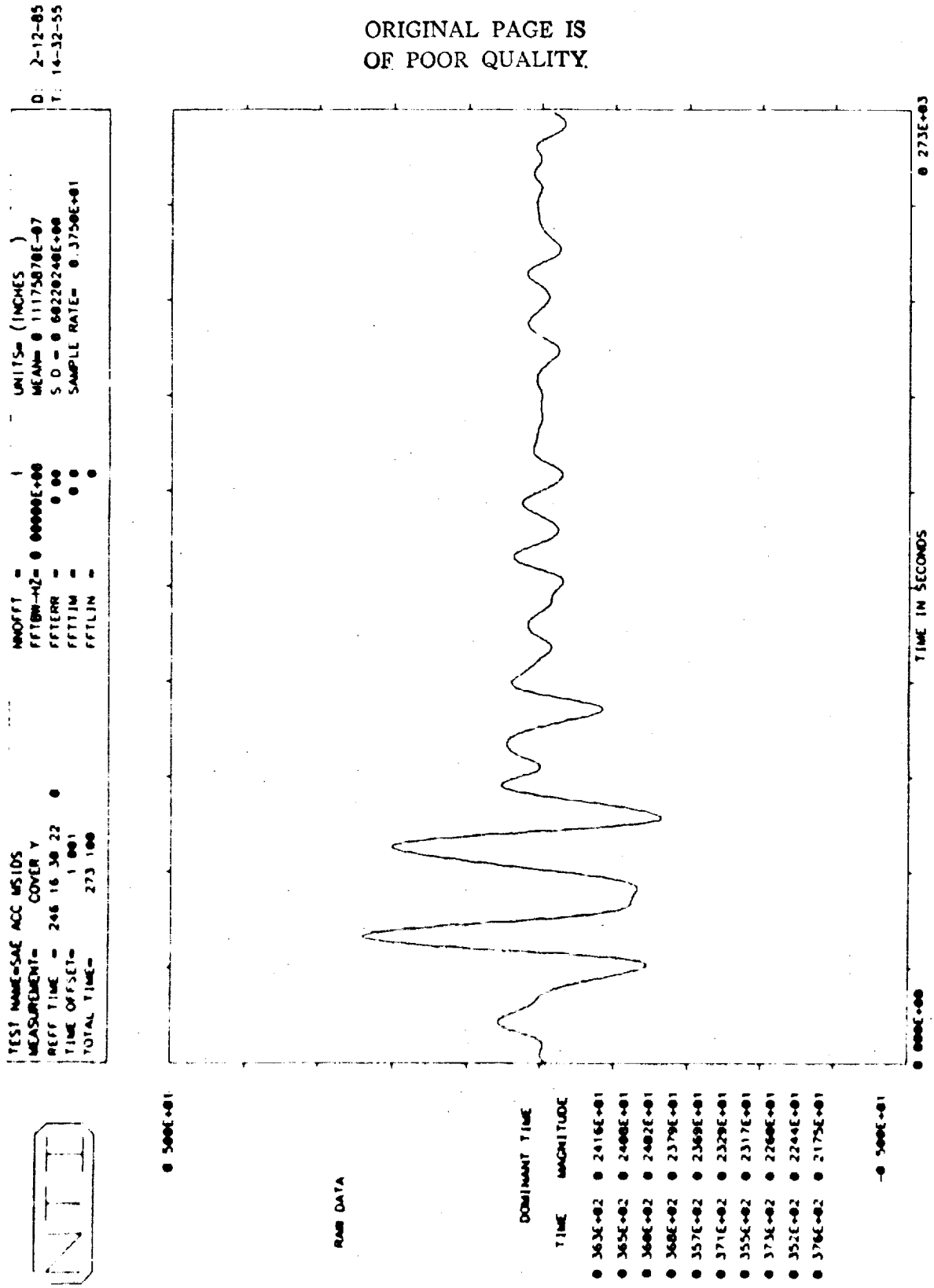

TEST NAME=SAE ACC MSIDS
MEASUREMENT= COVER X2
REFF TIME = 246 16 30 22 0
TIME OFFSET= 1 001
TOTAL TIME= 273 100

NNOFFT = 1
FFTBW-HZ= 0 00000E+00
FFTERR = 0 00
FFTTIM = 0 0
FFTLIN = 0

UNITS= (INCHES)
MEAN=-0 38999130E-08
S D = 0 80060640E+00
SAMPLE RATE= 0 3750E+01

D: 2-12-85
T: 14-31-29

0 500E+01

RAW DATA

DOMINANT TIME

TIME	MAGNITUDE
0 736E+02	0 2592E+01
0 739E+02	0 2590E+01
0 824E+02	- 2582E+01
0 827E+02	- 2581E+01
0 733E+02	0 2573E+01
0 741E+02	0 2569E+01
0 821E+02	- 2558E+01
0 829E+02	- 2553E+01
0 731E+02	0 2536E+01
0 744E+02	0 2529E+01

-0 500E+01

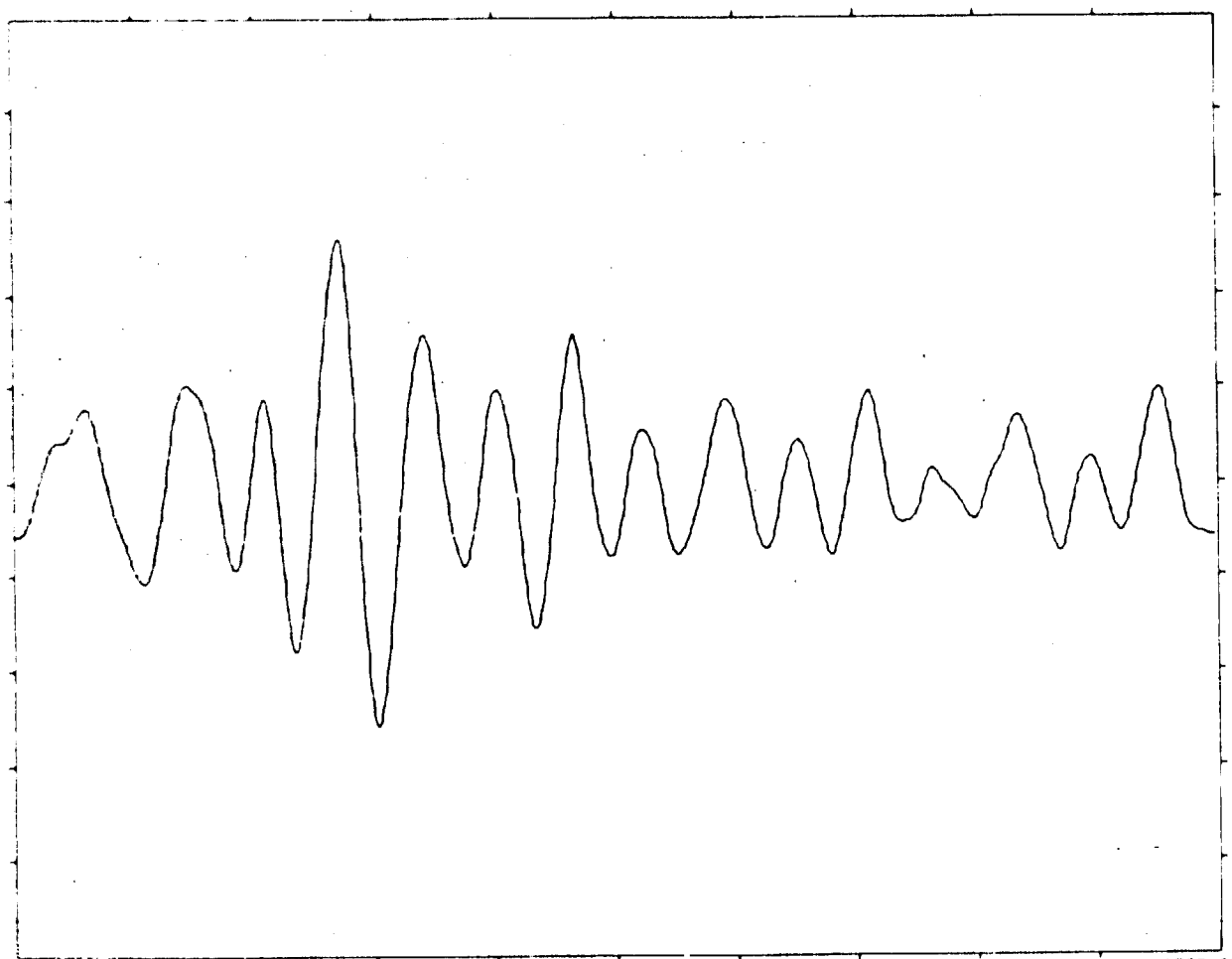

0 000E+00 TIME IN SECONDS 0 273E+03

TEST NAME=SAE ACC MSIDS
MEASUREMENT= COVER X1
REFF TIME = 246 17 23 4. 0
TIME OFFSET= 1 001
TOTAL TIME= 273 100

NNOFFT = 1
FFTBW-HZ= 0.00000E+00
FFTERR = 0 00
FFTTIM = 0 0
FFTLIN = 0

UNITS= (INCHES)
MEAN= 0 87675290E-09
S D = 0 69486960E+00
SAMPLE RATE= 0.3750E+01

D: 2-12-85
T: 14-34-22

0 500E+01

RAW DATA

DOMINANT TIME

TIME	MAGNITUDE
0 696E+02	0 2588E+01
0 699E+02	0 2587E+01
0 693E+02	0 2570E+01
0 701E+02	0 2568E+01
0 704E+02	0 2533E+01
0 691E+02	0 2533E+01
0 707E+02	0 2481E+01
0 688E+02	0 2475E+01
0 709E+02	0 2414E+01
0 685E+02	0 2395E+01

-0 500E+01

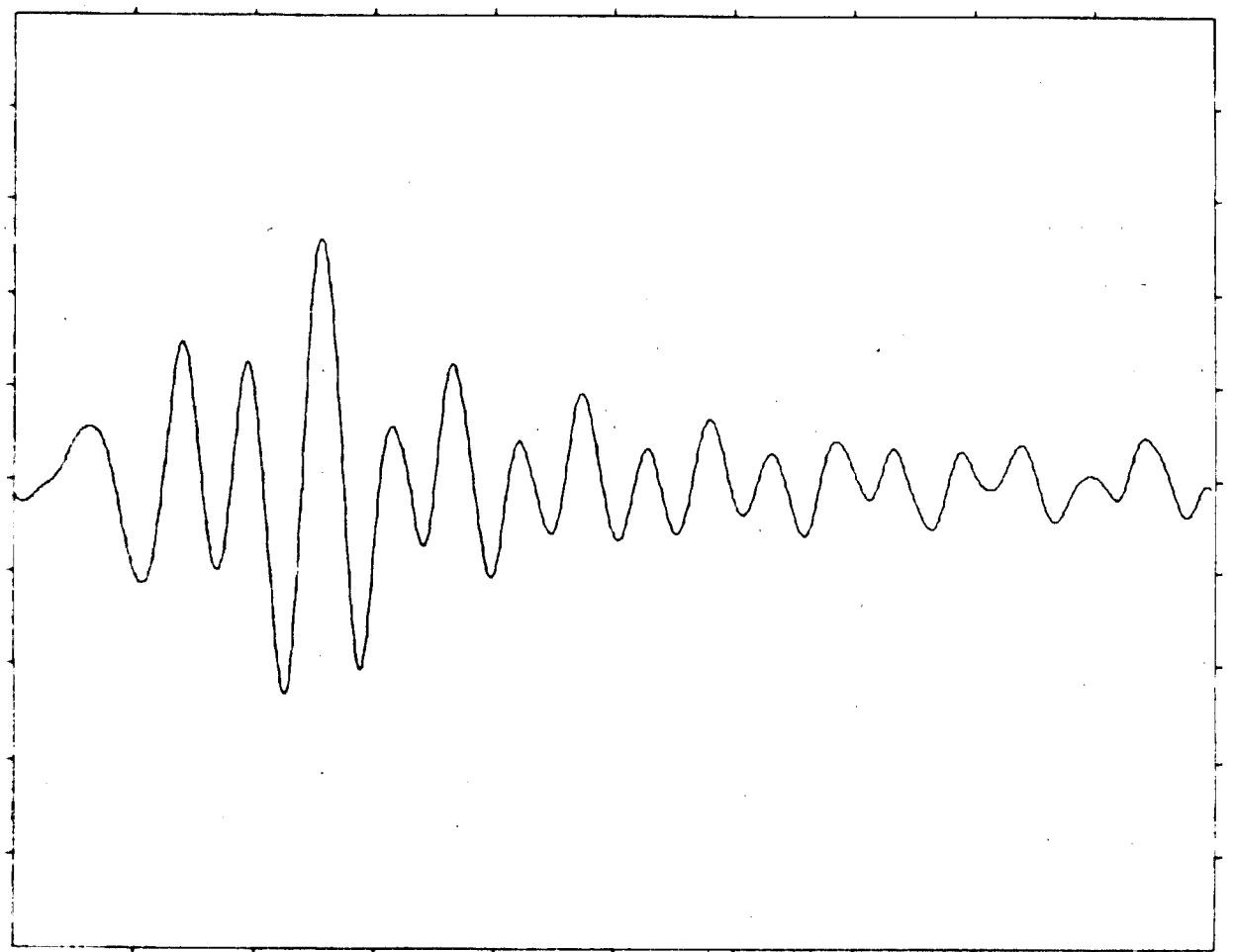

0 000E+00 TIME IN SECONDS 0 273E+03

ORIGINAL PAGE IS
OF POOR QUALITY

TEST NAME=SAE ACC MSIDS
MEASUREMENT= COVER Y
REF TIME = 246 17 23 4 0
TIME OFFSET= 1 001
TOTAL TIME= 273 100

NNOFFT = 1
FFTBW-HZ= 0 00000E+00
FFTERR = 0 00
FFTTIM = 0 0
FFTLIN = 0

UNITS= (INCHES)
MEAN=-0 63446350E-00
S D = 0 50356410E+00
SAMPLE RATE= 0 3750E+01

D: 2-12-85
T: 14-38- 5

0 500E+01

RAW DATA

TIME	MAGNITUDE
0 357E+02	0 2126E+01
0 355E+02	0 2124E+01
0 [illegible]	0 [illegible]
0 352E+02	0 2100E+01
0 [illegible]	0 2085E+01
0 349E+02	0 2074E+01
0 365E+02	0 2042E+01
0 347E+02	0 2023E+01
0 [illegible]	0 1984E+01
0 344E+02	0 1957E+01

-0 500E+01

0 000E+00 TIME IN SECONDS 0 273E+03

ORIGINAL PAGE IS
OF POOR QUALITY

ORIGINAL PAGE IS
OF POOR QUALITY

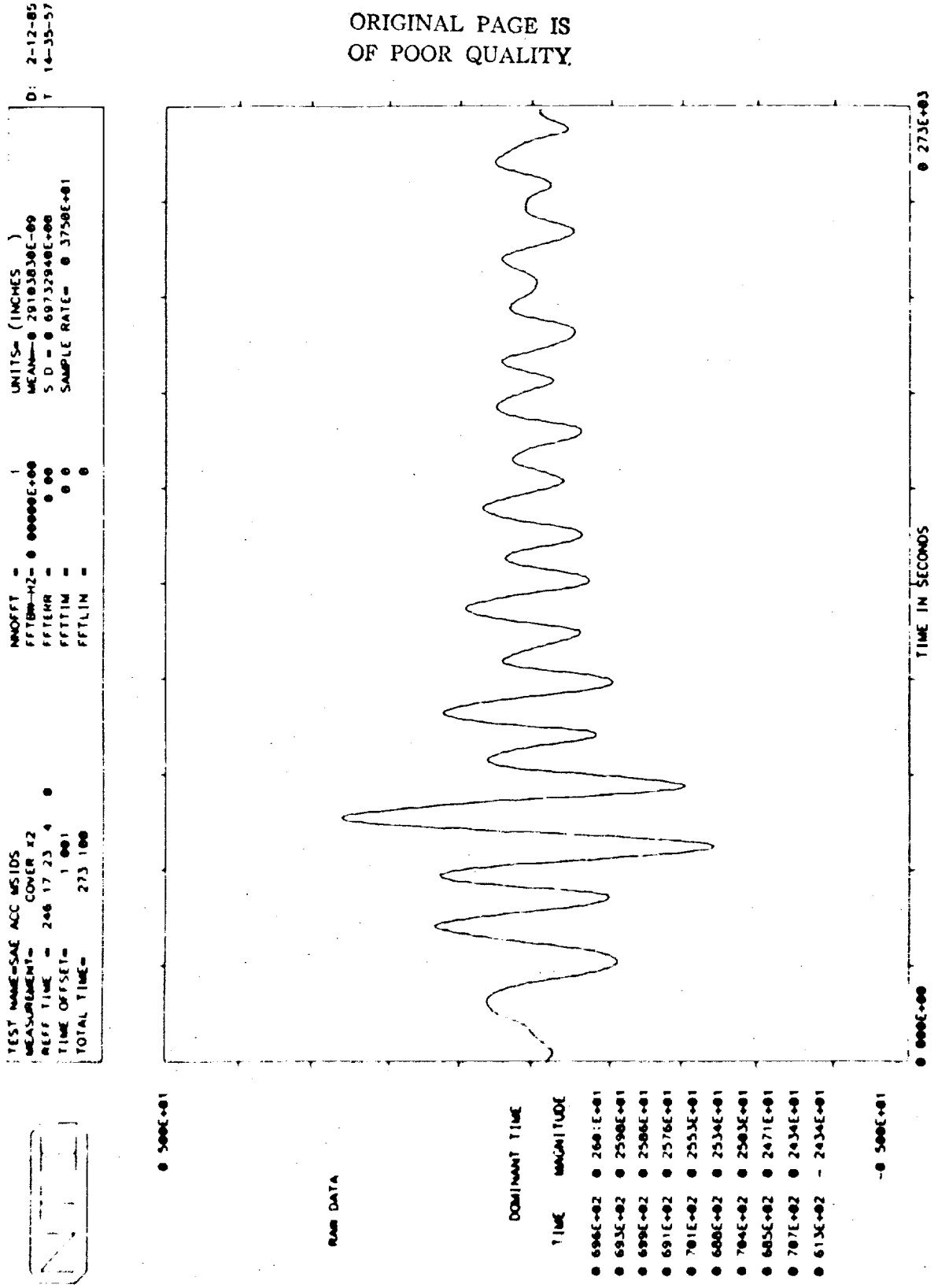

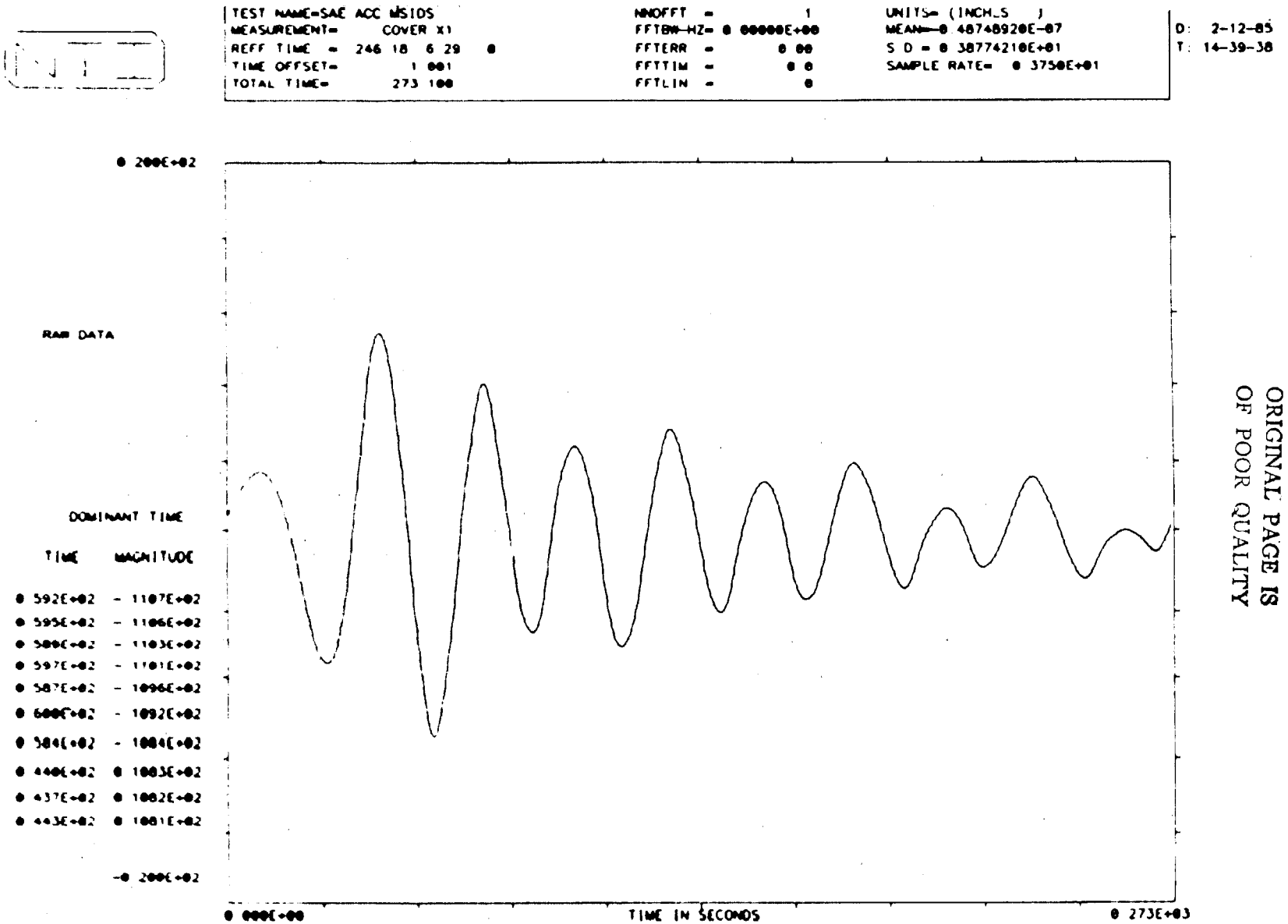

ORIGINAL PAGE IS
OF POOR QUALITY

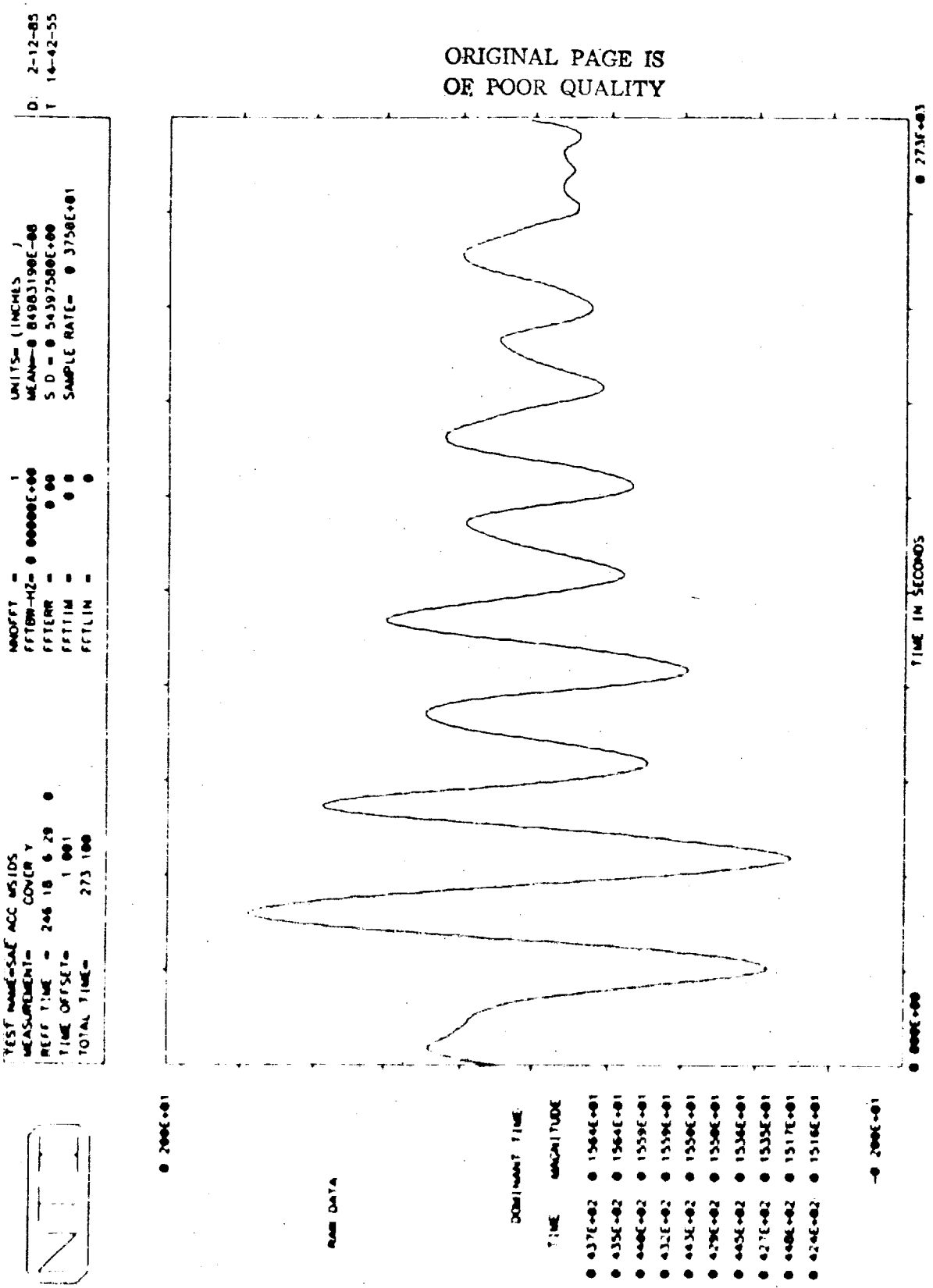

TEST NAME=SAE ACC MSIDS
MEASUREMENT= COVER #2
ACFF TIME = 246 18 6 29 0
TIME OFFSET= 1 001
TOTAL TIME= 273 100

NNOFFT = 1
FFT@0-HZ= 0 00000E+00
FFTERR = 0 00
FFTTIM = 0 0
FFTLIN = 0

UNITS= (INCHES)
MEAN=-0 52765250E-07
S D = 0 38333140E+01
SAMPLE RATE= 0 3750E+01

D: 2-12-85
T: 14-41- 8

0 200E+02

RAW DATA

DOMINANT TIME

TIME	MAGNITUDE
0 592E+02	- 1101E+02
0 595E+02	- 1100E+02
0 589E+02	- 1098E+02
0 597E+02	- 1094E+02
0 587E+02	- 1091E+02
0 600E+02	- 1084E+02
0 584E+02	- 1080E+02
0 437E+02	0 1070E+02
0 603E+02	- 1070E+02
0 440E+02	0 1070E+02

-0 200E+02

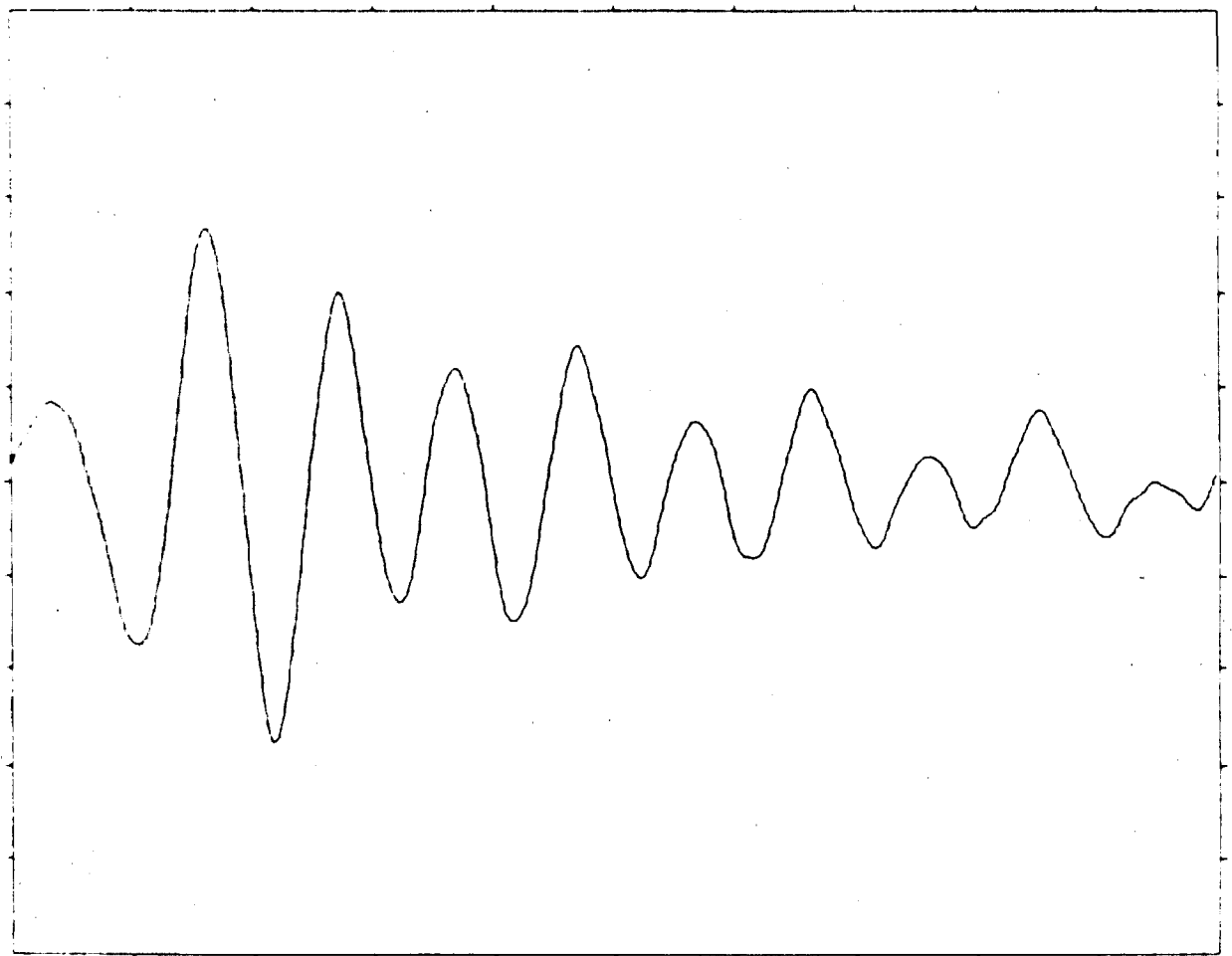

0 000E+00 TIME IN SECONDS 0 273E+03

ORIGINAL PAGE IS
OF POOR QUALITY

ORIGINAL PAGE IS
OF POOR QUALITY

TEST NAME=SAE ACC MSIDS
MEASUREMENT= COVER Y
BEFF TIME = 246 19 31 29 0
TIME OFFSET= 1 001
TOTAL TIME= 273 100

NNOFFT = 1
FFTBW-HZ= 0 00000E+00
FFTEHR = 0 00
FFTTIM = 0 0
FFTLIN = 0

UNITS= (INCHES)
MEAN=-0 65774660E-08
S D = 0 98075800E+00
SAMPLE RATE= 0 3750E+01

D 4-12-85
T 14-52-23

0 500E+01

RAW DATA

DOMINANT TIME

TIME	MAGNITUDE
0 397E+02	- 3436E+01
0 400E+02	- 3483E+01
0 395E+02	- 3487E+01
0 403E+02	- 3464E+01
0 39[illegible]E+02	- 3462E+01
0 389E+02	- 3423E+01
0 405E+02	- 3423E+01
0 387E+02	- 3369E+01
0 408E+02	- 3365E+01
0 384E+02	- 330[illegible]E+01

-0 500E+01

0 000E+00 TIME IN SECONDS 0 273E+03

ORIGINAL PAGE IS
OF POOR QUALITY

ORIGINAL PAGE IS
OF POOR QUALITY

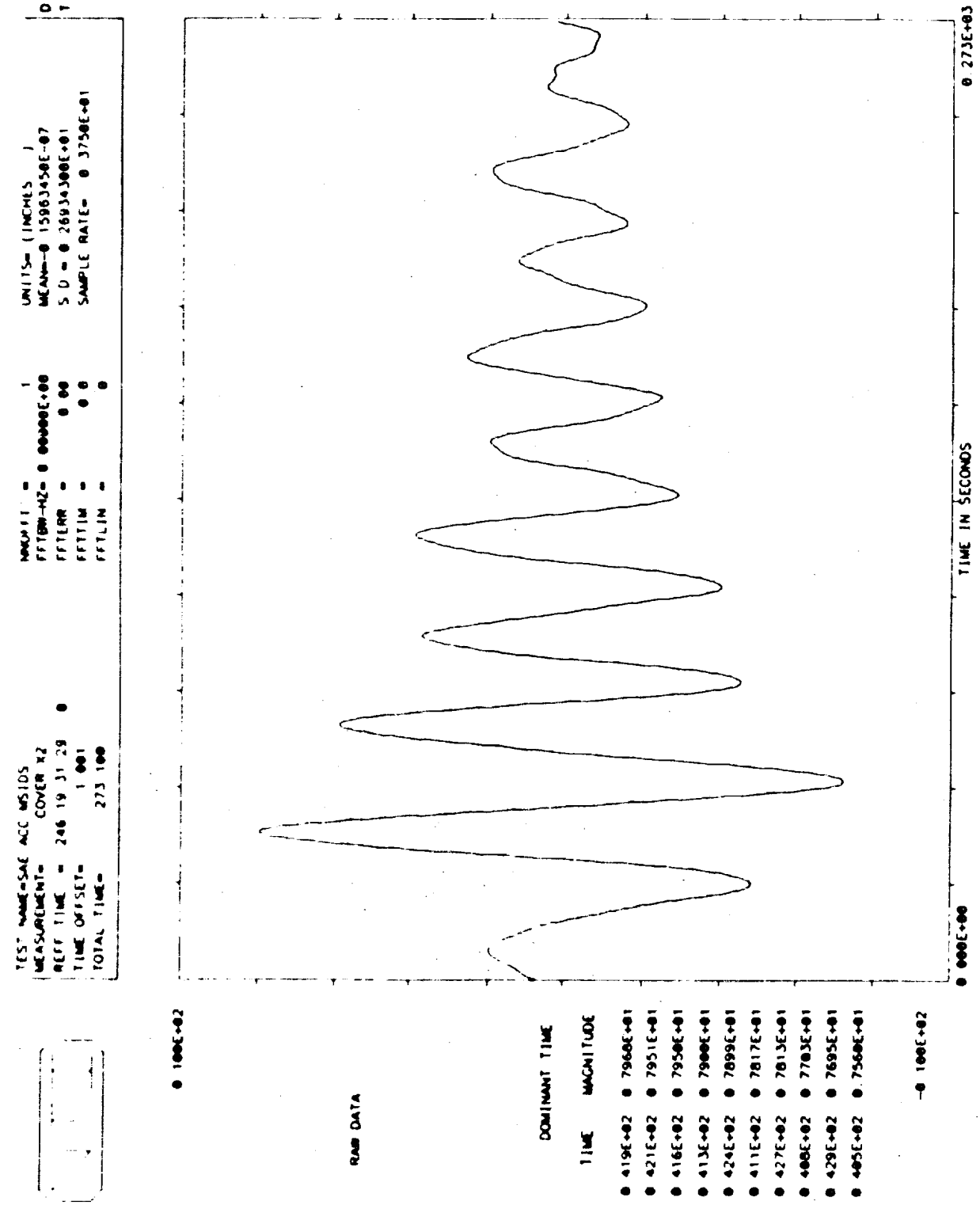

TEST NAME=SAE ACC MSIDS	NNOFFT = 1	UNITS= (INCHES)	D 2-12-85
MEASUREMENT= COVER X1	FFTBW-HZ= 0 00000E+00	MEAN=-0 16552800E-09	T 14-54-34
REFF TIME = 247 16 2 11 0	FFTERR = 0 00	S D = 0 51822070E+00	
TIME OFFSET= 1 001	FFTTIM = 0 0	SAMPLE RATE= 0 3750E+01	
TOTAL TIME= 273 100	FFTLIN = 0		

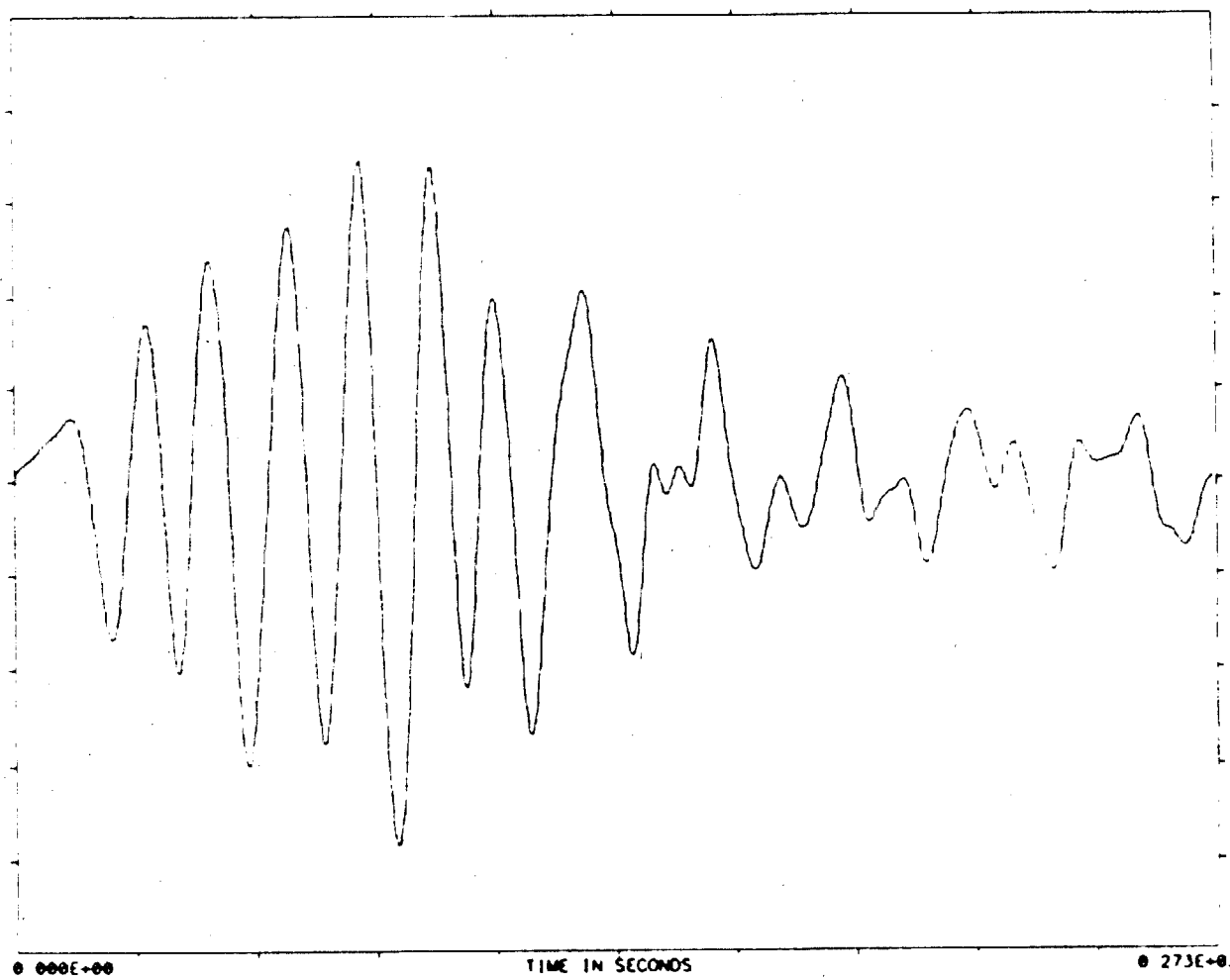

DOMINANT TIME

TIME	MAGNITUDE
0 867E+02	- 1532E+01
0 869E+02	- 1530E+01
0 864E+02	- 1522E+01
0 872E+02	- 1514E+01
0 861E+02	- 1499E+01
0 875E+02	- 1485E+01
0 859E+02	- 1464E+01
0 877E+02	- 1443E+01
0 856E+02	- 1418E+01
0 880E+02	- 1389E+01

ORIGINAL PAGE IS
OF POOR QUALITY

TEST NAME=SAE ACC MSIDS
MEASUREMENT= COVER Y
REFF TIME = 247 16 2 11 0
TIME OFFSET= 1 001
TOTAL TIME= 273 100

NNOFFT = 1
FFTBW-HZ= 0.00000E+00
FFTERR = 0 00
FFTTIM = 0 0
FFTLIN = 0

UNITS= (INCHES)
MEAN=-0 63955670E-00
S D = 0 48496500E+00
SAMPLE RATE= 0 3750E+01

D: 2-12-85
T: 14-57-23

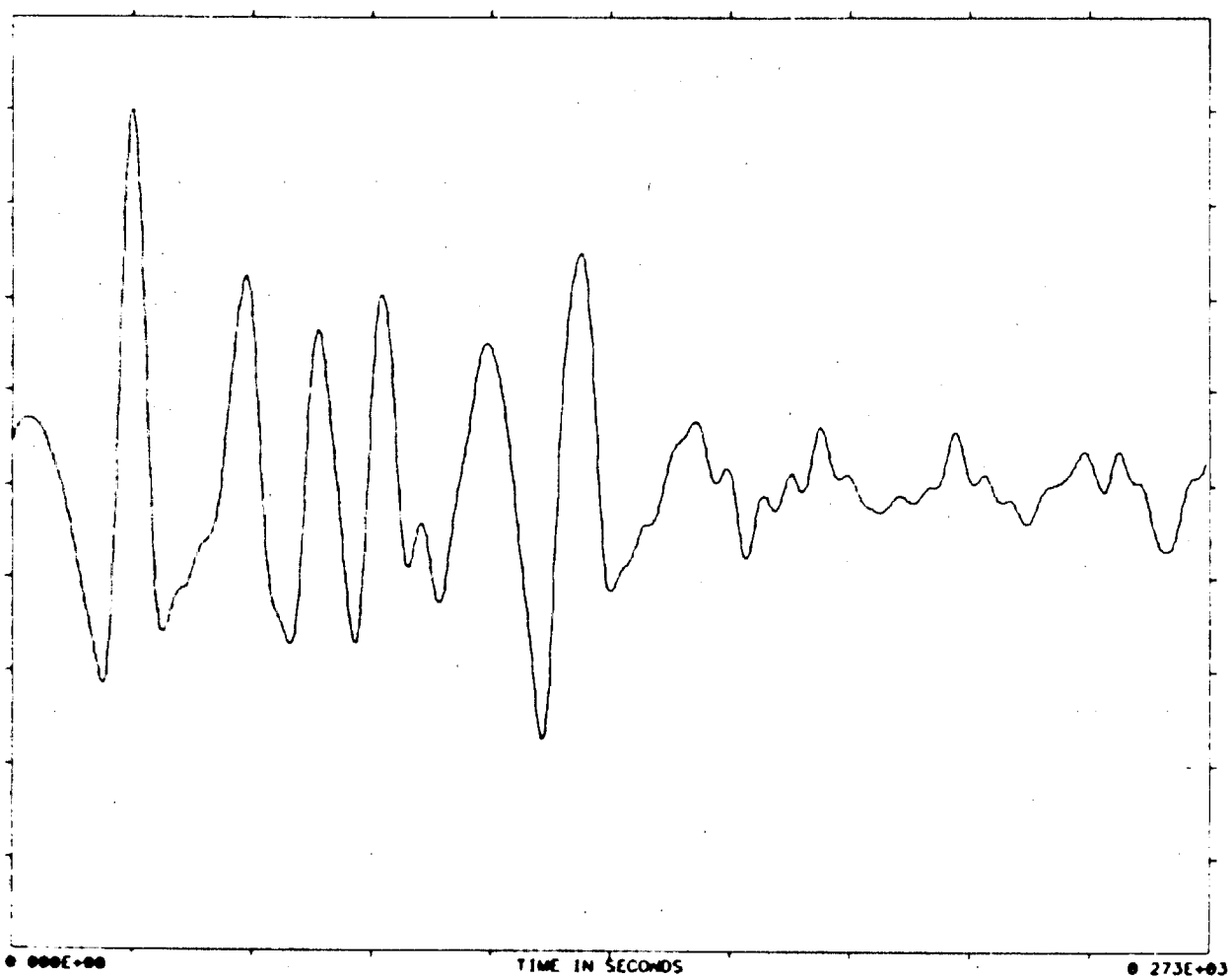

DOMINANT TIME

TIME	MAGNITUDE
0 272E+02	0 1602E+01
0 275E+02	0 1601E+01
0 269E+02	0 1584E+01
0 277E+02	0 1578E+01
0 267E+02	0 1544E+01
0 280E+02	0 1534E+01
0 264E+02	0 1483E+01
0 283E+02	0 1472E+01
0 261E+02	0 1403E+01
0 285E+02	0 1393E+01

TEST NAME=SAE ACC MSIDS	NNOFFT = 1	UNITS= (INCHES)	D: 2-12-85
MEASUREMENT= COVER X2	FFTBW-HZ= 0.00000E+00	MEAN=-0.40890000E-00	T: 14-55-58
REFF TIME = 247 16 2 11 0	FFTERR = 0 00	S D = 0.51644898E+00	
TIME OFFSET= 1 001	FFTTIM = 0 0	SAMPLE RATE= 0.3750E+01	
TOTAL TIME= 273 100	FFTLIN = 0		

0.200E+01

RAW DATA

-0.200E+01

DOMINANT TIME

TIME	MAGNITUDE
0.864E+02	- 1432E+01
0.867E+02	- 1430E+01
0.861E+02	- 1419E+01
0.869E+02	- 1413E+01
0.779E+02	0 1407E+01
0.776E+02	0 1402E+01
0.781E+02	0 1400E+01
0.859E+02	- 1390E+01
0.872E+02	- 1384E+01
0.773E+02	0 1383E+01

0.000E+00 TIME IN SECONDS 0.273E+03

ORIGINAL PAGE IS
OF POOR QUALITY

ORIGINAL PAGE IS
OF POOR QUALITY

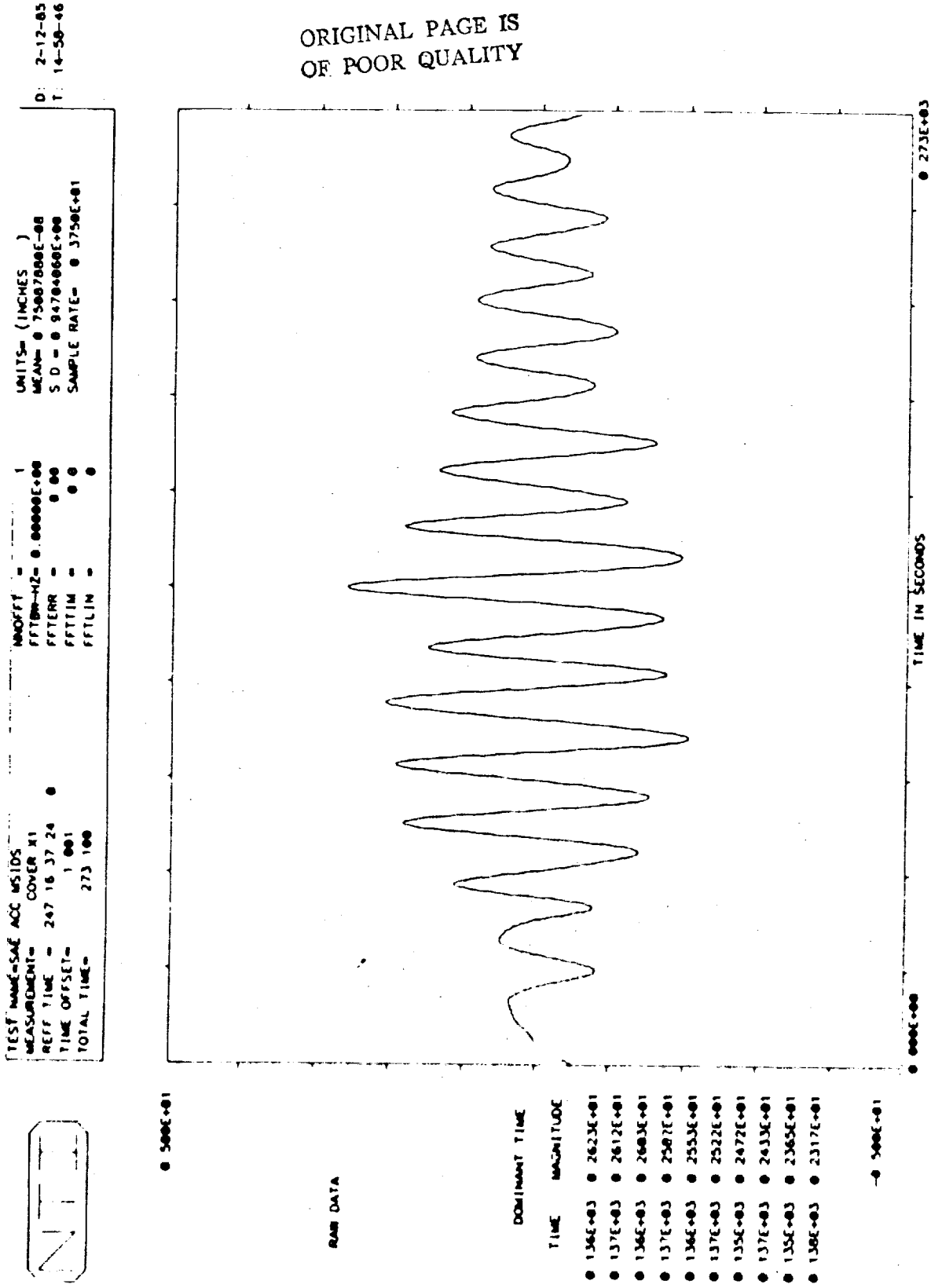

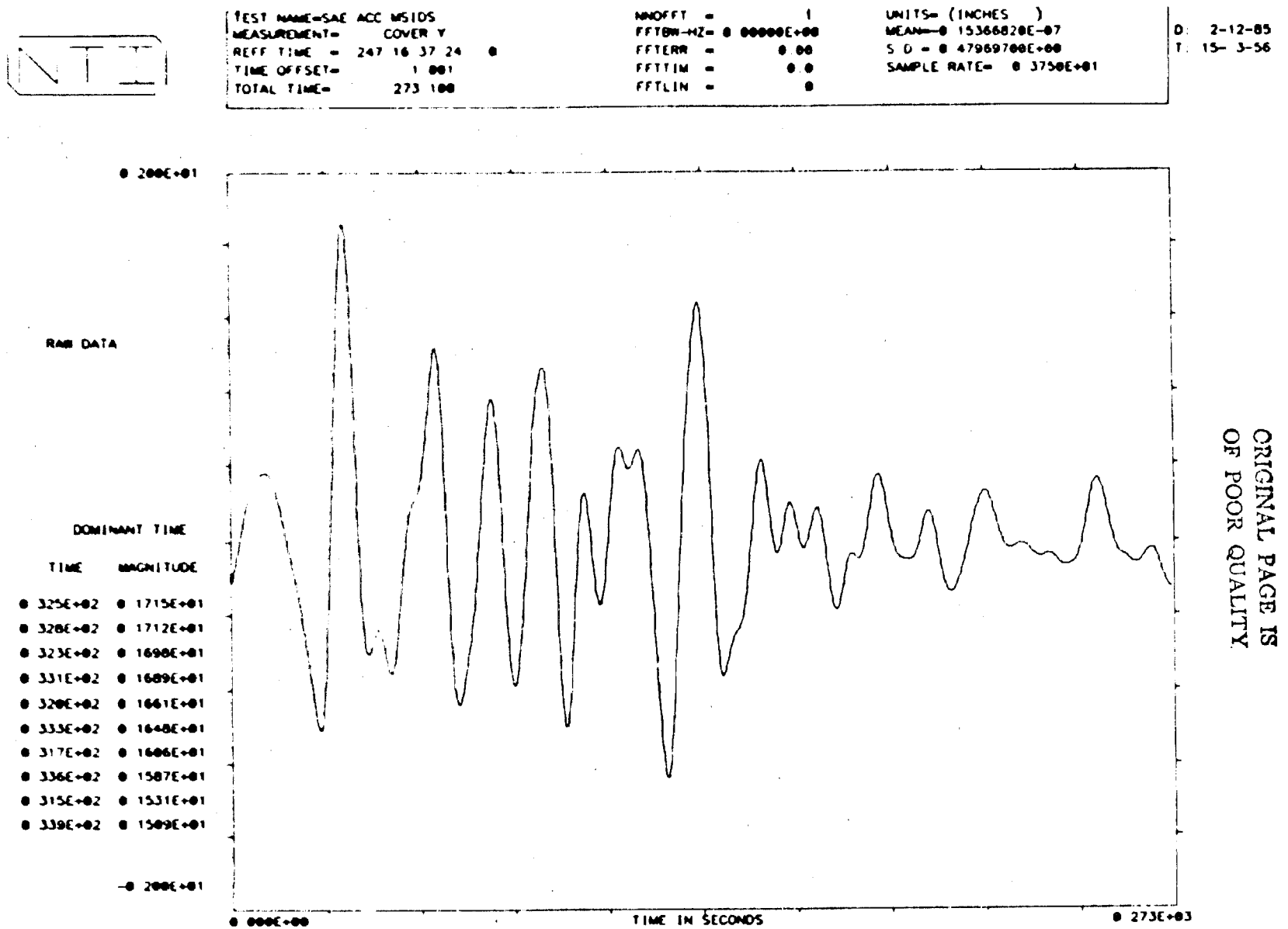

ORIGINAL PAGE IS
OF POOR QUALITY

ORIGINAL PAGE IS
OF POOR QUALITY

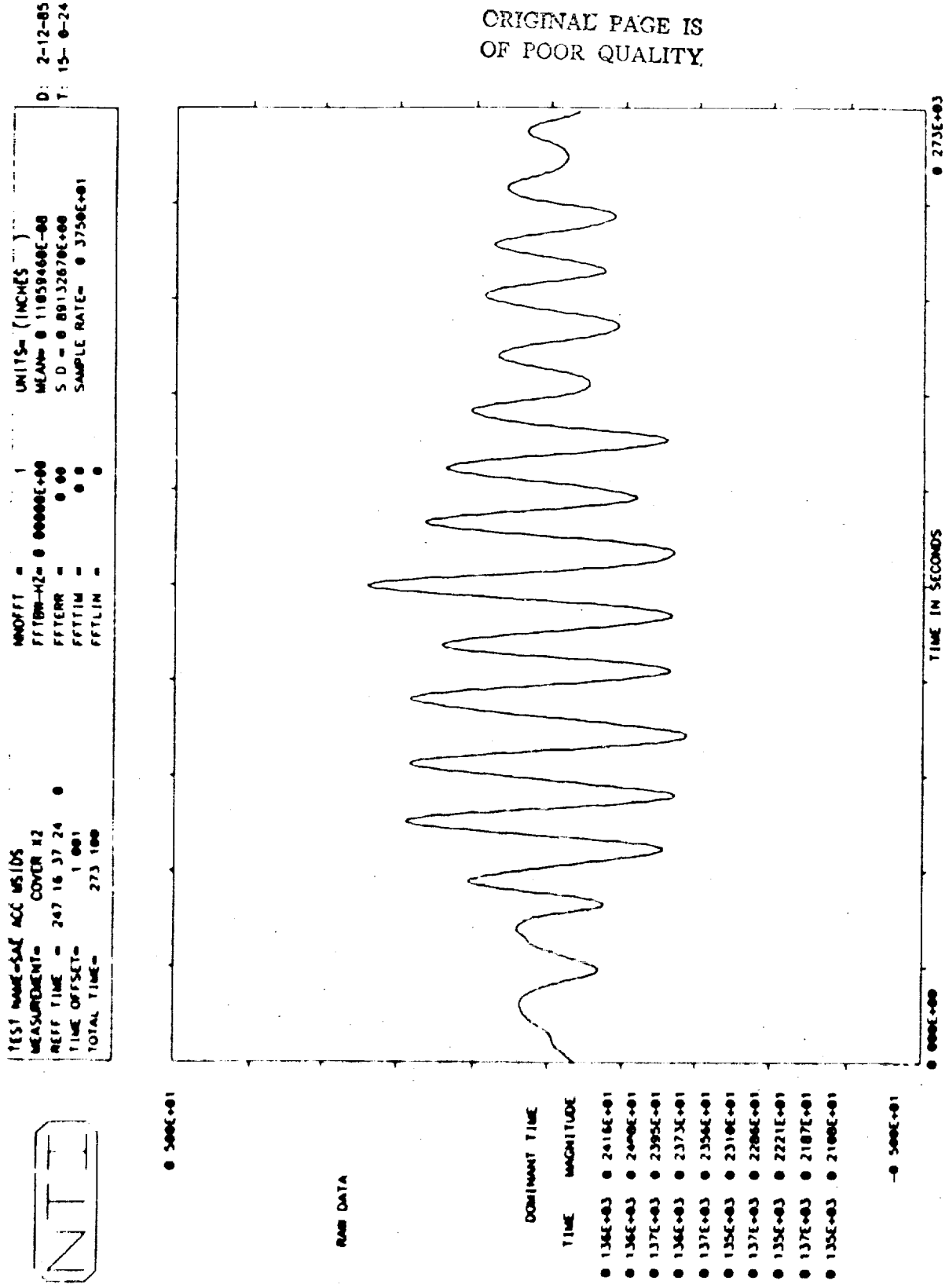

TEST NAME=SAE ACC MSIDS
MEASUREMENT= COVER h1
REFF TIME = 247 17 32 39 0
TIME OFFSET= 1 001
TOTAL TIME= 273 100

NNOFFT = 1
FFTBW-HZ= 0 00000E+00
FFTERR = 0 00
FFTTIM = 0 0
FFTLIN = 0

UNITS= (INCHES)
MEAN= 0 74851420E-00
S D = 0 20390000E+00
SAMPLE RATE= 0 3750E+01

D: 2-13-85
T 7-27-22

0 100E+01

RAW DATA

DOMINANT TIME

TIME	MAGNITUDE
0 523E+02	- 6564E+00
0 525E+02	- 6515E+00
0 520E+02	- 6457E+00
0 528E+02	- 6312E+00
0 424E+02	0 6273E+00
0 427E+02	0 6240E+00
0 421E+02	0 6206E+00
0 517E+02	- 6205E+00
0 429E+02	0 6107E+00
0 419E+02	0 6036E+00

-0 100E+01

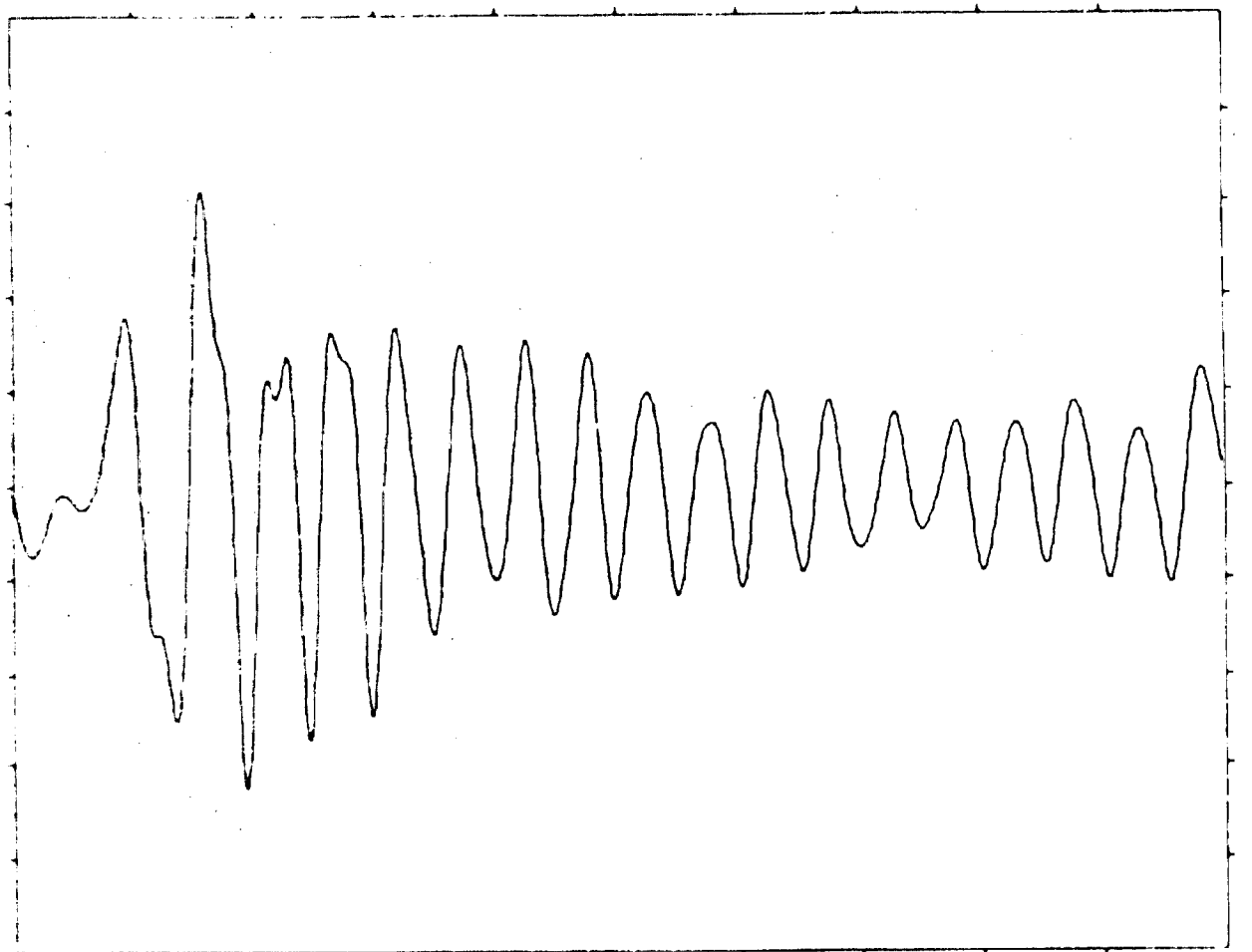

0 000E+00 TIME IN SECONDS 0 273E+03

ORIGINAL PAGE IS
OF POOR QUALITY

ORIGINAL PAGE IS
OF POOR QUALITY

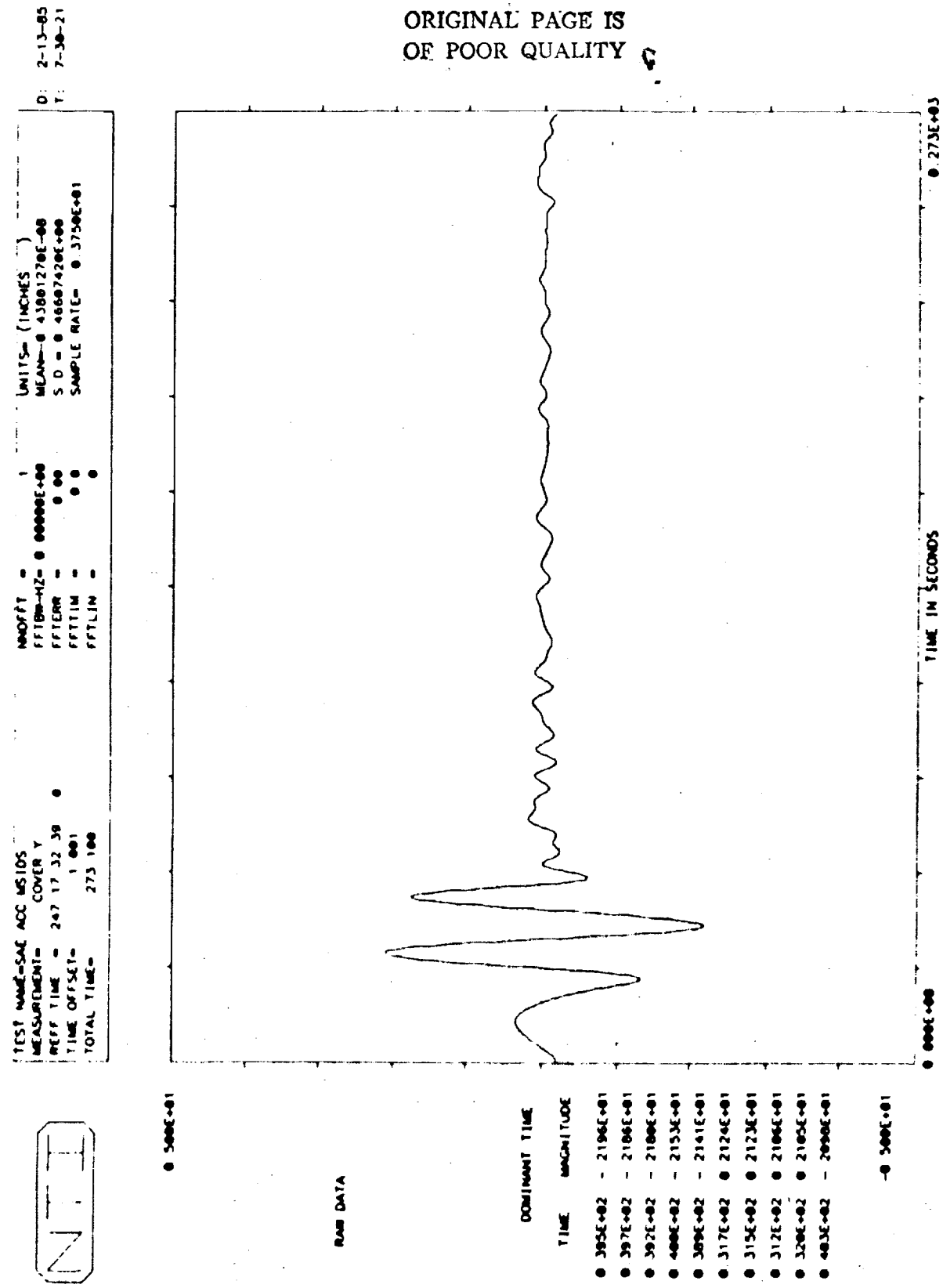

TEST NAME=SAE ACC MSIDS		NNOFFT =	1	UNITS= (INCHES)	
MEASUREMENT=	COVER X2	FFTBW-HZ=	0.00000E+00	MEAN=-0.55661080E-09	D: 2-13-85
REFF TIME =	247 17 32 30 0	FFTERR =	0 00	S D = 0.21415340E+00	T: 7-29- 3
TIME OFFSET=	1 001	FFTTIM =	0 0	SAMPLE RATE= 0.3750E+01	
TOTAL TIME=	273 100	FFTLIN =	0		

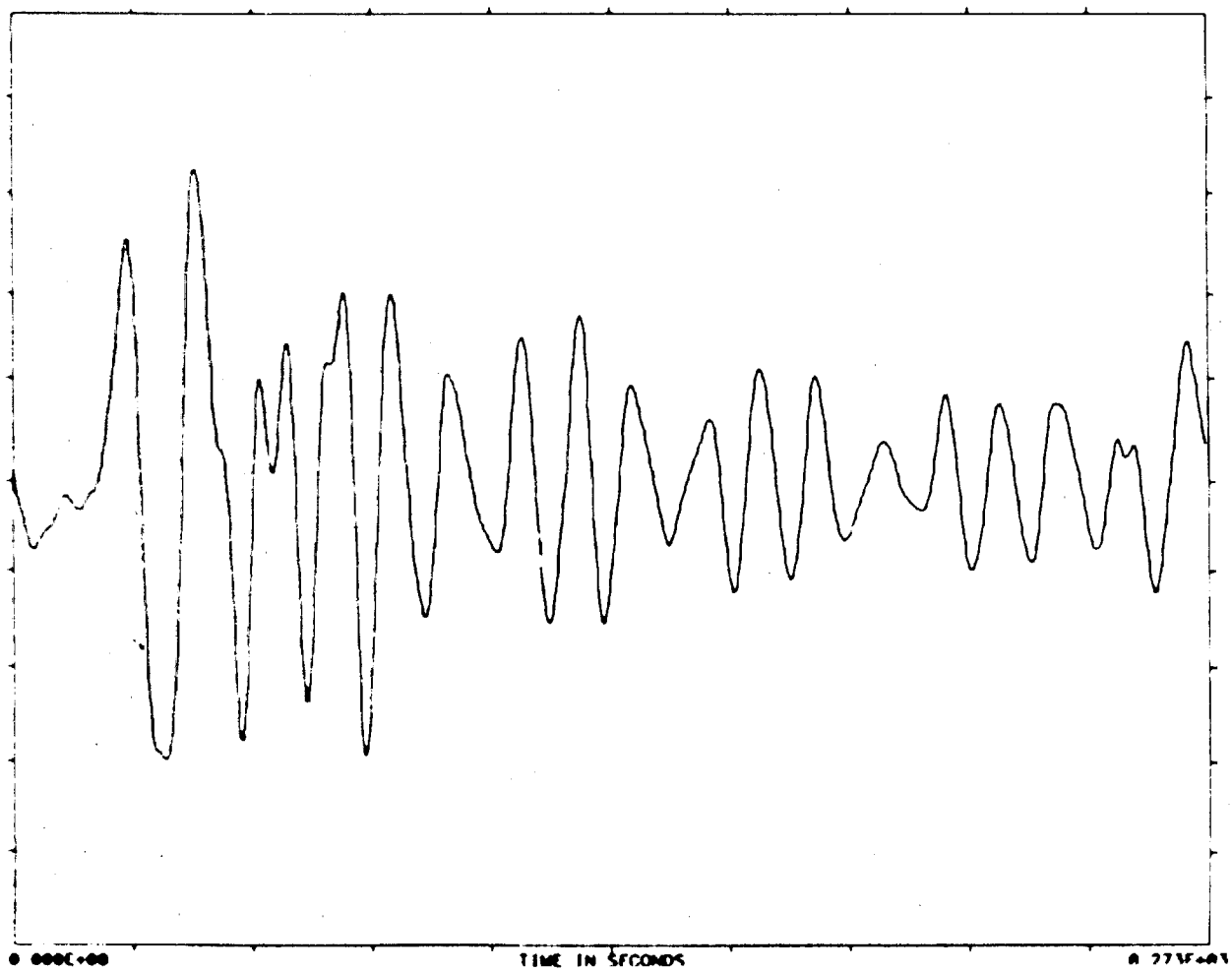

DOMINANT TIME

TIME	MAGNITUDE
0.416E+02	0.644E+00
0.413E+02	0.642?E+00
0.419E+02	0.641?E+00
0.421E+02	0.634?E+00
0.411E+02	0.633?E+00
0.424E+02	0.623?E+00
0.408E+02	0.615?E+00
0.427E+02	0.000?E+00
0.347E+02	-.590?E+00
0.349E+02	-.596?E+00

ORIGINAL PAGE IS
OF POOR QUALITY

ORIGINAL PAGE IS
OF POOR QUALITY

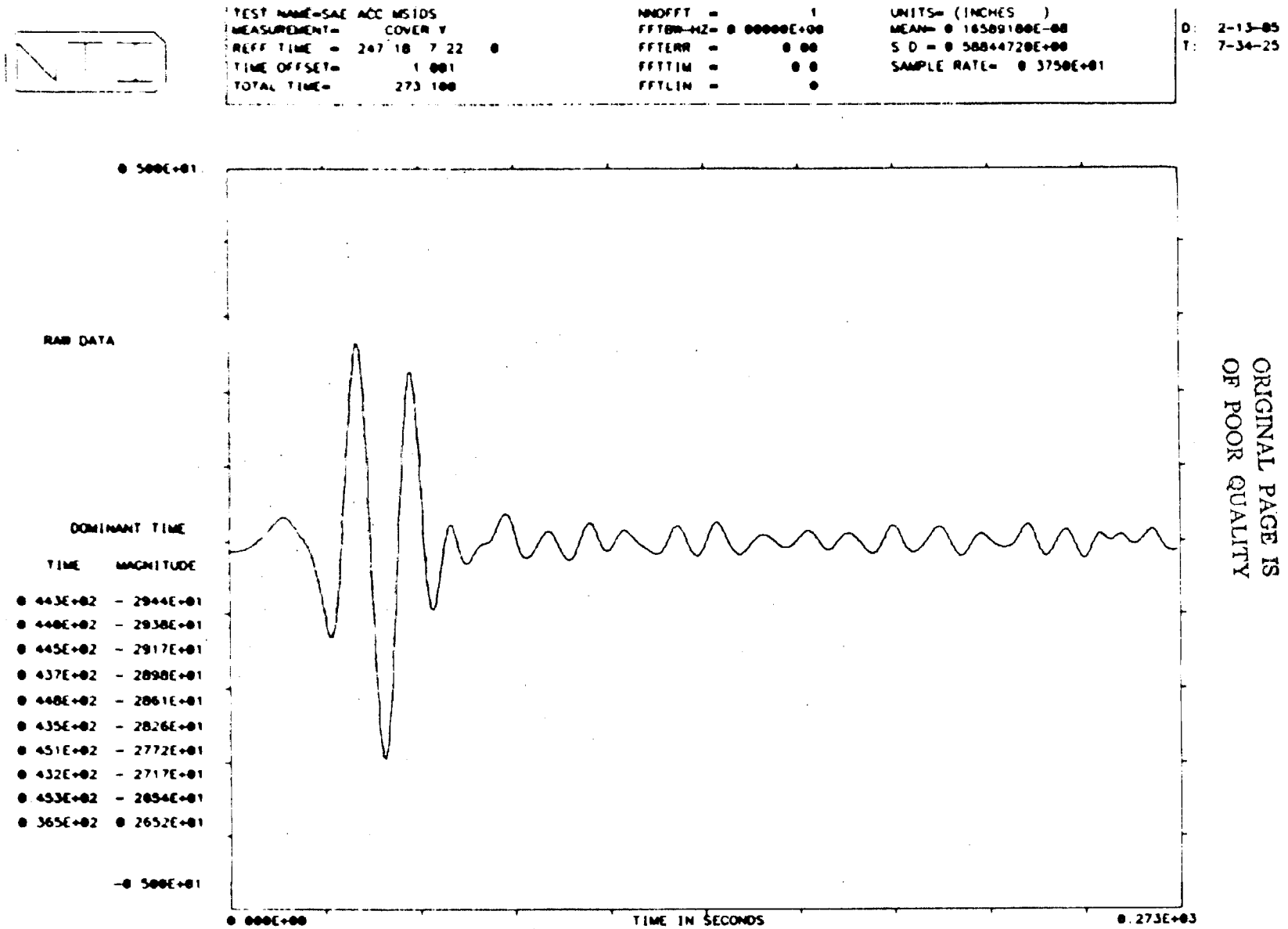

ORIGINAL PAGE IS
OF POOR QUALITY

ORIGINAL PAGE IS
OF POOR QUALITY

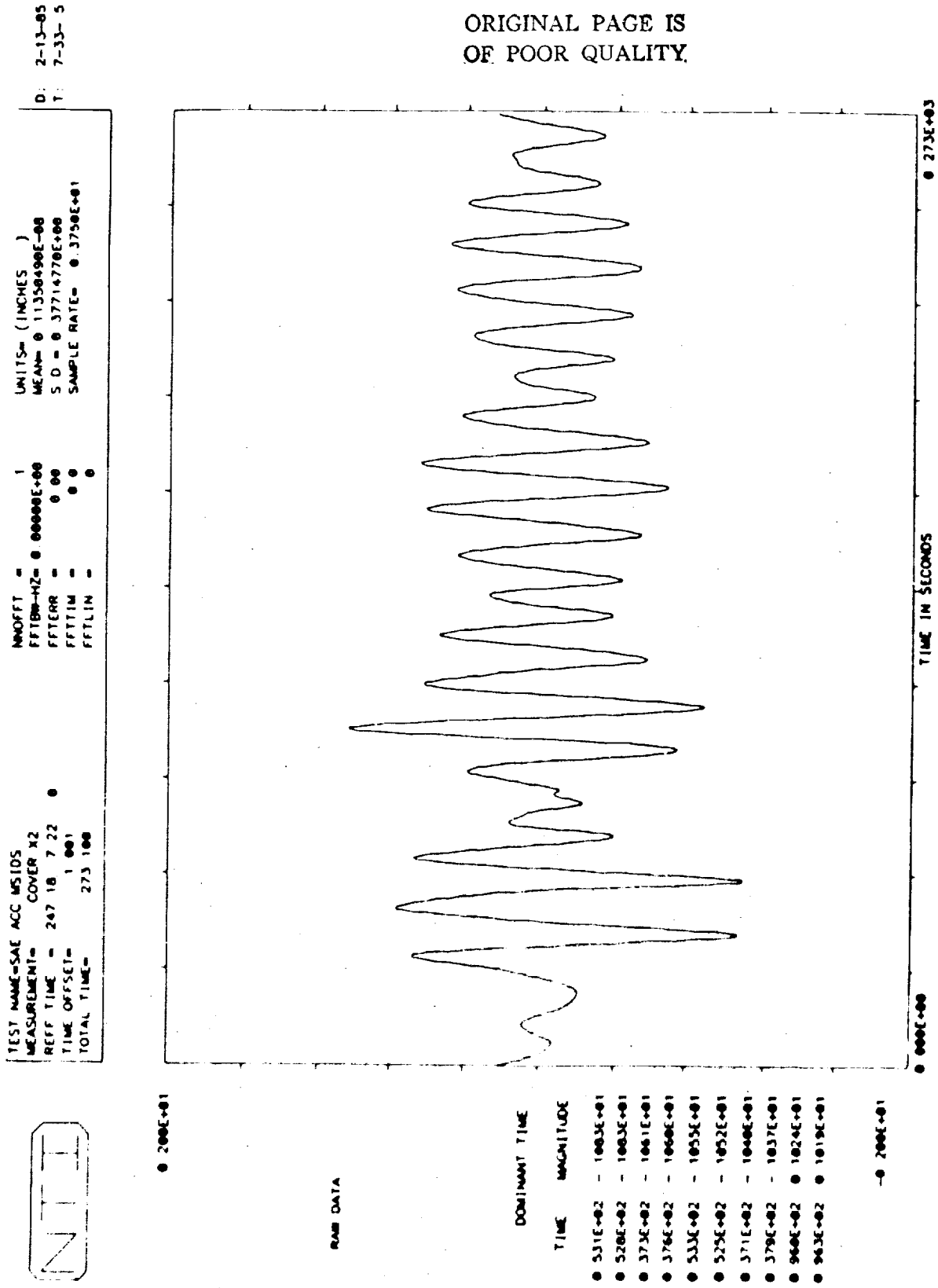

Final Report

LMSC-F087173

Appendix F
Computed Mast Tip Accelerations

ORIGINAL PAGE IS
OF POOR QUALITY

SIMULATED ACCELERATION HISTORIES

REFERENCE GMT = 245 19:25:44 6 – FILE 5

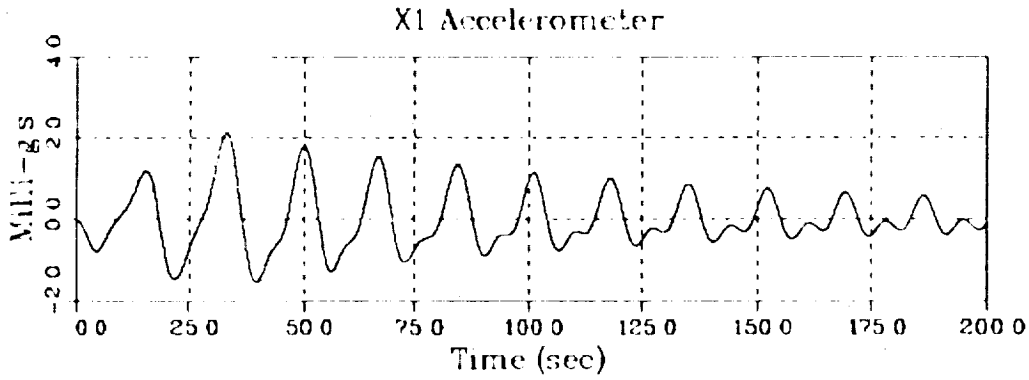

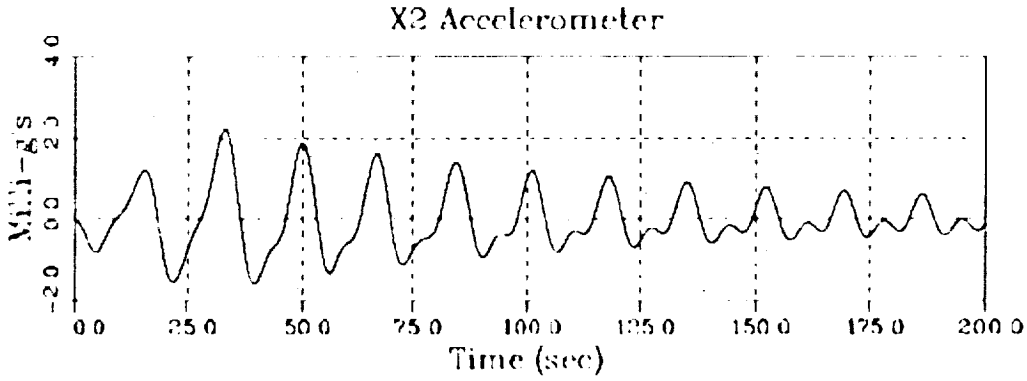

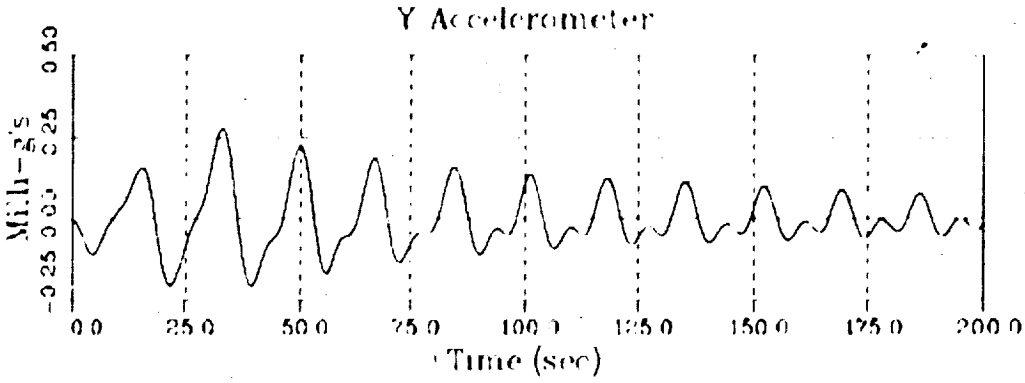

ORIGINAL PAGE IS
OF POOR QUALITY

SIMULATED ACCELERATION HISTORIES

REFERENCE GMT = 245:20:13:45.9 – FILE 6

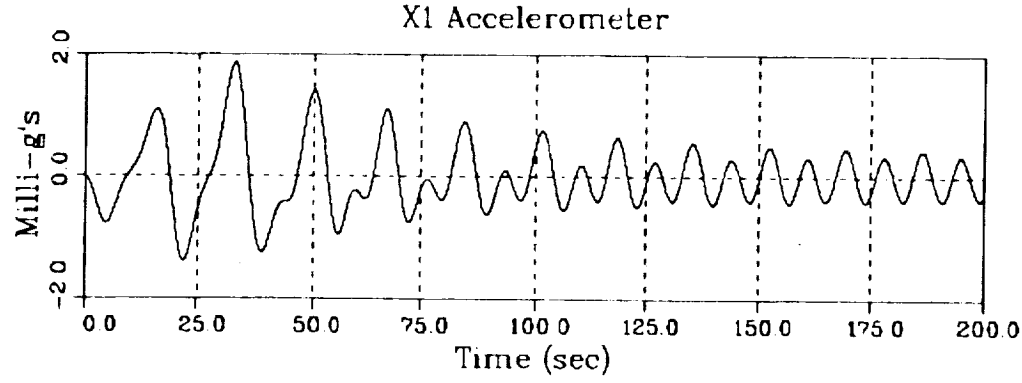

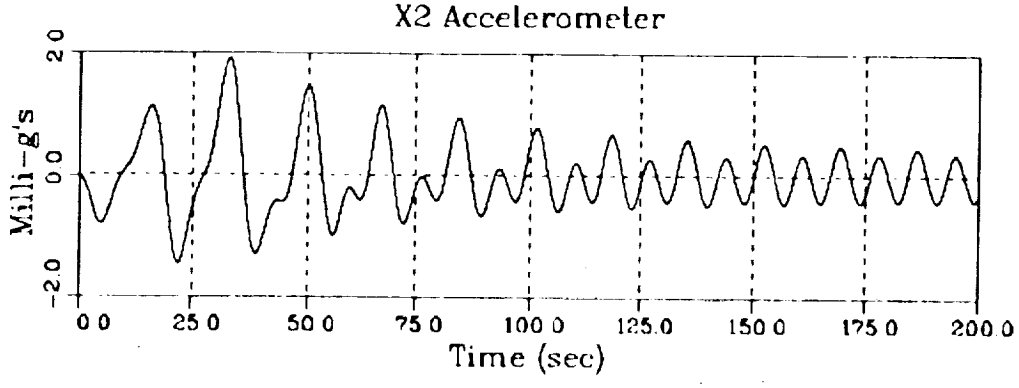

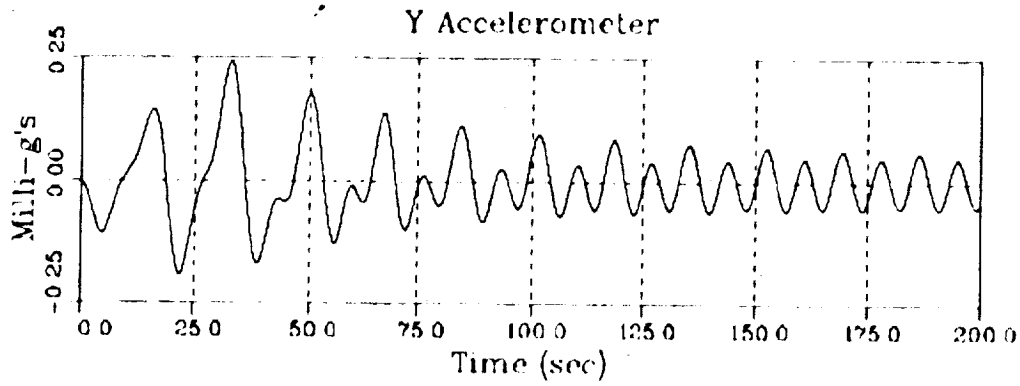

ORIGINAL PAGE IS
OF POOR QUALITY

SIMULATED ACCELERATION HISTORIES

REFERENCE GMT 245:20:13:45.9 FILE 6 (with IC's)

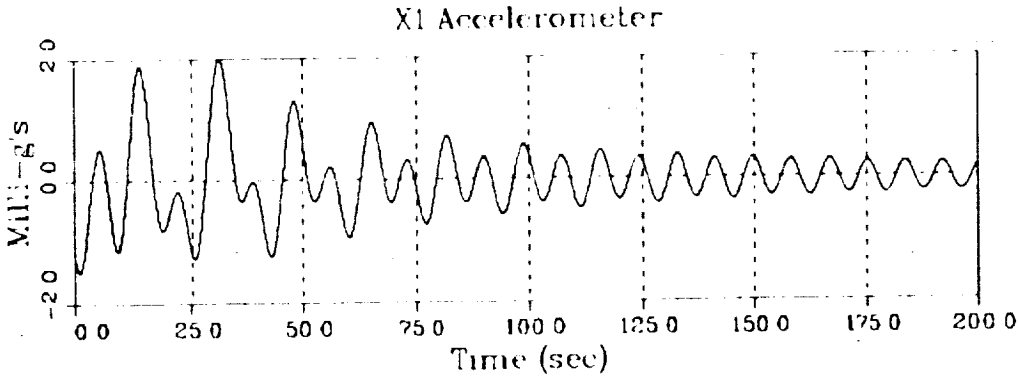

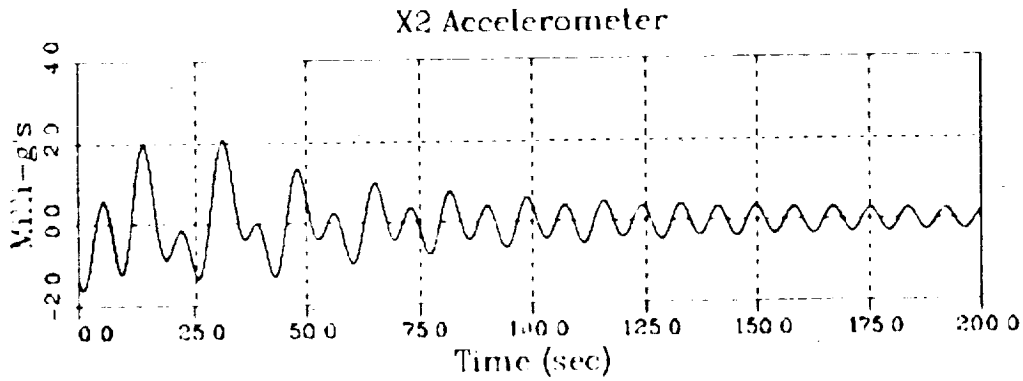

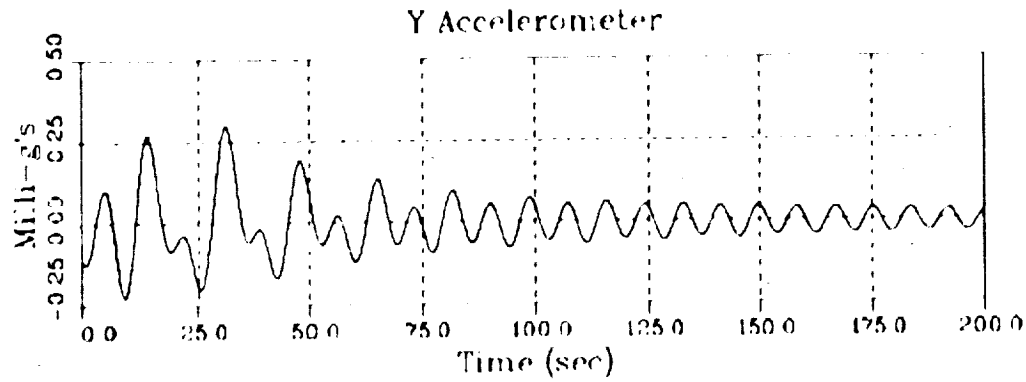

ORIGINAL PAGE IS
OF POOR QUALITY

SIMULATED ACCELERATION HISTORIES

REFERENCE GMT = 246:13:29:43.7 – FILE 10

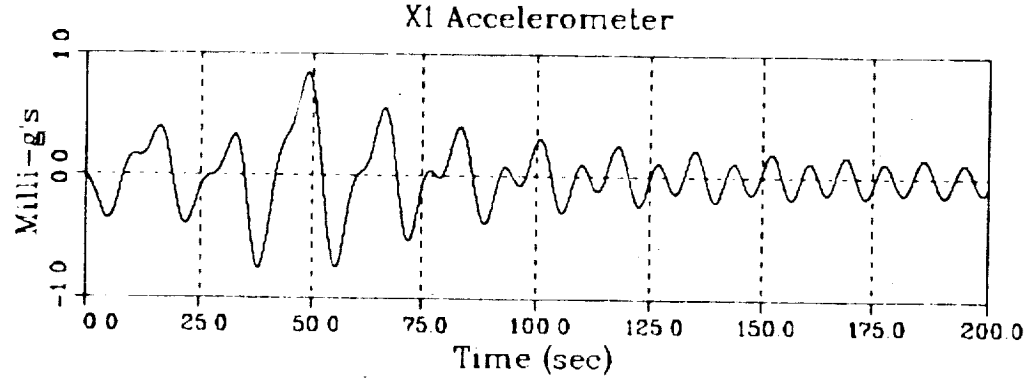

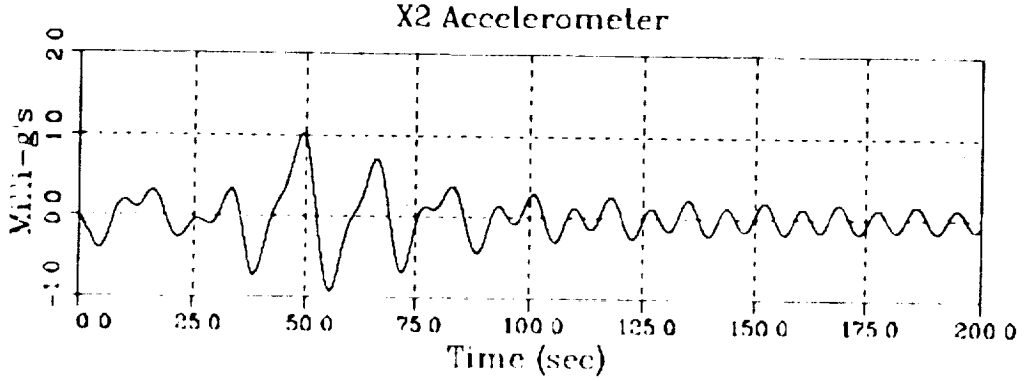

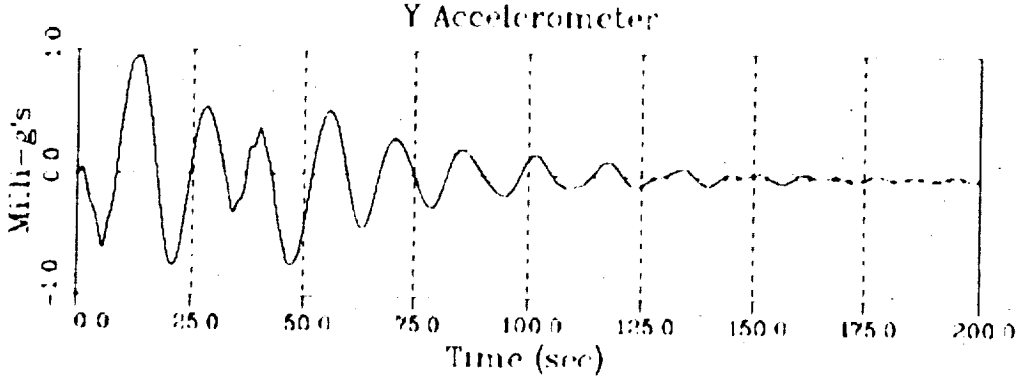

ORIGINAL PAGE IS
OF POOR QUALITY

SIMULATED ACCELERATION HISTORIES

REFERENCE GMT 246:14:22: 9.9 FILE 11

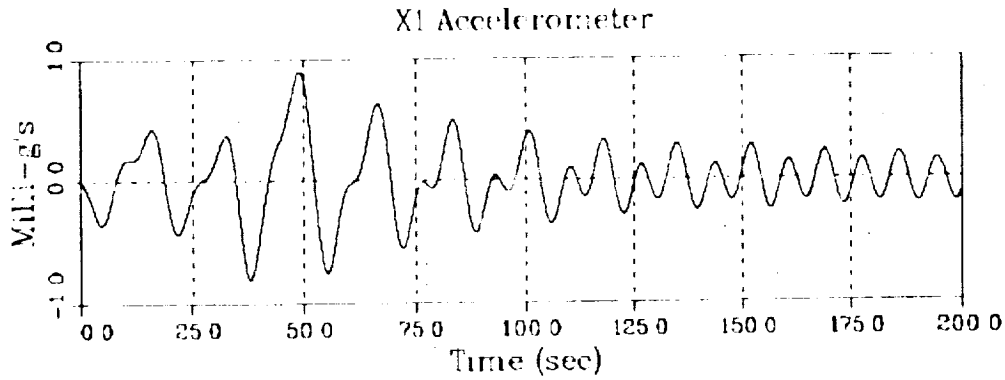

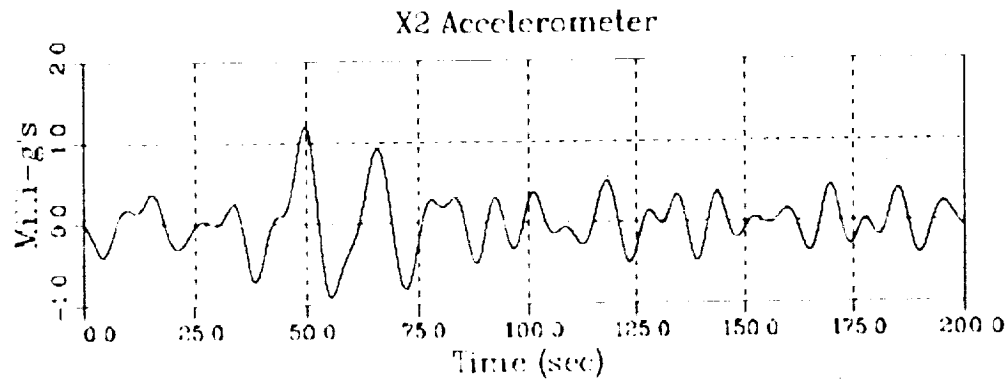

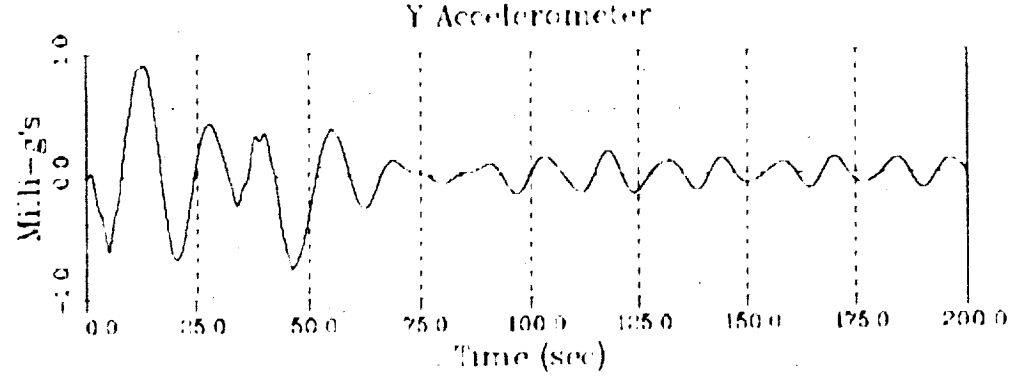

ORIGINAL PAGE IS
OF POOR QUALITY

SIMULATED ACCELERATION HISTORIES

REFERENCE GMT = 246:15:0:42.4 – FILE 12

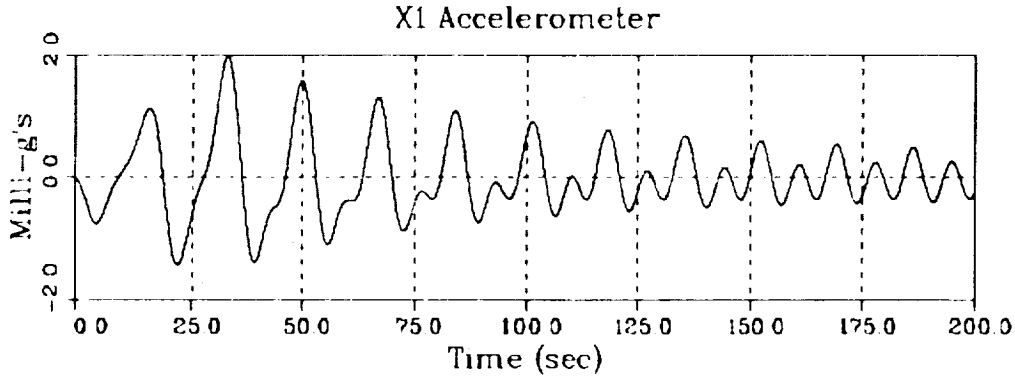

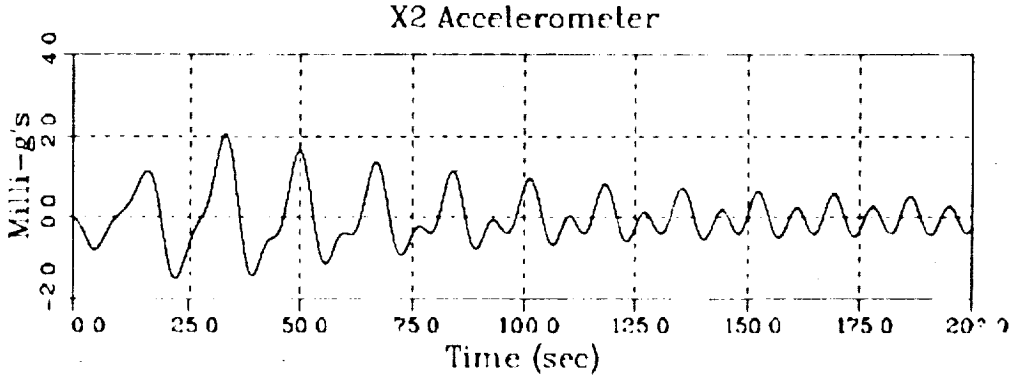

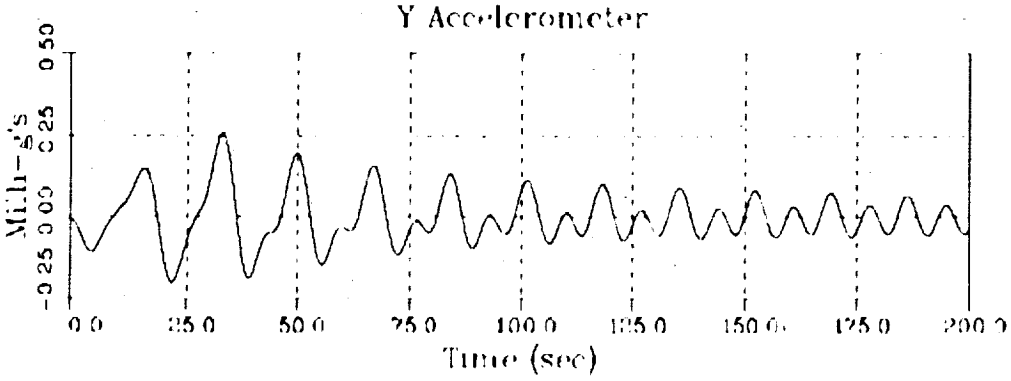

ORIGINAL PAGE IS
OF POOR QUALITY

SIMULATED ACCELERATION HISTORIES

REFERENCE GMT - 246:15:52:50.1 - FILE 13

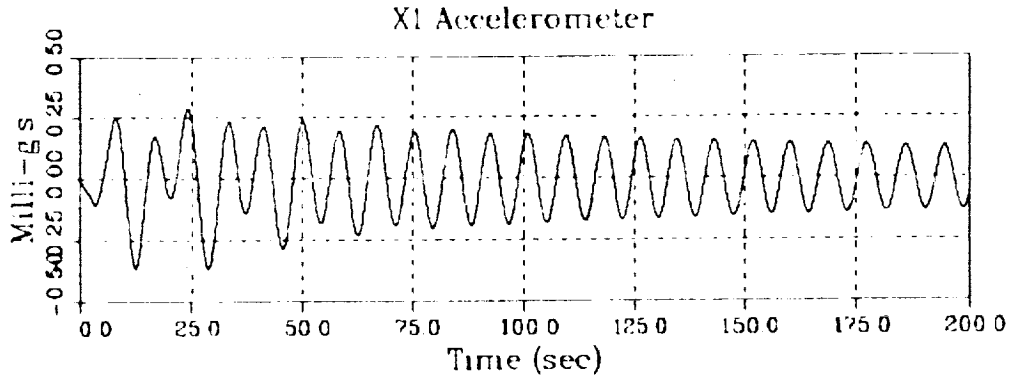

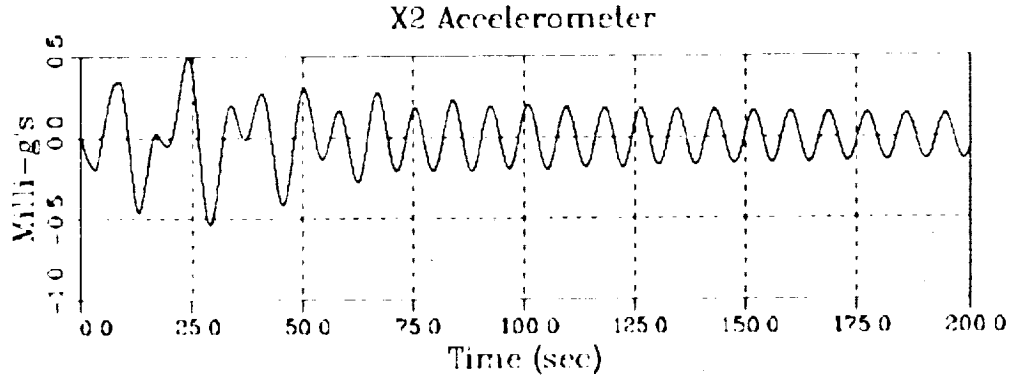

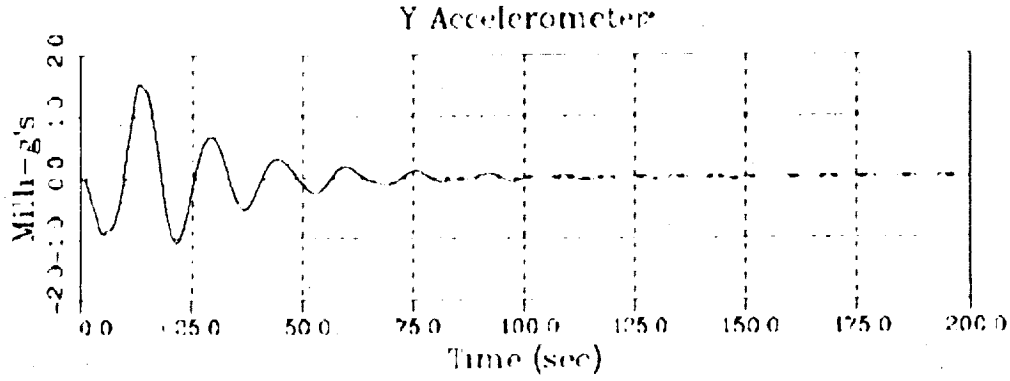

ORIGINAL PAGE IS
OF POOR QUALITY

SIMULATED ACCELERATION HISTORIES

REFERENCE GMT - 246:16:30:43.8 - FILE 14

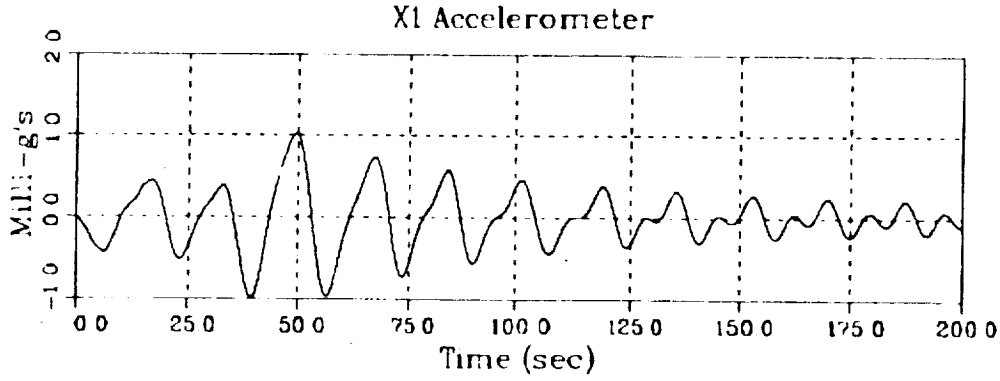

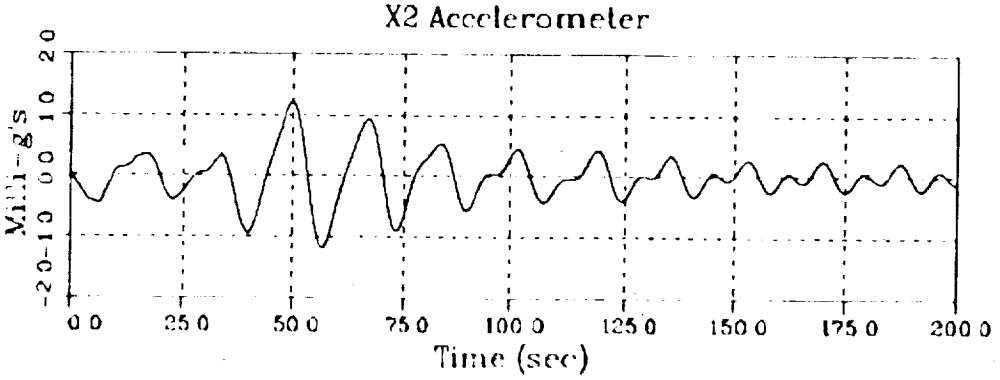

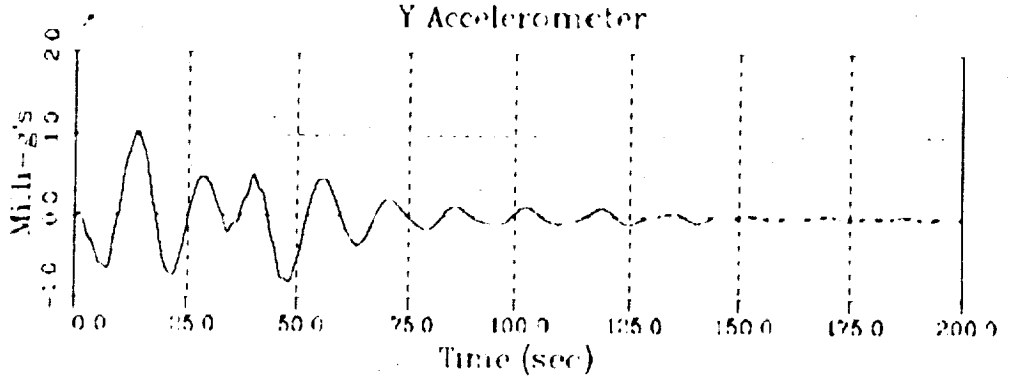

ORIGINAL PAGE IS
OF POOR QUALITY

SIMULATED ACCELERATION HISTORIES

REFERENCE GMT = 246 17:23:23.6 FILE 15

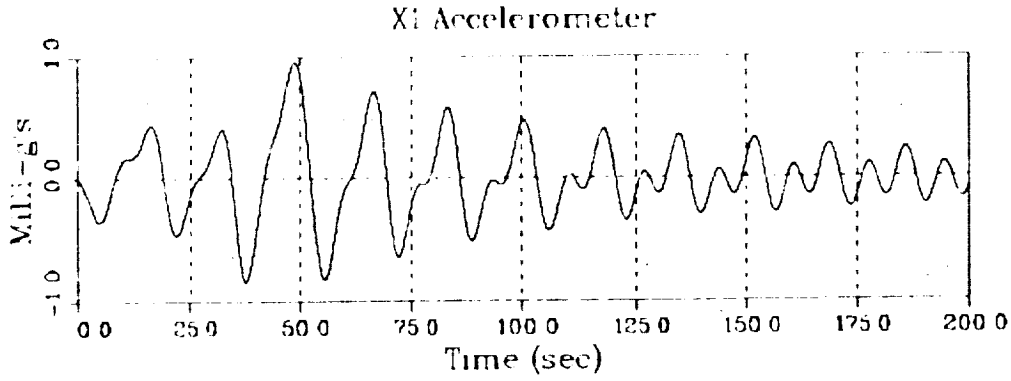

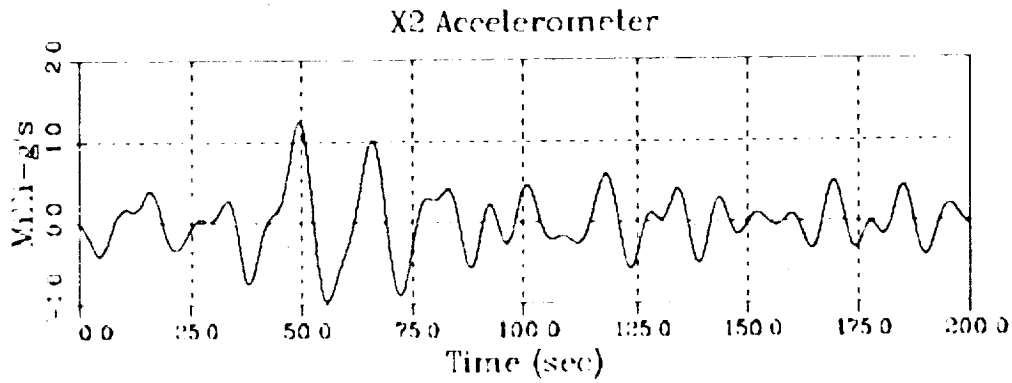

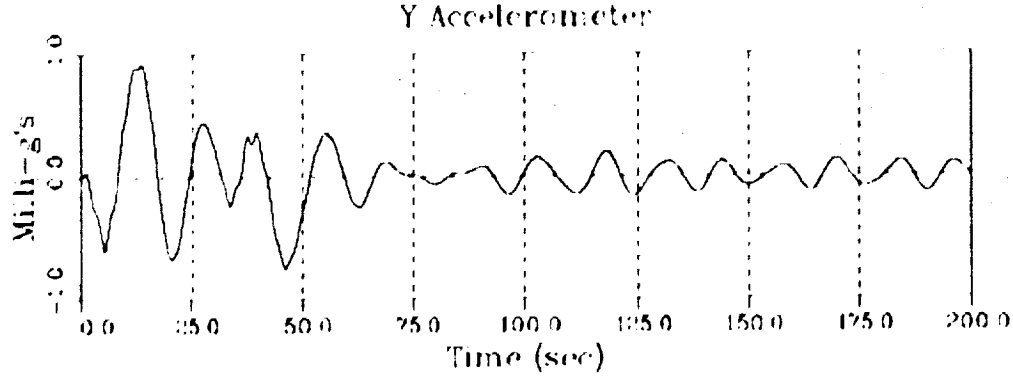

ORIGINAL PAGE IS
OF POOR QUALITY

SIMULATED ACCELERATION HISTORIES

REFERENCE GMT = 246 18 6 44 3 FILE 17

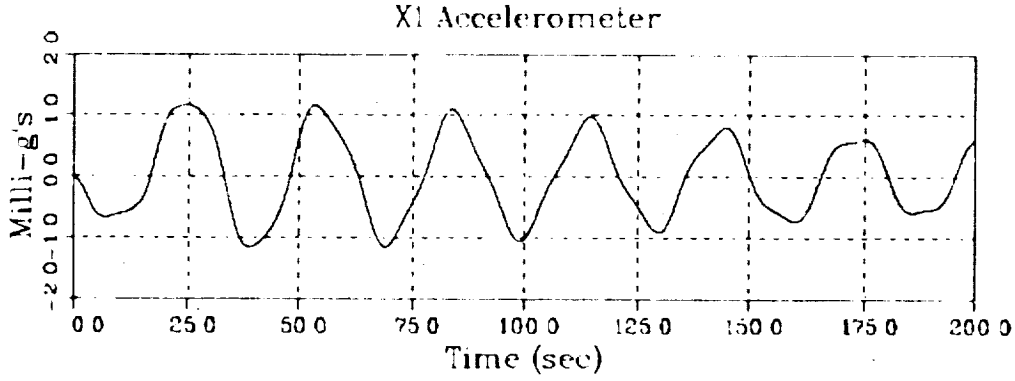

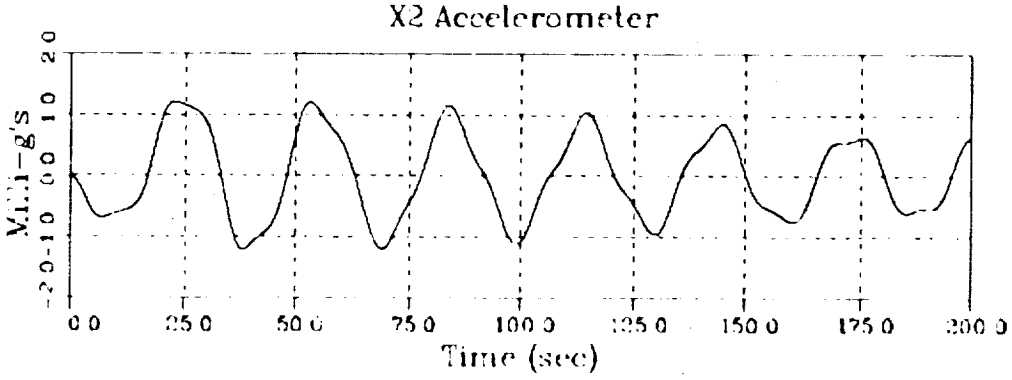

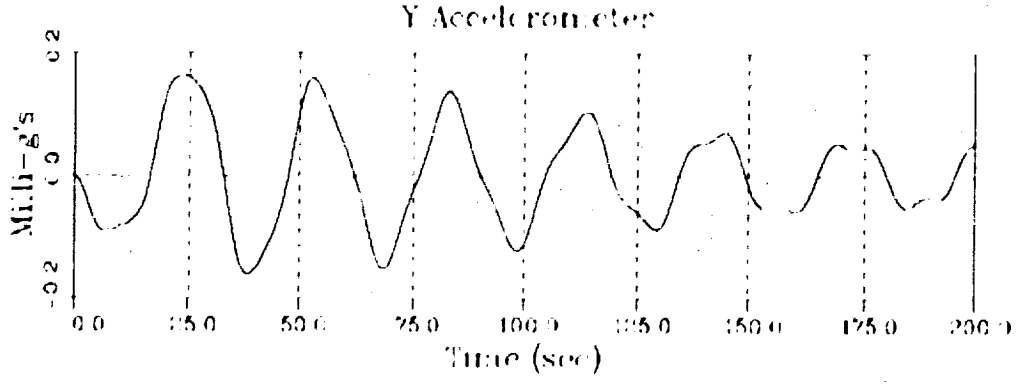

ORIGINAL PAGE IS
OF POOR QUALITY

SIMULATED ACCELERATION HISTORIES

REFERENCE GMT 246:19:31:47.1 FILE 20

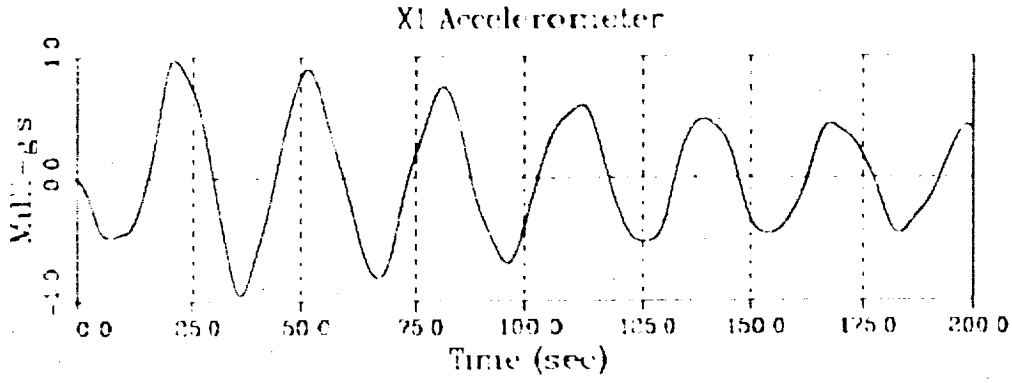

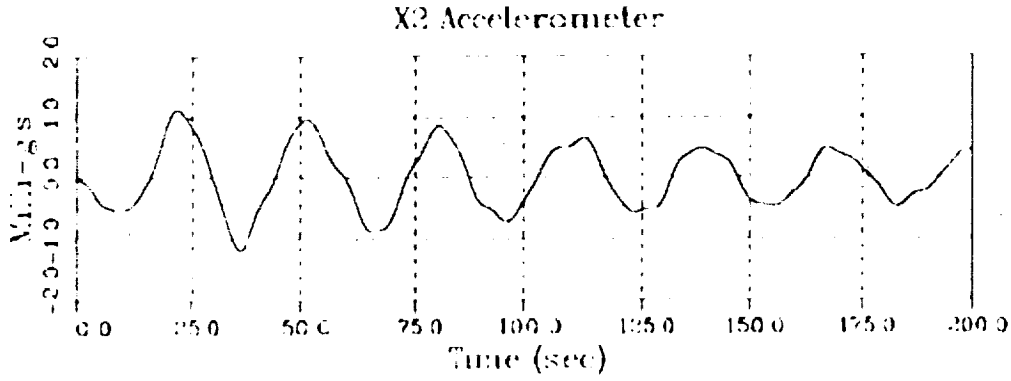

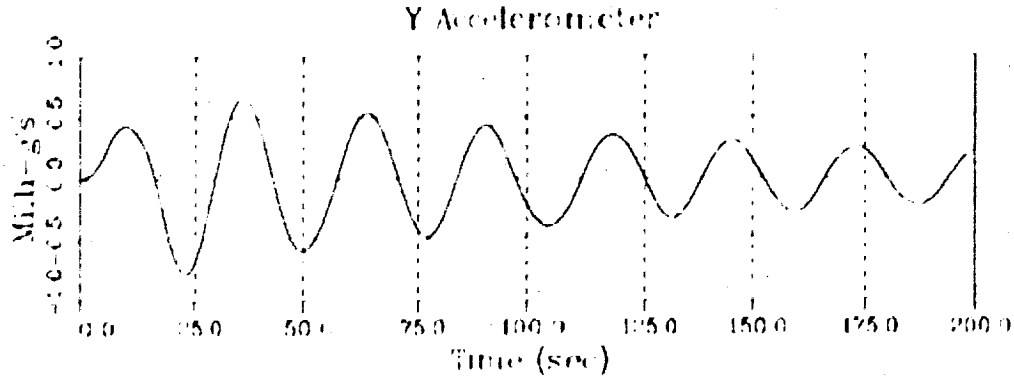

ORIGINAL PAGE IS
OF POOR QUALITY

SIMULATED ACCELERATION HISTORIES

REFERENCE GMT = 247 16 22 07 FILE 26

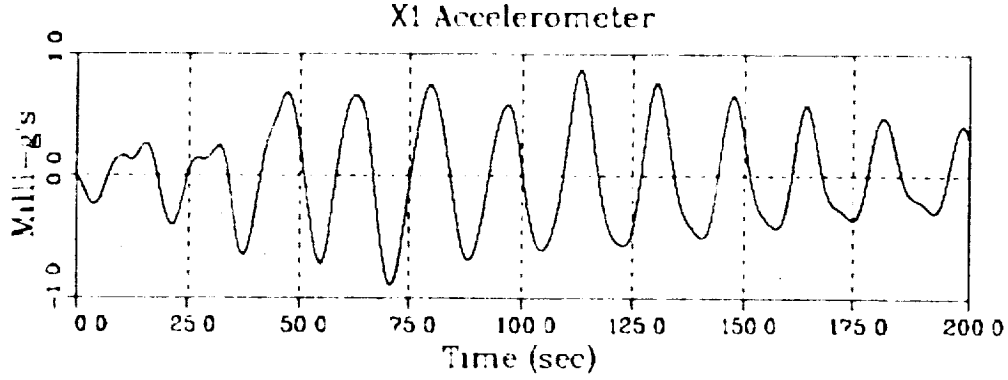

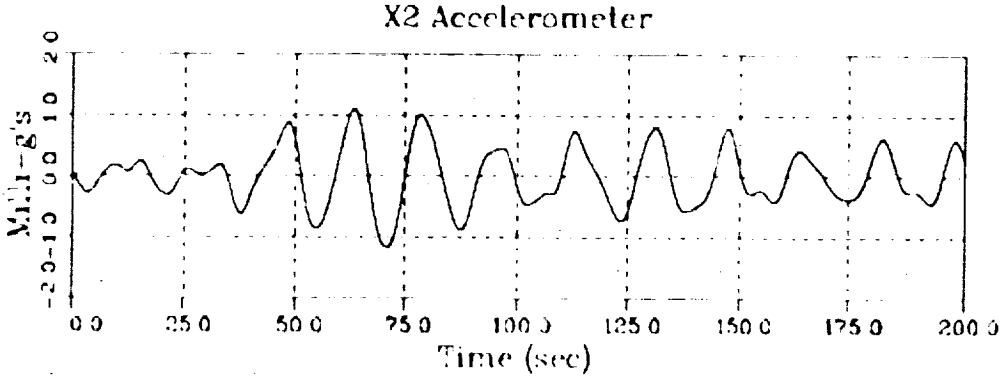

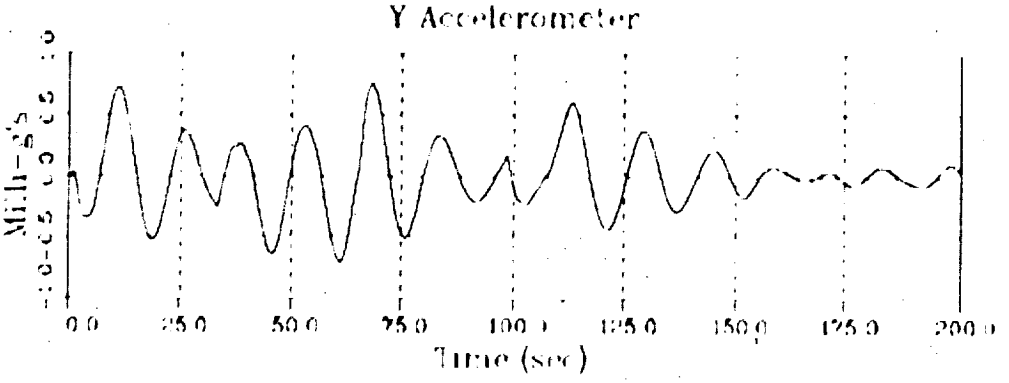

ORIGINAL PAGE IS
OE POOR QUALITY

SIMULATED ACCELERATION HISTORIES

REFERENCE GMT 247 16:37:49.4 FILE 37

X1 Accelerometer

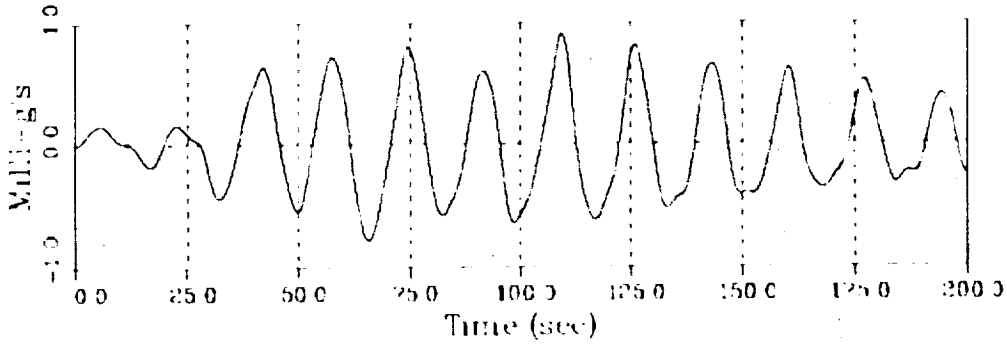

X2 Accelerometer

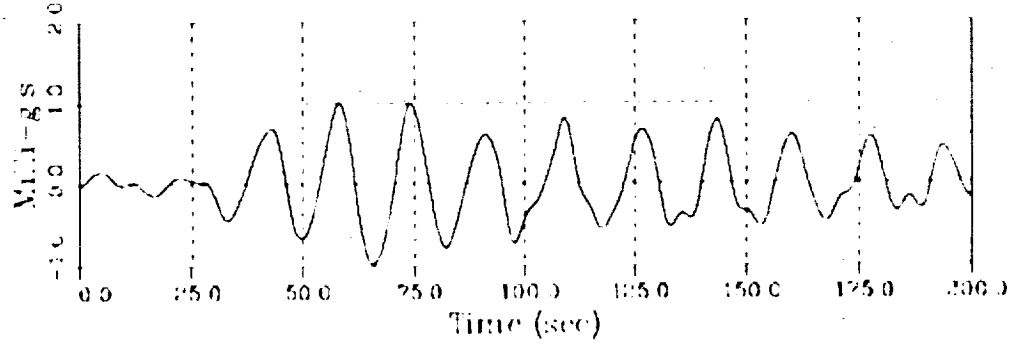

Y Accelerometer

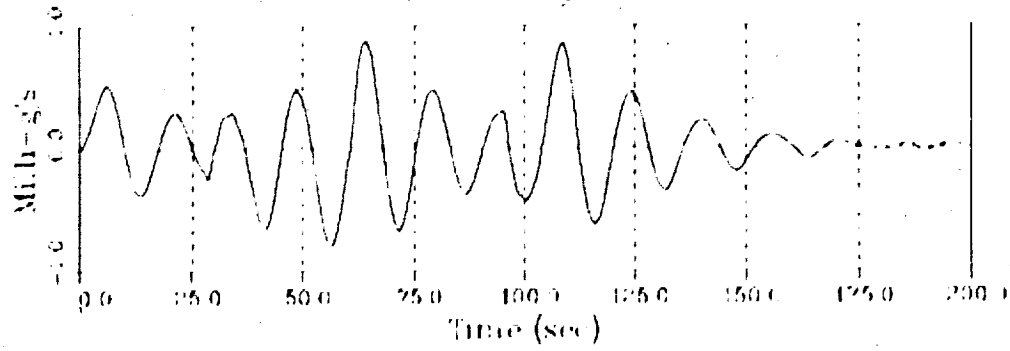

ORIGINAL PAGE IS
OF POOR QUALITY

SIMULATED ACCELERATION HISTORIES

REFERENCE GMT 247:17:32:58.4 FILE 28

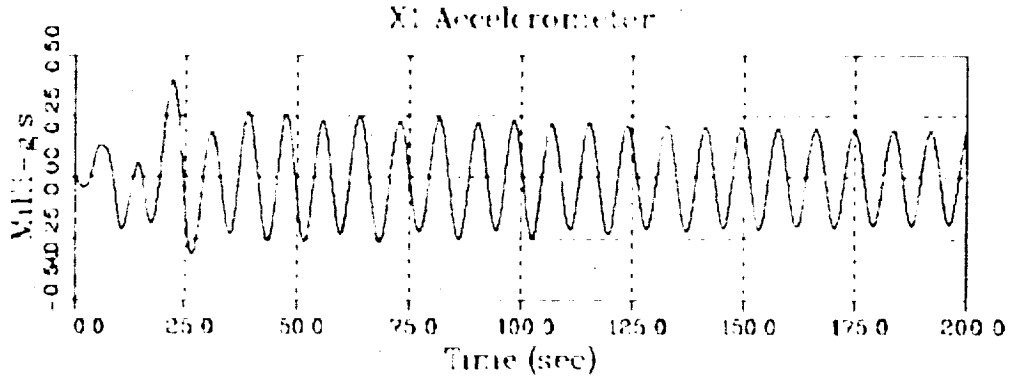

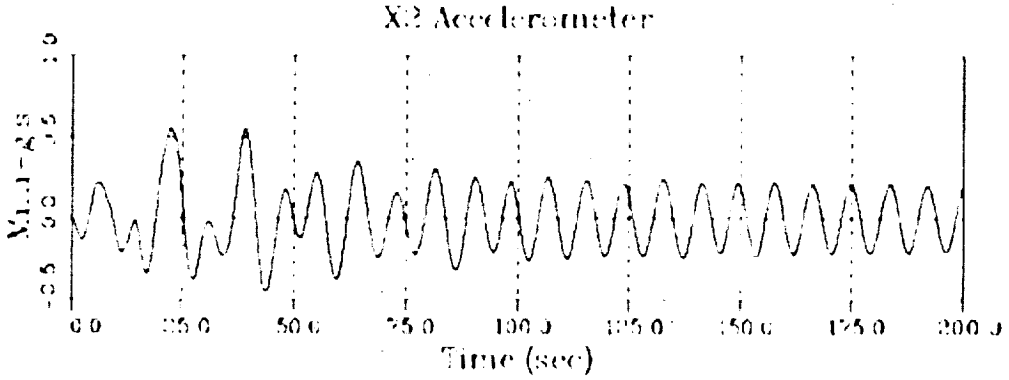

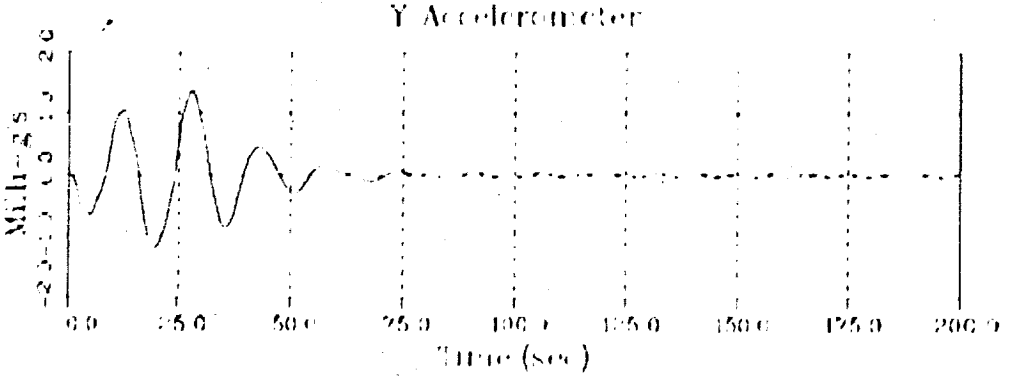

ORIGINAL PAGE IS
OF POOR QUALITY

SIMULATED ACCELERATION HISTORIES

REFERENCE GMT = 247 18 7:45 0 FILE 29

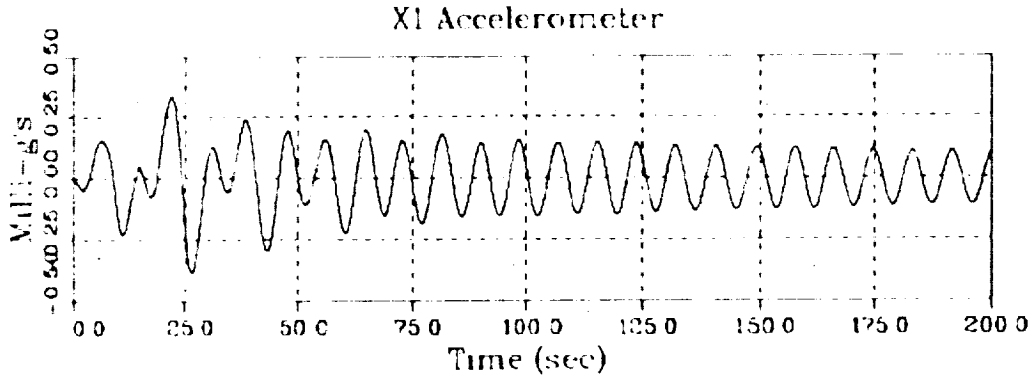

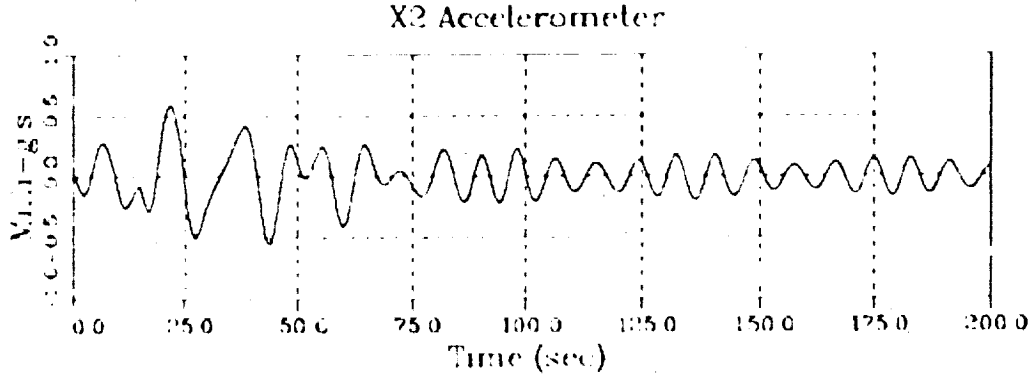

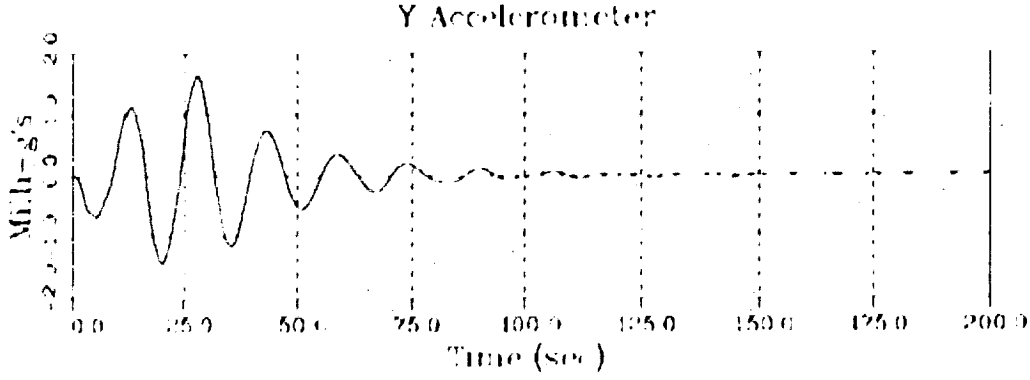

Final Report

LMSC-F087173

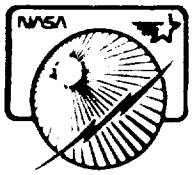

Appendix G
Computed Mast Tip Displacements

SIMULATED TIP DISPLACEMENT HISTORIES

REFERENCE GMT = 245 19:25:44.6 - FILE 5

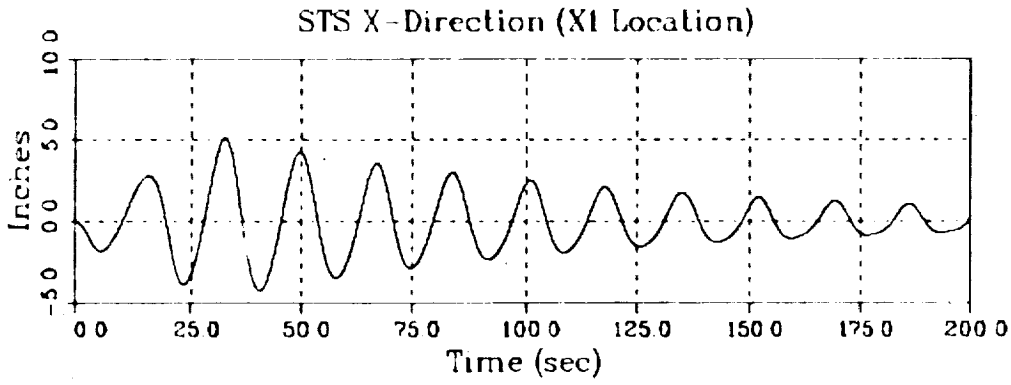

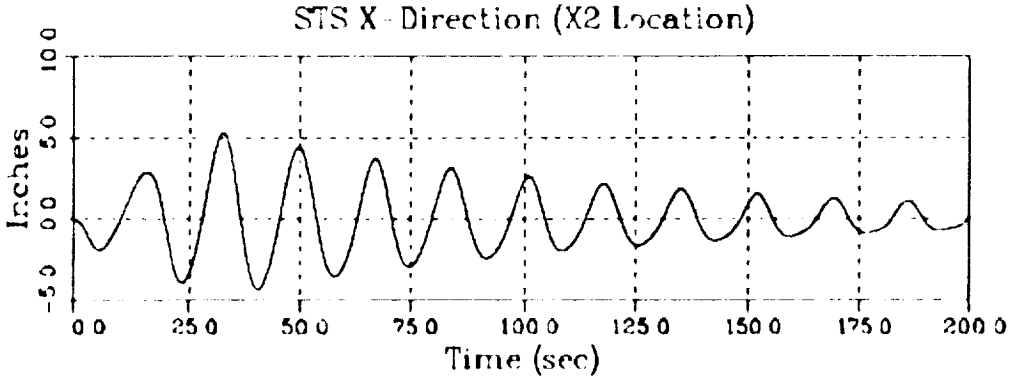

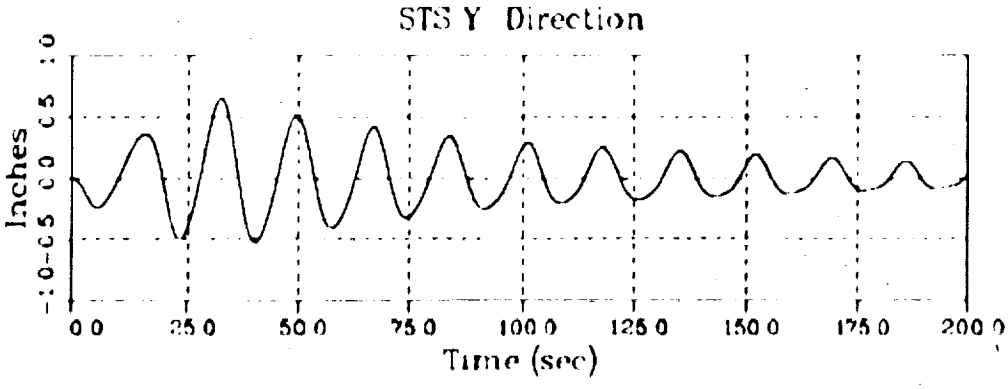

SIMULATED TIP DISPLACEMENT HISTORIES

REFERENCE GMT = 245:20:13:45.9 - FILE 6

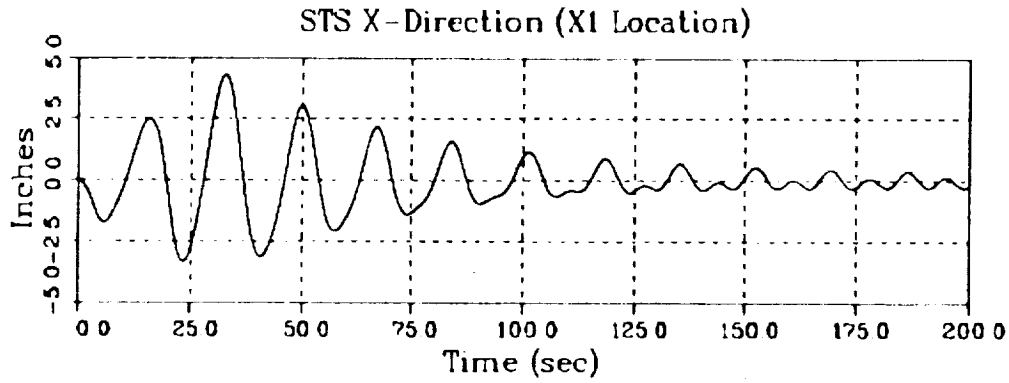

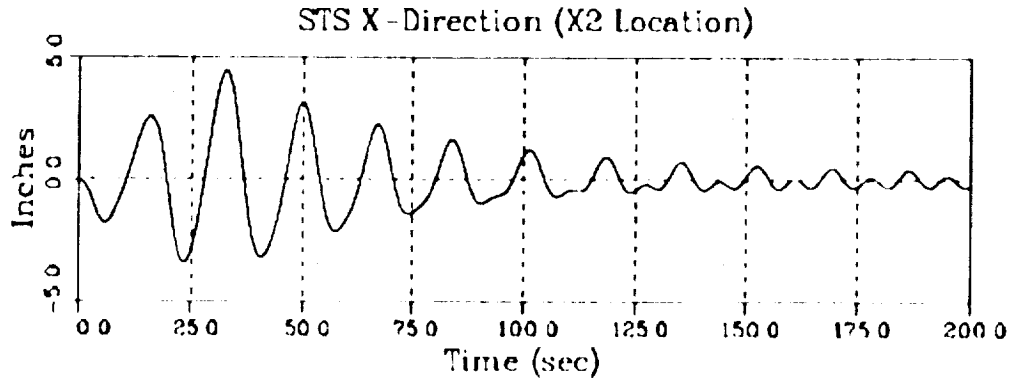

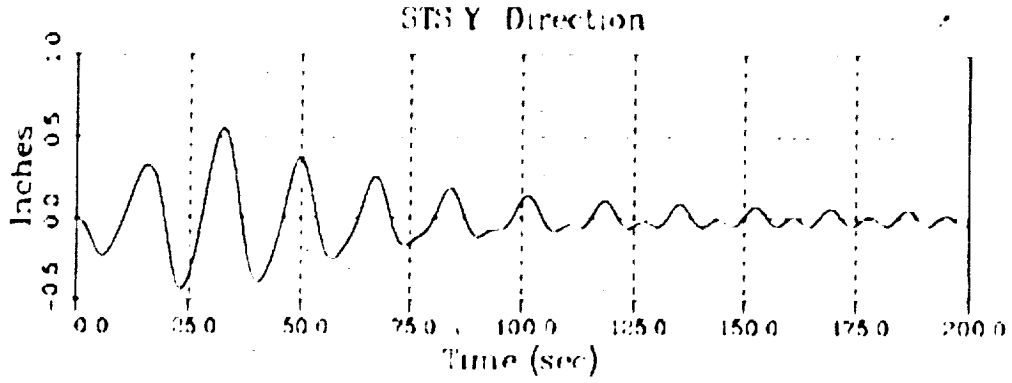

ORIGINAL PAGE IS
OF POOR QUALITY

SIMULATED TIP DISPLACEMENT HISTORIES

REFERENCE GMT – 245:20:13:45.9 – FILE 6 (with I.C.'s)

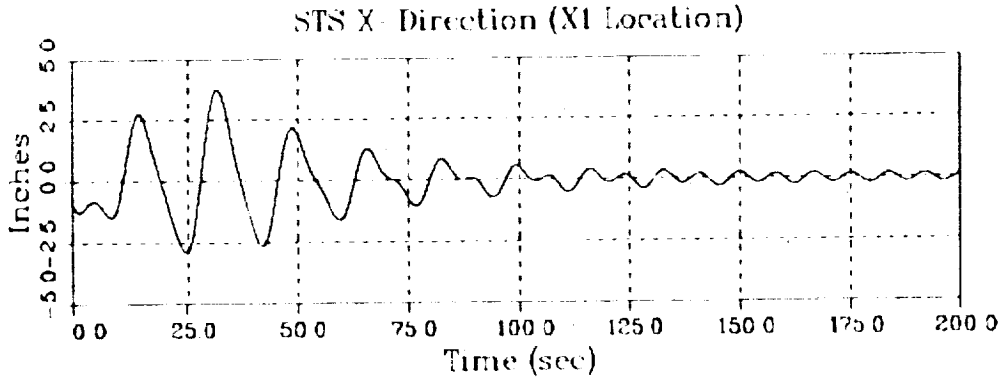

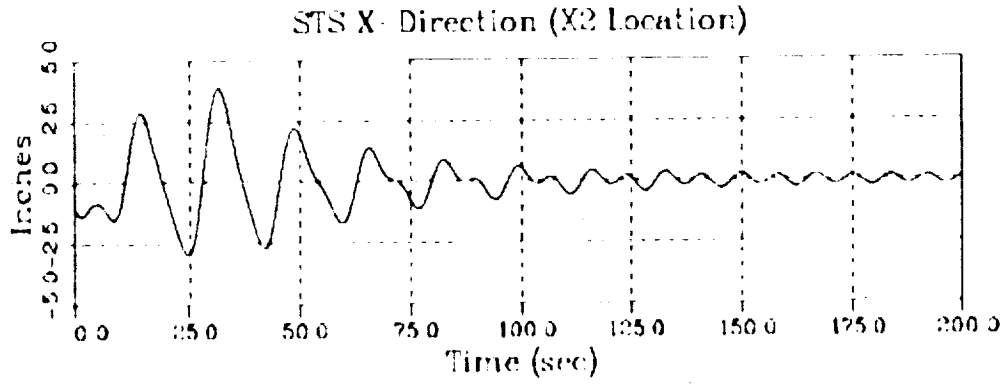

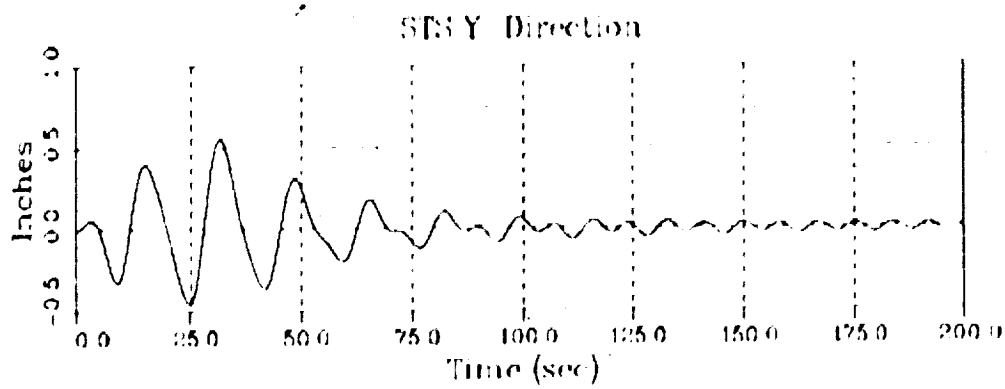

SIMULATED TIP DISPLACEMENT HISTORIES

REFERENCE GMT 246:13:29:43.7 FILE 10

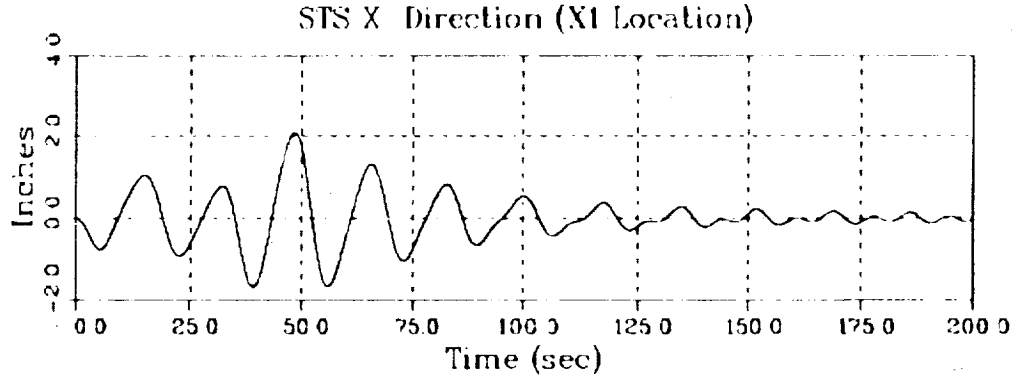

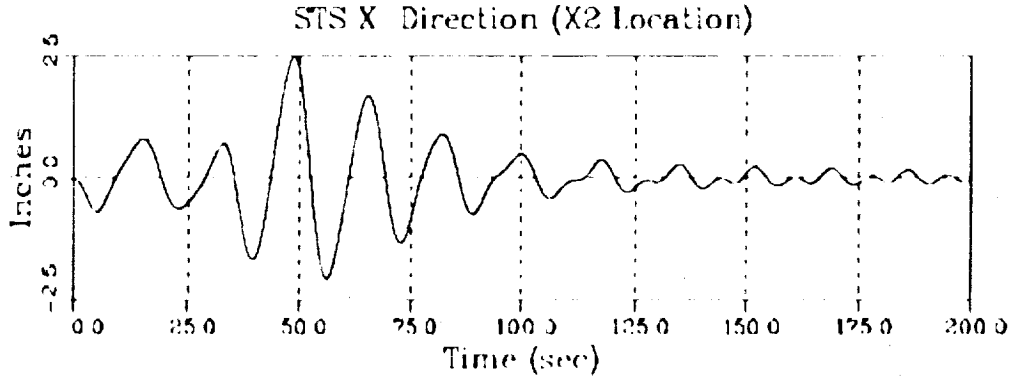

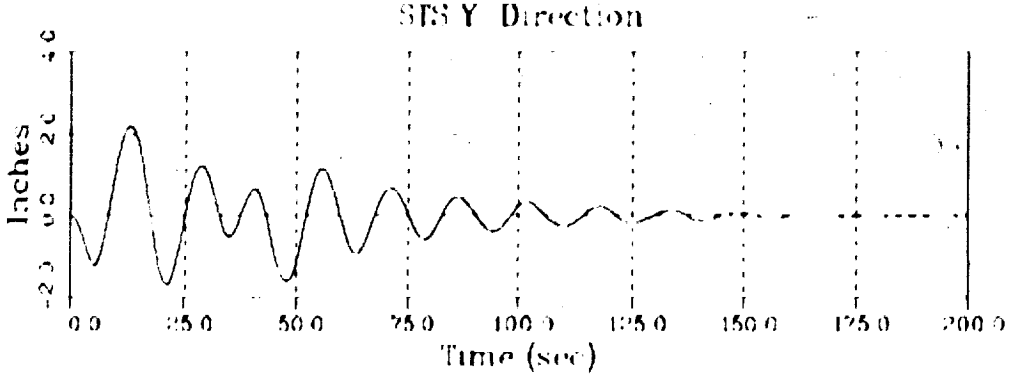

ORIGINAL PAGE IS
OF POOR QUALITY

SIMULATED TIP DISPLACEMENT HISTORIES

REFERENCE GMT 246:14:22: 9.9 FILE 11

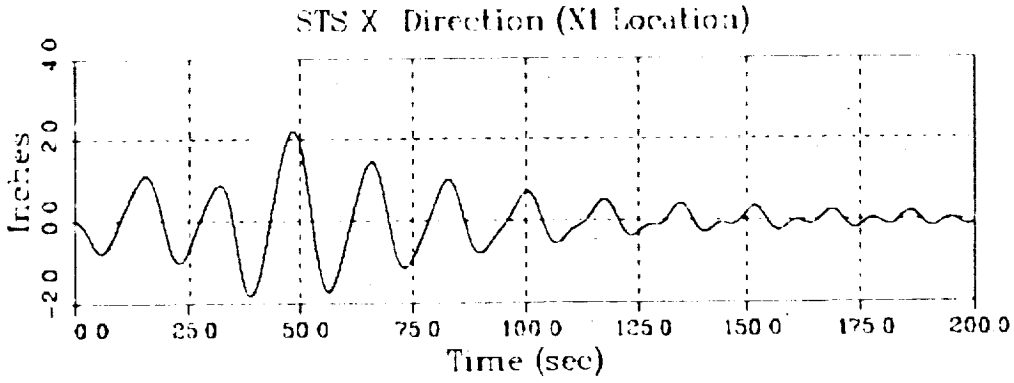

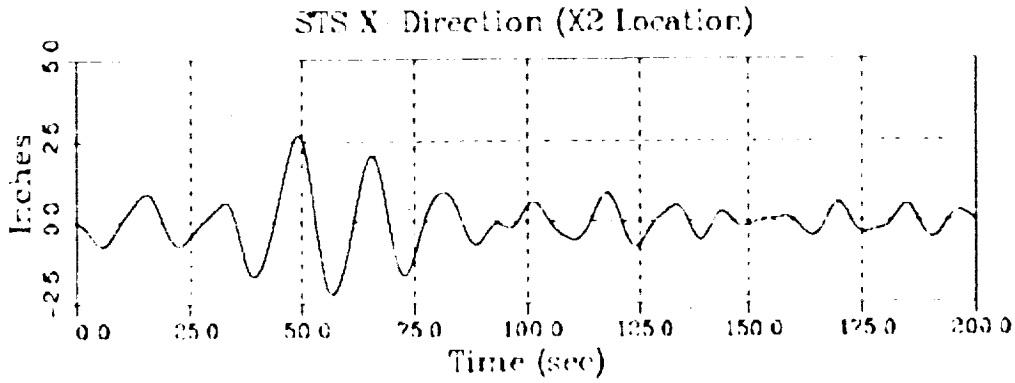

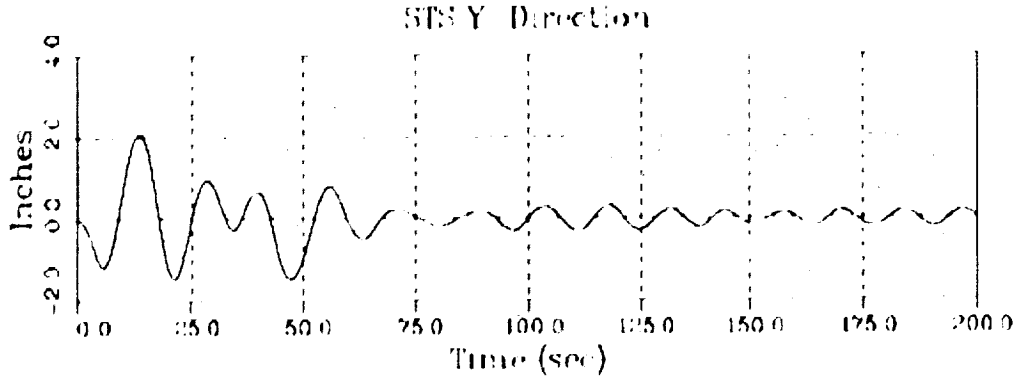

ORIGINAL PAGE IS
OF POOR QUALITY

SIMULATED TIP DISPLACEMENT HISTORIES

REFERENCE GMT - 246:15:04:24 FILE 12

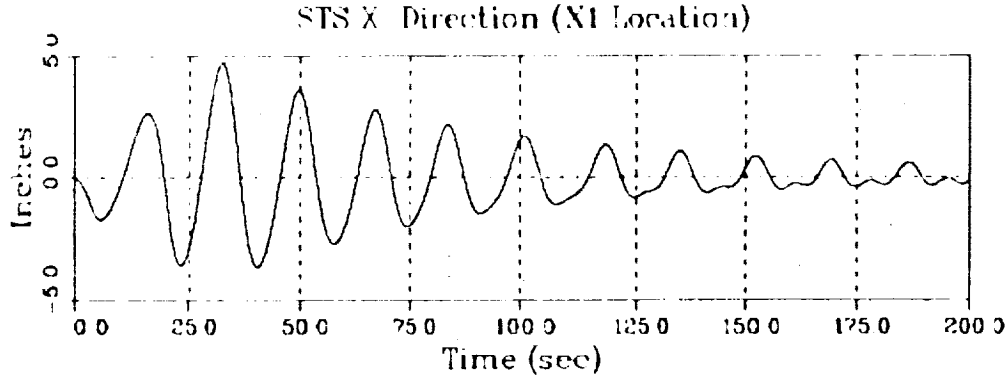

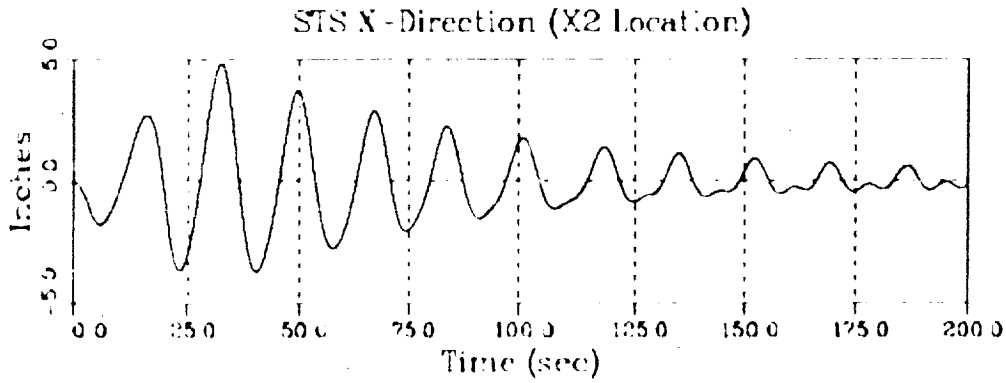

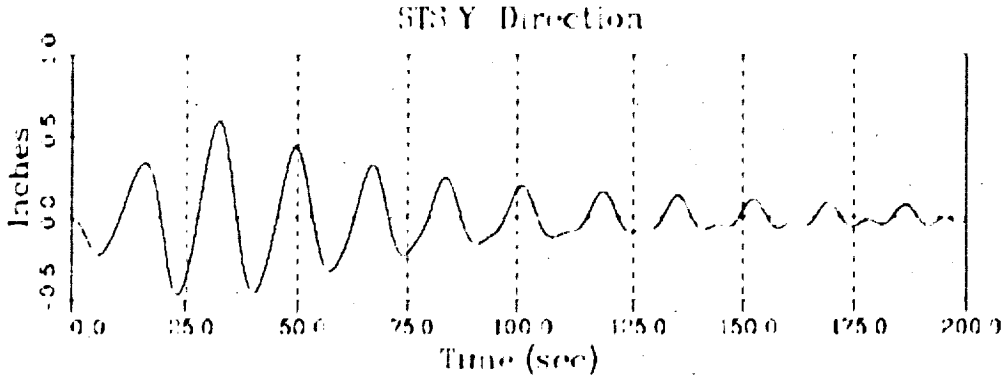

ORIGINAL PAGE IS
OF POOR QUALITY

SIMULATED TIP DISPLACEMENT HISTORIES

REFERENCE GMT 246:15:52:50.1 FILE 13

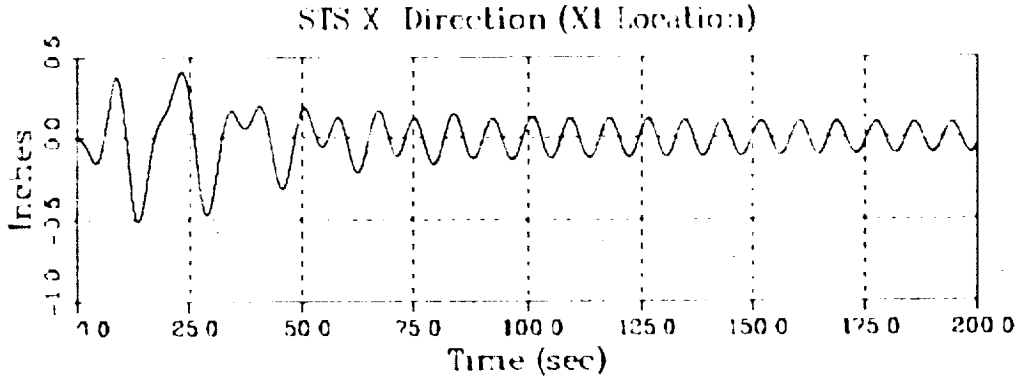

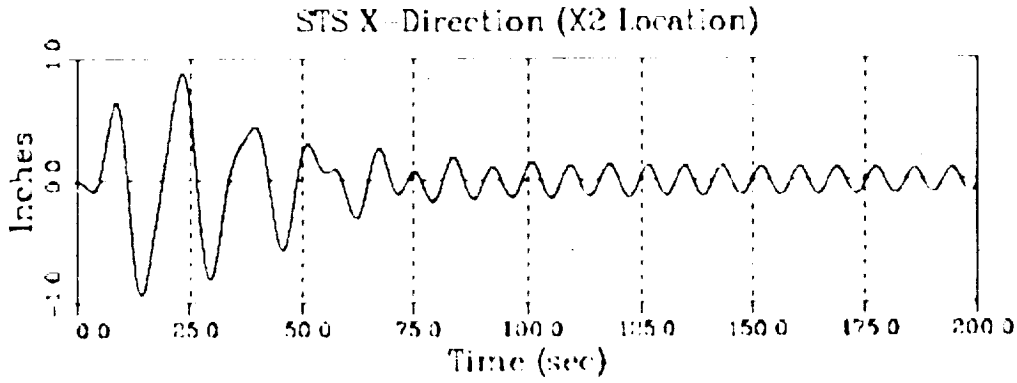

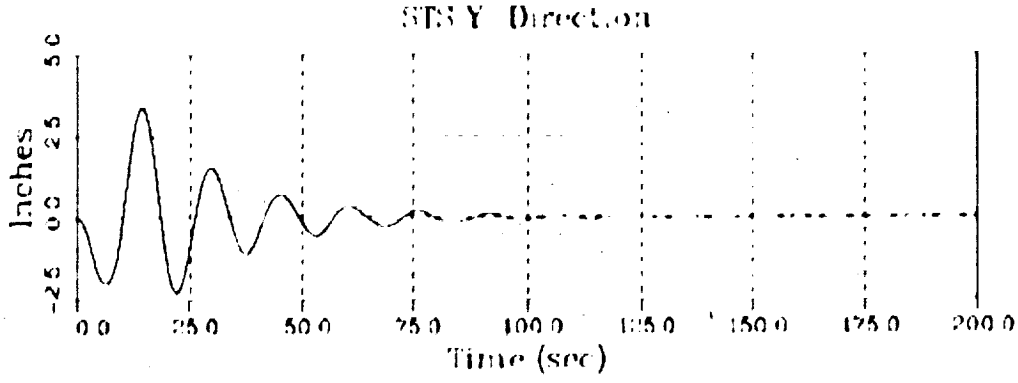

SIMULATED TIP DISPLACEMENT HISTORIES

REFERENCE GMT = 246:16 30:43.8 – FILE 14

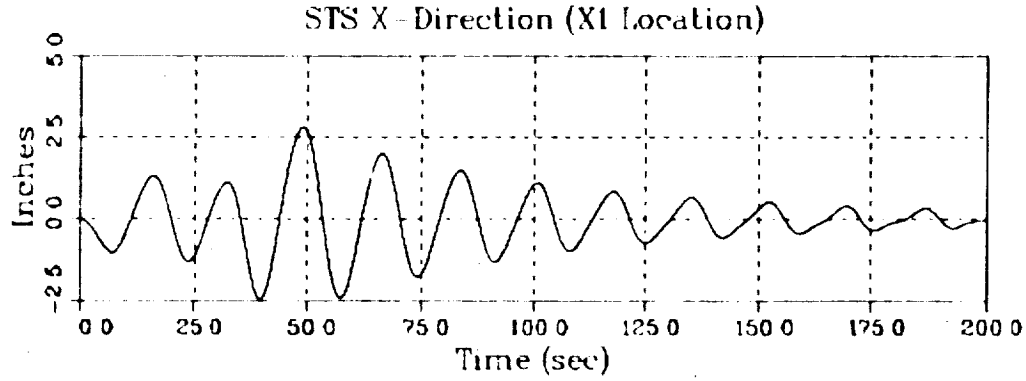

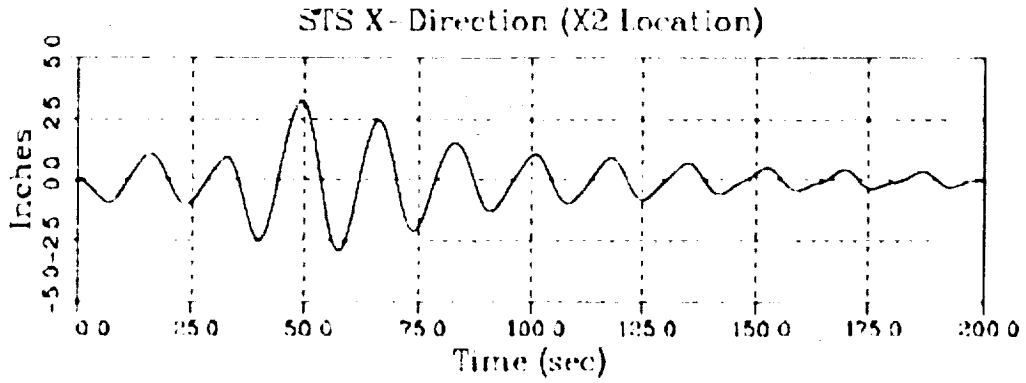

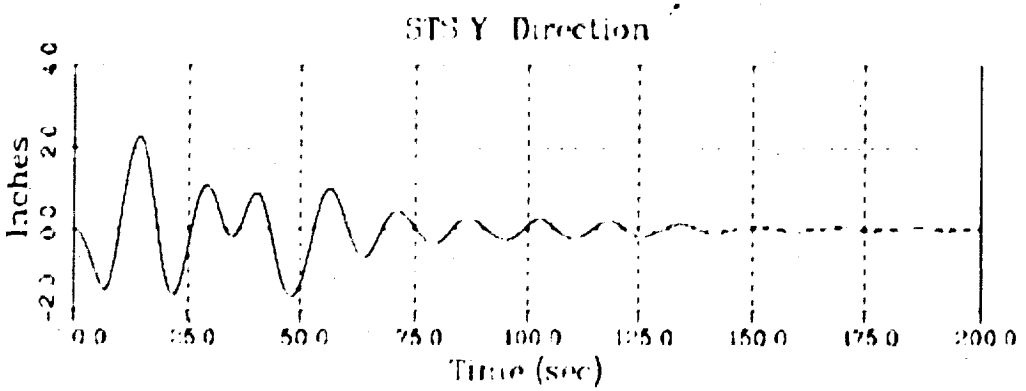

ORIGINAL PAGE IS
OF POOR QUALITY

SIMULATED TIP DISPLACEMENT HISTORIES

REFERENCE GMT = 246 17:23:23.6 - FILE 15

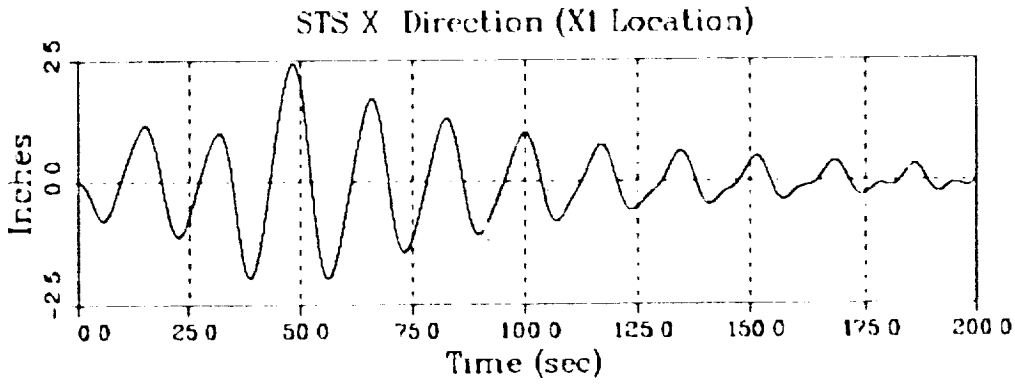

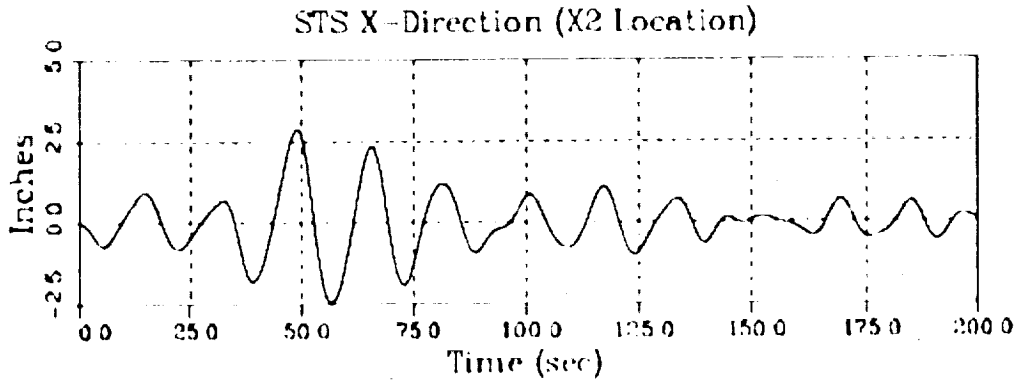

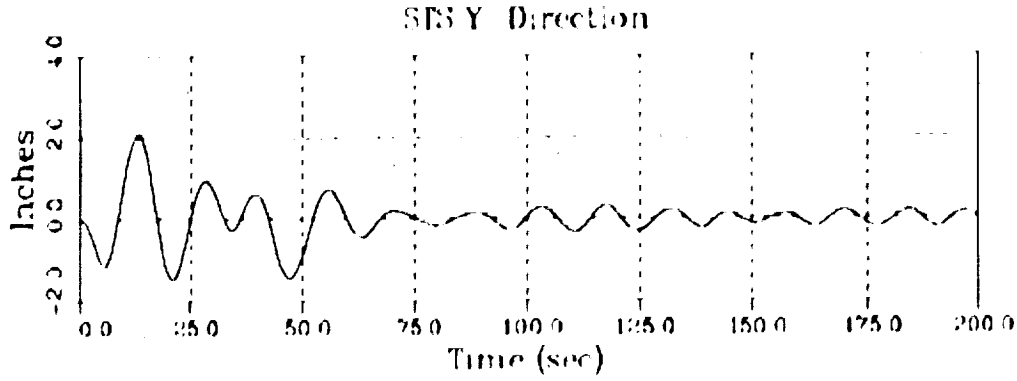

ORIGINAL PAGE IS
OF POOR QUALITY

SIMULATED TIP DISPLACEMENT HISTORIES

REFERENCE GMT – 246 18 6 44 3 FILE 17

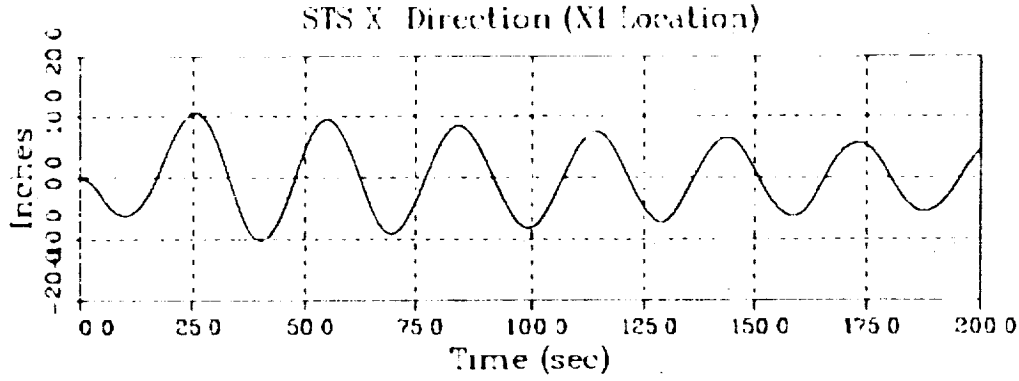

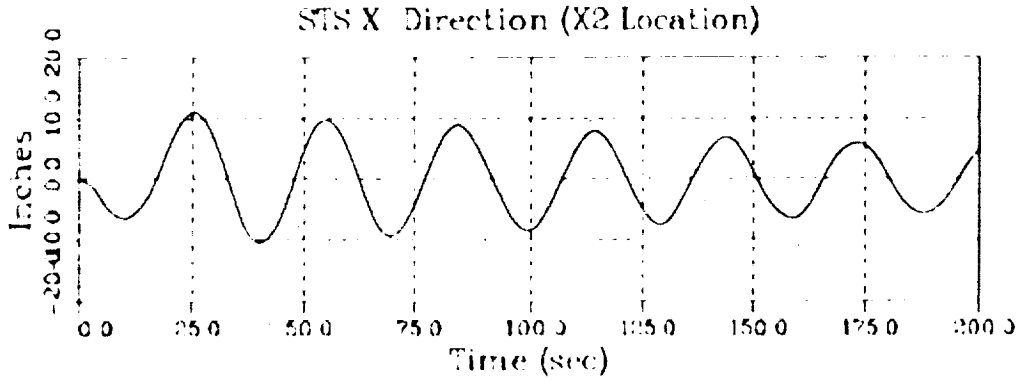

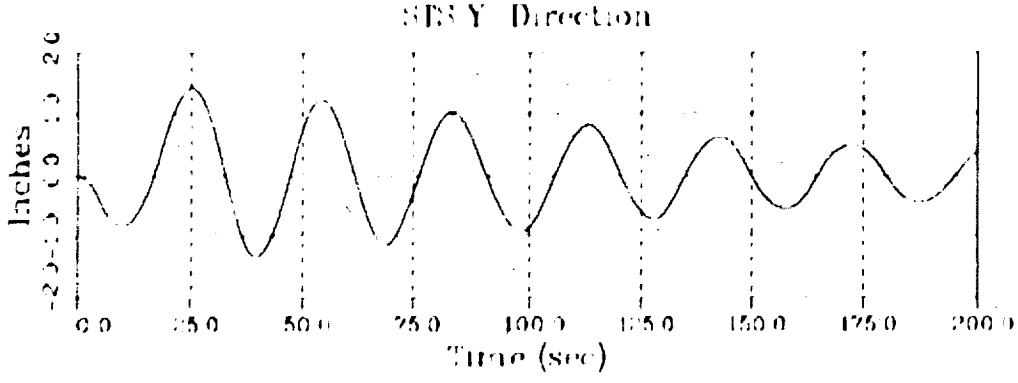

ORIGINAL PAGE IS
OF POOR QUALITY

SIMULATED TIP DISPLACEMENT HISTORIES

REFERENCE GMT = 246:19:31:47.4 FILE 20

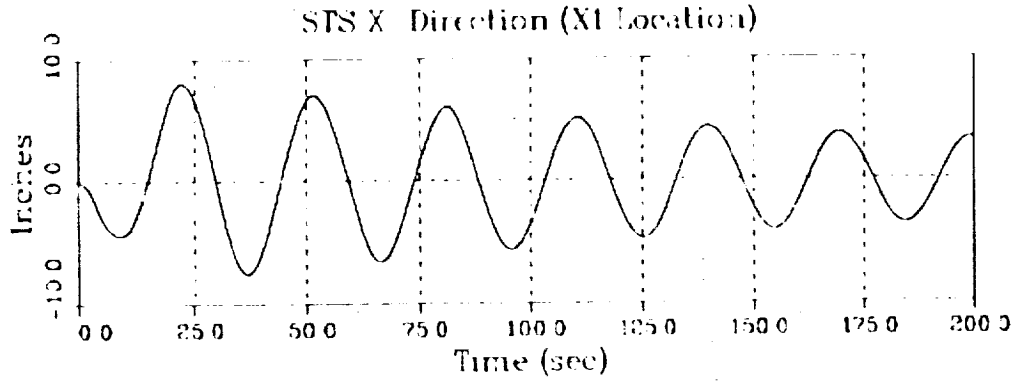

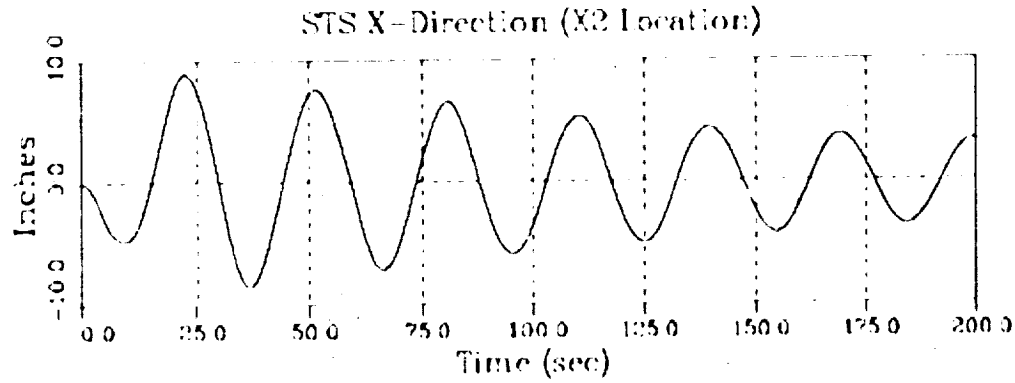

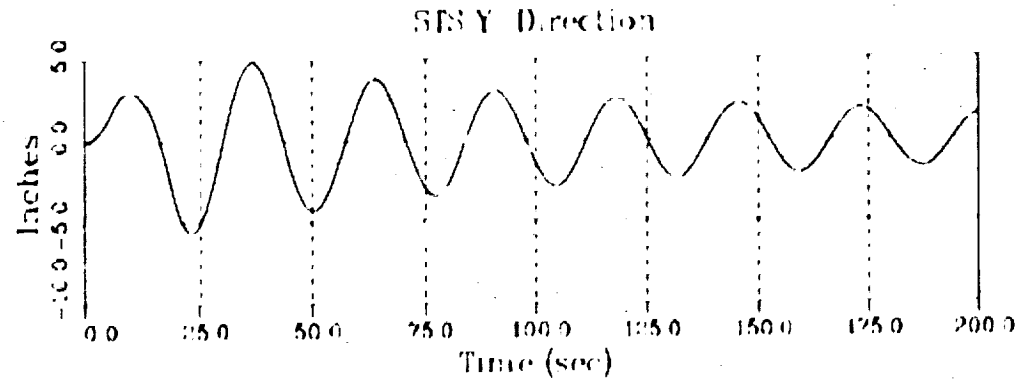

ORIGINAL PAGE IS
OF POOR QUALITY

SIMULATED TIP DISPLACEMENT HISTORIES

REFERENCE GMT 247 16: 22 07 FILE 26

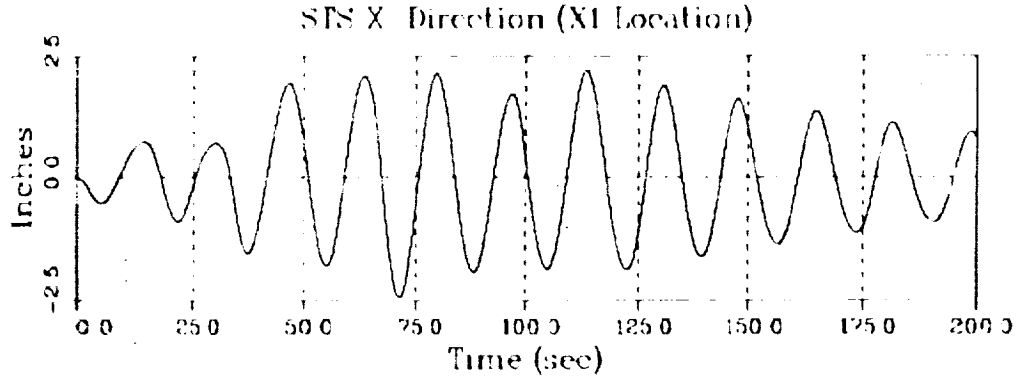

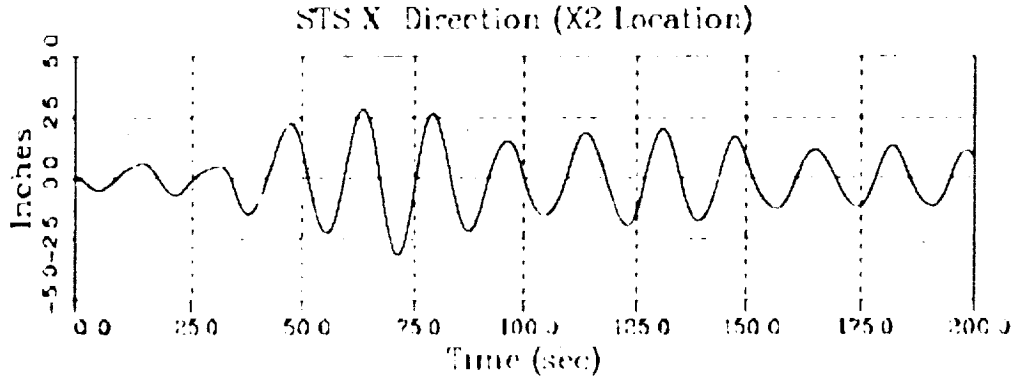

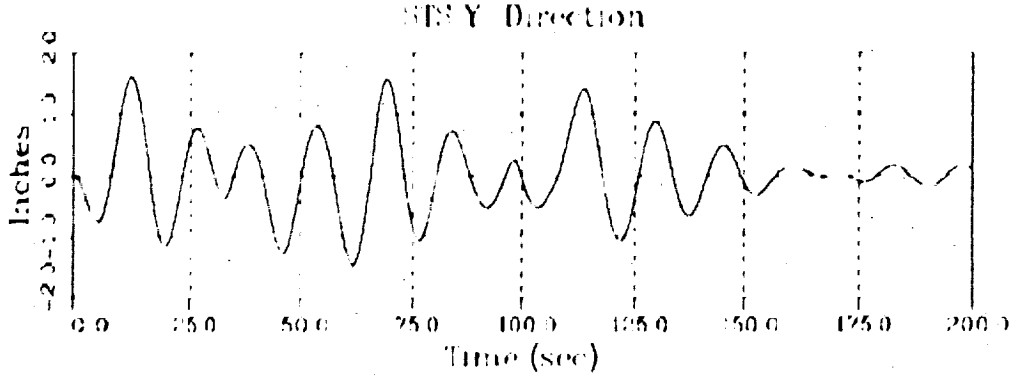

ORIGINAL PAGE IS
OF POOR QUALITY

SIMULATED TIP DISPLACEMENT HISTORIES

REFERENCE GMT 247:16:37:49.4 FILE 37

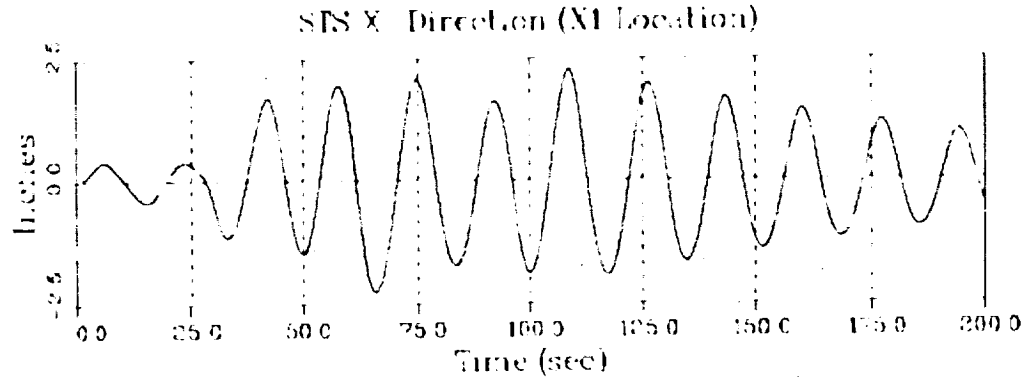

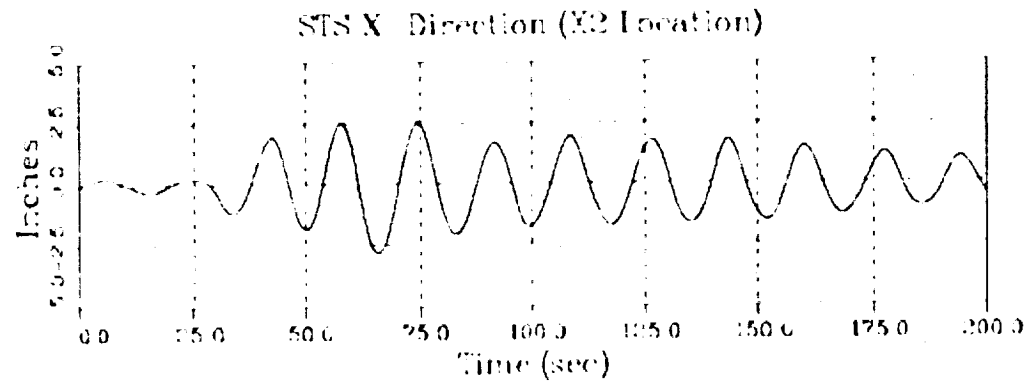

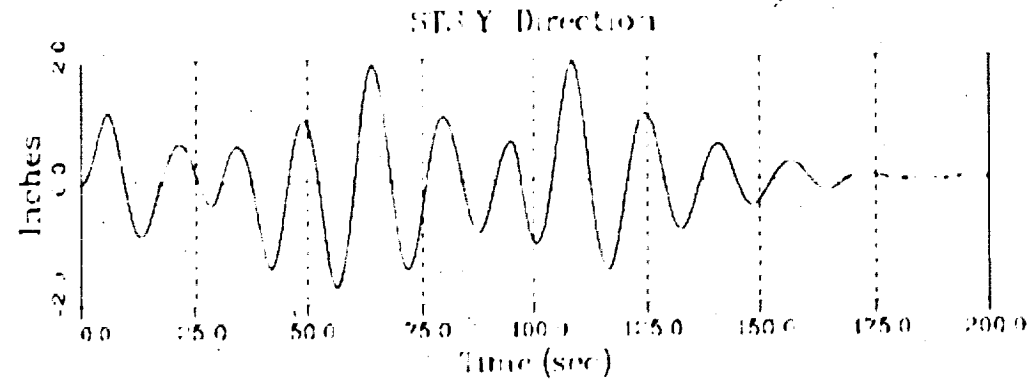

ORIGINAL PAGE IS
OF POOR QUALITY

SIMULATED TIP DISPLACEMENT HISTORIES

REFERENCE GMT = 247 17:32:58.4 FILE 28

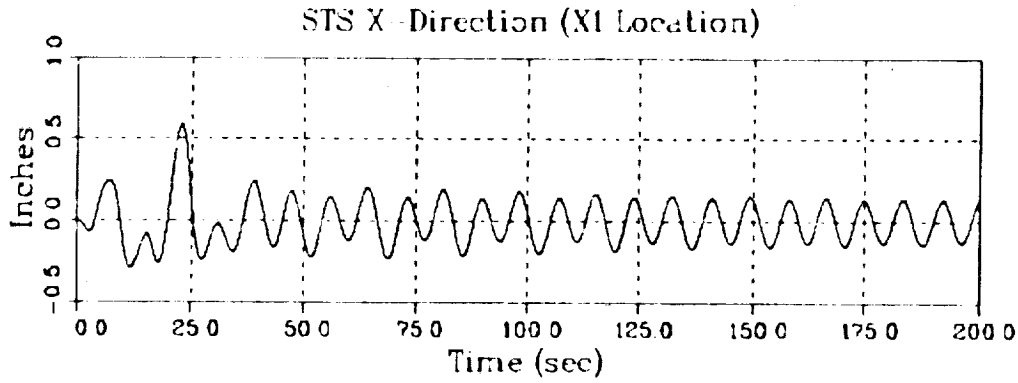

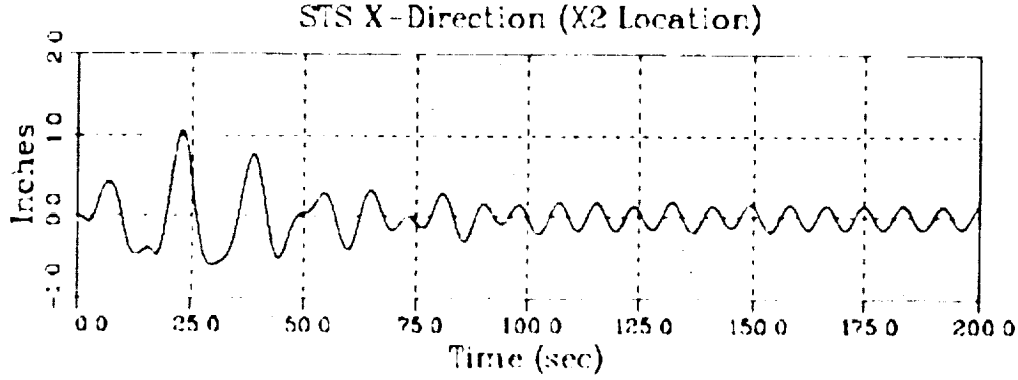

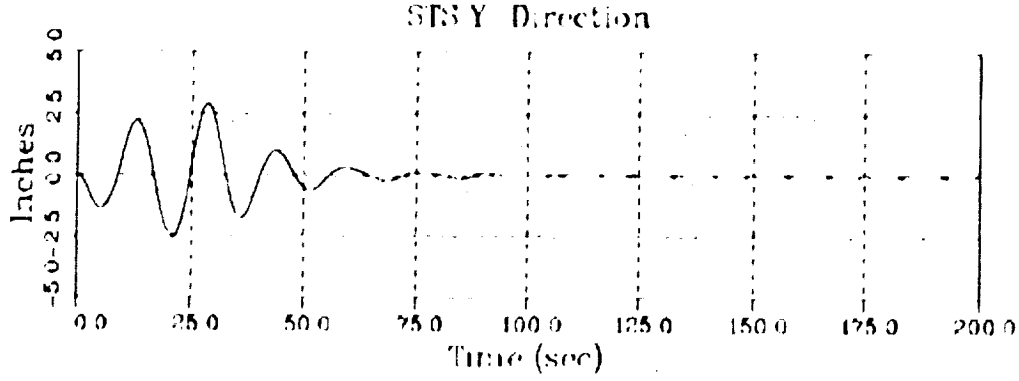

ORIGINAL PAGE IS
OF POOR QUALITY

SIMULATED TIP DISPLACEMENT HISTORIES

REFERENCE GMT = 247:18:7:45.6 - FILE 29